Springer Series on Atomic, Optical and Plasma Physics 72

Valeriy Astapenko

Polarization Bremsstrahlung on Atoms, Plasmas, Nanostructures and Solids

Springer

Springer Series on

ATOMIC, OPTICAL, AND PLASMA PHYSICS 72

For further volumes:
http://www.springer.com/series/411

Springer Series on

ATOMIC, OPTICAL, AND PLASMA PHYSICS

The Springer Series on Atomic, Optical, and Plasma Physics covers in a comprehensive manner theory and experiment in the entire field of atoms and molecules and their interaction with electromagnetic radiation. Books in the series provide a rich source of new ideas and techniques with wide applications in fields such as chemistry, materials science, astrophysics, surface science, plasma technology, advanced optics, aeronomy, and engineering. Laser physics is a particular connecting theme that has provided much of the continuing impetus for new developments in the field. The purpose of the series is to cover the gap between standard undergraduate textbooks and the research literature with emphasis on the fundamental ideas, methods, techniques, and results in the field.

Please view available titles in *Springer Series on Atomic, Optical, and Plasma Physics* on series homepage http://www.springer.com/series/411

Valeriy Astapenko

Polarization Bremsstrahlung on Atoms, Plasmas, Nanostructures and Solids

With 151 Figures

Springer

Valeriy Astapenko
Moscow Institute of Physics and Technology
Dolgogoprudnyi, Moscow region
Moscow, Russia

ISSN 1615-5653
ISBN 978-3-642-34081-9 ISBN 978-3-642-34082-6 (eBook)
DOI 10.1007/978-3-642-34082-6
Springer Heidelberg New York Dordrecht London

Library of Congress Control Number: 2012955486

Printed on acid-free paper

Springer is part of Springer Science+Business Media (www.springer.com)

to my teacher Victor Buimistrov

Contents

Chapter 1
Genesis of the Concept of Polarization Bremsstrahlung

1.1 Definition and Physics of Polarization Bremsstrahlung

Polarization bremsstrahlung (PBs) is a fundamental radiative process arising in scattering of a charged particle by a target with internal degrees of freedom [1]. An elementary example of PBs is radiation of an electron on an atom. In this case internal degrees of freedom correspond to bound electrons of an atom that can reradiate an electromagnetic eigenfield of an incident particle (in this case of an electron). This process is presented in Fig. 1.1 together with ordinary bremsstrahlung (OBs) that is also called static bremsstrahlung (SBs).

In Fig. 1.1 the dotted arrows show a real bremsstrahlung photon, the solid thick arrow shows a virtual photon of the eigenfield of an incident particle, the solid curve shows the trajectory of an incident particle.

It will be recalled that OBs results from acceleration of a charged particle in the field of a target. If an electron is scattered by a "bare" nucleus, bremsstrahlung (Bs) will proceed only by an ordinary (static) channel if nuclear degrees of freedom are neglected. In case of the presence of bound electrons, PBs arises together with OBs. To take into account the polarization channel, it is necessary to consider atomic electrons "on a par" with an incident electron, that is, as an independent dynamic degree of freedom able to participate "fully" in electromagnetic processes. At early stages of the theory of Bs on an atom an approximate model was used, within the framework of which bound electrons were replaced with the static distribution of electron charge. In other words, their role reduced exclusively to screening an atomic nucleus. So this model is called *the screening approximation*. In the screening approximation the polarization Bs channel is absent since atomic electrons are prevented from reradiating the electromagnetic field of an incident particle. But the fact is that atomic electrons are excited as a result of collision with a charged particle incident on an atom and can transform the energy of this excitation to the energy of a bremsstrahlung photon. It is significant that in this case the matter is so-called virtual excitation, when an electron is in a state with a

V. Astapenko, *Polarization Bremsstrahlung on Atoms, Plasmas, Nanostructures and Solids*, Springer Series on Atomic, Optical, and Plasma Physics 72,
DOI 10.1007/978-3-642-34082-6_1, © Springer-Verlag Berlin Heidelberg 2013

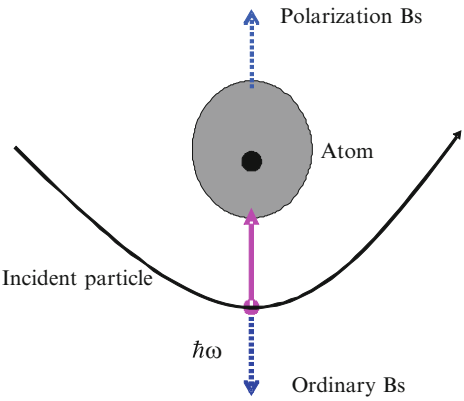

Fig. 1.1 Two channels of bremsstrahlung of an incident particle on an atom

higher energy that does not conform to the stationary state of an electron in the field of the atomic core.

It is possible to give PBs a double interpretation. First, this process can be represented as the conversion (reradiation) of a virtual photon making the eigenfield of an incident charge to a real photon on the electron subsystem of a target. This interpretation goes back to the method of equivalent photons that was for the first time applied by E. Fermi to calculate cross-sections of excitation of an atom by charged particles even before development of quantum mechanics. In the case under consideration PBs results from scattering of a virtual photon by atomic electrons to a real photon. This approach is especially descriptive in case of a relativistic incident particle, the electromagnetic field of which in its structure is close to the field of a free electromagnetic wave corresponding to radiation in an empty space. Another interpretation treats PBs as radiation arising as a result of induction of a variable dipole moment in the target core during scattering of a charged particle. The radiating dipole moment is proportional to the dynamic polarizability of a target at a specified frequency, so arising radiation is called polarization radiation. It is called bremsstrahlung since its energy, as in case of ordinary Bs, is drawn from the kinetic energy of an incident particle that is slowed down after emission of a photon.

Besides PBs on an atom, PBs on negative ions, positive ions with an electron core, on Debye spheres in plasma, on a solid body (amorphous, crystalline, polycrystalline), clusters, nanoparticles, etc. is possible.

In the presence of radiation an inverse bremsstrahlung effect by the polarization channel is also possible, when the energy of a radiation field is absorbed by an electron scattered by an atom (ion) as a result of "pumping" through the electron core of a target. Then the field energy decreases, and the electron is accelerated. In case of a reverse energy flow, on the contrary, the electron is slowed down, and the field is strengthened.

It should be emphasized that PBs and SBs arise in the same elementary radiative process. In terms of quantum mechanics this means that in obtaining the probability of total Bs it is necessary to sum their amplitudes. Hence it follows that the total

probability of the process contains an interference summand corresponding to interchannel interference during Bs. This summand is particularly important in case of bremsstrahlung of nonrelativistic electrons.

1.2 Analogs of Polarization Bremsstrahlung in a Medium

The term "polarization bremsstrahlung" was invented for radiation during scattering of a charged particle by an atom in 1985 [1]. Until then different scientific groups used three terms: dynamic Bs (V.M. Buimistrov's group), atomic Bs (M.Ya. Amus'ya with co-workers), and polarization Bs (B.A. Zon).

For radiation resulting from the conversion of the eigenfield of charged particles on Debye spheres in plasma A.V. Akopyan and V.N. Tsytovich [2] proposed the term "transient bremsstrahlung". The origin of this name is connected with the fact that PBs in plasma can be described as transient scattering of virtual photons to real photons by the Debye "coat". The correspondence between transient Bs and polarization (dynamic) Bs was established in the V.A. Astapenko's thesis [3], in which it was shown that transient Bs is nothing but polarization Bs on Debye coats surrounding ions in plasma.

Another analog of PBs is parametric X-radiation arising in scattering of a charged particle in a single crystal. This term was invented by Ya.B. Fainberg and N.A. Khizhnyak.

In works of N.N. Nasonov it was shown that parametric X-radiation represents a coherent part of PBs in a crystal in the spectral range, in which the high-frequency approximation for dynamic polarizability of crystal atoms is true.

Finally, another realization of PBs is emission of a charged particle on nonuniformities of dielectric permittivity of a medium that was studied theoretically by S.P. Kapitsa [4]. This emission results from scattering of the eigenfield of a charge in a substance that is caused by the nonuniformity of electron density of a target resulting in nonuniformity of dielectric permittivity.

From the above it is seen that the interpretation of PBs as the process of scattering of virtual photons is applicable to a wide range of phenomena both on atomic particles and on condensed media, in plasma, and in nanomaterials.

To summarize, the polarization mechanism is a basis for the consistent microscopic description of related radiative phenomena, in which the conversion of a virtual photon to a real photon on target electrons occurs (Table 1.1).

1.3 Main Properties and Characteristic Features of Polarization Bremsstrahlung

Since the mechanism of initiation of a polarization channel differs from the mechanism of initiation of ordinary Bs, PBs has a number of distinguishing characteristic features (Table 1.2).

Table 1.1 Synonyms of the term "PBs" and analogs of PBs in a medium

Radiation on an atom	Dynamic Bs (V.M. Buimistrov with co-workers)
	Atomic Bs (M.Ya. Amus'ya with co-workers)
	Polarization Bs (B.A. Zon)
Radiation in plasma	Transient Bs (V.N. Tsytovich, A.V. Akopyan)
Radiation in a condensed medium	Parametric X-radiation (Ya.B. Fainberg and N.A. Khizhnyak)
	Radiation on random nonuniformities (S.P. Kapitsa)

Table 1.2 Characteristic features of ordinary and polarization bremsstrahlung

Static Bs	Polarization Bs
Caused by acceleration of a charge in the field of a target	Caused by a variable dipole moment induced in the target core
Formed at short distances from a target	Formed at long distances from a target
The intensity is inversely proportional to the squared mass of an incident particle	The intensity does not depend on the mass of an incident particle
Has an acute angular distribution for relativistic incident particles	Has a dipole angular distribution for relativistic incident particles
The spectrum is defined by the potential of a target	The spectrum is defined by the dynamic polarizability of a target

The most essential distinction between these mechanisms of radiation is that the intensity of OBs is inversely proportional to the squared mass of an incident charged particle, and the intensity of PBs does not depend on this mass (as a first approximation).

Another distinction shows itself for relativistic charged particles: OBs has a narrow angular distribution along the velocity of a scattered charge, and the angular distribution of PBs is of a dipole nature.

In the relativistic case the PBs cross-section increases logarithmically with the energy of an incident particle, and the SBs cross-section does not depend on energy in the relativistic limit.

Another important distinction is that OBs is formed at short distances from a scattering center, and PBs is formed at large distances. So the polarization channel is more sensitive to the spatial structure of a target than the static mechanism of Bs. Based on this fact is the possibility to develop new methods of material diagnostics using PBs.

The OBs spectrum is defined by the potential of a target, while the spectral PBs cross-section is proportional to the squared dynamic polarizability of a target. This property of the polarization channel can be used to determine eigenfrequencies and strengths of oscillators of electron transitions of a target.

1.4 Theoretical Fundamentals Concerning Polarization Bremsstrahlung

Polarization bremsstrahlung results from virtual excitation of bound electrons of a target under the action of a variable electric field produced by an incident particle. Corresponding to the virtual excitation of a system in terms of the second-order perturbation theory is summation over intermediate energy states of the electron core of a target. Generally speaking, this summation covers the region of the discrete and continuous energy spectra. If the frequency of an emitted photon approaches one of eigenfrequencies corresponding to the transition of target electrons between bound states, the resonance increase of the PBs cross-section occurs. In this case *resonant polarization bremsstrahlung* takes place. The described situation arises in scattering of electrons by ions in the UV and X-ray (in case of multiply charged ions) ranges. Besides, it takes place in scattering of electrons by alkali and alkali-earth atoms in the visible spectrum. Corresponding to the resonance process is a resonance in the frequency dependence of the dynamic polarizability of a target. Such a resonance is absent in the X-ray frequency range for targets consisting of neutral atoms because of the low oscillator strength of bound-bound transitions in this case and influence of electron collective effects.

As already noted, an important characteristic feature of PBs is the independence of its cross-section from the mass of an incident particle, while ordinary bremsstrahlung (OBs) of heavy particles caused by acceleration of a charge in the electric field of the target is suppressed. The OBs cross-section is inversely proportional to the squared mass of an emitting particle. The independence of the PBs cross-section from the mass of an incident particle is connected with the nature itself of this phenomenon. The virtual photon of the charge eigenfield is defined by the velocity and the impact parameter and does not depend on mass.

Within the framework of the classical trajectory description it can be said that PBs is formed at distances exceeding the size of the electron core of a target since with smaller impact parameters the coherence of reradiation of a virtual photon of an incident particle eigenfield to a real photon is lost. On the contrary, OBs in scattering of an electron by a neutral atom corresponds to small impact parameters and occurs in the region of space where the scattering center field is the strongest. The trajectory approach loses its obviousness in charge scattering in an extended medium. Then it is better to use the conjugate space, in which the role of distance is played by a wave vector transferred from an incident particle to a target: the more is the transferred wave vector, the less is a corresponding spatial scale. In such an approach it can be asserted that the most contribution to the integrated cross-section of PBs on an isolated atomic particle is made by transferred wave vectors smaller than the inverse radius of a target.

In case of electron scattering in a condensed substance and in plasma, PBs with transfer of energy-momentum to collective excitations (phonons, plasmons, polaritons) as well as to the whole sample as a unit is possible. The latter case is realized in scattering of a charged particle in single-crystal and polycrystalline targets, when together with pair (incoherent) interaction processes with transfer of a

momentum (or a wave vector) to the whole crystal lattice are possible. In this situation the transferred wave vector is equal to one of the vectors of the reciprocal crystal lattice, and the yield of PBs photons is proportional to the squared concentration of medium atoms. Coherent PBs in a single crystal occurs at fixed frequencies defined by the reciprocal lattice vector and the incident particle velocity. It can be interpreted as the Bragg scattering of a virtual photon of the incident particle eigenfield by the crystal planes of a target. Thus the PBs spectrum in a regular structure has a set of sharp maxima (coherent peaks). When going to a polycrystal, it is necessary to average the PBs probability over possible orientations of microcrystallites. As a result, coherent peaks in the PBs spectrum disappear, and instead of them a stepped structure appears that is caused by sequential "turning-off" of the reciprocal lattice vector contribution to radiation as the bremsstrahlung photon energy growths.

Besides the coherent component of PBs, in crystalline targets at the nonzero temperature of a medium an incoherent radiation channel arises that is caused by lattice thermal vibrations. The incoherent component of PBs prevails in the high-frequency spectral range where the process is accompanied by transfer of reciprocal lattice vectors of high magnitudes from an incident particle to a target. Such processes are rather sensitive to the deviation of the lattice structure from the ideal structure.

PBs both of nonrelativistic and of relativistic electrons scattered by isolated centers of force has a dipole pattern, while OBs of a relativistic charge in this case is directed along its velocity. This is connected with the fact that a real photon during PBs is produced as a result of scattering of a virtual photon by nonrelativistic electrons of a target. If the radiation coherence length L_{coh} is introduced as a distance at which the detachment of a real photon from the eigenfield of a charged particle occurs, it can be shown that this value reaches macroscopic sizes for incident particles with the high Lorentz factor $\gamma = 1\Big/\sqrt{1-(\mathrm{v}/c)^2} >> 1$ (v is the velocity of an incident particle, c is the velocity of light in free space) $L_{coh} \approx \gamma^2 \lambda$ (λ is wavelength of emitted photon).

The coherence length of PBs in pair interaction remains being of the order of the radiation wavelength. This causes the absence of the density effect for PBs in disordered structures. It will be recalled that the density effect in OBs shows itself in reduction of process intensity as a result of increasing phase velocity of electromagnetic waves in a medium with the plasma dielectric permittivity (which is less than unity). This increase results in the fact that a real photon is detached from the incident particle eigenfield faster than it would occur in vacuum, which results in reduction of the OBs cross-section. This effect was for the first time predicted by M.L. Ter-Mikaelyan [5]. It is responsible for decreasing OBs intensity in the low-frequency range $\omega < \gamma\, \omega_{pe}$ (ω_{pe} is electronic the plasma frequency).

For applications of PBs spectroscopy as a physical basis for diagnostics of materials including nanostructured media, it should be noted that it is the formation of PBs at large impact parameters (or at low transferred momenta) that makes it sensitive to interatomic correlations. This ultimately makes it possible to obtain information on a target structure based on the analysis of spectral and angular dependences of PBs.

1.5 Polarization Bremsstrahlung in Atoms, Solids and Nanostructures

The consistent theory of PBs on an atom based on the quantum-mechanical approach has arisen in the works of V.M. Buimistrov, M.Ya. Amus'ya, and B.A. Zon [1, 6–10]. The historically first were the works of V.M. Buimistrov [6] and V.M. Buimistrov in co-author with L.I. Trakhtenberg [7]. In the first of the cited works PBs that was called dynamic Bs of a nonrelativistic electron was calculated in the resonant approximation, when the frequency of an emitted photon is close to one of the eigenfrequencies of an atom. In this case it was possible to retain one summand of the sum over virtual transitions of bound atomic electrons.

In the paper [7] a special method of summation of the perturbation theory series was used in calculation of the cross-section of PBs of an electron scattered by a hydrogen atom. As a result, it has been possible to describe the PBs spectrum in a wide frequency range, but not only in the region of resonance frequencies. In the work [10] the process was considered in the high-frequency approximation, when it is possible to carry out the approximate summation of the perturbation theory series. Within the framework of the consistent quantum-mechanical formalism in this work the static Bs channel was also taken into account. It was shown that in the high-frequency limit the cancellation of the contribution of the polarization channel and the screening effect of atomic electrons in the OBs amplitude occurs. As a result, the process proceeds as on a "bare" nucleus. This effect was called the effect of atom stripping during Bs (stripping approximation), or the descreening effect. Further it was shown that in case of multielectron atoms the "stripping" approximation gives a good conformity with the result of the more exact approach in a wide frequency range, but not only in the high-frequency limit. In the papers [6–10] an incident electron was assumed to be nonrelativistic, but fast enough, so it was possible to use the Born approximation for its interaction with an atom.

In the work of M.Ya. Amus'ya with co-authors [8] an incident electron, on the contrary, was assumed to be slow, and the inverse bremsstrahlung effect was calculated, that is, the absorption of a photon of the external electromagnetic field by an electron scattered by an atom. The contribution both of ordinary and of polarization Bs was taken into account, and in the latter case for calculation of an amplitude a special version of the many-particle perturbation theory was used: the random phase approximation with exchange. It was shown that the contribution of the polarization channel is rather essential and can exceed the contribution of the ordinary mechanism of the bremsstrahlung effect even far from resonance frequencies.

In the B.A. Zon's work [9] in the description of the amplitude of PBs on an atom in the Born-Bethe approximation the dynamic polarizability of an atom was used for the first time, which was an essential step in the development of the PBs theory since this has opened a possibility to use well-developed methods of calculation of atomic polarizability for description of the polarization channel.

The description of PBs in plasma in the approach of V.N. Tsytovich [2] was based on the use of the classical formalism for nonlinear current arising in scattering of charged particles in plasma. Nonlinear current radiation as a result of scattering processes of two types, Compton and transient, was considered. Compton scattering is accompanied by transfer of the momentum excess during radiation to plasma electrons and corresponds to ordinary Bs. Transient scattering is connected with transfer of the momentum excess to plasma ions, when a photon is emitted by a coherently vibrating charge of the Debye sphere, and corresponds to PBs. The consideration of PBs in plasma within the framework of the quantum-mechanical approach was given in the thesis [3] with the use of the method of the dynamic form factor of plasma components that was finally expressed in terms of different components of the plasma dielectric permittivity.

PBs on an amorphous target within the framework of the approach based on classical electrodynamics was studied theoretically in the paper [11]. A similar method was used in the work [12] in calculation of the spectrum of Bs of relativistic electrons in a polycrystal with account for of the polarization channel. In the cited paper it was shown that the PBs spectrum contains maxima corresponding to the fulfilment of the Bragg condition in scattering of a virtual photon to a real photon by a polycrystalline target. The position of the maximum is defined by the electron velocity and the vector of the reciprocal lattice of the polycrystal. With increasing velocity of an incident electron the spectral maximum is shifted towards higher photon energies. The PBs intensity at the maximum exceeds the intensity of ordinary Bs.

PBs of a nonrelativistic heavy charged particle on a thin polycrystalline target was calculated in the work [13] by the methods of quantum mechanics without considering photoabsorption and loss of energy of an incident particle in a substance. In this case the OBs intensity is negligible since it is inversely proportional to the squared charge mass. It was shown that in contrast to the relativistic case the significant contribution to the photon yield by the polarization channel is made by the incoherent summand in the PBs amplitude connected with transfer of the energy-momentum excess in binary collisions. The contribution of the coherent mechanism of PBs, when a momentum is transferred to the whole crystal lattice as a unit, is the most essential in the low-frequency part of the spectrum. An important feature of PBs of a nonrelativistic charge in a polycrystal is the presence of frequency steps in the spectrum connected with “turning-off” of the contribution of one of the reciprocal lattice vectors to the process. The position of the frequency step is defined by the reciprocal lattice vector and the velocity of an incident particle and thus carries information on the target properties.

PBs of a nonrelativistic electron in a thin polycrystalline target was calculated in the paper [14] in the stripping approximation with account for of the contributions of both channels to the process. It was shown that the spectrum of total Bs contains “frequency steps” arising due to the contribution of the coherent part of PBs to radiation.

As already noted, experiments on investigation of PBs in a condensed medium were carried out mainly with the use of relativistic electrons with an energy of

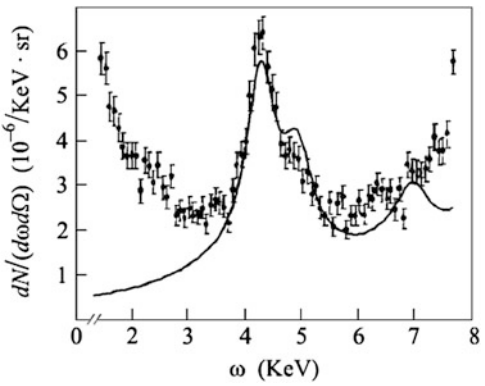

Fig. 1.2 The measured (*points*) and calculated (*solid curve*) spectra of PBs of an electron with an energy of 7 MeV from a copper foil [16]

several MeV. In this case the polarization channel shows itself as maxima on the spectral dependence of bremsstrahlung photon yield. For example, in the work [15] the spectrum of Bs of an electron with the energy of 2.4 MeV scattered in a polycrystalline aluminum target was recorded. The position of the spectral maximum of radiation falling on photon energy of 4 KeV was clearly located. The comparison with the calculation based on the approach [12] showed a good conformity between the experimental and theoretical data. In the process of this work in the paper [16] the measurements of the PBs spectra for electrons with the energy of 7 MeV scattered in polycrystalline films of aluminum, copper, and nickel were carried out, and the detailed quantitative comparison of the experimental and calculated data was presented. A good conformity between the theory and the experiment was obtained, which is demonstrated for a copper target by Fig. 1.2.

In the central part of this figure the major peak caused by the polarization channel is located. The low-frequency part of the spectrum is an exponential background. In the high-frequency wing there is a peak of the copper *K*-line with a maximum at 8.025 eV. In the spectrum there is also a background peak of the *K*-line of iron at 6.4 KeV. On the right side of the central peak of PBs there is a second peak. Fitting the spectrum with the Gauss distribution gives the position of peaks: 4.267 eV and 4.886 eV. The third peak of PBs should show itself according to calculations in a range of photon energies about 7 KeV. However, in this case it is difficult to discern this peak in the spectrum in view of its position at the rise of the copper *K*-line peak that surpasses PBs in intensity by more than two orders of magnitude.

Thus in case of scattering of relativistic electrons in polycrystalline targets a reliable experimental evidence of substantiality of the PBs contribution to the yield of X-ray photons is obtained, and the characteristic features of the polarization channel spectrum are reproduced by calculation within the framework of a corresponding theoretical approach [12].

The initial stage of theoretical and experimental investigations of PBs and a number of related processes was summed up in the review [17] and the monograph [18].

The book [18] (Chap. 7) contains also the theoretical description of PBs in collisions of electrons with metal clusters and fullerenes. The emphasis is on the spectra in the visible wavelength range, where radiation has characteristic maxima connected with collective excitations of the electron subsystem of a target. These collective excitations are caused by variations of the electron density of valence (in case of fullerenes) and delocalized (in case of metal clusters) electrons, by which a virtual photon of an incident particle is scattered to a real bremsstrahlung photon. The said variations occur in a thin near-surface layer of the target, the thickness a of which is of the order of the atom size and is supposed to be much lesser than the cluster radius R. In the interior of the cluster electron density is compensated by the positive charge of ions. The construction of the theory in the case under consideration is significantly simplified due to the presence of the small parameter a/R that makes it possible to use a simple model expression for the form-factor of the target $F(q)$.

The generalized polarizability of the target $\alpha(\omega, q)$ necessary for calculation of the PBs cross-section in the Born approximation, as a rule, is calculated in the multiplicative approximation, in which $\alpha(\omega, q) = \alpha(\omega)\,\tilde{F}(q)$, where $\alpha(\omega)$ is the dipole dynamic polarizability, $\tilde{F}(q)$ is the normalized form factor of the target representing a spatial Fourier transform of electron density distribution. The above equation was proved in the paper [19] with the use of calculations made within the framework of the quantum-mechanical random phase exchange approximation for a case of multielectron atoms.

The dynamic polarizability of metal clusters and fullerenes was calculated in the resonant approximation [18, 20], when the function $\alpha(\omega)$ has a resonance at the plasma frequency ω_p:

$$\alpha(\omega) = R^3\,\frac{\omega_p^2}{\omega_p^2 - \omega^2 - i\,\omega\,\Gamma}, \tag{1.1}$$

where Γ is the damping constant. The plasma frequency is defined by the number of delocalized electrons N_e and the target radius R. The formula for plasma frequency used in [18, 20] in case of a metal cluster in atomic units ($e = m_e = \hbar = 1$) looks like: $\omega_p = \sqrt{N_e/R^3}$, in case of a fullerene $\omega_p = \sqrt{2\,N_e/3\,R^3}$.

For metal clusters the photon energy at the plasma frequency depending on the size of a cluster changes from 2 to 5 eV. For the fullerene C_{60} this energy is much more and is 19 eV.

It should be noted that the radius of the fullerene C_{60} is 0.35 nm (about 6 a.u.), and the radius of a carbon atom is less than 0.1 nm. The form factor for cluster targets can be calculated in the general form in view of the fact that PBs results from scattering of a virtual photon of the incident particle eigenfield in a thin near-surface layer. Substituting the equation $|\mathbf{r}_a| \approx R$ ($\mathbf{r}_a$ is the radius vector of a cluster atom) in the expression for the form factor, we can find: $F(q) = \frac{3 j_1(qR)}{qR}$ ($j_1(x)$ is the first-order spherical Bessel function). This expression is true for the transferred vectors q of not too high magnitudes that satisfy the inequality: $q << 1/a$.

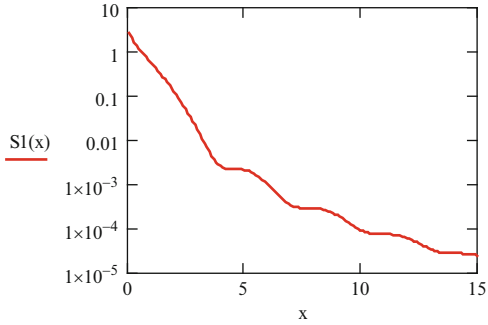

Fig. 1.3 The plot of the function $S_1(x)$ defining, together with the target polarizability, the dependence of the PBs cross-section on the size of a nanocluster

The expression for the spectral cross-section of PBs of a nonrelativistic electron on a nanocluster (in atomic units) looks like [18, 20]:

$$\omega \frac{d\sigma^{PB}}{d\omega} = \frac{16\,\omega^4}{3\,c^3\,\mathrm{v}^2}\,|\alpha(\omega)|^2\,[S_1(R\ q_{\min}) - S_1(R\ q_{\max})], \tag{1.2}$$

where $q_{\min} = \frac{m\mathrm{v}}{\hbar}\left(1 - \sqrt{1 - \frac{2\hbar\omega}{m\mathrm{v}^2}}\right), q_{\max} = \frac{m\mathrm{v}}{\hbar}\left(1 + \sqrt{1 - \frac{2\hbar\omega}{m\mathrm{v}^2}}\right)$ are the magnitudes of the minimum and maximum wave vectors transferred from an incident particle to the target, and

$$S_1(x) = \frac{1}{8\,x^6}\left[6 + 9\,x^2 - \left(12\,x + 2\,x^3 - 4\,x^5\right)\,\sin\left(2\,x\right) - \left(6 - 3\,x^2 + 2\,x^4\right)\right.$$
$$\left.\times\,\cos\left(2\,x\right) - 8\,x^6\,Ci\left(2\,x\right)\right] \tag{1.3}$$

is the function arising after integration with respect to the momentum transferred from an electron to the target, $Ci(x) = \gamma + \ln x + \int_0^x \frac{\cos t - 1}{t}\,dt$ is the integral cosine ($\gamma \cong 0.577$ is the Euler constant). According to the formula (1.2), the function $S_1(x)$, together with the target polarizability (1.1), defines the dependence of the PBs cross-section on the size of a nanocluster.

It should be noted that far from the kinematic boundary, when $\hbar\,\omega << m\,\mathrm{v}^2/2$, we have $q_{\min} \approx \omega/\mathrm{v}$ and $q_{\max} \approx 2\,m\,\mathrm{v}/\hbar$. In this case $q_{\min} << q_{\max}$ and according to the plot of Fig. 1.3, the inequality $S_1(R\ q_{\min}) >> S_1(R\ q_{\max})$ is true, so it is possible to retain only the first summand in the square brackets on the right of the Eq. 1.2. In the limit $R\ q_{\min} << 1$ the formula (1.3) gives $S_1(x) \approx -\ln(2\,R\,q_{\min}) \cong \ln(\mathrm{v}/2\,\omega\,R)$, and (1.2) and (1.3) give the result known from the theory of PBs on an atom.

Presented in the book [18] and the review [20] are the results of calculations (in the first Born approximation for interaction of an incident particle with a target) of spectral cross-sections of PBs arising in scattering of electrons by metal clusters and fullerenes.

For a case of collision of an electron with fullerenes it was shown that the maximum of the spectral PBs cross-section is reached in fulfilment of the condition

$v = v_{max} \approx R\,\omega_p$, where v is the initial velocity of a scattered electron. The value of the optimum velocity v_{max} for the fullerene C_{60} is about 3.5 a.u., which corresponds to the energy of 167 eV. At such an electron energy the maximum of the spectral cross-section of PBs on the fullerene C_{60} falls on a photon energy about 19 eV, and the calculated value of the cross-section $\omega\, d\sigma/d\omega$ at a corresponding frequency is about 10^{-19} cm^2 (about $3.6{\cdot}10^{-3}$ atomic cross-section units). The width of the maximum in the spectrum of PBs on the fullerene is defined by the value of the ratio $\Gamma/\omega_p \approx 0.6$. The high value of this ratio is caused by the fact that the energy of plasmon resonance in a fullerene is more than the potential of ionization of its atoms, so the ionization processes (bound-free transitions) make a substantial contribution to damping of collective oscillations in a fullerene.

With decreasing electron velocity the maximum of the PBs cross-section is shifted towards lower photon energies. Thus at an electron velocity of 1.5 a.u. (an energy of 30.6 eV) the cross-section maximum is reached at a bremsstrahlung photon energy of 11.5 eV and is about $1.8{\cdot}10^{-20}$ cm^2. With increasing electron velocity the cross-section maximum is shifted to the high-frequency range. In this case the right resonance arm is amplified since the suppression of the PBs spectrum (due to the influence of the target form factor) occurs then at higher frequencies. The calculation of the spectral cross-section of PBs on a fullerene for an electron velocity of 7 a.u. gives a maximum cross-section value of $7{\cdot}10^{-20}$ cm^2 at a bremsstrahlung photon energy of 20 eV. At low velocities the process cross-section as a function of the bremsstrahlung photon energy oscillates. These oscillations are connected with the diffraction of the incident particle eigenfield on the target and are seen on the plot of Fig. 1.3 for the function $S_1(x)$.

The calculation of the velocity dependence of the cross-section of PBs on a fullerene shows that the cross-section maximum at the plasma frequency is reached at an electron velocity of 3.5 a.u. A corresponding curve shows a sharp dip with decreasing velocity, which is caused by the influence of the target form factor. At high velocities rather smooth reduction of the cross-section occurs, which is connected with the presence of the squared electron velocity in the denominator of the expression for the PBs cross-section.

The numerical analysis presented in [18] and [20] shows that the angular distribution of PBs in scattering of an electron by a fullerene depends on electron velocity. At the maximum of the frequency and velocity dependences ($\hbar\,\omega = 19$ eV, $v = 3.5$ a.u.) this distribution has a maximum at a radiation angle of 90°. At low velocities including the optimum velocity PBs is defined mainly by plasmon oscillations occurring in parallel with the velocity of an incident electron. At high electron energies the main role is played by transferred momenta perpendicular to the direction of incident particle motion, which corresponds to the maximum of PBs along or antiparallel to the electron velocity (the radiation angle is 0° or 180°).

The results of calculations of spectral, angular, and velocity dependences of the cross-section of PBs of an electron scattered by a metal nanoparticle are presented in the publications [18] and [20]. In particular, a cluster was considered that

contained 40 sodium atoms (Na_{40}). In this case the relative width of resonance is $\Gamma/\omega_p \approx 0.2$. The small value of this ratio is caused by the fact that the energy of plasmon resonance in a metal cluster is less than the potential of ionization of its atoms. So bound-free transitions (ionization) do not make a contribution to the process of plasma oscillation damping. As a result, the frequency dependence of the cross-section of PBs on a metal cluster near the plasmon resonance is defined mainly by the dynamic polarizability of a target.

The numerical analysis [18, 20] shows that the optimum value of electron velocity to reach the maximum in the spectral cross-section of PBs on the cluster Na_{40} at the plasmon resonance frequency ($\hbar\omega_p = 2.85$ eV) is 1.5 a.u. (30.6 eV). In this case the value $\omega\, d\sigma/d\omega$ is $2.8{\cdot}10^{-19}$ cm^2 (0.01 atomic cross-section units). With changing velocity the position of the maximum practically does not change, and the cross-section value decreases. Thus in case of twofold decrease or increase of incident particle velocity the cross-section of PBs at the maximum of the spectral dependence decreases approximately by half. Also given in the cited works are the calculations of the cross-section of PBs of an electron with the energy of 13.6 eV scattered by clusters containing 10^2, 10^3, 10^4, and 10^5 atoms. The photon energy at the maximum is practically the same for all types of clusters, and the maximum cross-section grows from $8{\cdot}10^{-19}$ to $4{\cdot}10^{-17}$ cm^2.

From the presented results it follows that the number of spectral oscillations of the cross-section grows with increasing size of the cluster, and these oscillations are most manifested in the low-frequency wing. With increasing size of the cluster the optimum value of the velocity of an incident electron at which the cross-section has maximum also increases.

It should be noted that the use of the model expression for polarizability in the region of plasmon resonance (1.1) in description of PBs on metal clusters with a great number of atoms (10^3 and more) seems inadequate. In this case it is more preferable to use the Mi theory based on the introduction of the dielectric permittivity of a target substance.

The ratio of the PBs cross-section to the ordinary bremsstrahlung cross-section is given by the expression [18, 20]:

$$\frac{d\sigma^{PB}}{d\sigma^{OB}} \propto N_e \left(\frac{\omega_p}{\Gamma}\right)^2 S_1\left(\frac{\omega_p R}{\mathrm{v}}\right), \tag{1.4}$$

that is, is defined mainly by the number of delocalized electrons and by the ratio ω_p/Γ that for fullerenes is 1.67, and for metal clusters is five and more. The argument of the function $S_1(x)$ in case of optimum values of parameters for a fullerene is 1.3, and the value of the function itself is about 0.36. In case of metal nanoclusters the argument of $S_1(x)$ does not exceed 0.2, and accordingly the value of the function itself is $S_1(x) \geq 2$.

In view of the presented values of the magnitudes included in the formula (1.4), it is possible to conclude that PBs of electrons on fullerenes and metal nanoclusters in the region of plasmon resonance surpasses the contribution of ordinary

bremsstrahlung in order of magnitude. The proportionality of the ratio of the PBs and OBs cross-sections to the number of delocalized electrons following from Eq. 1.4 is a consequence of coherent reradiation of a virtual photon of an incident particle by fullerenes and nanoclusters in the wavelength range under consideration.

PBs as a means of diagnostics of the fullerene structure was discussed in the paper [21] on the basis of calculation of the form-factor defining the intensity of radiation by the polarization channel. In contrast to the publications [18, 20], the work [21] considered the kiloelectron-volt range of bremsstrahlung photon energies, where the oscillations of PBs intensity increasing with decreasing photon energy should also show themselves. These oscillations are explained by the interference of contributions to the process from different sites of a fullerene. The calculations carried out in the paper [21] are based on the approximate approach, the main disadvantage of which is the absence of integration with respect to the wave vector **q** transferred from an incident particle to a target as well as inexact recording the value of the latter: $q \approx 2\,(\omega/c)\,\sin(\theta/2)$, where θ is the radiation angle. Actually, in calculation of the total PBs intensity it is necessary to sum the contribution to the process from all angles of electron scattering by a target, which corresponds to integration with respect to the wave vector magnitude from ω/v to $m\,\mathrm{v}/\hbar$. Another assumption made in the cited work consists in neglecting the bond of fullerene electrons with the nuclei of carbon atoms. This assumption in the spectral range under consideration is quite correct if valence electrons of atoms making a fullerene are concerned. But it is not so obvious for electrons of inner shells (K-electrons).

References

1. Tsytovich, V.N., Oiringel, I.M. (eds.): Polarization Bremsstrahlung. Plenum Press, New York (1991)
2. Tsytovich, V.N., Akopyan, A.V.: Bremsstrahlung in a nonequilibrium plasma. Sov. J. Plasma Phys. **1**(4), 371 (1975)
3. Astapenko, V.A.: Emission and absorption of photons in multiparticle interactions. Ph.D. Thesis. MIPT, Moscow (1985) (in Russian)
4. Kapitsa, S.P.: Radiation of charge moving in inhomogeneous medium. Sov. Phys. JETP **12**, 954 (1961)
5. Ter-Mikaelian, M.: High Energy Electromagnetic Processes in Condensed Media. Wiley, New York (1972)
6. Buimistrov, V.M.: Resonant Bremsstrahlung and absorption of photons. Ukr. Fiz. Zh. **17**, 640 (1972)
7. Buimistrov, V.M., Trakhtenberg, L.I.: Bremsstrahlung cross section in scattering of an electron by a hydrogen atom. Sov. Phys. JETP **42**, 55 (1975)
8. Amusia, M.Y., Baltenkov, A.S., Paiziev, A.A.: Bremsstrahlung of electrons on atoms with allowance for polarizability. JETP Lett. **24**, 332 (1976)
9. Zon, B.A.: Bremsstrahlung in collisions between electrons and atoms. Sov. Phys. JETP **46**, 65 (1977)

10. Buimistrov, V.M., Trakhtenberg, L.I.: The role of atomic electrons in bremsstrahlung. Sov. Phys. JETP **46**, 447 (1977)
11. Nasonov, N.N., Safronov, A.G.: Polarization bremsstrahlung of a relativistic charge in condensed matter. Sov. Phys. JTP **37**, 973 (1992)
12. Nasonov, N.N.: Collective effects in the polarization bremsstrahlung of relativistic electrons in condensed media. NIM B **145**, 19 (1998)
13. Astapenko, V.A.: Polarization Bremsstrahlung of heavy charged particles in polycrystal. JETP **99**, 958 (2004)
14. Astapenko, V.A., Buimistrov, V.M., Nasonov, N.N., Krotov, Y.A.: Polarization bremsstrahlung from non-relativistic electrons penetrating a polycrystalline target. Phys. Lett. A **332/3**, 298 (2004)
15. Blashevich, S., Chepurnov, A., Grishin, V., et al.: Polarization bremsstrahlung of relativistic electrons in aluminium. Phys. Lett. A **254**, 230 (1999)
16. Astapenko, V.A., Kubankin, A.S., Nasonov, N.N., et al.: Measurement of the polarization bremsstrahlung of relativistic electrons in polycrystalline targets. JETP Lett. **84**, 281 (2006)
17. Astapenko, V.A., Bureeva, L.A., Lisitsa, V.S.: Polarization effects in atomic transitions. Phys. Usp. **45**, 149 (2002)
18. Korol', A.V., Lyalin, A.G., Solov'ev, A.V.: Polarization Bremsstrahlung. S.-Peterb. Gos. Pedagog. Univ., St. Petersburg (2004) (in Russian)
19. Korol, A.V., Lyalin, A.G., Obolenskii, O.I., et al.: The role of the polarization mechanism for emission of radiation by atoms over a broad photon frequency range. JETP **87**, 251 (1998)
20. Lyalin, A.G., Solov'yov, A.V.: Polarizational bremsstrahlung from atomic clusters. Rad. Phys. Chem. **75**, 1358 (2006)
21. Grishin, V.K.: Polarization bremsstrahlung as a means of diagnostics of fullerenes. Vestnik MGU **2**, 69 (2004) (in Russian)

Chapter 2
Quantum-Electrodynamics Approach to Description of Bremsstrahlung of a Fast Charged Particle on an Atom with Account for the Polarization Channel

In this chapter with the use of the consistent quantum-electrodynamic approach the cross-section of bremsstrahlung of a fast charged particle on a one-electron and multielectron atom was obtained and analyzed within the framework of the first Born approximation.

In this section, unless otherwise indicated, we use the relativistic system of units, in which $\hbar = c = 1$ ($\hbar$ is the Planck constant, c is the velocity of light in vacuum).

2.1 Amplitude of Bremsstrahlung of a Relativistic Charged Particle on a One-Electron Atom

In this paragraph the expression for the amplitude of Bs of a relativistic incident particle (IP) on a one-electron (hydrogen-like) atom is derived within the framework of the consistent quantum-electrodynamic approach.

Let us consider the collision of a relativistic charged particle (the charge e_0, the mass m_0, the initial energy $\varepsilon_i = \sqrt{p_i^2 + m_0^2}$) in the state $|p_i\rangle$ with a hydrogen-like atom being in the state $|n_i\rangle$ with the energy E_i. (It will be recalled that the symbol $|\psi\rangle$ means the Dirac ket vector corresponding to the wave function ψ.)

As a result of collision, the IP goes to the state $|n_f\rangle$ with the energy $\varepsilon_f = \sqrt{p_f^2 + m_0^2}$, a bremsstrahlung photon with the frequency ω and the wave vector $\mathbf{k}$ is emitted, and the atom goes to the state $|n_f\rangle$ with the energy E_f.

We assume that the incident particle satisfies the Dirac equation. Besides, we consider satisfied the Born condition for IP velocities before (v_i) and after (v_f) collision with a target (Z is the atomic nucleus charge):

$$Z e_0 << \mathrm{v}_{i,f}. \tag{2.1}$$

V. Astapenko, *Polarization Bremsstrahlung on Atoms, Plasmas, Nanostructures and Solids*, Springer Series on Atomic, Optical, and Plasma Physics 72,
DOI 10.1007/978-3-642-34082-6_2, © Springer-Verlag Berlin Heidelberg 2013

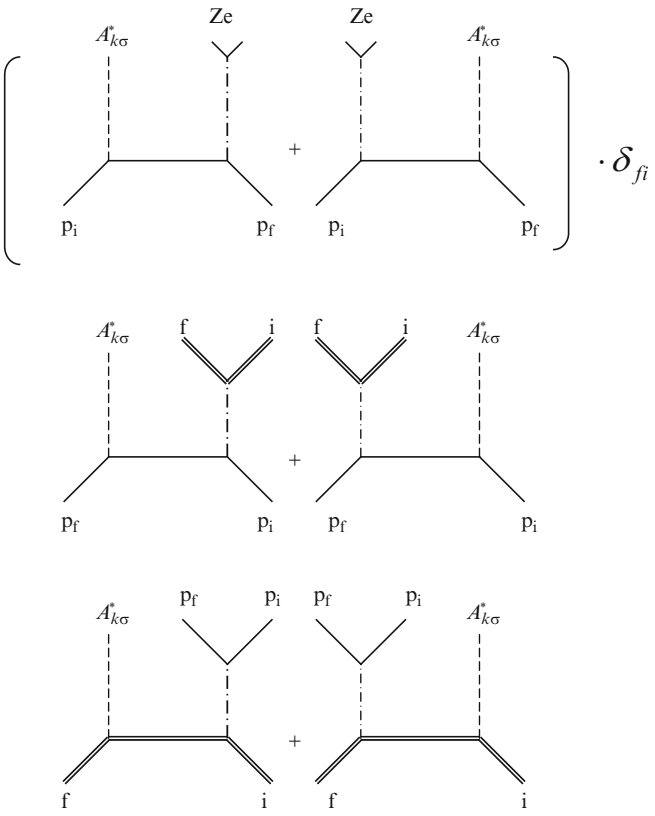

Fig. 2.1 The diagrams describing the amplitude of bremsstrahlung on an atom in the third order of the perturbation theory

In this case the IP is described by a plane wave in contrast to the exact solution of the Dirac equation in the external nuclear field that is necessary to describe a bound electron of an atom. In the case that an incident particle is an electron, this makes it possible also to neglect exchange summands in the process amplitude.

Let us use the standard quantum-electrodynamic perturbation theory for a scattering operator [1]. In its lower order of interaction between an IP and an atomic electron with an electromagnetic field we have a graphic expression for the Bs amplitude (Fig. 2.1).

In Fig. 2.1 the single lines correspond to the wave functions and the propagator of an incident particle, the double lines correspond to an atomic electron in the nuclear field, δ_{fi} is the Kronecker symbol. It will be recalled that the propagator (or the propagation function) describes the amplitude of probability of particle propagation from one spatio-temporal point to another. The wavy line means the electromagnetic field: the photon propagator and the wave function of a free photon $A_{\mathbf{k}\sigma}$ ($\mathbf{k}$ is the wave vector, σ is the photon polarization index).

The analytical expression for the amplitude of total Bs corresponding to the diagrams shown in Fig. 2.1 represents the sum of static and polarization terms:

$$M_{fi} = M_{fi}^{st} + M_{fi}^{pol} \tag{2.2}$$

The first summand in Eq. 2.2 corresponds to the ordinary (static) channel, its expression looks like:

$$M_{fi}^{st} = -\frac{4\pi e_0^2 e}{q^2} A_{\mathrm{k},\sigma}^{\mu *} \left[Z g^{0\nu} \langle f|i\rangle - j_{fi}^{\nu}(\mathbf{q}) \right] G_{\nu\mu}(p_1, p_2), \tag{2.3}$$

where

$$G_{\nu\mu}(p_1, p_2) = \frac{\bar{u}_f}{\sqrt{2\,\varepsilon_f}} \left[\gamma_\nu \frac{\gamma p_2 + m_0}{p_2^2 - m_0^2} \gamma_\mu + \gamma_\mu \frac{\gamma p_1 + m_0}{p_{12}^2 - m_0^2} \gamma_\nu \right] \frac{u_i}{\sqrt{2\,\varepsilon_i}} \tag{2.4}$$

is the propagator of a free electron. In the formulas (2.3) and (2.4) the following designations are used:

$q_1 = p_f - p_i$, $q = q_1 + k$, $p_2 = p_f + k$, $p_1 = p_i - k$, $A_{\mathbf{k},\sigma} = \sqrt{2\pi/\omega}\, e_{\mathbf{k},\sigma}$,

$|p\rangle = \dfrac{u(p,s)}{\sqrt{2\varepsilon}} \exp(-ipx)$, $j_{n'n}^{\mu}(\mathbf{k}) = \langle n'|\gamma^\mu \exp(-i\mathbf{kr})|n\rangle$, $a = a^\mu = \{a^0, \mathbf{a}\}$,

$ab = a^\mu b_\mu = a^0 b_0 - \mathbf{ab}$, $\mu, \nu = 0 \div 3$.

The metric, normalization and designations in the formula (2.3) are analogous to those used in the book [1]: $g_{\mu\nu}$ is the metric tensor, γ^μ are the Dirac matrices. The normalization of bispinors: $\bar{u}u = u^+\gamma^0 u = 2\,m_0$ corresponds to the normalization of the wave function of an incident charge to one particle in the main region with a unit volume. The wave function of a photon $A_{\mathbf{k}\sigma}$ is also normalized to one photon in the main region, $e_{\mathbf{k}\sigma}$ is the polarization 4-vector that in the laboratory system of coordinates satisfies the three-dimensionally transverse gauge: $e_{\mathbf{k}\sigma} = \{0; \mathbf{e}_{\mathbf{k}\sigma}\}$, $\mathbf{k}\mathbf{e}_{\mathbf{k}\sigma} = 0$. n, f, i is the set of quantum numbers defining a stationary state of an atom.

The second summand in the formula (2.2) corresponds to the polarization channel. We have for it [2, Chap. 5]:

$$M_{fi}^{pol} = \frac{4\pi}{q_1^2} A_{\sigma\nu\mathbf{k}}^{*} \sum_n \left[\frac{j_{n_f n}^{\nu}(\mathbf{k}) j_{n n_i}^{\mu}(\mathbf{q}_1)}{E_f - E_n + \omega \pm i0} + \frac{j_{n_f n}^{\mu}(\mathbf{q}_1) j_{n n_i}^{\mu}(\mathbf{k})}{E_i - E_n - \omega \pm i0} \right] \frac{\bar{u}_f \gamma_\mu u_i}{2\sqrt{\varepsilon_f \varepsilon_i}} \tag{2.5}$$

The sum over intermediate states extends both to the positive ($+i\,0$) and to the negative ($-i\,0$) energy spectrum of an atomic electron.

Let us analyze the diagrams of Fig. 2.1 and their associated formulas (2.3) and (2.5). The first four graphic summands and their associated expression for the static amplitude (Eq. 2.3) in the case that an atomic electron does not change its state give the classical Bethe-Heitler result [3] – bremsstrahlung of a relativistic electron in

the static nuclear field and the atomic electron field screening it (the screening approximation). If in these terms of the process amplitude all possible final states of an atomic electron are taken into account, we will obtain the Lamb and Wheeler result [4]. The Fourier transform of the time part of the transitional current 4-vector at $f = i$ gives an ordinary form factor of charge screening. Its space part is a current (magnetic) summand of screening and can be essential in Bs with excitation of deep atomic shells for high nuclear charges.

It should be noted that the consistent electrodynamic approach to the relativistic problem of Bs on an atom even in the ordinary static part of the process amplitude leads to results supplementing the Bethe-Heitler theory: to taking into account a possibility of change of an atomic state and to appearance of a current additive in the form factor caused by the space components of the transitional current 4-vector for an atomic electron.

The last two graphic summands in Fig. 2.1 and their associated expression (2.5) describe the emission of a bremsstrahlung photon by an atomic electron in collision of an IP with an atom. These terms appear if an atomic electron is considered as a peer dynamic particle interacting with an electromagnetic field, including the electromagnetic field of vacuum. The contribution to total bremsstrahlung given by these summands is called polarization bremsstrahlung since it is defined by the dynamic polarization of an atom in the IP field.

A characteristic feature of the polarization summand of the amplitude of Bs on an atom is the presence of sums over intermediate states of an atomic electron with resonant energy denominators. And the relativistic (for a bound electron) problem in addition to the resonance in the electronic spectrum of atomic states has a resonant denominator in the positron part of the sum, when $\omega = \varepsilon_i - \varepsilon_n^{(-)} \approx 2m$. However, we will restrict ourselves to the frequency range $\omega << m$.

The total Bs cross-section contains also the interference contribution of the static and polarization channels. But, as it will be seen from the following, its value for a relativistic IP is small.

It is of interest to trace two passages to the limit in the expression (2.2). Let us assume at first that a nucleus is absent ($Z = 0$). In this case the first two diagrams presented in Fig. 2.1 will disappear. In the remaining four diagrams it is necessary to replace the double lines describing an atomic electron in the nuclear field by single lines (describing a free electron). Then these diagrams go to the graphic representation of the process of IP emission on a free electron that is well known in quantum electrodynamics. In this case the first pair of diagrams describes the contribution of an incident particle to Bs in its scattering by an electron, and the second pair of diagrams describes the contribution of a recoil electron to the process.

In the high-frequency range ($\omega >> m$) in case of an incident electron a result is obtained that is known from quantum electrodynamics: recoil electron emission can be neglected, in this case a fast electron emits at a slow unit charge as at an immobile one. It should be noted that to obtain the said passage to the limit, it is

necessary to take into account all possible excitations of an atom both in the discrete spectrum and in the continuous spectrum.

In another limiting case, when an atomic electron is absent, the last four diagrams in Fig. 2.1 disappear, and the process amplitude comes to bremsstrahlung on a "bare" nucleus.

From the diagrams of Fig. 2.1 it is seen that the ordinary (static or Bethe-Heitler) and polarization summands of the amplitude differently depend on the mass and charge of an IP. Really, $M_{fi}^{st} \propto e_0^2 e/m_0$, and $M_{fi}^{pol} \propto e_0 e^2/m$, and static Bs disappears with the IP mass tending to infinity, while the polarization summand remains finite. The change of the sign of the incident particle charge does not change the static amplitude and changes the sign of the polarization amplitude, which results in changing sign of the interference summand of the total cross-section of Bs on an atom.

Let us consider a case of a nonrelativistic atomic electron ($Z<<137$, $\left|E_{i,f} - m\right| << m$). If, besides, $\omega << m$, the expression (2.5) can be transformed to the form containing only nonrelativistic characteristics of an atomic electron.

Really, at $Z << 137$ we have the following passage to the limit for the components of the current 4-vector:

$$j_{fn}^{\mu}(\mathbf{q}_1) = \int d\mathbf{r}\, \varphi_f^* \{1, \vec{\alpha}\} \varphi_n \exp(-i\,\mathbf{q}_1 \mathbf{r}) \approx \left\{ \int d\mathbf{r}\, \varphi_f^* \exp(-i\,\mathbf{q}_1 \mathbf{r}) \varphi_n; \int d\mathbf{r}\, \varphi_f^* \hat{j}(\mathbf{q}_1) \varphi_n \right\}, \tag{2.6}$$

here

$$\hat{j}(\mathbf{q}) = \exp(-i\,\mathbf{qr}) \frac{(-i\nabla)}{2m} + \frac{(-i\nabla)}{2m} \exp(-i\,\mathbf{qr}) \tag{2.7}$$

is the nonrelativistic expression for the spatial Fourier transform of the current density operator, ∇ is the vector differential operator.

The approximate Eq. 2.6 corresponds to the formal expansion of atomic bispinors to the large (~ 1) and small (~ v_a) spinors and to following neglect of spin additives.

Thus in the polarization term of the amplitude (Eq. 2.5) in the sum over intermediate states with positive energy the transition to the nonrelativistic description comes to replacement of relativistic expressions for transitional currents by their nonrelativistic analogs. The sum over intermediate states with negative energy can be transformed if it is assumed that the main contribution to it is made by states, the energy of which satisfies the inequality $||E_n^{(-)}| - m| << m$. In view of the fact that $\left|E_{f,i} - m\right| << m$ and $\omega << m$, the energy denominators in the summands with negative energy can be replaced by the value $2\,m$. Further, using the projection operator $\left(m - \hat{H}_a\right)/2m$ ($\hat{H}_a$ is the atomic Hamiltonian) for the space of wave

functions with negative energy, it is possible to extend summation to the whole energy spectrum of an atomic electron. For this purpose we assume:

$$\left(m - \hat{H}_a\right)/2m = \left(1 - \gamma^0\right)/2$$

$$\gamma^0 \left|n^{\pm}\right\rangle = \pm \left|n^{\pm}\right\rangle,$$

then

$$\sum_{E_n<0} \approx \frac{1}{2m} \langle f| \exp(-i\,\mathbf{qr}) \left(\gamma^\mu \frac{(1-\gamma^0)}{2} \gamma^\nu + \gamma^\nu \frac{(1-\gamma^0)}{2} \gamma^\mu \right) |i\rangle, \tag{2.8}$$

and in view of the permutation relation $\gamma^\mu\gamma^\nu + \gamma^\nu\gamma^\mu = 2\,\delta^{\mu\nu}$ we will obtain:

$$\sum_{E_n<0} \approx \frac{\delta^{\mu\nu}}{m} \langle f| \exp(-i\,\mathbf{qr}) |i\rangle = \frac{\delta^{\mu\nu}}{m}\, j_{fi}^{(0)}(\mathbf{q}). \tag{2.9}$$

Thus the polarization term of the amplitude for a nonrelativistic atomic electron looks like:

$$M_{fi}^{pol} = \frac{4\,\pi\, e_0 e^2}{q_1^2} A_{\mathbf{k}\sigma}^{\nu *} \sum_{E_n>0} \left[\frac{j_{fn}^{\nu}(\mathbf{k}) j_{ni}^{\mu}(\mathbf{q}_1)}{\omega_{fn} + \omega + i0} + \frac{j_{fn}^{\mu}(\mathbf{q}_1) j_{ni}^{\nu}}{\omega_{in} - \omega + i0} + \frac{\delta^{\mu\nu}}{m} j_{fi}^{\,0}(\mathbf{q}) \right] \frac{\bar{u}_f \gamma_\mu u_i}{2\sqrt{\varepsilon_f \varepsilon_i}}. \tag{2.10}$$

The expression (2.10) in case of a nonrelativistic IP leads to the known result of the nonrelativistic theory of PBs [2]:

$$M_{fi}^{pol} = \frac{4\,\pi\, e_0\, e^2}{q_1^2} \sqrt{\frac{2\,\pi}{\omega}} \sum_n \left\{ \frac{\mathbf{e}_{\mathbf{k}\sigma}^* \mathbf{j}_{fn}(\mathbf{k})\, j_{ni}^0(\mathbf{q}_1)}{\omega_{fn} + \omega + i0} + \frac{j_{fn}^0(\mathbf{q}_1)\, \mathbf{e}_{\mathbf{k}\sigma} \mathbf{j}_{ni}(\mathbf{k})}{\omega_{in} - \omega + i0} \right\}. \tag{2.11}$$

To derive the formula (2.11) from (2.10), it is necessary to suppose (neglecting spin effects):

$$\bar{u}_f\, \gamma^\mu\, u_i / 2\sqrt{\varepsilon_i \varepsilon_f} \approx \{1, \mathbf{v}_0\}, \quad |\mathbf{q}_1| << \left|\mathbf{p}_{i,f}\right|.$$

2.2 Amplitude of Bremsstrahlung of a Fast Charged Particle on a Multielectron Atom

The consistent quantum-electrodynamic consideration of PBs of a relativistic IP on a multielectron atom is complicated by the necessity to take into account the interaction between atomic electrons in the relativistic formalism as well as by

the problem of summation over states with negative energy for a multielectron system. At the same time calculation for nonrelativistic atomic electrons can be considerably simplified if from the very beginning a nonrelativistic atomic Hamiltonian is used and an incident particle is replaced by the electromagnetic field it produces (by a set of virtual photons).

Let us justify a possibility of such a replacement. Let the free IP field operator $\hat{\varphi}(x)$ ($x = \{t, \mathbf{r}\}$) satisfy the Dirac equation:

$$(\gamma\, p - m_0)\hat{\varphi}(x) = 0. \tag{2.12}$$

We will assume that for the operator of the electron-positron field of atomic electrons $\hat{\psi}(x)$ the Dirac equation with interaction is true:

$$\left[\gamma\left(p + e\,A^{ext}(x) + e\,\hat{A}^{ae}\right) - m\right]\hat{\psi}(x) = 0, \tag{2.13}$$

where $A^{ext}(x)$ is the potential of the external nuclear field, $\hat{A}^{ae}(x)$ is the operator of the electromagnetic field produced by atomic electrons that satisfies the Maxwell equation:

$$\partial^{\nu}\partial_{\mu}\hat{A}^{ae\,\mu}(x) - \partial^{\mu}\partial_{\mu}\hat{A}^{ae\,\nu}(x) = 4\,\pi\,e\,\hat{j}^{\nu}(x), \tag{2.14}$$

where $\hat{j}^{\nu}(x) = \hat{\bar{\psi}}(x)\,\gamma^{\nu}\,\hat{\psi}(x)$ is the operator of atomic electron current, summation is supposed over twice-repeating indices.

Thus it is supposed that the interaction between atomic electrons is taken into account in $\hat{\psi}(x)$.

Let us represent the state vectors for the system of fields (of atomic electrons, an incident particle, an electromagnetic field) as the product: $\left|\Phi_j\right\rangle = |j\rangle\left|\varphi_j\right\rangle|n_{\mathbf{k}\sigma}\rangle$, where $|j\rangle$ is the state vector for atomic electrons interacting among themselves, $\left|\varphi_j\right\rangle$ is the state vector for a free incident particle, $|n_{\mathbf{k}\sigma}\rangle$ is the state vector for an electromagnetic field. The equation for the system state vector $|\Phi\rangle$ in the interaction representation looks like:

$$i\partial|\Phi\rangle/\partial t = \int dr\,\left[e_0\hat{J}^{\nu}(x) - e\,\hat{j}^{\nu}(x)\right]\hat{A}_{\nu}(x)\,|\Phi\rangle,$$

where

$$\hat{J}^{\nu}(x) = \hat{\bar{\varphi}}(x)\,\gamma^{\nu}\,\hat{\varphi}(x)$$

is the four-dimensional vector of the operator of incident particle current density.

$$\hat{S} = T\,\exp\left\{-i\int dx\,\hat{A}_{\nu}(x)\,\left[e_0\,\hat{J}^{\nu}(x) - e\,\hat{j}^{\nu}(x)\right]\right\}, \tag{2.15}$$

where T is the chronological ordering symbol.

The PBs amplitude in the lower order of the perturbation theory is described by the third term in the expansion of the scattering operator $\hat{S}$ (here for short we use the designation $x_i \equiv i$):

$$\hat{S}_3 = (-i)^3 e^2 e_0 \int d1\, d2\, d3\, T\left\{\hat{A}_\nu(1)\hat{j}^\nu(1)\,\hat{A}_\mu(2)\hat{j}^\mu(2)\,\hat{A}_\lambda(3)\hat{J}^\lambda(3)\right\}. \tag{2.16}$$

In obtaining this formula similar summands resulting from rearrangement of integration variables were reduced. Hereafter we consider that there is no exchange between an incident particle and atomic electrons. Using the commutativity of corresponding operators, the expression (2.16) for the scattering operator in the third order of the perturbation theory can be rewritten as:

$$\hat{S}_3 = (-i)^2 \int d1 d2 \hat{A}_\nu(1) T\left\{e^2 \hat{j}^\nu(1)\hat{j}^\mu(2)\right\} \int d3 e_0 D_{\mu\lambda}(2,3)\hat{J}^\lambda(3), \tag{2.17}$$

where $D_{\mu\lambda}(2,3) = iT\langle 0|\hat{A}_\mu(2)\,\hat{A}_\lambda(3)|0\rangle$ is the photon propagator.

In the formula (2.17) one unpaired $\hat{A}$ -operator is retained, which corresponds to the one-photon change of the electromagnetic field.

By matrixing the scattering operator $\hat{S}$ with respect to the initial and final states of the system we obtain:

$$S^{pol}_{3,fi} = (-i)^2 \int d1\, d2\, A^*_{\mathbf{k}\sigma\nu}(1)\, L^{\nu\mu}_{fi}(1,2)\, A^{(0)}_{\mu,fi}(2), \tag{2.18}$$

where

$$L^{\nu\mu}_{fi}(1,2) = e^2 \langle f|T\left\{\hat{j}^\nu(1)\hat{j}^\mu(2)\right\}|i\rangle \tag{2.19}$$

is the relativistic analog of the tensor of electromagnetic field scattering by an atom;

$$A^{(0)}_{\mu,fi}(2) = -e_0 \int d3 D_{\mu\nu}(2,3)\left\langle \varphi_f|\hat{J}^\nu(3)|\varphi_i\right\rangle \tag{2.20}$$

is the 4-potential of a virtual photon produced by an incident particle in the process of scattering: $|\varphi_i\rangle \rightarrow \left|\varphi_f\right\rangle$. It should be noted that the potential of a virtual photon $A^{(0)}{}_{fi}$ could be found from the Maxwell equations (2.14) if on their right side the matrix element of the IP transitional current operator $\left\langle \varphi_f\right|\hat{J}^\mu(3)\,|\varphi_i\rangle$ is substituted.

The formula (2.18) for the amplitude of PBs allows its interpretation as a process of scattering (conversion) of a virtual photon $A^{(0)}{}_{fi}$ by atomic electrons to a real photon.

It is easy to show that the same expression for the PBs amplitude can be obtained from another form of the interaction Hamiltonian:

$$V' = -e \int d\mathbf{r} \left\{ \hat{A}_v(x) + A^{(0)}_{fi,v}(x) \right\} \hat{j}^v(x). \tag{2.21}$$

Here an incident particle is replaced by the electromagnetic field $A^{(0)}_{fi}$ it produces and thus it is excluded from consideration as a dynamical degree of freedom. The field $A^{(0)}_{fi}$ can be considered a specified field determined by the Eq. 2.20 – the prescribed current approximation. Then the PBs amplitude is obtained by the standard method in the second order of the perturbation theory. After calculation of a corresponding matrix element we find for it:

$$S'^{pol}_{2,fi} = (-i)^2 \int d1\, d2\, A^*_{\mathbf{k}\sigma,v}(1) \langle f | T \left\{ e^2 \hat{j}^v(1) \hat{j}^\mu(2) \right\} | i \rangle A^{(0)}{}_{fi}(2). \tag{2.22}$$

From comparison of the formulas (2.18) and (2.22) it follows:

$$S^{pol}_{3,fi} = S'^{pol}_{2,fi}.$$

Thus the PBs amplitude can be calculated (with fixed initial and final IP states) with replacing an incident particle by the field it produces with the help of formula (2.20). Then in the case under consideration for nonrelativistic atomic electrons a single relativistic degree of freedom – an incident particle – will be excluded, and it is possible to use the nonrelativistic formalism to calculate the Bs amplitude.

It should be noted that replacement of a particle by its field is widely used also in calculation of Bethe-Heitler Bs by the equivalent photon method, when in the IP rest frame the atomic field is replaced by equivalent photons that are Compton-scattered to bremsstrahlung photons by an incident particle.

Let us calculate, replacing an IP by its field, the PBs amplitude for a nonrelativistic multielectron atom ($Z<<137$) with neglected exchange of incident and bound electrons. We use the axial gauge of the electromagnetic potential ($A_0 = 0$). The nonrelativistic Hamiltonian of perturbation of atomic electrons by the electromagnetic field looks like:

$$V = \frac{e}{2m} \sum_j \left\{ \hat{\mathbf{p}}_j \hat{\mathbf{A}}(\mathbf{r}_j, t) + \hat{\mathbf{A}}(\mathbf{r}_j, t)\, \hat{\mathbf{p}}_j + e\, \hat{\mathbf{A}}^2(\mathbf{r}_j, t) \right\}, \tag{2.23}$$

where $\hat{\mathbf{p}}_j = -i\nabla_j$, $\hat{\mathbf{A}} = \hat{\mathbf{A}}^{ph} + \mathbf{A}^{(0)}_{fi}$ is the sum vector-potential, the operator $\hat{\mathbf{A}}^{ph}$ describes the photon field ($kx = \omega t - \mathbf{kr}$, $\omega = |\mathbf{k}|$),

$$\hat{\mathbf{A}}^{ph}(x) = \sum_{\mathbf{k},\sigma} \sqrt{\frac{2\pi}{\omega}} \left\{ \mathbf{e}_{\mathbf{k},\sigma}\, \hat{c}_{\mathbf{k},\sigma}\, \exp(-ikx) + \mathbf{e}^*{}_{\mathbf{k},\sigma}\, \hat{c}^+{}_{\mathbf{k},\sigma}\, \exp(ikx) \right\}, \tag{2.24}$$

where $\mathbf{e}_{\mathbf{k},\sigma}$ is the unit vector of photon polarization, $c^{+}_{\mathbf{k},\sigma}, c_{\mathbf{k},\sigma}$ are the operators of birth and destruction of photons; $\mathbf{A}^{(0)}_{fi}$ is given by the formula (2.20) – this is an external field produced by an incident particle.

Going to the interaction representation $\hat{V}_{\text{int}} = \exp\left(i\hat{H}_a t\right) V \exp\left(-i\hat{H}_a t\right)$ (the photon field is already written in the interaction representation), we have for the scattering operator:

$$\hat{S} = T\ \exp\left\{ -i \int_{-\infty}^{\infty} \hat{V}_{\text{int}}(t)\, dt \right\}. \tag{2.25}$$

The contribution to the PBs amplitude in the lower order of the perturbation theory (in the second order with respect to an electron charge) is made by the first and second terms of the expansion S, the zeroth term of this expansion – one – corresponds to the unchanged state of the system. In the first-order term the contribution to the process is made by the summand containing the squared sum vector potential, in the first-order term in perturbation the contribution is made by the summand containing $\hat{\mathbf{p}}\hat{\mathbf{A}} + \hat{\mathbf{A}}\hat{\mathbf{p}}$. According to the physical picture of PBs, it is necessary to take into account terms containing the mixed product $\hat{\mathbf{A}}_{ph}$ and $\mathbf{A}^{(0)}_{fi}$. So the matrix element of the process is represented as

$$S^{pol}_{fi} = S^{(1)}_{fi} + S^{(2)}_{fi},$$

here

$$S^{(1)}_{fi} = -i\langle \Phi_f | \int_{-\infty}^{\infty} dt \exp(iH_a t) \frac{e^2}{2m} \sum_{j=1}^{N} 2\hat{\mathbf{A}}^{ph}(\mathbf{r}_j, t)\mathbf{A}^{(0)}_{fi}(\mathbf{r}_j, t) \exp(-iH_a t)|\Phi_i\rangle, \tag{2.26}$$

with $|\Phi_j\rangle = |j\rangle\, |n_{\mathbf{k},\sigma}\rangle$ since an incident particle is already taken into account in $\mathbf{A}^{(0)}_{fi}$.

From the relation (2.26) we find

$$S^{(1)}_{fi} = -2i\pi\delta\left(\varepsilon_f + E_f + \omega - \varepsilon_i - E_i\right)\sqrt{\frac{2\pi}{\omega}}\, \mathbf{e}^{*}_{\mathbf{k},\sigma}\mathbf{A}^{(0)}_{fi}(q_1)\langle f| \sum_{j=1}^{N} \exp\left(-i\mathbf{q}\mathbf{r}_j\right)|i\rangle \frac{e^2}{m}, \tag{2.27}$$

where $\mathbf{A}^{(0)}_{fi}(q_1)$ is the spatio-temporal Fourier transform of the incident particle field calculated on the four-dimensional vector $q_1 = \left\{\varepsilon_f - \varepsilon_i,\ \mathbf{p}_f - \mathbf{p}_i\right\}$. Spin effects are neglected. By analogy, for $S^{(2)}_{fi}$ we have the expression:

$$S_{fi}^{(2)} = -\frac{1}{2}\left\langle \Phi_f \middle| T \int\int dt\, dt'\, \hat{V}_{\text{int}}(t)\, \hat{V}_{\text{int}}(t') \middle| \Phi_i \right\rangle. \tag{2.28}$$

After simple transformations the matrix element of the scattering operator $S_{fi}^{(2)}$ is brought to the form:

$$S_{fi}^{2} = -e^2 2\pi\delta(\Delta E_i)\sqrt{\frac{2\pi}{\omega}}\, e^{*}_{\mathrm{k},\sigma,\mathrm{l}}\, A^{(0)}_{fi,s}(q_1)\langle f| \int d\tau \exp(i\omega\tau)\hat{j}^{l}(\mathbf{k},\tau)\hat{j}^{s}(\mathbf{q}_1)|i\rangle, \tag{2.29}$$

where

$$j^{l}(\mathbf{k},\tau) = \exp(iH_a\tau)\frac{1}{2m}\sum_{j=1}^{N}\left\{\hat{p}_j^{l}\exp\left(-i\mathbf{k}\mathbf{r}_j\right) + \exp\left(-i\mathbf{k}\mathbf{r}_j\right)\hat{p}_j^{l}\right\}\exp(-iH_a\tau)$$

is the spatial Fourier transform of the operator of atomic electron current in the interaction representation.

Summing the matrix elements $S_{fi}^{(1)}$ and $S_{fi}^{(2)}$, we obtain the PBs amplitude as:

$$S_{fi}^{pol} = 2\pi i\delta\left(\varepsilon_f + E_f + \omega - \varepsilon_i - E_i\right)\left(q_1^0\right)^2\sqrt{\frac{2\pi}{\omega}}\, e^{*}_{k,\sigma,l}A^{(0)}_{fi,s}(q_1)\langle f|\hat{c}^{ls}(k,\mathbf{q}_1)|i\rangle, \tag{2.30}$$

where

$$q_1^0 = \varepsilon_f - \varepsilon_i$$

is the change of IP energy during the process.

In the expression (2.30) $\hat{c}^{ls}(k,\mathbf{q}_1)$ is the operator of electromagnetic field scattering by an atom in the nonrelativistic (for atomic electrons) approximation that can be represented in the following form:

$$\hat{c}^{ls}(k,\mathbf{q}_1) = \frac{e^2}{m\left(q_1^0\right)^2}\left[im\int_{-\infty}^{\infty} d\tau \exp(i\omega\tau)T\left\{\hat{j}^{l}(\mathbf{k},\tau)\hat{j}^{s}(\mathbf{q}_1,0)\right\} - \delta^{ls}\hat{n}(\mathbf{q})\right], \tag{2.31}$$

where $\hat{n}(\mathbf{q}) = \sum_{j=1}^{N}\exp\left(-i\,\mathbf{q}\mathbf{r}_j\right)$ is the Fourier transform of the operator of atom electron density.

Analyzing the initial relativistic expression, from which Eq. 2.31 follows, it can be said that the first summand in the square brackets in Eq. 2.31 arises from the sum over the positive part of the atomic electron spectrum and describes scattering of an electromagnetic field by the atomic electron current. The second summand in

Eq. 2.31 arises after folding of the sum over states of the negative energy spectrum and describes field scattering by the atomic electron charge.

Let us write the matrix element $c_{fi}^{ls}(k,\mathbf{q}_1)$ in terms of the sum over intermediate states of atomic electrons:

$$c_{fi}^{ls}(k,\mathbf{q}_1)=\frac{e^2}{m\left(q_1^0\right)^2}\left\{m\sum_n\left[\frac{j_{fn}^l(\mathbf{k})j_{ni}^s(\mathbf{q}_1)}{\omega_{fn}+\omega+i0}+\frac{j_{fn}^s(\mathbf{q}_1)j_{ni}^l(\mathbf{k})}{\omega_{in}-\omega+i0}\right]-\delta^{ls}\,n_{fi}(\mathbf{q})\right\}. \tag{2.32}$$

In case of the spherically symmetric state $|i\rangle$ and within the framework of the dipole approximation (for $f=i$, $\mathbf{k}=\mathbf{q}_1=0$), from the formula (2.32) it follows:

$$c_{ii}^{ls}(\mathbf{q}_1,\mathbf{k}\to 0)\to\alpha(\omega)\,\delta^{ls}=\delta^{ls}\,\frac{e^2}{m}\sum_n\frac{f_{in}}{\omega_{in}^2-\omega^2}, \tag{2.33}$$

where $\alpha(\omega)$ is the dipole polarizability of an atom, f_{in} is the oscillator strength for the transition $i\to n$. In the formulas (2.30), (2.31), (2.32) and (2.33) it is implied that the bremsstrahlung photon frequency detuning Δ from resonance is great enough, so that: $\Delta=\left|\omega-\omega_{f(i)n}\right|>>\Gamma_{f(i)n}$, where $\Gamma_{f(i)n}$ is the line width for the transition $n\to f(i)$. Otherwise in these expressions it is necessary to take into account the line width for corresponding transitions.

It is well seen that the obtained expression for the PBs amplitude (Eq. 2.30) corresponds to its interpretation as a process of scattering of the incident particle eigenfield by atomic electrons to a bremsstrahlung photon.

Now let us calculate the amplitude of static (ordinary) bremsstrahlung (due to emission of a photon by an incident particle) taking into account possible excitation of atomic electrons. We use again the interpretation of bremsstrahlung as a process of scattering of a virtual photon to a real photon. Now virtual photons are produced by an atom (by a nucleus and bound electrons). For an atom at rest and nonrelativistic atomic electrons, virtual photons produced by them are mainly longitudinal. In this case it is convenient to use the Coulomb gauge of the electromagnetic potential ($\mathrm{div}\mathbf{A}=0$) since then it is possible to take into account only its time component. The space components describe in the Coulomb gauge the transverse part of the field and in the case under consideration are small. The time component of the potential of a virtual photon produced by an atom according to Eq. 2.20 is

$$A_{fi}^0=-\int d1'\,D_{00}(1,1')\,\langle f|\hat{J}^0(1')|i\rangle, \tag{2.34}$$

where

$$\hat{J}^0(1)=Ze\delta(\mathbf{r}_1-\mathbf{r}_0)-e\sum_{j=1}^{N}\delta\left(\mathbf{r}_1-\mathbf{r}_j\right)$$

is the atomic charge density operator in the coordinate representation ($\mathbf{r}_0$ is the radius vector of a nucleus). According to the standard rules of quantum electrodynamics [1], it is easy to obtain the expression for the static bremsstrahlung amplitude:

$$S_{fi}^{st} = -2\pi i\sqrt{\frac{2\pi}{\omega}}\, e_0^2 e_{k,\sigma,\mathrm{v}}^{*}\mathrm{T}^{v}\left(p_{f,i};k\right)A_{fi}^{0}(q)\delta\left(\varepsilon_f + E_f + \omega - \varepsilon_i - E_i\right). \tag{2.35}$$

Here the following designations are introduced:

$$\mathrm{T}^{v} = \frac{\bar{u}_f}{\sqrt{2\varepsilon_f}}\left\{\gamma^{v}\frac{p_f\gamma + \gamma k + m_0}{\left(p_f + k\right)^2 - m_0^2}\gamma^{0} + \gamma^{0}\frac{p_i\gamma - \gamma k + m_0}{\left(p_i - k\right)^2 - m_0^2}\gamma^{v}\right\}\frac{\bar{u}_i}{\sqrt{2\varepsilon_i}}, \tag{2.36}$$

$$A_{fi}^{0}(\mathbf{q}) = \left(4\pi/\mathbf{q}^2\right)\left\{\delta_{fi}Ze - en_{fi}(\mathbf{q})\right\}. \tag{2.37}$$

Physically Eq. 2.37 describes the screened potential of a nucleus, and Eq. 2.36 describes scattering of an electromagnetic field by an incident particle.

Thus the total amplitude of Bs of a relativistic incident particle on a nonrelativistic atom ($Z << 137$) in view of the polarization mechanism and possible excitation of atomic electrons with neglected spin effects looks like:

$$S_{fi}^{Br} = S_{fi}^{st} + S_{fi}^{pol}, \tag{2.38}$$

where S_{fi}^{pol} and S_{fi}^{st} are given respectively by the formulas (2.30) and (2.35).

2.3 Total Bremsstrahlung of a Fast Charged Particle on an Atom

2.3.1 General Expression for the Process Cross-Section

Based on the obtained expression for the amplitude, we will write the expression for the spectral Bs cross-section [1]:

$$\frac{d\sigma^{Br}(\omega)}{d\omega} = \frac{\varepsilon_i}{|\mathbf{p}_i|}\sum_{f,\sigma}\frac{d\Omega_{\mathbf{k}}}{(2\pi)^3}\frac{d\mathbf{q}}{(2\pi)^3}\lim_{T\to\infty}\frac{\left|S_{fi}^{Br}\left(\sigma;\mathbf{p}_{f,i};\mathbf{k}\right)\right|}{T}, \tag{2.39}$$

here $d\Omega_{\mathbf{k}}$ is the solid angle around the direction of the photon wave vector $\mathbf{k}$, T is the parameter having time meaning, summation is made over polarizations of an emitted photon (σ) and final states of an atom ($|f\rangle$). As before, we consider an

incident particle to be a Born particle, and the initial state of an atom to be nondegenerate.

In view of the explicit form of S_{fi}^{Br} the formula (2.39) can be rewritten:

$$\frac{d\sigma^{Br}(\omega)}{d\omega} = \frac{\varepsilon_i}{|\mathbf{p}_i|}\sum_{f,\sigma}\omega^2\frac{d\Omega_{\mathbf{k}}}{(2\pi)^3}\frac{d\mathbf{q}}{(2\pi)^3}2\pi\delta(\Delta\mathrm{E}) \times\frac{2\pi}{\omega}\left|e^*_{\mathbf{k}\sigma,l}\left\{e_0^2T^l\frac{4\pi}{q^2}\left(Ze\delta_{fi}-en_{fi}(\mathbf{q})\right)+\left(q_1^0\right)^2c_{fi}^{ls}A^0_{fi,s}\right\}\right|^2 \tag{2.40}$$

or

$$\frac{d\sigma^{Br}(\omega)}{d\omega} = \frac{d\sigma^{st}}{d\omega}+\frac{d\sigma^{pol}}{d\omega}+\frac{d\sigma^{\mathrm{int}}}{d\omega}. \tag{2.41}$$

The last term in Eq. 2.41 describes the interference of the static and polarization Bs, T^l and c_{fi}^{ls} are given by the formulas (2.36) and (2.32) of the previous paragraph.

Hereafter we assume that $|\mathbf{q}_1|<<|\mathbf{p}_{f,i}|$ – the motion of an IP is weakly disturbed during bremsstrahlung. So in the following formulas we use one value of IP velocity: $\mathrm{v}_i \cong \mathrm{v}_f \equiv \mathrm{v}_0$. Then for the vector potential of the virtual photon field $A_{fi}^{(0)}$ we have the expression:

$$\mathbf{A}^{(0)}(q) \simeq \frac{4\pi\, e_0}{q^0}\,\frac{\mathbf{v}_0\; q^0/c^2-\mathbf{q}}{\left(q^0/c\right)^2-\mathbf{q}^2}\,\delta\left(q^0-\mathbf{q}\mathbf{v}\right), \tag{2.42}$$

where $\mathbf{v}_0$ is the velocity of an incident particle.

In the same approximation for the function T (see the definition (2.36)) we obtain:

$$\mathbf{T} = \frac{\mathbf{q}_1}{m_0\,\gamma\,(\omega-\mathbf{k}\mathbf{v}_0)}, \quad \gamma = \varepsilon_i/m_0. \tag{2.43}$$

The obtained expression (2.40) for the cross-section of bremsstrahlung on an atom is the most general. With neglected internal degrees of freedom for an IP and an atomic nucleus it describes consistently the contribution of atomic electrons to the Bs process.

For the static Bs cross-section from Eq. 2.40 after simple transformations we find:

$$\frac{d\sigma^{st}}{d\omega} = \frac{\omega}{\mathrm{v}_0}\int\frac{d\Omega_{\mathbf{k}}\,d\mathbf{q}}{(2\pi)^4}\int dt\, e^{it\left(\omega+q_1^0\right)}\sum_{\sigma}\left|\mathbf{e}^*_{\mathbf{k},\sigma}\,\mathbf{T}\right|^2 \times\frac{e_0^4\,e^2}{\mathbf{q}^2}\,\langle i|(Z-\hat{n}(-\mathbf{q}))\,(Z-\hat{n}(\mathbf{q},t))|i\rangle. \tag{2.44}$$

If the energy of excitation of atomic electrons can be neglected in comparison with the frequency of an emitted photon ω, then in the formula (2.44) it is possible to assume $\hat{n}(\mathbf{q},t) \approx \hat{n}(\mathbf{q},0)$:

$$\frac{d\sigma^{st}}{d\omega} = \frac{\omega}{\mathrm{v}_0}\int \frac{d\Omega_{\mathbf{k}}\, d\mathbf{q}}{(2\pi)^3}\,\delta\left(q_1^0+\omega\right)\left[\mathbf{n}\,\mathbf{T}\right]^2 \frac{e_0^4\, e^2}{\mathbf{q}^2}\,\langle i||Z-\hat{n}(\mathbf{q})|^2|i\rangle, \quad \mathbf{n}=\frac{\mathbf{k}}{k}. \tag{2.45}$$

In derivation of (2.45) the equation was used: $\sum\limits_{\sigma} e^*_{\mathbf{k}\sigma,l}\, e_{\mathbf{k}\sigma,s} = \delta_{ls} - n_l\, n_s$.

The expression (2.45) agrees with the result of Lamb and Wheeler [4] who for the first time consistently took into consideration the contribution of excitation of atomic electrons to static bremsstrahlung.

In case of a heavy IP $(m_0 >> m)$ the first summand under the modulus sign in the formula (2.40) can be neglected in comparison with the second summand since $|\mathbf{T}| \propto 1/m_0$, while $\mathbf{A}^{(0)}(\mathbf{q})$ and $\hat{c}^{ls}(k,\mathbf{q}_1)$ do not depend on the IP mass. Then the total cross-section of Bs on an atom comes to the PBs cross-section, for which from Eq. 2.40 we find:

$$\frac{d\sigma^{pol}}{d\omega} = \frac{\omega}{\mathrm{v}_0}\int \frac{d\Omega_{\mathbf{k}}\, d\mathbf{q}}{(2\pi)^5}\left(\delta_{ls}-n_l\, n_s\right)\left(q_1^0\right)^4 A^{(0)}_{fi,s'}(q_1)\,A^{(0)}_{fi,l'}(q_1)\int dt\, e^{iq^0t}\langle i|\hat{c}^{sl'*}(0)\,\hat{c}^{ls'}(t)|i\rangle, \tag{2.46}$$

where

$$\hat{c}^{ls}(t) = \exp(i\,H_a\,t)\,\hat{c}^{ls}(0)\,\exp(-i\,H_a\,t) \tag{2.47}$$

is the operator of electromagnetic field scattering by an atom in the Heisenberg representation.

Thus the polarization bremsstrahlung cross-section summed over all final states of atomic electrons is expressed in terms of the correlation function of the operator of electromagnetic field scattering by an atom that can be written as

$$Kc_{ii}(t) \equiv \langle i|\hat{c}^{lsl*}(0)\,\hat{c}^{ls'}(t)|i\rangle,$$

where summation is supposed over twice-repeating indices.

2.3.2 PBs Without Excitation of a Target

Let us consider PBs without excitation of an atom ("elastic" PBs). Its cross-section is given by the summand with $f = i$ in the second term under the modulus sign in the formula (2.40):

$$\frac{d\sigma^{pol}_{ii}}{d\omega} = \frac{\omega}{\mathrm{v}_0}\int \frac{d\Omega_{\mathbf{k}}\, d\mathbf{q}}{(2\pi)^4}\left(\delta_{ls}-n_l\, n_s\right)\left(q_1^0\right)^4 A^{(0)}_{h}(q_1)\,A^{(0)}_{r}(q_1)\,\delta\left(q_1^0+\omega\right)\langle i|\hat{c}^{lh}|i\rangle\langle i|\hat{c}^{sr*}|i\rangle. \tag{2.48}$$

At first we consider the spectral range $\omega << p_a \, \mathrm{v}_0$ ($p_a \approx Z^{1/3} \, m \, e^2$ is the characteristic atomic momentum). Then the main contribution to the process under consideration will be made by the moduli $|\mathbf{q}_1| << p_a$ permitted by the energy conservation law. Otherwise ($|\mathbf{q}_1| >> p_a$) PBs with excitation and ionization of an atom should prevail. So in this case for the scattering tensor the dipole approximation can be used:

$$c_{ii}^{lh}(k, \mathbf{q}_1) \to \delta^{lh} \, \alpha_i(\omega) \, \theta(p_a - |\mathbf{q}_1|), \tag{2.49}$$

and instead of Eq. 2.48 we will obtain:

$$\frac{d\sigma_{ii}^{pol}}{d\omega} \approx \frac{\omega}{\mathrm{v}_0} \int \frac{d\Omega_{\mathbf{k}} \, d\mathbf{q}}{(2\pi)^4} \left[\mathbf{n} \, \mathbf{A}^{(0)}(q_1)\right]^2 \delta\left(q^0\right) \theta(p_a - |\mathbf{q}_1|) \left|\omega^2 \, \alpha_i(\omega)\right|^2, \quad \omega < p_a \, \mathrm{v}_0. \tag{2.50}$$

It should be noted that the used approximation corresponds to the Born-Bethe approximation in the theory of atomic excitation by electron impact.

From the formula (2.50) we find the following expression for the frequency-angular distribution of elastic PBs in the frequency range under consideration:

$$\frac{d\sigma_{ii}^{pol}(\omega, \vartheta)}{d\omega} = \frac{2 \, e_0^2}{\mathrm{v}_0^2} \frac{d\omega}{\omega} \left|\omega^2 \, \alpha_i(\omega)\right|^2 \left(1 + \cos^2\vartheta\right) \, \sin\vartheta \, d\vartheta \, \ln\left(\frac{\gamma \, p_a \, \mathrm{v}_0}{\omega}\right), \tag{2.51}$$

where ϑ is the angle between the initial IP velocity vector and the bremsstrahlung photon wave vector (radiation angle).

In derivation of the formula (2.51) summands of the order of one were neglected in comparison with the large logarithm (the large logarithm approximation).

From the expression (2.51) two corollaries follow:

1. In contrast to static Bs, polarization Bs of an ultrarelativistic IP ($\gamma >> 1$) in the frequency range $\omega < p_a \, \mathrm{v}_0$ is not directional, but is of a dipole nature,
2. The PBs cross-section grows logarithmically with IP energy in the ultrarelativistic limit at $\omega < p_a \, \mathrm{v}_0$.

These characteristic features of PBs of a relativistic IP allow descriptive physical interpretation. The logarithmic growth of the PBs cross-section with IP energy is connected with the features of the spatial structure of the electromagnetic eigenfield of a relativistic charged particle. The spatial distribution of the potential of this field at the frequency ω is given by the formula:

$$A^{(0)}(\omega) \propto \exp\left(i \, \frac{\omega}{\mathrm{v}_0} \, (z - \mathrm{v}_0 \, t) - i \frac{\omega \, \rho}{\gamma \, \mathrm{v}_0}\right), \tag{2.52}$$

here z, ρ are the cylindrical coordinates of the IP field.

Thus we obtain the lateral dimension of the field $\rho_{\max} \approx \gamma\, v_0/\omega$, and accordingly for the minimum transferred transverse momentum we have $|\mathbf{q}_\perp|_{\min} \approx \omega/\gamma\, v_0$. Hence from the formula for the spectral PBs cross-section (in the Born approximation): $d\,\sigma^{pol}(\omega) \propto \ln\left(|\mathbf{q}_\perp|_{\max}/|\mathbf{q}_\perp|_{\min}\right)$ the second PBs property follows that is noted here. It should be noted that in case of static Bs on a neutral atom the maximum size of a field scattered by an IP to a bremsstrahlung photon is defined by the size of an atom.

2.3.3 High-Frequency Limit

Now we will consider "elastic" PBs (without change of an atomic state) in the frequency range $I << \omega << m$ (I is the atomic ionization potential). In this case it is possible to use the high-frequency asymptotics for the scattering operator:

$$\hat{c}^{ls}(k, \mathbf{q}_1) \approx -\frac{e^2}{m\left(q_1^0\right)^2}\,\hat{n}(\mathbf{q})\left\{\delta^{ls} + \frac{q_1^l\, q_1^s}{2\,m\,\omega}\right\}, \quad I << \omega << m. \tag{2.53}$$

The formula (2.53) is obtained with the use of the expansion into a series of the matrix element c_{fi}^{ls} (Eq. 2.32) in terms of the powers of the ratio $|\omega_{jn}|/\omega \quad (j = f, i)$, the summands in the sum over intermediate states with $|\omega_{jn}| > \omega$ making a small contribution to c_{fi}^{ls} at $\omega >> I$. Substituting the formula (2.53) in Eq. 2.48, we find:

$$\frac{d\sigma_{ii}^{pol}}{d\omega} = \frac{\omega}{v_0}\int \frac{d\Omega_{\mathbf{k}}\, d\mathbf{q}}{(2\pi)^4}\;\delta\left(q^0\right)\left(\frac{e^2}{m}\right)^2 |n_{ii}(\mathbf{q})|^2\left[\mathbf{n}, \left(\mathbf{A}^{(0)}(\mathbf{q}) + \frac{\mathbf{q}_1\left(\mathbf{q}_1 \mathbf{A}^{(0)}(\mathbf{q}_1)\right)}{2\,m\,\omega}\right)\right]^2, \quad I << \omega << m. \tag{2.54}$$

To simplify the calculations, we consider that $\gamma >> 1$, then the IP field is mainly transverse and $\mathbf{q}_1\, \mathbf{A}^{(0)}(\mathbf{q}_1) = 0$. We use the approximation of *exponential* screening of an atomic nucleus to calculate the spectral PBs cross-section. Then:

$$n_{ii}(\mathbf{q}) = \frac{N}{\left(1 + \mathbf{q}^2/p_a^2\right)}. \tag{2.55}$$

Here N is the number of atomic electrons (for a neutral atom, naturally, $N = Z$). The value $n_{ii}(\mathbf{q})$ represents the (static) form factor of the atomic core in the state $|i\rangle$.

Using Eq. 2.55 and the relation $\alpha_i(\omega) \to \alpha_\infty(\omega) = -N\,e^2/m\,\omega^2$ to estimate the spectral PBs cross-section in a high-frequency range, we find for three spectral

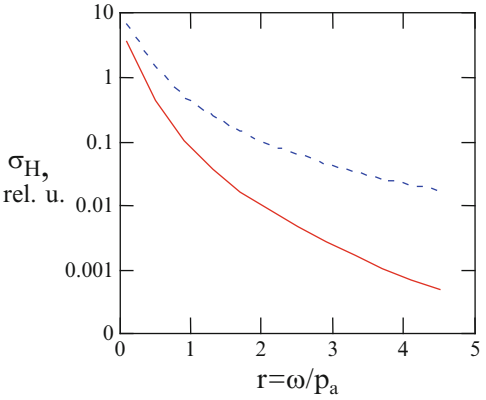

Fig. 2.2 The spectral cross-section of PBs of a relativistic electron on a hydrogen atom in the high-frequency region $\omega >> I = 0.5$ a.u. as a function of the parameter $r = \omega/p_a$ for two values of the relativistic factor: $\gamma = 2$ (*solid line*), $\gamma = 10$ (*dotted line*)

ranges after integration with respect to the solid angle of photon escape and the transferred momentum the following expressions:

$$\frac{d\sigma_{ii}^{pol}}{d\omega} = \frac{16}{3} N^2 \frac{e^4 e_0^2}{m^2 \omega} \ln\left(\frac{\gamma p_a}{\omega}\right) \quad I << \omega << p_a, \tag{2.56}$$

$$\frac{d\sigma_{ii}^{pol}}{d\omega} = 2N^2 \frac{e^4 e_0^2}{m^2 \omega} \left(\frac{p_a}{\omega}\right)^2 \ln(\gamma) \quad p_a << \omega << \gamma^2 p_a, \tag{2.57}$$

$$\frac{d\sigma_{ii}^{pol}}{d\omega} = 4N^2 \frac{e^4 e_0^2}{m^2 \omega} \left(\frac{p_a}{\omega}\right)^2 \left(\frac{\gamma^2 p_a}{\omega}\right)^2 \quad \gamma^2 p_a << \omega << m. \tag{2.58}$$

The formulas (2.56), (2.57), and (2.58) are low-sensitive to a specific type of nucleus screening by atomic electrons. The spectral cross-section (2.56) can be obtained from the formula (2.51) since in this frequency range the dipole approximation for interaction of an IP with an atomic core (and especially with a photon) is still true.

The spectral cross-section of PBs of a relativistic electron on a hydrogen atom in a high-frequency range calculated by the formulas (2.56) and (2.57) is presented in Fig. 2.2 for two values of the relativistic factor γ.

From the given figure it follows that the cross-section of PBs of a relativistic electron in the high-frequency range $\omega > p_a$ decreases with growing frequency. Physically this is a consequence of coherence loss for interaction of a virtual photon of the IP field with an atomic electron. From mathematical point of view, this decrease is defined by reduction of the atomic form factor $n_{ii}(\mathbf{q})$ with growing magnitude of the transferred wave vector $|\mathbf{q}| > p_a$. Another conclusion of Fig. 2.2 is the growth of the PBs cross-section with increasing energy of a relativistic incident particle (of the relativistic factor γ).

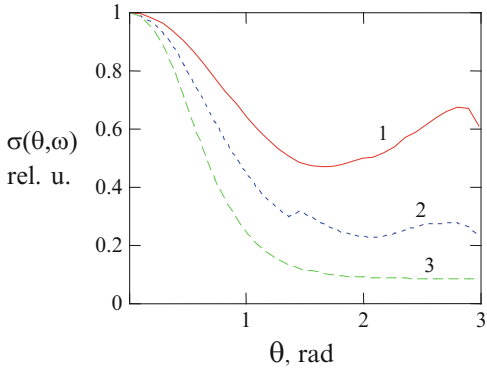

Fig. 2.3 The angular dependence of PBs on an atom (Z = 30) in the high-frequency approximation for different frequencies of a bremsstrahlung photon: ω = 5 keV (*curve 1*), ω =15 keV (*curve 2*), ω = 50 keV (*curve 3*), the IP velocity is: v = 0.9 c

The frequency range of Eq. 2.57 is characteristic for ultrarelativistic incident particles. In this range the compensation of a momentum transferred from an IP to an atom due to a photon momentum is possible. As the analysis shows, this is true only for small enough radiation angles: $\vartheta \leq \sqrt{p_a/\omega} \approx \sqrt{\lambda/R_a}, \quad R_a \approx p_a^{-1}$. This inequation follows from the condition of smallness of a momentum transferred to a target during Bs in comparison with an atomic momentum: $\omega\,(1 - \mathrm{v}_0\,\cos(\vartheta)) \leq p_a\,\mathrm{v}_0$.

Thus in the frequency range of Eq. 2.57 PBs gains directionality, and in calculation of the process cross-section it is necessary to take into account a photon momentum.

The angular diagram of PBs of a relativistic electron on a hydrogen atom in the high-frequency limit is presented in Fig. 2.3 for different values of bremsstrahlung photon energy.

It is seen that with growing energy of a bremsstrahlung photon the angular distribution of PBs of a relativistic electron is narrowed.

In the frequency range of Eq. 2.58 (if it exists) a momentum transferred from an IP to the atomic core at any radiation angles is more than the characteristic atomic momentum, and PBs is strongly suppressed as it follows from the form of the static atomic form factor (2.57). Physically this means that with large momenta transferred to an atom ($|\mathbf{q}| >> p_a$) that are characteristic for this frequency range inelastic PBs channels prevail that are accompanied by excitation and ionization of an atomic electron.

It should be noted that in the above "elastic" PBs the contribution of all atomic electrons to radiation is coherent, so the process cross-section is proportional to the squared number of atomic electrons. This circumstance can be explained as follows. During elastic PBs, when the state of the atomic core does not change, an electron charge, remaining localized in the atom, shows itself as the charge of one particle Ne (at $\lambda > R_a$). Therefore the amplitude of its interaction with an electromagnetic field is proportional to Ne, and the cross-section is proportional to $(Ne)^2$.

Let us return to the total PBs cross-section that takes into account excitation of atomic electrons – the formula (2.46). To obtain the spectral PBs cross-section in the explicit form in the general case does not seem possible. Let us consider some particular, but practically important situations.

Let the frequency ω be such that the main contribution to the cross-section that is differential with respect to a transferred momentum is made by $|\mathbf{q}_1| << p_a$. (This in particular takes place in experiments on agreement (see [5]) if a scattered electron is observed at small scattering angles). Then the dipole approximation for interaction of an IP with the atomic core is true, and it is possible to integrate with respect to $\mathbf{q}$ in view of the explicit form of $\mathbf{A}^{(0)}(q)$ (Eq. 2.42). Taking into account the spherical symmetry of the state $|i\rangle$, we obtain after a number of transformations for the spectral PBs cross-section the following expression (we assume that $\omega_{si} < p_a \mathrm{v}_0 - \omega$):

$$\frac{d\sigma_{fi}^{pol}}{d\omega} = \frac{16\, e_0^2}{9\, \mathrm{v}_0^2} \sum_{m,l,f} \omega^3 \, |\langle f|\hat{c}_{ml}(\omega)|i\rangle|^2 \, \ln\left(\frac{\gamma\, p_a\, \mathrm{v}_0}{\omega + \omega_{fi}}\right). \tag{2.59}$$

It should be noted that the summand in the formula (2.59) with $f = i$ gives the spectral cross-section of elastic PBs following also from the formula (2.51) after integration with respect to the angle of photon escape.

2.3.4 Near-Resonant PBs

Let us consider a case of the near-resonance frequency ω, when the following inequation is satisfied: $\Gamma_{nf} << |\omega - \omega_{nf}| << \omega$, here ω_{nf} and Γ_{nf} are the eigenfrequency and the line width for the transition $n \to f$ between two states of the discrete spectrum of the atomic core. Then in the expression for the matrix element from the operator of electromagnetic field scattering by an atom (Eq. 2.32) one resonant summand can be separated that makes the main contribution to the amplitude, and the imaginary part of the scattering tensor can be neglected in comparison with the real part. Then in the sum over f on the right side of the Eq. 2.59 one resonant summand remains.

After summation over the projections of the total momentum of resonant states we find for a singlet initial state:

$$\frac{d\sigma_{fi}^{res}}{d\omega} = \frac{4\, e_0^2\, e^4}{3\, \mathbf{v}_0^2\, m^2} \left(\frac{\omega}{\Delta}\right)^2 \frac{f_{in}}{\omega_{ni}} \left(2J_f + 1\right) f_{fn} \ln\left(\frac{\gamma\, p_a\, \mathrm{v}_0}{\omega + \omega_{\mathrm{fi}}}\right) \quad \Delta = \omega - \omega_{nf}$$
$$\omega >> |\Delta| >> \Gamma_{fn}, \tag{2.60}$$

here f_{ik} is the oscillator strength for the transition $i \to k$, J_f is the quantum number of the total angular momentum of an atom in the state $|f\rangle$.

Following from the expression (2.60) for $f = i$ is the formula for "elastic" near-resonance PBs that was studied in detail earlier [2].

The case $f \neq i$ was studied in the paper of V.M. Buimistrov and L.I. Trakhtenberg [6] from the standpoint of the prospect of obtaining radiation amplification based on the PBs effect.

Given in the author's work [7] is the generalization of the spectrum of near-resonant PBs to the case of the energy-band structure of a target in the elementary isotropic effective mass approximation.

In this situation the scattering tensor can be represented as:

$$c^{hl}(k,q) = \int\limits_{\Omega_{Br}} \frac{d\vec{\kappa}}{(2\pi)^3} \frac{e^2}{\omega^2} \frac{j^h_{vc}(\mathbf{k},\vec{\kappa})\, j^l_{cv}(\mathbf{q},\vec{\kappa})}{\omega - \omega_{cv}(\vec{\kappa}) + i\,\Gamma_{cv}/2}. \tag{2.61}$$

Here integration is performed with respect to the quasi-momentum of electrons $\vec{\kappa}$ in the Brillouin zone Ω_{Br}, $\omega_{cv}(\vec{\kappa}) = \varepsilon_c(\vec{\kappa}) - \varepsilon_{vc}(\vec{\kappa})$ is the difference of electron energies in the conduction band and in the valence band. Then we will assume that transitional current weakly depends on an electron quasi-momentum. In the general case it is necessary to perform integration in the formula (2.61) in view of the dispersion law $\varepsilon_{c,v}(\vec{\kappa})$. We will consider the approximation of parabolic bands, in which: $\varepsilon_{v,c}(\vec{\kappa}) = \varepsilon^0_{v,c} \mp \vec{\kappa}^2 \big/ 2\, m_{v,c}$, $m_{v,c}$ are the effective masses of electrons near the valence band top and the conduction band bottom. Then after averaging over photon polarizations for the spectral intensity of PBs the following expression can be obtained:

$$\frac{dW^{pol}}{d\omega} = B(\omega)\, |J(\Delta)|^2, \tag{2.62}$$

where

$$B(\omega) = \int \frac{d\mathbf{q}}{(2\pi)^{10}}\, \mu^3_{cv}\, e^4 \left[\mathbf{n}\, \mathbf{j}_{vc}(\mathbf{k})\right]^2 \left(\mathbf{A}(q)\, \mathbf{j}_{cv}(\mathbf{q})\right)^2,$$

$$J(\Delta) = \begin{cases} 1 - \frac{\sqrt{|\Delta|}}{a}\, arctg\left(\frac{a}{\sqrt{|\Delta|}}\right), & \Delta<0 \\ 1 + \frac{\sqrt{\Delta}}{2a} \ln\left|\frac{a-\sqrt{\Delta}}{a+\sqrt{\Delta}}\right|, & \Delta>0 \end{cases}$$

$$\Delta = \omega - \left(\varepsilon^0_c - \varepsilon^0_v\right), \quad \mu^{-1}_{cv} = m^{-1}_c + m^{-1}_v, \quad a \approx N_v^{1/3} \Big/ \mu^{1/2}_{cv}, \quad \mathbf{n} = \mathbf{k}/|\mathbf{k}|,$$

N_v is the concentration of the valence band electrons. The target parameter is a^2, it is proportional to the energy of localization of a quasi-particle with the reduced mass μ_{cv} in the volume N_v^{-1}, its value is accordingly of the order of the permitted band width.

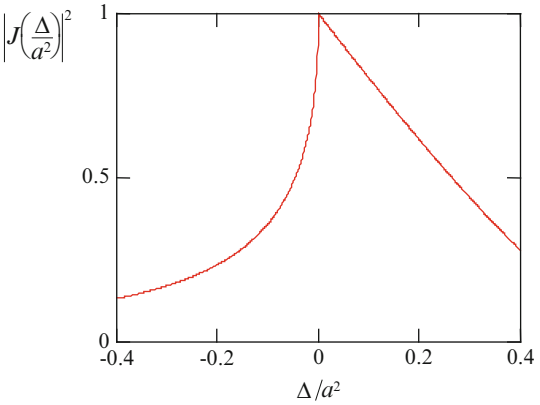

Fig. 2.4 The plot of the function $|J(x)|^2$ describing the spectrum of near-resonance PBs for a case of the energy-band structure of a target in the isotropic effective mass approximation

In the formula (2.62) it is assumed that $a^2 \neq |\Delta|$, otherwise it is necessary to take into account the imaginary additive in the expression for the scattering tensor (2.61).

The function $B(\omega)$ has no resonance peculiarities for the case under consideration: $\omega < v_0/d$ (d is the lattice constant), so the frequency peculiarities of the PBs spectrum are described by the function $|J(\Delta)|^2$, the plot of which is presented in Fig. 2.4 for the case of practical interest $\Delta < a^2$ ($a^2 = N_v^{2/3}/\mu_{cv}$).

From this figure it follows in particular that the spectrum of near-resonance PBs for the energy-band structure of a target has a pronounced asymmetry: for frequencies smaller than the energy gap width (negative detunings from resonance Δ) the PBs intensity falls more steeply than for positive detunings. This circumstance is quite expected since positive detunings correspond to the virtual transition to the conduction band, and negative detunings correspond to the virtual transition to the band gap.

The function $J(\Delta)$ itself for detunings under consideration is positive ($\Delta < a^2$), which corresponds to destructive interference with the static Bs channel. For high detunings $\Delta > a^2$ this function is negative, and interchannel interference is constructive.

It should be noted that in the limit $a^2 << |\Delta|$ in the expression (2.62) the multiplier $|\omega_{cv}/\Delta|^2$ appears that is characteristic for near-resonant PBs on one atom.

It is significant that if $\omega < \omega_{cv}$ and $|\Delta| > \Gamma_{cv}$, a cascade process connected with real filling of the conduction band is impossible.

2.3.5 PBs with Target Excitation

Now we will calculate the PBs cross-section with excitation (including ionization) of an atom for $m >> \omega >> I$. Substituting the expression for $\hat{c}^{lh}$ in this spectral range Eq. 2.53 in the formula (2.48), we find

$$\frac{d\sigma_{ii}^{pol}}{d\omega} = \frac{\omega}{\mathrm{v}_0}\int \frac{d\Omega_{\mathbf{k}}\, d\mathbf{q}}{(2\pi)^4}\left(\frac{e^2}{m}\right)^2 \left[\mathbf{n},\ \left(\mathbf{A}^{(0)}(q_1) + \frac{\mathbf{q}_1\left(\mathbf{q}_1\,\mathbf{A}^{(0)}(q_1)\right)}{2m\omega}\right)\right]^2 S_{ii}(q). \quad (2.63)$$

Here the value is introduced:

$$S_{ii}(q) = \frac{1}{2\pi}\int\limits_{-\infty}^{\infty} dt\ \exp\left(iq^0 t\right)\langle i|\hat{n}|(-\mathbf{q})\hat{n}(\mathbf{q},t)|i\rangle| \quad (2.64)$$

that we will call the dynamic form factor according to the terminology accepted for description of effects in a media. For simplicity we assume further $q_1 \approx q$, so neglecting summands of the order of $(p_a/\omega)^2$ in comparison with one at $\omega >> p_a$; at $\omega < p_a$ the dipole approximation is true, so the magnitudes $|\mathbf{q}|$ and $|\mathbf{k}|$ can be neglected in comparison with p_a. As seen from Eq. 2.63, for calculation of the spectral PBs cross-section it is necessary to know the explicit form of the $\mathbf{q}$ and q^0 functional dependence of S_{ii}.

With further tracing only qualitative moments in mind, here we use for calculations the simplest analytical approximation of $S_{ii}(q)$:

$$S_{ii}(q) \approx \theta(|\mathbf{q}| - p_a)\,\delta\left(q^0 + \frac{\mathbf{q}_1^2}{2m}\right) N + \theta(p_a - |\mathbf{q}|)\,\delta\left(q^0\right) N^2, \quad (2.65)$$

where N is the number of electrons in an atom.

The approximate Eq. 2.65 can be obtained after a number of transformations, taking into account the explicit form of the electron density operator being an operator of shift in the momentum space and corresponding permutation relations.

The physical meaning of two summands in Eq. 2.65 is transparent: the first summand describes processes with ionization of the atomic core, when a transferred momentum is large, in this case the contribution of bound electrons is incoherent and part of energy is carried away by a knocked-on electron. The second summand describes the coherent process, when a momentum transferred to the core from an IP is small, and the atom remains in the former state. In the latter case the recoil momentum takes over a massive nucleus, and coherence takes place since the phase of electromagnetic interaction of the IP with the target core changes little at distances of the order of the atomic radius.

From the formulas (2.63) and (2.65) it is easy to find the spectral PBs cross-section in the approximation under consideration:

$$\frac{d\sigma_{ii}^{pol}}{d\omega} = \frac{16e_0^2e^4}{3m^2\mathrm{v}_0^2}\left\{\theta(p_a\mathrm{v}_0 - \omega)\left[N^2\ \ln\left(\frac{\gamma p_a \mathrm{v}_0}{\omega}\right) + N\ln\left(\frac{m_0\mathrm{v}_0}{p_\mathrm{a}}\right)\right]\right.$$
$$\left. + \theta(\omega - p_a\mathrm{v}_0)\,N\ \ln\left(\frac{\gamma m_0\mathrm{v}_0^2}{\omega}\right)\right\}. \quad (2.66)$$

The obtained expression allows descriptive physical interpretation. At $\omega<p_a v_0$ (the summand in the square brackets) PBs proceeds both without excitation of an atom (if $|\mathbf{q}|<p_a$) and with its ionization (at $|\mathbf{q}|>p_a$). And in the first case PBs is coherent by the contribution of atomic electrons to the process (the cross-section is proportional to N^2), in the second case PBs is incoherent (the cross-section is proportional to the number of atomic electrons N). In the spectral range $\omega>p_a v_0$ – the second summand in the braces in Eq. 2.66 – the law of conservation of energy-momentum permits only $|\mathbf{q}|>p_a$, so PBs proceeds mainly with atomic ionization, and its cross-section is proportional to N.

It is essential that the total PBs cross-section (2.66) taking into account excitation and ionization of an atom admits a correct passage to the limit to the case $Z = 0$, corresponding to which is the equation $p_a = 0$ in the formula (2.66). Then the summand in the square brackets describing "elastic" PBs disappears, and the remaining last term in the braces describes emission of a slow free recoil electron in collision with a relativistic charged particle as it must be according to the physical picture of the process. It should be noted that this passage to the limit does not take place for the "elastic" PBs cross-section since in the absence of a nucleus the process becomes fundamentally inelastic – an atomic electron takes over a momentum excess and increases its energy.

Let us compare integrated (with respect to the scattering and radiation angles) cross-sections of the polarization and static Bs channels. Corresponding cross-sections look most simple in the quasi-classical ($\varepsilon_{f,i}>>\omega$) and ultrarelativistic ($\gamma>>1$) limits and in the region of frequencies exceeding the atomic ionization potential.

Thus in the spectral range $p_a v_0>\omega>>I$ the main contribution to both Bs channels is made by the "elastic" summands (without excitation of the atomic core) (we assume $Z, N>>1$):

$$\frac{d\sigma_{ii}^{pol}}{d\omega} = \frac{16N^2e^6}{3m^2\omega}\ln\left(\frac{\gamma p_a}{\omega}\right), \tag{2.67}$$

$$\frac{d\sigma_{ii}^{st}}{d\omega} = \frac{16Z^2e^6}{3m^2\omega}\ln\left(\frac{m}{p_a}\right), \tag{2.68}$$

that (in case of $Z = N$) differ only by logarithmic factors, though they have (in the ultrarelativistic case) essentially different radiation patterns.

Let us write out the cross-sections of inelastic static and polarization Bs in the spectral range where the main contribution to PBs is made by the processes with atomic ionization:

$$\frac{d\sigma_{nonel}^{pol}}{d\omega} = \frac{16Ne^6}{3m^2\omega}\ln\left(\frac{\varepsilon}{\omega}\right), \tag{2.69}$$

$$\frac{d\sigma^{stl}_{nonel}}{d\omega} = \frac{16Ne^6}{3m^2\omega}\ln\left(\frac{m}{p_a}\right), \quad \gamma >> \sqrt{\frac{\omega}{p_a}}. \tag{2.70}$$

Thus in the frequency range $p_a\, \mathrm{v}_0 << \omega << m$ the cross-sections of elastic static and elastic polarization Bs differ only by logarithmic factors, and inelastic summands of the cross-section corresponding to them are close in value up to $\omega \approx m$.

At $\omega >> m$ the space part of the 4-momentum transferred to an atom is great, and atomic electrons can to a good accuracy be considered free, which gives the result known in quantum electrodynamics when a recoil electron emits ω/m times less than a fast electron. Thus the contribution of the polarization summand to the total cross-section of Bs of an electron on an atom in the region of high ($\omega >> m$) frequencies is negligibly small in comparison with the contribution of the static summand.

All aforesaid is true also for the case of Bs of an ultrarelativistic positron on an atom, when the sign of the polarization summand of the amplitude changes to the opposite. But, as for an electron, due to different dependences of the static and polarization summands on radiation angles their interference can be neglected and thereby the total cross-section of Bs of an ultrarelativistic particle can be represented as the sum of two summands (polarization and static).

2.3.6 Channel Interference

Now let us consider the summand in the cross-section of Bs on a neutral atom describing the interference of the static and polarization channels. As follows from the analysis of angular dependences, this interference is low for an ultrarelativistic incident particle. So here we will consider an incident particle to be nonrelativistic, but still a Born particle. Let us neglect excitation of an atom during bremsstrahlung. Then from Eq. 2.40 in view of Eqs. 2.42 and 2.43 it can be obtained for the interference summand in the cross-section:

$$\frac{d\sigma^{\mathrm{int}}_{ii}}{d\omega} \approx \frac{32\, e_0^2\, \omega^3}{3\, \mathrm{v}_0^2} \int\limits_{\omega/\mathrm{v}_0}^{|\mathbf{q}_1|_{\max}} \frac{|e\, e_0|}{m_0\, \omega}\, \mathrm{Re}\{c_{ii}(\omega; |\mathbf{q}_1|)\}\, (Z - n_{ii}(\mathbf{q}_1))\, \frac{d|\mathbf{q}_1|}{|\mathbf{q}_1|}. \tag{2.71}$$

In derivation of Eq. 2.71 it was taken into account that for a nonrelativistic IP $|\mathbf{q}_1| \geq \omega/\mathrm{v}_0 >> |\mathbf{k}|$. We call attention to the fact that the contribution to interference is made only by the real part of the diagonal matrix element from the operator of electromagnetic field scattering by an atom (Eq. 2.31). For the elementary approximation of the scattering tensor (2.49) from the formula (2.71) we have approximately:

$$\frac{d\sigma_{ii}^{\text{int}}}{d\omega} \approx \frac{32\left|e_0^2 e\right|}{3m_0 \mathrm{v}_0^2}\,\omega^2\,\{\mathrm{Re}[\alpha_i(\omega)]\}\int\limits_{p^*}^{p_a}\frac{(Z-n_{ii}(|\mathbf{q}_1|))}{|\mathbf{q}_1|}d|\mathbf{q}_1|, \tag{2.72}$$

$p^* = \max\{p_{\min},\ \omega/\mathrm{v}_0\}$, where $p_{\min}$ is the characteristic momentum of outer shell electrons, p_a is the characteristic momentum of atomic electrons making the main contribution to atomic polarizability at the frequency under consideration ω. From Eq. 2.72 it follows that the interference term in the Bs cross-section can be noticeable if the greatest contribution to polarizability is made by the inner atomic shell with comparable cross-sections of PBs and SBs. This takes place, for example, for Bs of electrons on neutral xenon for frequencies near the potential of ionization of the $4f$ -subshell.

The radiation spectrum of xenon in case of passage of an electron beam through it was recorded in the work [8]. A shift of the frequency maximum from the value calculated without considering interference to 20 eV was found. This discrepancy was explained by the fact that the velocity of electrons in a beam is probably not high enough for the Born approximation to work "well". On the other hand, a reason of shift can be an interference term in the total Bs cross-section that was not taken into account. And if an IP is heavy or ultrarelativistic, the expected value of shift should be small due to the smallness of the interference summand in these cases.

For an ultrarelativistic IP the theory results in an additional possibility of interest: the value of shift of the Bs frequency maximum relative to the potential of ionization of a corresponding atomic subshell sharply depends on the angle of photon emission, which is caused by essentially different patterns of the static and polarization Bs channels in the ultrarelativistic case.

It should be noted that the above brief analysis of channel interference relates to Bs of a Born IP on a neutral atom, where, generally speaking, interference effects in the Bs cross-section integrated with respect to the angle of incident particle scattering are low due to different regions of space of channel formation: corresponding to the static channel are large angles of IP scattering and respectively small distances to a nucleus, corresponding to the polarization channel are small scattering angles and large distances.

Thus interference effects in Bs on a neutral atom can show themselves most strongly in the Bs cross-section differential with respect to the angle of IP scattering, which was shown in the work [9]. The situation is different for Bs on ions for strongly inelastic scattering of electrons of moderate energies, when channel interference is found to be essential also in the integrated process cross-section.

2.4 Polarization Bremsstrahlung of a Fast Charged Particle on an Atom in the Local Plasma Approximation

The spectral PBs cross-sections in the high-frequency limit obtained in the previous paragraph in Eqs. 2.56, 2.57, and 2.58 are true for the frequencies $\omega >> I$, where I is the characteristic atomic ionization potential (it will be recalled that in this chapter

we use the relativistic system of units, in which $\hbar = c = 1$). In case of a multielectron atom this value is of rather indefinite nature, so the domain of applicability of the high-frequency approximation requires its refinement.

At the same time it is for a multielectron atom that polarization effects in Bs should be the most essential. And the calculation of the dynamic polarizability of a multielectron atom defining the PBs cross-section is an intricate quantum-mechanical problem that has to be solved anew for each specific target.

In this connection it seems to be useful to apply simple universal models suitable for estimation of the value of the polarization Bs cross-section and for revealing general qualitative regularities of this process.

One of such models is the method of local electron density (or local plasma frequency) that was first proposed by Brandt and Lundqvist for calculation of the cross-section of photoabsorption by multielectron atoms [10].

In this section this method is used to describe PBs of a fast (including relativistic) charged particle on a neutral multielectron atom, the distribution of electron density in which is given by the statistical Thomas-Fermi model.

It should be noted that the use of the local plasma frequency method for calculation of the polarizability of a Thomas-Fermi atom is intrinsically consistent since the physical representations underlying both models are analogous.

The advantages of the used approach are also that it is most adequate just for those frequencies and distances, at which the significant role is played by multielectron effects, the description of which within the framework of the consistent quantum-mechanical consideration is difficult and laborious.

2.4.1 *Polarizability of a Thomas-Fermi Atom in the Local Plasma Frequency Approximation*

Within the framework of the Brandt-Lundqvist model the expression for the dynamic polarizability of an atom looks like:

$$\alpha(\omega) = \int_0^\infty \frac{\omega_p^2(r)\, r^2\, dr}{\omega_p^2(r) - \omega^2 - i0}, \tag{2.73}$$

where $\omega_p(r) = \sqrt{4\,\pi\, e^2\, n(r)/m}$ is the local plasma frequency depending on the local electron density of the electron core $n(r)$, r is the distance from a point under consideration to an atomic nucleus.

Hereafter for the function $n(r)$ the Thomas-Fermi approximation will be used that gives [11]:

$$n(r) = n_{TF}(r) = Z^2 f(r/r_{TF}), \quad f(x) = \frac{32}{9\,\pi^3}\left(\frac{\chi(x)}{x}\right)^{3/2}, \tag{2.74}$$

where $r_{TF} = b\,a_0/Z^{1/3}$ is the Thomas-Fermi radius ($b = (9\,\pi^2/128)^{1/3} \cong 0.8853$, a_0 is the Bohr radius, Z is the nuclear charge), $\chi(x)$ is the Thomas-Fermi function.

The expression (2.71) can be transformed to the form revealing the scaling law (scaling) with respect to the parameter $v = \hbar\,\omega/2\,Ry\,Z$ ($Ry = 13.6\ \ eV$) having the meaning of dimensionless (reduced) frequency:

$$\alpha(v) = r_{TF}^3\,\beta(v) = \frac{b^3\,a_0^3}{Z}\,\beta(v). \tag{2.75}$$

Here the dimensionless complex function $\beta(v)$ (the reduced polarizability of a Thomas-Fermi atom) is introduced, the imaginary part of which is (the prime means differentiation with respect to the argument x):

$$\mathrm{Im}\{\beta(v)\} = \pi\,\frac{f(x_v)\,x_v^2}{|f'(x_v)|}, \tag{2.76}$$

and the real part can be calculated by the "punctured" Kramers-Kronig relation:

$$\mathrm{Re}\{\beta(v)\} = \frac{2}{\pi}\int_0^\infty \frac{[\mathrm{Im}\{\beta(v)\} - \mathrm{Im}\{\beta(\tilde{v})\}]\,\tilde{v}d\tilde{v}}{v^2 - \tilde{v}^2}. \tag{2.77}$$

In the formulas (2.76), (2.77) the value x_v is determined by solution of the equation:

$$4\,\pi f(x) = v^2 \tag{2.78}$$

that describes the resonance of the radiated frequency with the local plasma frequency at some value of the parameter x (the reduced distance to a nucleus).

The expression (2.76) is obtained from the determination of the dynamic (Eq. 2.73) and reduced (Eq. 2.75) polarizabilities with the use of the known Sokhotsky formula.

It should be noted that the numerical calculation of dimensionless polarizability directly by the formulas (2.73), (2.74), and (2.75) is found to be difficult for low frequencies ($v<1$) in view of the singularity of a corresponding integrand and slow decrease of Thomas-Fermi electron density (2.74) with distance. As a result, the numerical integration loses accuracy. So it is proved to be preferably to use the formulas (2.76), (2.77), and (2.78) for calculation of the reduced polarizability $\beta(v)$.

The ratio $g(v)$ of the modulus of the function $\beta(v)$ to the modulus of its high-frequency limit ($\beta_\infty(v) = -b^{-3}v^{-2}$) is presented in Fig. 2.5.

Given in the same figure is the corresponding ratio for a krypton atom restored by the data of the work [12], in which the dynamic polarizability of an atom was calculated by the quantum-mechanical method within the framework of the random phase exchange approximation.

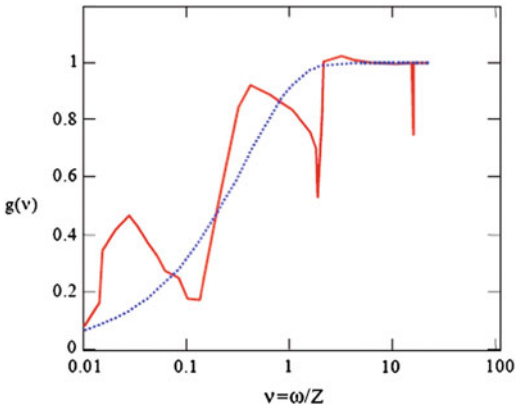

Fig. 2.5 The dynamic polarizability moduli normalized to their high-frequency limit as functions of the dimensionless frequency $v = \hbar\omega/2ZRy$ for a krypton atom: *solid curve* – by the data of the work [12], *dotted curve* – calculation for a Thomas-Fermi atom in the local electron density model

It is seen that the function $g(v) = v^2\,|\beta(v)|$ for a Thomas-Fermi atom smoothly describes the spectral peculiarities of the dynamic polarizability of a krypton atom connected with the shell structure of an atom and approaches its high-frequency limit for $v>10$.

However, it should be remembered that in the range of low frequencies $v<0.1$ the used approximation becomes inadequate since, on the one hand, the local plasma frequency approximation "works" badly for polarizability of an atom Eq. (2.73), and on the other hand, the contribution to polarizability at these frequencies is made by the peripheral regions of an atom, where the statistical model is inapplicable. Really, calculation by the formula (2.78) gives: $x_{0.1} = 3.4$, $x_1 = 0.64$, and $x_{10} = 0.053$, at the same time the region of truth of the statistical model in the variable x is determined by the inequation $Z^{-2/3} << x << Z^{1/3}$.

So in further consideration we will restrict ourselves to the range $v>0.1$. It should be noted that for $Z \approx 50$ this corresponds to the photon energies $\omega>130$ eV, which exceeds considerably the potential of ionization of the outer electron shell of a neutral atom, so the electron core can be considered "defrozen". Besides, in this frequency range, as seen from the above values of x_v, the inequation $x_v \leq 3.4$ is true. The boundary reduced radius of a neutral atom calculated in the Thomas-Fermi-Dirac model (with consideration for exchange) according to the paper [13] is well approximated by the formula $x_0 = 4Z^{0.4}$. Thus in our case $(Z>>1)$ $x_v<<x_0$, and conclusions of further consideration practically do not depend on refinements of the initial statistical Thomas-Fermi model, they are also true for ions with low enough degree of ionization if the condition $x_0(Z_i/Z)>>x_v$ is satisfied, which is confirmed by calculations carried out.

Good agreement of the magnitude of the dynamic polarizability of a Thomas-Fermi atom calculated in the local electron density approximation with the results of quantum-mechanical calculations [12], as seen from Fig. 2.5, takes place for the values of the dimensionless frequency: $v>2$. Both approaches give the same value of frequency for the maximum of the function $g(v)$: $v_{\max} \approx 0.5$ or $\hbar\omega_{\max} \approx 490\ eV$,

so that $\hbar\omega_{\max} >> I_p(Kr) = 14\ eV$, and the electron core of a krypton atom can be considered "defrozen".

The latter circumstance serves as a qualitative justification of adequacy of using the local plasma frequency approximation for calculation of the dynamic polarizability of an atom in the spectral range under consideration: $v \geq v_{\max}$.

It is interesting to note that even in the region of the maximum of the function $g(v) = v^2\,|\beta(v)|$ ($v_{\max} \approx 0.5$), where, generally speaking, the quantum features of motion of atomic electrons are essential, the distinction in the results of quantum-mechanical and statistical calculations of the dynamic polarizability of a krypton atom is less than 30 %.

The most distinction in results (about 47 %), as seen from Fig. 2.5, takes place for $v \approx 1$, that is, for frequencies near the potential of ionization of the $2p$ -subshell of a krypton atom. This fact is quite natural since neither the statistical model of a Thomas-Fermi atom nor the local plasma frequency approximation takes into account the shell structure of an atom, but they render the smoothed behavior of corresponding dependences.

Thus it can be stated that the model approximations used in this section for calculation of the dynamic polarizability of an atom are in good conformity with the results of quantum-mechanical calculations and at the same time are of a universal nature.

2.4.2 *Cross-Section of Polarization Bs of a Fast Charged Particle on a Thomas-Fermi Atom*

The spectral cross-section of polarization Bs of a fast electron on an atom within the framework of the first Born approximation is described by the expression (2.46) that for a process without excitation of a target, as it was shown in the previous paragraph, can be simplified to the form:

$$\frac{d\sigma^{PB}}{d\omega} = \frac{\omega^5}{(2\,\pi)^3\,\mathrm{v}} \int d\Omega_{\mathbf{n}}\, d\mathbf{q}\, |\alpha(\omega,\, \mathbf{q} + \mathbf{k})|^2\, [\mathbf{n}\,\mathbf{A}(q)]^2\, \delta(\omega + \mathbf{q}\mathbf{v}), \tag{2.79}$$

here $d\Omega_{\mathbf{n}}$ is the solid angle in the direction of photon emission, $\mathbf{k},\ \omega$ are the wave vector and the frequency of a bremsstrahlung photon, $\mathbf{q} = \mathbf{p}_f - \mathbf{p}_i$ is the change of an incident particle momentum, $\mathbf{A}(q)$ is the spatio-temporal Fourier transform of the vector-potential of the incident particle electromagnetic field that in the axial gauge ($A_0 = 0$) is given by the expression (2.42).

The key value in the formula (2.79) – $\alpha(\omega,\, \mathbf{q} + \mathbf{k})$ – is the nondipole dynamic polarizability of an atom, to calculate which the above approach is used.

It should be noted that the formula (2.79) is of a classical nature, it does not include the Planck constant, and it can be obtained within the framework of the

classical calculation of the PBs cross-section for a uniformly moving charge after summation over the impact parameter.

Hereafter for calculation of the Bs cross-section we will restrict ourselves to the Born-Bethe approximation, in which it can be assumed:

$$\alpha(\omega, q) = \alpha(\omega)\,\theta(p_a - q), \tag{2.80}$$

here $\theta(x)$ is the Heaviside function (a unit "step"). As a characteristic atomic momentum, we will use the Thomas-Fermi momentum $p_a = Z^{1/3}/(b\,a_0)$.

In the Born-Bethe approximation (2.80) the integral in the formula (2.79) is calculated analytically. The result, however, is found to be cumbersome. So we will give here the formula in the general writing representing the spectral cross-section of polarization Bs in terms of the single integral with respect to the value of a transferred momentum. In this expression there are two characteristic frequency ranges that are explicitly separated: $\omega < p_a\,\mathrm{v}$ is the "low-frequency" range and $\omega > p_a\,\mathrm{v}$ is the "high-frequency" range:

$$\begin{aligned}\frac{d\sigma^{PB}}{d\omega} = \frac{4\omega^3}{\mathrm{v}^2}\,|\alpha(\omega)|^2 \Bigg\{ &\theta\left(\frac{p_a \mathrm{v}}{1+\mathrm{v}} - \omega\right)[H_1(\omega, p_a - \omega) + H_2(\omega)] \\ &+\theta\left(\omega - \frac{p_a \mathrm{v}}{1+\mathrm{v}}\right) H_1\left(\omega, \frac{\omega}{\mathrm{v}}\right)\Bigg\},\end{aligned} \tag{2.81}$$

where

$$\begin{aligned}G_1 = &\frac{p_a^2 - (q-\omega)^2}{2\,\omega q}\left[\omega^2\,\mathrm{v}^2 + q^2 - \frac{5}{2}\,\omega^2 + \frac{\omega^4}{2\,q^2\,\mathrm{v}^2}\right] \\ &-\frac{1}{3}\left[\left(\frac{p_a^2 - (q-\omega)^2}{2\,\omega q}\right)^3 + 1\right]\left[q^2 - \frac{5}{2}\,\omega^2 + \frac{3\,\omega^4}{2\,q^2\,\mathrm{v}^2}\right]\end{aligned}$$

and

$$G_2 = 2\,\omega^2\left(\mathrm{v}^2 - \frac{5}{3}\right) + \frac{4}{3}\,q^2.$$

The formula (2.81) in the frequency range $\omega < p_a\,\mathrm{v}$, when the contribution to the cross-section is made by the first summand in the braces, is reduced to the known expression for the spectral cross-section of polarization Bs of a relativistic incident electron [2] (see also the formula (2.51) for the spectral-angular PBs cross-section):

$$\frac{d\sigma^{PB}}{d\omega} = \frac{16\,\omega^3\,|\alpha(\omega)|^2}{3\,\mathrm{v}^2}\ln\left(\frac{2\,\gamma\,p_a\,\mathrm{v}}{\omega\,(1+\mathrm{v})}\right), \qquad \omega < p_a\,\mathrm{v}. \tag{2.82}$$

Here $\gamma = (1 - \mathrm{v}^2)^{-1/2}$ is the relativistic factor, $\alpha(\omega)$ is the *dipole* dynamic polarizability of a target atom.

Going in the formula (2.82) to dimensionless variables with the use of the Eq. 2.75 and the determination of the Thomas-Fermi radius, we obtain the following expression for the spectral cross-section of polarization Bs:

$$d\sigma^{PB}(\nu) = \frac{16\,Z^2\,b^6}{3\,\mathrm{v}^2}\left|\nu^2\,\beta(\nu)\right|^2\frac{d\nu}{\nu}\ln\left(\frac{2\,\gamma\,\mathrm{v}}{\nu\,a_0\,(1+\mathrm{v})\,Z^{2/3}}\right) = Z^2\,d\tilde{\sigma}^{PB}(\nu). \quad (2.83)$$

In the formula (2.83) the function $d\tilde{\sigma}^{PB}(\nu)$ is introduced that is naturally can be called the *reduced cross-section* of the process since for this function in the case under consideration for polarization Bs of a fast incident particle approximate scaling with respect to the parameter ω/Z takes place, while the nuclear charge dependence is only logarithmic.

From the expression (2.83) it follows in particular that the spectral cross-section of polarization Bs of a Thomas-Fermi atom (accurate to the logarithmic factor) grows quadratically with increasing nuclear charge if in this case the dimensionless frequency ν does not change.

It should be noted that in case of a hydrogen-like ion, when scaling with respect to the parameter $\nu_H = \omega/Z^2$ takes place, the spectral cross-section of PBs of a fast particle in the Born approximation does not depend at all on a nuclear charge for the specified value of the dimensionless frequency ν_H, while the spectral cross-section of static Bs grows quadratically with increasing Z (accurate to the logarithmic factor).

Thus the used model predicts amplification of polarization effects in Bs of a fast particle on a neutral atom with increasing charge of the nucleus of the latter.

The spectral cross-section of ordinary (static) Bs in view of screening of the nuclear field [2] in case of weakly inelastic electron scattering is given by the expression:

$$d\sigma^{OB}(\omega) = \frac{16\,Z^2}{3\,\mathrm{v}^2}\frac{d\omega}{\omega}\ln\left\{\frac{\nu}{p_a}\right\}, \quad \omega < p_a\,\mathrm{v}. \quad (2.84)$$

The ratio of the cross-sections determined by the formulas (2.83) and (2.84) makes it possible to find the R-factor in the frequency range under consideration ($\omega < p_a\,\mathrm{v}$) and in the relativistic limit ($\mathrm{v} \cong 1$):

$$R(\nu, Z, \gamma) \equiv \frac{d\sigma^{PB}}{d\sigma^{OB}} = b^6\left|\nu^2\,\beta(\nu)\right|^2\frac{\ln\left\{\frac{137\,\gamma}{\nu\,Z^{2/3}}\right\}}{\ln\left\{\frac{137}{Z^{1/3}}\right\}}, \quad \nu < \frac{137}{Z^{2/3}}. \quad (2.85)$$

The results of calculation of the R-factor as a function of the dimensionless frequency ν for different values of the charge Z and the relativistic factor γ in the

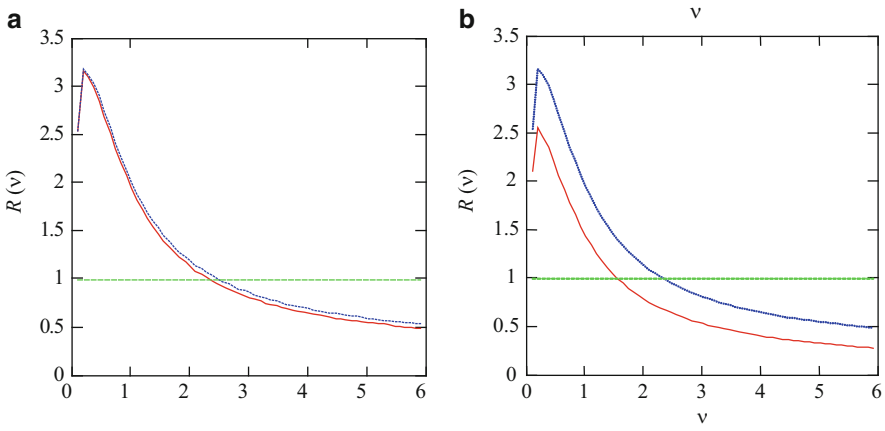

Fig. 2.6 The dependences of the R-factor on the reduced frequency v calculated for Bs of a fast electron on a Thomas-Fermi atom with the nuclear charge Z: (**a**) *solid curve* – $\gamma = 10$, $Z = 60$; *dotted curve* – $\gamma = 10$, $Z = 30$; (**b**) *solid curve* – $Z = 60$, $\gamma = 3$; *dotted curve* – $Z = 60$, $\gamma = 10$

range $v < 137/Z^{2/3}$ are presented in Fig. 2.6. It should be noted that corresponding to these values of the dimensionless frequency v (for the nuclear charges $Z \approx 50$) are the photon energies $\hbar\omega < 14$ keV.

It is seen that the value of the R-factor of a relativistic incident electron in a wide frequency range is about one and for $\omega \approx ZRy$ ($\nu = 0.5$) reaches its maximum value about $2.5 \div 3$. In this case the "sublogarithmic" influence of a nuclear charge on scaling with respect to Z is vanishingly small, and the influence of the relativistic factor is more significant.

It should be noted that the interference of the polarization and static Bs channels in case of a relativistic charged particle is small in view of different radiation patterns: the ordinary channel gives high-directivity radiation to a cone with an angle of the order of $1/\gamma$ [1], and the angular distribution of polarization Bs for the frequencies $\omega < p_a v$ is of a dipole nature [2].

In the case under consideration for weakly inelastic scattering of a Born charged particle in the frequency range $\omega < p_a \nu$ the main contribution to Bs is made by small scattering angles, when the influence of effects of penetration of an incident particle into the electron core of an atom is small.

The said circumstance results in different frequency dependences of the polarization Bs cross-section for different degrees of inelasticity of incident electron scattering. In case of the process considered in this chapter, the spectral maximum of the polarization Bs cross-section is considerably shifted to the region of high frequencies and falls with growing Bs frequency more slowly than corresponding spectral dependences in emission of photons of threshold energies.

In the frequency range $\omega > p_a \nu$ the law of conservation of energy-momentum conditions the necessity of penetration of an incident charged particle into the electron core of a target. So reradiation of a virtual photon of the scattered electron

eigenfield to a real photon on atomic electrons loses coherent behavior. As a result, the spectral cross-section of polarization Bs is found to be suppressed in comparison with the cross-section of ordinary Bs.

It should be noted that in the high-frequency region $\omega > p_a$ v the dimensionless frequency ν satisfies the inequation $\nu > 10$ (we assume that $Z \geq 30$), and, as seen from Fig. 2.5, the reduced polarizability of a Thomas-Fermi atom is close to its high-frequency limit: $\beta(\nu) \approx \beta_\infty(\nu) = -b^{-3}\nu^{-2}$. The frequency dependence of the polarization Bs cross-section in this case is defined mainly by the integral with respect to the angular variables and the value of the transferred momentum q in the formula (2.79).

The formula (2.82) in the frequency range $\omega > p_a$ v becomes untrue, and for determination of the polarization Bs cross-section it is necessary to proceed from the general expression (2.81). In this case the contribution is made by the second summand in the braces of Eq. 2.81. The analysis shows that in the expression for the spectral cross-section the multiplier $(p_a/\omega)^2$ appears that defines the smallness of the polarization channel contribution to the total spectral Bs cross-section. However, the spectral-angular cross-section of polarization Bs in the region of photon emission angles $\gamma^{-1} < \vartheta \leq \sqrt{p_a/\omega}$ exceeds the corresponding cross-section of the static channel.

The carried out consideration shows in particular that the characteristic potential of ionization of a multielectron atom included in the definition of the region of truth of the high-frequency approximation (see Eq. 2.53) can be represented as: $I(Z) = 2\,\zeta\, Z\, Ry$, that is, increases linearly with growing charge of the nucleus of a target atom. In this formula the constant $\zeta \geq 5$ is introduced, the exact value of which is not determined and depends on accuracy, with which it is required to calculate the process cross-section.

Thus in this paragraph within the framework of the local electron density method and the Thomas-Fermi model the universal description of polarization Bs of a fast Born charged particle on a multielectron atom ($Z >> 1$) in the region of energies of bremsstrahlung photons $\omega > 100$ eV is given. It is shown that the R-factor defining the relative value of the polarization channel contribution to the total Bs cross-section has approximate scaling with respect to the parameter ω/Z and at the frequencies $\omega_{\max} \approx Z\, Ry$ reaches its maximum value $R_{\max}(\gamma) = 2.5 \div 3$ that grows logarithmically with the energy of an incident particle.

The decrease of the R-factor with growing energy of an emitted photon in the low-frequency region $\omega < p_a$ v is most pronounced up to frequencies of the order of $20\, Z\, Ry$, when the magnitude of the polarizability of a Thomas-Fermi atom decreases when going to its high-frequency asymptotics.

In the spectral range $10\, Z\, Ry < \omega < p_a$ v the decrease of the R-factor and polarization Bs intensity has weak logarithmic behavior and is caused by reduction of the maximum impact parameter.

In the high-frequency range $\omega > p_a$ v the frequency change of polarization Bs intensity is defined mainly by kinematic factors and by violation of coherence of reradiation of a virtual photon to a real photon on atomic electrons. In this case the

decrease of spectral intensity becomes power-like. At the same time the pattern of radiation by the polarization channel is narrowed, so that $\vartheta \leq \sqrt{p_a/\omega}$, and in the frequency range $p_a<\omega<\gamma^2 p_a$ there is the region of Bs angles: $\gamma^{-1}<\vartheta \leq \sqrt{p_a/\omega}$, in which the polarization mechanism prevails over the ordinary (static) mechanism of radiation.

2.5 Incoherent Polarization Bremsstrahlung of a Fast Charged Particle on an Atom in the High-Frequency Approximation

In this paragraph within the framework of the high-frequency approximation for the operator of electromagnetic field scattering the universal description of incoherent polarization Bs of a fast charged particle on a multielectron atom is obtained. The PBs cross-section is expressed in terms of the Compton profile of X-ray scattering, for which a voluminous calculation material is available. The obtained universal representation for the process cross-section is justified both for the statistical atom model and on the basis of established approximate scaling of Hartree-Fock Compton profiles.

This paragraph is the refinement, supplement, and generalization of the consideration of PBs with atomic ionization carried out in the Sect. 2.3 to the case of taking into account atomic electron binding in the initial state.

2.5.1 Connection of the Dynamic Form Factor with the Compton Profile of an Atom

In Sect. 2.3 the expression (2.63) was obtained for the cross-section of high-frequency PBs ($m>>\omega>> I$) of a fast charged particle in terms of the dynamic form factor (DFF) of a target (Eq. 2.64).

The approximate expression for the DFF (2.65) and the formula following from it for the PBs cross-section (2.66) give a qualitative idea of the process, separating two characteristic frequency ranges.

In the low-frequency range ($\omega < p_a \mathrm{v}_0$) PBs is coherent by the contribution of atomic electrons, the process proceeds without excitation of a target, and the cross-section is proportional to the squared number of atomic electrons.

In the high-frequency range ($\omega > p_a \mathrm{v}_0$) radiation with ionization of a target prevails, and the PBs cross-section is proportional to the number of electrons in an atom.

In the latter case the (incoherent) DFF of an atom is represented as the sum of the DFF of electron subshells of the atom:

$$S(q) = \sum_{n,l} S_{nl}(q). \tag{2.86}$$

Let us transform the expression for the dynamic form factor of the electron subshell (Eq. 2.64) using the expansion in terms of the total system of wave functions.

Then we will use the fact that in the frequency range under consideration $\omega > p_a \, v_0$ momenta transferred from an incident particle to a target far exceed the characteristic atomic momentum. Then the wave functions of the continuous spectrum making the main contribution to the DFF can be to a good accuracy approximated by plane waves, and the expression for the DFF of the electron subshell is represented as:

$$S_{nl}(q) = \int \frac{d\mathbf{p}}{4\pi} \, \delta\left(q^0 + \frac{(\mathbf{p}-\mathbf{q})^2}{2} - \varepsilon_{nl}\right) |R_{nl}(p)|^2, \tag{2.87}$$

here $q^0 = \omega + \mathbf{q}_1 \, \mathbf{v} + \mathbf{q}_1^2/2m$ is the energy of a nonrelativistic IP transferred to the target, (m is its mass); $\mathbf{q}_1 = \mathbf{p}_f^{IP} - \mathbf{p}_i^{IP}$ is the change of the incident particle momentum (here the upper index is introduced for IP momenta to distinguish them from atomic electron momenta), $\mathbf{q} = \mathbf{q}_1 + \mathbf{k}$ is the momentum transferred to the target; ε_{nl} is the energy of the electron subshell under consideration (n, l are the principal and orbital quantum numbers). In the formula (2.87) the function $R_{nl}(p)$ is introduced that represents the spatial Fourier transform of a normalized radial wave function of the nl-state determined by the formula:

$$R_{nl}(p) = \sqrt{\frac{2}{\pi}} \int_0^\infty R_{nl}(r) \, j_l(p\,r) \, r^2 dr, \tag{2.88}$$

$j_l(p\,r)$ is the spherical Bessel function of the first kind.

2.5.2 *Impulse Approximation*

The delta function in the formula (2.86) describes the law of conservation of energy in the PBs process with target ionization. In the expression (2.86) we went from summation over the finite momentum of an atomic electron to summation over the momentum of the Fourier expansion of the wave function of the electron subshell under consideration. In the impulse approximation this value coincides with the initial momentum of an atomic electron. Thus, if it is assumed that:

$$p^2/2 = \varepsilon_{nl}, \tag{2.89}$$

we come to the impulse approximation widely used in calculations of the Compton effect on atoms.

Really, in fulfilment of Eq. 2.89 the DFF of the electron subshell (Eq. 2.86) can be represented as:

$$S_{nl}^{(IA)}(q) = \frac{1}{|\mathbf{q}|} J_{nl}\left(Q = -\frac{q^0 + \mathbf{q}^2/2}{|\mathbf{q}|}\right). \tag{2.90}$$

Here the Compton profile of the electron subshell $J_{nl}(Q)$ [14, 15] is introduced that is determined according to the formula:

$$J_{nl}(Q) = \frac{1}{2} \int_Q^\infty |R_{nl}(p)|^2 p\, dp. \tag{2.91}$$

This value is tabulated for all subshells of all elements in [14] with the use of the Hartree-Fock and Dirac-Hartree-Fock wave functions.

The formulas (2.86) and (2.90) give the representation of an incoherent DFF in terms of the Compton profile in the impulse approximation.

Beyond the framework of the impulse approximation instead of the formula (2.90) it is possible to obtain from Eq. 2.86 the following representation for the dynamic form factor of an atom in terms of its Compton profile:

$$S_{nl}(q) = \frac{1}{2|\mathbf{q}|} \left\{ J_{nl}\left(-|\mathbf{q}| + \sqrt{2(-q^0 + \varepsilon_{nl})}\right) - J_{nl}\left(|\mathbf{q}| + \sqrt{2(-q^0 + \varepsilon_{nl})}\right) \right\}. \tag{2.92}$$

Using the tabulated values of the Compton profile [14] makes it possible with the formulas (2.86), (2.92), and (2.63) to calculate the cross-sections of incoherent PBs of various elements.

2.5.3 *Compton Profile Within the Framework of Statistical Atom Models*

For universalization of the dependence of PBs cross-sections on the charge of an atomic nucleus, it is of interest to obtain an expression for the Compton profile within the framework of the statistical model.

Let us introduce an "effective" one-electron radial wave function of an atom in the statistical model, connecting it with the radial density of distribution of the electron charge $\rho_{stat}(r)$ by the formula:

$$R_{stat}(r) = \sqrt{\rho_{stat}(r)/Z}. \tag{2.93}$$

Then, considering the distribution of electron density in an atom spherically symmetrical, it is possible to obtain from Eqs. 2.88, 2.91, and 2.93 for the Compton profile in the statistical approximation (in terms of one electron) the following expression:

$$J^{(1)}_{stat}(q) = \frac{1}{\pi Z} \int\limits_{q}^{\infty} \frac{dp}{p} \left| \int\limits_{0}^{\infty} \sqrt{\rho_{stat}(r)}\, \sin(pr)\, r\, dr \right|^2 . \tag{2.94}$$

In the elementary case of exponential screening, when the radial electron density in an atom looks like:

$$\rho_{\exp}(r) = \frac{4Z}{r_{TF}^3}\, e^{-2r/r_{TF}}, \tag{2.95}$$

the following expression for the Compton profile (Eq. 2.94) can be obtained:

$$J^{(1)}_{\exp}(q) = \frac{8\, r_{TF}}{3\pi} \frac{1}{\left(1 + (q\, r_{TF})^2\right)^3} . \tag{2.96}$$

By analogy, for the reduced Compton profile of an atom in the Thomas-Fermi model we have:

$$\tilde{J}_{TF}(\tilde{q}) = \frac{1}{\pi} \int\limits_{\tilde{q}}^{\infty} \frac{|g_{TF}(\tilde{p})|^2}{\tilde{p}}\, d\tilde{p}, \tag{2.97}$$

introduced here is the spatial Fourier transform of the square root of the normalized Thomas-Fermi density:

$$g_{TF}(\tilde{p}) = \int\limits_{0}^{\infty} (\chi(x))^{3/4} \sin(\tilde{p}\, x)\, x^{1/4} dx. \tag{2.98}$$

The obtained reduced Compton profiles satisfy the necessary normalizing condition:

$$\int\limits_{0}^{\infty} \tilde{J}_{stat}(\tilde{q})\, d\tilde{q} = \int\limits_{0}^{\infty} J^{(1)}_{stat}(q)\, dq = 0.5. \tag{2.99}$$

As seen from the formulas (2.96), (2.97), the normalized Compton profile of an atom in statistical models depends only on the reduced momentum $\tilde{q} = q\, r_{TF} = q/p_{TF}$.

Presented in Fig. 2.7 are the dependences of normalized Compton profiles of an atom on the reduced momentum $\tilde{q}$ calculated within the framework of statistical models and by the data of the Hartree-Fock calculations [14] for argon and krypton atoms. It is seen that the Thomas-Fermi Compton profile in the region of small transferred momenta exceeds appreciably values obtained within the framework of other models, which is explained by not fast enough decrease of the Thomas-Fermi electron density with distance. At the same time the exponential screening model

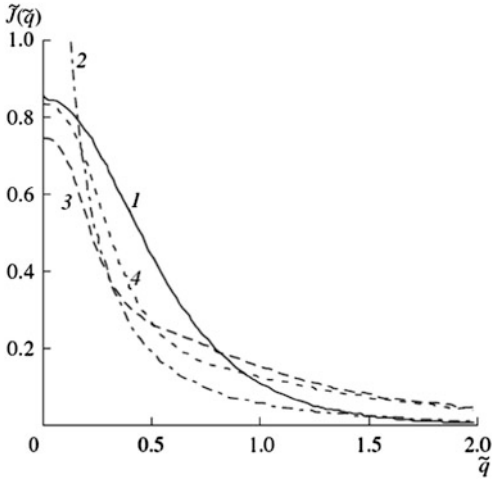

Fig. 2.7 The dependences of the normalized Compton profile on the reduced transferred momentum obtained within the framework of different models: (*1*) exponential screening; (*2*) Hartree-Fock calculation for an argon atom; (*3*) Hartree-Fock calculation for a krypton atom; (*4*) Thomas-Fermi model

gives quite satisfactory approximation to the results of more exact calculations [14] with the use of the Hartree-Fock wave functions.

Following from this figure, in particular, is approximate scaling of normalized Hartree-Fock Compton profiles as functions of the reduced momentum.

2.5.4 *Cross-Section of Incoherent PBs of a Nonrelativistic Born Particle*

The expression for the spectral cross-section of PBs of a nonrelativistic Born charged particle in the high-frequency range $m>>\omega>>I$ integrated with respect to the solid angle of photon emission can be obtained from the formula (2.63). In the ordinary (Gaussian) system of units it looks like:

$$d\sigma(\omega) = \frac{8}{3\,\pi}\,\frac{e^4\,e_0^2}{m_e^2\,\mathrm{v}\,\hbar\,c^3}\,\frac{d\omega}{\omega}\int\!\!\int d\Omega_{\mathbf{q}}\,dq\,S\left(q^0,\,\mathbf{q}\right), \tag{2.100}$$

where $e_0 = Z_0\,e$ is the IP charge.

In derivation of (Eq. 2.100) the expression for the vector potential of the eigenfield of a nonrelativistic IP in the axial gauge was used, and it was assumed that $\mathbf{q} = \mathbf{q}_1$.

It should be noted that in the approximation of quasi-free (at rest) atomic electrons the incoherent DFF of a target is given by the equation:

$$S_{free}^{ncoh}(q) = \frac{Z}{q\,\mathrm{v}}\,\delta\left(\frac{\omega + \mathbf{q}\,\mathbf{v} + \mathbf{q}^2/(2\,\mu)}{q\,\mathrm{v}}\right), \tag{2.101}$$

where μ is the reduced mass of an electron and an IP, Z is the number of atomic electrons equal to the nuclear charge.

Substituting the expression (2.92) for the incoherent DFF summed over all electron subshells of an atom in the formula (2.100), we come to the following representation of the spectral PBs cross-section in the frequency range $\omega > p_a \, \mathrm{v}_0$:

$$d\sigma(\omega, \mathrm{v}, m) = \sqrt[3]{Z} Z_0^2 \, d\tilde{\sigma}\left(\frac{\omega}{p_{TF}^2}, \frac{\mathrm{v}}{p_{TF}}, m\right). \tag{2.102}$$

Introduced here is the reduced cross-section $d\tilde{\sigma}$ depending on the frequency of an emitted photon and the IP velocity normalized accordingly to the characteristic momentum of a Thomas-Fermi atom.

The reduced cross-section is expressed in terms of the normalized Compton profile of an atom by the formulas:

$$d\tilde{\sigma}(\tilde{\omega}, \tilde{\mathrm{v}}, m) = \sigma_0 \frac{b^2}{\tilde{\mathrm{v}}^2} \frac{d\tilde{\omega}}{\tilde{\omega}} I(\tilde{\omega}, \tilde{\mathrm{v}}, m) \tag{2.103}$$

$$I(\tilde{\omega}, \tilde{\mathrm{v}}, m) = \int_{q_{\min}}^{q_{\max}} \frac{d\tilde{q}}{\tilde{q}} \int_{-\mathrm{v}}^{-\mathrm{v}_m} \left\{ \tilde{J}\left(-\tilde{q} + \sqrt{-2\tilde{q}^0}\right) - \tilde{J}\left(\tilde{q} + \sqrt{-2\tilde{q}^0}\right) \right\} d(\mathrm{v} \cos(\mathbf{q}\,\mathbf{v})), \tag{2.104}$$

here $\mathrm{v}_m = \left(\tilde{\omega} + \tilde{q}^2/2m\right)/\tilde{q}$, $\mathrm{b} = 0.8853$.

The upper and lower limits of integration with respect to the magnitude of the transferred momentum in the integral (2.104) are defined by the condition $\mathrm{v}_m < \mathrm{v}$.

The dimensional cross-section σ_0 included in the expression (2.103) is:

$$\sigma_0 = \frac{16}{3} \frac{e^6}{m_e^2 \hbar \, c^3} = 2.074 \cdot 10^{-6} \, \text{a.u.} \tag{2.105}$$

Here we used the Gaussian system of units.

Thus the formulas (2.102), (2.103), (2.104), and (2.105) reveal the scaling law for the cross-section of incoherent PBs of a fast (but nonrelativistic) charged particle on a multielectron atom and express the process cross-section in terms of the normalized Compton profile of X-ray scattering. This cross-section (accurate to the multiplier $\sqrt[3]{Z}$) depends on the frequency of an emitted photon and the IP velocity nondimensionalized with the use of the Thomas-Fermi momentum.

It should be noted that though, strictly speaking, scaling Eqs. 2.102, 2.103, 2.104, and 2.105 is obtained within the framework of the statistical model of an atom, it is also approximately true for a Hartree-Fock atom in view of the above approximate scaling of normalized Compton profiles (see Fig. 2.7).

We will give for comparison a corresponding expression for the cross-section of incoherent PBs on a hydrogen-like ion with the charge Z:

$$d\sigma_H(\omega, \mathrm{v}, m) = Z^{-1}\, b^{-2}\, d\tilde{\sigma}\left(\frac{\omega}{p_H^2}, \frac{\mathrm{v}}{p_H}, m\right), \tag{2.106}$$

where $p_H = Z$ a.u. is the characteristic momentum of a hydrogen-like atom.

The found expression (2.102) for the cross-section of high-frequency PBs with atomic ionization refines and supplements the result of Eq. 2.69 obtained with the use of the DFF in the model of free atomic electrons (Eq. 2.101) that can also be represented in the form (2.102) and (2.103), if it is assumed that:

$$I_{free}(\tilde{\omega}, \tilde{\mathrm{v}}, \mu) = \ln\left\{\frac{1 + \sqrt{1 - 2\,\tilde{\omega}/(\mu\,\tilde{\mathrm{v}}^2)}}{1 - \sqrt{1 - 2\,\tilde{\omega}/(\mu\,\tilde{\mathrm{v}}^2)}}\right\}. \tag{2.107}$$

Shown in Fig. 2.8 are the spectral dependences of the value $\omega\,\frac{d\sigma}{d\omega}$ calculated within the framework of different approximations, including the model of free atomic electrons, for incoherent PBs of a proton. It is seen that the main difference of the models shows itself in the frequency range $\omega > \omega^* = \mu\,\mathrm{v}^2/2$, that is, behind the "cutoff" frequency for PBs on free electrons.

From kinematic considerations it is clear that the "cutoff" frequency for PBs of an electron, other things being equal, is half the value for PBs of a proton (because of the difference in reduced masses), this situation supplements the conclusion drawn earlier about the PBs cross-section independence of the mass of an incident particle.

The reduction of the cross-section with growing PBs frequency in the exponential screening model occurs appreciably faster than for the Hartree-Fock Compton profile, which follows also from Fig. 2.7. For frequencies smaller than the "cutoff" frequency the Hartree-Fock consideration of binding of atomic electrons in the initial state results in a somewhat smaller cross-section value in comparison with the model of free atomic electrons.

Let us note the close similarity of the dependences in Fig. 2.8 with corresponding spectral cross-sections for radiation ionization from the theoretical work [16]. In this work for description of incoherent PBs (radiation ionization) a similar approach was used, based on the use of the nondiagonal atomic form factor $F_{n,W}(q)$ that was calculated earlier in connection with the problem of ionization of atoms and excitation of characteristic X-rays.

Shown in Fig. 2.9 are the dependences of the value $\omega\, d\sigma/d\omega$ of incoherent PBs of a proton on a krypton atom on the proton velocity for three values of bremsstrahlung photon energy – 3.78 keV, 7.57 keV, and 11.35 keV.

It is seen that the velocity dependences of cross-section have maxima. These maxima are shifted to the region of higher velocities with growing bremsstrahlung

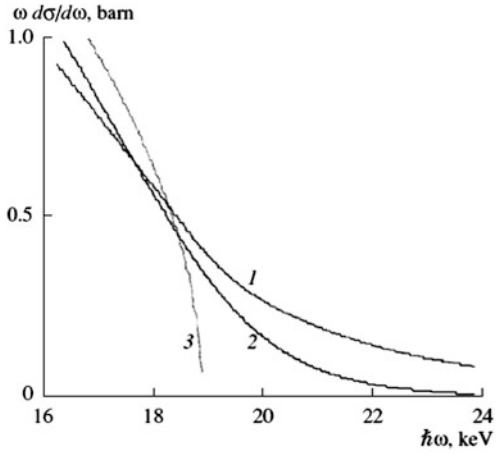

Fig. 2.8 The spectral cross-section of incoherent PBs of a proton with an energy of 34 MeV on a krypton atom near the "cutoff" frequency calculated within the framework of different approximations for the electron density of an atom: Hartree-Fock calculation (*curve 1*), exponential screening (*curve 2*), approximation of free atomic electrons (*curve 3*)

photon energy. A corresponding formula relating the bremsstrahlung photon frequency and the optimum value of proton velocity in atomic units looks like:

$$v_{opt} = 1.89\sqrt{\omega} \tag{2.108}$$

It is essential that the relation (2.108) does not depend on the charge of an atomic nucleus in contrast to the analogous dependence for coherent PBs, when there is a linear connection between the optimum velocity and radiated frequency through the radius of the atomic subshell making the greatest contribution to the process.

2.5.5 *Comparison of Cross-Sections of Incoherent and Coherent PBs*

Now we will analyze the relation between the cross-sections of coherent and incoherent PBs.

We will calculate the cross-section of the coherent process within the framework of the exponential screening model for the electron density of the target core. A corresponding expression can be obtained from the formula (2.63) if it is taken into account that the DFF of an atom in this case is reduced to the ordinary static form factor being a Fourier transform of electron density.

After standard transformations including integration with respect to the solid angles of an emitted photon and a transferred momentum, for the cross-section of coherent PBs of a nonrelativistic Born particle we have the following expression (in atomic units):

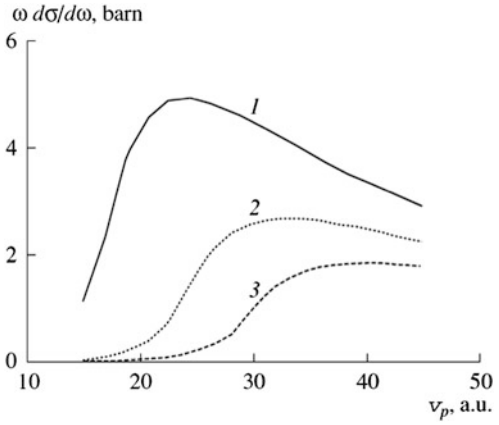

Fig. 2.9 Incoherent PBs of a proton on a krypton atom as a function of the proton velocity for three values of bremsstrahlung photon energy: $\hbar\omega = 3.78$ keV (*curve 1*), $\hbar\omega = 7.57$ keV (*curve 2*), $\hbar\omega = 11.35$ keV (*curve 3*)

$$d\sigma_{coh}^{(\exp)}(\omega) = \frac{16}{3}\frac{Z^{4/3}}{\tilde{\mathrm{v}}^2 c^3} b^2 \int_{\tilde{q}_{\min}}^{\tilde{q}_{\max}} \frac{1}{\left(1+\tilde{q}^2/2\right)^4}\frac{d\tilde{q}}{\tilde{q}}\frac{d\omega}{\omega}. \tag{2.109}$$

In the integral of the expression (2.109) there are the same limits of integration with respect to the transferred momentum as in the formula (2.104). "Tilde" above the sign of the transferred momentum and of the IP velocity, as before, means normalization to the momentum (velocity) of a Thomas-Fermi atom.

The integral in the Eq. 2.109 is taken in quadratures, but a corresponding expression is rather cumbersome. For a heavy IP the upper limit of integration can be replaced by infinity, then for the integral with respect to the reduced transferred momentum we have:

$$I_{coh}^{(\exp)}(\tilde{\omega}, \tilde{\mathrm{v}}) = \frac{11 + 54\left(\frac{\tilde{\mathrm{v}}}{\tilde{\omega}}\right)^2 + 72\left(\frac{\tilde{\mathrm{v}}}{\tilde{\omega}}\right)^4}{12\left(1+2\left(\frac{\tilde{\mathrm{v}}}{\tilde{\omega}}\right)^2\right)^3} - \frac{11}{12} + \frac{1}{2}\ln\left(1+2\left(\frac{\tilde{\mathrm{v}}}{\tilde{\omega}}\right)^2\right). \tag{2.110}$$

It should be noted that in the limit $\mathrm{v}\, p_{TF} << \omega$ $(*)$ from the formula (2.110) the asymptotics follow:

$$I_{coh}^{(\exp)}(\tilde{\omega}, \tilde{\mathrm{v}}) \cong 2\left(\tilde{\mathrm{v}}/\tilde{\omega}\right)^8. \tag{2.111}$$

The inequation (*) can be rewritten as: $\omega >> 0.125\, Z^{2/3}$ keV, whence it follows that it is satisfied for all Z in the kiloelectron-volt range of bremsstrahlung photon energies.

From the formulas (2.109), (2.110), and (2.111) we obtain for the coherent PBs cross-section in the exponential screening approximation and the high-frequency limit $\omega >> 0.125\, Z^{2/3}$ keV:

$$d\sigma_{coh}^{(\exp)}(\omega) = \frac{32\,b^2}{3\,c^3}\,Z^{4/3}\,\frac{\tilde{\mathrm{v}}^6}{\tilde{\omega}^8}\,\frac{d\omega}{\omega}. \tag{2.112}$$

For correct estimation of the relation between the cross-sections of coherent and incoherent processes it is important to emphasize that a simple exponential approximation underestimates considerably the contribution of the K-shell to coherent PBs on a multielectron atom in a high-frequency range. Really, the radius of the orbit nearest to the nucleus is approximately $Z^{2/3}$ times less than the Thomas-Fermi radius, so the corresponding integral in the formula (2.109) results in reduction of the spectral cross-section at higher frequencies than this takes place for the Thomas-Fermi radius.

To take into account the contribution of the K-shell, we rewrite the formula (2.109) as follows ($Z>>1$):

$$d\sigma_{coh}^{(\exp)}(\omega) = \frac{16}{3}\,\frac{Z^{4/3}}{\tilde{\mathrm{v}}^2\,c^3}\,b^2\,\frac{d\omega}{\omega}\left\{I_{coh}^{(\exp)}(\tilde{\omega},\,\tilde{\mathrm{v}}) + \frac{4}{Z^2}\,I_{coh}^{(\exp)}(\tilde{\omega},\,\tilde{\mathrm{v}}\,(p_K(Z)/p_{TF}))\right\}, \tag{2.113}$$

introduced here is the momentum of the atomic K-shell $p_K(Z)$.

The expression (2.113) is a universal (common for all nuclear charges) representation of the cross-section of coherent PBs of a fast particle obtained in the exponential electron density model with individual consideration of the contribution of the K-shell to radiation.

The results of calculation of the spectral cross-sections of coherent and incoherent PBs of a proton on a krypton atom for two values of proton velocity are presented in Fig. 2.10.

From this figure it follows in particular that the prevalence of the incoherent process over the coherent process can take place at high enough velocities of an incident particle since in this case the "cutoff frequency" for radiation ionization is shifted to the region of high frequencies, in which the contribution of most of atomic electrons to coherent PBs is already small.

Thus in this paragraph within the framework of the high-frequency approximation for the operator of electromagnetic field scattering the universal description of incoherent PBs of a fast charged particle on a multielectron atom was obtained. The process cross-section is expressed in terms of the Compton profile of X-ray scattering.

The basis for the obtained universal description is approximate scaling of the reduced Compton profile of X-ray scattering by a neutral atom for high enough nuclear charges ($Z \geq 20$) that was found in this work.

Based on the derived formulas and within the framework of different approximations for electron density of the electron core of a target, the spectral and velocity dependences of the cross-section of incoherent PBs of a proton on a multielectron atom were analyzed.

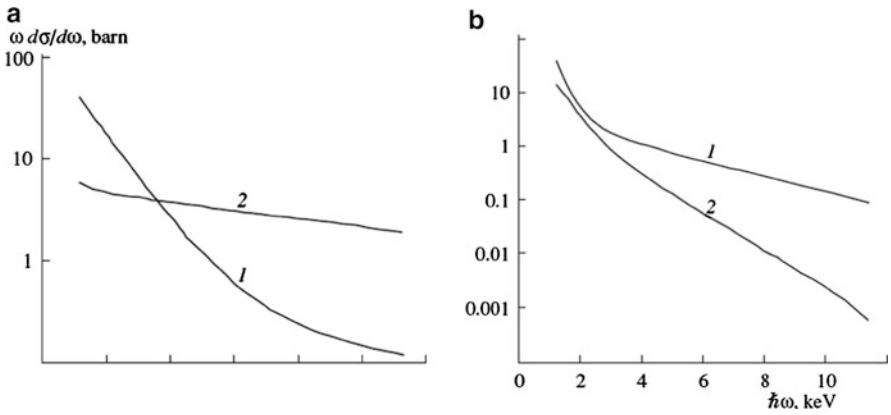

Fig. 2.10 The spectral cross-sections of coherent (*curves 1*) and incoherent (*curves 2*) polarization bremsstrahlung of a proton on a krypton atom for different proton velocities: (**a**) $v^{IP} = 10\,v_{TF} = 3$ 7.3 a.u., (**b**) $v^{IP} = 3v_{TF} = 11.2$ a.u.

It was shown that for a specified PBs frequency there is an optimum velocity of an incident particle, at which the process cross-section has maximum. The value of optimum velocity grows as the square root of frequency.

The carried out comparison of the cross-sections of coherent and incoherent processes has shown that for high enough velocities of an incident particle there is a frequency range of prevalence of PBs with atomic ionization over coherent PBs.

References

1. Berestetskii, V.B., Lifshitz, E.M., Pitaevskii, L.P.: Quantum Electrodynamics. Elsevier, Oxford (1982)
2. Tsytovich, V.N., Oiringel, I.M. (eds.): Polarization Bremsstrahlung. Plenum Press, New York (1991)
3. Bethe, H., Heitler, W.: On stopping of fast particles and on creation of positive electrons. Proc. Roy. Soc. Lond. A **146**, 83 (1934)
4. Wheeler, J., Lamb, W.: Influence of atomic electrons on radiation and pair production. Phys. Rev. **55**, 858 (1939)
5. Mason, N.J.: Laser-assisted electron-atom collisions. Rep. Prog. Phys. **56**, 1275 (1993)
6. Buimistrov, V.M., Trakhtenberg, L.I.: Free electron transition and light amplification. Opt. Commun. **8**, 289 (1973)
7. Astapenko, V.A.: Spectrum of polarization bremsstrahlung in a solid near its absorption edge. Sov. Phys. JETP **72**, 92 (1991)
8. Verkhovtseva, E.T., Gnatchenko, E.V., Pogrebnjak, P.S.: Investigation of the connection between giant resonances and atomic bremsstrahlung. J. Phys. B **16**, L613 (1983)
9. Trakhtenberg, L.I.: Resonant emission and absorption of photons during triple collision between electron, photon and atom. Opt. Spectr. **44**, 510 (1978)
10. Brandt, W., Lundqvist, S.: Atomic oscillations in the statistical approximation. Phys. Rev. **139**, A612 (1965)

11. Landau, L.D., Lifshits, E.M.: Quantum Mechanics. Nauka, Moscow (1989) (in Russian)
12. Korol', A.V., Lyalin, A.G., Obolenskii, O.I., Solov'yov, A.V.: The role of the polarization mechanism for emission of radiation by atoms over a broad photon frequency range. Sov. Phys. JETP **84**, 229 (1998)
13. Ulantsev, A.D., Shevelko, V.P.: Static multipole polarizability of atoms and ions in the Thomas-Fermi model. Opt. Spectr. **65**, 590 (1988)
14. Biggs, F., Mendelsohn, L.B., Mann, J.B.: Hartree-Fock Compton profiles for the elements. At. Data Nucl. Data Tables **16**, 201 (1975)
15. Bergstrom, P.M., Pratt Jr., R.H.: An overview of the theories used in compton scattering calculations. Radiat. Phys. Chem. **50**, 3 (1997)
16. Ishii, K., Morita, S.: Continuum X-ray produced by light-ion-atom collisions. Phys. Rev. A **30**, 2278 (1984)

Chapter 3
Quasi-Classical Theory of Bremsstrahlung on an Atom and an Ion with a Core

The quasi-classical theory of Bs on atoms and ions plays an important role in a number of applications such as radiation in partially ionized plasma, low-temperature plasma, gas discharge, absorption of radiation by plasma media, etc.

Stated in this chapter is the theory of spontaneous Bs, including the polarization channel, in scattering of electrons by atoms and ions with a core with fulfilment of the quasi-classical condition

$$\frac{Z e^2}{\hbar \mathrm{v}} \geq 1, \tag{3.1}$$

where Z is the charge number of an atom (ion), v is the electron velocity. In this chapter the Gaussian system of units is used.

As seen from the formula (3.1), a quasi-classical electron should be rather slow in contrast to a Born electron, for which the inequation (2.1) reverse of the relation (3.1) is true. It should be noted that the Born inequation is "strong", and the quasi-classical inequation is "weak".

The condition (3.1) is realized, for example, for low-temperature plasma. In this case by the charge number of an atomic (ion) nucleus and the electron velocity their average values defined by the state of a substance should be meant.

3.1 Classical Consideration in the Approximation of Straight Trajectories

3.1.1 Ordinary (Static) Bremsstrahlung

As is known, emission of a photon in scattering of a charged particle on an atom (ion, molecule, cluster, etc.) is called *bremsstrahlung*. The initial and final states of an emitting particle in this process belong to the continuous spectrum, and radiant

V. Astapenko, *Polarization Bremsstrahlung on Atoms, Plasmas, Nanostructures and Solids*, Springer Series on Atomic, Optical, and Plasma Physics 72,
DOI 10.1007/978-3-642-34082-6_3, © Springer-Verlag Berlin Heidelberg 2013

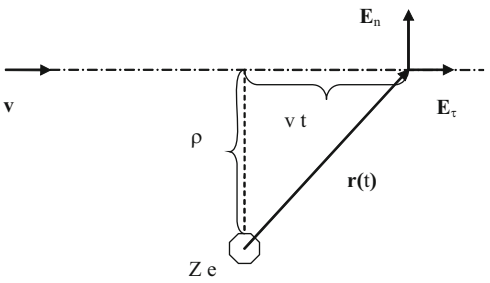

Fig. 3.1 The diagram of electron scattering by a nucleus in the approximation of straight trajectories, ρ is the impact parameter

energy is got from its kinetic energy. Let us consider at first the most simple case, when a nonrelativistic electron is scattered by a "bare" nucleus (that is, a nucleus without bound electrons) with the charge number Z. We use the classical expression for the power of dipole radiation Q in terms of the acceleration of a scattered electron $\mathbf{w}$ (the acceleration of a nucleus can be neglected due to its large mass) [1]:

$$Q(t) = \frac{2\,e^2}{3\,c^3}\,\mathbf{w}^2(t). \tag{3.2}$$

The total energy of bremsstrahlung for the whole time of collision is:

$$\Delta \mathrm{E} = \frac{4\,e^2}{3\,c^3}\int\limits_0^\infty |\mathbf{w}(\omega)|^2\,\frac{d\omega}{2\,\pi}. \tag{3.3}$$

In derivation of Eq. 3.3 the relation was used:

$$\int\limits_{-\infty}^{\infty} f^2(t)\,dt = 2\int\limits_0^\infty |f(\omega)|^2\,\frac{d\omega}{2\,\pi}, \tag{3.4}$$

where $f(t)$ is the real function of time, $f(\omega)$ is its Fourier component.

To calculate the Fourier component of the acceleration $\mathbf{w}(\omega)$, it is necessary to concretize the character of motion of a particle. It is well known that in case of a central force field the moment of momentum of an electron is $M = m\,\mathrm{v}\,\rho$, where v is the electron velocity (infinitely far from the nucleus), ρ is the impact parameter (see Fig. 3.1).

Thus the motion of a particle in the potential $U(r = |\mathbf{r}|)$ is characterized by two values: the initial velocity and the impact parameter, so the Fourier component of acceleration depends also on ρ: $\mathbf{w}(\omega) \to \mathbf{w}_\rho(\omega)$. For the last value we have:

$$\mathbf{w}_\rho(\omega) = \frac{e}{m}\,\mathbf{E}(\omega, \rho), \tag{3.5}$$

where $\mathbf{E}(\omega, \rho)$ is the Fourier component of the intensity of the nuclear electric field acting on a scattered electron with a specified impact parameter.

Let us calculate $\mathbf{E}(\omega, \rho)$ in the approximation *of straight trajectories* of electron motion. This approximation is true for "distant" collisions, when $\rho > a_C$ ($a_C = Z\,e^2/m\,\mathrm{v}^2$ is the Coulomb length). It should be noted that this approach was used by E. Fermi in calculation of excitation of atoms by charged particles [2]. Using the elementary electrodynamic formulas, we find for the Fourier component of nuclear electric field intensity:

$$\mathbf{E}(\omega, \rho) = \frac{2\,Z\,e}{\rho\,\mathrm{v}} \left\{ F\left(\frac{\omega\,\rho}{\mathrm{v}}\right) \mathbf{e}_n - iF'\left(\frac{\omega\,\rho}{\mathrm{v}}\right) \mathbf{e}_\tau \right\}, \tag{3.6}$$

where $\mathbf{e}_{n,\,\tau}$ are the normal and tangent (with respect to the velocity vector $\mathbf{v}$) unit vectors (see Fig. 3.1);

$$F(\zeta) = \int_0^\infty \frac{\cos(\zeta\,x)}{(1+x^2)^{3/2}}\,dx, \tag{3.7}$$

the prime designates differentiation with respect to the argument.

From the formula (3.3) in view of Eq. 3.5 the following expression for bremsstrahlung energy differential with respect to the photon frequency:

$$\frac{d\mathrm{E}_\rho}{d\omega} = \frac{2\;e^4}{3\,\pi\,m^2\,c^3}\,|\mathbf{E}(\omega, \rho)|^2. \tag{3.8}$$

The probability of bremsstrahlung in scattering of an electron with a specified impact parameter and frequency is related to the energy of Eq. 3.8 by the relation:

$$\frac{dW_\rho}{d\omega} = \frac{1}{\hbar\,\omega}\,\frac{d\mathrm{E}_\rho}{d\omega}, \tag{3.9}$$

and spectral cross-section of the process is:

$$\frac{d\sigma}{d\omega} = 2\,\pi \int_{\rho\,\mathrm{min}}^{\rho\,\mathrm{max}} \frac{dW_\rho}{d\omega}\,\rho\,d\rho, \tag{3.10}$$

where ρ_{min}, ρ_{max} are the minimum and maximum impact parameters. Assembling the formulas (3.8), (3.9) and (3.10), we obtain:

$$\frac{d\sigma}{d\omega} = \frac{4\;e^4}{3\;m^2\,c^3\,\hbar\,\omega} \int_{\rho\,\mathrm{min}}^{\rho\,\mathrm{max}} |\mathbf{E}(\omega, \rho)|^2\,\rho\,d\rho. \tag{3.11}$$

Hence in the approximation of straight trajectories we have for the spectral cross-section of bremsstrahlung of an electron on a "bare" nucleus:

$$\frac{d\sigma}{d\omega} = \frac{16\,Z^2\ e^6}{3\ m^2\,\mathrm{v}^2\,c^3\,\hbar\,\omega} \int\limits_{\rho\,\min}^{\rho\,\max} \frac{d\rho}{\rho} \left\{ F^2\left(\frac{\omega\,\rho}{\mathrm{v}}\right) + F'^2\left(\frac{\omega\,\rho}{\mathrm{v}}\right) \right\}, \tag{3.12}$$

where the function $F(\zeta)$ is given by the formula (3.7).

The classical consideration is found to be not sufficient to determine the limits of integration in Eq. 3.12 with respect to the impact parameter. For this purpose it is necessary to involve quantum considerations. Thus the minimum value $\rho_{\min}$ is defined by the de Broglie wavelength of a scattered electron:

$$\rho_{\min} \approx \lambda\!\!\!^{-}_{DB} = \frac{\hbar}{m\,\mathrm{v}}. \tag{3.13}$$

The relation (3.13) reflects the fact that the location of a quantum particle can not be determined more precisely than the spatial "diffusiveness" of its wave function that is characterized by the de Broglie wavelength. To determine the maximum impact parameter $\rho_{\max}$, it is necessary to use the energy conservation law in bremsstrahlung and the connection of change of a momentum of an incident electron with the value ρ: $\Delta p \approx \hbar/\rho$, then it is possible to obtain:

$$\rho_{\max} \approx \frac{\mathrm{v}}{\omega}. \tag{3.14}$$

In derivation of Eq. 3.14 the energy conservation law was used in the form $\hbar\,\omega = \mathbf{v}\ \boldsymbol{\Delta}\mathbf{p}$ true for small changes of the electron momentum $|\boldsymbol{\Delta}\mathbf{p}| \ll p$, which corresponds to the approximation of straight trajectories. This approximation realized in case of distant collisions $\rho > a_C$ implies the weakness of interaction of an incident particle with a target nucleus. It is natural that in weak interaction mainly low-frequency photons will be emitted. It can be shown that a corresponding condition looks like: $\omega < \omega_C$, where $\omega_C = \mathrm{v}/a_C$ is the Coulomb frequency. In the low-frequency region the argument of the function $F(\zeta)$ and of its derivative $F'(\zeta)$ is less than one: $\zeta = \omega\,\rho/\mathrm{v} < 1$, so, as it follows from the definition (3.7), it is possible to use the following approximate equations: $F(\zeta) \approx 1$ and $F'(\zeta) \approx 0$. As a result, instead of Eq. 3.12 we have:

$$\frac{d\sigma}{d\omega} = \frac{16\,Z^2\ e^6}{3\ m^2\,\mathrm{v}^2\,c^3\,\hbar\,\omega} \ln\left(\frac{\rho_{\max}}{\rho_{\min}}\right). \tag{3.15}$$

It is easy to generalize the obtained expression to an arbitrary scattered charged particle, for which the used approximations are fulfilled. For this purpose in the formulas (3.2) and (3.5) it is necessary to make replacements: $e \to e_p$, $m \to m_p$, where e_p, m_p are the charge and the mass of an incident particle. Then in view of

Eqs. 3.13 and 3.14 we come from Eq. 3.15 to the final expression for spectral bremsstrahlung of a nonrelativistic charged particle on a "bare" nucleus in the low-frequency approximation ($\hbar\,\omega << m_p\,\mathrm{v}^2/2$):

$$\frac{d\sigma}{d\omega} = \frac{16\,Z^2\;e^2\,e_p^4}{3\;m_p^2\,\mathrm{v}^2\,c^3\;\hbar\,\omega}\,\ln\left(\frac{m_p\,\mathrm{v}^2}{\hbar\,\omega}\right). \tag{3.16}$$

From the obtained equation it follows that the bremsstrahlung cross-section is *inversely proportional to the squared mass of an incident particle*. Thus, when going from light charged particles (electron, positron) to heavy particles (proton, alpha particle, etc.), the cross-section of the process under consideration decreases more than million times. This conclusion led to the well-known statement that heavy charged particles do not emit bremsstrahlung photons. As it will be clear from the following, this statement needs considerable correction.

The spectral intensity of emission is equal to the process cross-section multiplied by the incident particle flux and the energy of an emitted photon, so Eq. 3.16 gives:

$$\frac{dI}{d\omega} = \frac{16\,Z^2\;e^2\,e_p^4}{3\;m_p^2\,\mathrm{v}\,c^3}\,\ln\left(\frac{m_p\,\mathrm{v}^2}{\hbar\,\omega}\right). \tag{3.17}$$

As was already said, the formulas (3.16) and (3.17) were obtained in the approximation of distant collisions corresponding to emission of low-frequency photons. The contribution to bremsstrahlung of high-frequency photons $\omega > \omega_C$ is made by close collisions $\rho < a_C$ corresponding to *strongly curved trajectories*. The spectral cross-section and the intensity of bremsstrahlung of an electron in this case are described by the Kramers formulas:

$$\frac{d\sigma^{(Kram)}}{d\omega} = \frac{16\,\pi\,Z^2\;e^6}{3\,\sqrt{3}\;m^2\,\mathrm{v}^2\,c^3\;\hbar\,\omega}, \tag{3.18}$$

$$\frac{dI^{(Kram)}}{d\omega} = \frac{16\,\pi\,Z^2\;e^6}{3\,\sqrt{3}\;m^2\,\mathrm{v}\,c^3}. \tag{3.19}$$

The right side of the Eq. 3.19 does not include the Planck constant, which is indicative of the purely classical nature of this expression.

The formulas for bremsstrahlung of an electron scattered by the Coulomb center *beyond the approximation of straight trajectories* can be obtained by corresponding replacement of the Fourier transform of the electric field intensity $\mathbf{E}(\omega, \rho)$ by the function corresponding to motion in the Coulomb potential. This problem for a case of static Bs is considered in detail in the review [3] within the framework of so-called Kramers electrodynamics for motion of electrons along strongly curved trajectories.

It is interesting to note that the Kramers formulas (3.18) and (3.19) describe not only bremsstrahlung, but also photorecombination, when the final state of an emitting electron belongs to the discrete ion spectrum, that is, is bound. The said circumstance is a consequence of the fact that emission in the high-frequency limit $\omega > \omega_C$ is "gathered" from a section of the trajectory of the most approach to a nucleus, so an emitting electron "does not know" where it gets after emission of a photon.

The expressions (3.16) and (3.17) are obtained within the framework of the classical consideration with quantum "insertions" (3.13) and (3.14). It is clear that such an approach is not consistent, but its important advantage is physical transparency and mathematical simplicity. It is pertinent to note here that the use of the quantum-mechanical formalism within the framework of the *Born approximation* results in the same formulas for the cross-section and intensity of bremsstrahlung of low-frequency photons as Eqs. 3.16 and 3.17.

The criterion of the Born approximation (in the Gaussian system of units) is given by the inequation:

$$\frac{Z\left|e\,e_p\right|}{\hbar\,\mathrm{v}} << 1, \tag{3.20}$$

that is, corresponds to fast enough incident particles. The condition (3.20) allows calculation of the scattering cross-section by the perturbation theory with the ratio $Z\left|e\,e_p\right|/\hbar\,\mathrm{v}$ serving as a small parameter of the theory. The possibility of classical consideration is given by the inequation reverse of (3.20), so the above agreement of results is connected with the use of the approximation of straight trajectories, when the influence of a target on an electron is low as in the case of the Born approximation.

When going to bremsstrahlung on an atom, it is necessary to take into account the screening effect of bound electrons, which results in the replacement

$$\rho_{\max} \to \min(\mathrm{v}/\omega,\ r_a), \tag{3.21}$$

(r_a is the atomic radius) in the expressions for the cross-section and intensity of the process. Really, for the impact parameters $\rho > r_a$ the atomic field is close to zero, so the acceleration of an incident particle is negligible, and together with it, according to Eq. 3.2, bremsstrahlung is also absent. It is clear that screening is essential for low enough frequencies $\omega < \mathrm{v}/r_a$, otherwise an incident particle should fly close enough to a nucleus to emit a photon of a specified frequency.

In case of bremsstrahlung on multielectron atoms, when the Thomas-Fermi model "works", the Thomas-Fermi radius can be used as an atomic radius: $r_a \approx r_{TF} = a_B\, b/\sqrt[3]{Z}$, where $a_B \approx 0.53$ Å is the Bohr radius, Z is the charge number of the atomic nucleus, $b \cong 0.8553$ is the constant.

The replacement of Eq. 3.21 corresponds to the *screening approximation* in the bremsstrahlung theory used by Bethe and Heitler [4] in generalization of formulas for the process cross-section to an atomic case.

Physically the screening approximation means the replacement of atomic electrons by the distribution of electrostatic charge screening a nucleus. Thus bound electrons are excluded from consideration as a dynamic degree of freedom that can be excited during bremsstrahlung and can reradiate the electromagnetic field of an incident particle. Actually in emission of high-energy photons the energy-momentum excess can be transferred to atomic electrons, resulting in their excitation and ionization.

3.1.2 Polarization Bremsstrahlung

Besides the above real excitation, atomic electrons in case of collision of an atom with a charged particle can be excited *virtually*. Virtual excitation corresponds to appearance of a variable dipole moment in the atom that, according to the fundamentals of electrodynamics, should radiate electromagnetic waves. Such a process is called *polarization bremsstrahlung* since it is connected with the dynamic polarizability of an atom. The dynamic polarizability of an atom is considered in detail in Appendix 1. The dynamic polarizability of an atom together with the external variable field defines a radiating dipole moment.

Another interpretation can be given to polarization bremsstrahlung as a process of scattering of the eigenfield of an incident particle (a virtual photon) to the radiation field (a real photon) by atomic electrons. Polarization bremsstrahlung is an additional channel of radiation in charge scattering by a target having a system of bound electrons. We will call ordinary bremsstrahlung existing also on a "bare" nucleus ordinary or static bremsstrahlung. The last term implies that this channel is a single channel in the model of static distribution of electron charge of bound electrons.

Let us derive the formulas for polarization bremsstrahlung of a fast charged particle on an atom, considering the atom to be an elementary dipole with the polarizability $\alpha(\omega)$ (see Appendix 1, the formula (A.3) for connection of an induced dipole moment and the electric field strength).

For description of motion of an incident particle we use, as above, the classical approach and the approximation of straight trajectories. Again we proceed from the formula for the power of dipole radiation, but this time we will write it in terms of the dipole moment of the radiating system:

$$Q(t) = \frac{2}{3\,c^3}\left|\ddot{\mathbf{d}}(t)\right|^2. \tag{3.22}$$

Here two dots designate the second time derivative. Integrating the Eq. 3.22 with respect to time and using the formula (3.37) for the squared second derivative of the dipole moment, we come to the expression for the total energy of polarization bremsstrahlung for the whole time of collision corresponding to the impact parameter ρ:

$$\Delta \mathrm{E} = \frac{4\,e^2}{3\,c^3} \int\limits_0^\infty \omega^4 \left|\alpha(\omega)\,\mathbf{E}^{(p)}(\omega,\,\rho)\right|^2 \frac{d\omega}{2\,\pi}, \tag{3.23}$$

where $\mathbf{E}^{(p)}(\omega, \rho)$ is the Fourier component of the intensity of the electric field of an incident charged particle at the location of the atom. In derivation of this formula the relation was used: $\ddot{\mathbf{d}}(\omega) = -\omega^2\,\mathbf{d}(\omega)$ that follows from determination of the Fourier components.

Going from the total radiated energy to the spectral cross-section, as it was done in derivation of the formula (3.11), we obtain for polarization bremsstrahlung the following expression:

$$\frac{d\sigma^{PB}}{d\omega} = \frac{4\,\omega^3\,|\alpha(\omega)|^2}{3\;c^3\;\hbar} \int\limits_{\tilde{\rho}\,\mathrm{min}}^{\tilde{\rho}\,\mathrm{max}} \left|\mathbf{E}^{(p)}(\omega,\rho)\right|^2 \rho\,d\rho. \tag{3.24}$$

The upper limit of integration in this formula following from the energy conservation law is determined by the Eq. 3.14, the same as for static bremsstrahlung. The lower limit of integration is much different. In the elementary dipole approximation under consideration it is defined by the size of an atom:

$$\tilde{\rho}_{\mathrm{min}} = r_a. \tag{3.25}$$

As the analysis shows, scattering at low impact parameters $\rho < r_a$ makes a small contribution to the polarization bremsstrahlung cross-section since then coherence in reradiation of the eigenfield of an incident particle by atomic electrons to a real photon is lost.

From Fig. 3.1 it is easy to see that the Fourier component of the intensity of the electric field of an incident particle in the approximation of straight trajectories can be calculated by the formula similar to Eq. 3.6 with replacement of the nuclear charge by the incident particle (projectile) charge. As a result, for the intensity $\mathbf{E}^{(p)}(\omega, \rho)$ we have:

$$\mathbf{E}^{(p)}(\omega,\rho) = \frac{2\,e_p}{\rho\,\mathrm{v}} \left\{-F\left(\frac{\omega\,\rho}{\mathrm{v}}\right)\mathbf{e}_n + i\,F'\left(\frac{\omega\,\rho}{\mathrm{v}}\right)\mathbf{e}_\tau\right\}, \tag{3.26}$$

where $\mathbf{e}_n, \mathbf{e}_\tau$ are the normal and tangent unit vectors, the function $F(\zeta)$ is given by the Eq. 3.7. Shown in Fig. 3.2 is the modulus of the normal and tangential components of the electric field Eq. 3.26 as well as the entire spectrum $H(\nu) = \sqrt{F^2(\nu) + F'^2(\nu)}$ as a function of the dimensionless frequency $\nu = \omega\,\rho/\mathrm{v}$.

From Fig. 3.2 it is seen that the main contribution to the spectral function $H(\nu)$ in the region of its high values is made by the normal component of the electric field of an electron, and the spectrum width is of the order of the ratio v/ρ.

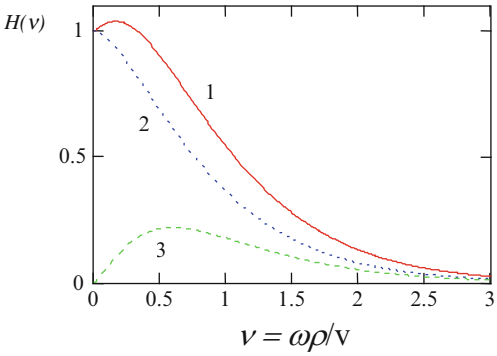

Fig. 3.2 The spectrum of the electric field of an incident particle (Eq. 3.26) as a function of the dimensionless frequency: *1* – entire spectrum, *2* – of the normal component of the field, *3* – of the tangent component of the field

Substituting Eq. 3.26 in Eq. 3.24, we obtain the spectral cross-section of polarization bremsstrahlung in the used approximation:

$$\frac{d\sigma^{PB}}{d\omega} = \frac{16\, e_p^2\, \omega^3\, |\alpha(\omega)|^2}{3\, \mathrm{v}^2\, c^3\, \hbar} \int_{r_a}^{\mathrm{v}/\omega} \frac{d\rho}{\rho} \left\{ F^2\left(\frac{\omega\, \rho}{\mathrm{v}}\right) + F'^2\left(\frac{\omega\, \rho}{\mathrm{v}}\right) \right\}. \tag{3.27}$$

Hence for intensity we find:

$$\frac{dI^{PB}}{d\omega} = \frac{16\, e_p^2\, \omega^4\, |\alpha(\omega)|^2}{3\, \mathrm{v}\, c^3} \int_{r_a}^{\mathrm{v}/\omega} \frac{d\rho}{\rho} \left\{ F^2\left(\frac{\omega\, \rho}{\mathrm{v}}\right) + F'^2\left(\frac{\omega\, \rho}{\mathrm{v}}\right) \right\}. \tag{3.28}$$

It should be noted that the formula (3.28) does not contain the Planck constant, which is indicative of its classical nature.

In the limit of low frequencies, when $F(\zeta) \approx 1$ and $F'(\zeta) \approx 0$, the formula (3.27) gives:

$$\frac{d\sigma^{PB}}{d\omega} = \frac{16\, e_p^2\, \omega^3\, |\alpha(\omega)|^2}{3\, \mathrm{v}^2\, c^3\, \hbar} \ln\left(\frac{\mathrm{v}}{\omega\, r_a}\right). \tag{3.29}$$

This expression is true for the frequencies $\omega < \mathrm{v}/r_a$, otherwise it is necessary to use the formula (3.27). Calculation, however, shows that in the frequency range $\omega > \mathrm{v}/r_a$ polarization bremsstrahlung is low.

The cross-section of Eq. 3.29 can be obtained within the framework of the quantum approach in case of truth of the Born approximation Eq. 3.20, that is, for fast (but nonrelativistic) incident particles.

It must be emphasized that the polarization bremsstrahlung cross-sections (3.27), (3.29) do not depend on the mass of an incident particle in contrast to the static bremsstrahlung cross-section (3.17). Thus the statement long existing in

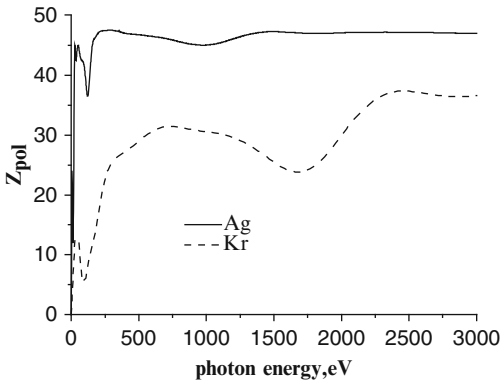

Fig. 3.3 The spectral dependence of the polarization charge of silver and krypton atoms

physics that heavy charged particles do not emit bremsstrahlung photons does not extend to the polarization channel. This circumstance is connected with the fact that the static bremsstrahlung cross-section is proportional to the squared acceleration of an incident particle, while the polarization channel cross-section the does not depend on this acceleration.

The polarization bremsstrahlung cross-section (3.29) can be obtained from the static process cross-section (3.16) with the use of replacements $m_p \to m, e_p^4 \to e^2\, e_p^2$, $\rho_{\min} \to \tilde{\rho}_{\min}$, and

$$Z \to Z_{pol}(\omega), \tag{3.30}$$

where

$$Z_{pol}(\omega) = \frac{m\,\omega^2}{e^2}\,|\alpha(\omega)| \tag{3.31}$$

is the effective polarization atomic charge (in the units of the electron charge e).

The polarization charge characterizes the ability of the electron core of an atom to emit a photon under the action of an ac field. In contrast to an ordinary charge, the polarization charge depends on the radiation frequency. The frequency dependence of the polarization charges of silver and krypton atoms is presented in Fig. 3.3.

From this figure it is seen that in the high-frequency range the polarization charge is equal to the number of bound electrons of an atom (or the charge number of its nucleus). This circumstance follows from the definition (3.31) and the formula for high-frequency polarizability (A.16). In the region of low frequencies $\omega \to 0$ the polarization charge according to Eq. 3.31 decreases quadratically since then the atomic polarizability is equal to its static value (A.15), that is, does not depend on frequency. Finally, in the intermediate spectral range the polarization charge is a nonmonotonic function that reflects the features of the energy spectrum of an atom. For example, a wide "dip" on the dashed curve of Fig. 3.3 in a range

of 1,600–1,750 eV corresponds to the energy of binding of $2p$ -electrons in a krypton atom. The minimum in the region of low frequencies corresponds to virtual excitation of subshells of an atom with the principal quantum number $n = 3$. Thus the spectral cross-section of polarization bremsstrahlung reflects the dynamics of the atomic core as a function of frequency.

In the high-frequency limit, when $\omega >> \omega_a$ (ω_a is the characteristic frequency of excitation of an atom in the discrete spectrum), but still $\omega < \mathrm{v}/r_a$, $\alpha(\omega) \approx -Z\,e^2/m\,\omega^2$ ($Z_{pol}(\omega) = Z$), and the formula (3.29) gives:

$$\frac{d\sigma^{PB}}{d\omega} = \frac{16\,Z^2\,e^4\,e_p^2}{3\,m^2\mathrm{v}^2\,c^3\hbar\,\omega}\,\ln\left(\frac{\mathrm{v}}{\omega\,r_a}\right). \tag{3.32}$$

Curiously, in case of an incident electron (positron) the obtained expression differs from the formula for the static bremsstrahlung cross-section (3.17) only by a logarithmic factor.

Now we will consider a resonant case, when the bremsstrahlung frequency is close to one of eigenfrequencies of an atom $\omega \approx \omega_0$, and dynamic polarizability looks like:

$$\alpha(\omega \approx \omega_0) \cong \frac{e^2}{m}\,\frac{f_0}{\omega_0^2 - \omega^2 - 2\,i\,\omega\,\delta_0}. \tag{3.33}$$

This expression for resonant polarizability follows from the general formula (A.14), if in it one resonant summand is retained, in which $\omega_{nm} \equiv \omega_0, f_{nm} \equiv f_0$ and $\delta_{nm} \equiv \gamma_0$. Substituting the formula (3.31) in Eq. 3.29, we obtain:

$$\frac{d\sigma^{res}}{d\omega} = \frac{4}{3}\,\frac{e_p^2}{\hbar\,c}\,\left(\frac{c}{\mathrm{v}}\right)^2\,\frac{r_e^2 f_0^2\,\omega_0}{(\omega_0 - \omega)^2 + \delta_0^2}\,\ln\left(\frac{\mathrm{v}}{\omega\,r_a}\right), \tag{3.34}$$

where $r_e = e^2/m\,c^2 \approx 2.8 \cdot 10^{-13}$ cm is the electron classical radius.

From the expression (3.34) it is seen that resonance polarization bremsstrahlung has a sharp maximum at the frequency $\omega = \omega_0$ if $\delta_0 << \omega_0$. The last inequation is satisfied in case of excitation of electrons of the outer atomic shell in the discrete spectrum, so for a neutral atom the energies of resonant photons are about 10 eV and less. In case of multiply charged ions having a system of bound electrons (an electron core) these energies can be much higher and reach a value of the order of several keV. Then, however, the transition damping constant equal to the Einstein coefficient A_{mn} is also great, and therefore the resonance becomes not such sharp. At frequencies corresponding to virtual excitation of inner atomic shells the resonance structure in the spectral dependence of the dynamic polarizability $\alpha(\omega)$ disappears. Instead of it, on the spectral curves "dips" arise that correspond to the beginning of photoionization of the atomic subshell (see Fig. 3.3).

3.2 Bremsstrahlung of Quasi-Classical Electrons in the Local Plasma Approximation for the Electron Core of a Target

The local plasma model (the Brandt-Lundqvist approximation [5]) for the polarizability of a multielectron target was considered in Sect. 2.4 (Sect. 2.4.1). This model was proposed for description of multielectron atoms, in which the electron–electron interaction in a specified (wide enough) spectral range can play a role comparable to the electron-nucleus interaction.

The Brandt-Lundqvist approximation can be considered as an elementary classical analog of the quantum-mechanical random phase exchange approximation widely used for taking into account electron–electron correlations in atomic physics. The main idea of this method is that electron–electron correlation effects are expressed in terms of the dynamic polarizability of the atomic core.

Such calculations in respect to the problem of calculation of the cross-section of polarization bremsstrahlung on an atom in a wide frequency range were carried out in the work [6] for electrons of kilovolt energies scattered by a krypton atom. It should be noted that such calculations represent a rather intricate numerical problem since wave functions of atomic electrons already in the zeroth approximation are the solutions of the Hartree-Fock integro-differential equations.

The high reliability of results obtained within the framework of the random phase exchange approximation shows the reverse side of the medal in necessity to carry out laborious calculations for each specific target and in difficulty of obtaining qualitative regularities "working" in a wide enough range of variation of problem parameters.

The purpose of this chapter is to develop semiquantitative methods of calculation of polarization effects in radiative processes on multielectron targets and to carry out the analysis of qualitative regularities of the said processes on their basis.

The main advantage of the used approach consists in its calculating simplicity and physical obviousness. Making no pretence of the exact quantitative description of the phenomenon, the method used in this chapter can be considered as an additional (to consistent quantum-mechanical calculations) method of description of polarization-interference effects on multielectron systems.

3.2.1 Polarizability of an Atom in the Brandt-Lundqvist Model

The dipole polarizability of an atom (or other multielectron system) is given within the framework of the local plasma frequency model by the formula (2.73) that can be rewritten as

$$\alpha^{BL}(\omega) = \int_0^{R_0} \frac{\omega_p^2(r)\, r^2\, dr}{\omega_p^2(r) - \omega^2 - i\,\delta} = \int \beta^{BL}(r,\omega)\; d\mathbf{r}, \tag{3.35}$$

where $\omega_p(r) = \sqrt{4\pi e^2 n(r)/m}$ is the local plasma frequency depending on the local electron density of the electron core $n(r)$, r is the distance from a point under consideration to the atomic nucleus, R_0 is the atomic radius. Here and further the spherical symmetry of the system is assumed, so $n(\mathbf{r}) = n(r)$.

The Eq. 3.35 gives the expression for dynamic polarizability as the volume integral of some dimensionless function $\beta^{BL}(r, \omega)$:

$$\beta^{BL}(r, \omega) = \frac{\omega_p^2(r)/4\,\pi}{\omega_p^2(r) - \omega^2 - i\,\delta}$$

that is natural to be called the *spatial density of the dynamic polarizability* of a target in the Brandt-Lundqvist approximation. This value in the local approximation under consideration is a liaison between the induced atomic polarization at the specified frequency $\mathbf{P}(r, \omega)$ and the strength of the external electric field $\mathbf{E}(r, \omega)$ causing this polarization, the cause and effect being taken at one point of space (local approximation):

$$\mathbf{P}(r, \omega) = \beta(r, \omega)\,\mathbf{E}(r, \omega). \tag{3.36}$$

In writing Eq. 3.36 it is assumed that the target has a spherical symmetry.

It should be noted that the expression (3.35) can be rewritten as the frequency integral if the spectral density of the oscillator strength is duly introduced by the formula

$$\frac{df}{d\omega} = \frac{m\,\omega^2}{e^2} r_p^2(\omega) \frac{dr_p(\omega)}{d\omega}, \tag{3.37}$$

where the function $r_p(\omega)$ is determined by solution of the equation

$$\omega = \omega_p(r). \tag{3.38}$$

Thus the dynamic polarizability in the Brandt-Lundqvist model can be formally presented in the characteristic quantum-mechanical form. The remaining difference consists in the fact that the Eq. 3.35 does not describe the contribution of the discrete spectrum to the atomic polarizability, which is natural since the local plasma frequency approximation is an essentially classical approximation. It should be noted that the contribution of the discrete spectrum is most essential for alkali-like ions and is small for systems with filled electron shells.

As easily seen from the formula (3.35), the high-frequency dynamic polarizability in the Brandt-Lundqvist model has correct asymptotics agreeing with the result of the quantum-mechanical calculation:

$$\alpha^{hf}(\omega) = -\frac{e^2\,N_e}{m\,\omega^2}, \tag{3.39}$$

where N_e is the full number of target electrons (see Appendix 1, the formula (A.16))

Table 3.1 Static polarizabilities of atoms and ions with filled shells (a.u.)

Atom (ion)	ArI	KrI	XeI	KII	RbII	CsII	SrIII	BaIII
α_0^{exp}	11	17	27	7.5	12	16.3	6.6	11.4
α_0^{var}	19.3	26.8	30.9	9.1	14.3	17.8	8.7	11.4
α_0^{VSh}		21.1	25.5	6.6	11.9	15.3	7.5	9.7
α_0^{BL}	22	24	27	8.6	11.6	13.5	7	8.4

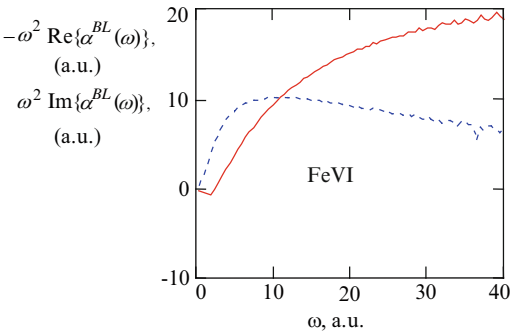

Fig. 3.4 The frequency dependences of the real (*solid line*) and imaginary (*dotted line*) parts of the dynamic polarizability of the iron ion calculated within the framework of the local plasma model

Given in Table 3.1 is the comparison of the values of static polarizabilities of atoms and ions (in atomic units) with filled electron shells calculated by different methods within the framework of the statistical description of an atom with experimental data (α_0^{exp}).

Here: α_0^{var} is the calculation by the variational method [7], α_0^{VSh} is the calculation of Vinogradov and Shevel'ko [8], $\alpha_0^{BL} = R_0^3/3$ is the calculation in the Brandt-Lundqvist model [5].

In calculations of static polarizability in the Brandt-Lundqvist model the radius of an atom (ion) was used that was calculated in view of the correlation allowance in the Thomas-Fermi-Dirac model.

From the given table it follows that in most cases for static polarizability the Brandt-Lundqvist method gives a satisfactory fit to the experiment for atoms (ions) with filled shells.

So from the analysis of low-frequency and high-frequency limits it can be expected that the use of the Brandt-Lundqvist model in the first approximation gives a reasonable approximation for the dynamic polarizability of an atom (ion).

Given in Fig. 3.4 are the frequency dependences of the values $\omega^2\,\mathrm{Re}\{\alpha(\omega)\}$ and $\omega^2\,\mathrm{Im}\{\alpha(\omega)\}$ for a FeVI ion calculated in the Brandt-Lundqvist approximation in a wide frequency range. The comparison with analogous dependences calculated in the random phase exchange approximation for a multielectron atom [6] shows that the calculation in the Brandt-Lundqvist model qualitatively correctly describes the

smoothed functions $\omega^2 \operatorname{Re}\{\alpha(\omega)\}$, $\omega^2 \operatorname{Im}\{\alpha(\omega)\}$ without considering peculiarities caused by the shell structure of an atom (maxima and minima near the thresholds of ionization of subshells).

Besides the Thomas-Fermi model for description of distribution of electron density of an atom, a number of improved models is used, such as the Thomas-Fermi-Dirac model and the Lenz-Jensen model [7]. Within the framework of these models the radius of a neutral atom R_0 is found to be a finite quantity in contrast to the Thomas-Fermi model, in which $R_0 \to \infty$. Moreover, for description of electron subshells the Slater wave functions are used that are distinguished by simplicity and ease in carrying out analytical calculations. These functions look like:

$$P_\gamma(r) = \sqrt{\frac{(2\beta)^{2\mu+1}}{\Gamma(2\mu+1)}} r^\mu e^{-\beta r}, \tag{3.40}$$

where $\gamma = (nl)$ is the set of quantum numbers characterizing an electronic state, β, μ are the Slater parameters that are chosen in a special manner to satisfy the experimental data on the energy of corresponding shells. The wave functions (3.40) are normalized, have correct asymptotics at long distances. With the use of the functions (3.40) the radial distribution of electron density of an atom in the Slater approximation can be obtained as

$$n(r) = \sum_\gamma N_\gamma P_\gamma^2(r). \tag{3.41}$$

The Slater electron density as well as the densities of other models of the atomic core can be used in calculation of the dynamic polarizability of an atom in the local plasma frequency approximation (3.35).

In more detail the methods of description of the core of multielectron atoms and ions, including statistical models, are stated in Appendix 2.

The results of calculation of the real and imaginary parts of the dipole dynamic polarizability of a krypton atom within the framework of the local plasma frequency method by the formula (3.35) with the use of electron density according to Slater and Lenz-Jensen are presented in Fig. 3.5. Shown in the same figure are the results of calculation of corresponding values in the quantum-mechanical random phase exchange approximation carried out in the work [6].

It is seen that the dynamic polarizability of a krypton atom calculated in the local plasma frequency model for Lenz-Jensen electron density in a smoothed manner renders the quantum-mechanical features of the frequency behavior of dynamic polarizability that are most pronounced near the potentials of ionization of electron subshells. Using the Slater wave functions within the framework of this model makes it possible to detect to some extent spectral fluctuations of polarizability near the potentials of ionization of electron subshells. In this case, however, the universality of description characteristic for the statistical model of an atom is violated.

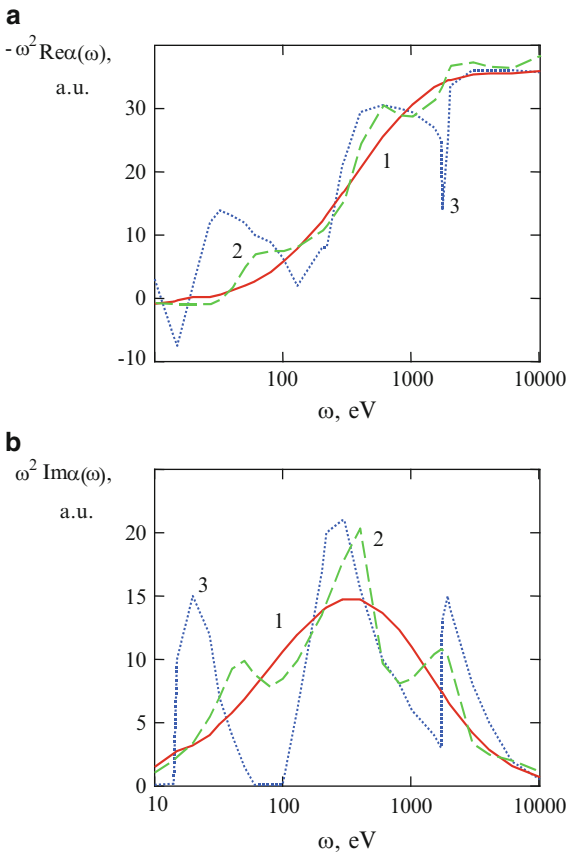

Fig. 3.5 The frequency dependences of the real (**a**) and imaginary (**b**) parts of the polarizability of a krypton atom calculated in different approximations: in the local plasma frequency approximation for Lenz-Jensen electron density (*1*), for Slater electron density (*2*), and in the random phase exchange approximation (*3*)

With the use of the formula (3.35) and the statistical model of an atom (see Appendix 2) for dynamic polarizability the following expression can be obtained:

$$\alpha(\omega, Z) = r_{TF}^3 \tilde{\alpha}\left(\frac{\omega}{Z}\right) = \frac{b^3 a_0^3}{Z} \tilde{\alpha}\left(\frac{\omega}{Z}\right), \tag{3.42}$$

$$\tilde{\alpha}(v) = \int_0^{x_0} \frac{4\pi f(x) x^2 \, dx}{4\pi f(x) - v^2 - i0}, \tag{3.43}$$

where $r_{TF} = b a_0 / Z^{1/3}$ is the Thomas-Fermi radius, Z is the charge of the atomic nucleus, a_0 is the Bohr radius, $b \cong 0.8853$, $\tilde{\alpha}(v)$ is the dimensionless polarizability as a function of the reduced frequency $v = \hbar\omega / 2Ry\, Z$, ($Ry = 13.6$ eV), $x_0 = R_0 / r_{TF}$ is the reduced atomic radius, $f(x)$ is the universal function describing the distribution of the electron density $n(r)$ in an atom within the framework of the statistical model according to the formula $n(r) = Z^2 f(r / r_{TF})$.

The explicit expressions for the function $f(x)$ for a number of statistical models, including the Thomas-Fermi and Lenz-Jensen models, are given in Appendix 2. For example, for the Lenz-Jensen function the formula (A.46) is true. Though the Thomas-Fermi function $\chi(x)$, in terms of which the concentration of atomic electrons (A.45) and the atomic potential are expressed, has no analytical representation, for this formula there are good approximations obtained by A. Sommerfeld. These approximations, both for neutral atoms and for multielectron ions, are also given in Appendix 2 (see the formulas (A.48), (A.49) (A.50)).

It must be emphasized that the dimensionless polarizability $\tilde{\alpha}(v)$ does not depend on the charge of an atomic nucleus. Thus the representation of the dynamic polarizability of a statistical atom (3.42) and (3.43) reveals the scaling law for this value with respect to the parameter v.

Let us give the high-frequency asymptotics of the dimensionless polarizability following from the formulas (3.42) and (3.43) with the help of the explicit form of the function $f(x)$ for the distribution of the Thomas-Fermi and Lenz-Jensen electron density (see Appendix 2). For the imaginary part of the dimensionless polarizability $\tilde{\alpha}(v)$ we have:

$$\mathrm{Im}\left\{\tilde{\alpha}^{T-F}(v \to \infty)\right\} \to \frac{4.35}{v^4}, \tag{3.44}$$

$$\mathrm{Im}\left\{\tilde{\alpha}^{L-J}(v \to \infty)\right\} \to \frac{4.615}{v^4}. \tag{3.45}$$

From the formulas (3.44) and (3.45) it is seen that the above statistical models give a close result for the imaginary part of polarizability. The high-frequency asymptotics of the real part of the dimensionless polarizability $\tilde{\alpha}(v)$ in both models of electron density of the atomic core look like

$$\mathrm{Re}\{\tilde{\alpha}(v \to \infty)\} \to -\frac{b^{-3}}{v^2}, \tag{3.46}$$

which is in the qualitative agreement with the general formula (3.39). From comparison of the expressions (3.44), (3.45) and (3.46) it follows in particular that at high frequencies the imaginary part of polarizability decreases much more rapidly than its real part.

Thus using the Brandt-Lundqvist model seems justified for the qualitative description of polarization effects on multielectron ions and atoms for frequencies $\omega \approx Z$ and more.

In the low-frequency range the use of the plasma-statistical approach can require some correction due to the fact that the potential of ionization of an atom within the framework of statistical models has an underestimated value, especially for targets with filled shells, so the characteristic features of the frequency dependence $\alpha(\omega)$ are found to be shifted to the region of low frequencies. So in calculation of cross-sections in the low-frequency range with the use of the Brandt-Lundqvist model for

the dynamic polarizability of a target it is worthwhile to shift the frequency dependence of polarizability to the region of high frequencies, so that the maximum of its imaginary part falls on the potential of ionization of an atom.

3.2.2 Polarization Potential in the Bremsstrahlung Theory

For calculation of the polarization bremsstrahlung cross-section we will introduce into consideration the potential of interaction of an incident particle with an ion being in the external uniform electromagnetic field $\mathbf{E}(\omega)$. This potential looks like

$$V_{pol}(\mathbf{R},\omega) = \int d\mathbf{r}\, \frac{\delta\rho(\mathbf{r},\omega)}{|\mathbf{r}-\mathbf{R}|}, \tag{3.47}$$

here $\delta\rho(\mathbf{r},\omega)$ is the spatial density of perturbation of an electron charge induced in the ion core under the action of the external field, $\mathbf{R}$ is the radius vector of an incident particle (IP).

It should be noted that the proposed approach is suited also for calculation of spontaneous processes: in this case by $\mathbf{E}(\omega)$ the field of quantum fluctuations should be understood.

The electron charge density perturbation $\delta\rho(\mathbf{r},\omega)$ is related with the polarization density induced in the ion core:

$$\delta\rho(\mathbf{r},\omega) = \text{div}\ \mathbf{P}(\mathbf{r},\omega). \tag{3.48}$$

The value $\mathbf{P}(\mathbf{r},\omega)$ in the *local approximation* is given by the formula (3.36).

The distribution of electron density in an atom (ion) everywhere in what follows we will assume to be spherically symmetric.

Assembling the written-out formulas and using the expansion of the reciprocal distance $|\mathbf{r}-\mathbf{R}|^{-1}$ in terms of spherical harmonics, after simple algebraic transformations and integration with respect to angular variables we obtain for the polarization potential in the local approximation the following expression:

$$V_{pol}(\mathbf{R},\omega) = e\frac{\mathbf{R}\mathbf{E}(\omega)}{R^3}\int_0^R \beta\,(r,\omega)\ 4\pi r^2 dr. \tag{3.49}$$

It is essential that this formula describes the *nondipole* potential of interaction of an IP with a perturbed ion core, which manifests itself in the presence of the magnitude of the IP radius vector in the upper limit of integration. This circumstance has a simple electrostatic interpretation: an external charge interacts only with part of the electron cloud inside the sphere of radius R.

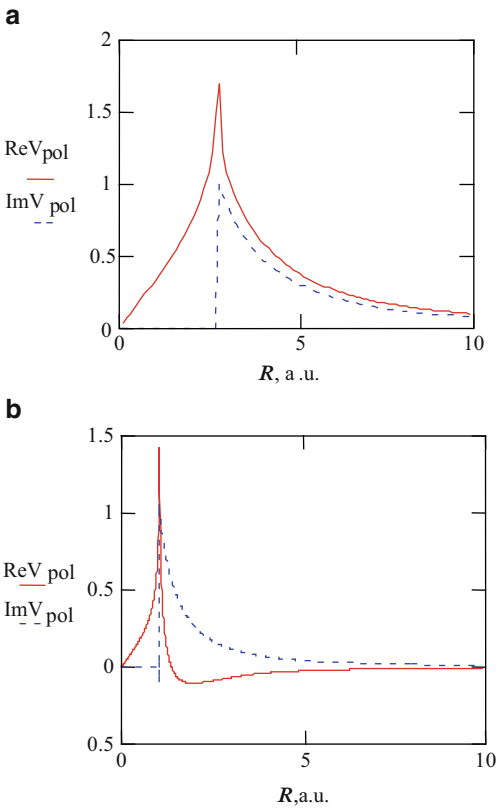

Fig. 3.6 The real and imaginary parts of the polarization potential normalized to the amplitude of the electromagnetic field at frequencies (**a**) $\omega = 0.9$ a.u., (**b**) $\omega = 3$ a.u. as functions of the distance to the nucleus of a *KII* ion. Calculation in the Brandt-Lundqvist approximation [5] with the use of the Thomas-Fermi-Dirac electron density

Thus the obtained polarization potential (Eq. 3.49) describes the effects connected with penetration of an IP into the ion core.

Presented in Fig. 3.6a, b are the results of calculation of the real and imaginary parts of the polarization potential normalized to the amplitude of the external electric field for a *KII* ion. The calculation was made in the local plasma approximation with the use of the electron density of the ion core in the Thomas-Fermi-Dirac model for two frequencies of the electromagnetic field $\omega = 0.9$ a.u. (a), 3 a.u. (b) by the formula (3.43). In both cases the real part of the polarization potential has a maximum at a distance determined by the Eq. 3.38. At this distance the local dielectric permittivity of a target becomes zero and at the same time an imaginary additive to the polarization potential appears. It is seen from the figure that the distance $r_p(\omega)$ (see Eq. 3.38) decreases with growing frequency. The function $r_p(\omega)$ in the Thomas-Fermi-Dirac model is monotonically decreasing since the spatial density of electron distribution in this model grows monotonically.

It is interesting to note that for any finite frequency $(0 < \omega < \infty)$ there is some distance to a nucleus $r_0(\omega)$ (and $r_0(\omega) > r_p(\omega)$), at which the real part of the polarization potential changes a sign. If it is taken into account that the interaction force is equal to the derivative of the potential taken with the minus sign, it can be

concluded from the form of the curves in Fig. 3.6 that at short enough distances from the nucleus an IP is effectively attracted to the target under the action of its polarization. At the same time at long distances the polarization interaction corresponds to repulsion.

Using the expression for the polarization potential (Eq. 3.49), it is possible to obtain the formula for a dipole moment induced in the ion core by a scattered particle if it is taken into account that:

$$V_{pol}(\mathbf{R},\,\omega) = -\mathbf{E}(\omega)\,\mathbf{D}_{pol}(\mathbf{R},\,\omega). \tag{3.50}$$

From comparison of Eqs. 3.49 and 3.50 we find

$$\mathbf{D}_{pol}(\mathbf{R},\omega) = -e_p\,\frac{\mathbf{R}}{R^3}\int\limits_0^R \beta\,(r,\omega)\,4\,\pi\,r^2\,dr. \tag{3.51}$$

The dipole moment $\mathbf{D}_{pol}(\mathbf{R},\omega)$ induced in the atomic core is a function of the external field frequency and the radius vector of an incident particle $\mathbf{R}$.

In view of the explicit expression for the spatial density of polarizability (3.35) from the formula (3.51) we find for the real and imaginary parts of the polarization dipole moment

$$\mathrm{Re}\left\{\mathbf{D}^{BL}(\omega,\,\mathbf{R})\right\} = e\,\frac{\mathbf{R}}{R^3}\,V.P.\int\limits_0^R \frac{\omega_p^2(r)\,r^2 dr}{\omega_p^2(r)-\omega^2}, \tag{3.52}$$

$$\mathrm{Im}\left\{\mathbf{D}^{BL}(\omega,\mathbf{R})\right\} = e\,\frac{\mathbf{R}}{R^3}\,\frac{\pi}{2}\,\omega^2\,\frac{r_p^2(\omega)}{\left|d\omega_p\left(r_p\right)/dr\right|}\,\theta\left(R-r_p(\omega)\right), \tag{3.53}$$

where $\theta(x)$ is the Heaviside theta function, $V.P.$ is the symbol of the principal integral value.

The total radiating dipole moment of the system IP + atom (ion) is:

$$\mathbf{D}_{tot}(\mathbf{R},\omega) = e_p\,\mathbf{R} - e_p\,\frac{\mathbf{R}}{R^3}\int\limits_0^R \beta\,(r,\omega)\,4\,\pi\,r^2\,dr. \tag{3.54}$$

It should be noted that following from the Eq. 3.54 is the simple relation between the static and polarization dipole moments in the approximation under consideration:

$$\mathbf{D}_{pol}(\mathbf{R},\omega) = \left\{-\frac{1}{R^3}\int\limits_0^R \beta\,(r,\omega)\,4\,\pi\,r^2\,dr\right\}\mathbf{D}_{st}(\mathbf{R},\omega).$$

The formula (3.54) is a primary formula for carrying out numerical calculations of polarization effects in the local approximation. It corresponds to consideration of two channels of the process: static (the first summand in Eq. 3.54) and polarization (the second summand). Since these summands enter into the expression for the total radiating dipole moment of the system target + IP, the expression (3.54), being substituted in the standard formula for the process cross-section or corresponding intensity, will describe also interference effects connected with the interaction of channels.

3.3 Polarization Bremsstrahlung on a Multielectron Ion in the Approximation of Classical Motion of an Incident Particle

As was already noted, the Born parameter η characterizing the motion of plasma electrons under conditions of thermodynamically equilibrium plasma is more or of the order of one:

$$\eta = \frac{Ze^2}{\hbar \mathrm{v}} \geq 1. \tag{3.55}$$

The inequation (3.55) is the reverse of the Born condition and corresponds (in the strong inequality limit) to the quasi-classical approximation for IP motion. It is within the framework of quasi-classics (or, more precisely, of the semiclassical approach) that V.I. Kogans with coworkers [9, 10] have carried out the detailed analysis of the static channel of bremsstrahlung on multielectron atoms and ions. The so-called rotation approximation has been developed that allows rather simple calculation of spectral cross-sections of main radiation processes including photorecombination as well.

The comparison with quantum-mechanical numerical calculations [11] has shown high accuracy of the semiclassical approach and in particular of the rotation approximation in the theory of static Bs.

So it seems natural to use the semiclassical approach also in investigation of polarization Bs on a multielectron ion and to design on its basis the generalization of the rotation approximation including the description of the polarization channel.

As known [12], in classical consideration of a collisional-radiative process the value κ is introduced that is called effective radiation by the formula

$$\kappa = \int_0^\infty \Delta \mathrm{E}(\rho)\, 2\,\pi\,\rho\, d\rho, \tag{3.56}$$

here $\Delta \mathrm{E}(\rho)$ is the total radiation of one IP with the specified impact parameter ρ.

Further we will be interested also in spectral effective radiation $d\kappa(\omega)/d\omega$, the expression for which in the dipole approximation for interaction with an electromagnetic field for a spontaneous process looks like

$$\frac{d\kappa(\omega)}{d\omega} = \frac{4\,\omega^4}{3\,c^3} \int\limits_0^\infty |\mathbf{D}(\omega,\rho)|^2 \rho d\rho, \tag{3.57}$$

where $\mathbf{D}(\omega,\rho)$ is the Fourier transform of the radiating dipole moment of the system at the frequency ω calculated along the trajectory of an IP characterized by the impact parameter ρ.

Between the value $d\kappa/d\omega$ and the spectral cross-section of bremsstrahlung $d\sigma/d\omega$ there is a simple connection:

$$\frac{d\kappa}{d\omega} = \hbar\omega \frac{d\sigma}{d\omega}.$$

To take into account interference-polarization effects, as $\mathbf{D}(\omega,\rho)$, further we will use the temporal Fourier transform of the total dipole moment

$$\mathbf{D}_{tot}(\omega,\rho) = \int\limits_{-\infty}^{+\infty} \mathbf{D}_{tot}(\mathbf{R}(t,\rho,\mathrm{v_i}),\omega) e^{i\omega t} dt, \tag{3.58}$$

in which the function $\mathbf{D}_{tot}(\mathbf{R},\omega)$ is given by the expression (3.54). It should be noted that the dimensionalities of $\mathbf{D}_{tot}(\mathbf{R},\omega)$ and $\mathbf{D}_{tot}(\omega,\rho)$ do not agree: the first value has the dimensionality of the electric dipole moment, and the second value has the dimensionality of its Fourier transform.

Thus in classical calculation of spectral effective radiation it is necessary to know the law of IP motion:

$$\mathbf{R} = \mathbf{R}(t,\rho,\mathrm{v_i}), \tag{3.59}$$

here $\mathrm{v_i}$ is the initial IP velocity.

In investigation of strongly inelastic processes of scattering corresponding to IP motion along strongly curved trajectories it is convenient to express the temporal Fourier transform of the dipole moment of an IP (the first summand of the formula (3.54)) in terms of the Fourier transform of the force acting on the IP on the side of a target. Then from Eq. 3.54 the following expression for the Fourier transform of the total radiating dipole moment of the system (the formula (3.58)) can be obtained:

$$\mathbf{D}_{tot}(\omega,\rho) = \frac{e_p}{m_p\,\omega^2} \left\{ \frac{\mathbf{R}}{R} \frac{dU(R)}{dR} \right\}_{\omega,\rho} - e_p \left\{ \frac{\mathbf{R}}{R^3} \int\limits_0^R \beta(r,\omega)\, 4\,\pi\, r^2 dr \right\}_{\omega,\rho}. \tag{3.60}$$

Here the braces designate taking the Fourier transform in view of the dependence Eq. 3.59.

Thus the expressions (3.56), (3.57), and (3.60) give the formal solution of the problem under consideration. Further simplification of these formulas is impossible since the dependence Eq. 3.59 for IP motion in the Thomas-Fermi potential (and its modifications) has no analytical description (in contrast to motion in the Coulomb field).

To carry out numerical calculations, it is convenient from the independent time variable (t) to go to the independent variable R – the distance from an IP to the nucleus. For this purpose we will use the standard representation of trajectory time and angle of rotation of the IP radius vector in terms of R and the parameters ρ and $\mathrm{v_i}$:

$$t(R,\rho,\mathrm{v_i}) = \int\limits_{r_{\min}(\rho,\mathrm{v_i})}^{\mathrm{R}} \frac{\mathrm{dR}}{\mathrm{v_r}(R,\rho,\mathrm{v_i})} \tag{3.61}$$

$$\varphi(R,\rho,\mathrm{v_i}) = \rho\,\mathrm{v_i} \int\limits_{r_{\min}(\rho,\mathrm{v_i})}^{\mathrm{R}} \frac{\mathrm{dR}}{\mathrm{v_r}(R,\rho,\mathrm{v_i})\,R^2}, \tag{3.62}$$

here $\mathrm{v_r}(R,\rho,\mathrm{v_i})$ is the radial IP velocity, the expression for which looks like

$$\mathrm{v_r}(R,\rho,\mathrm{v_i}) = \sqrt{\mathrm{v_i^2} + 2|U|/m_p - \mathrm{v_i^2}\rho^2/R^2}, \tag{3.63}$$

$r_{\min}(\rho,\mathrm{v_i})$ is the minimum distance of IP approach to the center of the scattering potential determined by solution of the equation

$$\mathrm{v_r}(R,\rho,\mathrm{v_i}) = 0. \tag{3.64}$$

Using the Eqs. 3.60, 3.61, 3.62, and 3.63, it is possible to calculate the Cartesian projections (on the focal axes of coordinates – see Fig. 3.7) of the Fourier transform of the radiating dipole moment of the system according to the formulas:

$$\left(\mathbf{D}_{pol}\right)_x(\omega,\rho) = 2\int\limits_{r_{\min}}^{\infty} \cos(\varphi(R,\rho))\,\cos(\omega\,t(R,\rho))\,D_p(\omega,R)\,\frac{dR}{\mathrm{v_r}(R,\rho)}, \tag{3.65}$$

where $D_p(\omega,R)$ is the magnitude of the vector (3.51).

The expression for $\left(\mathbf{D}_{pol}\right)_y$ is obtained by replacement in Eq. 3.65 of cosines by sines.

The diagram of IP scattering by an atom (ion) with indication of the coordinate axes and the angle φ is presented in Fig. 3.7.

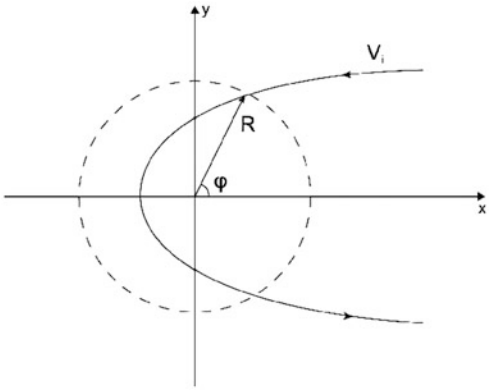

Fig. 3.7 Scattering of an incident particle by a target with the electron core

We will give the results of calculations of spectral effective radiation for electron scattering by a *KII* ion for the following values of parameters $v_i = 1.4$ a.u., $\omega = 0.9$ a.u. The choice of these values is caused by the fact that under conditions of thermodynamically equilibrium plasma of most interest is emission of thermal energy electrons (of the order of the ion ionization potential) of photons with an energy close to the initial IP energy. (The potential of ionization of a *KII* ion is 1.16 a.u.)

To calculate the dipole moment induced in the ion core, we will use the target polarizability density in the Brandt-Lundqvist approximation (the formula (3.35)) shifted in frequency to the value $\Delta\omega = 0.6$ a.u. towards high frequencies. Then the frequency dependence of the dynamic polarizability of the ion core will be approximated to its quantum-mechanical analog.

The electron density of the ion core defining the local plasma frequency was calculated on the basis of numerical integration of the Thomas-Fermi-Dirac equation (with exchange and correlation allowances) with the use of the reduced ionic radius $x_0 = 8.91$ relative units. It will be recalled that the reduced ionic radius is the ratio of the ionic radius R_0 to the Thomas-Fermi radius $a_{TF} = 0.8853/Z^{1/3}$ a.u. In this case the "local plasma radius" (see Eq. 3.38) is $r_p(\omega) = 2.77$ a.u.

Let us introduce into consideration the characteristic radius of radiation in the Kramers limit – $r_{ef}(\omega, v_i)$ – (see [13]), being the solution of the equation

$$\frac{v_i^2}{2} + \frac{|U(r)|}{m_p} = \frac{\omega^2 r^2}{2}. \tag{3.66}$$

This value defines the effective distance of radiation by the static channel. It is essential that in the Kramers limit the value $r_{ef}(\omega, v_i)$ grows with initial velocity.

For the reduced values of parameters and the distribution of electron density of the ion core of a *KII* ion in the Thomas-Fermi-Dirac model we have: $r_{ef}(\omega, v_i) = 1.98$ a.u.

To clarify the appropriateness of using the quasi-classical approach, it should be noted that besides the "global" criterion of quasi-classics (Eq. 3.55), there is also a local criterion that in a three-dimensional case looks like:

$$\eta^{loc}(r) = \frac{\hbar\ \mathrm{div}(\mathbf{p}(\mathbf{r}))}{p^2(\mathbf{r})} << 1. \tag{3.67a}$$

The expression for the local parameter (3.67a) can be rewritten within the framework of the rotation approximation [10] as follows:

$$\eta^{loc}\left(r_{ef}\right) = \hat{\lambda}\left(r_{ef}\right)/r_{ef} << 1, \tag{3.67b}$$

here r_{ef} is given by the formula (3.66). The value (Eq. 3.67b) in the case under consideration is: $\eta^{loc}\left(r_{ef}\right) = 0.22$.

For a special case of a Thomas-Fermi atom (ion) in [10] the analog of the "global" parameter (3.55) was obtained, the reciprocal of which $\varepsilon = 1/\eta$ is given by the formula

$$\varepsilon = \frac{E\, a_{TF}}{Z\, e^2} \equiv 32.6\ \frac{E(\kappa\mathrm{eV})}{Z^{4/3}} \tag{3.67c}$$

Hence for the IP velocity $\mathrm{v_i} = 1.4$ a.u. we find: $\varepsilon = 0.017 << 1$.

Thus the values of the parameters of motion of an IP and a target ion under consideration satisfy the conditions of the quasi-classical approximation for the static Bs spectrum.

The condition of subline quasi-classicity (radiation from the trajectory with a fixed impact parameter ρ) can be written as:

$$\rho\ \mathrm{v_i} \approx \sqrt{l(l+1)} \approx l + 1/2 >> 1. \tag{3.68}$$

The condition (3.68) in our case gives $\rho >> 1$ a.u.

Shown in Fig. 3.8 are the dependences of integrands in the definition of the Fourier transforms of the x- and y-components of the dipole moment induced in the core of a *KII* ion (the real part) on the distance to the nucleus for two values of the impact parameter: (a) $\rho = 1.75$ a.u. and (b) $\rho = 3$ a.u.

In the first case the y-projection of the real part of the induced dipole moment is maximum ($\mathrm{Re}D_y = 2.92$ a.u., $\mathrm{Re}D_x = 1.1$ a.u.), in the second case the x-projection is maximum ($\mathrm{Re}D_x = 2.4$ a.u., $\mathrm{Re}D_y = 1.59$ a.u.).

From Fig. 3.8 it follows in particular that the maximum of the x-component of the dipole moment is reached at the minimum (for the given impact parameter) distance to the ion nucleus. The maximum of the y-component falls on the distance equal to the "plasma" radius $r_p(\omega)$ (for those impact parameters, for which the inequation $r_{\min}(\rho) < r_p(\omega)$ is satisfied).

From Fig. 3.8b it is seen that the integrand for the x-component sharply grows if the equation $r_{\min}(\rho) = r_p(\omega)$ takes place. This equation separates the trajectory of IP motion, at which polarization Bs caused by the x-component of the dipole moment induced in the ion core has maximum.

Let us represent the dependence of the projections of the dipole moments on the impact parameter ρ as a table (Table 3.2).

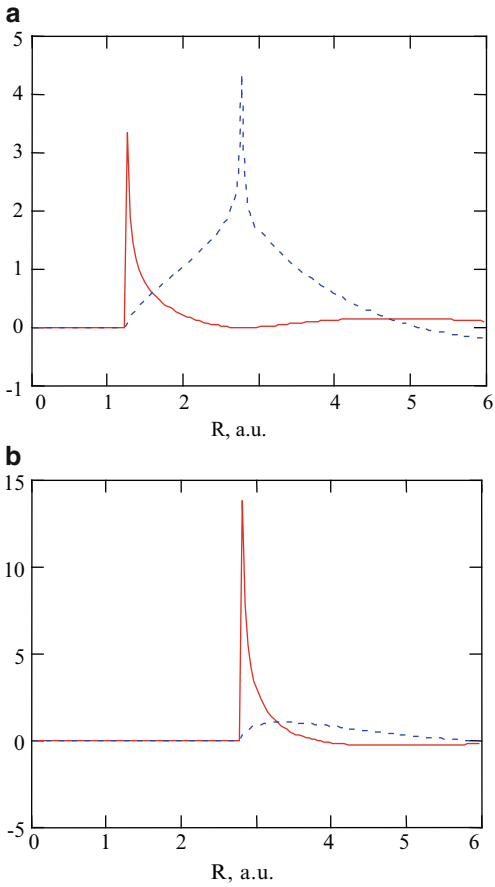

Fig. 3.8 Integrands in the definition of the Fourier transforms of the *x*- (*solid curve*) and *y*- (*dotted curve*) components of the induced dipole moment (the real part) in the core of a *KII* ion ($\omega = 0.9$ a.u., $E = 1$ a.u.) as functions of the distance to the nucleus for the impact parameters: (a) $\rho = 1.75$ a.u. and (**b**) $\rho = 3$ a.u.

Table 3.2 Projections of dipole moments as functions of impact parameter [a.u.]

ρ	1	1.5	2	2.5	3	4	5	6
r_{min}	0.163	0.8	1.58	2.2	2.74	3.76	4.75	5.7
$ReDp_x$	−0.1	1.48	1.0	1.48	2.4	0.73	0.36	0.16
$ReDp_y$	−1.59	2.1	2.9	2.4	1.7	0.86	0.33	0.17
$ImDp_x$	−0.37	1.15	−0.03	−0.22	1.05	0.88	0.29	0.13
$ImDp_y$	−1	0.54	1.1	1.25	1.33	0.68	0.3	0.14

The parameters of calculation were corrected by the conformity of results for the Coulomb potential to exact analytical expressions for the scattering angle.

The calculation in the statistical Thomas-Fermi-Dirac potential shows that for impact parameters lesser than 1.4 a.u. the scattering angle exceeds 180°, which corresponds to beginning of the phenomenon of IP twisting around the target.

On the other hand, for these impact parameters the condition of subline quasi-classical condition is violated, which nevertheless is found to be inessential for

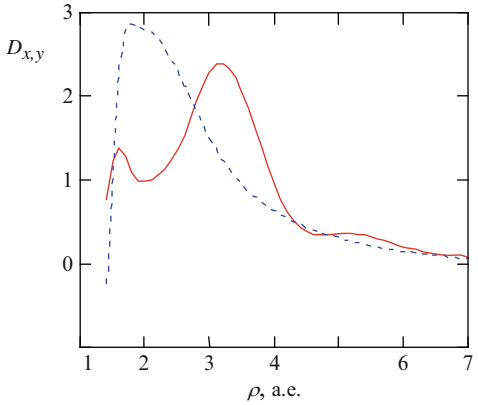

Fig. 3.9 The dependences on the impact parameter of the *x*- (*solid curve*) and *y*- (*dotted curve*) components of the dipole moment induced in the *KII* ion core (the real part) at the frequency $\omega = 0.9$ a.u. in the Brandt-Lundqvist model [5] and the quasi-classical approximation for IP motion

Table 3.3 Effective radiation by the static and polarization channels [a.u.]

Projections, channels	*x*-projection real	imaginary	*y*-projection real	imaginary	Total for each channel
Static	$8.84 \cdot 10^{-6}$		$2.9 \cdot 10^{-6}$		$1.17 \cdot 10^{-5}$
Polarization.	$5.3 \cdot 10^{-6}$	$1.5 \cdot 10^{-6}$	$5.4 \cdot 10^{-6}$	$2.4 \cdot 10^{-6}$	$1.46 \cdot 10^{-5}$

calculation of the polarization channel since small distances to the nucleus make a small contribution to it.

The contribution of these impact parameters ($\rho \leq 1.4$) to effective radiation by the polarization channel is about 1 %.

The obtained dependences of the Fourier transforms $\mathrm{Re}\, D_{x,y}(\omega, \rho)$ on the impact parameter ρ are presented in Fig. 3.9. From this figure it follows in particular that the maximum of the *x*-component of the induced dipole moment in the ion core falls on the impact parameter $\rho_{\max}$ that is approximately equal to the "plasma" radius r_p.

The results of calculation of the values of effective radiation (in atomic units) by the static and polarization bremsstrahlung channels with subdivision to the contributions of the *x*- and *y*-projections are given in Table 3.3.

From Table 3.3 it is seen that in the polarization channel the contribution of the *y*-projection of the dipole moment induced in the core is comparable (and even somewhat exceeds) the contribution of the *x*-projection in contrast to the relation of these contributions to radiation by the static channel. This circumstance is a consequence of the effect of penetration of an IP into the core of a target. This penetration more strongly acts on the *x*-projection, reducing it, than on the *y*-projection. Formally this can be explained by the fact that in motion of an IP along one of the halves of its trajectory its *x*-coordinate changes a sign when crossing the abscissa of the point of

location of the target nucleus, and the y-coordinate is constant-sign and approaches its zero value only at the point of turn of radial IP motion (see Fig. 3.7).

Let us introduce the R-factor characterizing the relative contribution of the polarization channel to bremsstrahlung by the formula:

$$R(\omega) = \frac{d\kappa^{pol}(\omega)}{d\kappa^{st}(\omega)}. \tag{3.69}$$

From the data of Table 3.3 the value of the R-factor in the case under consideration can be determined:

$$\{R\}^{BL}_{clas}(\,\omega = 0.9 \text{ a.u.}, \rho_{\min} = 1.4\,\text{a.u.}) = 1.24. \tag{3.70a}$$

It should be noted that in the value of effective radiation by the static channel an uncertainty remains that is connected with the problem of choosing the lower limit of integration with respect to the impact parameter in the formula (3.36).

For comparative estimation of the relative value of the polarization channel we will use the result of calculation of the static channel contribution within the framework of the rotation approximation (see the paper [10]).

The calculation in the Thomas-Fermi-Dirac model for spectral effective radiation by the static channel gives:

$$\left\{\frac{d\kappa^{rot}_{st}}{d\omega}\right\}_{TFD}(KII,\ \omega = 0.9 \text{ a.u.}) = 5.46 \times 10^{-5}\,\text{a.u.}$$

Hence it follows that the R-factor within the framework of the rotation approximation is:

$$\{R\}^{BL,rot}_{clas,TFD}(KII,\ \omega = 0.9 \text{ a.u.}) = 2.67. \tag{3.70b}$$

However, it should be remembered that the Thomas-Fermi-Dirac model within the framework of the rotation approximation somewhat overestimates the result just for frequencies $\omega \leq 1$ a.u. since in this case the effective radius of radiation r_{ef} (see 3.66) is found to be of the order of the boundary size of an ion, where the statistical model has the greatest error.

So for more correct estimation of effective radiation within the framework of the rotation approximation we use the ion potential in the Slater approximation. Then instead of Eq. 3.70b it can be obtained:

$$\left\{\frac{d\kappa^{rot}_{st}}{d\omega}\right\}_{Slater}(KII,\ \omega = 0.9 \text{ a.u.}) = 4.72 \times 10^{-6}\,\text{a.u.},$$

and correspondingly:

$$\{R\}^{BL,rot}_{clas,Slater}(KII,\ \omega = 0.9 \text{ a.u.}) = 3.1. \tag{3.70c}$$

Thus it can be concluded that the classical estimation for the above values of parameters gives the following lower boundary for the value of the R-factor at a frequency near the potential of ionization of a KII ion for IP of threshold energies (T is the IP energy):

$$R\big(KII,\ \hbar\omega \approx I_p \approx T\big) \geq 2 \tag{3.71}$$

and therefore the contribution of the polarization channel exceeds appreciably the contribution of the static channel to effective radiation of bremsstrahlung.

This conclusion is rather essential since it relates to characteristic "plasma" frequencies (of the order of the ion ionization potential) and a strongly inelastic process, when radiated energy is of the order of the initial IP energy. It is just the situation that is characteristic for Bs in plasma.

3.4 Polarization-Interference Effects in the High-Frequency Limit

From the consideration of effective radiation in collision of an IP with a structural target that was carried out in the previous paragraph within the framework of the classical description of IP motion it follows that the calculation by the obtained formulas is a multistep problem requiring trivariate integration with a singular integrand even for the spectral cross-section. The calculation of the total bremsstrahlung loss, accordingly, results in a quadrivariate integral.

As is known, for static Bs the calculation of total effective radiation is simplified considerably since it is possible to carry out a number of integrations analytically, and the resultant expression (in case of the central potential of scattering) is a single integral, from which all temporal characteristics of IP motion dropped out.

If the polarization channel is taken into account, the situation changes cardinally since the frequency dependence of target polarization in the general case does not allow frequency integration in the expression for total effective polarization radiation.

Assembling the formulas (3.56), (3.57), (3.58), (3.59), and (3.60), we obtain for the total bremsstrahlung loss by the polarization channel in the local plasma frequency approximation:

$$\kappa_{pol} = \frac{4\,e_p^2}{3\,c^3} \int_0^{m_p v_i^2/2\hbar} \omega^4 d\omega \int_0^{\infty} \rho d\rho \left| \int_{-\infty}^{+\infty} dt\, e^{i\omega t} \frac{\mathbf{R}(t,\rho)}{R(t,\rho)^3} \int_0^{R(t,\rho)} \beta(r,\omega)\, 4\pi r^2 dr \right|^2. \tag{3.72}$$

The upper limit of frequency integration reflecting the presence of a short-wavelength limit in Bs is a corollary of quantum relations (the semiclassical approximation [9]) introduced into the classical consideration.

It should be noted that in calculation of the temporal Fourier transform in the formula (3.72) it is possible from time integration to go to integration with respect to the variable distance of an IP to the nucleus R if the radial velocity of IP motion by the formula (3.63) is introduced and the dependences (3.61), (3.62) for the trajectory time and the angle of IP rotation are used.

The description of polarization-interference effects in Bs on a multielectron ion (atom) is simplified considerably in the high-frequency limit, that is, for frequencies much more than the characteristic frequencies of electrons of a target ion. As a result, it appears to be possible to carry out analytical transformations of the formulas describing polarization Bs and to give their descriptive physical interpretation.

Most considerably simplified is the expression for total effective radiation (total bremsstrahlung loss of energy).

Really, in the high-frequency limit the spatial density of the polarizability of the target electron core will be written as:

$$\beta^{hf}(r,\omega) = -\frac{e^2\, n(r)}{m\,\omega^2}. \tag{3.73}$$

It should be noted that the value (3.73) is dimensionless since the concentration of the electron core $n(r)$ has the dimensionality of the reciprocal volume.

For the radiating dipole moment of the core (the polarization channel) with the use of the formulas (3.51) and (3.73) we find the following simple expression:

$$\mathbf{D}^{hf}_{pol}(\mathbf{R},\omega) = e_p \frac{\mathbf{R}}{R^3} \frac{e^2}{m\,\omega^2} N(R), \tag{3.74}$$

here

$$N(R) = \int_0^R n(r)\, 4\,\pi\, r^2\, dr \tag{3.75}$$

is the number of target electrons inside the sphere of the radius R. It should be recalled that R is a distance from an IP to the nucleus of the target.

The physical meaning of Eqs. 3.74 and 3.75 is that the contribution to polarization Bs is made only by the electron density of the target inside the said sphere. The latter is the reflection of the electrostatic fact that a charge placed inside the uniformly charged spherical layer will not experience the Coulomb force. This is true for the process under consideration without real excitation of target electrons since then the core electrons are equivalent to the charge distribution that does not change its geometrical form.

Substituting Eqs. 3.73 in 3.72 results in reduction of frequency degrees, and as a result, changing the order of integration, we obtain:

$$\kappa_{pol}^{hf} = \frac{4\,e_p^2\,e^4}{3\,c^3\,m^2}\int\limits_0^\infty \rho d\rho \int\int dt dt' \int\limits_0^{\mathrm{v}_i^2/2} e^{i\omega(t-t')} d\omega \frac{\mathbf{R}(t)\mathbf{R}(t')}{R^3(t)R^3(t')} N(R(t))N(R(t')). \quad (3.76)$$

Then we use the equation

$$\mathrm{Re}\left\{\int\limits_0^\infty e^{i\omega(t-t')}d\omega\right\} = \pi\delta(t-t').$$

The upper limit here is assumed to be equal to infinity according to the quasi-classical condition $\hbar \to 0$. Going in the formula (3.76) to the integration variable R (after such a replacement the lower limit of integration becomes equal to $r_{\min}(\rho)$, and the result is multiplied by 2 due to the parity of the integrand in the formula (3.76) relative to the change of a time sign) and performing integration with respect to the impact parameter ρ, we find:

$$\kappa_{pol}^{hf} = \frac{8\,\pi\,e^2}{3\,c^3\,m^2\,\mathrm{v}_i}\int\limits_0^\infty f_{pol}^2(r)\sqrt{1-\frac{2U(r)}{m_p\mathrm{v}_i^2}}\,r^2 dr. \quad (3.77)$$

The value $f_{pol}(r)$ appearing here, that is natural to be called polarization force, is determined by the equation:

$$f_{pol}(r) = e_p\,e\frac{N(r)}{r^2}. \quad (3.78)$$

This force (repulsion) acts on an IP on the side of target electrons located inside the sphere of the radius R. With the same force (according to the Newton's third law) the IP accelerates target electrons moving as a single cloud of negative charge, causing polarization Bs.

Let us give here also the expression for total effective radiation by the static channel (see [9]):

$$\kappa_{st} = \frac{8\,\pi\,e_p^2}{3\,c^3\,m_p^2\,\mathrm{v}_i}\int\limits_0^\infty \left(\frac{dU(r)}{dr}\right)^2\sqrt{1-\frac{2\,U(r)}{m_p\mathrm{v}_i^2}}\,r^2 dr. \quad (3.79)$$

It is well seen that the formulas (3.77), (3.79) have a quite similar structure, only the last expression includes the ordinary "static" force:

$$f_{st}(r) = -\frac{dU(r)}{dr}. \quad (3.80)$$

In spite of significant similarity of the Eqs. 3.77 and 3.79, there is also a significant difference between them: the integral of Eq. 3.77 is divergent at the lower limit (in a quasi-classical case as $\int_0 r^{-5/2} dr$) and requires a "cutoff".

The "polarization" integral of Eq. 3.79 at the lower limit is convergent. This is a corollary of taking into account the penetration of an IP into the target core, with the result that the effective electron charge of a ion defining radiation by the polarization channel in the high-frequency limit under consideration decreases.

As a cutoff radius for static effective radiation (3.79), the effective radius of radiation (the formula (3.66)) $r_{ef}(\omega)$ at a frequency corresponding to the initial IP energy is chosen: $\hbar\omega = m\mathrm{v}_i^2/2$.

The formulas (3.76) and (3.77) describe the contribution of each channel to the effective cross-section individually. In fact, in the high-frequency limit under consideration interchannel interference is found to be rather considerable. For total effective radiation of an *electron* the following expression can be obtained in much the same way as this was done above:

$$\kappa_{tot}^{hf} = \frac{8\pi e^2}{3c^3 m^2 \mathrm{v}_i} \int_0^\infty \left(f_{st}(r) - f_{pol}(r)\right)^2 \sqrt{1 - \frac{2U(r)}{m\,\mathrm{v}_i^2}}\, r^2 dr. \tag{3.81}$$

If an effective static charge for an incident electron is introduced by the formula:

$$Z_{ef}(r) = e^{-2} \left| \frac{dU(r)}{dr} \right| r^2, \tag{3.82}$$

then instead of Eq. 3.81 we have:

$$\kappa_{tot}^{hf} = \frac{8\,\pi\, e^6}{3c^3\, m^2\, \mathrm{v}_i} \int_0^\infty \left(N(r) + Z_{ef}(r)\right)^2 \sqrt{1 - \frac{2U(r)}{m\,\mathrm{v}_i^2}}\, r^{-2} dr. \tag{3.83}$$

Hence it is seen that total effective radiation including interchannel interference in the high-frequency limit is defined by the total charge

$$Z = N(r) + Z_{ef}(r) \tag{3.84}$$

that is equal to the charge of the ion nucleus.

To illustrate this fact, given in Fig. 3.10 are the radial dependences of effective polarization (curve 1), static (curve 2), and total (curve 3) charges for a *KII* ion calculated in the Slater model. It is seen that the total charge (3.84) is really equal to the charge of the ion nucleus.

This circumstance is an analog of the effect of atom "stripping" that was for the first time established in the Born approximation [14] for a case of quasi-classical IP motion with penetration into the target core.

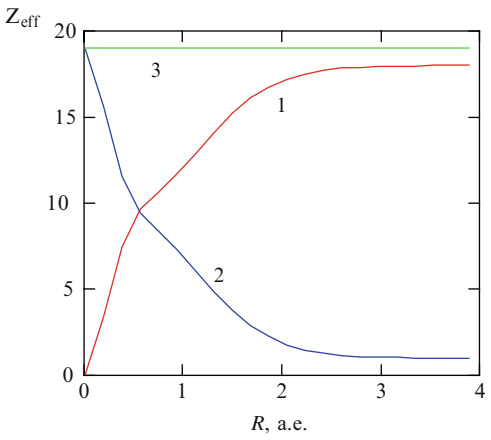

Fig. 3.10 The radial dependences of effective (*1*) polarization, (*2*) static, and (*3*) total charges for a *KII* ion calculated in the Slater model

From Fig. 3.10 it is seen also that the values of effective static and polarization charges are compared for a *KII* ion at a distance about 0.6 a.u. from the nucleus. At longer distances the "polarization" force prevails, at shorter distances the "static" force prevails. In this case it should be remembered that the high-frequency approximation under consideration is true for high enough frequencies

$$\omega > \tilde{\omega}.$$

The analysis shows that the characteristic frequency $\tilde{\omega}$ for a *KII* ion is about 15–20 a.u. (for higher frequencies the polarizability of the target core is close to its high-frequency limit). The effective radii of radiation determined by the Eq. 3.66 in this frequency range satisfy the inequation $r_{ef} < 0.4$ a.u. So the "static" force always exceeds the "polarization" force in the region of truth of the high-frequency approximation.

3.5 Description of Polarization Effects Within the Framework of the Generalized Rotation Approximation

The aim of this paragraph is to simplify the expression for polarization Bs to simple enough calculation formulas. This will allow carrying out numerical estimations of the process cross-sections by the order of magnitude in a wide frequency range in a single manner for any nuclear charges and degrees of target ion ionization and, moreover, it makes it possible to establish qualitative regularities of a phenomenon without resorting to cumbersome calculations. The consistent approach (naturally, within the framework of the plasma model for polarizability) does not allow obtaining simple calculation formulas for *spectral* effective radiation even in the high-frequency limit.

At the same time, as was already said above, in the theory of static Bs there is a rather effective method of approximate calculation of intensity of radiation of a quasi-classical particle, so-called rotation approximation [10], that from the standpoint of the result was found to be more adequate than the consistent classical consideration.

The physical basis of this approach is in the space limitation of a region responsible for radiation by an IP of photons with high enough frequency. The high-frequency behavior, more precisely, the "Kramers behavior", is understood from the standpoint of fulfilment of the inequation [3]:

$$\omega > \omega_{ef}^{Coul} = \frac{m_p \mathrm{v_i}^3}{Z_{ef}\, e_p^2}. \tag{3.85}$$

In this case an IP radiates mainly near the point of turn of its radial motion. It should be noted that quantitatively the rotation approximation also gives a reasonable result in the case $\omega \approx \omega_{ef}^{Coul}$.

For the Bs cross-section integrated with respect to the impact parameter the effective distance (r_{ef}) depends only on the radiated frequency and the target potential and is determined by the Eq. 3.66.

Formally the rotation approximation corresponds to "introduction" into the Eq. 3.60 for total effective static Bs of the delta function of the difference of frequencies ω and the IP rotation frequency at the distance r_{ef}:

$$\omega_{rot}(r) = \frac{\sqrt{\mathrm{v_i}^2 + 2\left|U(r)/m_p\right|}}{r}. \tag{3.86}$$

Thus we come to the following formula for spectral effective radiation *in the rotation approximation* [10]:

$$\left\{\frac{d\kappa_{st}(\omega)}{d\omega}\right\}_{rot} = \frac{8\pi\, e_p^2}{3\, c^3\, m_p^2\, \mathrm{v}_i} \int\limits_0^\infty \left(\frac{dU(r)}{dr}\right)^2 \sqrt{1 - \frac{U(r)}{m_p \mathrm{v}_i^2/2}}\ \delta(\omega - \omega_{rot}(r))\, r^2 dr. \tag{3.87}$$

It seems attractive to generalize the rotation approximation for taking into account radiation by the polarization channel as well.

This is hardly possible to be done strictly since even the static rotation approximation Eq. 3.87 is obtained on the basis of intuitive considerations. So the approach developed below is qualitative, pretending only to the numerical estimation of cross-sections by the order of magnitude.

In the formula (3.87) the information on the vector nature of the radiating dipole moment of an IP is lost. It is connected with the fact that in the high-frequency approximation Eq. 3.85 the main contribution to the process cross-section is made by the x-component of the IP dipole moment. The situation is different for the

polarization channel: for the parameters given in Table 3.3 the contributions of both projections are approximately equal. Therefore in generalization of the rotation approximation for taking into account the polarization channel it is necessary to take into account the features of spatial formation of both Cartesian projections of the dipole moment of the ion core on the axis of the focal system of coordinates.

As seen from Fig. 3.9, the Fourier component of the y-projection of the radiating dipole moment of the target core is defined by the distances of the order of $r_p(\omega)$ (see the formula (3.38)), while the x-component is defined by the distances of most IP approach to the target $r_{\min}$ (the Eq. 3.66).

So it is natural to do the following generalization of the rotation approximation to the polarization channel:

$$\left\{\frac{d\kappa_{pol}(\omega)}{d\omega}\right\}_{rot} = \left\{\frac{d\kappa_{pol}(\omega)}{d\omega}\right\}_{x}^{rot} + \left\{\frac{d\kappa_{pol}(\omega)}{d\omega}\right\}_{y}^{rot}, \tag{3.88}$$

here

$$\left\{\frac{d\kappa_{pol}}{d\omega}\right\}_{x}^{rot} = \frac{8\,\pi\,e^2}{3\,m^2\,c^3\,\mathrm{v_i^2}} \left[\frac{\left|f_x^{pol}(\omega,R)\right|^2 \mathrm{v_r}(R,\rho=0)}{|d\omega_{rot}/dR|}\,R^2\right]_{R=r_{ef}(\omega)} \tag{3.88a}$$

and

$$\left\{\frac{d\kappa_{pol}}{d\omega}\right\}_{y}^{rot} = \frac{8\,\pi\,e^2}{3\,m^2\,c^3\,\mathrm{v_i^2}} \left[\frac{\left|f_y^{pol}(\omega,R)\right|^2 \mathrm{v_r}(R,\rho=0)}{|d\omega_{p}/dR|}\,R^2\right]_{R=r_{p}(\omega)}. \tag{3.88b}$$

The expression for the projection depending on the polarization force frequency is the generalization of the high-frequency analog:

$$f_{x,y}^{pol}(\omega,R) = e_p\,\frac{m\,\omega^2\,R_{x,y}}{e\,R^3}\int_0^R \beta(r,\omega)\;4\pi\,r^2 dr. \tag{3.89}$$

Quantitatively the use of the formula (3.89) instead of Eq. 3.78 means elimination of the abnormally great contribution of low frequencies to the cross-section of polarization Bs arising in case of using the high-frequency approximation near the threshold of target ionization.

It should be noted that the formula (3.89) can be also rewritten in the form similar to Eq. 3.78:

$$f_{x,y}^{pol} = e\,e_p\,\frac{R_{x,y}}{R^3}\;N_{ef}(R,\omega), \tag{3.90}$$

here

$$N_{ef}(R,\omega) = \frac{m\,\omega^2}{e^2}\left|\int_0^R \beta(r,\omega)\,4\,\pi\,r^2\,dr\right| \tag{3.91}$$

is the effective electron charge depending on the frequency and distance to the target nucleus and defining the cross-section of Bs by the polarization channel.

The above formulas for the polarization Bs channel correspond to the simple physical interpretation of this process in the spirit of classical electrodynamics as radiation arising due to acceleration of the effective electron charge of a target under the action of a force from the side of a scattered IP.

According to subdivision of spectral effective radiation by the polarization channel into the sum of contributions of two projections of the induced dipole moment of the target for the spectral R-factor determined by the relation (3.69), within the framework of the generalized rotation approximation it can be written:

$$R^{rot}(\omega) = \frac{1}{2}\left(R_x^{rot}(\omega) + R_y^{rot}(\omega)\right). \tag{3.92}$$

The numerical coefficient in Eq. 3.92 arose due to approximate replacement of the mean squares of sine and cosine of the angle of IP rotation (see Eq. 3.62) by 0.5.

Given in Fig. 3.11a are the frequency dependences of three types of the R-factors appearing in the formula (3.92) for a *KII* ion and threshold energies of an IP. It is essential that the values of the R-factors are compared far from the threshold of target ionization. Near the threshold (for IP energies under consideration) the contribution of the y-component prevails.

The analysis within the framework of the approximation under consideration shows that with growing IP energy the relative contribution of the x-component increases, reaching its maximum value at the energy ($T = m_p\,\mathrm{v}_i^2/2$) determined by the equation:

$$r_{ef}(\omega, T) = r_p(\omega) \tag{3.93}$$

The physical meaning of the formula (3.93) is clear: the generalized rotation approximation predicts the optimum value of initial energy of an IP, at which the effective radius of radiation by the static channel coincides with the "plasma" radius corresponding to the maximum of the spatial density of target polarizability at the given frequency ω. For $\hbar\,\omega = 24.5$ eV the IP energy satisfying the Eq. 3.93 is $T_{opt} = 75$ eV in scattering by a *KII* ion.

Using this model makes it possible to answer an important question: beginning from what frequencies does the high-frequency approximation for the polarization Bs channel work? The comparison of calculation results in the generalized rotation approximation with the high-frequency spectral R-factor is given in Fig. 3.11b.

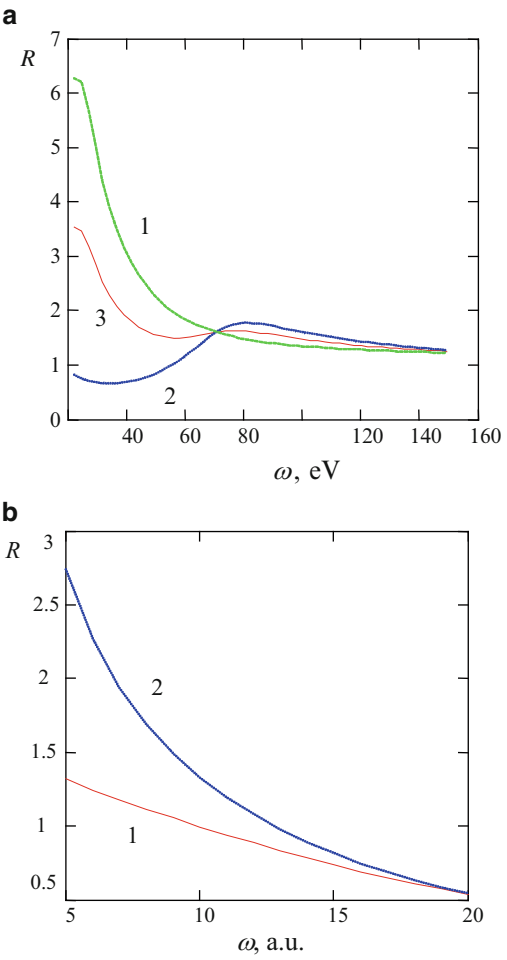

Fig. 3.11 (a) The frequency dependence of the R-factor in different versions of the generalized rotation approximation, when in the PBs cross-section are separated: *1* – "plasma" radius, *2* – effective radius of the static channel, *3* – their half-sum. (**b**) The comparison of the R-factor calculated in the generalized rotation approximation (*1*) with the high-frequency R-factor (*2*) for threshold energies of an IP in its scattering by a *KII* ion

From this figure it is seen that the high-frequency approximation in scattering of an IP of threshold energy by a *KII* ion is true for $\omega > \omega^{rot} = 20$ a.u. With growing IP energy the value ω^{rot} increases.

Let us give the results of calculation of total effective radiation by the polarization channel with the use of the generalized rotation approximation. The corresponding expression (in a somewhat simplified version) looks like:

$$\kappa^{pol}(T) = \frac{8\pi\, e_p^2\, e^4}{3\, c^3 \sqrt{2\, m_p\, T}} \int\limits_{r_{\min}(T)}^{\infty} N_{ef}^2(R,\ \omega_{rot}(R,T)) \sqrt{1 - \frac{U(R)}{T}}\, R^{-2}\, dR, \qquad (3.94)$$

here $r_{\min}(T) = r_{ef}(T,T)$.

Table 3.4 Effective radiation by different channels of a quasi-classical electron on a *KII* ion depending on IP energy

T, a.u. IP energy	3	4	5	10	20
$r_{\min}(T)$, a.u.	1.9	0.95	0.85	0.6	0.42
$\kappa^{st}(T)$ 10^5, a.u. rotation approximation	0.58	0.74	0.86	1.12	1.26
$\kappa^{pol}(T)$ 10^5, a.u. generalized rotation approximation	0.56	0.73	0.86	1.14	1.15
$\kappa^{pol}(T)$ 10^5, a.u. high-frequency approximation	13.2	10	9	5.4	3.2

Though the integral in the formula (3.94) is convergent, we introduced a "cutoff" at the same lower limit as for the static channel since the "non-classical" region of small distances to a nucleus makes a significant contribution for Thomas-Fermi electron distribution overestimating the real electron density near the nucleus. The results of numerical estimations on the basis of the obtained expressions are presented in Table 3.4

In the second line of the table the values of the lower limit in the integrals of Eqs. 3.80 and 3.60 determining total effective radiation by the polarization and static channels are given. It is characteristic for the quasi-classical limit that this value rather weakly decreases with growing IP energy. This defines the weak dependence of total effective radiation on IP energy.

From the calculations carried out within the framework of the generalized rotation approximation it follows that for quasi-classical energies of an incident particle (in terms of fulfilment of the inequations (3.55)) the values of total effective radiation of an electron on a *KII* ion by the static and polarization channels are much the same. The high-frequency approximation overestimates considerably the contribution of the polarization channel, in particular for low IP energies.

The developed approach allows numerical estimations of the contributions of both Bs channels for a wide range of parameters: the charges of ion nuclei Z, the degree of their ionization $q = Z_i/Z$, the frequency of radiation. For this purpose it is convenient to use the Sommerfeld analytical model for the Thomas-Fermi function [7] (see the formulas (A.48) and (A.49)) that makes it possible to carry out calculations rather simply. The results of calculations of the spectral Bs characteristics in the generalized rotation approximation for a wide frequency range and IP of threshold energies ($\hbar\omega \approx T$) are presented in Fig. 3.12a, b.

Following from Fig. 3.12 are the important corollaries of calculations within the framework of the generalized rotation approximation. The contributions of the polarization and static channels to the spectral cross-section of Bs on a *KII* ion for electrons of threshold energies are compared ($R = 1$) at the frequency $\omega^* = 10$ a.u. The maximum of the R-factor is reached for frequencies of the order of the target ionization potential. In this case the generalized rotation approximation gives the following value for the R-factor: $R^{rot}_{\max} \approx 3$. It should be noted that this value represents a lower estimate since the Brandt-Lundqvist model underestimates the value of polarizability.

In the model under consideration the R-factor depends on IP energy (T), growing with T. This has a simple qualitative explanation. With the increase of energy

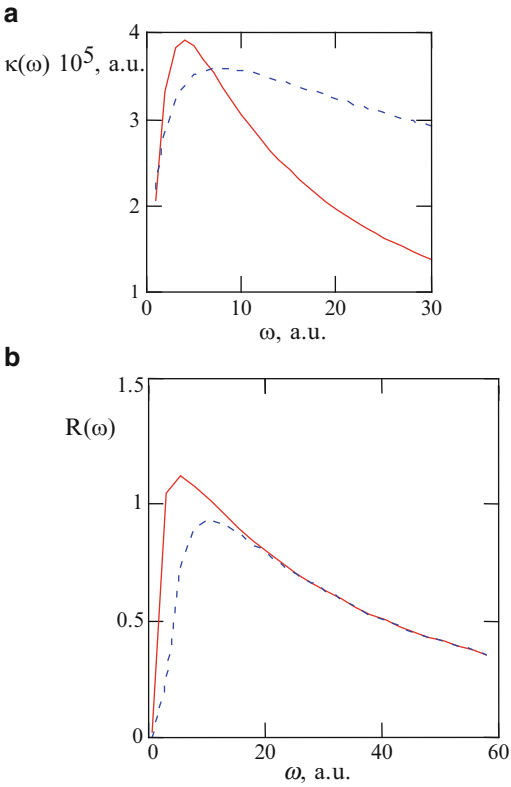

Fig. 3.12 The calculations in the generalized rotation approximation: (a) The spectral dependences of effective radiation of IP of threshold energies by the polarization (*solid curve*) and static (*dotted curve*) channels for $Z = 60$, $q = 0.05$. (**b**) The spectral R-factor for different degrees of ionization: $q = 0.1$ (*solid curve*), $q = 0.2$ (*dotted curve*) and $Z = 60$

(limited by the conditions of usability of the rotation and quasi-classical approximations) the effective radius of the static channel increases: as a result, the effective charge of an ion decreases, the effective electron charge of the core grows.

Given in Fig. 3.12a are the frequency dependences of effective radiation by the polarization (solid curve) and static (dotted curve) channels for a Thomas-Fermi ion (the charge of the nucleus is $Z = 60$, the degree of ionization is $q = 0.05$) up to the kiloelectron-volt energy of a bremsstrahlung photon. It is seen that both dependences have a maximum, and for the polarization channel it is shifted towards lower frequencies. With growing energy of a bremsstrahlung photon effective radiation by the polarization channel (after achievement of the maximum) decreases faster than by the static channel. This is connected with the effect of penetration of an IP into the electron core of a target ion, which, on the one hand, results in increase of the effective charge of the ion defining static Bs, and on the other hand, reduces the dynamic (nondipole) polarizability of the ion core causing polarization Bs.

Presented in Fig. 3.12b are the spectral R-factors for two values of degree of ion ionization: $q = 0.1$ (solid curve), $q = 0.2$ (dotted curve) and the charge of the ion nucleus $Z = 60$. It is seen that the maximum of the R-factor for an ion of lower

charge is reached at lower frequencies, the value of the maximum R-factor is more in magnitude for an ion of a lower degree of ionization. This is explained by higher effective charge and lower nondipole polarizability for an ion of higher charge. With growing photon energy these distinctions (for a multielectron ion) are smoothed, and the values of the R-factors of ions under consideration at higher frequencies are equalized.

Thus it is possible to make a conclusion about the important role of effects of penetration of a radiating electron into the target core for correct description of Bs on multielectron ions of IP of threshold energies. Without considering this phenomenon a qualitatively incorrect result is obtained. For example, the R-factor with growing frequency will tend to the value $1 - q$ (equal to the ratio of the number of bound electrons to the nuclear charge), but not to zero as it should be according to the physics of the process.

Presented in Fig. 3.13a, b are the dependences of the spectral R-factor on the ion charge for different Bs frequencies (a) and nuclear charges (b) calculated for IP of threshold energies. This figure demonstrates the presence (within the framework of the generalized rotation approximation used here) of the optimum ion charge $Z_i^{opt}e$, at which the value of the R-factor (at a frequency characteristic for a given ion) is maximum. This circumstance is a nontrivial fact. Really, for a one-electron ion (and in the case $q \approx 1$) the function $R(Z_i)$ is monotonically decreasing since then the value defining the R-factor is proportional to the reciprocal ion charge: $\omega^2\alpha(\omega)/Z_i(\omega) \propto 1/Z_i$ (for frequencies of the order of the ion ionization potential).

For a multielectron ion the behavior of this dependence is unobvious, and in the general case an answer can be given only within the framework of the approximate description of Bs.

From Fig. 3.13a it follows that the optimum charge $Z_i^{opt}\,e$ grows with decreasing frequency of radiation, and the maximum value of the R-factor in this case somewhat decreases. With growing charge of the ion nucleus (Fig. 3.13b) the value $Z_i^{opt}\,e$ is shifted to the region of high values, and the value of the R-factor appreciably increases. At the same time for low ion charges the R-factors calculated at corresponding (different!) characteristic frequencies do not depend on the nuclear charge.

Let us apply the obtained formulas for calculation of spectral effective radiation in scattering of an electron with an energy of 1 and 10 keV by tungsten ions with different charges. The corresponding diagrams are given in Figs. 3.14 and 3.15. From the given figure it follows that the static channel prevails over the polarization channel throughout the region of frequencies.

With growing IP energy, as seen from Fig. 3.15, a spectral range from 350 to 750 keV takes place, in which the polarization channel prevails over the static channel. According to Figs. 3.14 and 3.15, effective radiation by the polarization channel has a maximum in the low-frequency region of the spectrum that is shifted to the region of high photon energies with increasing IP energy.

Presented in Fig. 3.16 are the calculations of the spectral R-factor (3.69) for Bs of different energies on tungsten ions.

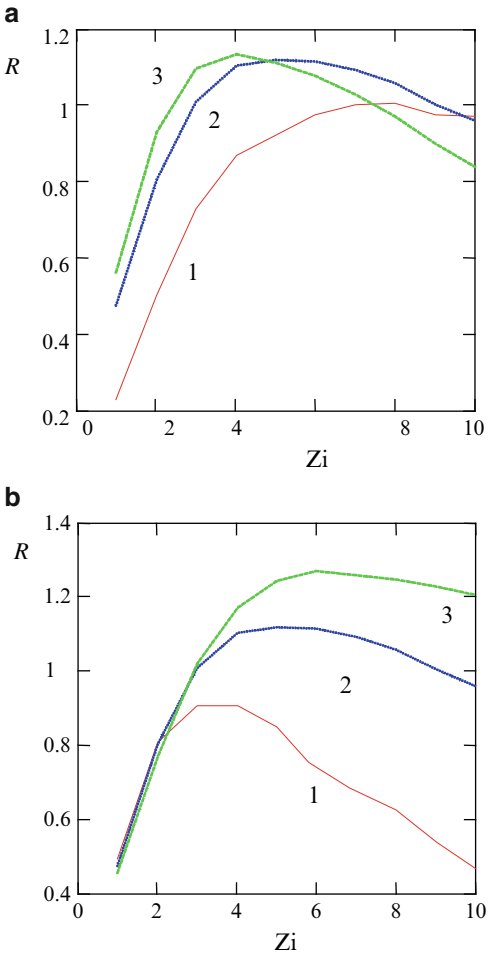

Fig. 3.13 Calculations in the generalized rotation approximation of the dependences of the R-factor on the ion charge at a fixed frequency multiple of the target ionization frequency in the Thomas-Fermi model $\hbar\,\omega = k\,I_p^{TF}$. (a) as functions of the ion charge at different frequencies: $1 - k = 1, 2 - k = 2, 3 - k = 3$. (**b**) the same at the fixed frequency ($\hbar\,\omega = 2\,I_p^{TF}$) for different charges of the ion nucleus: $1 - Z = 30$, $2 - Z = 60$, $3 - Z = 90$

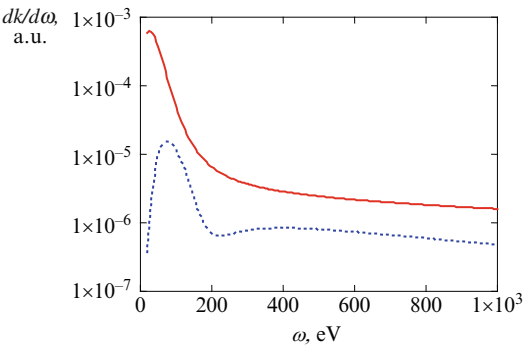

Fig. 3.14 The spectrum of effective radiation in scattering of an electron of energy 1 keV by a tungsten ion with the charge $Z_i = 20$: *solid curve* – static channel, *dotted curve* – polarization channel

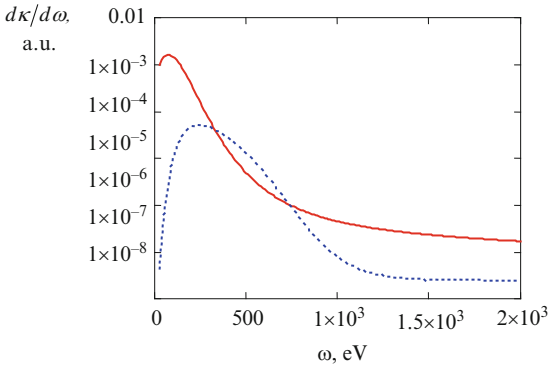

Fig. 3.15 The spectrum of effective radiation in scattering of an electron of energy 10 keV by a tungsten ion with the charge $Z_i = 38$: *solid curve* – static channel, *dotted curve* – polarization channel

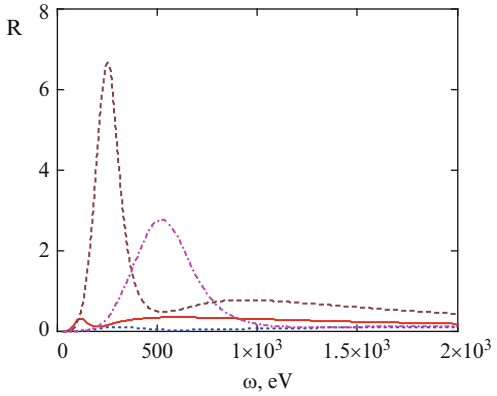

Fig. 3.16 The spectral *R*-factor for Bs on tungsten at different ion charges and IP energies: *solid curve* – Z_i =20, E = 1 keV; *dotted curve* – Z_i =38, E = 1 keV; *dashed curve* – Z_i =20, E = 10 keV; *dash-and-dot curve* – Z_i =38, E =10 keV

It is seen that with growing IP energy (10 keV) the contribution of PBs grows especially for rather low ion charges Z_i =20, when the maximum $R_{max} = 6.8$ is observed in a low-frequency range of the order of 200 keV. With increasing ion charge (at the same IP energy of 10 keV) the maximum of the spectral *R*-factor is shifted to the region of high photon energies (about 500 keV), becoming in this case more wide. In case of low IP energies (1 keV) the *R*-factor is less than one throughout the spectral range for the considered tungsten ions. This is explained by deep penetration of an IP into the ion core for emission of a photon at a low IP energy (1 keV).

Thus the use of the generalized rotation approximation in the description of polarization effects for IP of threshold energies on multielectron ions is found to be rather effective for revealing qualitative regularities of behavior of both Bs channels.

At the end of this paragraph we will make a useful remark on determination of the effective charge of an ion in the rotation approximation $Z_{ef}^{rot}\, e$ (e is the elementary charge) that, in particular, can be used in estimation of effective radiation by the static channel on the basis of the known Kramers formula:

$$\frac{d\kappa^{(Kram)}}{d\omega} = \frac{16\,\pi\, Z_{ef}^2\; e^6}{3\,\sqrt{3}\; m^2\, \mathrm{v}^2\, c^3}\,. \tag{3.95}$$

The matter is that the simple use of the formula (3.79) with substitution of the effective radius of radiation in it leads, generally speaking, to an incorrect result.

The correct expression for the charge number Z_{ef}^{rot} can be obtained from Eq. 3.87 with the use of simple algebraic transformations, it looks like:

$$Z_{ef}^{rot} = \left\{ \frac{r^2\; |dU/dr|}{e\;\sqrt{e^2 + |dU/dr|/(m\,\omega^2 r)}} \right\}_{r=r_{ef}(\omega,T)}, \tag{3.96}$$

where e is the elementary charge.

For Bs on a *KII* ion in the Thomas-Fermi-Dirac model from Eq. 3.96 we find: $Z_{ef}^{rot}(\omega = 0.9\ \text{a.u.},\ T = 1\ \text{a.u.}) = 1.83$ and, accordingly, $d\kappa^{Kr}\big(\omega, Z_{ef}\big)/d\omega = 6.3 \times 10^{-6}$ a.u..

References

1. Landau, L.D., Lifshits, E.M.: The Classical Theory of Fields, 4th edn. Pergamon, New York (1975)
2. Fermi, E.: Uber die Theorie des Stossen zwishen Atomen und electrisch geladenen Teilchen. Z. Physik **29**, 315 (1924)
3. Kogan, V.I., Kukushkin, A.B., Lisitsa, V.S.: Kramers electrodynamics and electron-atomic radiative-collisional processes. Phys. Rep. **213**, 1 (1992)
4. Bethe, H., Heitler, W.: On stopping of fast particles and on creation of positive electrons. Proc. Roy. Soc. Lond. A **146**, 83 (1934)
5. Brandt, W., Lundqvist, S.: Atomic oscillations in the statistical approximation. Phys. Rev. **139**, A612–A617 (1965)
6. Korol', A.V., Lyalin, A.G., Obolenskii, O.I., Solov'yov, A.V.: The role of the polarization mechanism for emission of radiation by atoms over a broad photon frequency range. JETP **87**, 251 (1998)
7. Gombas, P.: Die Statistische Theorie des Atoms und ihre Anwendungen. Springer, Wien (1949)
8. Vinogradov, A.V., Shevelko, V.P.: Static dipole polarizability of atoms and ions in Thomas-Fermi model. Trudy FIAN **119**, 158 (1980) (in Russian)
9. Gervids, V.I., Kogan, V.I.: Penetration and screening effects in electron bremsstrahlung on ions. JETP Lett. **22**, 142 (1975)
10. Kogan, V.I., Kukushkin, A.B.: The emission from quasi-classical electrons in an atomic potential. Sov. Phys. JETP **60**, 665 (1984)

11. Pratt, R.H., Tseng, H.K.: Tip region of the bremsstrahlung spectrum from incident electrons of kinetic energy 50 keV–1.84 MeV. Phys. Rev. A **11**, 1797 (1975)
12. Buimistrov, V.M., Trakhtenberg, L.I.: The role of atomic electrons in bremsstrahlung. Sov. Phys. JETP **46**, 447 (1977)

Chapter 4
Bremsstrahlung in Plasma with Account for the Polarization Channel

4.1 Total and Spectral Intensities of Radiation of Quasi-Classical Electrons on Atoms and Ions

At the beginning of this chapter we summarize the general expressions describing bremsstrahlung of quasi-classical electrons on targets both having an electron core and representing a "bare" atomic nucleus.

4.1.1 Main Expressions

According to classical electrodynamics, the instantaneous (at a given instant of time t) power of dipole radiation of the charge e is expressed by the formula

$$Q(t) = \frac{2\,e^2}{3\,c^3}|\ddot{\mathbf{r}}(t)|^2, \tag{4.1}$$

where c is the velocity of light in free space, $\ddot{\mathbf{r}}(t)$ is the charge acceleration. The dipole behavior of radiation means that its wavelength is much longer than the characteristic dimensions of the radiating system. In this section we will be interested in radiation in infinite motion of a charged particle. Then the trajectory of motion will be characterized by the impact parameter ρ: $\mathbf{r} = \mathbf{r}(t, \rho)$. Knowing the instant radiation power, it is possible to calculate the total energy of the electromagnetic field radiated in charge scattering by the external potential with the specified impact parameter ρ:

$$\Delta E(\rho) = \int\limits_{-\infty}^{\infty} Q(t, \rho)\, dt. \tag{4.2}$$

V. Astapenko, *Polarization Bremsstrahlung on Atoms, Plasmas, Nanostructures and Solids*, Springer Series on Atomic, Optical, and Plasma Physics 72,
DOI 10.1007/978-3-642-34082-6_4, © Springer-Verlag Berlin Heidelberg 2013

In classical physics for characterization of the radiative process the special value κ is introduced that is called *effective radiation* and is determined by the following equation:

$$\kappa = \int_0^\infty \Delta E(\rho)\, 2\,\pi\,\rho\, d\rho. \tag{4.3}$$

Appearing here is the total energy $\Delta E(\rho)$ radiated during charge scattering that is given by the expressions (4.1) and (4.2). Effective radiation describes the contribution to the process of all possible trajectories of charge motion characterized by different impact parameters and orientations of orbit planes (the multiplier $2\,\pi$). For transformation of the formula (4.3) we will use the known relation:

$$\int_{-\infty}^{\infty} f^2(t)\, dt = \frac{1}{\pi} \int_0^\infty |f(\omega)|^2 d\omega, \tag{4.4}$$

where $f(t)$ is the real time function, $f(\omega)$ is its Fourier transform. In our case $f(t) = |\ddot{\mathbf{r}}(t)|$, then $f(\omega) = \omega^2 |\mathbf{r}(\omega)|$ according to the property of the Fourier transform of a derivative. In view of Eq. 4.4, the formulas (4.1), (4.2), and (4.3) give

$$\kappa = \int_0^\infty \frac{d\kappa}{d\omega} d\omega, \tag{4.5}$$

where $d\kappa/d\omega$ is spectral effective radiation, for which the equation is true:

$$\frac{d\kappa}{d\omega} = \frac{4\,e^2\,\omega^4}{3\,c^3} \int_0^\infty |\mathbf{r}(\omega, \rho)|^2\, \rho\, d\rho. \tag{4.6}$$

As seen from the above formulas, effective radiation has a dimensionality of energy multiplied by area. To obtain the expression for radiation power, effective radiation should be multiplied by the density of the flux of charged particles (electrons) scattered by the potential $j = n\,\mathrm{v}$ (n is the concentration of incident particles, v is their velocity far from the scattering center):

$$dQ/d\omega = (d\kappa/d\omega)\, j.$$

Then for the spectral radiation power we obtain

$$\frac{dQ}{d\omega} = \frac{4\,e^2\,\omega^4}{3\,c^3}\, n\,\mathrm{v} \int_0^\infty |\mathbf{r}(\omega, \rho)|^2\, \rho\, d\rho. \tag{4.7}$$

The total radiation power in charge scattering by the external potential will be obtained after taking an integral of Eq. 4.7 with respect to positive frequencies up to the maximum frequency $\omega_{\max} = E/\hbar$ defined by the energy conservation law:

$$Q = \int_0^{\omega_{\max}} \frac{dQ}{d\omega}\, d\omega. \tag{4.8}$$

In case of a spherically symmetric potential it is possible to obtain a closure for the total radiation power with the use of the formulas (4.1), (4.2), and (4.3). For this purpose we will use the Newton's second law that in the field of central conservative forces looks like

$$\ddot{\mathbf{r}}(t) = -\frac{1}{m}\,\frac{\mathbf{r}}{r}\,\frac{dU}{dr}. \tag{4.9}$$

Substituting Eq. 4.9 in Eq. 4.1, we find

$$Q(t) = \frac{2\,e^2}{3\,m^2\,c^3}\left|U_r'(r(t))\right|^2, \tag{4.10}$$

where $r(t)$ is given by the motion trajectory, and the prime means a derivative with respect to the radius vector magnitude. Then for the total radiated energy from Eqs.4.10 and 4.2 we have

$$\Delta E(\rho) = \frac{4\,e^2}{3\,m^2\,c^3}\int_{r_{\min}}^{\infty} \left|U_r'\right|^2 \frac{dr}{\mathrm{v}_r(r,\rho)}. \tag{4.11}$$

In this equation we went from time integration to integration with respect to the radius vector magnitude using the replacement $dt = dr/\mathrm{v}_r$, where $\mathrm{v_r}$ is the radial velocity of a particle (3.63) depending on the distance to the potential center and the impact parameter ρ. Substituting Eq. 4.11 in Eq. 4.3, integrating with respect to $d\rho$, and going to the radiation power by multiplying by the density of the flux of incident electrons $j_e = n_e\,\mathrm{v}_e$, we find

$$Q = \kappa\, n_e\, \mathrm{v}_e = \frac{8\,\pi\,e^2\,n_e}{3\,m_e^2\,c^3\,\mathrm{v}_e}\int_0^{\infty} r^2\left|U_r'\right|^2\sqrt{\mathrm{v}_e^2 - \frac{2}{m_e}\,U(r)}\,dr. \tag{4.12}$$

Here is taken into account that $E = m\,\mathrm{v}_e^2/2$. For the Coulomb attractive potential the formula (4.12) gives

$$Q_{Coul} = \frac{8\,\pi\,e^6\,n_e}{3\,m_e^2\,c^3\,\mathrm{v}_e}\int_0^{\infty} r^{-2}\sqrt{\mathrm{v}_e^2 + \frac{2\,Z\,e^2}{m_e\,r}}\,dr. \tag{4.13}$$

Hence it is seen that the total intensity of radiation of charge scattering by the Coulomb potential calculated within the framework of classical physics *diverges* at small distances from the potential center as $r^{-3/2}$. This difficulty of the classical theory is a matter of principle since it results from neglect of wave properties of particles. To overcome it, the lower limit of integration in the formulas (4.12) and (4.13) should be replaced by the de Broglie wavelength for an electron:

$$r_{\min} = \lambda\!\!\!^{-}_{DB} = \frac{\hbar}{m_e \mathrm{v}_e}. \tag{4.14}$$

This replacement means taking into account the fact that the distance between an incident particle and the potential center can not be determined more precisely than its de Broglie wavelength $\lambda\!\!\!^{-}_{DB}$. This value characterizes the diffusiveness of a particle trajectory due to its intrinsic wave properties. It should be noted that in case of the Coulomb repulsive potential, when the potential energy is positive, the minimum distance will be determined from the non-negativity constraint for the radicand on the right side of the Eq. 4.12, that is

$$r_{\min} = \frac{2Ze^2}{m_e \mathrm{v}_e^2}. \tag{4.15}$$

4.1.2 High-Frequency Radiation. Kramers Electrodynamics

In scattering of an electron with the initial velocity v_e by the external potential $U(r)$ it is possible to determine scale distances and frequencies characterizing this scattering. The scale distance $r = a$ is determined by the relation ($E = m_e \mathrm{v}_e^2/2$)

$$E \approx |U(a)|. \tag{4.16}$$

The formula (4.16) has a simple physical meaning: at a characteristic distance the initial energy of an electron and the magnitude of its potential energy are compared. At distances $r>>a$ the effect of the potential on the electron motion is low. In the opposite limit $r<<a$ the initial energy of an electron can be neglected in comparison with its potential energy. In case of the Coulomb potential the characteristic length scale is called the *Coulomb length*:

$$a_{Coul} = \frac{Ze^2}{m_e \mathrm{v}_e^2}. \tag{4.17}$$

The squared Coulomb length defines the cross-section of elastic scattering of charges and a number of other collisional characteristics. It can be separated in the

formula (4.13) describing the radiation power in scattering in the Coulomb field. The Coulomb length (accurate to the multiplier) is equal to the minimum distance in scattering in the repulsive potential (4.15).

The characteristic scattering frequency is given by the ratio of the initial velocity of an electron and the characteristic length: $\tilde{\omega} = \mathrm{v}_e / a_{Coul}$. In case of the Coulomb field this gives

$$\tilde{\omega} \equiv \omega_{Coul} = \frac{m\,\mathrm{v}_e^3}{Z\,e^2}. \tag{4.18}$$

The Coulomb frequency (4.18) defines the characteristic frequency of electron radiation in the Coulomb field. High-frequency radiation

$$\omega >> \omega_{Coul} \tag{4.19}$$

has its specific features. Let us consider them by the example of the Coulomb attractive potential. Rigorous analysis based on the exact solution of the equations of charge motion in the Coulomb field shows that radiation in the high-frequency range Eq. 4.19 is "gathered" from the trajectory section near the turning point $r \approx r_{\min}$, where the acceleration of a particle is maximum. Then the radiated frequency is close to the frequency of rotation (the angular velocity) of a charge on the section of the trajectory of the most approach:

$$\omega \approx \omega_{rot}(r_{\min}) = \frac{\mathrm{v}(r_{\min})}{r_{\min}}. \tag{4.20}$$

It should be noted that on the section under consideration the radial electron velocity is equal to zero, so it coincides with the azimuthal velocity, therefore

$$\mathrm{v}(r_{\min}) = \frac{\rho\,\mathrm{v}_e}{r_{\min}}. \tag{4.21}$$

The Eq. 4.21 follows from the angular momentum conservation law in the spherically symmetric potential. For the Coulomb field of attraction we have

$$r_{\min}(\rho) = a_{Coul}\left[\sqrt{1 + \frac{\rho^2}{a_{Coul}^2}} - 1\right]. \tag{4.22}$$

If Eqs. 4.21 and 4.22 are substituted in the right side of the Eq. 4.20, then in view of the definition (4.18) it can be seen that the inequation (4.19) is satisfied only for low impact parameters:

$$\rho << a_{Coul}. \tag{4.23}$$

Thus high-frequency radiation of Eq. 4.19 occurs on trajectories of charge motion with a low impact parameter, when a particle at the point of the maximum

approach has a high enough rotational velocity (4.20) to radiate an electromagnetic wave of a specified frequency.

It should be noted that in the case (4.23) charge scattering occurs at large angles $\theta \approx \pi$. The last relation follows from the connection between the impact parameter and the angle of scattering in the Coulomb field $a_{Coul} = \rho\,\mathrm{tg}(\theta/2)$. Thus corresponding to high-frequency radiation of Eq. 4.19 is the motion *along strongly curved trajectories* with low impact parameters. The features of collisional-radiative processes under such conditions are described by the *Kramers electrodynamics*. From the above it follows that in the case (Eq. 4.19) under consideration, when the inequation (4.23) is satisfied, for the minimum distance from a scattering particle to the potential center the approximate equation is true:

$$r_{\min}(\rho << a_{Coul}) \approx \frac{\rho^2}{2\,a_{Coul}} << \rho. \tag{4.24}$$

The obtained relation follows from Eq. 4.22. Substituting Eqs. 4.21, 4.24 in the formula (4.20), we come to the following estimation:

$$\omega \approx \omega_{rot}(r_{\min}) \approx 4\left(\frac{a_{Coul}}{\rho}\right)^3 \omega_{Coul}. \tag{4.25}$$

Since $\rho << a_{Coul}$ are considered, from Eq. 4.25 the inequation (4.19) follows, that is, radiation really occurs at a frequency much higher than the characteristic Coulomb frequency.

4.1.3 Total Radiation Power

The expression for the total (throughout the spectral range) power of radiation arising as a result of electron scattering by an atom (ion) can be obtained by integrating the expression (3.87) with respect to frequency in view of the presence of a delta function and by multiplying it by the electron flow density. As a result, in the quasi-classical approximation for plasma electron motion we find

$$Q = \frac{8\,\pi\,e^2\,n_e}{3\,m_e^2\,c^3\,\mathrm{v}_e} \int\limits_{\dot{z}_{DB}}^{\infty} r^2 |f(r)|^2 \sqrt{\mathrm{v}_e^2 - \frac{2}{m_e}\,U(r)}\,dr, \tag{4.26}$$

where $f(r)$ is the force causing radiation of electromagnetic waves. In the case that this is the ordinary ("static") force $f_{st}(r) = -dU/dr$, the expression (4.26) describes the intensity of radiation by the "static" channel, when the core of a target is supposed to be "frozen". And if $f(r)$ is the polarization force (3.78), the power (Eq. 4.26) corresponds to the polarization channel of radiation. It will be recalled

that in the quasi-classical limit bremsstrahlung and recombination radiation are described by a common expression, and the difference is that the photon energy in recombination radiation is more than the initial electron energy.

4.2 Bremsstrahlung of Thermal Electrons on the Debye Sphere Around an Ion in Plasma

In plasma, besides polarization bremsstrahlung of electrons on atoms and ions, it is necessary, generally speaking, to take into account radiation caused by the presence of the Debye sphere around ions. This radiation arises with impact parameters that are more than the ion size that in this case can be considered to be the point size. The point ion together with the Debye sphere formed by plasma electrons is a peculiar atom, with the essential difference that instead of bound electrons its "nucleus" (ion) is screened by plasma electrons that are free. Nevertheless, the said analogy makes it possible for description of PBs on the Debye sphere to use the approach developed for radiation in electron-atom collisions.

PBs on the Debye sphere was for the first time considered by V.N. Tsytovich and A.V. Akopyan for a case of fast (superthermal) electrons moving along straight-line trajectories. This kind of polarization Bs in the original works [1, 2] was called *transient Bs*.

In this section we will consider polarization Bs in the limit opposite in electron motion velocity (when the inequation (3.1) is satisfied), which is more adequate for plasma electrons, the characteristic velocity of which is of the order of the thermal velocity.

To obtain effective radiation by the polarization channel, we use the expression (4.26), in which it is necessary to substitute the formula for the polarization force (3.78) and the Debye potential of an ion in plasma:

$$U_D(r) = -\frac{Z_i\, e^2}{r}\, \exp(-r/r_D), \tag{4.27}$$

here r_D is the Debye radius. After simple algebraic transformations with the use of the relation $Q = \kappa\, n_e\, \mathrm{v}_e$, assuming that $m_e \mathrm{v}_e^2/2 = T$ (T is the temperature of plasma electrons in energy units), the expression for effective radiation by the polarization channel can be written as:

$$\kappa_{pol}^{D} = \frac{8\pi\, e^6}{3 m_e\, c^3 \sqrt{2\, m_e\, T}}\, \frac{Z_i^2}{r_D}\, \Phi\left(\frac{2a_T}{r_D}\right), \tag{4.28}$$

here the function is introduced:

$$\Phi(x) = \int_0^\infty \frac{dr}{r^2}\, \left[1 - e^{-r}\,(1+r)\right]^2 \sqrt{1 + \frac{x}{r} e^{-r}}. \tag{4.29}$$

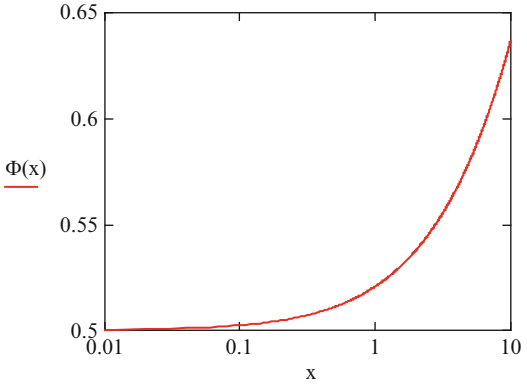

Fig. 4.1 The function Φ(x) defining PBs of thermal electrons on the Debye sphere in plasma

The parameter $a_T = Z_i\, e^2/2T$ is the Coulomb length in scattering of an electron with the energy T by an ion with the charge $Z_i\, e$. The plot of this function is presented in Fig. 4.1.

It should be noted that the ratio $\xi = 2a_T/r_D$ is proportional to the nonideality parameter (the ratio of average potential energy to average kinetic energy) for plasma. For ideal plasma one has $\xi << 1$. And if $\xi > 1$, the condition of idealness ($n_e r_D^3 >> 1$) is violated, and the nature of screening of an ion in plasma will change too.

As seen from Fig. 4.1, the function (4.29) grows very slowly with its growing argument, its derivative at zero is: $\Phi'(0) = 0.025$, so for all cases of practical interest it is possible to suppose $\Phi = 0.5$. Therefore from the expression (4.28) it follows:

$$\kappa_{pol}^{D} = \frac{4\pi\, e^6}{3m_e\, c^3 \sqrt{2\, m_e\, T}} \frac{Z_i^2}{r_D}\ . \tag{4.30}$$

The formula (4.30) that is true for arbitrary quasi-classical motion of an electron after multiplication by the electron flow density coincides (in terms of one ion) with the expression for the total power radiated by the polarization channel that for the first time was obtained by V.N. Tsytovich for *straight-flight* electrons [1].

Thus it can be concluded that under conditions of ideal plasma the nature of motion of an electron weakly influences its radiation by the *polarization* channel.

For effective static radiation in the Coulomb field of the ion from the formula (4.12) in view of the integral "cutoff" at the lower limit of Eq. 4.14 it can be obtained:

$$\kappa_{st} = \frac{8\pi\, Z_i\, e^6\, \sqrt{T/Ry}}{9\, c^3\, m_e\, \hbar} \left[\left(\frac{x_m + 2}{x_m} \right)^{3/2} - 1 \right], \tag{4.31}$$

where $x_m = \left(2\sqrt{T/Ry}/Z_i\right)^{2/3}$, $Ry = 13.6$ eV. In the limit $x_m << 1$ the expression (4.31) is simplified to the form:

$$\kappa_{st} = \frac{8\sqrt{2}\,\pi}{9}\,\frac{Z_i^2\,e^6}{\hbar\,m_e\,c^3}. \tag{4.32}$$

It should be noted that the Planck constant in the quasi-classical equations (4.31 and 4.32 arose because of its presence at the lower limit of the "cutoff" of the integral in Eq. 4.12 with respect to distance (Eq. 4.14). The expression (4.32) differs from the Kramers formula for effective radiation that can be obtained from Eq. 5.76 by the multiplier $\sqrt{2/3} \simeq 0.816$.

From the formulas (4.32) and (4.30) with the use of the expression for the electron Debye radius $r_D = \sqrt{T/4\,\pi\,e^2\,n_e}$ we find for the ratio of the contributions of the polarization and static channels:

$$\Re^D(n_e, T) = \frac{\kappa_{pol}^D}{\kappa_{st}} \cong 3\,\frac{\sqrt{n_e/n_a}}{(T/2\,Ry)}, \tag{4.33}$$

where $n_a = a_B^{-3} \simeq 6.8 \cdot 10^{24}$ cm^{-3} is the atomic concentration. As seen from Eq. 4.33, for the appreciable contribution of polarization effects to Bs on an ion with Debye screening plasma should be as dense and cold as possible.

Let us perform a numerical estimation of the value $\Re$ for laser plasma with the following parameters: $n_e \approx 7{\cdot}10^{18}$ cm^{-3}, $T \approx 1$ eV, then $\Re \approx 10$ %. And if $n_e \approx 7{\cdot}10^{20}$ cm^{-3}, then $\Re \approx 100$ %, but then the plasma parameter becomes less than one, and plasma becomes nonideal.

It is of interest to estimate the contribution of polarization Bs for plasma of the inner regions of Sun: $n_e \approx 5.7{\cdot}10^{25}$ cm^{-3}, $T \approx 1{,}550$ eV. For these values with the use of Eq. 4.33 we find: $\Re \approx 15$ %.

Let us write out the expression for the ratio $\Re$ in terms of the Debye number (the parameter of plasma idealness) $N_D = (4\pi/3)\,r_D^3\,n_e$:

$$\Re(n, N_D) \approx 1.24\,\frac{(n/n_a)^{1/6}}{N_D^{2/3}}. \tag{4.34}$$

Hence it is seen that for the fixed parameter of plasma idealness N_D the ratio $\Re$ is a very weak function of the concentration of plasma electrons.

From the consideration carried out it follows that the contribution of polarization effects to the total bremsstrahlung loss of plasma electrons on the Debye sphere surrounding an ion in nondegenerate plasma can be comparable with the contribution of ordinary (static) Bs only for cold and dense enough plasma, when the idealness parameter N_D is of the order of one. Otherwise the ratio of the contributions of the polarization and static channels does not exceed 10–15 %.

For spectral effective PBs within the framework of the rotation approximation (3.88a) (neglecting the y-component of the polarization force) and the explicit expression for the derivative $|d\omega_{rot}/dR|$ following from the formula

$$\omega_{rot}(R) = \frac{\sqrt{v_e^2 + 2\,|U_D(R)/m_e|}}{R}, \tag{4.35}$$

the expression can be obtained:

$$\frac{d\kappa_{pol}^{(rot)}}{d\omega} = \frac{8\,\pi\,\hbar\,\left|f_{pol}\left(r_{ef}(\omega)\right)\right|^2}{3\,m_e^2\,c^3\,\sqrt{2\,T/m_e}}\,\frac{r_{ef}^4(\omega)}{1 + \left|U_D'\left(r_{ef}(\omega)\right)\right|/\left(m_e\,\omega^2\,r_{ef}(\omega)\right)}, \tag{4.36}$$

where $U_D' = dU_D/dr$, $r_{ef}(\omega)$ is the effective distance, at which radiation of electromagnetic waves of a specified frequency occurs, it is given by solution of the Eq. 3.66, in which it is necessary to suppose $U \to U_D$, $m_p \to m_e$ and $v_i \to v_e$.

To calculate the polarization force $f_{pol}(r)$ determined by the formula (3.78), we will use the expression for electron concentration in the Debye sphere as a function of the distance to an ion:

$$n_e(r) = \frac{Z_i}{4\,\pi\,r_D^2}\,\frac{\exp(-r/r_D)}{r}. \tag{4.37}$$

Hence for the effective electron charge causing PBs – $N_{pol}(R,\omega)$ we find:

$$N_{pol}(R,\,\omega) = N_e(R) = 4\,\pi\int_0^R n_e(r)\,r^2\,dr = \\ = Z_i\,[1 - (1 + R/r_D)\,\exp(-R/r_D)]. \tag{4.38}$$

Here the value R is a current distance from a radiating electron to an ion in electron motion in its orbit. The physical meaning of Eq. 4.38 is that PBs is formed by the part of an electron charge screening a plasma ion that is in the sphere of radius R since this charge interacts with an incident electron in a coherent manner (as a unit). It should be noted that in this case the polarization charge does not depend on frequency and $N_{pol}(R>>r_D,\,\omega) = Z_i$, that is, at long distances between a radiating electron and an ion the whole electron charge of the Debye sphere takes part in formation of PBs.

The expression for spectral effective radiation by the static channel within the framework of the rotation approximation will be determined by the equation similar to Eq. 4.36 accurate to the replacement of the polarization force by the ordinary ("static") force representing the derivative of the potential (4.27) with respect to the radius vector ($f_{st} = U_D'$):

$$\frac{d\kappa_{st}^{(rot)}}{d\omega} = \frac{8\,\pi\,\hbar\,\left|U_D'\left(r_{ef}(\omega)\right)\right|^2}{3\,m_e^2\,c^3\,\sqrt{2\,T/m_e}}\,\frac{r_{ef}^4(\omega)}{1 + \left|U_D'\left(r_{ef}(\omega)\right)\right|/\left(m_e\,\omega^2\,r_{ef}(\omega)\right)}. \tag{4.39}$$

Here and further the condition $\omega >> \omega_{pe}$ providing propagation of a transverse electromagnetic wave in plasma is supposed to be satisfied.

For the quantitative characteristic of the PBs contribution to bremsstrahlung in electron scattering by a point ion in plasma we will introduce the spectral R-factor in the rotation approximation:

$$R^{(rot)}(\omega) = \frac{d\kappa_{pol}^{(rot)}(\omega)}{d\kappa_{st}^{(rot)}(\omega)} = \left[\frac{f_{pol}\left(r_{ef}(\omega)\right)}{f_{st}\left(r_{ef}(\omega)\right)}\right]^2 = \left[\frac{N_e\left(r_{ef}(\omega)\right)}{r_{ef}^2(\omega)\, U_D'\left(r_{ef}(\omega)\right)}\right]^2. \tag{4.40}$$

Substituting here the expressions for $N_e(R)$ (Eq. 4.38) and U_D (Eq. 4.27), we find

$$R^{(rot)}(\omega) = \left[1 - \frac{\exp\left(r_{ef}(\omega)/r_D\right)}{1 + r_{ef}(\omega)/r_D}\right]^2 \approx \left(r_{ef}(\omega) < r_D\right) \approx \frac{1}{4}\left(\frac{r_{ef}(\omega)}{r_D}\right)^4. \tag{4.41}$$

In derivation of Eq. 4.41 the inequality $r_{ef}(\omega) < r_D$ is used that is true for ideal plasma in the frequency range $\omega \geq \omega_{Coul}$, where ω_{Coul} is the Coulomb frequency determined by the formula (4.18).

The numerical estimation based on Eq. 4.41 indicates that in the case under consideration the contribution of the polarization channel to bremsstrahlung is small and is about 1 %.

With the use of the above expressions it can be shown that

$$\frac{d\kappa_{pol}^{(rot)}}{d\omega} \propto \omega^{-\frac{8}{3}}. \tag{4.42}$$

This dependence somewhat differs from the similar dependence given in the book [2] for fast superthermal electrons in the frequency range $\omega > \gamma^2(\mathrm{v}/\mathrm{v}_{Te})\,\omega_{pe}$ (v is the velocity of a fast electron, v_{Te} is the thermal velocity of plasma electrons, ω_{pe} is the electron plasma frequency)

$$\frac{d\kappa_{pol}}{d\omega} \propto \omega^{-4}. \tag{4.43}$$

4.3 Bremsstrahlung of Fast Electrons in Plasma

Radiation in scattering of electrons by ions in plasma was considered in Chap. 3 within the framework of the quasi-classical approximation, the criterion of which is given in the general case by the inequation (3.67a) and by the relation (3.1) in case of the Coulomb potential. In the quasi-classical approximation it can be considered that the motion of an electron in radiation of electromagnetic waves occurs along a

specified trajectory defined by the potential of a target. This situation is typical for low-temperature plasma, in which the condition of quasi-classicity (Eq. 3.67a) is satisfied.

In consideration of bremsstrahlung of fast (superthermal) particles, including relativistic particles, an opposite approximation is adequate that is called the Born approximation, the criterion of which is the inequation that is inverse for Eq. 3.1:

$$\frac{Z\,e^2}{\hbar\,\mathrm{v}} << 1, \tag{4.44}$$

where v is the electron velocity, Z is the charge number of the nucleus of an atom (ion). It should be noted that the inequation (4.44) is strong, and the inequation (3.1) is weak. Physically the Born condition corresponds to the weak disturbance of motion of a scattered particle under the action of the target potential.

4.3.1 Polarization Bremsstrahlung of a Fast Charged Particle in Plasma

As was already noted in Chap. 1, PBs can be considered as the conversion of a virtual photon of the eigenfield of an incident particle to a real photon on electrons of a medium. This interpretation becomes especially obvious for fast charged particles, the eigenfield of which approaches the field of a free electromagnetic wave. Plasma electrons in the frequency range $\omega >> \omega_{pe}$ are quasi-free. (Here we do not consider bound electrons of ions, and plasma is considered to be ideal.) Therefore for description of PBs of a fast charged particle in plasma it is possible to use the results obtained in Chap. 2 for bremsstrahlung on an atom in the high-frequency limit (2.54). Really, for quasi-free electrons the eigenfrequency can be assumed to be equal to the plasma frequency, and then the condition of high-frequency in the spectral range under consideration is satisfied automatically. From the aforesaid it follows that in going from an atom to plasma, in the expression for the PBs cross-section (2.54) instead of the dynamic form factor of an atom it is necessary to put the DFF of the electron component of plasma and to neglect the second summand in the parentheses of the formula (2.54). As a result, we have

$$\frac{d\sigma^{pol}_{plas}}{d\omega\, d\Omega_{\mathbf{k}}} = r_e^2 \frac{\omega}{\mathrm{v}\, c\, \hbar} \int \frac{d\mathbf{q}}{(2\pi)^4} \left[\mathbf{n},\, \tilde{\mathbf{A}}^{(p)}(q_1)\right]^2 \tilde{S}_e\left(q^0, \mathbf{q}\right) V, \tag{4.45}$$

where V is the volume of plasma, in which PBs is generated, $\tilde{\mathbf{A}}^{(p)}(q_1)$ is the vector potential of an incident particle (without a frequency delta function).

The normalized dynamic form factor of the electron component is [3]

$$\tilde{S}_e(q) = \left|\frac{\varepsilon^{l(i)}(q)}{\varepsilon^{l}(q)}\right|^2 |\delta n_e(q)|^2 + z_i^2 \left|\frac{1-\varepsilon^{l(e)}(q)}{\varepsilon^{l}(q)}\right|^2 |\delta n_i(q)|^2, \tag{4.46}$$

where

$$\left|\delta n_{e,i}(q)\right|^2 = \frac{n_{e,i}}{\sqrt{2\pi}\,\mathrm{v}_{Te}\,|\mathbf{q}|}\exp\left(-\frac{(q^0)^2}{2\,\mathbf{q}^2\,\mathrm{v}_{Te,i}^2}\right) \tag{4.47}$$

are the spatio-temporal Fourier transforms of the squared thermal fluctuations of the electron and ionic components of plasma calculated on the four-dimensional wave vector $q = (q^0, \mathbf{q})$, $n_{e,i}$ are the average concentrations of electrons and ions.

The functions $\varepsilon^{l(e)}(q)$, $\varepsilon^{l(i)}(q)$ and $\varepsilon^{l}(q)$ represent the longitudinal part of the dielectric permittivity of plasma components (electrons and ions) and of the whole plasma.

The DFF of plasma components and the longitudinal part of the dielectric permittivity of plasma are considered in detail in Appendix 3.

In the spectral range under consideration $\omega >> \omega_{pe}$ the dielectric permittivity of plasma at the frequency of an emitted photon ω is close to unity. Nevertheless, in case of relativistic particles, when the Lorentz factor $\gamma >> 1$, in description of an electromagnetic field in a medium the dielectric permittivity, generally speaking, should be taken into account due to the presence of a resonant denominator in the formula for the vector potential (4.48). In the case under consideration it can be supposed that $\varepsilon^{(l)}(q_1) \cong \varepsilon^{(t)}(q_1) = \varepsilon\left(q_1^0\right)$ since the inequality $\left|q_1^0\right| \approx \omega >> |\mathbf{k}|\mathrm{v}_{Te}$ is satisfied. Then the vector potential of the electromagnetic field of an IP is given by the formula (2.42) from the second chapter with the replacement $q \to q_1$ and in view of the dielectric permittivity of a medium:

$$\mathbf{A}^{(p)}(q_1) = \left(\frac{4\,\pi\,c\,e_0}{q_1^0\,\varepsilon(q_1)}\right)\frac{\varepsilon(q_1)\left(q_1^0/c^2\right)\mathbf{v} - \mathbf{q}_1}{\varepsilon(q_1)\left(q_1^0/c\right)^2 - \mathbf{q}_1^2}\,\delta\left(q_1^0 - \mathbf{q}_1\,\mathbf{v}\right). \tag{4.48}$$

The first summand on the right side of Eq. 4.46 after substitution in the expression for the cross-section (4.45) corresponds to bremsstrahlung with transfer of the momentum excess to a plasma electron. Let us call this radiation *Compton* Bs by analogy with Compton X-ray scattering by an atom, when the energy-momentum excess is carried away by an ionized atomic electron. In the case under consideration the role of X-radiation is played by a virtual photon of the eigenfield of an incident particle. It should be noted that the term Compton Bs in the works [1, 2] was used in a different sense – for description of static Bs in a medium. In view of the aforesaid, our use of this term seems more adequate.

The numerical analysis shows that in calculation of the cross-section of PBs in plasma the replacement can be made to a high accuracy:

$$\frac{1}{\sqrt{2\pi}\,\mathrm{v}_T\,|\mathbf{q}|}\exp\left(-\frac{(q^0)^2}{2\,\mathbf{q}^2\,\mathrm{v}_T^2}\right) \to \delta\left(q^0\right). \tag{4.49}$$

Then the expression for the cross-section of Compton Bs takes the form

$$\frac{d\sigma^{(CB)}}{d\omega\, d\Omega_{\mathbf{k}}} = N_e\, r_e^2\, \frac{e_0^2}{\hbar\,\omega}\, \frac{c}{\mathrm{v}} \times \int \frac{d\mathbf{q}}{\pi^2}\, \delta((\mathbf{q}-\mathbf{k})\mathbf{v}+\omega)\, \frac{\left[\mathbf{n},\, \mathbf{v}\varepsilon(\omega)\left(\omega/c^2\right)-\mathbf{q}\right]^2}{\left(\mathbf{q}^2-2\mathbf{q}\,\mathbf{k}\right)^2} \left(\frac{\mathbf{q}^2\, r_{De}^2}{1+\mathbf{q}^2\, r_{De}^2}\right)^2, \tag{4.50}$$

where N_e is the number of plasma electrons in the volume of interaction, r_{De} is the electron Debye radius, $|\mathbf{k}| = (\omega/c)\,\sqrt{\varepsilon(\omega)}$. It should be noted that the last multiplier on the right side of this equation "cuts off" integration with respect to the transferred wave vector from below: $|\mathbf{q}| > r_{De}^{-1}$. Physically this means that scattering with low transfer of a momentum does not make a contribution to Compton Bs since then an IP interacts not with an individual plasma electron, but with the Debye sphere as a single formation.

Integration with respect to the solid angle of the transferred wave vector $d\Omega_{\mathbf{q}}$ in Eq. 4.50 can be performed in the general form if the function is introduced:

$$I_\varphi(q,\mathrm{v},\omega,\theta) = \frac{q^3\,\mathrm{v}}{2\,\pi} \int d\Omega_{\mathbf{q}}\, \delta(\omega-\mathbf{k}\mathbf{v}+\mathbf{q}\mathbf{v})\, \frac{\left[\mathbf{n},\, \omega\,\mathbf{v}\,\varepsilon(\omega)/c^2-\mathbf{q}\right]^2}{\left(\mathbf{q}^2-2\,\mathbf{k}\,\mathbf{q}\right)^2}. \tag{4.51}$$

Then instead of the Eq. 4.50 we have:

$$\frac{d\sigma^{(CB)}}{d\omega\, d\Omega_{\mathbf{k}}} = \frac{2}{\pi} N_e\, r_e^2\, \frac{e_0^2}{\hbar\,\omega}\, \frac{c}{\mathrm{v}^2} \int_{x_{\min}(\theta)}^{x_{\max}(\omega)} \left(\frac{x^2\,(\omega\, r_{De}/c)^2}{1+x^2\,(\omega\, r_{De}/c)^2}\right)^2 \tilde{I}_\varphi(x,\beta,\theta)\, \frac{dx}{x}. \tag{4.52}$$

Here $x_{\max} = \mu\, c^2\, \beta/\hbar\,\omega$, $x_{\min} = q_{\min}\dfrac{c}{\omega} = \beta^{-1} - \cos\theta$, the function $\tilde{I}_\varphi(x,\beta,\theta)$ is given by the formula

$$\tilde{I}_\varphi(x,\beta,\theta) = \frac{x^2 f_1(x,\beta,\theta)}{\Delta^{3/2}(x,\beta,\theta)} + \frac{x^2}{4}\left[\frac{f_2(x,\beta,\theta)}{\Delta^{1/2}(x,\beta,\theta)} - 1\right], \tag{4.53}$$

where

$$f_1 = \left(x^2 + 2\,\cos(\theta)\, x_{\min}\right)\left[\left(x^2 - {x_{\min}}^2\right)\cos^2\theta + (x_{\min}-\beta)^2 \sin^2\theta\right] + 4\,\sin^2\theta\,\cos\theta\,(x_{\min}-\beta)\left(x^2-{x_{\min}}^2\right)$$

and

$$f_2 = x^2 + 2\,\cos(\theta)\,x_{\min},\; x_{\min} = q_{\min}\frac{c}{\omega} = \beta^{-1} - \cos\theta,$$
$$\Delta = \left(x^2 - 2\left(1 - \frac{\cos\theta}{\beta}\right)\right)^2 + 4\frac{1-\beta^2}{\beta^2}\sin^2\theta.$$

It should be noted that in the nonrelativistic limit v<<c the integral of Eq. 4.51 looks like:

$$I_\varphi(q, \mathrm{v}, \omega, \theta) \cong \frac{1+\cos^2\theta}{2} + \left(\frac{\omega}{q\,\mathrm{v}}\right)^2 \frac{1-3\cos^2\theta}{2}. \tag{4.53a}$$

Compton bremsstrahlung in case of an atomic target corresponds to PBs with atomic ionization.

The second summand in the equation for the normalized DFF of the electron component of plasma (4.46) after substitution in the expression for the cross-section (4.45) corresponds to polarization Bs on the Debye sphere around a plasma ion. This radiation in the original works [1, 2] was called *transient* bremsstrahlung. In the process of transient Bs the energy-momentum excess is transferred to a heavy ion, and emission of a photon occurs as a result of interaction of the electron Debye sphere as a whole with the electromagnetic field. In view of the explicit form of the longitudinal part of the dielectric permittivity of plasma (A.68), (A.69) and the passage to the limit (4.50) for the spectral-angular cross-section of transient Bs from Eqs. 4.45, 4.48 we obtain

$$\frac{d\sigma^{(TrB)}}{d\omega\, d\Omega_{\mathbf{k}}} = N_i\, z_i^2 r_e^2 \frac{e_0^2}{\hbar\,\omega}\frac{c}{\mathrm{v}} \times \int \frac{d\mathbf{q}}{\pi^2} \frac{\left[\mathbf{n},\, \mathbf{v}\left(\omega\,\varepsilon(\omega)/c^2\right) - \mathbf{q}\right]^2}{\left(\mathbf{q}^2 - 2\mathbf{q}\,\mathbf{k}\right)^2} \frac{\delta((\mathbf{q}-\mathbf{k})\mathbf{v} + \omega)}{\left(1 + \mathbf{q}^2 r_{De}^2\right)^2}, \tag{4.54}$$

where N_i is the number of plasma ions in the volume of interaction. Hence it is seen that the main contribution to transient Bs is made by low values of the transferred wave vector $|\mathbf{q}|<r_{De}^{-1}$ that correspond in the classical pattern of the process to high impact parameters $\rho>r_{De}$. It is in such a case that a fast electron interacts in a coherent manner with electrons screening an ion in plasma. The coherence of interaction manifests itself in the fact that the process cross-section (4.54) is proportional to the squared number of electrons of the Debye sphere equal to the charge of a plasma ion. Thus transient Bs can be interpreted as radiation of the Debye sphere oscillating in the ac field produced by a fast electron during scattering.

For the spectral cross-section of transient Bs from Eq. 4.54 we have:

$$\frac{d\sigma^{(TrB)}}{d\omega} = \frac{1}{\pi^2} N_i\, z_i^2 r_e^2 \frac{e_0^2}{\hbar\,\omega}\frac{c}{\mathrm{v}^2}\,\Im^{(Tr)}, \tag{4.55}$$

where the dimensionless integral is introduced:

$$\Im^{(Tr)} = \mathrm{v}\int d\mathbf{q}\int d\Omega_{\mathbf{k}}\,\frac{\left[\mathbf{n},\,\mathbf{v}\left(\omega\,\varepsilon(\omega)/c^2\right)-\mathbf{q}\right]^2}{\left(\mathbf{q}^2-2\mathbf{q}\,\mathbf{k}\right)^2}\,\frac{\delta((\mathbf{q}-\mathbf{k})\mathbf{v}+\omega)}{\left(1+\mathbf{q}^2\,r_{De}^2\right)^2}. \tag{4.56}$$

To calculate the integral of Eq. 4.56, it is convenient to make the replacement of the variable: $\mathbf{q}=\kappa+\mathbf{k}$, where $\kappa=\left(\mathbf{p}_f-\mathbf{p}_i\right)/\hbar$. Then after integration with respect to the angular variables we have:

$$\Im^{(Tr)} = \frac{2\,\pi^2}{r_{De}^4\,k}\int\limits_{\omega/\mathrm{v}}^{\kappa_{\max}}\frac{d\kappa}{\kappa^2\left(\kappa^2-k^2\right)^2}\left\{\frac{\omega^2\,\mathrm{v}^2\,k\,r_{De}^2}{\tilde{c}^4}\left(\kappa^2-\frac{\omega^2}{\mathrm{v}^2}\right)g(\kappa)+\frac{1}{2\,k\,r_{De}^2}\,f(\kappa)\right\}, \tag{4.57}$$

$$g(\kappa) = \frac{1}{1+r_{De}^2\left(\kappa-k\right)^2}-\frac{1}{1+r_{De}^2\left(\kappa+k\right)^2}, \tag{4.58}$$

$$\begin{aligned} f(\kappa) = &\left(\frac{\omega^2\,\mathrm{v}^2}{2\,\tilde{c}^4}-\kappa^2-2\,\frac{\omega^2}{\tilde{c}^2}-\frac{3\,\omega^4}{2\,\tilde{c}^4\,\kappa^2}\right)\\ &\times\left[4\,\kappa\,k\,r_{De}^2+\left(1+r_{De}^2\left(\kappa^2+k^2\right)\right)\ln\frac{1+r_{De}^2\left(\kappa-k\right)^2}{1+r_{De}^2\left(\kappa+k\right)^2}\right], \end{aligned} \tag{4.59}$$

where $\tilde{c}=c/\sqrt{\varepsilon}$ is the phase velocity of light in a medium, $\kappa_{\max}=\mu\,\mathrm{v}/\hbar, k=\sqrt{\varepsilon}\,\omega/c$.

The analysis of the expressions (4.55), (4.56), (4.57), (4.58), and (4.59) shows that it is possible to separate three characteristic frequency ranges for the spectral cross-section of transient Bs of a relativistic ($\mathrm{v}\simeq c$) incident particle.

1. In the spectral range $\omega_{pe}<<\omega<\mathrm{v}/r_{De}=(\mathrm{v}/\mathrm{v}_{Te})\,\omega_{pe}$ (strong screening) that exists in case of a fast particle ($\mathrm{v}>>\mathrm{v}_{Te}$), the integral of Eq. 4.57 is simplified to the form

$$\Im^{(Tr)} \simeq \frac{16}{3}\,\pi^2\,\ln\left(\frac{c}{r_{De}\,\omega\sqrt{\left(c/\mathrm{v}\right)^2-\varepsilon(\omega)}}\right),$$

and the cross-section (4.55) in the relativistic limit is:

$$\frac{d\sigma^{(TrB)}}{d\omega} = \frac{16}{3}\,N_i\,z_i^2\,r_e^2\,\frac{e_0^2}{\hbar\,\omega}\,\frac{c}{\mathrm{v}^2}\,\ln\left(\frac{\gamma\,c\,\omega_{pe}}{\mathrm{v}_{Te}\sqrt{\omega^2+\gamma^2\,\omega_{pe}^2}}\right). \tag{4.60}$$

In derivation of Eq. 4.60 it was assumed that $\varepsilon(\omega) = 1 - \left(\omega_{pe}/\omega\right)^2$ and $r_{De} = \mathrm{v}_{Te}/\omega_{pe}$.

2. In the range $(\mathrm{v}/\mathrm{v}_{Te})\,\omega_{pe} << \omega < \gamma^2(\mathrm{v}/\mathrm{v}_{Te})\,\omega_{pe}$ (intermediate screening) we have:

$$\frac{d\sigma^{(TrB)}}{d\omega} = 2N_i\, z_i^2\, r_e^2\, \frac{e_0^2}{\hbar\,\omega}\, \frac{c}{\mathrm{v}^2} \left(\frac{\mathrm{v}\,\omega_{pe}}{\mathrm{v}_{Te}\,\omega}\right)^2 \ln\left(\frac{2\gamma\,\omega}{\sqrt{\omega^2 + \gamma^2\,\omega_{pe}^2}}\right). \tag{4.61}$$

3. In the high-frequency range $\gamma^2(\mathrm{v}/\mathrm{v}_{Te})\,\omega_{pe} << \omega$ (weak screening) the equation is true:

$$\frac{d\sigma^{(TrB)}}{d\omega} = 4N_i\, z_i^2\, r_e^2\, \frac{e_0^2}{\hbar\,\omega}\, \frac{c}{\mathrm{v}^2} \left(\frac{\mathrm{v}\,\omega_{pe}}{\mathrm{v}_{Te}\,\omega}\right)^2 \left(\frac{\gamma^2\mathrm{v}\,\omega_{pe}}{\mathrm{v}_{Te}\,\omega}\right)^2. \tag{4.62}$$

Let us comment the expressions (4.60), (4.61), and (4.62) that for the intensity of Bs of an ultrarelativistic electron in plasma were for the first time obtained in the work [2].

In the low-frequency spectral range (1) for all radiation angles θ the inequality (the case of strong screening) takes place:

$$q_{\min}\, r_{De} < 1. \tag{4.63}$$

It will be recalled that $q_{\min} = \omega/\mathrm{v} - k\cos\theta$ is the minimum wave vector transferred from an incident particle to plasma. The condition (4.63) within the framework of the classical picture of the process means that the law of conservation of energy-momentum permits such impact parameters, at which a particle during radiation flies at distances from an ion that are more than the Debye radius. In such a case the coherent interaction of the IP with the Debye sphere takes place: the electron charge screening an ion in plasma oscillates as a unit under the action of the alternating field of the incident particle and emits a bremsstrahlung photon. The phrase "strong screening" means that the Debye radius is small enough from the standpoint of fulfilment of the inequation (4.63).

In the spectral range (1) the intensity of transient Bs

$$\frac{dI^{(TrB)}}{d\omega} \propto \hbar\,\omega\, \frac{d\sigma^{(TrB)}}{d\omega}$$

weakly depends on frequency: in the range $\omega < \gamma\,\omega_{pe}$ there is no frequency dependence at all, and for the high frequencies $\gamma\,\omega_{pe} < \omega < (\mathrm{v}/\mathrm{v}_{Te})\,\omega_{pe}$ (under the assumption that $\mathrm{v}/\mathrm{v}_{Te} > \gamma$) this dependence is only logarithmic.

In going to the second (2) spectral range $(\mathrm{v}/\mathrm{v}_{Te})\,\omega_{pe} << \omega < \gamma^2(\mathrm{v}/\mathrm{v}_{Te})\,\omega_{pe}$ – intermediate screening – the inequation (4.63) providing the coherence of interaction of an IP with the Debye sphere is satisfied only for small radiation angles

$$\theta < \frac{\mathrm{v}\,\omega_{pe}}{\mathrm{v}_{Te}\,\omega}, \tag{4.64}$$

which results in appearance of the small multiplier $\left(\mathrm{v}\,\omega_{pe}/\mathrm{v}_{Te}\,\omega\right)^2$ in the formula for the cross-section. As a result, the intensity of transient Bs in the range under consideration decreases as the squared frequency. Physically (4.64) separates the region of radiation angles, for which a considerable part of the transferred wave vector is carried away by a photon, so $q_{\min} \sim \omega/(\gamma^2 \mathrm{v})$. As a result, the impact parameter permitted by the law of conservation of energy-momentum exceeds the Debye radius, and the interaction of the IP with the Debye sphere is of a coherent nature.

Finally, in the high-frequency range (3) – weak screening – the law of conservation of energy-momentum permits only small impact parameters, lesser than the Debye radius. In this case, "from the point of view of an IP", for all radiation angles the Debye sphere is a rather friable formation, so the interaction of a radiating particle during PBs occurs most likely with each plasma electron taken separately. The process loses coherence, the intensity of radiation decreases as the fourth power of frequency.

4.3.2 *Static Bremsstrahlung of a Fast Charged Particle in Plasma*

We will give the formulas for the spectral cross-section of static Bs (ordinary bremsstrahlung) in the limits of weak and strong screening obtained in the work [1] for a relativistic incident electron. These expressions can also be derived within the framework of the formalism stated in Chap. 2 in view of the influence of the dielectric permittivity of a medium on an electromagnetic field.

Static Bs represents scattering of the eigenfield of a target (a virtual photon) by an incident particle to a bremsstrahlung photon. Hence it is seen that in SBs there is no analogy with Compton scattering as in PBs with ionization of an atom. Therefore the term *Compton Bs* in relation to SBs introduced in the works [1, 2] seems to us not quite appropriate. As stated above, we use this term to designate polarization Bs on plasma electrons in case of a high transferred momentum that can be interpreted as Compton scattering of a virtual photon by the Debye sphere. It should be noted that this analogy can not be understood literally since plasma electrons are free, and atomic electrons are bound.

In the limit of weak screening $q_{\min} r_{De} > 1$, when $\gamma^2 (\mathrm{v}/\mathrm{v}_{Te})\,\omega_{pe} << \omega$, for the spectral cross-section of static Bs to the logarithmic accuracy the expression is true [2]:

$$\frac{d\sigma^{(st)}}{d\omega} = \frac{16}{3} N_i z_i^2 r_e^2 \left(\frac{m}{m_0}\right)^2 \frac{e_0^2}{\hbar\,\omega} \frac{c}{\mathrm{v}^2} \ln\left(\frac{\gamma^2 m c^2}{\hbar\,\omega}\right). \tag{4.65}$$

Implied by the logarithmic accuracy is the approximation, in which the value of the order of one is neglected in comparison with a large logarithm. In this case the argument of the logarithm on the right side of Eq. 4.65 is supposed to be much more than one.

It should be noted that in case of an incident electron ($m_0 = m$) the SBs cross-section (4.65) only by the logarithmed expression differs from the cross-section of transient Bs (4.60) that, however, "works" in another spectral range.

In case of strong screening $q_{\min} r_{De} < 1$ corresponding to the frequency range $\omega_{pe} << \omega << \gamma^2 (\mathrm{v}/\mathrm{v}_{Te})\, \omega_{pe}$, for the static Bs cross-section it can be obtained [2]:

$$\frac{d\sigma^{(st)}}{d\omega} = \frac{16}{3} N_i z_i^2 r_e^2 \frac{e_0^2}{\hbar\,\omega} \left(\frac{m}{m_0}\right)^2 \frac{c}{\mathrm{v}^2} \frac{\omega^2}{\omega^2 + \gamma^2\,\omega_{pe}^2} \ln\left(\frac{m\,c\,\mathrm{v}_{Te}}{\hbar\,\omega_{pe}}\right). \tag{4.66}$$

In derivation of Eq. 4.66 the expression $\varepsilon(\omega) = 1 - \left(\omega_{pe}/\omega\right)^2$ for the dielectric permittivity of plasma was used.

Let us pay attention to the multiplier $(m/m_0)^2$ in the expressions for the SBs cross-section (m_0 is the IP mass) that makes SBs of heavy particles negligible. This multiplier is absent in case of PBs since then the conversion of a virtual photon to a real photon occurs on electrons (either atomic or plasma electrons).

An important point in the formula (4.66) is the presence of the multiplier $\omega^2 \Big/ \left(\omega^2 + \gamma^2\,\omega_{pe}^2\right)$ that for the frequencies $\omega < \gamma\,\omega_{pe}$ reduces the cross-section of SBs in plasma $\left(\gamma\,\omega_{pe}/\omega\right)^2$ times. This circumstance is called the *density effect* in bremsstrahlung in a medium (or the Ter-Mikaelyan density effect [4]) since the reduction of the cross-section is proportional to the electron concentration in a substance ($\omega_{pe}^2 \sim n_e$). The density effect under consideration is connected with the increase of the phase velocity of light in plasma $\tilde{c} = c \Big/ \sqrt{1 - \left(\omega_{pe}^2/\omega^2\right)} > c$, which results in reduction of the time of detachment of a bremsstrahlung photon from the eigenfield of a relativistic charged particle.

As seen from the expression (4.60), the density effect in transient Bs does not show itself. This is explained by the fact that in case of PBs the conversion of a virtual photon to a real photon occurs on nonrelativistic electrons of plasma, so the increase of the phase velocity of light in a medium has no effect on the cross-section value.

Thus in the spectral range $\omega < \min\left\{\gamma\,\omega_{pe},\ (\mathrm{v}/\mathrm{v}_{Te})\,\omega_{pe}\right\}$ transient Bs of relativistic electrons in plasma surpasses static Bs suppressed by the density effect.

In case of Bs of thermal electrons in plasma ($\mathrm{v} \sim \mathrm{v}_{Te}$) the static channel of radiation, as a rule, prevails since the characteristic distance, at which radiation of a bremsstrahlung photon occurs, is found to be less than the Debye radius (see Eq. 4.41).

It should be noted that the obtained expressions for the cross-sections of PBs and SBs are applicable not only for plasma, but also in the high-frequency range

$\omega >> I_a/\hbar$ (I_a is the potential of ionization of substance atoms), when the plasma formula for the dielectric permittivity of a medium "works", accurate to replacement of plasma parameters by substance parameters.

4.4 Bremsstrahlung in Dense Plasma in the "Hard-Sphere" Model

In case of dense and rather cold plasma, when the electron concentration reaches solid-state values, the Debye model of electron distribution (4.38) defining Bs on a screened plasma ion becomes inadequate, so it is necessary to use other approaches. One of the most popular recent methods of description of dense plasma is so-called "hard-sphere" model that will be used in this paragraph for calculation of Bs in the local plasma approximation [5].

4.4.1 Hard-Sphere Model in Dense Plasma

Under the action of short energy momenta of high intensity on a solid body fast ionization of atoms occurs, in which the electron-ion system has no time to shatter forming plasma with a particle concentration up to 10^{22} cm^{-3}. Under these conditions Debye screening of an ion by plasma electrons is modified, so the formula (4.37) for the distribution of the electron concentration around a plasma ion fails.

In the hard-sphere model it is supposed that plasma consists of ions screened both by bound and by free electrons, and the radial derivative of the electron concentration on the sphere surface is equal to zero. This boundary condition corresponds to the zero electric potential on the sphere surface in contrast to the Debye distribution (4.37). The electric charge of the hard sphere is also equal to zero. The hard spheres in plasma form a close-packed ensemble similarly to the solid-state case. The radius of the hard sphere depends on the ion concentration n_i by the formula

$$R_0 = \sqrt[3]{\frac{3}{4\,\pi\, n_i}}. \tag{4.67}$$

For example, for the solid-state ion concentration $n_i = 10^{22}$ cm^{-3} we have $R_0 = 2.88$ Å. In this case the electron plasma frequency is $\omega_{pe} \simeq 13.4$ eV (naturally, plasma is assumed to be electrically neutral). In contrast to the Debye radius ($r_{De} = \sqrt{T_e/4\,\pi\, e^2\, n_e}$), the hard sphere radius does not depend on plasma temperature. Presented in Fig. 4.2 in the log-log scale are the dependences of the values of the hard sphere radius and the Debye radius (for two temperatures) as functions of the ion concentration. From this figure it follows that the Debye radius decreases faster with growing ion concentration than the hard sphere radius, which, however, immediately follows from the definition of these radii.

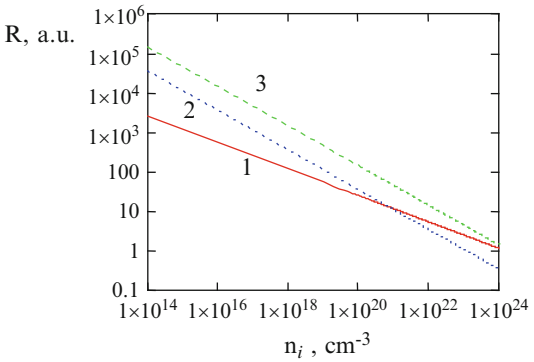

Fig. 4.2 The dependences of the hard-sphere radius and the Debye radius (for two temperatures) on ion concentration: (*1*) – hard-sphere radius; (*2*) – Debye radius for T = 3 a.u.; (*3*) – Debye radius for T = 50 a.u.

The distribution of the electron density inside the hard sphere around an ion with the charge number Z_i is determined *ab initio* by solution of the quantum-mechanical problem [6] with specified boundary conditions and the temperature T defining the velocity distribution of free electrons inside the hard sphere. Within the framework of this model, generally speaking, two types of electron distributions take place: $n_{be}^{hs}(r, T, Z_i)$ for bound electrons and $n_{fe}^{hs}(r, T, Z_i)$ for free electrons that depend on plasma temperature.

The most simple model using the concept of hard sphere is the model of the uniform distribution of electron density:

$$n_{ue}^{hs}(r) = n_e\,\theta(R_0 - r), \tag{4.68}$$

where $\theta(r)$ is the Heaviside step function, $n_e = Z_i\,n_i$ is the average concentration of plasma electrons.

The Debye distribution of the electron concentration around an ion in plasma is given by the formula (4.37)

$$n_D(r) = \frac{Z_i}{4\,\pi\,r_{De}^2}\,\frac{\exp(-r/r_{De})}{r},$$

where $r_{De} = \sqrt{T_e/4\,\pi\,e^2\,n_e}$ is the Debye radius, that can be obtained from the Poisson equation for the Debye potential (4.27).

Shown in Fig. 4.3 are the radial distributions of the electron concentration around an Al^{13+} ion calculated within the framework of different models and temperatures for the average ion concentration $n_i = 10^{22}$ cm^{-3}. It will be recalled that the atomic unit of concentration is $n_a \cong 6.8 \times 10^{24}$ cm^{-3}. The distribution of the electron concentration in the hard-sphere model for different temperatures and average ion concentrations used in this chapter is kindly given by Xiangdong Li (private communication). From the figure it follows in particular that with growing temperature the electron distribution inside the hard sphere approaches the uniform distribution (Eq. 4.68).

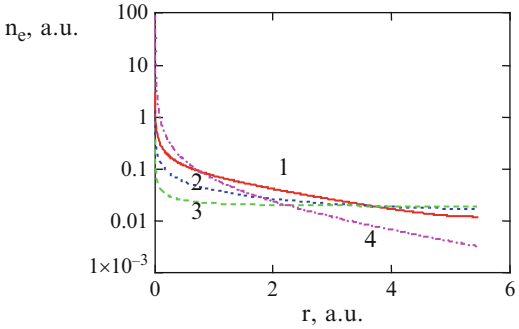

Fig. 4.3 The radial dependence of the electron concentration inside the hard sphere around an Al^{13+} ion in plasma calculated in different models: *solid curve* (*1*) – hard-sphere model, T = 0.3 a.u., *dotted curve* (*2*) – hard-sphere model, T = 3 a.u., *dashed curve* (*3*) – hard-sphere model, T = 50 a.u., *dash-and-dot curve* (*4*) – Debye model, T = 3 a.u.

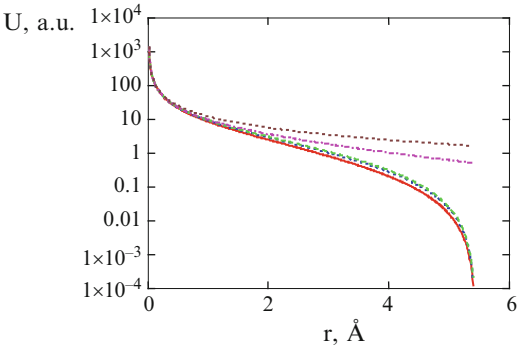

Fig. 4.4 The radial dependence of the electric potential inside the hard sphere in plasma: *solid curve* – hard-sphere model, T = 0.3 a.u., *dotted curve* – hard-sphere model, T = 3 a.u., *dashed curve* – hard-sphere model, T = 50 a.u., *dash-and-dot curve* – Debye model, T = 3 a.u., *top dotted curve* – Debye model, T = 50 a.u.

The radial distribution of the electric potential around an Al^{13+} ion inside the hard sphere in plasma with $n_i = 10^{22}$ cm^{-3} is also shown in Fig. 4.4 for the hard-sphere model and the Debye model for different temperatures.

It is seen that, as it follows from the definition of a hard sphere in dense plasma, the electric potential at its boundary tends to zero, while the Debye potential at the boundary of this sphere differs from zero.

4.4.2 Form Factor of the Hard Sphere in Dense Plasma

The cross-section of polarization bremsstrahlung is defined by the generalized polarizability of a target $\alpha(\omega, \mathbf{q}_1)$ (for example, see the formula (2.79)), where ω

is the frequency of a bremsstrahlung photon, $\mathbf{q}_1 = \mathbf{q} + \mathbf{k}$ is the wave vector transferred to the target, $\mathbf{q} = \left(\mathbf{p}_f - \mathbf{p}_i\right)/\hbar$, $\mathbf{p}_{i,f}$ are the initial and finite momenta of an IP. The calculation of the generalized polarizability of the target is an intricate quantum-mechanical problem, so in case of fast incident particles so-called multiplicative approximation is used:

$$\alpha(\omega, \mathbf{q}_1) \approx \alpha(\omega)\, \tilde{F}(\mathbf{q}_1), \tag{4.69}$$

where $\alpha(\omega)$ is the dipole dynamic polarizability of the target, $\tilde{F}(\mathbf{q}_1)$ is the normalized form factor of the target $\tilde{F}(0) = 1$ representing the spatial Fourier transform of the electron density of the target:

$$\tilde{F}(\mathbf{q}_1) = \frac{1}{Z_i} \int n(\mathbf{r})\, \exp(i\, \mathbf{q}_1\, \mathbf{r})\, d\mathbf{r}, \tag{4.70}$$

where Z_i is the charge number of a plasma ion, $n(\mathbf{r})$ is the distribution of the electron concentration in the hard sphere.

It should be noted that in case of atoms, ions and a hard sphere in plasma the spherical symmetry takes place, so vectors appearing in the Eq. 4.70 can be replaced by their magnitudes.

Thus according to Eq. 4.70, the normalized form factor of the target is defined by the distribution of the electron density in it.

It should be noted that in the Born-Bethe approximation the normalized form factor of the hard sphere in plasma is given by the simple formula:

$$\tilde{F}^{B-B}(q_1) = \theta\left(R_0^{-1} - q_1\right), \tag{4.71}$$

where $\theta(x)$ is the Heaviside function.

In the model of the uniform distribution of electrons (Eq. 4.68) the normalized form factor of the hard sphere can be calculated in the analytical form:

$$\tilde{F}_u(q_1) = 3\, \frac{j_1(q_1 R_0)}{q_1\, R_0}, \tag{4.72}$$

where $j_1(x)$ is the spherical Bessel function of the first kind.

The form factor for the Debye distribution of electrons (Eq. 4.37) looks like

$$\tilde{F}_D(q_1) = \frac{1}{1 + (q_1\, r_{De})^2}, \tag{4.73}$$

where r_{De} is the electron Debye radius.

Presented in Fig. 4.5 are the results of calculations of the squared function $\tilde{F}(\mathbf{q}_1)$ of the hard sphere for different distributions of the electron concentration for the

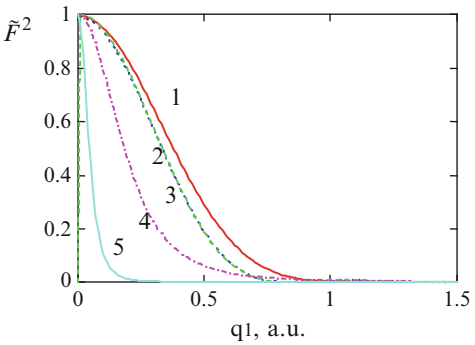

Fig. 4.5 The squared normalized form factor for the distribution of free electrons in the hard sphere calculated in different models, the X-axis in a.u., the Y-axis is dimensionless: (*1*) – *ab initio* calculation for T = 0.3 a.u., (*2*) – *ab initio* calculation for T = 50 a.u., (*3*) – for uniform distribution of electrons inside the hard sphere, (*4*) – Debye model for T = 3 a.u., (*5*) – Debye model for T = 50 a.u., $n_i = 10^{22}$ cm^{-3}

average concentration of Al^{13+} aluminum ions equal to $n_i = 10^{22}$ cm^{-3} and for several temperatures.

It is seen that the form factor of *ab initio* calculation for high temperature (T = 50 a.u.) practically coincides with the form factor of the uniform distribution of the electron concentration inside the hard sphere (4.68). The fastest decrease with growing transferred wave vector takes place for the form factor corresponding to the Debye distribution for high temperature. The slowest decrease of the form factor takes place for *ab initio* calculation of the electron concentration at the lowest considered temperature (T = 0.3 a.u.).

4.4.3 Polarization Charge Around an Ion in Dense Plasma

As was noted in Chap. 3, for description of polarization bremsstrahlung by analogy with ordinary Bs it is convenient to introduce a dimensionless quantity (the polarization charge of a target) characterizing the efficiency of reradiation of a virtual photon to a real photon of PBs by the electron core of a target. The polarization charge can be determined with the use of the formula

$$Z_{pol}(\omega) = \frac{m\,\omega^2}{e^2}\,|\alpha(\omega)| \tag{4.74}$$

that includes the dynamic polarizability of the target $\alpha(\omega)$. In contrast to the ordinary charge number of the target nucleus, the polarization charge is a function of the frequency of a photon emitted by the polarization channel. These dependences for silver and krypton atoms are presented in Fig. 3.3. It is seen that

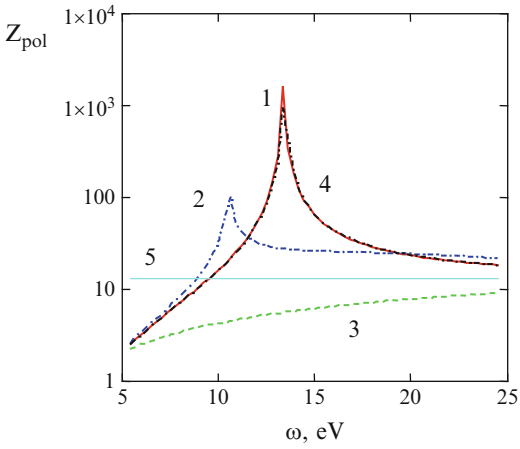

Fig. 4.6 The frequency dependences of the polarization charge of the hard sphere in plasma with different electron density distributions and the high-frequency limit of the polarization charge for Al^{+13}, $n_i = 10^{22}$ cm^{-3} (*1*) – T = 50 a.u., (*2*) – T = 0.3 a. u., (*3*) – Debye model; (*4*) – uniform electron density distribution, (*5*) – high-frequency limit of polarization charge

they have a nonmonotonic behavior with peculiarities near the potentials of ionization of electron shells of atoms.

The spectral dependences of the polarization charge of the hard sphere around an Al^{13+} aluminum ion in plasma with the concentration $n_i = 10^{22}$ cm^{-3} calculated within the framework of different approaches are presented in Fig. 4.6.

It is seen that *ab initio* calculations (Xiangdong Li, private communication) predict the presence of a spectral maximum in a range from 10 to 14 eV (depending on plasma temperature). With growing temperature the spectral maximum of the polarization charge is shifted to the high-frequency region, and at the temperature $T = 50$ a.u. (1,360 eV) the spectrum of the polarization charge obtained on the basis of *ab initio* calculations practically coincides with that for the uniform distribution of the electron charge inside the hard sphere (Eq. 4.68). In this case the position of the spectral maximum of the polarization charge is practically equal to the electron plasma frequency at the specified concentration $\omega_{pe} \simeq 13.4$ eV. It is seen that the polarization charge in the Debye model (curve 3) is a monotonically increasing function of the photon energy without a maximum.

4.4.4 *Cross-Sections of Polarization and Static Bs of Fast Electrons in Dense Plasma (in the Hard-Sphere Model)*

Looking most simply is the cross-section of PBs of a nonrelativistic Born electron on the hard sphere in plasma in the Born-Bethe approximation for the form factor (4.71).

$$\omega \frac{d\sigma_{pol}^{B-B}}{d\omega} = \frac{16}{3} \frac{Z_{pol}^2(\omega)\, e^6}{m^2 \mathrm{v}^2 \hbar\, c^3} \ln\left(\frac{\mathrm{v}}{\omega R_0}\right), \tag{4.75}$$

where v is the initial velocity of a fast electron, $Z_{pol}(\omega)$ is the polarization charge of the hard sphere (4.74). It is obvious that the formula (4.75) is true if the logarithmed expression is more than one:

$$\frac{\mathrm{v}}{\omega R_0} > 1 \rightarrow \omega < \frac{\mathrm{v}}{R_0} \equiv \omega_{\max}^{B-B}, \tag{4.76}$$

which imposes restriction on the PBs frequency in the Bethe-Born model.

The expression for the cross-section of SBs of a fast electron in the Bethe-Born approximation is obtained by replacement on the right side of the Eq. 4.75 of the squared polarization charge $Z_{pol}^2(\omega) \rightarrow Z_i^2$ in the prelogarithmic factor and $\frac{\rho_{\max}}{\rho_{\min}} = \frac{\mathrm{v}}{\omega R_0} \rightarrow \frac{m\,\mathrm{v}\,R_0}{\hbar}$ in the logarithmed expression.

Another restriction of our consideration is inequality $\omega >> \omega_{pe}$ where ω_{pe} is plasma frequency corresponding to average electron concentration. In opposite case ($\omega \approx \omega_{pe}$) it is necessary to account for dielectric permittivity $\varepsilon(\omega, k)$ in the calculation of Bremsstrahlung cross-section in plasma.

As already noted, the formula (4.75) is true in the low-frequency limit $\omega < \mathrm{v}/R_0$ (Eq. 4.76). For higher frequencies the use of the form factor (Eq. 4.71) in the Born-Bethe approximation becomes inadequate. Then it is necessary to apply the Born approximation and the normalized form factor of the hard sphere in the general form Eq. 4.70. The corresponding expression looks like

$$\omega\,\frac{d\sigma_{pol}^{B}}{d\omega} = \frac{16}{3}\,\frac{Z_{pol}^2(\omega)\,e^6}{m^2\mathrm{v}^2\,\hbar\,c^3}\int\limits_{q_{1\min}}^{q_{1\max}} \tilde{F}^2(q_1)\,\frac{dq_1}{q_1}, \tag{4.77}$$

where $q_{1\max} = m\,\mathrm{v}/\hbar$ and $q_{1\min} = \omega/\mathrm{v}$ are the maximum and minimum wave vectors transferred from a fast electron to the target.

For ordinary (static) Bs of an electron on the hard sphere in the Born approximation the formula is true:

$$\omega\,\frac{d\sigma_{st}^{B}}{d\omega} = \frac{16}{3}\,\frac{Z_i^2\,e^6}{m^2\mathrm{v}^2\,\hbar\,c^3}\int\limits_{q_{1\min}}^{q_{1\max}} \left(1 - \tilde{F}(q_1)\right)^2\,\frac{dq_1}{q_1}, \tag{4.78}$$

where the limits of integration are the same as on the right side of the Eq. 4.77.

The expression (4.78) for static (ordinary) Bs can be obtained from the formula (2.45) with the function T (Eq. 2.43) in the nonrelativistic limit.

The formulas for PBs and SBs (4.76), (4.77), and (4.78) relate to arbitrary spherically symmetric targets with a specified polarization charge and the static form factor. The specificity of the situation under consideration consists in the concrete form of the functions $Z_{pol}^2(\omega)$ and $\tilde{F}(q_1)$ that for the hard-sphere model in plasma were studied in Sects. 4.4.3 and 4.4.2.

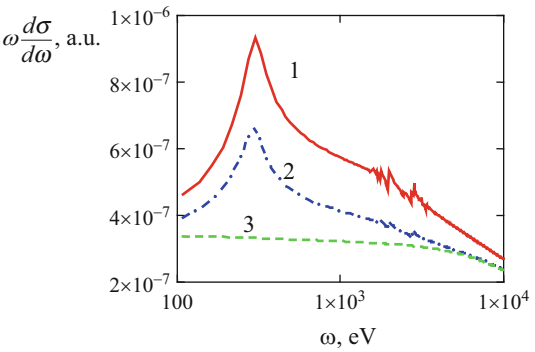

Fig. 4.7 The spectral cross-section of Bs on neon-like aluminum in dense plasma in a wide spectral range: *solid curve* (*1*) – total Bs, *dashed-dotted curve* (*2*) – sum Bs, *dashed curve* – SBs

As follows from the results of Chap. 2 (see Sect. 2.3), besides the polarization and static channels, in bremsstrahlung on targets with an electron core there is, generally speaking, an interference summand (the third summand in the equation below):

$$\frac{d\sigma_{tot}(\omega)}{d\omega} = \frac{d\sigma_{st}}{d\omega} + \frac{d\sigma_{pol}}{d\omega} + \frac{d\sigma_{\text{int}}}{d\omega}. \tag{4.79}$$

Neglecting the interference of the polarization and static channels, we have:

$$\frac{d\sigma_{sum}(\omega)}{d\omega} = \frac{d\sigma_{st}}{d\omega} + \frac{d\sigma_{pol}}{d\omega}, \tag{4.80}$$

where the total cross-section means the sum of the contributions of two Bs channels without the interference term.

Neglecting the interference summand in the cross-section of total spectral Bs can be justified for relativistic electrons, when the angular distribution of radiation of the polarization and static channels differ sharply. In the general case, taking into account the interference summand may be essential and influence the value and form of the spectrum of total Bs on targets with a core.

Presented in Fig. 4.7 are the spectral cross-sections of Bs in a wide range of bremsstrahlung photon energies corresponding to total (1), sum (2), and static (3) Bs of a fast electron (v = 50 a.u.) on a neon-like aluminum ion in dense plasma (Al^{3+}, $n_i = 10^{20}$ cm^{-3}) calculated within the framework of the Born approximation and the local plasma frequency model for the polarizability of the hard sphere.

From Fig. 4.7 it follows that taking into account the polarization channel results in this case in appearance of a spectral maximum in the Bs cross-section at a frequency of several hundreds of electron-volts, corresponding to virtual excitation of the electron core of a neon-like ion under the action of the fast electron field. It is seen that the interference of channels plays an appreciable role: when it is taken into account, at the maximum of the frequency dependence the cross-section of total Bs on a neon-like aluminum ion in dense plasma is approximately three times more than the cross-section of static Bs.

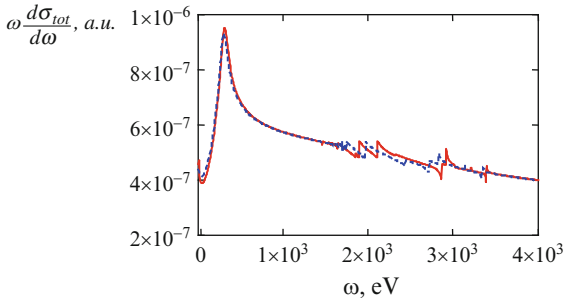

Fig. 4.8 The cross-section of total Bs of a fast electron (v = 50 a.u.) on neon-like aluminum in a wide spectral range for two values of plasma concentration: *solid curve* – $n_i = 10^{22}$ cm^{-3}, *dotted curve* – $n_i = 10^{20}$ cm^{-3}, plasma temperature T = 50 a.u.

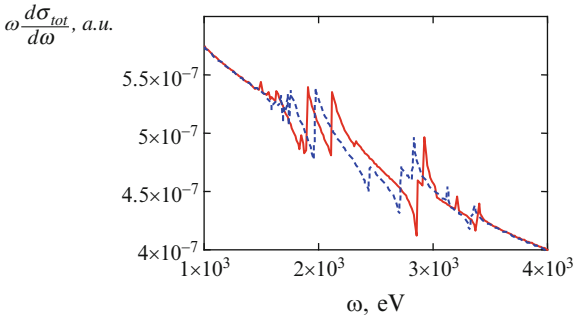

Fig. 4.9 The same as in Fig. 4.8 in the kiloelectron-volt range of bremsstrahlung photon energies

The spectral cross-section of total Bs of a fast electron (v = 50 a.u.) on neon-like aluminum in plasma with different values of ion concentration ($n_i = 10^{22}$ cm^{-3} and $n_i = 10^{20}$ cm^{-3}) and the temperature T = 50 a.u. in a wide spectral range (from 0 to 4 keV) is presented in Fig. 4.8.

The similar data are given in Fig. 4.9 in a range of bremsstrahlung photon energies from 1 to 4 keV, where the effect of the plasma electron concentration on the total Bs spectrum shows itself distinctly.

The calculation was carried out within the framework of the local plasma frequency method and the Born approximation for a fast electron with account for the interference between static and polarization Bs channels on the basis of *ab initio* data on electron distribution in the hard sphere in plasma. From Figs. 4.8 and 4.9 it follows that the calculation of total Bs of a fast electron on neon-like aluminum within the framework of the used approximations predicts an insignificant effect of plasma concentration on the process cross-section in the kiloelectron-volt range.

The local plasma frequency method makes it possible to describe in a single approach the contribution of bound and free electrons of the hard sphere to Bs.

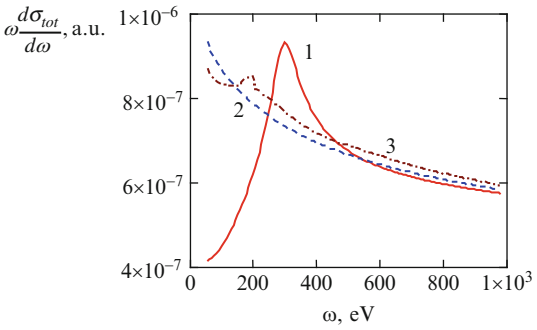

Fig. 4.10 The spectrum of total Bs of a fast electron on aluminum ions of different multiplicities in dense plasma: *curve 1* – neon-like aluminum, *curve 2* – helium-like aluminum, *curve 3* – fully ionized aluminum

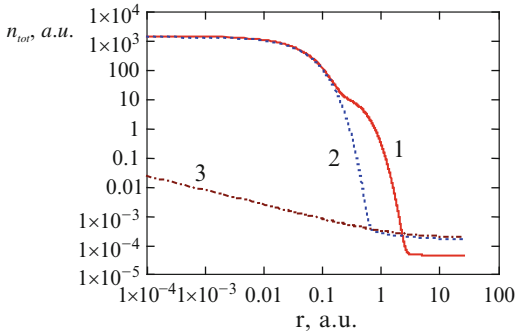

Fig. 4.11 The results of *ab initio* calculations of the distribution of the electron density inside the hard sphere in plasma with the concentration $n_i = 10^{20}$ cm^{-3} and the temperature T = 10 a.u. for different degrees of ionization of aluminum: *curve 1* – neon-like aluminum, *curve 2* – helium-like aluminum, *curve 3* – fully ionized aluminum

The results of calculation of the spectral cross-section of total Bs of a fast electron (v = 50 a.u.) on aluminum ions of different multiplicities are presented in Fig. 4.10 for the ion concentration $n_i = 10^{20}$ cm^{-3} and the plasma temperature T = 10 a.u.

Presented in the following Fig. 4.11 in the log-log scale (by both axes) are the distributions of total electron density for the same plasma concentration and different charge states of an aluminum ion.

Seen in Fig. 4.11 is the contribution of the second electron shell of neon-like aluminum on the background of the electron concentration of an Al^{11+} ion. The peripheral charge concentration is connected with free electrons inside the hard sphere. It is seen that at distances $r>1$ a.u. the concentration of free electrons in case of a fully ionized aluminum atom coincides with that for a helium-like aluminum ion. At the same time the contribution of free electrons in case of a neon-like aluminum ion at the periphery of the hard sphere is approximately an order of magnitude less than in two other cases.

From Fig. 4.10 it follows that in the spectral cross-section of total Bs of a fast electron on neon-like aluminum a maximum is found with the center at a photon energy about 350 eV. This peak is caused by the conversion of a virtual photon of a fast electron to a real photon on the electron core of an Al^{3+} ion. The spectral dependence of total Bs on a helium-like Al^{11+} ion in the approximation under consideration represents a monotonically decreasing curve without peculiarities. It is curious that the Bs spectrum in scattering of a fast electron by fully ionized aluminum has a peculiarity as a weak maximum at a bremsstrahlung photon energy of 190–200 eV. The growth of the Bs cross-section in the low-frequency range is connected with the contribution of free electrons to the polarization channel of the process (see Figs. 4.6, 4.7, 4.8, and 4.9). But the low-frequency spectral region ($\omega \approx \omega_{pe}$) is beyond the validity of our cross-section calculations as it was pointed above.

References

1. Tsytovich, V.N., Akopyan, A.V.: Bremsstrahlung in a nonequilibrium plasma. Sov. J. Plasma Phys. **1**(4), 371 (1975)
2. Tsytovich, V.N., Akopyan, A.V.: Transition bremsstrahlung of relativistic particles. JETP **44**, 87 (1976)
3. Lifshitz, E.M., Pitaevskii, L.P.: Statistical Physics, part 2. Pergamon Press, Oxford (1984)
4. Ter-Mikaelian, M.: High Energy Electromagnetic Processes in Condensed Media. Wiley, New York (1972)
5. Nguyen, H., Grumberg, J., Caby, M., et al.: Line broadening by hot and dense plasmas. Phys. Rev. A **24**, 438 (1981)
6. Xiangdong Li, Zhizhan Xu, Rosmej, F.B.: Exchange energy shift under dense plasma conditions. J. Phys. B. **39**, 3373 (2006)

Chapter 5
Bremsstrahlung of Fast Charged Particles in a Solid Body

5.1 Polarization Bremsstrahlung in a Single Crystal

5.1.1 General Expression for the Cross-Section of a Radiative Process on an Atomic Ensemble

The cross-section of a photoprocess on an atomic ensemble (in case of a monatomic target) can be represented in the following form [1]:

$$d\sigma_{target} = \left| \sum_j \exp\left(i\,\mathbf{q}\,\mathbf{r}_j\right) \right|^2 d\sigma_{atom}, \tag{5.1}$$

where summation is performed over all atoms of the target being in the volume of interaction, $d\sigma_{atom}$ is the differential cross-section of the process on one atom under consideration,

$$\mathbf{q} = \left(\mathbf{p}_f - \mathbf{p}_i\right)/\hbar + \mathbf{k}$$

is the wave vector transferred from an incident particle (IP) to the target, $\mathbf{p}_i$, $\mathbf{p}_f$ are the initial and final momenta of the IP, $\mathbf{k}$ is the wave vector of a photon. For a substance consisting of atoms of different kinds the formula (5.1) is obviously generalized.

The expressions for the cross-sections of bremsstrahlung of fast charged particles on an atom are given in Chap. 2 both for the static channel (see the formulas (2.43), (2.45)) and for the polarization channel (see Eqs. 2.42 and 2.50).

In the state of thermodynamic equilibrium the squared absolute value in the formula (5.1) should be correspondingly averaged:

V. Astapenko, *Polarization Bremsstrahlung on Atoms, Plasmas, Nanostructures and Solids*, Springer Series on Atomic, Optical, and Plasma Physics 72,
DOI 10.1007/978-3-642-34082-6_5, © Springer-Verlag Berlin Heidelberg 2013

$$\left|\sum_j \exp\left(i\,\mathbf{q}\,\mathbf{r}_j\right)\right|^2 \rightarrow \left\langle \sum_{j,\,j'} \exp\left(i\,\mathbf{q}\,\left(\mathbf{r}_j - \mathbf{r}_{j'}\right)\right)\right\rangle. \tag{5.2}$$

The angle brackets on the right side of the Eq. 5.2 imply thermodynamic averaging.

5.1.2 Structure Factor of a Three-Dimensional Crystal

The structure factor of a medium in a three-dimensional case (a three-dimensional single crystal, the angle brackets mean averaging over atomic positions) is [1]:

$$\left\langle \sum_{j,j'} \exp\left(i\,\mathbf{q}\,\left(\mathbf{r}_j - \mathbf{r}_{j'}\right)\right)\right\rangle = N\left(1 - \exp\left(-u^2\,q^2\right)\right) + N\,n_a\,(2\pi)^3 \sum_{\mathbf{g}} e^{-u^2\,g^2}\,|S(\mathbf{g})|^2\,\delta^{(3)}(\mathbf{q}-\mathbf{g}), \tag{5.3}$$

where $N = N_0\,N_{cell}$ is the full number of atoms in the volume of interaction, N_0 is the full number of cells in the volume of interaction, N_{cell} is the number of atoms in a unit cell, $\mathbf{g}$ is the wave vector of a reciprocal lattice, $n_a = N_{cell}/\Delta_{cell}$ is the volume concentration of atoms, Δ_{cell} is the volume of a unit cell.

In the formula (5.3) the value $S(\mathbf{q})$ is introduced – the *normalized* structure factor of a unit cell of a crystal on the wave vector q, $S(\mathbf{q}=0) = 1$, $\delta^{(3)}(\mathbf{q}) = \delta(q_x)\,\delta\left(q_y\right)\,\delta(q_z)$ is the three-dimensional delta function of the wave vector transferred to the target.

The first summand on the right side of the equation (5.3) describes incoherent scattering of an electromagnetic field by the atoms of a lattice. It is proportional to the number of atoms in the volume of interaction in the first degree. The second summand on the right side of (5.3) describes coherent scattering proportional to the squared concentration of atoms since $N = n_a\,V$.

As can be seen from the formula (5.3), coherent scattering takes place only when a wave vector transferred to a medium is equal to the reciprocal lattice vector $\mathbf{q} = \mathbf{g}$. Formally this circumstance manifests itself as the presence of delta functions in the coherent term. From the formula (5.3) it follows that in the limit of high transferred momenta, when $u^2\,q^2 > 1$, the incoherent component of the structure factor of the medium prevails. In case of fulfilment of the opposite inequation, the main contribution to the process is made by the coherent part of the structure factor of (5.3).

For a face-centered cubic lattice that corresponds to a number of metals such as aluminum, iron, copper, silver, and gold, the geometrical structure factor of a unit cell is equal to [2]:

$$S(\mathbf{g}) = \frac{1}{4}[1 + \cos[\pi\,(n_1 + n_2)] + \cos[\pi\,(n_3 + n_2)] + \cos[\pi\,(n_1 + n_3)]], \tag{5.4}$$

where $\mathbf{g} = n_1\,\mathbf{b}_1 + n_2\,\mathbf{b}_2 + n_3\,\mathbf{b}_3$; $\mathbf{b}_1,\ \mathbf{b}_2,\ \mathbf{b}_3$ are the basis vectors of the reciprocal lattice; $n_1,\ n_2,\ n_3$ are the integers. In case of a lattice *with the diamond structure* that silicon and germanium also have, instead of (5.4) we have:

$$S(\mathbf{g}) = \frac{1}{4}\cos\left[\frac{\pi}{4}\,(n_1 + n_2 + n_3)\right] \times [1 + \cos[\pi\,(n_1 + n_2)] + \cos[\pi\,(n_3 + n_2)] + \cos[\pi\,(n_1 + n_3)]]. \tag{5.5}$$

5.1.3 Cross-Section and Yield of Bremsstrahlung Photons

For convenience of comparison with an experiment, it is advisable to go from the cross-section of Bs on an atom to the differential yield of a number of photons per unit crystal length to the unit solid angle and in the unit frequency range:

$$\frac{dN}{d\omega\,d\Omega_{\mathbf{n}}\,dx} = \frac{d\sigma}{V\,d\omega\,d\Omega_{\mathbf{n}}}, \tag{5.6}$$

where V is the volume of interaction, N is the number of bremsstrahlung photons.

Hence with the use of the following formula

$$\frac{d\sigma_{ii}^{pol}}{d\omega\,d\Omega_{\mathbf{k}}} = \frac{2\,e_0^2\,\left|\,\omega^2\,\alpha_i(\omega)\right|^2}{\pi\,\mathrm{v}^2\,\mathrm{c}^3\,\hbar\omega}\int\limits_{q_{\min}}^{q_{\max}} I_\varphi(q,\mathrm{v},\omega,\theta)\,\tilde{F}_i^2(q)\,\frac{dq}{q} \tag{5.7}$$

for the cross-section of PBs on an atom, where the integral $I_\varphi(q,\mathrm{v},\omega,\theta)$ is given by the Eq. 4.53, in view of the coherent part of the structure factor of the medium (Eq. 5.3), the following expression can be obtained for the coherent part of PBs in a single crystal in case of a *nonrelativistic* incident electron (a nonrelativistic electron is considered here for simplicity of the formulas):

$$\frac{dN_{PB}^{(coh)}}{dx\,d\omega\,d\Omega_{\mathbf{k}}} = \frac{n_a^2\,e^2}{\pi\hbar\,\mathrm{v}\,c^3}\sum_{\mathbf{g}} S^2(\mathbf{g})\,\delta(\omega + \mathbf{g}\mathbf{v} - \mathbf{k}\mathbf{v})\,\omega^3\,|\alpha(\omega)|^2\,\exp\left(-u^2\,g^2\right)\tilde{F}_a^2(g)\,\frac{[\mathbf{s},\mathbf{g}]^2}{\mathbf{g}^4}, \tag{5.8}$$

where $\mathbf{s}$ is the unit vector in the direction of propagation of a photon, $\tilde{F}_a$ is the normalized form factor of a medium atom. The delta function appearing on the right side of this equation gives the relation between the frequency and the angle of

photon emission $\theta = \mathbf{v}\hat{}\mathbf{k}$ for the specified reciprocal lattice vector $\mathbf{g}$. As a result, the relationship is true:

$$\omega = -\frac{\mathbf{g}\,\mathbf{v}}{1 - \frac{\mathrm{v}}{c}\cos\theta}. \tag{5.9}$$

Here for generality the term with the ratio v/c in the denominator is retained.

The relation (5.9) defines the frequency-angular distribution of coherent PBs in scattering of a charged particle in a three-dimensional single crystal.

In the geometry of the process shown in Fig. 5.1 for the frequency of coherent PBs from the formula (5.9) we have in the nonrelativistic limit:

$$\omega_{\mathbf{g}} = \frac{2\pi\,\mathrm{v}}{d}\,[n_1\,\cos\alpha - \sin\alpha\,(n_2\,\cos\phi + n_3\,\sin\phi)], \tag{5.9a}$$

d is the crystal lattice constant, $n_1,\ n_2,\ n_3$ are the integers specifying the reciprocal lattice vector.

In the high-frequency spectral range, when $\alpha(\omega) \to -Z\,e^2/m\,\omega^2$, the expression for coherent PBs in a single crystal (Eq. 5.8) passes into the formula for X-ray parametric radiation [1].

With the use of the incoherent component of the structure factor of the crystal (Eq. 5.3) the incoherent part of PBs can be obtained. As a result, for the frequency-angular distribution of photon yield per unit trajectory length we have for a nonrelativistic incident electron:

$$\frac{dN_{pol}^{(incoh)}}{d\omega\,d\Omega_{\mathbf{k}}\,dx} = n_a\,\frac{e^2}{\hbar\,\omega}\,\frac{\left|\omega^2\alpha(\omega)\right|^2}{\pi\,\mathrm{v}^2\,c^3} \times \left(1 + \cos^2\theta\right)\int\limits_{q_{\min}}^{q_{\max}} \left(1 - \exp\left(-u^2\,q^2\right)\right)\tilde{F}_a^2(q)\ \frac{dq}{q}, \tag{5.10}$$

where $q_{\min} \simeq \omega/\mathrm{v}$, $q_{\max} = 2m\,\mathrm{v}/\hbar$ are the minimum and maximum wave vectors transferred from an incident electron to the medium.

Given in Fig. 5.2 are the intensities of different channels of PBs of an electron with a velocity of $1.5{\cdot}10^9$ cm/s scattered in a silicon single crystal as functions of the input angle α for $\varphi = \pi$ (see the definitions of the angles α and φ in Fig. 5.1). In Fig. 5.2 the solid curve represents coherent PBs; the dotted curve is for coherent PBs calculated with the high-frequency polarizability of atoms; the dashed curve is for incoherent PBs averaged over frequency with a relative resolution of 0.3 %.

It is seen that the intensity of coherent PBs calculated with the high-frequency polarizability $\alpha(\omega) = -Z\,e^2/m\,\omega^2$ does not depend on the angle of electron incoming into a single crystal. This circumstance is explained by the fact that in the high-frequency limit the polarization charge number proportional to $\left|\omega^2\alpha(\omega)\right|$

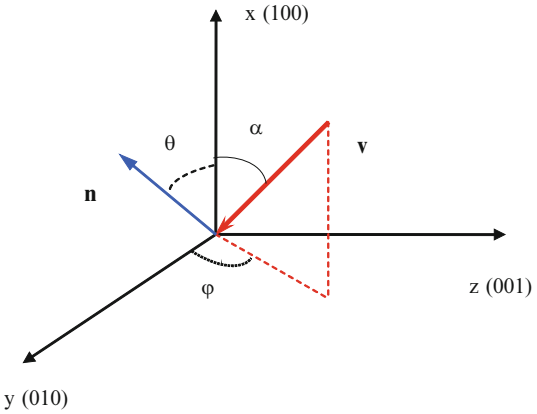

Fig. 5.1 The geometry of PBs in a single crystal

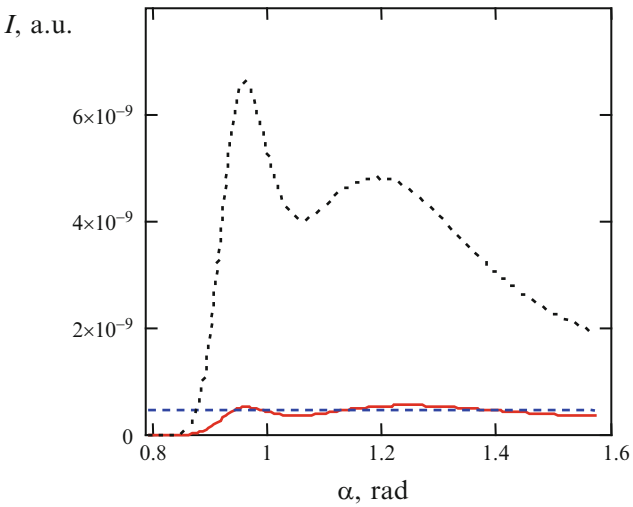

Fig. 5.2 The intensity of PBs of a nonrelativistic electron in a silicon single crystal as a function of the input angle (see the text)

does not depend on the radiation frequency. In calculation of the curves shown in Fig. 5.2 the contribution of 4-vectors of the reciprocal crystal lattice giving the identical dependence of radiation frequency on the input angle according to the Eq. 5.9 was taken into account.

Let us give here also the expressions describing total Bs of a *nonrelativistic* electron in a single crystal in view of the polarization and ordinary channels. For the coherent component of photon yield per unit trajectory length we have:

$$\frac{dN_{tot}^{(coh)}}{d\omega\, d\Omega_{\mathbf{k}}\, dx} = \frac{n_a^2\, Z^2 e^6}{\pi\, \hbar\omega\, \mathrm{v}\, m^2\, c^3} \times$$
$$\times \sum_{\mathbf{g}} S^2(\mathbf{g})\ \delta(\omega + \mathbf{gv} - \mathbf{kv}) \exp\left(-u^2\, g^2\right)$$
$$\times \left| 1 - \tilde{F}_a(q) - \frac{m\,\omega^2}{Z\, e^2}\, \alpha(\omega)\, \tilde{F}_a(g) \right|^2 \frac{[\mathbf{s}, \mathbf{g}]^2}{\mathbf{g}^4}. \qquad (5.11)$$

The incoherent component of total Bs of an electron is:

$$\frac{dN_{tot}^{(incoh)}}{d\omega\, d\Omega_{\mathbf{k}}\, dx} = n_a\, \frac{Z^2 e^6}{\hbar\,\omega}\, \frac{(1 + \cos^2\theta)}{\pi\, \mathrm{v}^2\, m^2\, c^3} \int_{q_{\min}}^{q_{\max}} \left(1 - \exp\left(-u^2\ q^2\right)\right)$$
$$\times \left| 1 - \tilde{F}_a(q) - \frac{m\,\omega^2}{Z\, e^2}\, \alpha(\omega)\, \tilde{F}_a(q) \right|^2 \frac{dq}{q}. \qquad (5.12)$$

On the right side of the Eqs. 5.11 and 5.12 the first two summands under the modulus sign describe the contribution of ordinary Bs to the process, and the third summand corresponds to PBs.

It should be noted that the coherent and incoherent components of bremsstrahlung do not interfere with each other.

From the formulas (5.11) and (5.12) it follows that in the high-frequency limit ($\alpha(\omega) \to -Z\, e^2/m\,\omega^2$) the second and third summands under the modulus sign cancel out, which corresponds to the *descreening effect* (or the effect of atom "stripping") in the process of Bs. It should be noted that this effect takes place only for a nonrelativistic incident electron.

For relativistic electrons in the most part of the spectral range the main contribution to the process is made by the coherent component of Bs, when the momentum excess from an incident particle is transferred to the crystal lattice as a whole. In the nonrelativistic case, generally speaking, the contributions of the coherent and incoherent Bs channels are comparable in value.

5.2 Polarization Bremsstrahlung in a Polycrystal

Serving as initial expressions for calculation of PBs of a fast charged particle in a polycrystal are the formulas (5.8) and (5.9). Going from a single crystal to a polycrystal consists in averaging the expression for the coherent component of PBs (5.8) over the solid angle of the reciprocal lattice vectors $\Omega_{\mathbf{g}}$ according to the equation

$$\left(\frac{dN}{d\omega\, d\Omega_{\mathbf{k}}\, dx}\right)_{polycr} = \int \frac{dN}{d\omega\, d\Omega_{\mathbf{k}}\, dx}\, \frac{d\Omega_{\mathbf{g}}}{4\,\pi}. \qquad (5.13)$$

It is obvious that such an averaging for the incoherent component of PBs (5.10) will not change the initial expression that does not depend on the vectors of the reciprocal lattice of a polycrystal. Therefore the expression for incoherent PBs in a polycrystal is given by the same formula (5.10) as in the case of a single-crystal target.

It should be noted that averaging by the formula (5.13) assumes that crystallites forming the polycrystal are of large enough size, so for each of them the expression for the structure factor of Eq. 5.3 is true.

After averaging the right side of the Eq. 5.8, with the use of Eq. 5.13 we obtain for the coherent component of PBs of a fast particle with the charge $Z_p\, e$ the following expression:

$$\left(\frac{dN}{d\omega\, d\Omega_k\, dx}\right)_{coh} = \frac{4\,\pi\, n_a^2\, Z_p^2\, e^2\, \omega^3}{\mathrm{v}^2\, c^3\, \hbar} \times$$
$$\times \sum_g N(g)\, \frac{\left|\alpha(\omega)\, \tilde{F}_a(g)\right|^2}{g^3}\, \exp\left(-g^2\, u^2\right)\, I_\varphi(g, \mathrm{v}, \omega, \theta)$$
$$\times\, \Theta\left(g\,\mathrm{v} - \omega\left(1 - \frac{\mathrm{v}}{c}\cos\theta\right)\right), \tag{5.14}$$

where $\Theta(x)$ is the Heaviside theta function that is equal to zero at a negative value of the argument and to one at a positive value. The theta function arose as a result of averaging over the solid angle $\mathbf{\Omega_g}$ of the delta function $\delta(\omega + \mathbf{gv} - \mathbf{kv})$ appearing in the expression (5.8). The kinematic integral $I_\varphi(g, \mathrm{v}, \omega, \theta)$ is given by the formulas (4.53), and in the nonrelativistic limit by the formula (4.53a). Introduced into the expression (5.14) is the charge number of an incident particle Z_p to describe PBs of a multiply charged ion, when $Z_p > 1$. It is obvious that in case of an electron $Z_p = -1$. Instead of summation over the reciprocal lattice vectors in the formula (5.8), on the right side of the Eq. 5.14 summation is carried out over the magnitudes of the reciprocal lattice vectors $g = |\mathbf{g}|$, $N(g)$ is the number of reciprocal crystal lattice vectors with a specified magnitude.

From the expression (5.14) it follows that in the spectrum of coherent PBs in a polycrystal spectral "steps" appear at frequencies defined by the magnitude of the reciprocal lattice vector g_j, by the velocity of an incident particle v and the radiation angle θ according to the equation:

$$\omega_j(\mathrm{v}, \theta) = \frac{g_j\, \mathrm{v}}{1 - \frac{\mathrm{v}}{c}\cos\theta} \tag{5.15}$$

Hence it is seen that in the nonrelativistic case $\mathrm{v} << c$ the frequency of the spectral step (Eq. 5.15) does not depend on the radiation angle and is directly proportional to the velocity of an incident particle.

An example of spectral steps in PBs on a polycrystalline target is presented in Fig. 5.3, in which the spectral dependence of PBs for scattering by a silver atom of an ion with the charge number $Z_p = 30$ and the velocity $\mathrm{v} = c/3$ is also given [3].

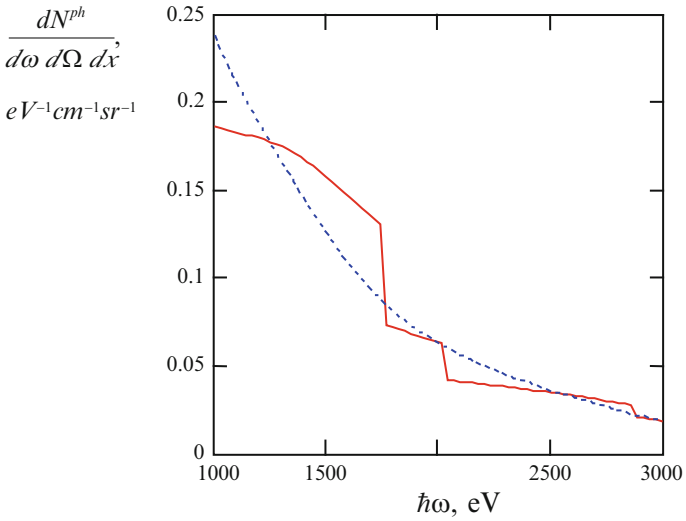

Fig. 5.3 PBs of a multiply charged ion in a silver polycrystal (*solid curve*) and on a silver atom (*dotted curve*)

For specified values of problem parameters (ion velocity and radiation angle), in the frequency range shown in Fig. 5.3 there are three frequency steps, the position of which is determined by the equation (5.15). For frequencies more than ω_j the contribution of the specified magnitude of the reciprocal lattice vector $\mathbf{g}$ to the process probability is equal to zero since the law of conservation of energy-momentum is not followed for it. As a result, a "frequency step" appears on the spectral dependence of yield of PBs photons. Since the frequency ω_j is defined by the magnitude of the vector $\mathbf{g}$, for which $S(\mathbf{g}) \neq 0$, the form of the spectrum of PBs in a polycrystal depends on the crystal structure of a target. For example, for a diamond-type crystal lattice the number of frequency steps will be less than for a face-centered lattice corresponding to silver. Really, in case of a diamond lattice there is an additional restriction for reciprocal lattice vectors, for which the structure factor of a unit cell is nonzero according to the formula (5.5).

The "manifestation" of the spectral step depends on the relation between the coherent and incoherent contributions to PBs. If incoherent PBs prevails, the frequency step will be "slurred over". To avoid this, the fulfilment of the condition is necessary:

$$g < \frac{1}{u}\left(1 - \frac{\mathrm{v}}{c}\cos\theta\right), \tag{5.16}$$

where u is the root-mean-square deviation of medium atoms from the equilibrium position. From the given inequation it follows that the stepped structure in the PBs spectrum for the specified magnitude of the reciprocal lattice vector will be more contrast for wide radiation angles θ. Really, with growing angle θ the minimum

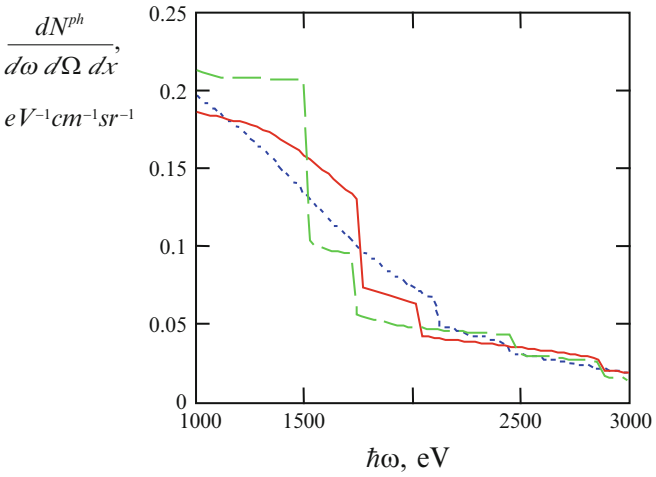

Fig. 5.4 The spectrum of PBs in a silver polycrystal for different radiation angles: *solid curve* – 90°, *dotted curve* – 60°, *dashed curve* – 120°

momentum transferred to a target increases and the contribution of the incoherent component of PBs decreases.

For reference we will give the formula for the root-mean-square deviation of crystal lattice atoms from their equilibrium position:

$$\langle u^2 \rangle = \frac{3\hbar^2}{4 M_a T_D} \left[1 + 4 \left(\frac{T}{T_D} \right)^2 \int_0^{T_D/T} \frac{y\, dy}{e^y - 1} \right], \tag{5.17}$$

where T_D is the Debye temperature in energy units, M_a is the mass of substance atoms. The Debye temperatures for aluminum, silicon, iron, and copper are respectively 418, 658, 467, and 339 K [1].

The dependence of the spectrum of PBs in a silver polycrystal on the angle of bremsstrahlung photon radiation is shown in Fig. 5.4.

From this figure it is seen that with increasing radiation angle the relative value of the "frequency jump" increases, and its position is shifted to the region of lower frequencies according to the formulas (5.15), and (5.16). Really, if the radiation angle is obtuse (the cosine is a negative value), then, as seen from the Eq. (5.16), the condition of "manifestation" of the spectral step is satisfied better than for smaller angles, when the cosine is equal to zero or takes on positive values. Physically this is connected with the fact that with growing radiation angle the relative contribution of the coherent component of PBs increases (in comparison with the incoherent component), and spectral steps, as seen from the expression (5.14), are caused just by coherent PBs. Thus the spectral steps are more noticeable for a radiation angle of 120° and are poorly discernible for a angle of 60°.

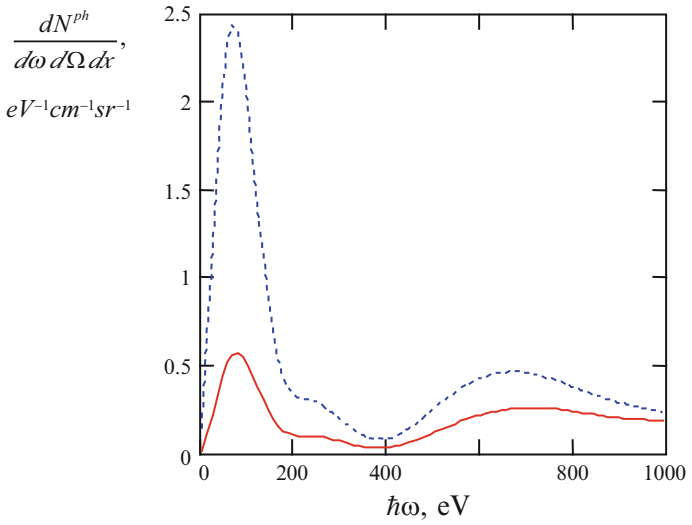

Fig. 5.5 PBs of an ion with the charge $Z_p = 30$ and the velocity $v = c/3$ in a silver polycrystal (*solid curve*) and on a silver atom (*dotted curve*) in the low-frequency range

In calculation of the spectrum of PBs in a silver polycrystal the following value of root-mean-square deviation of lattice ions from their equilibrium values $u_{Ag} = 0.087$Å was used. In the sum over the vectors of the reciprocal lattice with equal magnitudes that defines coherent PBs 50 summands were taken into account, for which $S(\mathbf{g}) \neq 0$. It should be noted that in taking into account 40 summands the result for photon yield (in an energy range from 1 to 10 keV) changes less than by 1 %.

Shown in Fig. 5.5 is the spectrum of PBs of a multiply charged ion $Z_p = 30$ with the velocity $v = c/3$ for a radiation angle of 90° in a silver polycrystal and on a silver atom in the low-frequency range.

In this case spectral steps are absent since the argument of the theta function in the formula (5.14) is positive for all $g \neq 0$. It is also seen that in this frequency range PBs in a polycrystal is *suppressed* in comparison with PBs on an isolated atom. This fact can be explained by superimposition of two circumstances. First, as seen from the formula (5.10), in the region of low frequencies $\omega < v/u$ the incoherent summand it small, and PBs is defined by the coherent component (Eq. 5.14). Second, momenta transferred to a target do not all make a contribution to coherent PBs in a polycrystal, but only those momenta, the magnitudes of which are equal to the magnitude of one of reciprocal lattice vectors. It is this fact that reduces the process intensity in comparison with radiation on an isolated atom, when the contribution to the process is made by all momenta transferred to a target that are permitted by the conservation law. For example, for the frequencies $\omega << v\, g$ the transferred momenta of small magnitude $\omega/v \leq q < g$ do not make a contribution to coherent PBs in a polycrystal, while it is just these momenta that play an important role in formation of PBs on an isolated atom.

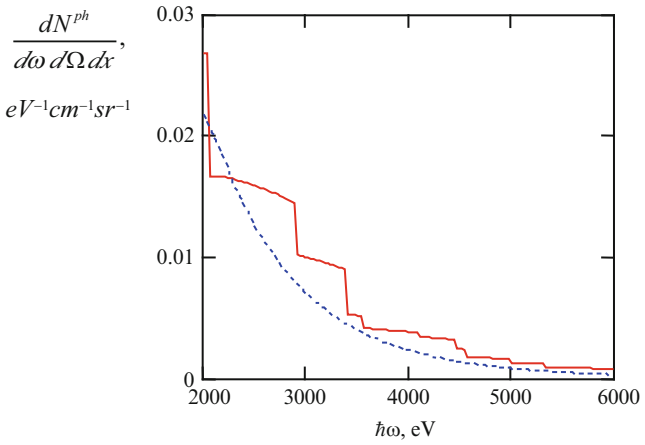

Fig. 5.6 The yield of PBs photons per unit trajectory length for an ion scattered in polycrystalline aluminum for different ion velocities: *solid curve* – v = c/3 (the ordinate is increased five times), *dotted curve* – v = c/20

The maxima of the frequency dependence in Fig. 5.5 are connected with the maxima of the imaginary part of the silver atom polarizability for photon energies close to the potentials of ionization of the shells *N* and *M*.

Presented in Fig. 5.6 is the dependence of the spectrum of PBs in an aluminum polycrystal on the velocity of an incident particle. The solid curve represents the radiation spectrum for a rather high value of the ion velocity (v = c/3).

With decreasing velocity, first, the contribution of the incoherent process increases, and second, the position of frequency steps is shifted to the low-frequency range.

Thus the position of a frequency step in the PBs spectrum can serve as a measure of energy of a scattered ion, and by the frequency shift ω_j it is possible to judge the energy loss for an incident particle. The dashed curve in Fig. 5.6 corresponds to the ion velocity equal to the velocity of protons with an energy of 1 MeV used in the experiments [4]. It is seen that in such an event the PBs spectrum does not contain a characteristic solid-state structure, but coincides with the spectrum of radiation on an isolated atom. It was this fact that took place in the experiments [4], in which no stepped spectrum structure was observed. This is explained by the fact that in case of low ion velocities the incoherent component of PBs prevails over the coherent component beginning with a photon energy of 500 eV. As a result, the stepped spectrum structure is found to be completely hidden behind the incoherent background.

Presented in Fig. 5.7 is the ratio of the contributions of the coherent and incoherent PBs channels for two values of energy (50 and 10 keV) of an electron scattered in polycrystalline copper, the radiation angle is 90°.

It will be recalled that coherent PBs corresponds to transfer of a momentum from an incident particle to a crystal lattice as a whole, and incoherent PBs arises during

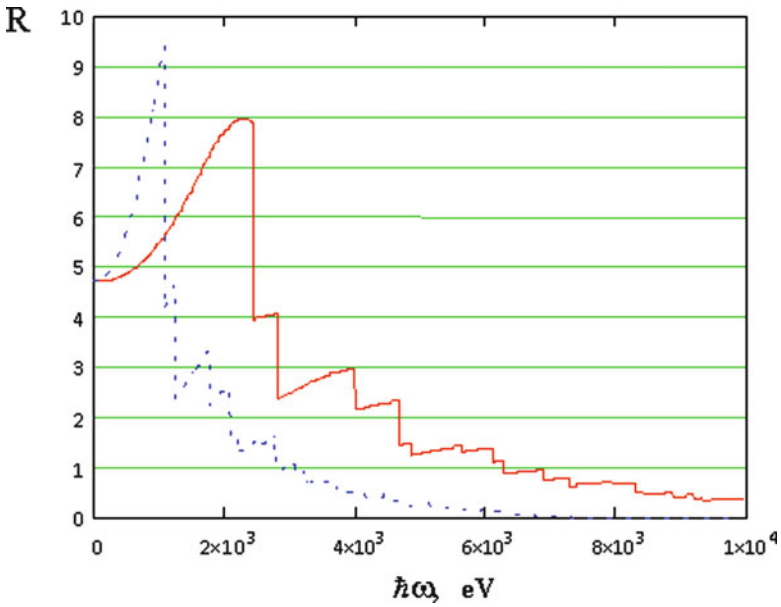

Fig. 5.7 The ratio of the coherent channel to the incoherent channel in PBs of an electron with an energy of 50 keV (*solid curve*) and 10 keV (*dash*-and-*dot curve*) scattered in copper

pair collisions between a scattered charge and target atoms. It is seen that in the low-frequency range coherent PBs prevails over incoherent PBs, for 50 keV electrons the contributions of both channels being compared at $\hbar\omega = 6.1$ keV and for 10 keV electrons at $\hbar\omega = 3$ keV. Thus the more is the velocity of an incident particle the wider is the spectral range of prevalence of coherent PBs over incoherent PBs.

In the high-frequency region of the PBs spectrum ($\hbar\omega > 10$ keV) characterized by high values of the momentum transferred to a target (or low values of the impact parameter) incoherent PBs prevails. Therefore the solid-state spectrum structure caused by the coherent interaction of an incident particle with the target becomes poorly discernible. As a result, the spectrum of PBs in a polycrystal approaches the spectrum on an isolated atom as it must be according to the physical picture of the process.

Thus for observation of frequency steps in the spectrum of PBs on a polycrystal it is necessary to use charged particles of high enough energy and to watch in the intermediate region of photon energy: from 1.5–2 to about 6 keV.

In the relativistic case in the PBs spectrum, instead of spectral steps, peaks are observed that correspond to the fulfilment of the Bragg condition for a virtual photon scattered by a polycrystalline target to a real photon. The maximum condition can be obtained from the formula (4.53) in the limit $\Delta \to 0$. Then we have $x_{\max} \approx 2\sin(\theta/2)$ or $\omega_g \approx g\,c/2\sin(\theta/2)$ – the frequency of a peak in the spectrum of PBs of a relativistic particle corresponding to the magnitude of the

reciprocal crystal lattice vector g. An analogous result was obtained in the N.N. Nasonov's work [5] within the framework of classical electrodynamics. Experimentally, the maxima of PBs of relativistic electrons in a polycrystalline target were for the first time recorded in the work [6] (see Fig. 2 of Chap. 1).

As was already said, the maxima in the spectrum of coherent PBs of a relativistic electron in a polycrystal correspond to Bragg scattering of virtual photons of its electromagnetic field by atomic planes. The Bragg condition for PBs in a polycrystal in the limit is expressed by the equation

$$\mathbf{k} - |\mathbf{k}| \frac{\mathbf{v}}{\mathrm{v}} = \mathbf{g}. \tag{5.18}$$

In writing Eq. 5.18 it was assumed that the wave vector of a virtual photon is directed along the velocity of an incident particle and is equal in magnitude to the wave vector of a real bremsstrahlung photon. This assumption is substantiated by the fact that the structure of the ultrarelativistic charge field is close to a plane wave with a wave vector parallel to the velocity of a particle. The graphic representation of the Eq. 5.18 is given in Fig. 5.8.

It should be noted that in case of a polycrystalline target for any radiation angle there will always be a crystallite, one of crystallographic planes of which is the bisector of the angle between the vectors **k** and **v** as shown in Fig. 5.8.

5.3 Polarization Bremsstrahlung in an Amorphous Medium

In case of PBs on an amorphous target, instead of the crystal structure factor (5.3) in the formula for the Bs cross-section (5.1) the following expression should be used:

$$S(\mathbf{q}) = {n_a}^{-1} \sum_{j,l} \left\langle \exp\left(i\,\mathbf{q}\,(\mathbf{r}_j - \mathbf{r}_l)\right)\right\rangle = 1 + n_a \int [g(r) - 1]\, \exp(i\,\mathbf{q}\,\mathbf{r})\, d\mathbf{r}. \tag{5.19}$$

The second equation in Eq. 5.19, where $g(r)$ is the pair correlation function for atoms, relates to an isotropic medium. For the structure factor of an amorphous substance in the "hard-sphere" approximation, when $g(r) = \Theta(r - D_a)$ (D_a is the mean diameter of an atom, $\Theta(x)$ is the theta function), from Eq. 5.19 it follows:

$$S_{amor}(q) = \left[1 - \sigma\, \frac{3 j_1(q D_a)}{q D_a}\right],\ \sigma = \frac{4\,\pi\, n_a {D_a}^3}{3}, \tag{5.20}$$

where $j_1(x)$ is the first-order spherical Bessel function. The second summand in the square brackets of the second equation (5.19) reflects the fact of destructive

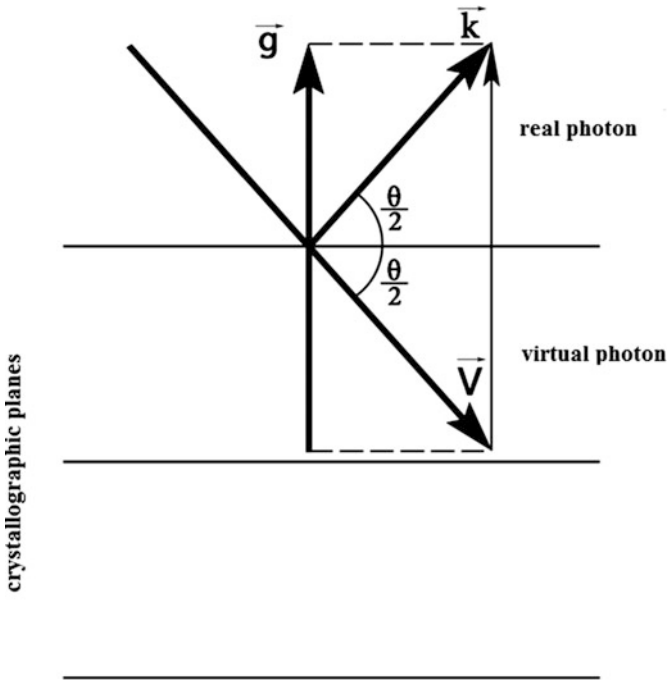

Fig. 5.8 The graphic representation of the Bragg condition for PBs of a relativistic particle scattered in a crystal

interference of the contributions of amorphous medium atoms to the total PBs intensity, with the result that the suppression of PBs occurs. It is obvious that the effect of PBs suppression connected with this interference is essential in the case that the parameter σ is close to one. Besides, for manifestation of this effect it is necessary that the argument of the spherical Bessel function $x = q D_a$ is less than one. Hence in view of the expression for the minimum momentum transferred to the medium $q_{\min} = (1 - (\mathrm{v}/\mathrm{c})\cos\theta)(\omega/\mathrm{v})$, we obtain:

$$\omega < \frac{\mathrm{v}}{D_a\,(1 - (\mathrm{v}/\tilde{c})\cos\theta)}, \tag{5.21}$$

where $\tilde{c}$ is the velocity of light in the target material. This inequation (with fulfilment of the condition $\sigma \approx 1$) determines the spectral range of suppression of PBs in an amorphous medium depending on the IP velocity and the angle of photon emission. Physically, corresponding to the condition (5.21) are such parameters of the problem, with which the contribution of small transferred momenta (high impact parameters) to the process is essential. Then PBs is of a collective nature, and mutual screening of different atoms reducing the process intensity occurs. This screening can be interpreted also as destructive interference of elementary PBs fields formed by individual atoms.

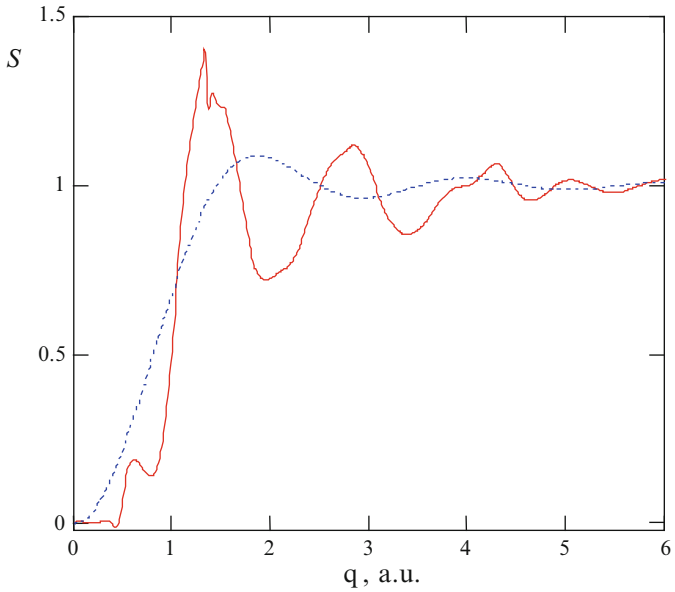

Fig. 5.9 The structure factor of amorphous silicon: *solid curve* – quantum-chemical calculation [7], *dotted curve* – calculation by the formula (5.20)

The use of the "hard-sphere" approximation (Eq. 5.20) for calculation of PBs intensity requires knowledge of the parameter $\sigma = 4\pi n_a D_a^3/3$. And if the concentration of atoms can be easily estimated from the known density of a substance, in determination of the mean atomic radius D_a being a model value there can be difficulties, especially in case of a medium with high atomic concentration. Let us illustrate the aforesaid by the example of the structure factor of liquid silicon, for which in the work [7] the results of quantum-chemical calculations are given. Calculated in [7], the dependence of the structure factor on the momentum transferred to the medium q at the melting temperature for silicon $T = 1410°\mathrm{C}$ is presented in Fig. 5.9 by the solid curve. Given in the same figure is the structure factor of liquid silicon calculated in the "hard-sphere" model for $\sigma = 1$ (dotted curve). This value of the parameter σ for the real density of liquid silicon $n_a = 5.446 \times 10^{22}$ cm^{-3} corresponds to the mean $D_a = 1.64$ Å that was used in construction of the dotted curve of Fig. 5.9. At the same time the tabular value of the silicon atomic diameter is $D_a = 2.36$ Å [8]. (It should be noted that the doubled Wigner-Seitz radius for the above concentration of silicon atoms is 3.27 Å). But with such a value of D_a the parameter $\sigma \cong 3$, so $S(q \to 0) < 0$, which is in contradiction with the positive definiteness of the structure factor of the medium.

A similar conclusion can be made for amorphous carbon and other condensed media of light atoms, when the model structure factor (5.20) causes a contradiction with the numerical values of the problem parameters. It should be noted that the pair

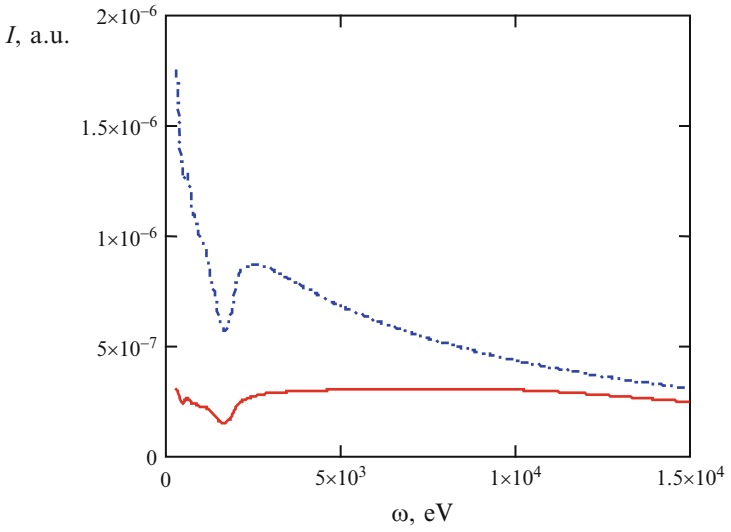

Fig. 5.10 The spectral intensity of PBs of an electron with $\gamma = 10$ on a target of amorphous silicon at the angle of radiation $\theta = 18°$: *solid curve* – radiation in amorphous silicon, *dash*-and-*dot curve* – PBs on an individual silicon atom

correlation function $g(r)$ used in the work [7] for determination of $S(q)$ differs noticeably from the theta function of the "hard-sphere" model. This difference is especially great at short distances $r \approx D_a$, where there is a maximum of the correlation function: $g \approx 2$. The last circumstance is indicative of the presence of a short-range order in liquid silicon at melting temperature.

Presented in Fig. 5.10 are the results of calculation of the spectrum of PBs in liquid silicon normalized to the concentration of medium atoms n_a and in scattering of an electron by an isolated atom. The plots of Fig. 5.10 are constructed for a relativistic electron with the Lorentz factor $\gamma = 10$ ($\gamma = \left(1 - (\mathrm{v}/c)^2\right)^{-1/2}$) and the angle of bremsstrahlung photon radiation $\theta = 18°$. The maximum of the spectral dependence for an isolated atom is caused by increasing polarization charge of a silicon atom, when the bremsstrahlung photon energy approaches the energy of ionization of the K-shell.

It is seen that the intensity of PBs in liquid silicon is much less than in the monatomic case throughout the range of photon energies due to destructive interference of contributions of different atoms discussed above. The calculation shows that for the larger radiation angle $\theta = 90°$ and the same other parameters the effect of PBs suppression takes place in the low-energy range $\hbar\,\omega < 3$ keV. This fact corresponds to the inequation (5.21) determining the region of essentiality of destructive interference in PBs. In the relativistic case with growing radiation angle the minimum momentum transferred to a medium increases and, as a result, the role of cooperative effects causing destructive interference decreases. Therefore

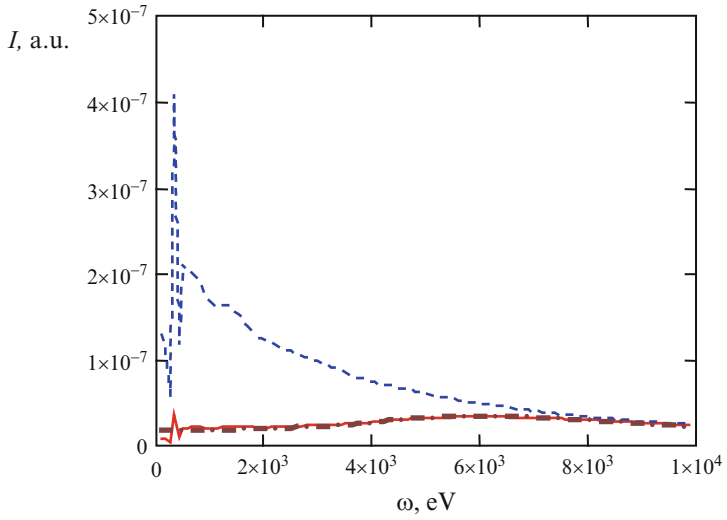

Fig. 5.11 The spectral intensity of PBs of a relativistic electron ($\gamma = 10$, $\theta = 45^\circ$) on a carbon target: *solid curve* – radiation on a target of amorphous carbon, *dotted curve* – PBs on a carbon atom, *dash*-and-*dot curve* – PBs on amorphous carbon in the high-frequency approximation

the effect of suppression of PBs intensity for large radiation angles occurs at lower frequencies, when the minimum transferred momentum is low enough, and in an elementary radiative act several medium atoms are involved.

In the experiment [9] that has shown the effect of suppression of PBs in an amorphous medium, radiation of an electron with an energy of 5–7 MeV scattered by a thin-film target of amorphous carbon was recorded. It is of interest to calculate the PBs intensity for experimental conditions [9] within the framework of the approach under consideration. The corresponding results are given in Fig. 5.11 for the Lorentz factor of a scattered electron $\gamma = 10$, the radiation angle 45°, the target density $\rho = 2.4$ g/cm^3, and the mean diameter of a carbon atom $D_a = 1.258$ Å, (at which $\sigma = 4\pi n_a D_a^3/3 = 1$).

Shown in the same figure are the results of calculation of the PBs intensity in amorphous carbon in the high-frequency approximation. From the form of the curves it follows that the suppression effect is most pronounced in the range of bremsstrahlung photon energies $\hbar\omega < 5$ keV, which corresponds to the experimental data of the work [9]. The maxima of the spectral dependences correspond to the binding energies for electrons of the K – and L-shells of a carbon atom – 296 and 16.6 eV. It is seen also that the high-frequency approximation well describes the process in a wide spectral range up to photon energies of 300 eV.

The analysis shows that the error of calculation of PBs intensity caused by inaccuracy of the model used for the structure factor of a medium depends on problem parameters. This error is most essential in the low-frequency range for large radiation angles, besides, it grows with increasing energy of an incident electron. The comparison of the results of calculation of PBs in liquid silicon

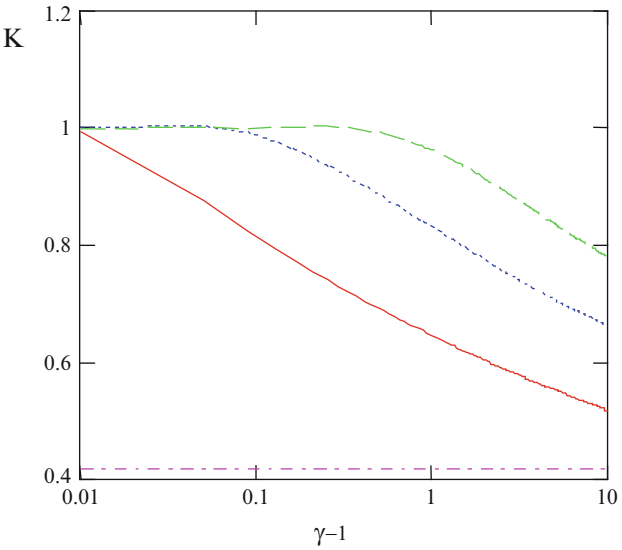

Fig. 5.12 The suppression ratio for PBs in amorphous silver as a function of the energy of an incident particle for the radiation angle $\theta = 18°$ and three values of bremsstrahlung photon energy: *solid curve* –$\hbar\omega = 300$ eV, *dotted curve* – $\hbar\omega = 1$ keV, *dashed curve* – $\hbar\omega = 3$ keV

obtained in the "hard-sphere" model and with the use of the quantum-chemical structure factor [7] gives a characteristic error no more than 20 % for $\gamma = 10$ and $\theta = 18°$. With growing radiation angle the calculation error increases, but the effect of PBs suppression itself decreases.

The effect of suppression of PBs in an amorphous medium in the X-ray range is essential only for relativistic incident particles. In case of a nonrelativistic electron beam it can be neglected, at least for bremsstrahlung photon energies more than 1 keV. This circumstance is illustrated by Fig. 5.12, where the X-axis corresponds to the energy of an incident particle normalized to the rest energy (for an electron to 511 keV), the Y-axis is the ratio of the intensity of PBs in an amorphous medium to the intensity of PBs on an atom.

Also shown in Fig. 5.12 is the straight line corresponding to the value of the PBs suppression ratio obtained in the limit of low transferred momenta: $K = 1 - \sigma = 0.417$. The suppression effect more strongly shows itself for lower photon energies, when the role of destructive interference of contributions of different atoms to the intensity of the process is great. In the low-frequency range PBs suppression occurs also for nonrelativistic incident particles, when $\gamma - 1 << 1$. For photons of high energies ($\omega > 1$ keV) the PBs intensity decreases noticeably only in case of high Lorentz factors γ. A characteristic feature of the curves in Fig. 5.12 is the presence of such inflection points γ^* that for $\gamma > \gamma^*$ the effect of PBs suppression begins. It should be noted that for large values of the Lorentz factor $\gamma > 10^4$ the suppression ratio becomes less than its limiting value $K = 1 - \sigma = 0.417$ (calculated to the logarithmic accuracy). This is connected with the density

effect in PBs, when the intensity of the process decreases as a result of screening of the IP eigenfield at $\varepsilon(\omega) < 1$ ($\varepsilon(\omega)$ is the dielectric permittivity of a medium). The last inequation for a silver target is satisfied in the range of photon energies: $\hbar\,\omega > 50$ eV.

A similar effect of suppression of PBs intensity in the low-frequency range takes place in scattering of a charged incident particle in a polycrystal [3] as was said in the previous section. As in case of an amorphous medium in a polycrystal for low transferred momenta $q < 2\,\pi/d$ (d is the lattice constant), the interference of the contributions of substance atoms to the intensity of the polarization channel is of a destructive nature, reducing the intensity of radiation. It should be noted that the appreciable value of the suppression ratio in an amorphous medium is possible only for relativistic incident particles (Fig. 5.12), while in a polycrystal the PBs intensity considerably decreases (times) in comparison with an isolated atom and in the nonrelativistic case [3].

The obtained expressions for the cross-section of Bs in different solid-state targets can be also used for estimation of intensity of radiation of secondary electrons produced in the target material by a primary electron beam, with corresponding replacement of kinematic parameters (velocity, photon energy, and radiation angle).

References

1. Ter-Mikaelian, M.: High Energy Electromagnetic Processes in Condensed Media. Wiley, New York (1972)
2. Animalu, A.O.E.: Intermediate Quantum Theory of Crystalline Solids. Prentice-Hall, New Jersey (1978)
3. Astapenko, V.A.: Polarization bremsstrahlung of heavy charged particles in polycrystal. JETP **99**, 958 (2004)
4. Ishii, K., Morita, S.: Continuum x-ray produced by light-ion-atom collisions. Phys. Rev. A **30**, 2278 (1984)
5. Nasonov, N.N.: Collective effects in the polarization bremsstrahlung of relativistic electrons in condensed media. NIM B **145**, 19 (1998)
6. Blashevich, S., Chepurnov, A., Grishin, V., et al.: Polarization bremsstrahlung of relativistic electrons in aluminium. Phys. Lett. A **254**, 230 (1999)
7. Stillinger, F.H., Weber, T.A.: Computer simulation of local order in condensed phases of silicon. Phys. Rev. B **31**, 5262 (1985)
8. Grigoriev, I.S., Meilihov, E.Z: Fisicheskie velichiny. Energoatomizdat, Moscow (1991) (in Russian)
9. Blashevich, S.V., Chepurnov, A.S., Grishin, V.K., et al.: Suppression of polarization bremsstrahlung of relativistic electrons moving through an amorphous carbon foil. Phys. Lett. A **211**, 309 (1996)

Chapter 6
Bremsstrahlung of Fast Charged Particles with an Electron Core in a Medium

6.1 Polarization Bremsstrahlung of a Hydrogen-Like Ion in a Crystal

6.1.1 Introductory Remarks

In scattering of a fast ion in a medium, ordinary (static) bremsstrahlung caused by acceleration of an incident particle (IP) in the field of a target is suppressed because of the high mass of an ion. So the prevailing mechanisms of photon emission in this case are connected with excitation (real or virtual) of electronic degrees of freedom of colliding particles. In emission of high-energy photons with an energy of the order of the IP kinetic energy, when a momentum transferred in collision is great in comparison with the characteristic momenta of bound electrons, considered as main mechanisms of radiation, as a rule, are processes with changing state of an electron subsystem. Among these processes are radiation ionization, emission of secondary electrons, and radiation electron capture [1]. In the spectral region far from the kinematic limit, when the characteristic transferred momentum is not great, and the photon frequency is of the order of the frequencies of excitation of bound electrons of colliding particles, it is necessary to take into account radiation caused by virtual excitation of electronic degrees of freedom without change of an electronic state. This kind of radiation defined by the dynamic polarizability of a target and an IP was called polarization bremsstrahlung [2].

PBs is a fundamental radiative process representing the conversion of the electromagnetic eigenfield (a virtual photon) of one of colliding particles to a real photon on the electron shell of another particle. In the case that both particles have electronic degrees of freedom, radiation can proceed by two channels according to on whose bound electrons the conversion of a virtual photon occurs. Thus, generally speaking, "target" PBs caused by the polarizability of target atoms (channel 1) and PBs of an incident particle caused by virtual excitation of an IP electron (channel 2) take place. The schematic representation of two PBs channels is shown in Fig. 6.1. It should be noted that the first PBs channel was studied by different authors both for a

V. Astapenko, *Polarization Bremsstrahlung on Atoms, Plasmas, Nanostructures and Solids*, Springer Series on Atomic, Optical, and Plasma Physics 72,
DOI 10.1007/978-3-642-34082-6_6,

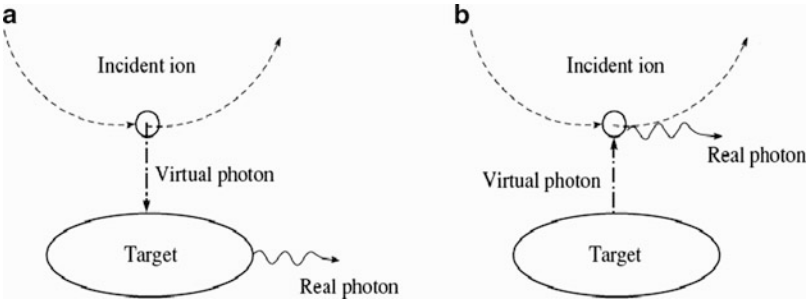

Fig. 6.1 (**a**) PBs by the first channel (target PBs), (**b**) PBs by the second channel (PBs from an IP)

case of collision of a pair of particles and in scattering in a medium [3–8]. The role of the second PBs channel is studied much less. Both PBs channels were first calculated in the works of M.Ya. Amus'ya with co-authors [2, Chap. 7].

In going to consideration of PBs of an ion with an electron core in a crystal, it is necessary to take into account collective effects caused by a possibility of coherent interaction of an IP with a target. This problem becomes especially urgent in connection with further improvement of methods of producing fast ion beams with specified characteristics including beams of multiply charged hydrogen-like ions [1]. Various aspects of interaction of such ions with a substance have been intensively studied in recent years [9, 10]. In particular, coherent excitation of a hydrogen-like argon ion in a single crystal was investigated experimentally [11], in which a momentum multiple of the momentum of a reciprocal lattice is transferred to a target (the Okorokov effect). Since PBs can be considered as a process of virtual excitation of a subsystem of bound electrons with their following radiation deexcitation, it is natural to expect that coherent effects such as the Okorokov effect are to show themselves in polarization bremsstrahlung as well.

6.1.2 Bremsstrahlung in a Polycrystal

The expression for PBs on a target due to virtual excitation of a medium electron in a polycrystal was derived in [5]. In this case the frequency-angular distribution of photon yield per unit length is given by the sum of the incoherent and coherent contributions:

$$\frac{dN_t}{dl\, d\omega\, d\Omega_{\mathbf{k}}} = \frac{dN_t^{(incoh)}}{dl\, d\omega\, d\Omega_{\mathbf{k}}} + \frac{dN_t^{(coh)}}{dl\, d\omega\, d\Omega_{\mathbf{k}}}. \tag{6.1}$$

Incoherent PBs on a target is described by the formula:

$$\frac{dN_t^{(incoh)}}{dl\, d\omega\, d\Omega_{\mathbf{k}}} = 2\, n_t\, \frac{e^2}{\hbar\,\omega}\, \frac{\left|\omega^2 \alpha_t(\omega)\right|^2}{\pi\, \mathrm{v}^2\, c^3} \times$$
$$\times \int\limits_{q_{\min}}^{q_{\max}} \left(1 - \exp\left(-u^2\, q^2\right)\right) \left[Z_{proj} - F_{proj}(q_{1c})\right]^2 F_t^2(q)\, I\varphi(q, \mathrm{v}, \omega, \theta)\, \frac{dq}{q}, \qquad (6.2)$$

where $n_t, \alpha_t(\omega), F_t(q)$ are the concentration, the dynamic polarizability, and the form factor of target atoms; $\mathbf{v}, Z_{proj}, F_{proj}$ are the velocity, the nuclear charge number, and the form factor of an incident ion (IP); $\omega, \mathbf{k}$ are the frequency and the wave vector of radiation in the target rest frame, θ is the angle between $\mathbf{v}$ and $\mathbf{k}$ in the same rest frame; $\hbar\mathbf{q}$ is the momentum transferred from an IP to the target, $\hbar\mathbf{q}_1$ is the change of the IP momentum, $\hbar\mathbf{q}_{1c}$ is the same value in the IP rest frame; u is the root-mean-square deviation of target atoms from the equilibrium position; c is the velocity of light; $q_{\min} = (1 - (\mathrm{v}/\mathrm{c})\, \cos\theta)\, (\omega/\mathrm{v}), q_{\max} = 2\,\mu\,\mathrm{v}$, μ is the target IP reduced mass;

$$I\varphi(q, \mathrm{v}, \omega, \theta) = \frac{q^3\, \mathrm{v}}{2\,\pi} \int d\Omega_{\mathbf{q}}\, \delta(\omega - \mathbf{k}\mathbf{v} + \mathbf{q}\mathbf{v})\, \frac{\left[\mathbf{s}, \omega\, \mathbf{v}/c^2 - \mathbf{q}\right]^2}{\left(\mathbf{q}^2 - 2\, \mathbf{k}\, \mathbf{q}\right)^2},\ \mathbf{s} = c\, \mathbf{k}/\omega, \quad (6.3)$$

is the integral with respect to the solid angle connected with the momentum transfer vector. This integral in the nonrelativistic limit takes the form

$$I\varphi(q, \mathrm{v}{<<}c, \omega, \theta) \cong \frac{1 + \cos^2\theta}{2} + \left(\frac{\omega}{q\,\mathrm{v}}\right)^2 \frac{1 - 3\cos^2\theta}{2}. \qquad (6.3a)$$

The formula (6.2) describes PBs on a target without excitation of bound electrons of the target and an IP – so-called "elastic" PBs.

The coherent part of PBs on a target is given by the following expression [5]:

$$\frac{dN_t^{(coh)}}{dl\, d\omega\, d\Omega_{\mathbf{k}}} = 2\, n_t^2\, \frac{e^2}{\hbar\,\omega}\, \frac{\left|\omega^2\ \alpha_t(\omega)\right|^2}{\pi\, \mathrm{v}^2\, c^3} \sum_g N(g)\ \Theta\left(g\mathrm{v} - \omega\left(1 - \frac{\mathrm{v}}{\mathrm{c}}\cos\theta\right)\right) \times$$
$$\times \frac{\exp(-u^2\, g^2)}{g^3}\, F_t^2(g)\, I\varphi(g, \mathrm{v}, \omega, \theta) \int\limits_0^{2\pi} \left[Z_{proj} - F_{proj}(g_{1c}(\phi))\right]^2 d\phi\ . \quad (6.4)$$

There is the sum over the magnitudes of the reciprocal lattice vectors $\mathbf{g}$, $N(g)$ is the number of these vectors with a specified magnitude g; φ is the azimuth angle of $\mathbf{g}$. In Eq. 6.4 averaging over the $\mathbf{g}$ direction is made to describe the contribution of all polycrystalline cells to the process. The theta function $\Theta(x)$ expresses the law of conservation of energy-momentum in radiation.

The expression for PBs of an IP (projectile) in a polycrystal can be derived with the use of the approach proposed in [2, Chap. 7] for description of PBs in atom-atom

collisions in the relativistic case. Generalization of this approach to scattering in a polycrystalline medium gives the following expression for the incoherent channel:

$$\frac{dN_{proj}^{(incoh)}}{dl\, d\omega\, d\Omega_{\mathbf{k}}} = n_t \frac{e^2}{\hbar\,\omega} \frac{\left|\omega\,\omega_c\,\alpha_{proj}(\omega_c)\right|^2}{\pi\,\mathrm{v}^2\,c^3}\left(1+\cos^2\theta_c\right)\times$$
$$\times \int\limits_{q_{\min}}^{q_{\max}} F_{proj}^2(q_{1c})[Z_t - F_t(q)]^2\left(1-\exp\left(-u^2\,q^2\right)\right)\frac{dq}{q}, \tag{6.5}$$

where $\alpha_{proj}(\omega_c)$ is the dynamic polarizability of an IP at the frequency in the IP rest frame and θ_c as a radiation angle in the IP rest frame. These values are connected with their analogs in the target rest frame according to the relations:

$$\omega_c = \gamma\,\omega\,(1-(\mathrm{v}/c)\,\cos\theta),\ \cos\theta_c = \frac{\cos\theta - \mathrm{v}/c}{1-(\mathrm{v}/c)\,\cos\theta}, \tag{6.6}$$

where $\gamma = 1/\sqrt{1-(\mathrm{v}/c)^2}$..

The coherent channel of PBs of an IP is described by the formula:

$$\frac{dN_{proj}^{(coh)}}{dl\, d\omega\, d\Omega_{\mathbf{k}}} = n_t^2 \frac{e^2}{\hbar\,\omega} \frac{\left|\omega\,\omega_c\,\alpha_{proj}(\omega_c)\right|^2}{\pi\,\mathrm{v}^2\,c^3}\left(1+\cos^2\theta_c\right)\times$$
$$\times \sum_g N(g)\ \Theta\left(g\mathrm{v} - \omega\left(1-\frac{\mathrm{v}}{\mathrm{c}}\cos\theta\right)\right)\frac{\exp(-u^2\,g^2)}{g^3}$$
$$\times\ [Z_t - F_t(g)]^2 \int\limits_0^{2\pi} F_{proj}^2(g_{1c}(\phi))\,d\phi\,. \tag{6.7}$$

Total PBs on an IP is given by the sum of Eqs. 6.5 and 6.7 as in the case of PBs on a target Eq. 6.1.

Let us consider a hydrogen-like incident ion. The eigenfrequencies of its bound electrons are given by the Bohr formula (the initial state of an IP electron is supposed to be the ground state):

$$\omega_n = Z_{proj}^2\,Ry\left(1-n^{-2}\right), \tag{6.8}$$

where Ry =13.6 eV and n is the principal quantum number. The IP form factor is

$$F_{proj}(q_1) = \frac{1}{\left(1+\left(a_{proj}\,q_1/2\right)^2\right)^2}, \tag{6.9}$$

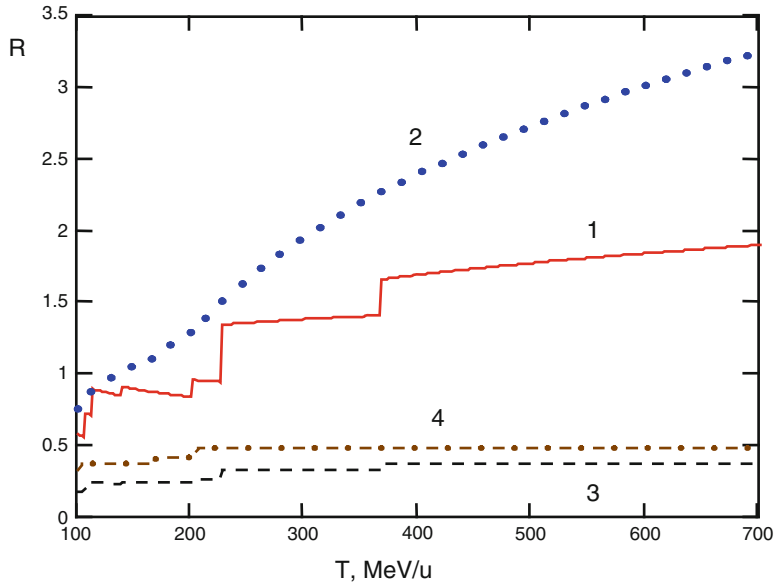

Fig. 6.2 The ratio between the coherent and incoherent contributions to PBs of an incident Ar^{17+} ion in aluminum: *1* – PBs on a target ($\theta = \pi/2$); *2* – PBs on a target ($\theta = \pi/6$); *3* – PBs on an IP ($\theta = \pi/2$); *4* – PBs on an IP ($\theta = \pi/6$)

where $a_{proj} = \hbar^2 / \left(Z_{proj}\, m\, e^2\right)$ is the Bohr radius. The general expression for the dynamic polarizability of an IP has the usual form:

$$\alpha_{proj}(\omega_c) = \frac{e^2}{m} \sum_n \frac{f_n}{\omega_n^2 - \omega_c^2}, \tag{6.10}$$

where f_n are the oscillator strengths that in case of a hydrogen-like ion have universal values independent of the charge number Z_{proj}. Small imaginary additives in the denominators on the right side of the Eq. 6.11 are omitted since further we do not consider the exact resonance when $\omega_c = \omega_n$.

At first, let us compare the contributions of the coherent and incoherent channels to PBs on a target and an IP. Figure 6.2 demonstrates this comparison for two values of radiation angles in case of scattering of a hydrogen-like argon ion in polycrystalline aluminum ($R = dN^{(coh)} / dN^{(incoh)}$).

The ratio R in Fig. 6.2 is shown as a function of the IP kinetic energy T for the specified photon energy $\hbar\omega = 6$ keV. The curves 1, 2 correspond to PBs on a target, the curves 3, 4 correspond to PBs on an IP. It can be seen from Fig. 6.2 that in case of PBs on a target the coherent channel prevails over the incoherent channel ($R > 1$), while for PBs on an IP there is an opposite situation ($R < 1$). The latter is due to the fact that in case of PBs on an IP an incident ion should approach the target nucleus to interact with it. But at such small distances the coherent interaction

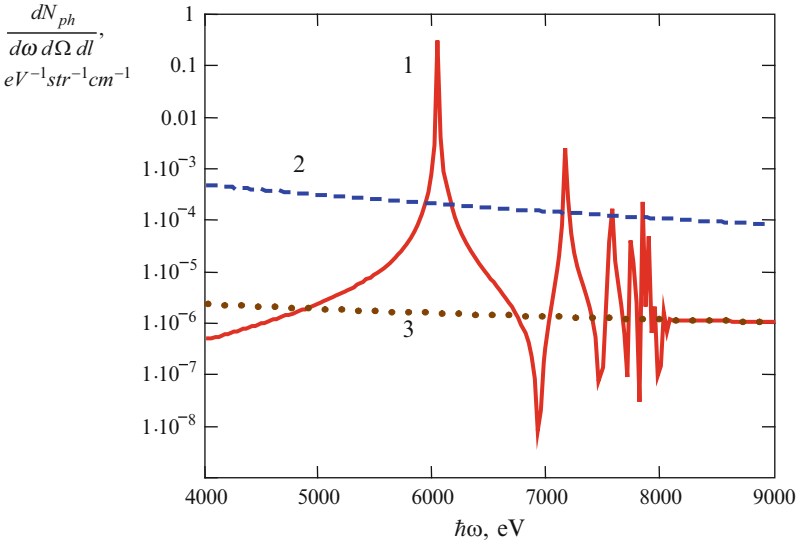

Fig. 6.3 The spectra of PBs of an Ar^{17+} ion in polycrystalline aluminum: *1* – PBs on an IP, *2* – PBs on a target, *3* – electron bremsstrahlung; T = 390 MeV/u ($\gamma = 1.42$), $\theta = \pi/6$

between an IP and the solid target is weak. During PBs on a target an incident ion interacts with target electrons. This interaction occurs at long distances (if the radiation frequency is not very high), so then coherent IP scattering by the target is strong enough. Coherent PBs leads to appearance of a distinct stepped structure on the curve 1. This structure is due to the presence of theta functions in the formulas (6.4), (6.7) that correspond to turning of the additional reciprocal lattice vector in the process with increasing IP kinetic energy.

Figure 6.3 demonstrates the spectra of PBs of an Ar^{17+} ion scattered in polycrystalline aluminum for the IP (curve 1) and target (curve 2) channels. There is also the spectrum of electron bremsstrahlung on the same target (curve 3).

In Fig. 6.3 the presence of sharp and relatively wide maxima in the spectrum of PBs on an IP can be seen (curve 1). These maxima correspond to fulfilment of the resonant conditions in the denominators of the expression for the dynamic polarizability of an IP (Eq. 6.10) in case of a hydrogen-like incident particle. Due to the Doppler effect (the first equation in Eq. 6.6), the resonance frequencies in the laboratory reference system depend on the IP energy and the radiation angle according to the formula

$$\omega_{\max}(n, \mathrm{v}, \theta) = \frac{\omega_n}{\gamma\,(1 - (\mathrm{v}/c)\,\cos\theta)}, \tag{6.11}$$

where ω_n is the eigenfrequency of a bound electron of an IP (Eq. 6.8), γ is the Lorentz factor. The first spectral maximum in Fig. 6.3 corresponds to virtual excitation of an IP electron to the excited state with $n = 2$. According to the formula (6.11), the resonant photon energy in this case (for specified values of T and θ) is

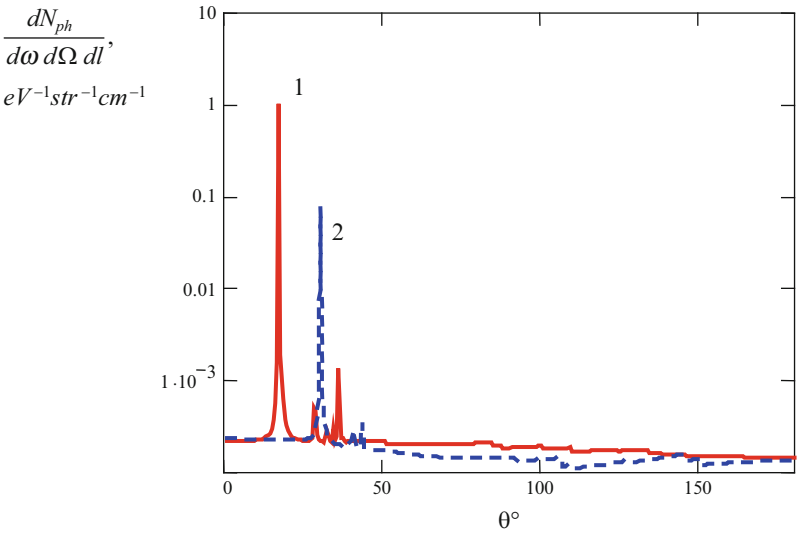

Fig. 6.4 The angular dependence of PBs on scattering of an Ar^{17+} ion in polycrystalline aluminum, $\hbar\omega = 6$ keV: *1* – T = 100 MeV/u, *2* – T = 390 MeV/u

6,041 eV, while in the IP rest frame it is equal to 3,305 eV. As can be seen from Fig. 6.3, in the vicinity of the maxima PBs on an IP strongly prevails over PBs on a target and electron bremsstrahlung. In the high-frequency limit the curves 1 and 3 coincide. This has a simple physical interpretation. A bound electron interacts with high-frequency radiation as a quasi-free electron. Therefore scattering of the IP eigenfield by an IP electron to a real high-energy photon occurs as by a free electron.

The angular dependence of PBs on scattering of an Ar^{17+} ion in polycrystalline aluminum ($\hbar\omega$ =6 keV) is shown in Fig. 6.4 for two values of IP kinetic energy.

There are also sharp maxima due to dependence of the resonance frequency in the target reference system on the radiation angle (Eq. 6.11). Radiation angles corresponding to the maxima in the angular PBs distribution are given by the formula:

$$\theta_{\max}(n,\omega,\mathrm{v}) = \arccos\left\{\frac{c}{\mathrm{v}}\left(1-\frac{\omega}{\gamma\,\omega_n}\right)\right\}, \tag{6.12}$$

where ω_n is the eigenfrequency of an IP electron (Eq. 6.8). It can be seen from Fig. 6.4 that the angles of the maxima increase with increasing IP kinetic energy.

Presented in Fig. 6.5 is PBs from hydrogen-like argon as a function of the IP kinetic energy for two values of the radiation angle. There are also sharp maxima in these dependences that have the same reason as in the case of the spectral-angular distribution of PBs. In this case, however, the first excitation frequency (Eq. 6.8) (n = 2) in the sum (Eq. 6.10) corresponds to the high-energy peaks on the curves 1, 2.

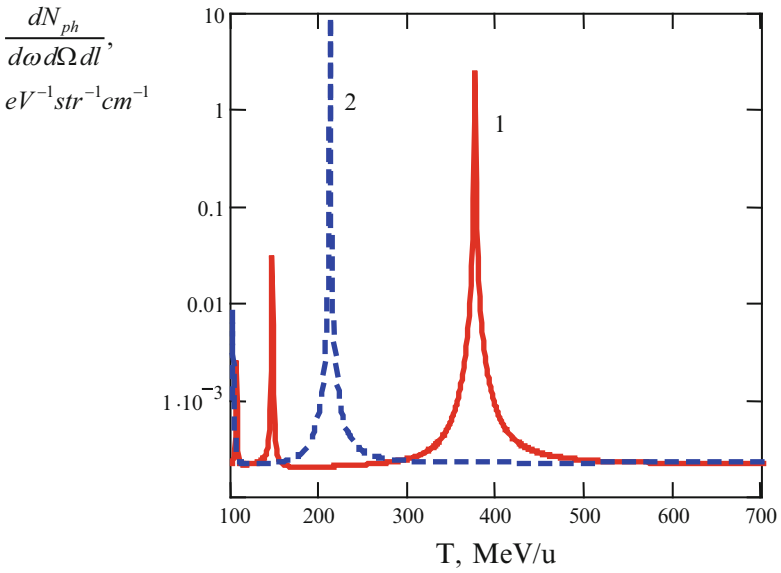

Fig. 6.5 PBs from an Ar^{17+} ion in polycrystalline aluminum as a function of the IP kinetic energy, $\hbar\omega = 6$ keV: *1* – $\theta = \pi/6$, *2* – $\theta = \pi/10$

This is due to the fact that the radiation frequency in the IP rest frame decreases with increasing IP kinetic energy according to the first formula (6.6).

It is shown that scattering of a fast multiply charged hydrogen-like ion in a polycrystalline target results in intense radiation that has a sharp frequency and angular dependence. This radiation arises due to scattering of the electromagnetic eigenfield of a target to a real photon by a bound electron of an IP (IP polarization bremsstrahlung). The PBs channel studied earlier due to scattering of the IP field to a real photon by target electrons may be called PBs on a target. In contrast to PBs on a target, the main contribution to PBs on an IP is made by the incoherent channel of the process. In this item it is demonstrated that the frequency-angular features of PBs on an IP strongly depend on the IP energy.

6.1.3 Bremsstrahlung in a Single Crystal

In this section we will consider a situation when a fast hydrogen-like ion with the velocity **v** is scattered in a single crystal and emits a PBs photon with the wave vector **k** in the geometry shown in Fig. 6.6.

The axes of the Cartesian coordinate system presented in this figure coincide with the crystallographic axes of the target. The ion velocity is supposed to be high enough, so that the first Born approximation for interaction of an IP with the target can be used. As was mentioned at the beginning of Chap. 6, in the case under consideration PBs proceeds by two channels: Eq. 6.13 due to virtual excitation of target electrons and Eq. 6.14 as a result of virtual excitation of the electron core of

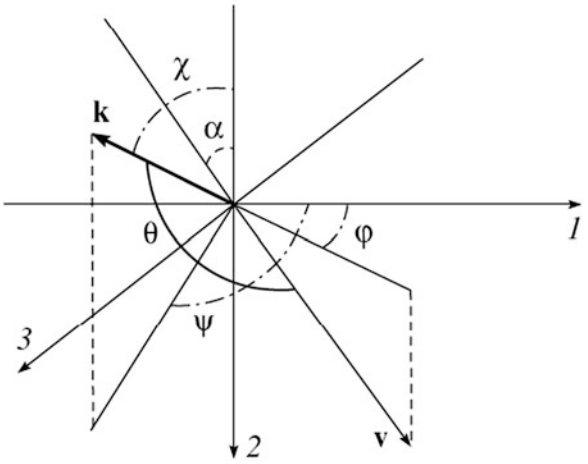

Fig. 6.6 The geometry of the process

an IP. In the first case scattering of the electromagnetic eigenfield of an incident ion to a real photon by target electrons occurs, and in the second case, on the contrary, there is scattering of the target eigenfield to a real photon by the electron core of an IP (Fig. 6.1). The expressions for the cross-sections of these channels can be obtained by summation of the contributions of PBs on different atoms (ions) of a substance. In the case under consideration with a crystalline target for each of the channels two types of the process are possible: the coherent process, when a momentum from an incident particle is transferred to the crystal lattice as a whole, and the incoherent process in case of pair interaction of an IP with atoms (ions) of a medium. Thus there are four kinds of PBs in consideration: coherent PBs on a target and an IP and incoherent PBs on a target and an IP.

To estimate the PBs value, it is convenient instead of the cross-section to use the number of photons emitted by an IP per unit length in the unit frequency range and to the unit solid angle. Then for coherent PBs by the first channel (Fig. 6.1a) the following expression can be obtained:

$$\frac{dN_t^{(coh)}}{dl\, d\omega\, d\Omega_{\mathbf{k}}} = \frac{n_t^2\, e^2}{\pi\, \hbar\, \mathrm{v}\, c^3} \sum_{\mathbf{g}} S^2(\mathbf{g})\ \delta(\omega + \mathbf{g}\mathbf{v} - \mathbf{k}\mathbf{v})\, \omega^3\, |\alpha_t(\omega)|^2 \times$$

$$\times \exp\left(-u^2\, g^2\right) \tilde{F}_t^2(g)\, \left[Z_{proj} - F_{proj}(g_{1c})\right]^2\, \frac{\left[\mathbf{s}, \omega\, \mathbf{v}/c^2 - \mathbf{g}\right]^2}{\left(\mathbf{g}^2 - 2\, \mathbf{k}\, \mathbf{g}\right)^2}. \quad (6.13)$$

Here the following designations are introduced: n_t is the concentration of target atoms, e is the elementary charge, c is the velocity of light, $S(\mathbf{g})$ is the geometrical structure factor of the crystal, $\mathbf{g}$ is the reciprocal lattice vector, ω is the frequency of a bremsstrahlung photon, $\alpha_t(\omega)$ is the dynamic polarizability of target atoms, u is the root-mean-square deviation of target atoms from the equilibrium position, $\tilde{F}_t(q)$ is the normalized form factor of medium atoms, Z_{proj} is the charge number of the IP nucleus, $F_{proj}(q)$ is the form factor of the IP electron core, $\mathbf{s} = c\,\mathbf{k}/\omega$ is the unit

vector in the direction of photon emission, $\mathbf{g}_1 = \mathbf{g} - \mathbf{k}$, $\mathbf{g}_{1c}$ is the reciprocal lattice vector in the reference system connected with an IP.

In derivation of the formula (6.13) integration with respect to the transferred wave vector $\mathbf{q}$ was performed in view of interaction of an IP with the target, which resulted in the equation $\mathbf{q} = \mathbf{g}$. The squared concentration of target atoms on the right side of the Eq. 6.13 is indicative of the coherent behavior of the process. The presence of the dynamic polarizability of target atoms in the formula (6.13) reflects the fact that photon emission results from induction of a variable dipole moment in target atoms during IP scattering. From the obtained expression it follows also that in the limit $u\,g > 1$ coherent PBs is low since then the coherence of IP interaction with a crystal lattice is violated.

The expression for incoherent PBs by the first channel looks like:

$$\frac{dN_t^{(incoh)}}{dl\,d\omega\,d\Omega_{\mathbf{k}}} = 2\,n_t\,\frac{e^2}{\hbar\,\omega}\,\frac{\left|\omega^2\alpha_t(\omega)\right|^2}{\pi\,\mathrm{v}^2\,c^3}\int\limits_{q_{\min}}^{q_{\max}}\left(1-\exp\left(-u^2\,q^2\right)\right)$$
$$\left[Z_{proj} - F_{proj}(q_{1c})\right]^2\,\tilde{F}_t^2(q)\,I\phi(q,\mathrm{v},\omega,\theta)\,\frac{dq}{q}, \tag{6.14}$$

where $q_{\min} = (1-(\mathrm{v}/\mathrm{c})\,\cos\theta)\,(\omega/\mathrm{v})$, $q_{\max} = 2\,\mu\,\mathrm{v}/\hbar$ are the minimum and maximum transferred vectors, μ is the reduced mass of an IP and an electron,

$$I\phi(q,\mathrm{v},\omega,\theta) = \frac{q^3\,\mathrm{v}}{2\,\pi}\int d\Omega_{\mathbf{q}}\,\delta(\omega - \mathbf{k}\mathbf{v} + \mathbf{q}\mathbf{v})\,\frac{\left[\mathbf{s},\,\omega\,\mathbf{v}/c^2 - \mathbf{q}\right]^2}{\left(\mathbf{q}^2 - 2\,\mathbf{k}\,\mathbf{q}\right)^2} \tag{6.15}$$

is the dimensionless integral that in the nonrelativistic limit is equal to:

$$I\phi(q,\mathrm{v}<<c,\omega,\theta) \cong \frac{1+\cos^2\theta}{2} + \left(\frac{\omega}{q\,\mathrm{v}}\right)^2\,\frac{1-3\cos^2\theta}{2}, \tag{6.16}$$

θ is the angle between the IP velocity vector and the wave vector of a bremsstrahlung photon (the radiation angle).

In contrast to coherent radiation (Eq. 6.13), incoherent PBs (Eq. 6.14) is proportional to the concentration of medium atoms in the first degree and grows with the parameter u.

With the use of the formulas for the cross-section of atom-atom PBs given in [2, Chap. 7] it is possible to obtain the following equation for the number of photons of coherent PBs in a single crystal by the second channel (Fig. 6.1b):

$$\frac{dN_{proj}^{(coh)}}{dl\,d\omega\,d\Omega_{\mathbf{k}}} = \frac{n_t^2\,e^2Z_t^2}{\pi\,\hbar\,\mathrm{v}\,c^3}\left(1+\cos^2\theta_c\right)\sum_{\mathbf{g}}S^2(\mathbf{g})\;\delta(\omega+\mathbf{g}\mathbf{v}-\mathbf{k}\mathbf{v})\,\omega\,\omega_c^2$$
$$\times\left|\alpha_{proj}(\omega_c)\right|^2\,\exp\left(-u^2\,g^2\right)F_{proj}^2(\mathbf{g}_{1c})\left[1-\tilde{F}_t(g)\right]^2/g^2, \tag{6.17}$$

where Z_t is the charge number of nuclei of medium atoms. Appearing in the formula (6.17), in contrast to coherent PBs by the first channel, is the dynamic polarizability of the IP electron core $\alpha_{proj}(\omega_c)$ at the photon frequency in the reference system connected with an incident particle:

$$\omega_c = \gamma\,\omega\,(1 - (\mathrm{v}/c)\,\cos\theta), \tag{6.18}$$

where $\gamma = 1/\sqrt{1-(\mathrm{v}/c)^2}$. is the Lorentz factor. The expression (6.17) includes also the cosine of the angle of photon emission in the IP reference system:

$$\cos\theta_c = \frac{\cos\theta - \mathrm{v}/c}{1 - (\mathrm{v}/c)\,\cos\theta}. \tag{6.19}$$

The formula for incoherent PBs by the second channel looks like:

$$\frac{dN_{proj}^{(incoh)}}{dl\,d\omega\,d\Omega_{\mathbf{k}}} = Z_t^2 n_t\,\frac{e^2}{\hbar\,\omega}\,\frac{\left|\omega\,\omega_c\,\alpha_{proj}(\omega_c)\right|^2}{\pi\,\mathrm{v}^2\,c^3}\left(1+\cos^2\theta_c\right) \times \int\limits_{q_{\min}}^{q_{\max}} F_{proj}^2(q_{1c})\left[1-\tilde{F}_t(q)\right]^2\left(1-\exp\left(-u^2\,q^2\right)\right)\frac{dq}{q}. \tag{6.20}$$

It should be noted that the form factors of medium atoms and IP are included in the formulas (6.17), (6.20) for the second PBs channel differently than in the analogous expressions (6.13), (6.14) for the first channel, which reflects the distinction in the processes of radiation by these channels (see Fig. 6.1).

The appreciable difference between the coherent and incoherent PBs channels is that in the coherent case the radiation frequency is fixed for specified IP velocity, angle of photon emission, and reciprocal lattice vector. This fact manifests itself in the presence of a delta function in the formulas (6.13), (6.17), whence the equation for the coherent radiation frequency ("coherent" frequency) follows:

$$\omega_{\mathbf{g}}(\mathbf{N}) = \frac{-g_0\mathbf{N}\mathbf{v}}{1-(\mathrm{v}/\mathrm{c})\cos\theta}, \tag{6.21}$$

where the integer vector $\mathbf{N} = (N_1, N_2, N_3)$ is introduced that is related to the reciprocal lattice vector by the formula $\mathbf{g} = g_0\,(N_1, N_2, N_3)$, where $g_0 = 2\,\pi/d$ (d is the lattice constant).

Since in the experiment the recording of photons is carried out with the use of a photodetector with a finite frequency resolution, let us integrate the obtained

expressions for coherent PBs (6.13), (6.17) using the spectral function of the photodetector that we will choose in the form [8]:

$$f_{sp}(\omega) = \frac{1}{\sqrt{\pi}} \exp\left(-\frac{(\omega - \omega_r)^2}{\Delta\omega^2} \right), \tag{6.22}$$

where $\omega_r = r\,\varepsilon$ is the central frequency of the rth channel, $\Delta\omega$ is the spectral resolution of the photodetector ($\varepsilon < \Delta\omega$).

After the said frequency integration we obtain the following expression for coherent PBs by the first channel (see Fig. 6.1) recorded in the rth channel of the photodetector [12]:

$$\left(\frac{dN_t^{(coh)}}{dl\, d\Omega_{\mathbf{k}}} \right)_r \cong \frac{n_t^2\, e^2}{\pi\, \sqrt{\pi}\, \hbar\, \mathrm{v}\, c^3} \sum_{\mathbf{N}} S^2(\mathbf{N})\, \omega_{\mathbf{g}}^{\mathbf{3}}(\mathbf{N}) \left| \alpha_t\big(\omega_{\mathbf{g}}(\mathbf{N})\big) \right|^2 \exp\Big(-(u\, g_0)^2\, \mathbf{N}^2 \Big)$$
$$\times \exp\left(-\frac{\big(\omega_r - \omega_{\mathbf{g}}(\mathbf{N})\big)^2}{\Delta\omega^2} \right) \tilde{F}_t^2(g_0|\mathbf{N}|) \left[Z_{proj} - F_{proj}(g_0|\mathbf{N}|) \right]^2$$
$$G(\mathbf{s}, \mathbf{v}, \mathbf{N}, g_0)\, \Theta(-\mathbf{v}\mathbf{N}), \tag{6.23}$$

$$G(\mathbf{s}, \mathbf{v}, \mathbf{N}, g_0) = \frac{\left[\mathbf{s},\, \omega_{\mathbf{g}}(\mathbf{N})\, \mathbf{v}/c^2 - g_0\, \mathbf{N} \right]^2}{\left(g_0^2\, \mathbf{N}^2 - 2\, g_0\, \omega_{\mathbf{g}}(\mathbf{N})\, (\mathbf{s}\, \mathbf{N}) \right)^2}, \tag{6.24}$$

and $\Theta(-\mathbf{v}\mathbf{N})$ is the Heaviside step function providing the positiveness of frequency of an emitted photon.

The expression for coherent PBs by the second channel integrated with the use of the spectral function of the photodetector (Eq. 6.22) looks like:

$$\left(\frac{dN_{proj}^{(coh)}}{dl\, d\Omega_{\mathbf{k}}} \right)_r = \frac{Z_t^2\, n_t^2\, e^2}{\pi\sqrt{\pi}\, \hbar\, \mathrm{v}\, c^3} \frac{g_0\, \gamma^2}{1 - (\mathrm{v}/c)\cos\theta} \left(1 + \cos^2\theta_c \right)$$
$$\sum_{\mathbf{N}} S^2(\mathbf{N})\ \ \Theta(-\mathbf{v}\mathbf{N})\, (-\mathbf{v}\mathbf{N})^3 \times \left| \alpha_{proj}(-\gamma\, g_0\, \mathbf{v}\mathbf{N}) \right|^2$$
$$\exp\Big(-(u\, g_0)^2\, \mathbf{N}^2 \Big)\ \exp\left(-\frac{\big(\omega_r - \omega_{\mathbf{g}}(\mathbf{N})\big)^2}{\Delta\omega^2} \right)$$
$$\times F_{proj}^2(g_{1c}) \left[1 - \tilde{F}_t(g_0 N) \right]^2 / \mathbf{N}^2. \tag{6.25}$$

Here the photon frequency in the reference system connected with an IP in the argument of the dynamic polarizability of an IP is written out in the explicit form in view of the Eqs. 6.18 and 6.21. In the formulas (6.23), (6.25) summation over the

reciprocal lattice vectors are replaced by summation over the components of the integer vector $\mathbf{N} = (N_1, N_2, N_3)$.

For incoherent PBs by the second channel after frequency integration with the spectral function of the photodetector (6.22) the following approximate expression can be obtained:

$$\left(\frac{dN_{proj}^{(incoh)}}{dl\, d\Omega_{\mathbf{k}}}\right)_r \approx \frac{Z_t^2 n_t e^2}{2\sqrt{\pi}\hbar\, c}\left(\frac{c}{\mathrm{v}}\right)^2 \frac{(1+\cos^2\theta_c)\, r_e^2}{\gamma^2(1-(\mathrm{v}/c)\cos\theta)^2} \sum_n \frac{\omega_n}{\Delta\omega_n} f_n^2$$
$$\times \exp\left\{-\frac{\left[\omega_r - \omega_n^{(lab)}(\mathrm{v},\theta)\right]^2}{\Delta\omega^2}\right\} \int\limits_{\omega_n/\gamma\,\mathrm{v}}^{2\mu\mathrm{v}} \left(1-\exp\left(-q^2u^2\right)\right)$$
$$F_{proj}^2(q_{1c})\left[1-\tilde{F}_t(q)\right]^2 dq/q, \tag{6.26}$$

where $\omega_n^{(lab)}(\mathrm{v},\theta) = \frac{\omega_n}{\gamma(1-(\mathrm{v}/c)\cos\theta)}$ is the IP eigenfrequency in the laboratory reference system connected with a target, $r_e = e^2/mc^2$ is the electron classical radius. The derivation of the formula (6.26) was carried out under the assumption that $\Delta\omega_n << \Delta\omega$ ($\Delta\omega_n$ is the spectral width of the line of the bound-bound transition in the electron core of an IP). Besides, in Eq. 6.26 the cross terms appearing in squaring the magnitude of the IP polarizability are omitted. For the polarizability of a bound electron the following standard expression is used:

$$\alpha_{proj}(\omega_c) = \frac{e^2}{m}\sum_n \frac{f_n}{\omega_n^2 - \omega_c^2 - i\,\omega_c\,\Delta\omega_n}, \tag{6.27}$$

where f_n, ω_n are the oscillator strengths and the eigenfrequencies of transitions of a bound electron of an IP from the ground state to the exited states. We assume that the IP core during the process is invariably in the 1 s-state.

The spectral dependence of incoherent "target" PBs (the first channel) is rather weak, so integration of its spectrum with the tool function of the photodetector (Eq. 6.22) will result in multiplication of the primary expression (6.14) by the parameter $\Delta\omega$.

Let us use the obtained formulas for calculation of spectral, velocity (on the IP velocity), and angular dependences of four kinds of PBs arising in scattering of a hydrogen-like Ar^{17+} argon ion in a silicon single crystal. In this case for the geometrical structure factor of the crystal the equation is true [13]:

$$S(\mathbf{g}) = \frac{1}{4}\cos\left[\frac{\pi}{4}(N_1+N_2+N_3)\right]\{1+\cos(\pi N_1)+\cos(\pi N_2)+\cos(\pi N_3)\}, \tag{6.28}$$

where N_j are the integers that mark out nonzero terms in the sum over $\mathbf{N}$ in the expression for coherent PBs (6.23), (6.25).

For the parameters of the polarizability of a bound electron of an IP being in the ground 1s-state and of its form factor we use the known hydrogen-like formulas [14]:

$$\omega_n = Z_{proj}^2 \frac{n^2-1}{2\,n^2} \text{ a.u.}, \; f_n = n^5 \frac{2^8\,(n-1)^{2n-4}}{3\,(n+1)^{2n+4}}, \tag{6.29}$$

$$F_{proj}(q_1) = \frac{1}{\left(1+\left(a_{proj}\,q_1/2\right)^2\right)^2}, \; a_{proj} = \hbar^2/\left(Z_{proj}\,m\,e^2\right). \tag{6.30}$$

In the formulas (6.29) n is the principal quantum number of the electron core of an IP. Fine splitting of energy levels is neglected. To be specific, in calculations the natural broadening of transitions of an IP electron in the discrete spectrum is assumed, then

$$\Delta\omega_n = A_n = Z_{proj}^4 \frac{2^7\,n\,(n-1)^{2n-2}}{9\,c^3\,(n+1)^{2n+2}} \text{ a.u.}, \tag{6.31}$$

where A_n is the Einstein coefficient for a spontaneous transition.

It should be noted that using the formulas (6.29) that take into account only transitions in the discrete spectrum is justified by the fact that the contribution of the second PBs channel from bound-free transitions in the IP core is small.

The calculation of the dynamic polarizability and form factors of target atoms is described in detail in the work [5].

Presented in Fig. 6.7 are the dependences of four kinds of PBs at the central frequency of the photodetector ω_r calculated by the formulas of the previous section for a case of scattering of a hydrogen-like Ar^{17+} argon ion (the IP velocity v =4 6.65 a.u.) incoming along the crystallographic axis 2 (the input angle $\alpha = 0$, see Fig. 6.2) into a silicon single crystal. For short, we will call these dependences spectral. The radiation angle θ is supposed to be 120°, and the spectral resolution of the photodetector is taken equal to 3 a.u. ($\Delta\omega$=81.6 eV). From the figure it follows that the spectra of coherent PBs by the first and second channels are sets of maxima, the position of which, according to the formula (6.21), is defined by the reciprocal lattice vector transferred from an IP to the target during PBs, by the IP velocity and the radiation angle. The width of these spectral maxima is connected with the width of the spectral resolution of the photodetector $\Delta\omega$, and the value is defined by the magnitude of the polarizability of target atoms and an IP electron at the coherent frequency (6.21).

The spectrum of incoherent PBs by the second channel is defined by the spectral dependence of the IP polarizability having sharp peaks at frequencies that in the IP reference system are close to the eigenfrequencies of excitation of a bound electron

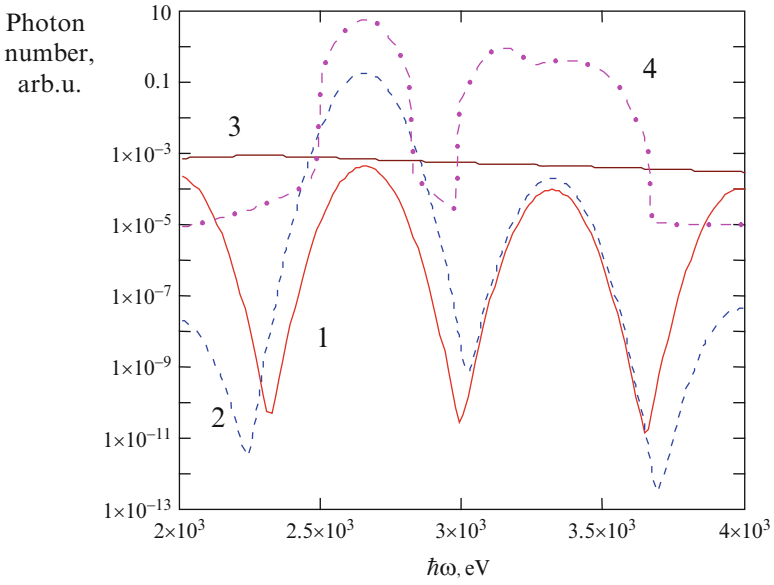

Fig. 6.7 The dependence of four kinds of PBs on photon energy at the central frequency of the photodetector in scattering of a hydrogen-like argon ion in a silicon single crystal (the ion velocity $v = 46.65$ a.u., the radiation angle $\theta = 120°$, the IP input angle $\alpha = 0$, the resolution of the photodetector $\Delta\omega$=81.6 eV): *1* – coherent PBs on a target, *2* – coherent PBs on an IP, *3* – incoherent PBs on a target, *4* – incoherent PBs on an IP

of a hydrogen-like ion. A corresponding condition for the frequency of a maximum in the spectrum of incoherent PBs by the second channel looks like:

$$\omega_{\max}(n, v, \theta) = \frac{\omega_n}{\gamma\,(1 - (v/c)\,\cos\theta)}. \tag{6.32}$$

The formula (6.32) is a condition of coincidence of the eigenfrequency of a bound electron of an IP in the laboratory reference system with the frequency of PBs recording. Owing to the Doppler effect, the eigenfrequency of the electron core of an IP in the laboratory system depends on the IP velocity and the radiation angle. The width of the discussed maxima, as in the coherent case, is defined by the value of the spectral resolution of the photodetector $\Delta\omega$.

It should be noted that in case of fast enough ions, following from the expression (6.32) is a possibility of radiation frequency tuning at the expense of change of the radiation angle, which may be found to be rather essential in practical applications of the phenomenon under consideration.

The spectrum of incoherent PBs by the first channel in the frequency range under consideration is described by a line weakly decreasing with growing frequency, close to the horizontal straight line. This is connected with the fact that the dynamic polarizability of target atoms defining this kind of PBs according to the formula

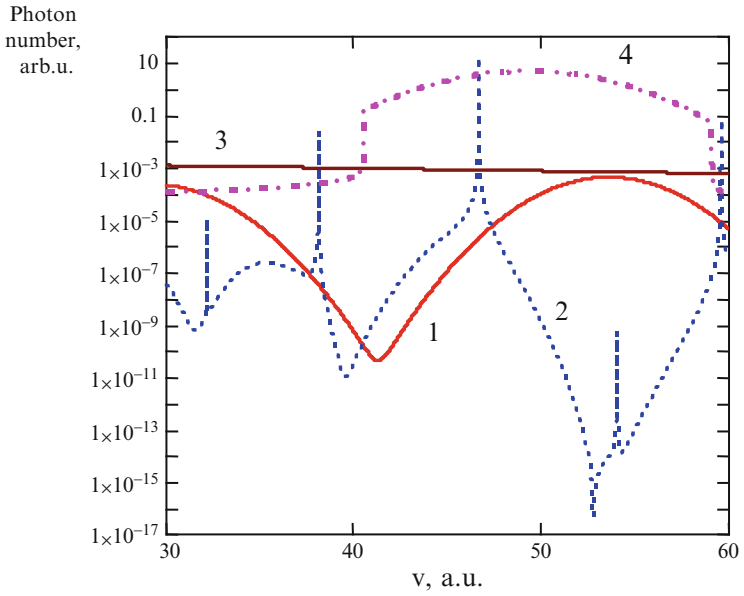

Fig. 6.8 The dependence on the velocity of an incident particle for four kinds of PBs in scattering of a hydrogen-like argon ion in a silicon single crystal (the photon energy at the central frequency of the photodetector $\hbar\omega_r = 2{,}448$ eV, the radiation angle $\theta = 135$, the IP input angle $\alpha = 0$, the resolution of the photodetector $\Delta\omega = 81.6$ eV): *1* – coherent PBs on a target, *2* – coherent PBs on an IP, *3* – incoherent PBs on a target, *4* – incoherent PBs on an IP

(6.14) depends rather weakly on the frequency in the spectral range presented in Fig. 6.7.

Figure 6.8 demonstrates the dependence of four kinds of PBs under consideration on the IP velocity for the bremsstrahlung photon energy at the central frequency of the photodetector $\hbar\omega_r = 2{,}445$ eV and a radiation angle of 135°. The input angle is supposed to be equal to zero, and the spectral width of the line of the photodetector resolution $\Delta\omega = 81.6$ eV.

From the figure it is seen that incoherent PBs by the first channel weakly depends on velocity. The velocity dependence of coherent PBs of the same channel is defined by the condition of equality of the frequency of recording the radiation and frequency of coherent radiation (Eq. 6.21). The maxima of the discussed dependence are connected with different reciprocal lattice vectors transferred from an IP to the target during coherent PBs. The width of these maxima is defined by the width of the spectral function of the photodetector (Eq. 6.22), and the value is defined by the dynamic polarizability of target atoms at the coherent frequency (6.21). It is seen that in the presented range incoherent PBs by the first channel everywhere prevails over coherent PBs.

The velocity dependence of incoherent PBs by the second channel has a wide maximum caused by the Doppler effect and the finite width of the spectral line of the photodetector. This maximum is connected with the fact that in view of fulfilment of

the condition $\Delta\omega_n << \Delta\omega$ the radiation frequency in the reference system connected with an IP is fixed and equal to one of the eigenfrequencies of a bound electron of an ion. When going to the laboratory reference system, the dependence of this resonance frequency on the IP velocity and the radiation angle appears, resulting in this maximum. The presented reasoning immediately follows from the expression (6.26).

A characteristic feature of Fig. 6.8 is the presence of sharp peaks in the velocity dependence of coherent PBs by the second channel. These peaks appear in case of equality of the coherent frequency (6.21) and one of the eigenfrequencies of a bound electron of an IP (the first equation in Eq. 6.29) converted to the laboratory reference system. This condition looks like:

$$\omega_{\max}(n, \mathrm{v}, \theta) \equiv \frac{\omega_n}{\gamma\,(1 - (\mathrm{v}/c)\,\cos\theta)} = \omega_{\mathbf{g}}(\mathbf{N}) \equiv \frac{-g_0 \mathbf{N}\mathbf{v}}{1 - (\mathrm{v}/\mathrm{c})\cos\theta}. \tag{6.33}$$

Hence the condition for the velocity value at the maximum of the velocity dependence follows:

$$\mathrm{v}_{\max}(n, \mathbf{N}, \alpha, \varphi) = \frac{c}{\sqrt{1 + \left(\frac{2\pi c}{\omega_n d}\right)^2 \left[N_1\,\sin\alpha\,\cos\varphi + N_2\,\sin\alpha\,\sin\varphi - N_3\,\cos\alpha\right]^2}}. \tag{6.34}$$

It should be noted that the velocity at the maximum does not depend on the angle of bremsstrahlung photon emission. In case of IP incoming along the crystallographic axis of the target ($\alpha = 0$) the expression (6.34) is simplified: the dependence only on the integer N_3 connected with the value of the transferred reciprocal lattice vector and on the eigenfrequency of an ion electron remains.

For maxima defined by the first eigenfrequency of an Ar^{17+} ion ($\omega_{n=2} = 3305$eV), from the Eq. 6.34 it is possible to obtain the table of values of IP velocity at the maxima of the velocity dependence of coherent PBs by the second channel (see Table 6.1).

Given in the second line of Table 6.1 are the values of coherent frequency (6.21) calculated for a radiation angle of 135°. The distinction of these values from the first eigenfrequency of an Ar^{17+} ion is connected with the Doppler effect.

In Fig. 6.8 four maxima corresponding to the values of IP velocity are well visible that are given in Table 6.1: 38.13, 46.656, and 59.579 a.u.. Also present in this figure are additional maxima of lesser values that are connected with equality of the coherent frequency (6.21) and other eigenfrequencies of the electron core of an IP (at $n>2$). The lesser value of these maxima is explained by the lesser value of oscillator strengths for virtual transitions to bound states of an IP electron with $n>2$.

The width of "velocity" maxima, as seen from Fig. 6.8, is rather small. It is defined by the value of spectral broadening of the line of the electron transition in the IP core that in the present calculation is supposed to be natural (see Eq. 6.31).

Table 6.1 Coherent frequency as a function of velocity in maximum for various N3 values

N_3	1	2	3	4	5
v_{max}, a.u.	112.751	80.372	59.579	46.656	38.13
$\hbar\omega_{\mathbf{g}}$, keV	1,187	1,892	2,276	2,505	2,652

Taking into account the additional mechanisms of broadening will result in broadening of corresponding velocity dependences.

From Fig. 6.8 it follows that for the parameters under consideration in the range of low velocities ($v < 42$ a.u.) incoherent Bs by the first channel prevails. For high IP velocities the main contribution to the process is made by incoherent PBs by the second channel, with the exception of rather narrow ranges near the values given in Table 6.1, where coherent PBs by the second channel prevails.

It should be noted that now rather high energy monochromaticity of an ion beam is achievable, at which the relative spread of IP velocity is fractions of a percent [1]. Therefore averaging over the spread of velocities in an ion beam should retain the main conclusions following from the given analysis of velocity dependences of different PBs kinds.

Presented in Fig. 6.9 are the angular dependences of considered kinds of PBs of an Ar^{17+} ion incoming into a silicon single crystal at a zero angle to the crystallographic axis for the IP velocity $v = 46.65$ a.u. and the bremsstrahlung photon energy $\hbar\omega_r = 2{,}448$ eV. The angular dependence of incoherent PBs by the first channel is manifested rather weakly.

The angular distributions of coherent PBs by both channels are similar: they have two maxima, and for wide angles maxima are more flat. The widths of these maxima are defined by the spectral resolution of the photodetector: they grow with $\Delta\omega$. Incoherent PBs by the second channel has a maximum in the region of wide radiation angles connected with fulfilment of the resonant condition in the polarizability of the electron core of an IP, when the conversion of the eigenfield of a target to a bremsstrahlung photon on a bound electron of an IP proceeds most effectively. On the whole, for specified values of IP velocity and bremsstrahlung photon energy incoherent PBs prevails in the angular dependence, and only in a rather narrow range of radiation angles near $\theta = 82^\circ$ prevailing is the contribution of coherent PBs by the first channel.

From the form of the angular dependences in Fig. 6.9 it follows that integration of the obtained expressions for PBs with the angular tool function of the photodetector may not change significantly the obtained result.

With increasing charge of the nucleus of a hydrogen-like ion the contribution of the second PBs channel to total radiation will decrease. This is connected, first, with growth of the IP eigenfield, which increases PBs by the first channel (see Eqs. 6.13, 6.14), and, second, with reduction of the polarizability of a bound electron of an IP. Really, in case of the natural broadening of the line (6.31) the sum over the principal quantum number in the formula (6.26) will contain the multiplier f_n/ω_n decreasing as Z_{proj}^{-2}. On the other hand, with growing Z_{proj} the spectral region of essentiality of PBs by the second channel will be shifted to the high-frequency region because of growing resonance frequencies of the polarizability of a hydrogen-like ion, whereas for low Z_{proj} this region

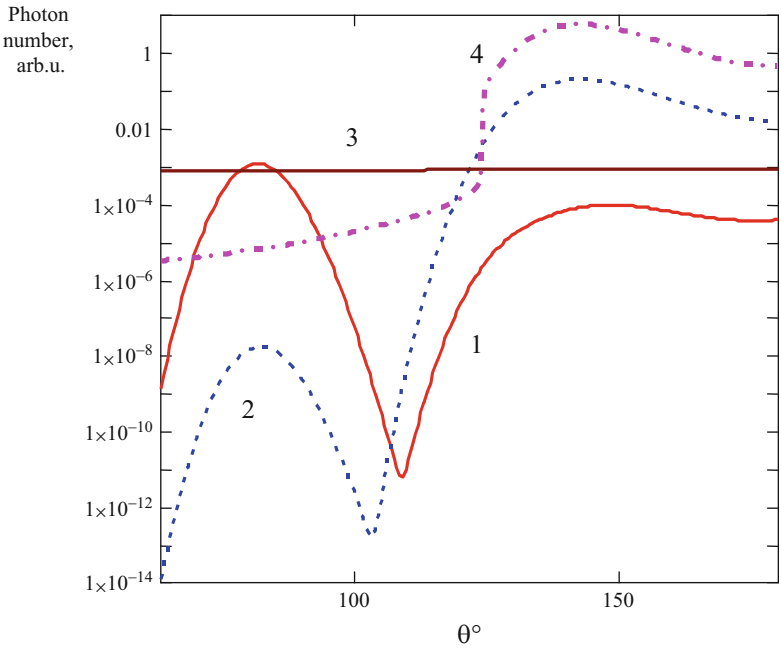

Fig. 6.9 The angular dependence of different kinds of PBs in scattering of a hydrogen-like argon ion in a silicon single crystal (the ion velocity v = 46.65 a.u., the photon energy $\hbar\omega_r$ = 2,448 eV, the input angle $\alpha = 0$, the resolution of the photodetector $\Delta\omega = 81.6$ eV): *1* – coherent PBs on a target, *2* – coherent PBs on an IP, *3* – incoherent PBs on a target, *4* – incoherent PBs on an IP

corresponds to vacuum ultraviolet radiation and soft X-rays. With growing charge of the nuclei of target atoms the relative contribution of the first and second PBs channels practically will not change, and radiation by each of the channels will increase proportionally.

6.2 Polarization Bremsstrahlung of a Fast Ion with an Electron Core in Plasma

In this paragraph within the framework of the first Born approximation polarization bremsstrahlung of a fast hydrogen-like ion in plasma is calculated and analyzed. The contribution of two channels to the process is taken into account: Eq. 6.35 of radiation due to conversion of the electromagnetic field of an ion to a real photon on plasma electrons and Eq. 6.36 of radiation as a result of virtual excitation of a bound electron of an ion (see Fig. 6.1a, b).

It is shown that the second channel of polarization bremsstrahlung has sharp peaks in the narrow spectral-angular range near the eigenfrequencies of the electron core of a fast ion, the spectral-angular dependence of radiation significantly depending on the velocity of an incident particle. The influence of plasma parameters on both polarization bremsstrahlung channels was investigated.

PBs of fast charged particles in plasma called transient Bs was for the first time investigated in the works of V.N. Tsytovich and A.V. Akopyan [15]. Further it was shown that this type of radiation is analogous to Bs in case of collision of charged particles with an atom that is caused by a variable dipole moment induced in the electron core of the atom by a scattered charged particle [2, Chap. 6]. PBs can arise also as a result of collision of neutral atoms or ions having an electron core. Then two channels of radiation are possible according to in which electron shell a radiating dipole moment is induced. Corresponding formulas for cross-sections in nonrelativistic and relativistic cases were obtained by M.Ya. Amus'ya with co-authors [2, Chap. 9].

Let us consider the process of emission of a transverse photon in scattering in plasma of an ion having a subsystem of bound electrons. By a transverse photon is meant the transverse mode of an electromagnetic field in plasma propagating also in vacuum in contrast to the longitudinal mode (plasmon). We assume that the ion velocity exceeds significantly the characteristic velocities of plasma particles and that the condition of the Born approximation for interaction of an IP with plasma particles is satisfied. Besides, we consider that the photon frequency $\omega > \gamma\,\omega_p$ (γ is the Lorentz factor of the IP, ω_p is the plasma frequency), then the influence of the density effect on Bs can be neglected.

As was already noted, the ordinary mechanism of Bs caused by acceleration of an IP in the target field is suppressed because of the high mass of an ion. As a result, the main radiative process is connected with the polarization mechanism of Bs. PBs in the case under consideration can proceed by two channels: (6.35) due to scattering of the IP eigenfield to a real photon on plasma electrons and Eq. 6.36 as a result of conversion of the eigenfield of plasma charges to a real photon on bound electrons of an IP. In both cases the energy of electromagnetic radiation is got from the kinetic energy of an IP, and the energy-momentum excess during the radiative process is absorbed by plasma ions. This interpretation assumes that the energy of plasma ions is insufficient to generate radiation of frequencies considered below.

6.2.1 *Polarization Bremsstrahlung Due to Virtual Excitation of Plasma Electrons (the First Channel)*

The expression for the differential cross-section of PBs in plasma by the first channel can be obtained within the framework of the approach described in [2, Chap. 6] that is based on the use of the formalism of the dynamic form factor of plasma components. The dimensionless PBs amplitude caused by the contribution of the jth plasma electron to the process under consideration is

$$T_{fi}^{PB} = 2\pi\, i\, \delta\left(\omega + \omega_{fi} + \mathbf{q}_1\mathbf{v}\right) \left(q_1^0\right)^2 \sqrt{\frac{2\,\pi}{\hbar\,\omega\,c^2\,V}}\, \frac{e^2}{m\,\omega^2} \left(\mathbf{e}_{\mathbf{k},\sigma}^{*},\, \mathbf{A}^{(pr)}(q_1)\right) \exp\left(i\,\mathbf{q}\,\mathbf{r}_j\right), \tag{6.35}$$

where V is the volume of quantization, $\mathbf{v}$ is the IP velocity and charge, $\hbar q = \hbar(q^0, \mathbf{q})$ is the four-dimensional energy-momentum vector transferred to plasma, $\hbar\omega_{fi}$ is the energy of excitation of a plasma electron during Bs, $q_1 = q - k = (1/\hbar)\left\{\varepsilon_f - \varepsilon_i,\ \mathbf{p}_f - \mathbf{p}_i\right\}$ is the four-dimensional wave vector proportional to the change of the IP energy-momentum, $k = (\omega/c,\ \mathbf{k})$ is the four-dimensional wave vector of a bremsstrahlung photon, $\mathbf{e}_{\mathbf{k},\sigma}$ is the unit vector of photon polarization,

$$\mathbf{A}^{(pr)}(q_1) = \frac{4\pi\, c e_{pr}}{q_1^0\, V}\, \frac{\mathbf{v}\, q_1^0/c^2 + \mathbf{q}_1}{\left(q_1^0/c\right)^2 - \mathbf{q}_1^2}, \qquad q_1^0 = \mathbf{q}_1\mathbf{v} \tag{6.36}$$

is the vector-potential of the IP field, $e_{pr} = Z_{pr}e$ is the IP charge. The axial gauge of the electromagnetic field is used, in which the scalar potential is equal to zero.

Summing the amplitude (Eq. 6.35) over all final states of a plasma electron $|f\rangle$, plasma electrons in the volume of quantization and polarizations of a bremsstrahlung photon σ, we find the following expression for the number of bremsstrahlung photons emitted by the first channel per unit IP trajectory length to the range of wave vectors $d\mathbf{k}$:

$$\frac{dN_{t\,\mathrm{arg}}}{dl\, d\omega\, d\Omega_{\mathbf{k}}} = \frac{1}{\pi^2}\, r_e^2\, \frac{c}{\mathrm{v}}\, \frac{e^2}{\hbar\,\omega} \int \left(Z_{pr} - F_{pr}(\mathbf{q})\right)^2 \frac{\left[\mathbf{s}, \omega\,\mathbf{v}/c^2 - \mathbf{q}\right]^2}{\left(\mathbf{q}^2 - 2\ \mathbf{k}\,\mathbf{q}\right)^2}\, S^{(ee)}\left(q^0, \mathbf{q}\right) d\mathbf{q}, \tag{6.37}$$

where Z_{pr}, $F_{pr}(\mathbf{q})$ are the charge number and the electron form factor of an IP, $r_e = e^2/mc^2$ is the electron classical radius, $\mathbf{s}$ is the unit vector in the direction of photon emission,

$$S^{(jl)}(q) = \frac{1}{2\,\pi} \int\limits_{-\infty}^{\infty} dt\, e^{i\,q^0\,t} \left\langle \hat{n}^{(j)}(\mathbf{q}, t)\, \hat{n}^{(l)}(-\mathbf{q}) \right\rangle \tag{6.38}$$

is the dynamic form factor corresponding to absorption of the four-momentum $\hbar q = \hbar(q^0, \mathbf{q})$ by plasma through interaction of the plasma components j and l. (For more details of the DFF of plasma components, see Appendix 3.)

PBs by the first channel is defined by the electron–electron DFF:

$$S^{(ee)}(q) = S_e^{(ee)}(q) + S_i^{(ee)}(q). \tag{6.39}$$

The first summand in the electron DFF (6.39) describes processes with transfer of the energy-momentum excess to the electron subsystem of plasma, the second summand does the same for the ionic subsystem. In the first case the conversion of the IP eigenfield occurs on individual plasma electrons (the incoherent process), and in the second case the conversion occurs on the Debye sphere screening a

plasma ion (the coherent process). Further we will be interested in coherent PBs. A corresponding component of the dynamic form factor of plasma $S_i^{(ee)}(q)$ in the limit $v>>v_{Ti}$ can be represented as:

$$S_i^{(ee)}(q) \cong n_i Z_i^2 \left| \frac{1-\varepsilon^{l(e)}(q)}{\varepsilon^l(q)} \right|^2 \delta(q^0), \tag{6.40}$$

where Z_i, n_i are the charge number and the concentration of plasma ions, $\varepsilon^{l(e)}(q)$, $\varepsilon^l(q)$ are the longitudinal dielectric permittivities of an electron plasma component and of plasma as a whole. The delta function in the Eq. 6.40 describes the energy conservation law with neglected recoil of a plasma ion. The coherent nature of the process is reflected in the quadratic dependence of $S_i^{(ee)}(q)$ on the number of electrons in the Debye sphere equal to Z_i. In the case under consideration for a fast IP ($v>>v_{Te}>>v_{Ti}$) we have

$$\varepsilon^{l(e)}(q) \cong \varepsilon^l(q=(0,\mathbf{q})) = 1 + \frac{1}{r_D^2\,\mathbf{q}^2}, \tag{6.41}$$

where r_D is the Debye radius. Then

$$S_i^{(ee)}(q) \cong n_i \left| \frac{Z_i}{1+r_D^2\,\mathbf{q}^2} \right|^2 \delta(q^0) = n_i\, |F_i(\mathbf{q})|^2\, \delta(q^0). \tag{6.42}$$

Here the form factor of the Debye sphere screening an ion in plasma is introduced by analogy with the atomic case that is by definition equal to:

$$F_i(\mathbf{q}) = \frac{Z_i}{1+r_D^2\,\mathbf{q}^2}, \tag{6.43}$$

so the spatial Fourier transform of the charge of a plasma ion on the wave vector $\mathbf{q}$ in the units of elementary charge is $Z_i - F_i(\mathbf{q})$. Substituting the expressions (6.42), (6.43) in the formula (6.37) and dividing by the concentration of ions, we obtain the expression for the differential cross-section of PBs on the Debye sphere ("target" PBs) with transfer of the energy-momentum excess to a plasma ion:

$$\frac{d\sigma_{t\,\mathrm{arg}}^{PB}}{d\omega\, d\Omega_{\mathbf{k}}} = \frac{2Z_i^2}{\pi\,\omega}\,\frac{v_a\, c}{v^2}\, r_e^2 \int\limits_{q_{\min}}^{q_{\max}} \frac{\left(Z_{pr} - F_{pr}(\mathbf{q})\right)^2 I_\phi(q,v,\omega,\theta)\, dq}{\left(1+r_D^2\,q^2\right)^2 q}, \tag{6.44}$$

where $v_a = e^2/\hbar$, $q = |\mathbf{q}|$, $\theta = \mathbf{k}^\wedge\mathbf{v}$ is the radiation angle, and

$$I_\phi(q,v,\omega,\theta) = \frac{q^3\, v}{2\,\pi} \int d\Omega_{\mathbf{q}}\, \delta(\omega - \mathbf{k}\mathbf{v} + \mathbf{q}\mathbf{v})\, \frac{\left[\mathbf{s}, \omega\,\mathbf{v}/c^2 - \mathbf{q}\right]^2}{\left(\mathbf{q}^2 - 2\,\mathbf{k}\,\mathbf{q}\right)^2} \tag{6.45}$$

is the kinematic integral that in the nonrelativistic limit is

$$I_\phi(q, \mathrm{v}<<c, \omega, \theta) \cong \frac{1+\cos^2\theta}{2} + \left(\frac{\omega}{q\,\mathrm{v}}\right)^2 \frac{1-3\cos^2\theta}{2}. \tag{6.46}$$

6.2.2 *Polarization Bremsstrahlung as a Result of Virtual Excitation of the Electron Core of an IP (the Second Channel)*

For the differential cross-section of the second PBs channel with generalization of the formulas obtained by M.Ya. Amus'ya with co-authors [2, Chap. 9], in case of atom-atom and ion-ion collisions the following expression can be obtained:

$$\frac{d\sigma^{PB}_{proj}}{d\omega\, d\Omega_{\mathbf{k}}} = \frac{Z_i^2}{\pi} \frac{\mathrm{v}_a\, \omega\, \omega_c^2}{\mathrm{v}^2\, c^3} \left|\alpha_{proj}(\omega_c)\right|^2 \left(1+\cos^2\theta_c\right) I_{pl}(r_D), \tag{6.47}$$

where $\alpha_{proj}(\omega_c)$ is the dynamic polarizability of an incident particle,

$$\omega_c = \gamma\,\omega\,(1-(\mathrm{v}/c)\,\cos\theta),\ \cos\theta_c = \frac{\cos\theta - \mathrm{v}/c}{1-(\mathrm{v}/c)\,\cos\theta} \tag{6.48}$$

are the frequency and the cosine of the radiation angle in the reference system connected with an incident particle,

$$I_{pl}(r_D) = \int\limits_{r_D\, q_{\min}}^{r_D\, q_{\max}} \frac{x^3\, F_{pr}(x/r_D)\, dx}{\left(1+x^2\right)^2}, \tag{6.49}$$

$$q_{\min} = \frac{\omega}{\mathrm{v}}(1-(\mathrm{v}/\mathrm{c})\,\cos\theta),\ q_{\max} = \frac{2\,\mu\,\mathrm{v}}{\hbar}, \tag{6.50}$$

where μ is the reduced mass of an IP and a plasma ion. In derivation of the formula (6.47) the expression for the form factor of the Debye sphere (Eq. 6.43) was used, by which the above generalization of the formulas of the work [2, Chap. 9] to the plasma case is achieved.

Further we will consider a case of a *hydrogen-like* incident ion. Then for the dynamic polarizability of an IP we have:

$$\alpha_{proj}(\omega) = \frac{e^2}{m} \sum_n \frac{f_n}{\omega_n^2 - \omega^2 - i\omega\delta_n}, \tag{6.51}$$

where

$$\omega_n = Z_{pr}^2 \frac{Ry}{\hbar}\left(1 - \frac{1}{n^2}\right) \tag{6.52}$$

are the eigenfrequencies of a bound electron of an IP, f_n are the oscillator strengths, δ_n are the damping constants. A characteristic feature of the dynamic polarizability of a hydrogen-like ion is the presence of sharp resonances at $\omega \approx \omega_n$ since $\omega_n >> \delta_n$. The electron form factor for the ground state of a hydrogen-like IP is

$$F_{pr}(q) = \frac{1}{\left(1 + (a\,q/2)^2\right)^2}, \tag{6.53}$$

where $a = \hbar^2/\left(Z_{pr}\, me^2\right)$. Substituting Eq. 6.53 in the formula (6.49), we find

$$I_{pl}(r_D, a) = \int\limits_{r_D\, q_{\min}}^{r_D\, q_{\max}} \frac{x^3\, dx}{\left(1 + x^2\right)^2 \left(1 + (a/2\, r_D)^2\, x^2\right)^4}. \tag{6.54}$$

It should be noted that in the limit $r_D >> a$ characteristic for nondegenerate plasma the approximate equation is true:

$$I_{pl}(r_D >> a) \approx \ln\left(\frac{2\, r_D}{a\,\sqrt{1 + r_D^2\, q_{\min}^2}}\right) - \frac{17 + 11\, r_D^2\, q_{\min}^2}{12 + 12 r_D^2\, q_{\min}^2}. \tag{6.55}$$

The cross-section of ordinary Bs of an electron in plasma in the frequency range under consideration $m\,\mathrm{v}^2/2\,\hbar >> \omega > \gamma\,\omega_p$ can be obtained if in the formula (6.47) the function $\alpha_{proj}(\omega_c)$ is replaced by the dynamic polarizability of a free electron, and instead of the integral $I_{pl}(r_D)$, $\ln(m\,\mathrm{v}\, r_D/\hbar)$ is substituted. As a result, we find

$$\frac{d\sigma_e^{OB}}{d\omega\, d\Omega_{\mathbf{k}}} = \frac{Z_i^2}{\pi}\, r_e^2\, \frac{\mathrm{v}_a\, c}{\mathrm{v}^2}\, \frac{1 + \cos^2\theta_c}{\gamma^2\,(1 - (\mathrm{v}/c)\,\cos\theta)^2}\, \ln\left(\frac{m\,\mathrm{v}\, r_D}{\hbar}\right). \tag{6.56}$$

Now let us consider some limiting cases of the above expressions for the cross-sections of PBs by the first and second channels. In the nonrelativistic case (v) in the frequency range $\omega < \mathrm{v}/r_D$ the formulas (6.44), (6.46) give

$$\frac{d\sigma_{t\,\mathrm{arg}}^{PB}(\omega < \mathrm{v}/r_D)}{d\omega\, d\Omega_{\mathbf{k}}} = \frac{2Z_i^2}{\pi}\, \frac{\left(Z_{pr} - 1\right)^2}{\mathrm{v}^2\, c^3\, \omega}\, \left(1 + \cos^2\theta\right) \ln\left(\frac{\mathrm{v}}{\omega\, r_D}\right). \tag{6.57}$$

In the opposite case of high enough frequencies $\omega > \mathrm{v}/r_D$, for the differential cross-section by the first channel we have

$$\frac{d\sigma^{PB}_{t\,\mathrm{arg}}(\omega > \mathrm{v}/r_D)}{d\omega\, d\Omega_{\mathbf{k}}} = \frac{Z_i^2}{2\pi}\left(Z_{pr}-1\right)^2\left(1+\cos^2\theta\right)\frac{\mathrm{v}^2}{c^3\,\omega^5\,r_D^4}\,. \tag{6.58}$$

The obtained expression contains the small multiplier $(\mathrm{v}/\omega\, r_D)^4$ that describes the suppression of PBs on the Debye cloud in the frequency range under consideration. This suppression is connected with the loss of coherence of conversion of a virtual photon to a real photon on the electron charge of the Debye sphere if $\lambda < r_D$ (λ is the wavelength of a bremsstrahlung photon).

In the low-frequency limit $\omega < \mathrm{v}/r_D$ in case of nondegenerate plasma the inequation $\omega < Z_{pr}^2 Ry$ is satisfied. Then for the IP polarizability it is possible to use the static approximation that for a hydrogen-like ion gives $\alpha_{proj}(0) = a_B^3 \Big/ Z_{pr}^4$, where a_B is the Bohr radius. Substituting this expression in the formula for the cross-section of PBs by the second channel (Eq. 6.47), we obtain:

$$\frac{d\sigma^{PB}_{proj}\left(\omega < Z_{pr}^2 Ry\right)}{d\omega\, d\Omega_{\mathbf{k}}} = \frac{81}{4\pi}\frac{Z_i^2}{Z_{pr}^4}a_B^6\frac{\omega^3\,\mathrm{v}_a}{\mathrm{v}^2\,c^3}\frac{\left(1-(\mathrm{v}/c)\,\cos\theta\right)^2}{1-(\mathrm{v}/c)^2}\left(1+\cos^2\theta_c\right)\,\ln\!\left(\frac{r_D}{a}\right). \tag{6.59}$$

In case of fulfilment of the inequation $\delta_n << |\omega_c - \omega_n| << \omega_n$ for the dynamic polarizability of an IP the resonant approximation "works". Then for the differential cross-section of PBs by the second channel the formula is true:

$$\frac{d\sigma^{PB}_{proj}(\omega_c \approx \omega_n)}{d\omega\, d\Omega_{\mathbf{k}}} \cong \frac{Z_i^2}{2\pi}\frac{r_e^2}{\omega}\frac{\mathrm{v}_a\, c}{\mathrm{v}^2}\frac{f_n^2}{\left[\frac{\omega_n}{\omega}-\gamma\left(1-\frac{\mathrm{v}}{c}\cos\theta\right)\right]^2}\left(1+\cos^2\theta_c\right)I_{pl}(r_D), \tag{6.60}$$

following from which is the presence of sharp peaks in the frequency-angular PBs distribution caused by conversion of fluctuations of the electric field of plasma to a real photon on a bound electron of a hydrogen-like IP. The frequency of a peak depends on the angle of photon emission the and IP energy according to the equation:

$$\omega_{\max}(n,\mathrm{v},\theta) = \frac{\omega_n}{\gamma\left(1-(\mathrm{v}/c)\cos\theta\right)}. \tag{6.61}$$

At a fixed PBs frequency the maximum in the angular distribution of the process is defined by the angle

$$\theta_{\max}(n,\omega,\mathrm{v}) = \arccos\left\{\frac{c}{\mathrm{v}}\left(1-\frac{\omega}{\gamma\,\omega_n}\right)\right\}. \tag{6.62}$$

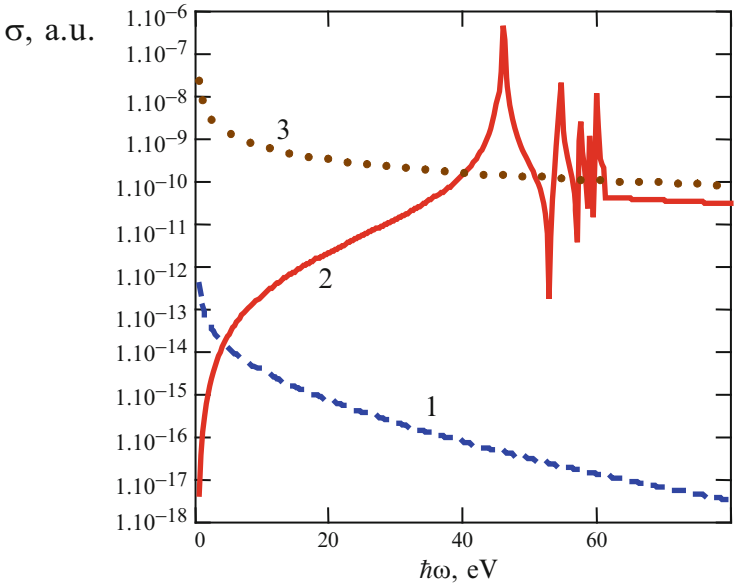

Fig. 6.10 The spectrum of PBs by the first channel (*curve 1*), by the second channel (*curve 2*) of a He^+ ion and the spectrum of ordinary Bs of an electron (*curve 3*) in nondegenerate plasma ($r_D = 5{\cdot}10^{-6}$ cm): v = $1.98{\cdot}10^{10}$ cm/s, $\theta = \pi/3$

From the Eq. 6.62 it follows in particular that the angular maximum occurs in fulfilment of the inequations

$$\gamma\left(1-\frac{\mathrm{v}}{c}\right)\omega_n \le \omega \le \gamma\left(1+\frac{\mathrm{v}}{c}\right)\omega_n. \tag{6.63}$$

Beyond the said spectral range the angular dependence of the cross-section of resonant PBs by the second channel has a monotonic behavior.

Calculated by the formulas (6.44), (6.47) the spectra of two PBs channels in scattering of a hydrogen-like helium ion (v = 90a.u.) in nondegenerate plasma ($r_D = 10^3$ a.u.) (curves 1, 2) are presented in Fig. 6.10 together with the spectrum of ordinary Bs of an electron (curve 3) for the radiation angle $\theta = \pi/3$.

It is seen that PBs caused by conversion of the electric field of a plasma ion on a bound electron of an IP to a bremsstrahlung photon (the second channel) has sharp maxima at frequencies described by the formula (6.61), corresponding to resonances of the dynamic polarizability of an IP. PBs by the second channel prevails everywhere, with the exception of the narrow region of low frequencies. At $\omega \to 0$ the spectral cross-section of the second channel decreases according to the formula (6.59) as the third power of frequency. At the same time the cross-section of the first PBs channel rapidly decreases with growing frequency because of the loss of coherence in reradiation of the IP eigenfield by electrons of the Debye sphere to a bremsstrahlung photon. This circumstance is connected with the high value of the

Debye radius in nondegenerate plasma $r_D >> a_B$, so the inequation $\omega > \mathrm{v}/r_D$ is satisfied in the overwhelming part of the spectral range, and the low value of the process cross-section in this case is predicted by the formula (6.58). Thus the spectral regions of essentiality of two PBs channels in nondegenerate plasma are much spaced due to the high value of the Debye radius. It should be noted that in the region of high frequencies, when the inequation $\omega_c > Z_{pr}^2 Ry$ is satisfied, the cross-sections of PBs of a hydrogen-like ion by the second channel and of ordinary Bs of an electron are close in value. This is connected with the fact that in the region of high frequencies the dynamic polarizability of an IP is close to that for a free electron.

With growing IP velocity the spectral maxima of PBs by the second channel are shifted to the region of lower frequencies, and the cross-section of the second channel decreases not so rapidly. Similar changes of the spectra occur with reduction of the radiation angle.

The spectral Bs cross-sections in scattering of a hydrogen-like carbon ion in degenerate plasma are presented in Fig. 6.11. Since in this case the Thomas-Fermi radius is much less than the Debye radius of nondegenerate plasma, the spectral ranges of essentiality of both PBs channels intersect. The second PBs channel, as before, prevails near the resonances of the dynamic polarizability of an IP.

The angular dependence of total PBs (the sum of both channels) in scattering of a hydrogen-like helium ion ($\mathrm{v} = 90$ a.u.) in nondegenerate plasma is presented in Fig. 6.12 for the frequency $\omega = 1.7$ a.u. (46.24 eV). From Fig. 6.12 it follows that the angular dependence of PBs of a hydrogen-like ion in plasma has sharp maxima corresponding, according to the formula (6.62), to the resonant condition $\omega_c(\mathrm{v},\theta) \approx \omega_n$ if only the frequency of a bremsstrahlung photon in the laboratory reference system satisfies the inequations (6.63). These maxima are shifted to the region of small angles with growing IP velocity.

The dependence of PBs of a hydrogen-like carbon ion scattered in nondegenerate plasma on the IP velocity is presented in Fig. 6.13 for two radiation angles: $\theta = \pi/10$ and $\theta = \pi/6$. The bremsstrahlung photon energy is $\hbar\omega = 544$ eV.

Two sharp peaks on these curves correspond to the resonance of the dynamic polarizability of a carbon ion in excitation of its bound electron from the ground state to the first exited condition. It is seen that with growing radiation angle the position of the maximum is shifted to the region of higher velocities.

This circumstance is a corollary of the formulas (6.52), (6.61) determining the photon energy at the maximum of the spectral dependence of the PBs cross-section as a function of the radiation angle and the IP velocity. Following from them is the expression for the IP velocity at the maximum:

$$\mathrm{v}_{\max}^{(\pm)} = c\,\frac{\cos\theta \pm \sqrt{\cos^2\theta + \left[(\omega_n/\omega)^2 - 1\right]\left[(\omega_n/\omega)^2 + \cos^2\theta\right]}}{(\omega_n/\omega)^2 + \cos^2\theta}, \qquad (6.64)$$

where ω_n is the eigenfrequency of a bound electron of an IP that is given by the formula (6.52). The expression (6.64), naturally, is true for $\mathrm{v}_{\max}$. Depending on the

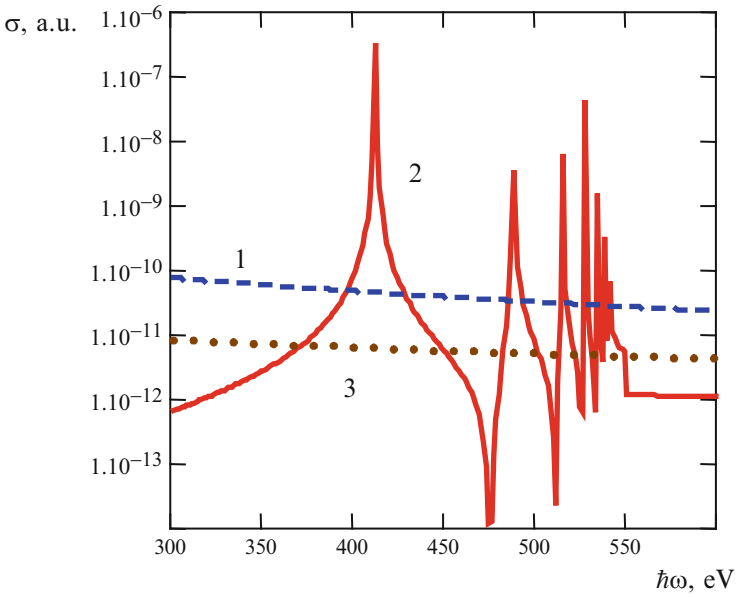

Fig. 6.11 The spectrum of PBs by the first channel (*curve 1*), by the second channel (*curve 2*) of a C^{+5} ion and the spectrum of ordinary Bs of an electron (*curve 3*) in degenerate plasma ($r_{TF} = 5{\cdot}10^{-9}$ cm): $v = 1.98{\cdot}10^{10}$ cm/s, $\theta = \pi/3$

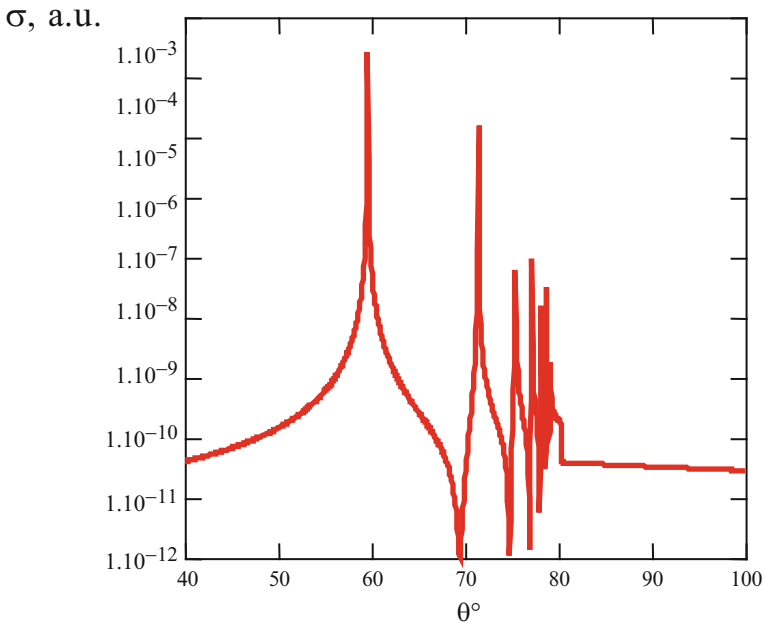

Fig. 6.12 The angular dependence of total PBs of a He^{+} ion ($v = 90$ a.u.) in nondegenerate plasma ($r_D = 5{\cdot}10^{-6}$ cm) for the bremsstrahlung photon energy $\hbar\omega = 46.24$ eV

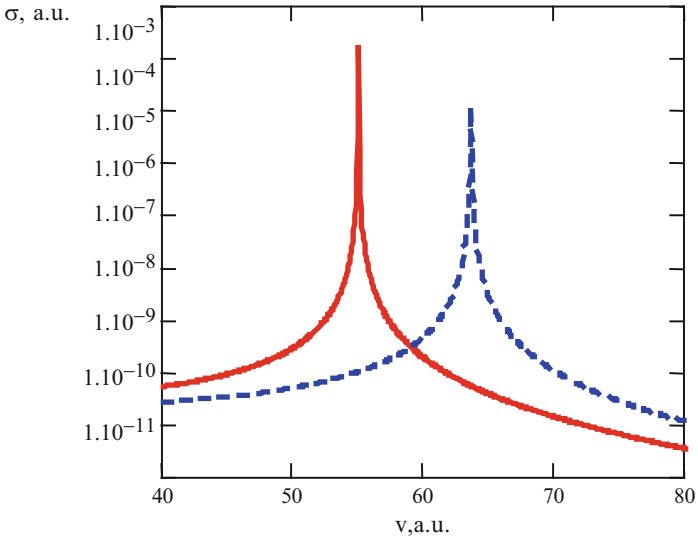

Fig. 6.13 The dependence of total PBs on the velocity of a C^{+5} ion ($\hbar\omega = 544$ eV) in nondegenerate plasma ($r_D = 5{\cdot}10^{-6}$ cm) for two radiation angles: *solid curve* – $\theta = \pi/10$, *dashed curve* – $\theta = \pi/6$

value of the ratio (ω_n/ω) and the radiation angle θ, the function $\sigma(v)$ can have two, one, or no maxima. For example, if the radicand on the right side of the Eq. 6.64 is equal to zero, it is obvious that $v_{max}^{(-)} = v_{max}^{(+)}$ – there is one maximum. Satisfying this condition is the relationship between the frequency and the radiation angle:

$$\omega = \frac{\omega_n}{\sin\theta} \equiv \omega^*. \tag{6.65}$$

In fulfilment of Eq. 6.65, following from Eq. 6.64 is a simple relation between the velocity at the maximum of the cross-section of PBs by the second channel and the radiation angle: $v_{max} = c\cos\theta$. At frequencies $\omega > \omega^*$ the PBs cross-section sharply decreases since the approximate equation $\omega_c \approx \omega_n$ resulting in a resonance in the dynamic polarizability of an IP ceases to be satisfied. With decreasing radiation frequency, when $\omega << \omega^*$, from the expression (6.64) the limiting dependences follow: $v_{max}^{(-)} \to 0$ and $v_{max}^{(+)} \to c$. Then the cross-section of PBs by the second channel is low in a wide range of IP velocities.

References

1. Eichler, J., Stöhlker, T.: Radiative electron capture in relativistic ion–atom collisions and the photoelectric effect in hydrogen-like high-Z systems. Phys. Rep. **439**, 499 (2007)
2. Tsytovich, V.N., Oiringel, I.M. (eds.): Polarization Bremsstrahlung. Plenum, New York (1991)

3. Nasonov, N.N.: Collective effects in the polarization bremsstrahlung of relativistic electrons in condensed media. NIM B **145**, 19 (1998)
4. Feranchuk, I.D., Ulyanenkov, A., Harada, J., Spencer, J.C.H.: Parametric x-ray radiation and coherent bremsstrahlung from nonrelativistic electrons in crystals. Phys. Rev. E **62**(4225) (2000)
5. Astapenko, V.A.: Polarization bremsstrahlung of heavy charged particles in polycrystal. JETP **99**, 958 (2004)
6. Astapenko, V.A., Buimistrov, V.M., Krotov, Y.A., Nasonov, N.N.: Polarization bremsstrahlung from non-relativistic electrons penetrating a polycrystalline target. Phys. Lett. A **332**, 298 (2004)
7. Astapenko, V.A., Nasonov, N.N.: Suppression of the polarization bremsstrahlung from a fast charged particle in an amorphous medium. JETP **103**, 553 (2006)
8. Baryshevsky, V.G., Batrakov, K.G., Feranchuk, I.D., et al.: Experimental observation of frequency tuning of x-ray radiation from nonrelativistic electrons in crystals. Phys. Lett. A **363**, 448 (2007)
9. Rzadkiewicz, J., Rosmej, O., Blazevic, A., et al.: Studies of the Kα X-ray spectra of low-density SiO_2 aerogel induced by Ca projectiles for different penetration depths. High Energy Density Phys. **3**, 233 (2007)
10. Hoffmann, D.H., Blazevic, A., Ni, P., et al.: Present and future perspectives for high energy density physics with intense heavy ion and laser beams. Laser Part. Beam. **23**, 47 (2005)
11. Azuma, T., Ito, T., Takabaysahi, Y., et al.: Resonant coherent excitation of hydrogen-like Ar ions to the n = 3 states. Physica Scripta **T92**, 61 (2001)
12. Astapenko, V.: Polarization bremsstrahlung from fast ions with the core in polycrystal. NIM B **266**, 3744 (2008)
13. Animalu, A.O.E.: Intermediate Quantum Theory of Crystalline Solids. Prentice-Hall, New Jersey (1978)
14. Bethe, H.A., Salpeter, E.E.: Quantum Mechanics of One and Two Electrons Atoms. Springer, Berlin (1957)
15. Tsytovich, V.N., Akopyan, A.V.: Bremsstrahlung in a nonequilibrium plasma. Sov. J. Plasma. Phys. **1**, 371 (1975)

Chapter 7
Investigation of Bremsstrahlung of Nonrelativistic Electrons in Thick and Thin Metal Targets

This chapter is dedicated to presentation of results of theoretical and experimental investigations of bremsstrahlung in scattering of nonrelativistic electrons with an energy of several tens of keV by solid-state targets carried out at the Collective Use Center of the Moscow Institute of Physics and Technology in 2009–2011.

In these investigations in interpretation of experimental results, besides the ordinary (static) mechanism of radiation, the polarization channel, coherent and incoherent electron scattering by a crystal lattice, electron energy loss in a medium, and absorption of bremsstrahlung photons in a substance material were taken into account.

7.1 Absorption of Photons in a Target Material

In case of thick enough targets, the thickness of which exceeds the photon absorption path in a target material, the integrated yield of bremsstrahlung photons that is recorded by a photodetector will be to a great extent defined by the said absorption. Therefore for calculation of the integrated yield of bremsstrahlung photons from a target it is important to know the frequency dependence of the photoabsorption coefficient $\mu(\omega)$ for a given substance.

Presented in Fig. 7.1 is the spectral dependence of the photon path length $L_{ph}(\omega) = 1/\mu(\omega)$ and the electron path length in copper for an initial electron energy of 30 keV. The data for the frequency dependence of the photoabsorption coefficient for copper $\mu(\omega)$ are taken from the site of the American National Institute of Standard [1].

The effect of photon absorption in a target material can be taken into account using the Bouguer law, following from which is a simple expression for the dependence of radiation intensity in a medium on the path length x that radiation has passed in a target material:

$$I(x) = I(0)\,\exp(-\mu x). \tag{7.1}$$

The Y-axis (in μm) in Fig. 7.1 is plotted in the logarithmic scale. Shown for comparison in the same figure as a straight line is the path length of an electron with

V. Astapenko, *Polarization Bremsstrahlung on Atoms, Plasmas, Nanostructures and Solids*, Springer Series on Atomic, Optical, and Plasma Physics 72,
DOI 10.1007/978-3-642-34082-6_7, © Springer-Verlag Berlin Heidelberg 2013

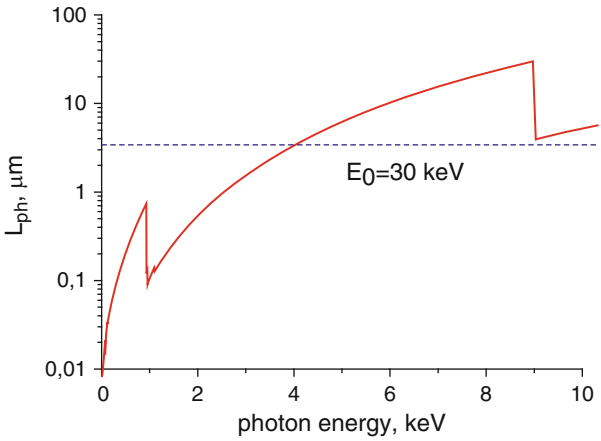

Fig. 7.1 The photon path length in copper (*solid curve*) as a function of the photon energy

the energy of 30 keV in copper (3.4 μm) to a stop due to inelastic collisions with medium atoms.

The minima of the photoabsorption path curve correspond to the electron binding energies for the *L*- and *K*-shells of a copper atom (about 1 and 9 keV respectively). It is seen that up to a photon energy of 4 keV the photoabsorption path in copper is less than the path length of an electron with the energy of 30 keV, that is, in this range of energies the photon yield is defined by photoabsorption in a target material.

In thick targets at frequencies near the minima of the photoabsorption curve presented in Fig. 7.1 the maximum integrated yield of bremsstrahlung photons can be expected.

7.2 Analytical Approach to Simulation of the Bremsstrahlung Photon Yield from a Metal Target

The polarization mechanism of Bs was studied rather fully theoretically and partially experimentally for atomic targets and for radiation of relativistic charges in thin films [2–7]. In the first case there are no medium effects at all, and in the second case in calculation of the process this influence was usually taken into account in the first order of the perturbation theory. The situation is quite different in consideration of Bs of nonrelativistic electrons in solid-state targets in the soft and moderate X-ray bands: $\hbar\omega = 0.1 \div 10$ keV. Then the bremsstrahlung photon yield will experience a significant influence of scattering and electron energy loss as well as of absorption of electromagnetic radiation in the substance. The said situation takes place in a number of technical applications (in X-ray tubes, electron microscopes, microwave devices), when the polarization mechanism of Bs is usually not taken into account [8].

7.2.1 Expressions for the Number of Photons per Unit Target Length

The spectral-angular distribution of Bs photons appearing in scattering of a non-relativistic electron in a thick metal target was simulated with the use of the following expression:

$$\frac{dN_{ph}}{d\omega\, d\Omega} = \int\int d\tilde{\chi}\, d\varphi \frac{\exp\left(-\tilde{\chi}^2\right)}{\pi\sqrt{\pi}} \int\limits_{E_{\min}(\omega,L,E_0)}^{E_0} \frac{dN_{tot}(E,\omega,\theta)}{d\omega\, d\Omega_{\mathbf{k}}\, dx} \times \exp\left(-\frac{\mu(\omega)\, x(E,E_0)}{\cos\beta}\right)\left(-\frac{dx}{dE}\right) dE, \tag{7.2}$$

where φ is the azimuth angle of the electron trajectory plane, $\tilde{\chi} = \chi \Big/ \sqrt{\langle\chi^2\rangle}$, χ is the angle of electron scattering in a target material, $\langle\chi^2\rangle$ is the mean-square angle of electron scattering, $\frac{dN_{tot}(E,\omega,\theta)}{d\omega\, d\Omega_{\mathbf{k}}\, dx}$ is the full number of photons with the frequency ω emitted by an electron with the energy E per unit path length in metal in a specified spectral-angular range, E_0 is the initial electron energy, β is the angle between the normal to the target surface and the direction to the photodetector (the viewing angle). In the formula (7.2) $E_{\min}(\omega, L, E_0)$ is the minimum electron energy at the output of the target, at which emission of a photon of a specified frequency is still possible, $\mu(\omega)$ is the photoabsorption coefficient in the target material, L is the target thickness, dx/dE is the value of reciprocal loss of electron energy per unit length. As seen from the Eq. 7.2, in calculation of photon yield integration with respect to the path length is replaced by integration with respect to the electron energy E, and summation over trajectories is carried out with the use of the Gaussian function determining the probability of electron scattering to the specified angle χ.

The formula (7.2) is true for distances between the radiation region and the photodetector that are much more than the size of the interaction region as well as for small enough electron scattering angles χ. In this approximation the angle of Bs photon emission θ for the normal incidence of an electron on the target surface is related to other angular parameters of the problem as follows:

$$\theta(\beta,\varphi,E,\tilde{\chi}) = \arccos\left[\frac{\cos(\beta)\,\cos(\varphi)\, tg\left(\tilde{\chi}\sqrt{\langle\chi^2(E)\rangle}\right) - \sin(\beta)}{\sqrt{1 + tg^2\left(\tilde{\chi}\sqrt{\langle\chi^2(E)\rangle}\right)}}\right], \tag{7.3}$$

As a target, we will further take a copper plate with a thickness from several nanometers to several microns. The mean-square angle of scattering of an electron with specified energy in copper (here energy is measured in kiloelectron-volts, the scattering angle is measured in radians) is

$$\left\langle \chi^2(E) \right\rangle \cong \frac{0.654}{E} \ln(25\,E),\ E>>0.3\,\text{keV}. \tag{7.4}$$

In the general case $\left\langle \chi^2(E) \right\rangle \cong \dfrac{0.07Z^{2/3}}{E} \ln\left(\dfrac{230\,E}{Z^{2/3}}\right)$ for $E>>0.035\,Z^{2/3}$ keV, where Z is the charge number of the nuclei of target atoms. The Eq. 7.4 is obtained with the use of the Born formula for the transport cross-section of electron scattering by an atom.

The approximation expression for the reciprocal value of energy loss per unit electron path in copper (the path is measured in centimeters, energy is measured in kiloelectron-volts) obtained with the use of the Bethe formula looks like:

$$\frac{dx}{dE} \cong -1.754\,x_{\max}(E_0)\,(E/E_0)^{0.754}, \tag{7.5}$$

where

$$x_{\max}(E_0) \cong 3.4 \cdot 10^{-4}\,(E_0/30)^{1.75} \tag{7.6}$$

is the path length in copper (in centimeters) of an electron with the specified initial energy E_0 (in kiloelectron-volts). From the Eq. 7.6 it follows in particular that for an initial energy of 30 keV the electron path length in copper is 3.4 μm. For comparison we will indicate that the path length in copper of an electron of this energy according to Kanaya-Okayama is 2.89 μm [10].

The lower limit of integration with respect to the electron energy in the formula (7.2) is:

$$E_{\min}(\omega, L, E_0) = \max\{\hbar\,\omega,\ E(L, E_0)\}. \tag{7.7}$$

The dependence of the energy of an electron scattered in copper on the path length and the initial energy is given by the approximate equation

$$E(x, E_0) \cong E_0 \left(1 - \frac{x}{x_{\max}(E_0)}\right)^{0.57}. \tag{7.8}$$

The inverse of the Eq. 7.8, the expression for the path length in the copper target of a electron with specified initial energy appearing on the right side of the Eq. 7.2 that can be obtained by solving the Eq. 7.5 looks like:

$$x(E, E_0) \cong x_{\max}(E_0) \left[1 - \left(\frac{E}{E_0}\right)^{1.754}\right]. \tag{7.9}$$

To calculate the spectral-angular distribution of bremsstrahlung photons emitted by an electron per unit path length, it is necessary to take into account that the interaction of an electron with a polycrystalline target can be of a coherent and incoherent nature.

In the coherent case an electron transfers to a target the wave vector $\mathbf{q}$ equal to the reciprocal lattice vector $\mathbf{g}$, that is, the interaction of an electron with all atoms of the target as a whole takes place. In the second case a photon is emitted in pair collision of an electron with a target atom. The detailed consideration of these problems is given in the work [5] and Chap. 5 of this monograph. Based on the analysis carried out in the cited paper, in the Born approximation for interaction of an incident electron with a target the necessary formulas can be obtained. For example, the spectral-angular distribution of Bs photons emitted per unit path length in the process of coherent scattering of a nonrelativistic electron in a polycrystal is given by the expression:

$$\frac{dN_{tot}^{(coh)}}{d\omega\, d\mathbf{\Omega_k}\, dx} = \frac{n_a^2\, e^6}{\pi\, \hbar\omega\, \mathrm{v}\, m^2\, c^3} \times$$
$$\times \int \sum_{\mathbf{g}} S^2(\mathbf{g})\ \delta(\omega + \mathbf{gv} - \mathbf{kv})\ \exp\left(-u^2 g^2\right)$$
$$\times \left| Z\left(1 - \tilde{F}_a(g)\right) - \frac{m\,\omega^2}{e^2}\,\alpha(\omega)\,\tilde{F}_a(g) \right|^2 \frac{[\mathbf{s},\mathbf{g}]^2}{\mathbf{g}^4}\,\frac{d\mathbf{\Omega_g}}{4\,\pi}, \tag{7.10}$$

where n_a is the concentration of target atoms, e is the elementary charge, c is the velocity of light, m is the electron mass, v is the electron velocity, $S(\mathbf{g})$ is the geometrical structure factor of a crystal, $\mathbf{g}$ is the reciprocal lattice vector, ω is the bremsstrahlung photon frequency. In the formula (7.10) $\alpha(\omega)$ is the dynamic polarizability of target atoms, u is the root-mean-square deviation of target atoms from the equilibrium position (for copper $u = 0.077$ Å at $T = 293^{\circ}K$), $\tilde{F}_a(q)$ is the normalized form-factor of medium atoms, $\mathbf{s} = c\,\mathbf{k}/\omega$ is the unit vector in the direction of photon emission, $d\mathbf{\Omega_g}$ is the element of the solid angle around the direction of the reciprocal lattice vector $\mathbf{g}$.

On the right side of the Eq. 7.10 averaging over the directions of reciprocal lattice vectors is carried out, which corresponds to going from a single crystal to a polycrystalline target.

The expression (7.10) describes Bs of a nonrelativistic electron by the ordinary and polarization channels as well as inter-channel interference. A corresponding formula for ordinary Bs can be obtained from Eq. 7.10 if the polarizability of target atoms is supposed to be equal to zero:

$$\frac{dN_{OB}^{(coh)}}{d\omega\, d\mathbf{\Omega_k}\, dx} = \frac{n_a^2\, e^6\, Z^2}{\pi\, \hbar\omega\, \mathrm{v}\, m^2\, c^3} \times$$
$$\times \int \sum_{\mathbf{g}} S^2(\mathbf{g})\ \delta(\omega + \mathbf{gv} - \mathbf{kv})\ \exp\left(-u^2\, g^2\right) \left|\left(1 - \tilde{F}_a(g)\right)\right|^2 \frac{[\mathbf{s},\mathbf{g}]^2}{\mathbf{g}^4}\,\frac{d\mathbf{\Omega_g}}{4\,\pi}. \tag{7.11}$$

A similar expression for the frequency-angular distribution of coherent PBs per unit path length of a nonrelativistic electron in a polycrystal is obtained from Eq. 7.10 in the limit $Z = 0$.

Indicative of the coherent nature of Bs is the presence of the squared concentration of target atoms n_a^2 in the expressions (7.10) and (7.11).

For incoherent Bs in view of two channels we have:

$$\frac{dN_{tot}^{(incoh)}}{d\omega\, d\Omega_{\mathbf{k}}\, dx} = n_a\, \frac{e^6}{\hbar\,\omega}\, \frac{(1+\cos^2\theta)}{\pi\, \mathrm{v}^2\, m^2\, c^3} \int\limits_{q_{\min}}^{q_{\max}} \left(1-\exp\left(-u^2\, q^2\right)\right) \times \left| Z\left(1-\tilde{F}_a(q)\right) - \frac{m\,\omega^2}{e^2}\, \alpha(\omega)\, \tilde{F}_a(q) \right|^2 \frac{dq}{q}, \tag{7.12}$$

$$q_{\min} = (1-(\mathrm{v}/\mathrm{c})\,\cos\theta)\,(\omega/\mathrm{v}),\ q_{\max} = 2\,m\,\mathrm{v}/\hbar.$$

The frequency-angular distribution of incoherent ordinary Bs per unit path length of a nonrelativistic electron in a polycrystal is given by the equation:

$$\frac{dN_{OB}^{(incoh)}}{d\omega\, d\Omega_{\mathbf{k}}\, dx} = n_a\, \frac{Z^2\, e^6}{\hbar\,\omega}\, \frac{(1+\cos^2\theta)}{\pi\, \mathrm{v}^2\, m^2\, c^3} \int\limits_{q_{\min}}^{q_{\max}} \left(1-\exp\left(-u^2\, q^2\right)\right) \left|\left(1-\tilde{F}_a(q)\right)\right|^2 \frac{dq}{q} \tag{7.13}$$

that is obtained from Eq. 7.12 if $\alpha(\omega) = 0$ is assumed.

The total yield of Bs photons per unit length $\dfrac{dN_{tot}(E,\omega,\theta)}{d\omega\, d\Omega_{\mathbf{k}}\, dx}$ appearing in the formula (7.2) is equal to the sum of the coherent and incoherent contributions (7.10) and (7.12). The same is also true for the photon yield without considering the polarization channel $\dfrac{dN_{OB}(E,\omega,\theta)}{d\omega\, d\Omega_{\mathbf{k}}\, dx}$.

The squared value in the formulas (7.10) and (7.12) can be called the effective charge number of an atom:

$$Z_{eff}(\omega, q) = \left| Z\left(1-\tilde{F}_a(q)\right) - \frac{m\,\omega^2}{e^2}\, \alpha(\omega)\, \tilde{F}_a(q) \right|. \tag{7.14}$$

It depends on the photon frequency and the transferred wave vector. The effective charge number of Eq. 7.14 defines the intensity of Bs of a nonrelativistic electron on an atom in view of the ordinary and polarization channels as well as inter-channel interference. It is interesting to note that for high enough photon energies $\hbar\,\omega >> I_a$ (I_a is the potential of atomic ionization) the approximate equation $Z_{eff}(\omega, q) \approx Z$ is true. The replacement $Z_{eff}(\omega, q) \to Z$ in calculation of intensity of Bs of a nonrelativistic electron on an atom is called atom "stripping" [6] or the descreening approximation.

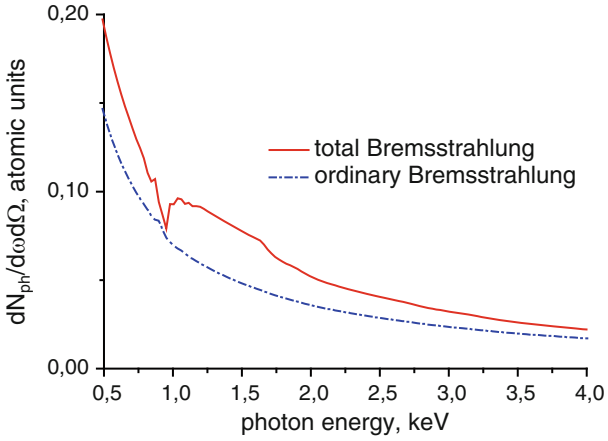

Fig. 7.2 The spectra of Bs of an electron with an initial energy of 30 keV from a thin (10 nm) copper target calculated with account for PBs (*solid curve*) and without its considering (*dash-and-dot curve*)

The value

$$Z_{pol}(\omega) = \left| \frac{m\,\omega^2}{e^2}\,\alpha(\omega) \right| \tag{7.15}$$

can be called the polarization charge number since it defines the polarization channel of Bs.

7.2.2 *Results of Numerical Simulation*

Let us use the obtained expressions for calculation of the yield of Bs photons in case of normal incidence of an electron beam on a copper target for a viewing angle of 35° with account for absorption of photons, energy loss, and electron scattering in the target material.

The spectra of total and ordinary Bs in scattering of an electron with an initial energy of 30 keV by a thin copper foil with a thickness of 10 nm are given in Fig. 7.2. In this case the target thickness is less than the path length of a photon and an electron, so photoabsorption and electron energy loss are negligible. From Fig. 7.2 it is seen that in contrast to the monotonically decreasing OBs spectrum, the spectrum of total Bs has a dip for photon energies about 1 keV followed by the flat maximum. These dip and maximum are connected with PBs and reflect the frequency dependence of the polarization charge of a copper atom (Eq. 7.15) near the threshold of ionization of the *L*-subshell.

It should be noted that without considering electron scattering in a target the Bs spectrum has "frequency steps" corresponding to "turning-off" of the contribution of a given reciprocal lattice vector to the process with growing photon energy [5].

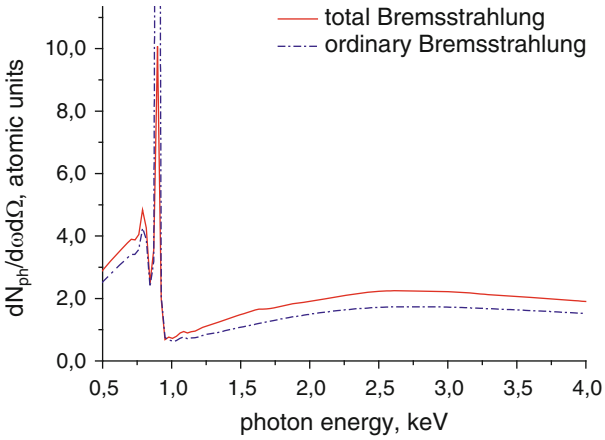

Fig. 7.3 The spectra of Bs of an electron with the initial energy $E_0 = 30$ (*solid curve*) and 12.7 keV (*dash-and-dot curve*) from a copper target with a thickness of 1 μm

These steps are connected with the contribution of coherent PBs. For problem parameters corresponding to Fig. 7.2, the first frequency step in the Bs spectrum falls on a photon energy about 1.7 keV, the second step falls on a photon energy about 1.9 keV. Electron scattering by target atoms results in "slurring" of frequency steps, so in Fig. 7.2 they are practically indiscernible.

The spectrum of ordinary Bs in case of a thin target far from the short-wavelength limit $\hbar\omega << E_0$ is well described by the dependence $E_0/\hbar\omega$ following from the simplest Bs consideration based on the use of the Kramers formula. This formula, generalized to taking into account electron energy loss in a thick target, looks like [8]:

$$\frac{dN_{ph}}{d\omega\, d\Omega} = k\, Z\, \frac{E_0 - \hbar\omega}{\hbar\omega}, \tag{7.16}$$

where k is the coefficient of proportionality. It should be noted that the Eq. 7.16 does not take into account the polarization Bs channel and absorption of radiation in a target and is true for a target thickness more than the electron path length in this target.

Presented in Fig. 7.3 are the results of calculation of the spectra of total Bs and OBs of an electron with an initial energy of 30 keV in a rather thick copper target ($L = 1$ μm), when $L > L_{ph}$. It is seen that in contrast to Fig. 7.2 both spectra are similar and differ only by absolute value. This circumstance is connected with the fact that in this case the Bs spectrum is defined mainly by the frequency dependence of photoabsorption identical for both Bs mechanisms.

The sharp maximum near a photon energy of 800 eV corresponds to the maximum of the photon path length in copper. The flat maximum of the Bs spectrum near a photon energy of 2.9 keV is connected with competition of two processes: the decrease of the photon yield per unit path length in a target and the increase of

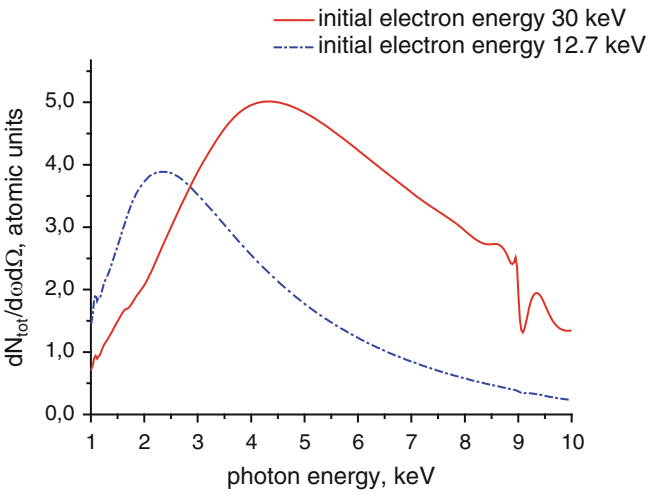

Fig. 7.4 The spectra of Bs of an electron with the initial energy $E_0 = 30$ (*solid curve*) and 12.7 keV (*dash-and-dot curve*) from a copper target with a thickness of 10 μm

the path length of a photon with its energy growing in a range from 1 to 9 keV. Thus the behavior of the Bs spectrum changes with changing target thickness from 10 nm to 1 μm, mainly due to the influence of photoabsorption.

In the analysis of experimental possibilities of investigation of the polarization channel contribution to the total yield of Bs photons it should be remembered that the strong *L*-line of characteristic copper radiation will mask Bs in an energy range of 900 eV–1.1 keV.

With changing initial energy of an electron the length of its path in a substance changes, which for thick enough targets should modify the Bs spectrum. This circumstance is illustrated by Fig. 7.4, shown in which are the spectral dependences of photon yield from a copper target with a thickness of 10 μm for electrons with an initial energy of 30 keV (solid curve) and 12.7 keV (dash-and-dot curve) in a wide range of photon energies from 1 to 10 keV.

It is seen that the Bs spectra in both cases have maxima, for the lower initial energy of an electron the maximum being shifted to the region of lower frequencies, and at a photon energy about 3 keV the spectral dependences intersect. The comparison of the spectra presented in Figs. 7.3 and 7.4 makes it possible to conclude that the spectral maxima are better manifested in radiation in a thicker target. The shift of the maxima of the curves is connected with the fact that at lower initial energy of an electron Bs is "gathered" from a smaller path length, so the influence of radiation absorption in the target is found to be weaker, and the photon yield in the long-wave spectral region is found to be higher. With growing photon energy in a range from 1 to 9 keV the photon path length becomes more than the electron path length in the target, which explains a higher photon yield for a higher initial energy of an electron.

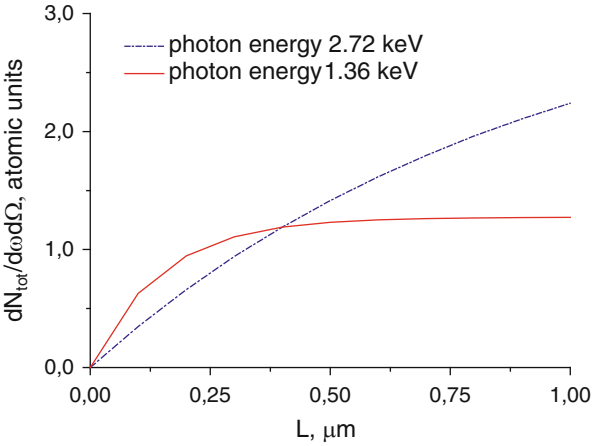

Fig. 7.5 The dependence of total Bs on the target thickness for two photon energies: 1.36 (*solid curve*) and 2.72 keV (*dash-and-dot curve*), and an initial electron energy of 30 keV

As can be seen from comparison of the path lengths of a photon and an electron in a substance, the position of these maxima is approximately described by solution of the equation

$$L_{ph}(\omega) = x_{\max}(E_0), \qquad (*)$$

that is, the photon absorption length at the maximum of the frequency dependence of the Bs yield $\omega_{\max}$ is equal to the electron path length in a target material. Appearance of maxima on the spectral curves for Bs in a thick target is explained by competition of influence of photoabsorption processes and electron energy loss on Bs yield from a target. For frequencies lower than $\omega_{\max}$ the yield of bremsstrahlung photons increases with growing frequency since the photoabsorption length in a target increases, remaining less than the electron path length. For frequencies higher than $\omega_{\max}$ the increase of the photoabsorption length is of no further consequence since the trajectory length is limited by the value $x_{\max}(E_0)$. As a result, the yield of photons begins to decrease with their growing energies since in this case the photon yield per unit path length decreases.

The calculation shows that the polarization channel of Bs of an electron with an initial energy of 30 keV makes the greatest contribution to the yield of a number of photons from a copper target (about 60 % in view of inter-channel interference) at a photon energy about 1.5 keV. With increasing photon energy the PBs contribution monotonically decreases, reaching 10 % for photons with the energy of 10 keV. With decreasing initial energy of an electron the maximum of the polarization contribution to Bs is shifted to the region of lower photon energies.

Presented in Fig. 7.5 are the dependences of Bs intensity for photons with an energy of 1.36 (solid curve) and 2.72 keV (dash-and-dot curve) on the thickness of a copper target for an initial electron energy of 30 keV. It is seen that for a lower photon energy the growth of Bs intensity with increasing target thickness goes to saturation more fast, which is connected with the influence of photoabsorption.

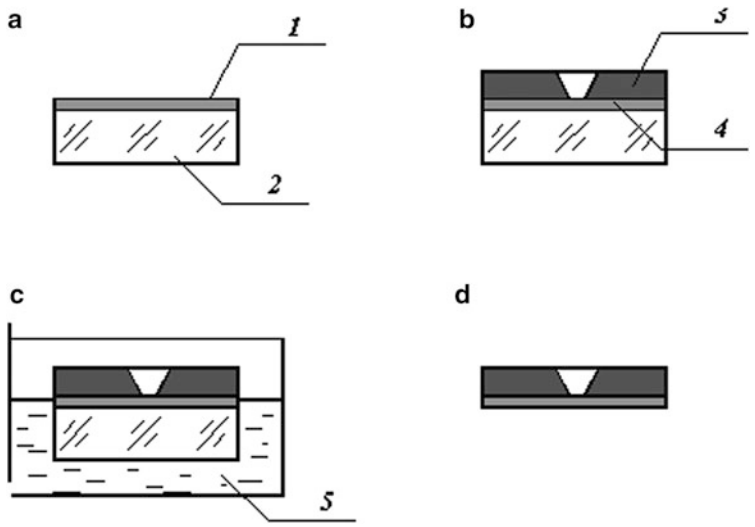

Fig. 7.6 The technology for production of thin films

The numerical analysis of the ratio of total Bs to the contribution of ordinary Bs depending on the target thickness, carried out within the framework of this approach, is indicative of weak dependence of the contribution of PBs of non-relativistic electrons scattered by a polycrystalline sample on its thickness.

7.3 Procedure of Manufacturing Thin Metal Films

For experiments, samples were required that were thin metal films. To avoid the negative influence of a substrate on results of measurements of tested object parameters, particular attention in the work was given to consideration of possibilities to manufacture free thin-film metal structures or metalized thin films of organic materials.

The development of technology for production of free films was coming to optimization of a number of operations reflected in Fig. 7.6.

The film of a metal (1), in particular of copper, was applied by vacuum evaporation to the polished surface of the substrate (2) of single-crystal potassium dihydrogen phosphate (KDP) (Fig. 7.6a). The diameter of the substrate was 20 mm, the thickness was 2 mm.

After coating, the ring (3) of D16T alloy was glued to the sample (Fig. 7.6b) with K400 adhesive (4). The inner diameter of the ring was equal to the diameter of the KDP substrate, its thickness was 3 mm, and the hole diameter was 1 mm. The obtained construction was partially immersed in the bath (Fig. 7.6c) with distilled water (5), so that the KDP substrate could be fully dissolved, but the solution did not get to the other side of the sample (to provide the convenience of following rinsing).

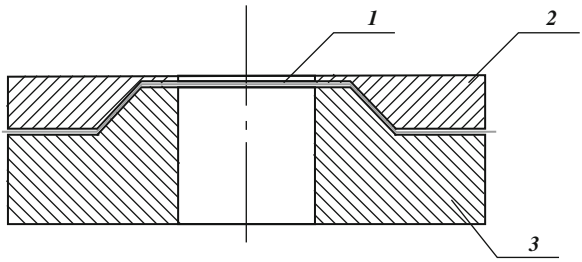

Fig. 7.7 The frame for application of a thin metal coating

A substrate material for application of a thin-film coating was chosen from considerations of its high water solubility. For example, at a temperature of 60 °C in 100 g of water up to 50 g of potassium dihydrogen phosphate is dissolved. At the same time it is possible to polish the surface of single-crystal substrates of this material with high quality necessary for coating.

After removal of the process substrate by etching, the film was carefully rinsed with distilled water. As a result, a sample of a thin-film membrane on a ring frame was obtained (Fig. 7.6d).

With the use of the described technology it was possible to obtain free metal films with a thickness of 1–3 μm. In case of large thicknesses there was a problem of cracking of films and their coming off the KDP substrate in the process of vacuum deposition. And films of a smaller thickness complicated the process of their rinsing in the absence of damages in operations of substrate removal.

To produce samples with a more thin metal layer, substrates were used that had the form of a thin-film lavsan membrane (1) pulled on the metal base in the form of a ring between the parts (2) and (3) with male and female cones (Fig. 7.7).

The lavsan film as a substrate for application of a metal coating was chosen to provide its minimum side effect on the results of measurements. This was achieved both by the minimum thickness of the film (3 μm) and by the nature of its material – polyethylene terephthalate (a monomer for its synthesis is a benzene ring with two COOH end groups). The film retains its properties up to 180 °C, which allows its use in the processes of deposition of metal coatings by the method of vacuum evaporation.

In the work two samples with copper layers deposited on lavsan were studied. The thickness of a metal layer was determined by the results of measurement of He-Ne laser light transmission by semitransparent samples.

To estimate the thickness of a metal coating by the known transmission coefficient T and reflection coefficient R, it is possible to use the formula following from the Bouguer law:

$$\exp(-2\,k_{ext}\,d) = \frac{I_p}{\tilde{I}_i} = \frac{I_p}{I_i - R\,I_i} = \frac{T}{1-R}, \tag{7.17}$$

introduced here is the extinction coefficient depending on a radiation wavelength:

$$k_{ext}(\lambda) = \frac{2\pi}{\lambda}\kappa(\lambda), \tag{7.18}$$

where $\kappa(\lambda)$ is the imaginary part of the refractive index of copper at a specified wavelength, d is the coating thickness.

At the wavelength of a He-Ne laser $\lambda = 633$ nm for copper we have: $\kappa \approx 3.45$ according to the data of the work [9], in which optical constants for noble metals and copper in a spectral range of 0.5–6.5 eV were measured with an error for the refractive index less than 0.02.

From the formulas (7.17) and (7.18) it is easy to find the expression for the film thickness:

$$d = \frac{\lambda}{4\pi\kappa(\lambda)} \ln\left\{\frac{1-R}{T}\right\}. \tag{7.19}$$

From the given formula it follows that, as it must be according to the physical meaning, the target thickness grows with decreasing imaginary part of the refractive index of a medium and the transmission coefficient of a coating.

In case of the first sample the transmission of the copper coating was 40 %, and the reflection was 12 %. In view of these data, from the formula (7.19) we find for the thickness of the first, more transparent, sample $d_1 = 11.5$ nm.

For a thicker coating produced by the above method when, according to the carried out measurements, $T < 0.0003$ and $R = 0.4$, the Eq. 7.19 gives the following lower estimate for the metal film thickness: $d_2 > 110$ nm.

7.3.1 Methods of Manufacturing Experimental Models

7.3.1.1 Thin-Film Evaporation

A glass substrate, previously washed and dried, is put in the BOC EDWARDS AUTO 500 vacuum evaporation system. Evaporation was carried out by the electron-beam method at a pressure of $2 \cdot 10^{-5}$ Torr. To obtain a smooth film, it is necessary to chose a mode, in which evaporation is intensive enough, but there is no bubble boiling yet. Presented in Fig. 7.8 is an example of an evaporated silver film.

7.3.1.2 Method of Shadow Evaporation

To obtain an island structure on the substrate surface, the method of shadow evaporation is used (Fig. 7.9).

The method is based on the fact that at the initial stage of formation of a film on the substrate surface the growth of separate islands of a material being evaporated occurs. Presented in Fig. 7.10 is an example of a structure obtained by shadow evaporation of indium.

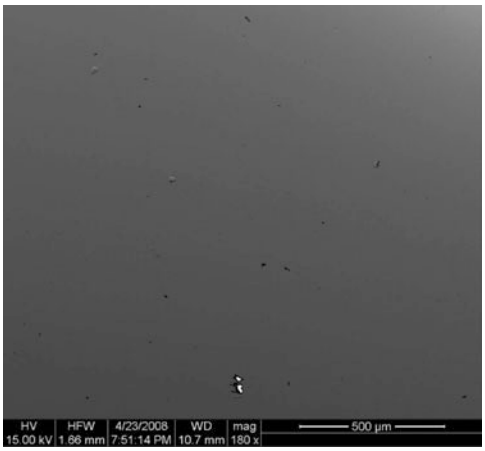

Fig. 7.8 An Ag film on glass

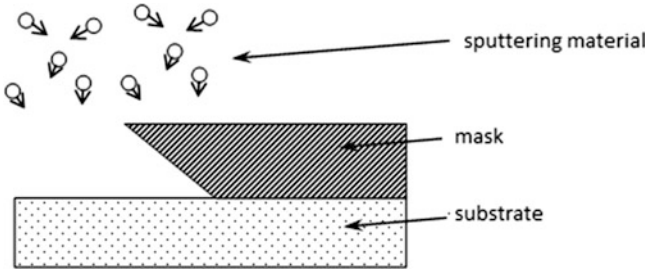

Fig. 7.9 Shadow evaporation

7.3.1.3 Technology for Manufacturing Membranes

On the polished surface of a potassium dideuterophosphate (DKDP) crystal a required film (in our case Ag) is evaporated (Fig. 7.11a). On the surface of the evaporated film a diaphragm is glued with epoxy adhesive (Fig. 7.11b). The obtained construction is immersed in water on special holders for several hours (Fig. 7.11c). Thus there remains a membrane "pulled" on the frame of the diaphragm (Fig. 7.11d).

7.4 Measurement of Bremsstrahlung Spectra for Electrons with Energies up to 30 keV Scattered in Metal Coatings

To measure spectra of X-radiation of nonrelativistic electrons scattered in a solid-state target, the FEI Quanta 200 scanning electron microscope was used. As a target, a standard specimen of copper was used at the preliminary stage of investigations. The measurements of the X-ray spectrum were carried out with the use of the EDAX energy dispersion spectrometer with a silicon-lithium crystal.

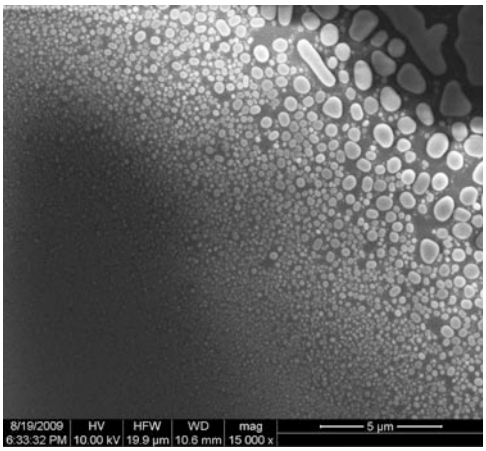

Fig. 7.10 The structure of the initial stage of growth of a condensed film

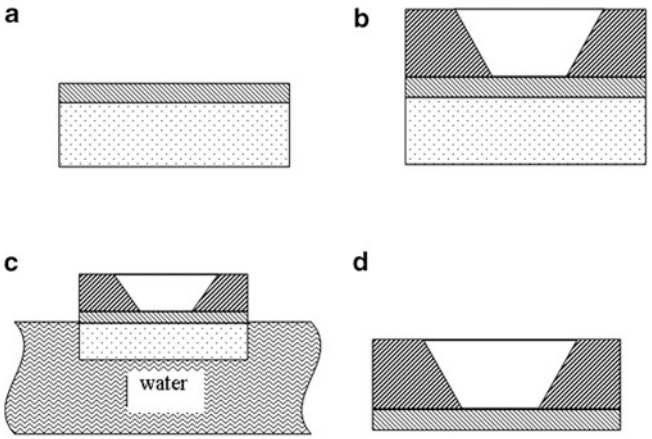

Fig. 7.11 Manufacture of membranes

The energy resolution of the spectrometer determined by the half-width of the characteristic manganese peak is 129 eV.

In Fig. 7.12 the diagram of the experimental system is presented.

An electron beam formed by the optics of the electron microscope after passing the final lens (1) was focused on the surface of the sample (6) at a right angle to the plane of the surface. Bremsstrahlung arising in the target was recorded by the energy dispersion spectrometer (4).

In taking X-ray spectra the flange focal distance (the distance between the objective lens and the sample) and the pressure in the chamber of the scanning electron microscope remained constant. The angle between the electron beam (3) and the direction to the spectrometer (4) was 35°.

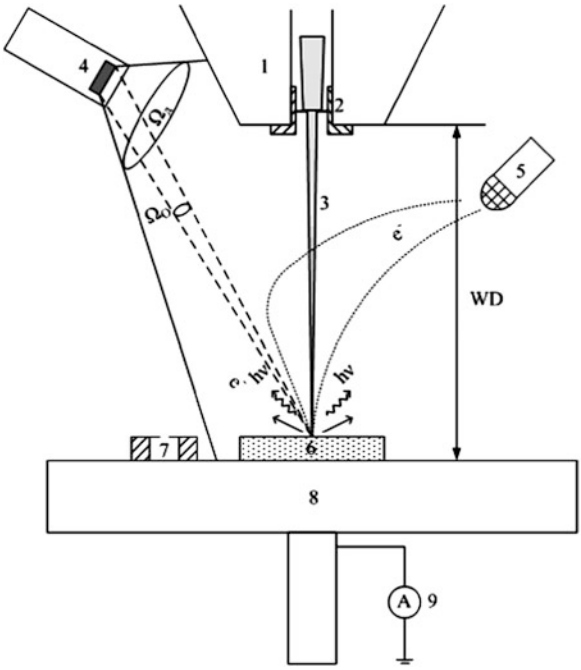

Fig. 7.12 The diagram of the experimental system: *1* final lens, *2* platinum diaphragm, *3* electron beam, *4* energy dispersion spectrometer, *5* true secondary electron detector, *6* sample, *7* Faraday cup, *8* objective table, *9* Keithley picoamperemeter

One of important parameters in taking X-ray spectra is the beam current. In case of current instability it is impossible to interpret the results of an experiment correctly, so for control of this parameter the method with the Faraday cup (7) was used. The Faraday cup is a fully enclosed, except for a small inlet hole, container. This construction prevents reflected and secondary electrons arising under the action of a primary beam from coming out. So the current flowing to the ground is exactly equal to the current of an incident beam and can be easily measured by a picoamperemeter. In our system the Keithley 6485 picoamperemeter (9) was used. The beam current was controlled before and after taking a spectrum. To be sure that during the experiment there were no jumps and sharp changes of current, an absorbed current was taken from the sample. In all obtained spectra the deviation of the beam current from the mean value does not exceed 1.5 %.

The results of measurements for different energies of the primary electron beam are given in Fig. 7.13 (averaging over five points).

X-radiation was recorded in a quantum energy range from 1 to 7.5 keV to avoid masking of Bs by an intensive peak of characteristic radiation of copper $L_{\alpha 1}$ with the energy of 933 eV. The peak that showed itself at the beginning of the spectrum corresponds to the characteristic line $K_{\alpha 1}$ for aluminum of 1,486 eV that is caused by the fact that part of electrons "shoots through" the copper film and begins to excite X-radiation in the substrate. The intensity of the aluminum peak increases with increasing energy of the primary electron beam since the depth of penetration of electrons grows.

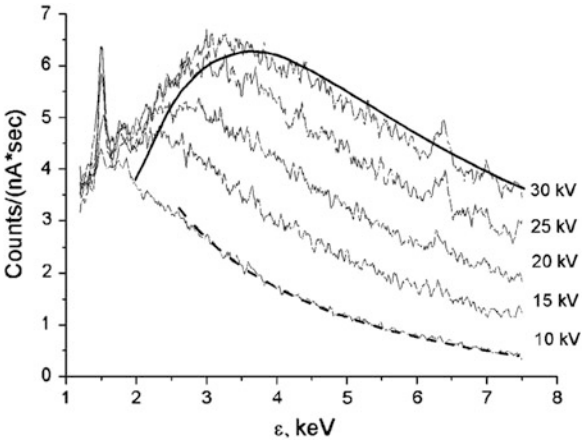

Fig. 7.13 The spectrum of X-radiation excited in a copper target with a thickness of 1 μm at an accelerating voltage from 10 to 30 kV

In the region of high energies (about 6.3 keV), most probably, showing itself is an "escape" peak connected with ionization of the *K*-shell of a silicon atom in the detector crystal by a photon of the *K*-line of copper, owing to which the spectrometer records a pulse with an energy equal to the difference of the energy of the characteristic peak of copper $Cu_{K\alpha}$ (8,037 eV) and the energy of ionization of the *K*-shell of a silicon atom (1,839 eV).

The bremsstrahlung spectrum has a form of a curve with a smooth maximum, the position of which is shifted to the region of high energies with increasing energy of primary electrons as described by the Eq. *. The dependence of intensity for energies of X-ray quanta to the right of the maximum and an electron beam energy of 10 keV (the dotted thickened curve in Fig. 7.13) can be approximated by the Kramers formula $I \propto (E_0 - \hbar\omega)/\hbar\omega$, where E_0 is the energy of the primary beam, $\hbar\omega$ is the energy of a X-ray quantum.

Throughout the region the experimental spectrum is approximated by the theoretical formula obtained with the use of the expressions of the subsection 7.2, under the assumption that the target thickness is 2 μm at an accelerating voltage of 30 kV (the solid curve in Fig. 7.13).

The results of measurements of the spectra of electron radiation on a copper film with a thickness of 100 nm are given in Fig. 7.14. The measurements of the X-ray spectrum were carried out with the EDAX energy dispersion spectrometer with an energy resolution of 129 eV. The results of measurements for different energies of the primary electron beam are given in Fig. 7.14 (averaging over seven points). X-radiation was recorded in a quantum energy range from 1 to 7.5 keV to avoid masking of Bs by an intensive peak of characteristic radiation of copper $L_{\alpha 1}$ with the energy of 933 eV.

The peak that showed itself at the beginning of the spectrum corresponds to the characteristic line K_α for aluminum of 1,486 eV that is caused by the fact that part of electrons "shoots through" the copper foil and begins to excite X-radiation in the substrate. The intensity of the aluminum peak increases with increasing energy of the primary electron beam since the number of electrons that passed through the foil

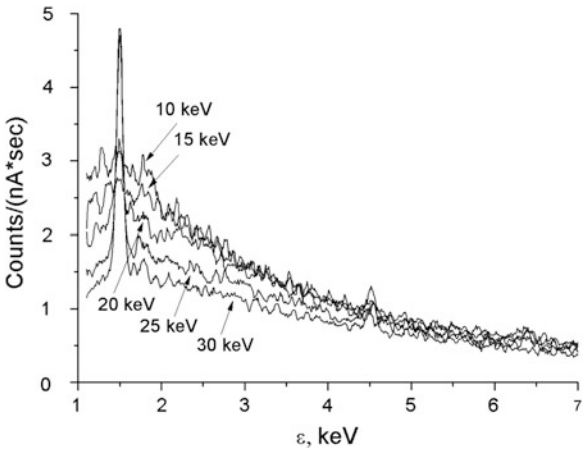

Fig. 7.14 The spectra of Bs from a 100-nm copper film taken at different accelerating voltages

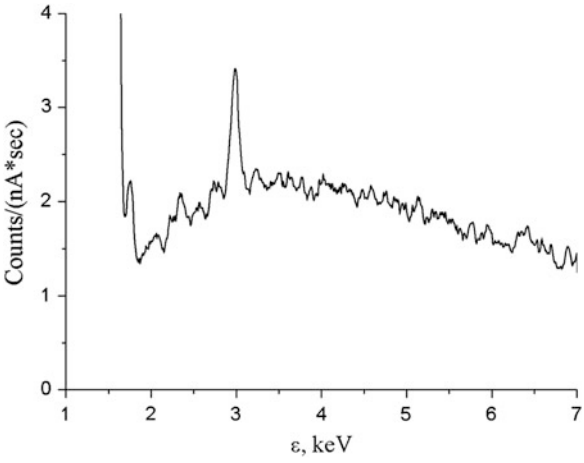

Fig. 7.15 The spectrum of Bs from a massive aluminum sample taken at an accelerating voltage of 30 kV

increases. On the spectrum a titanium peak ($Ti_{K\alpha}$) with an energy of 4,510 eV is also observed at all accelerating voltages, which is indicative of the presence of a titanium impurity in the foil. The bremsstrahlung spectrum has a form of a curve with a smooth maximum at the energy about 1,500 eV and does not depend on the accelerating voltage of the electron beam.

Presented in Fig. 7.15 is the spectrum of Bs from a massive aluminum sample taken at an accelerating voltage of the electron beam of 30 kV. The spectrum has a smooth maximum at the energy about 3,300 eV. At the beginning of the spectrum a section is seen that corresponds to the characteristic aluminum peak (K_α) with the energy of 1,486 eV. At the centre of the spectrum at the energy of 2,978 eV a double aluminum peak (K_α) is seen that is connected with the fact that the crystal of the energy dispersion spectrometer has no time to divide two quanta that came simultaneously.

Shown in Fig. 7.16 is the X-ray spectrum from a massive manganese target arising under the action on the target of electrons with the energy of 30 keV (the accelerating

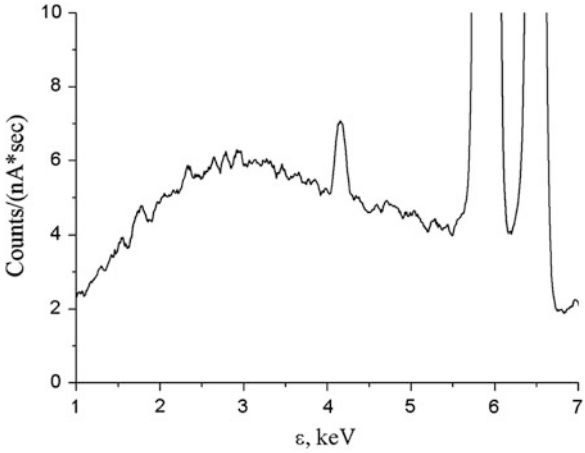

Fig. 7.16 The spectrum of Bs from a massive manganese sample taken at an accelerating voltage of 30 kV

voltage is 30 kV). The spectrum has a smooth maximum at a photon energy about 3 keV. At the end of the spectrum a section is seen that corresponds to the characteristic manganese peaks (K_α and K_β) with energies of 5,898 and 6,489 eV respectively.

At an energy of 4,059 eV a peak of loss of the characteristic line MnK_α is seen that is connected with ionization of the *K*-shell of a silicon atom in the detector crystal by a quantum of the *K*-line of manganese, owing to which the spectrometer records a pulse with an energy equal to the difference of the energy of the characteristic peak of manganese $Mn_{K\alpha}$ (5,898 eV) and the energy of ionization of the *K*-shell of a silicon atom (1,839 eV).

References

1. The NIST Webbook of Chemistry. See http://webbook.nist.gov/chemistry
2. Tsytovich, V.N., Oiringel, I.M. (eds.): Polarization Bremsstrahlung. Plenum, New York (1991)
3. Nasonov, N.N.: Collective effects in the polarization bremsstrahlung of relativistic electrons in condensed media. NIM B **145**, 19 (1998)
4. Feranchuk, I.D., Ulyanenkov, A., Harada, J., Spencer, J.C.H.: Parametric x-ray radiation and coherent bremsstrahlung from nonrelativistic electrons in crystals. Phys. Rev. E **62**, 4225 (2000)
5. Astapenko, V.A.: Polarization bremsstrahlung of heavy charged particles in polycrystal. JETP **99**, 958 (2004)
6. Astapenko, V.A., Buimistrov, V.M., Krotov, Y.A., Nasonov, N.N.: Polarization bremsstrahlung from non-relativistic electrons penetrating a polycrystalline target. Phys. Lett. A **332**, 298 (2004)
7. Astapenko, V.A., Nasonov, N.N.: Suppression of the polarization bremsstrahlung from a fast charged particle in an amorphous medium. JETP **103**, 553 (2006)
8. Goldstein, J., Newbury, D., Joy, D., Lyman, C., Echlin, P., Lifshin, E., Sawyer, L., Michael, J.: Scanning Electron Microscopy and X-Ray Microanalysis. Kluwer, New York (2003)
9. Johnson, P.B., Christy, R.W.: Optical constants of noble metals. Phys. Rev. B. **6**, 4370 (1972)

Chapter 8
Polarization Bremsstrahlung on Nanostructures

8.1 PBs on Atomic Clusters in a Wide Spectral Range

In Chap. 1 of this monograph the examples of calculation of PBs of an electron on a nanocluster in the low-frequency range were given, when the photon energy is from 1 to several tens of eV [1]. Here we will consider bremsstrahlung of a relativistic electron scattered on atomic clusters in a wide frequency range with an emphasis on the role of cooperative effects in the polarization and ordinary (static) channels of the process [2].

Let us calculate the intensity of the polarization and ordinary channels of Bs of a fast charged particle on a cluster within the framework of a simple model. The main assumptions of the used approach are reduced to the first Born approximation for interaction of an IP with a target and a jelly model for the form factor of the cluster.

Further we use the quasi-classical formula for the amplitude of static (ordinary) bremsstrahlung and the approximate expression for the generalized polarizability of cluster atoms.

With the use of the standard quantum-mechanical procedure (see details in the work [3]), for the differential intensity of Bs by each of the channels normalized to the number of atoms in a cluster N the following expression can be obtained:

$$\frac{dI}{d\omega\, d\Omega_{\mathbf{n}}} = \frac{1}{N} \int_{q_{\min}}^{q_{\max}} T(q)\, dq, \tag{8.1}$$

where $\mathbf{q} = \mathbf{p}_f - \mathbf{p}_i + \mathbf{k}$ is the momentum transferred to the target from an IP, $T(q)$ is the partial intensity of Bs, $d\Omega_{\mathbf{n}}$ is the solid angle in the direction of radiation, ω, $\mathbf{k}$ are the frequency and the wave vector of a photon, $\mathbf{p}_{i,f}$ are the initial and finite momenta of an incident particle. In this section the atomic system of units $\hbar = e = m_e = 1$ is used.

V. Astapenko, *Polarization Bremsstrahlung on Atoms, Plasmas, Nanostructures and Solids*, Springer Series on Atomic, Optical, and Plasma Physics 72,
DOI 10.1007/978-3-642-34082-6_8,

The partial intensity of PBs within the framework of the used approach can be represented as

$$T_{pol}(q) = \frac{2\,Z_p^2}{\pi\,c^3\,\mathrm{v}\,q}\,S(q,\,N)\,\left|Z_{pol}(\omega,\,q)\right|^2 I\phi(q,\,\mathrm{v},\,\omega,\,\theta), \tag{8.2}$$

where Z_p is the IP charge, c is the velocity of light, v is the velocity of an IP, $S(q,\,N)$ is the structure factor of the cluster, $Z_{pol}(\omega,\,q)$ is the effective polarization charge of cluster atoms, $I\phi(q,\mathrm{v},\omega,\theta)$ is the kinematic integral appearing as a result of integration with respect to the azimuth angle of the vector $\mathbf{q}$, $\theta = \mathbf{p}_i\hat{}\mathbf{k}$ is the angle of photon emission.

It should be noted that the expression (8.2) was obtained for a range of high enough frequencies, in which $\omega >> I_a$, where I_a is the potential of ionization of atoms forming the cluster. An opposite case of low frequencies $\omega < I_a$ was considered in the work [4].

For the structure factor of the cluster we will use the following model approximation:

$$S(q,N) = N^2\,F_J^2(q,N) + N\left(1 - F_J^2(q,N)\right), \tag{8.3}$$

where

$$F_J(q,N) = 3\,\frac{j_1(q\,r(N))}{q\,r(N)} \tag{8.4}$$

is the form factor of the spherical cluster in the jelly model normalized to one atom.

$$j_1(x) = \frac{\sin x}{x^2} - \frac{\cos x}{x} \tag{8.5}$$

is the spherical first-order Bessel function, $r(N)$ is the cluster radius depending on the number of atoms N that can be calculated by the formula:

$$r(N) = r_{WS}\,\sqrt[3]{N} = \sqrt[3]{\frac{3\,N}{4\,\pi\,n_a}}, \tag{8.6}$$

where r_{WS} is the Wigner–Seitz radius, n_a is the solid-state concentration of cluster atoms.

The first summand on the right side of the Eq. 8.3 is the coherent part of the structure factor of the cluster, the second summand is its incoherent part. It should be noted that the forms factor (Eq. 8.4) is normalized to the number of atoms by the spatial Fourier transform of probability of distribution of atoms in a cluster in the jelly model:

$$w_J(r,N) = \frac{3\,N\,\Theta(r(N) - r)}{4\,\pi\,r(N)^3}, \tag{8.7}$$

where $\Theta(x)$ is the Heaviside step function. In case of a monatomic cluster the structure factor (Eq. 8.4) is equal to one.

The polarization charge of cluster atoms can be represented as

$$Z_{pol}(\omega, q) = \omega^2 \left|\alpha(\omega, q)\right| \cong \omega^2 \left|\alpha(\omega)\right| \tilde{F}_a(q), \tag{8.8}$$

where $\alpha(\omega)$ and $\tilde{F}(q)$ are the dipole polarizability and the normalized form factor of an atom. These values were calculated by the method proposed in [5]. The imaginary part of the polarizability was determined with the use of the optical theorem in terms of the cross-section of photoabsorption of an atom by the data given at the site of the Berkeley National Laboratory. Then the real part of the polarizability was restored with the use of the Kramers-Kronig relation. The atomic form factor was calculated in the Slater approximation by the formula obtained in the paper [6].

The kinematic integral included in the partial intensity of PBs (Eq. 8.2) is determined by the equation

$$I\phi(q, \mathrm{v}, \omega, \theta) = \frac{AD - BE - CD}{\left(D^2 - E^2\right)^{3/2}} + \frac{CD}{E^2\sqrt{D^2 - E^2}} - \frac{C}{E^2}, \tag{8.9}$$

where A, B, C, D, E are rather cumbersome functions of the problem parameters, the explicit form of which is given in [5].

The approximate expression for the partial intensity of ordinary Bs in the quasi-classical approximation $\varepsilon_i >> \omega$ (ε_i is the initial IP energy) and the relativistic limit ($\mathrm{v} \approx \mathrm{c}$) looks like:

$$T_{st}(q) \cong \frac{2}{3\,\pi\, c^3\, \mathrm{v}\, q}\, S(q, N) \left(\frac{Z_p}{m_p}\right)^2 Z^2 \left(1 - F_a(q)\right)^2 \frac{\left(1 - (\mathrm{v}/\mathrm{c})^2\right)\left(1 + \cos^2\theta\right)}{\left(1 - (\mathrm{v}/\mathrm{c})\,\cos\theta\right)^2}, \tag{8.10}$$

where m_p is the IP mass, Z is the charge of an atomic nucleus. It should be noted that the relative error of the formula (8.10) for nonrelativistic IP velocities does not exceed 30 %.

The above formulas describe the intensities of two Bs channels in scattering of a fast charged particle by a cluster for high enough radiation frequencies $\omega >> I_a$. We neglect the inter-channel interference summand due to different dependence of PBs and SBs amplitudes on a transferred momentum, and in the relativistic case – on a radiation angle too.

Let us use the obtained formulas for calculation of intensity of Bs by the static and polarization channels in scattering of a fast electron by polyatomic clusters.

We will characterize the cooperative effects in Bs by the following ratio:

$$\xi = \frac{dI(N)}{dI(N = 1)}, \tag{8.11}$$

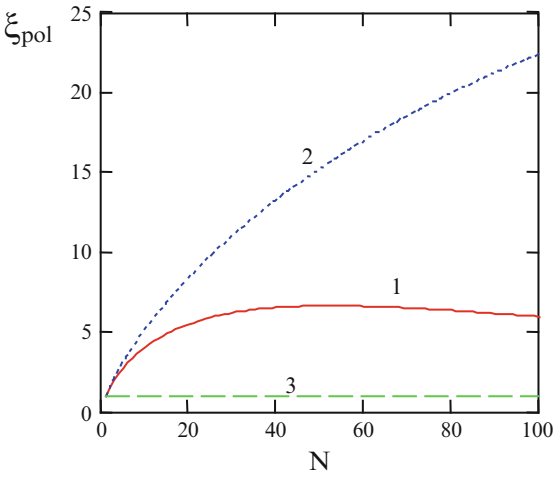

Fig. 8.1 Cooperative effects in PBs and SBs of an electron scattered by a copper cluster ($\gamma = 10$, $\hbar\omega = 1$ keV); *1* – PBs, $\theta = 1$ rad; *2* – PBs, $\theta = 0.5$ rad; *3* – SBs

where dI is the differential intensity of Bs by one of the channels normalized to the number of atoms in a cluster. In the absence of cooperative effects it is obvious that $\xi = 1$. In the opposite limiting case of constructive interference of contributions of cluster atoms to the Bs intensity we have: $\xi = \chi N$, $\chi < 1$. The coefficient χ takes into account the fact that transferred momenta essential in the process on an individual atom do not all make a considerable contribution to the coherent part of Bs on a cluster.

The dependence of the parameter ξ on the number of atoms in a copper cluster for both Bs channels is presented in Fig. 8.1. The bremsstrahlung photon energy is 1 keV, the Lorenz factor is $\gamma = 10$ ($\gamma = \left(1 - (\mathrm{v/c})^2\right)^{-1/2}$).

In case of the polarization channel the dependence $\xi(N)$ is given for two values of the radiation angle $\theta = 0.5,\ 1$ rad. From the figure it follows that cooperative effects are negligible for the static Bs channel and rather substantial for the polarization channel. The analysis shows that the value of cooperative effects in PBs grows noticeably with decreasing radiation angle. Besides, their role increases with growing IP energy and decreasing bremsstrahlung photon frequency. From the given curves and calculation data it follows that in case of the polarization channel, beginning from some value N_{sat} depending on the radiation angle and IP energy, the saturation of radiation intensity as a function of the number of atoms in a cluster takes place. The analysis shows that with decreasing radiation angle and growing IP energy the value N_{sat} grows.

For explanation of the listed regularities we will take into account the fact that, as follows from the formulas for the structure factor (Eqs. 8.3, 8.4, 8.5 and 8.6), constructive interference of contributions of different cluster atoms to the process takes place only for low enough values of the transferred momentum:

$$q < 1/r(N), \tag{8.12}$$

where $r(N)$ is the radius of the cluster (Eq. 8.6). Otherwise the structure factor of the cluster (normalized to the number of atoms) is equal to one, and cooperative effects are absent.

It is essential that the inequation (8.33) is incompatible with the condition

$$q > 1/r_a \tag{8.13}$$

defining the range of transferred momenta, in which ordinary Bs is not low in view of the obvious inequation $r(N) > r_a$ (r_a is the characteristic atomic radius). Hence a negligible value of cooperative effects in ordinary Bs on a cluster follows.

At the same time the partial amplitude of PBs is great in case of fulfilment of an inequation opposite to Eq. 8.13, so there is no analogous prohibition of cooperative effects in the polarization channel. Let us write out the expression for a minimum momentum transferred to the target from an IP, appearing in the integral (8.1):

$$q_{\min}(\omega, \mathrm{v}, \theta) = \frac{\omega}{\mathrm{v}} \left(1 - \frac{\mathrm{v}}{c} \cos\theta\right). \tag{8.14}$$

Following from the condition of essentiality of cooperative effects

$$q_{\min} < 1/r(N) \tag{8.15}$$

and the formula (8.6) for the cluster radius is the expression for the saturating value of the number of atoms in a cluster N_{sat}:

$$N_{sat} = \frac{4\,\pi\, n_a\, \mathrm{v}^3}{3\,\omega^3 \left(1 - \frac{\mathrm{v}}{\mathrm{c}} \cos\theta\right)^3}. \tag{8.16}$$

Following from Eq. 8.16 is the strong dependence of the value N_{sat} on the radiation angle and IP energy in the relativistic case. For example, for the parameters of Fig. 8.1 we have: $N_{sat}(\theta = 1\ rad) = 27$ and $N_{sat}(\theta = 0.5\ rad) = 1,312$.

The influence of cooperative effects on the angular dependence of PBs on a cluster is demonstrated by Fig. 8.2. Shown in this figure is the PBs intensity normalized to its value at a zero angle as a function of the radiation angle for different numbers of atoms in a copper cluster, including a monatomic case, at the photon energy of 5 keV and a Lorenz factor of 10.

It is seen that the angular distribution of PBs with growing number of atoms is narrowed, and its dependence on an angle in the limit of high values of the number N becomes nonmonotonic. This nonmonotonicity disappears in the nonrelativistic case with decreasing radiation frequency and grows with increasing number of atoms.

It should be noted that the said dependences in the angular distribution of PBs on clusters can be found experimentally only for heavy IP. In case of light IP (electron, positron), at small radiation angles the static channel prevails, cooperative effects in which are low.

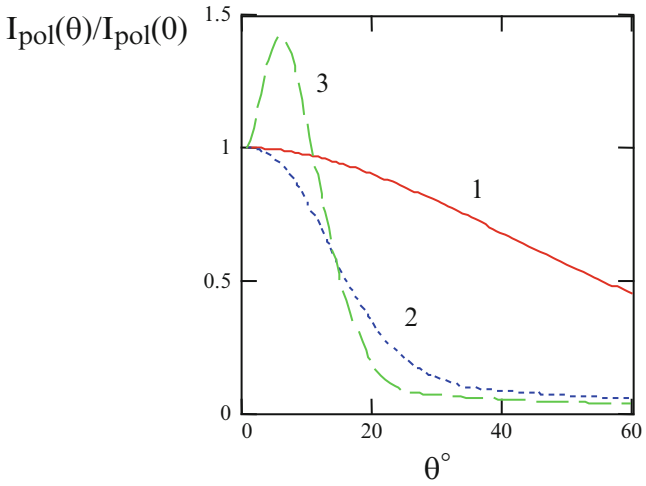

Fig. 8.2 The angular dependence of the normalized intensity of PBs of an electron on an individual atom (Eq. 8.22) and a copper cluster: N = 100 (Eq. 8.23), N = 1,000 (Eq. 8.24); $\hbar\omega = 5$ keV, $\gamma = 10$

To describe the relative contribution of PBs to the process, let us introduce the R-factor according to the equation:

$$R = \frac{dI_{pol}}{dI_{st}}. \tag{8.17}$$

The angular dependence of the R-factor of an electron with $\gamma = 10$ for a photon energy of 1 keV and different numbers of atoms in a copper cluster is presented in Fig. 8.3. It is seen that with increasing number of atoms the role of PBs grows. For example, for a monatomic case the angle, at which the intensities of PBs and SBs become equal, is 30°, and for $N = 100$ this angle is 10°.

Figure 8.4 demonstrates the influence of cooperative effects on the relative contribution of the polarization channel to emission of a fast electron ($\gamma = 10$) scattered by a copper cluster at different energies of a bremsstrahlung photon and a radiation angle of 15°.

The growth of the R-factor with increasing number of electrons in a cluster goes to saturation more fast for high photon energies according to the formula (8.16) for the value N_{sat}. Following from this figure is the strong dependence of the role of polarization effects on the cluster size, especially in the low-frequency range.

The condition of essentiality of cooperative effects in the spectrum of PBs on a cluster can be obtained from the inequation (8.15) in view of the explicit expression for the minimum momentum transferred to the target (Eq. 8.14). It looks like:

$$\omega < \omega_{\max} = \sqrt[3]{\frac{4\pi n_a}{3N}} \frac{\mathrm{v}}{1 - \frac{\mathrm{v}}{\mathrm{c}}\cos\theta}. \tag{8.18}$$

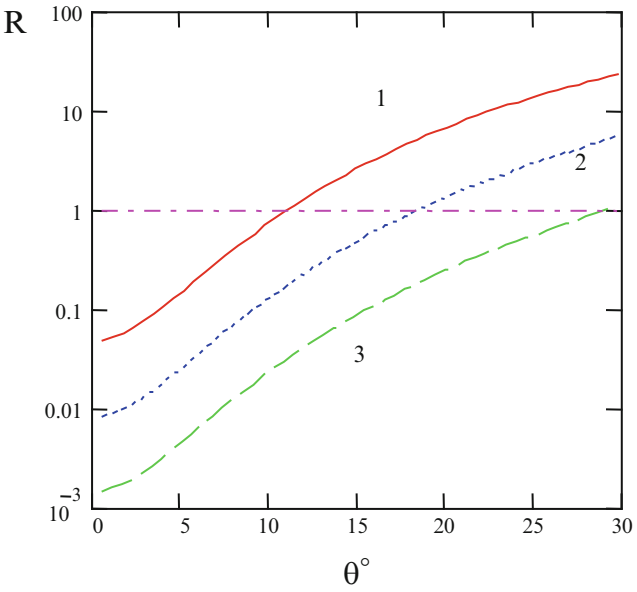

Fig. 8.3 The angular dependence of the *R*-factor for different numbers of atoms in a copper cluster including a monatomic case: $\hbar\omega = 1$ keV, $\gamma = 10$, *1* – N = 100, *2* – N = 10, *3* – N = 1

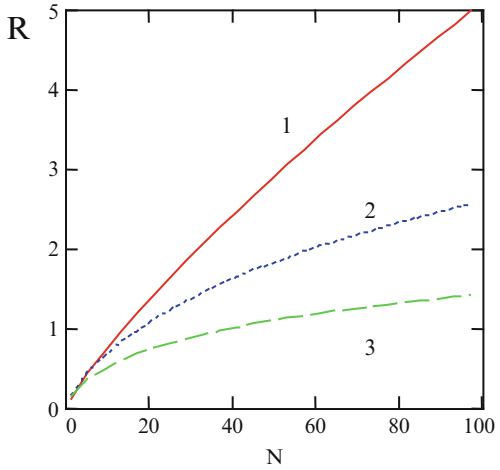

Fig. 8.4 The dependence of the *R*-factor on the number of atoms in a copper cluster for different frequencies *1* – $\hbar\omega = 500$ *eV*, *2* – $\hbar\omega = 2$ *keV*, *3* – $\hbar\omega = 3$ *keV*; $\gamma = 10$, $\theta = 15°$

For frequencies more than ω_{max} cooperative effects in Bs on a cluster are low.

In the nonrelativistic limit v<<c the maximum frequency of manifestation of cooperative effects does not depend on the radiation angle and is:

$$\omega_{\max}^{nrel} = \frac{\mathrm{v}}{r_{WS}\sqrt[3]{N}}. \tag{8.19}$$

The value of the Wigner–Seitz radius for metal clusters varies within $r_{WS} = 2 \div 4$, so the characteristic value of frequency (Eq. 8.19) for a mid-size cluster and an IP velocity about 10 a.u. is 1 a.u.

It should be noted that in the frequency a range $\omega < 1$ a.u. the calculation model used here becomes inadequate since then the dynamic polarizability of the cluster will be to a great extent defined by collective excitations of the cluster electrons. Such a situation for a nonrelativistic IP was considered in the work [7].

In the relativistic limit $\gamma >> 1$ it is convenient to represent the formula (8.18) in the form:

$$\omega_{\max} = \frac{1}{r_{WS}\sqrt[3]{N}} \frac{2\gamma^2}{4\gamma^2 \sin^2(\theta/2) + 1} \tag{8.20}$$

clearly demonstrating the dependence of the maximum frequency $\omega_{\max}$ on the IP energy. From the Eq. 8.20 it follows that in contrast to the nonrelativistic case, in the relativistic limit the influence of cooperative effects on the PBs spectrum is essentially defined by the angle of photon emission. For small angles and high values of the Lorenz factor of an IP the maximum frequency of manifestation of cooperative effects in PBs can reach high values. However, in this case it should be remembered that in the angular range $\theta < \gamma^{-2}$ in Bs of an electron (positron) the static channel prevails. So the question about a role of cooperative effects in the spectrum of Bs of a light charged particle on a cluster should be decided in view of concrete values of problem parameters. At the same time for Bs of heavy charged particles, when SBs is negligible, the spectral restriction on the role of cooperative effects in the relativistic a case is given by the frequency of Eq. 8.20.

The dependence of the spectrum of PBs on a copper cluster consisting of ten atoms on the IP energy is presented in Fig. 8.5 for a radiation angle of 0.5 rad.

It is seen that with growing Lorenz factor the intensity of radiation increases, and the maximum of the spectral dependence is shifted to the region of high frequencies. These changes are most pronounced in going from fast, but nonrelativistic IP to weakly relativistic particles. With further growth of the Lorent factor the spectrum of PBs on a cluster varies not so appreciably. With decreasing radiation angle the spectrum of PBs of relativistic IP is found to be more pulled into the region of high frequencies according to the formula (8.20), following from which is also the decrease of the maximum frequency with growing number of atoms in a cluster.

The intensity of total Bs and PBs in scattering of a nonrelativistic electron on a copper cluster and an individual atom as a function of the IP velocity is shown in Fig. 8.6 for the radiation angle $\theta = 1$ rad and the photon energy $\hbar\omega = 200$ eV. It is seen that in the nonrelativistic case there is the optimum value of the electron velocity $\mathrm{v}_{\mathrm{opt}}$, at which the intensity of PBs on a cluster is maximum. The dependence of this optimum velocity on the problem parameters is given by the expression:

$$\mathrm{v}_{\mathrm{opt}} = \omega r(N). \tag{8.21}$$

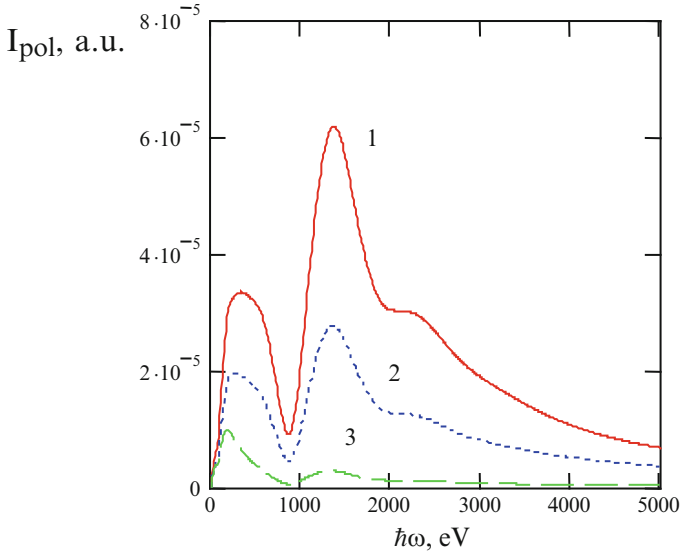

Fig. 8.5 The spectrum of PBs on a copper cluster (N = 10) for different values of the Lorentz factor and a radiation angle of 0.5 rad: *1* – $\gamma = 10^2$, *2* – $\gamma = 10$, *3* – $\gamma = 1.1$

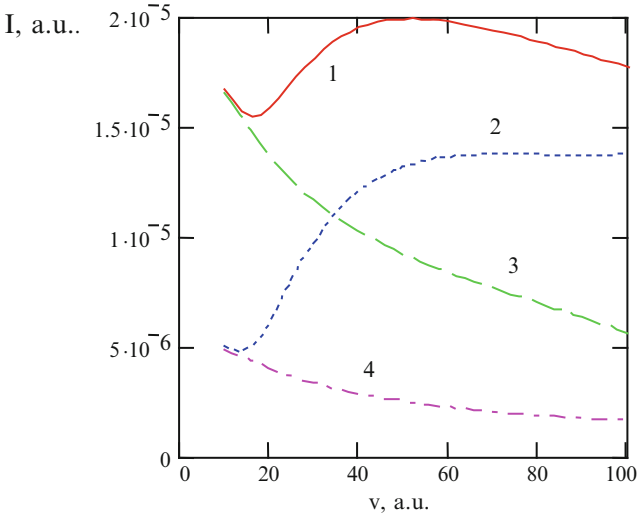

Fig. 8.6 The dependence of the Bs and PBs intensity on the electron velocity in the nonrelativistic case for a copper cluster (N = 20) and an individual atom, $\hbar\omega = 200$ eV, $\theta = 1$ rad. *1* – total Bs (N = 20), *2* – PBs (N = 20), *3* – total Bs (N = 1), *4* – PBs (N = 1)

In case of the process on an individual atom the cluster radius in Eq. 8.21 should be replaced by the characteristic atomic radius r_a. The given formula can be obtained with the use of the expression for the minimum transferred momentum (Eq. 8.14) in the case v<<c.

From the Eq. 8.21 it follows that with decreasing frequency and size of a cluster the value of the optimum velocity decreases. In particular, for the process on an individual atom and the photon energy $\hbar\omega = 200\,\text{eV}$ the value v_{opt} lies beyond the range of applicability of the Born approximation, so the velocity dependence of the Bs and PBs intensity looks like a monotonically decreasing curve. With growing number of atoms in a cluster the value of the optimum velocity increases as seen from the formulas (8.21) and (8.6).

With decreasing radiation angle the maximum in the velocity dependence of the Bs intensity disappears, and for PBs it becomes less pronounced. This is connected, on the one hand, with increasing contribution of the static channel to the process (see the formula (8.10)), and on the other hand, with growing value of the minimum transferred momentum (Eq. 8.14).

Figure 8.6 demonstrates the disappearance of cooperative effects with decreasing IP velocity: for the given photon energy (200 eV) the total Bs and PBs on a cluster and one atom coincide in the limit of low velocities.

In the high-frequency range the velocity dependence of the PBs intensity becomes monotonically increasing, which is connected with the natural restriction on the optimum IP velocity: $v_{opt}<137$. The monotonically increasing dependence of the PBs intensity on the IP energy is characteristic also for the relativistic case (with the exception of low frequencies not considered here).

Based on the analysis carried out in this section, it is possible to draw a conclusion about the essentiality of cooperative effects in Bs of a fast (including relativistic) charged particle scattered by a polyatomic cluster in a wide range of frequencies. These effects caused by constructive interference of the contributions of atoms to the process by the polarization channel result in nonlinear growth of the PBs intensity as a function of the number of atoms in a cluster. At the same time for the static Bs mechanism the contribution of different atoms to radiation is incoherent, which is caused by the smallness of impact parameters, on which SBs is formed.

It is shown that cooperative effects result in significant modification of the main characteristics of Bs on a cluster in comparison with a monatomic case. For example, in the high-frequency range with growing number of atoms the pattern of PBs is narrowed, and for large enough clusters the angular dependence of PBs of relativistic particles becomes nonmonotonic: a maximum appears with nonzero radiation angles.

With growing IP energy the maximum of the spectral distribution of PBs on a cluster is shifted to the region of high frequencies. The form of the high-frequency part of the spectrum in the relativistic case strongly depends on the radiation angle. With reduction of this angle the Bs intensity decreases with growing frequency much more slowly than for wide angles.

The analysis of the Bs intensity as a function of the IP velocity has shown that in the nonrelativistic case this dependence can be of different nature: from monotonically increasing to monotonically decreasing. In the relativistic limit the PBs intensity monotonically increases with IP energy. In the limit of low IP velocities the role of cooperative effects in Bs on a cluster becomes negligible.

The obtained results can be used in interpretation of experimental data on Bs of fast charged particles on clusters in the range of high enough photon energies.

8.2 PBs on Metal Nanospheres in a Dielectric Matrix

Metal nanoparticles of noble metals find use as nanomarkers for biological objects, for investigation of behavior of chemical and biological processes, as sensors for local optical environmental monitoring, for electrical control of light switching, for measurement of an electric charge, etc. [8]. In the said applications, as a rule, scattering of electromagnetic radiation in the spectral range corresponding to excitation of surface plasmons (the photon energy $\hbar\omega = 1 \div 4$ eV) is used.

Polarization bremsstrahlung (PBs) is a fundamental radiative process that can be interpreted as the conversion of the eigenfield of a charged particle on target electrons to a propagating electromagnetic wave [9]. Following from this interpretation is a possibility (by analogy with ordinary radiation) to use PBs for substance spectroscopy, in particular, for determination of parameters of metal nanoparticles.

In recent years works have appeared that are dedicated to the study of PBs as a basic process for nanomaterial diagnostics. For example, in the paper [10] a possibility to use this process for determination of a fullerene structure on the basis of calculation of a target form factor was discussed. PBs spectroscopy for diagnostics of polycrystalline and fine-grained media in the more general context of modification of the energy dispersion method was considered in the work [11]. We believe that PBs spectroscopy has also considerable promise as a physical method for metal nanosphere diagnostics.

8.2.1 General Formulas

In the Born approximation for interaction of an incident particle (IP) with a target in a dielectric medium the differential PBs cross-section is given by the expression [2] (in this section we use the Gaussian system of units):

$$\frac{d\sigma^{PB}}{d\omega\, d\Omega_{\mathbf{k}}} = \frac{2}{\pi}\frac{\omega^3}{c^3}\frac{e_p^2}{\hbar\,\mathrm{v}^2}\int\limits_{q_{\min}}^{q_{\max}} |\,\alpha(\omega,q)|^2\, I_\phi(q,\mathrm{v},\omega,\theta)\,\frac{dq}{q}, \tag{8.22}$$

where $d\Omega_{\mathbf{k}}$ is the element of a solid angle in the direction of radiation, c is the velocity of light, e_p is the IP charge, v is the IP velocity, $\alpha(\omega, q)$ is the generalized dynamic polarizability of the target, $\mathbf{k} = \sqrt{\varepsilon_m}\,(\omega/c)\,\mathbf{s}$ is the wave vector of a bremsstrahlung photon in a medium with the dielectric permittivity ε_m, θ is the angle between the

electron velocity vector and the wave vector of a bremsstrahlung photon (the radiation angle). The value $\mathbf{q} = \left(\mathbf{p}_f - \mathbf{p}_i + \mathbf{k}\right)/\hbar$ is the wave vector transferred from an IP to the target ($\mathbf{p}_{i,f}$ are the initial and finite momenta of an IP). The limits of integration on the right side of the Eq. 8.22 are $q_{\min} = (1 - (\mathrm{v}/\tilde{c})\cos\theta)(\omega/\mathrm{v})$, $q_{\max} = 2\mu\mathrm{v}/\hbar$, $\tilde{c} = c/\sqrt{\varepsilon_m}$ is the velocity of light in a medium. The dimensionless kinematic integral $I_\phi(q, \mathrm{v}, \omega, \theta)$ appearing in the formula (8.22) is determined by the equation

$$I_\phi(q, \mathrm{v}, \omega, \theta) = \frac{q^3\,\mathrm{v}}{2\pi}\int d\Omega_{\mathbf{q}}\,\delta(\omega - \mathbf{kv} + \mathbf{qv})\,\frac{\left[\mathbf{s}, \omega\,\varepsilon_m\,\mathbf{v}/c^2 - \mathbf{q}\right]^2}{\left(\mathbf{q}^2 - 2\,\mathbf{k}\,\mathbf{q}\right)^2}, \tag{8.23}$$

where $\mathbf{s}$ is the unit vector in the direction of photon emission. The solid-angle integral of the wave vector transferred to the target in the determination (8.23) can be calculated in elementary functions [5]. We do not give here a corresponding expression because of its cumbersomeness.

In the multiplicative approximation that well works for multielectron systems [12] the equation is true

$$\alpha(\omega, \mathbf{q}) = \alpha(\omega)\,\tilde{F}(q), \tag{8.24}$$

where $\alpha(\omega)$ is the dynamic polarizability, $\tilde{F}(q)$ is the normalized form factor of the target ($\tilde{F}(0) = 1$). Substituting the relation (8.24) in the formula (8.22) and using the expression for the radiation scattering cross-section in terms of the target polarizability

$$\sigma_{scat}(\omega) = \frac{8\pi}{3}\left(\frac{\omega}{c}\right)^4 |\alpha(\omega)|^2, \tag{8.25}$$

we find the representation of the cross-section of PBs on an isolated target in terms of the radiation scattering cross-section

$$\frac{d\sigma^{PB}}{d\omega\,d\Omega_{\mathbf{k}}} = \frac{3}{4\pi^2}\frac{c}{\mathrm{v}^2}\frac{e_p^2}{\hbar\omega}\,\sigma_{scat}(\omega)\int\limits_{q_{\min}}^{q_{\max}} \tilde{F}^2(q)\,I_\phi(q, \mathrm{v}, \omega, \theta)\,\frac{dq}{q}. \tag{8.26}$$

The convenient use of the expression (8.26) with regard to the analysis of PBs on metal nanospheres in a range of photon energies of 1–5 eV consists in the fact that the scattering cross-section $\sigma_{scat}(\omega)$ can be calculated using the Mie theory [13]. Within the framework of this theory the cross-section of radiation scattering by a metal sphere of the radius r_s placed in a dielectric medium looks like

$$\sigma_{scat}^{(Mie)}(\omega) = \frac{2\pi c^2}{\varepsilon_m\,\omega^2}\sum_{n=1}^{\infty}(2n+1)\left\{|a_n(x, mx, m)|^2 + |b_n(x, mx, m)|^2\right\}, \tag{8.27}$$

where $x = k\,r_s = \sqrt{\varepsilon_m}\,\frac{\omega}{c}\,r_s$ and $m = \sqrt{\varepsilon_s(\omega)/\varepsilon_m}$ are the parameters of the Mie theory, $\varepsilon_s(\omega)$ is the dielectric permittivity of the nanosphere material. The expansion coefficients a_n and b_n are

$$a_n(x,y,m) = \frac{\psi'_n(y)\,\psi_n(x) - m\,\psi'_n(x)\,\psi_n(y)}{\psi'_n(y)\,\zeta_n(x) - m\,\zeta'_n(x)\,\psi_n(y)}, \tag{8.28}$$

$$b_n(x,y,m) = \frac{m\,\psi'_n(y)\,\psi_n(x) - \psi'_n(y)\,\psi'_n(x)}{m\psi'_n(y)\,\zeta_n(x) - \zeta'_n(x)\,\psi_n(y)}, \tag{8.29}$$

$$\psi_n(z) = z\,j_n(z) = \sqrt{\frac{\pi\,z}{2}}J_{n+1/2}(z), \tag{8.30}$$

$$\zeta_n(z) = z\,h_n^{(1)}(z) = \sqrt{\frac{\pi\,z}{2}}H_{n+1/2}^{(1)}(z) \tag{8.31}$$

are the functions coined by Debye; $j_n(z), h_n^{(1)}(z)$ are the spherical Bessel and Hankel functions, $J_{n+1/2}(z)$ and $H_{n+1/2}^{(1)}(z)$ are the Bessel and Hankel functions.

The formula for the normalized form factor of a spherical target looks like [2]

$$\tilde{F}_s(q) = 3\,\frac{j_1(q\,r_s)}{q\,r_s}. \tag{8.32}$$

From this equation it follows in particular that $\tilde{F}_s(q=0) = 1$ and $\tilde{F}_s(q > 4/r_s) < 0.01$.

8.2.2 Results and Discussion

The spectral dependences of the PBs cross-section are presented in Fig. 8.7 for different nanosphere radii and in Fig. 8.8 for different velocities of an incident electron; the radiation angle in these figures is taken equal to 30°.

The maximum of the spectral dependence of the PBs cross-section shown in Fig. 8.7 is caused by excitation of a plasmon on the surface of the metal sphere under the action of the electric field of a scattered electron. From this figure it is seen that with increasing nanosphere radius the position of the spectral maximum of the PBs cross-section is shifted to the region of lower photon energies, and its width increases.

An analogous dependence takes place for the cross-section of radiation scattering by metal nanospheres [8], which is caused by a change of the resonance frequency of a surface plasmon ω_{res} with changing radius of the sphere. Really,

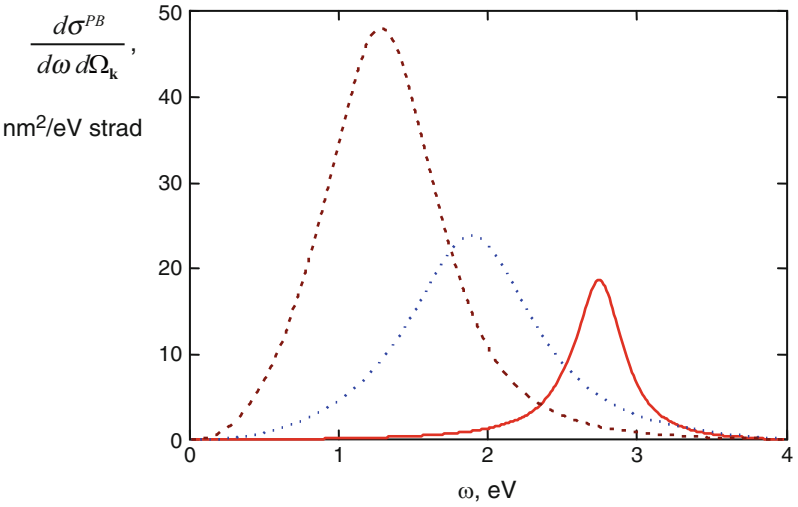

Fig. 8.7 The differential PBs cross-section for electron scattering by silver spheres with different radii in glass: *solid line* – $r_s = 30$ nm, *dotted line* – $r_s = 60$ nm, *dashed line* – $r_s = 90$ nm, $\theta = \pi/6$, $v = 50$ a.u.

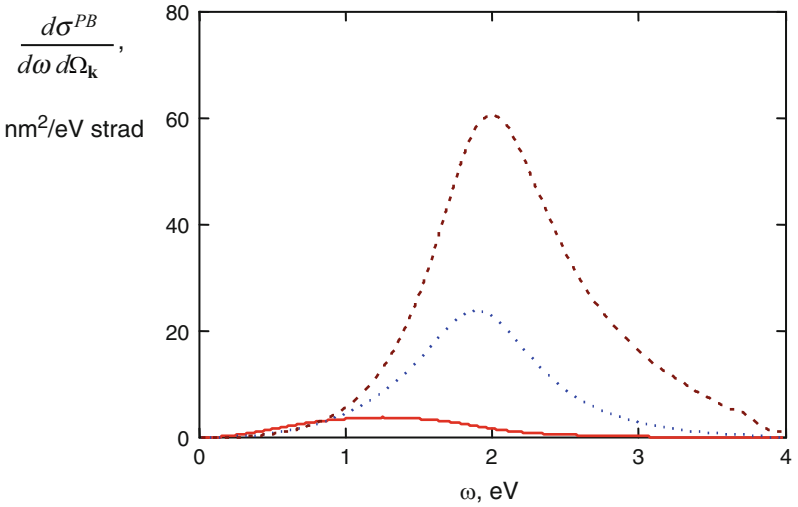

Fig. 8.8 The differential PBs cross-section for electrons with different velocities scattered by a silver sphere in glass: *solid line* – $v = 20$ a.u., *dotted line* – $v = 50$ a.u., *dashed line* – $v = 90$ a.u., $\theta = \pi/6$, $r_s = 60$ nm

the expression for the resonance frequency of a dipole plasmon on the sphere surface looks like

$$\omega_{res} \simeq \sqrt{\frac{\omega_p^2}{\varepsilon_\infty + 2\,\varepsilon_m} - \gamma^2}, \tag{8.33}$$

where ω_p is the plasma frequency of electrons of the sphere substance, γ is the damping constant of a surface plasmon, $\varepsilon_\infty - 1$ is the contribution of bound electrons to the dielectric permittivity of the metal. For large enough radii ($r_s > 30$ nm in case of a silver sphere) the damping constant becomes proportional to the cubed radius of the sphere $\gamma \propto r_s^3$, which defines a shift of the maximum of the radiation scattering and PBs cross-sections with increasing radius of the metal sphere.

Shown in Fig. 8.8 is the PBs cross-section as a function of the photon energy for different electron velocities and a silver sphere radius of 60 nm, the radiation angle is 30°. It is seen that for specified values of parameters the PBs cross-section with increasing electron velocity increases, and its spectral maximum is shifted to the region of higher frequencies. For small nanosphere radii $r_s < 20$ nm on the spectral curve of the PBs cross-section additional maxima appear that are caused by excitation of quadrupole and octupole surface plasmons.

It is seen that with approach of the electron velocity to the velocity of light in the glass matrix $\mathrm{v}* = \tilde{c} = c/\sqrt{\varepsilon_m} \simeq 91.33$ a.u. the velocity dependence of the PBs cross-section has singularity. Physically the said singularity corresponds to a possibility of radiation by an electron of a propagating electromagnetic field in a medium without scattering by a nanosphere. Besides, following from Fig. 8.9 is the presence of maxima on the velocity dependence of the PBs cross-section for small enough metal sphere radii. The value of electron velocity $\mathrm{v}_{\max}$ corresponding to these maxima decreases with decreasing radius according to the relation $\mathrm{v}_{\max} \propto \omega\, r_s$.

Oscillations of the PBs cross-section in Fig. 8.9 at low electron velocities arise due to the contribution to the process of transferred wave vectors of high magnitude: $q > 4/r_s$, when oscillations of the target form factor (Eq. 8.32) as functions of the argument $x = q\, r_s$ take place.

The dependence of the differential PBs cross-section on the nanosphere radius for different energies of a bremsstrahlung photon is demonstrated in Fig. 8.10 for an electron velocity of 50 a.u. and a radiation angle of 90°. It follows from Fig. 8.10 that with increasing photon energy the optimum radius of a nanoparticle, at which the PBs cross-section is maximum, decreases. In this case it turns out that the greatest value of the cross-section at the maximum of the radius dependence is reached for $\hbar\,\omega = 2.8$ eV.

Figure 8.11 demonstrates the narrowing of the angular dependence of the normalized PBs cross-section with increasing nanosphere radius for an IP velocity close to the velocity of light in a medium: $\mathrm{v} \to \tilde{c}$. The normalization of the cross-section was carried out to its value at a zero radiation angle. It is seen from this figure that for small nanosphere radii ($r_s = 10$ nm) the angular dependence of the PBs cross-section practically coincides with the angular dependence of linear dipole

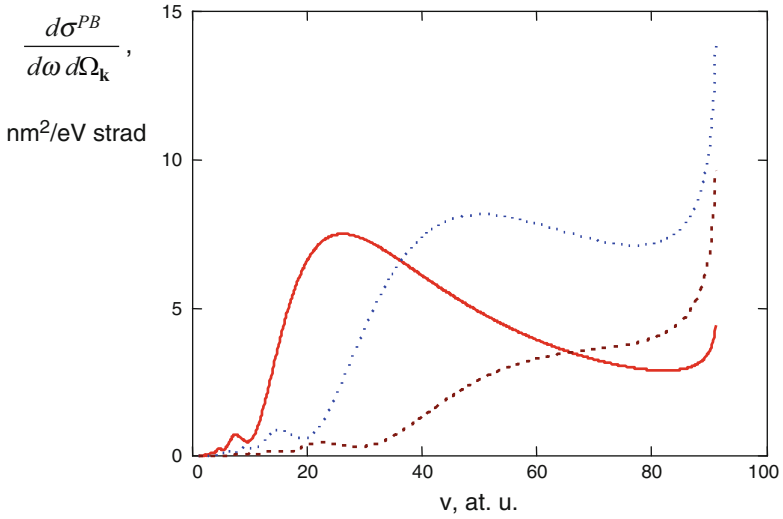

Fig. 8.9 The PBs cross-section for electron scattering by a silver sphere in glass as a function of the electron velocity for $\theta = \pi/2, \hbar\omega = 2.8$ eV. *Solid line* – $r_s = 20$ nm, *dotted line* – $r_s = 40$ nm, *dashed line* – $r_s = 60$ nm

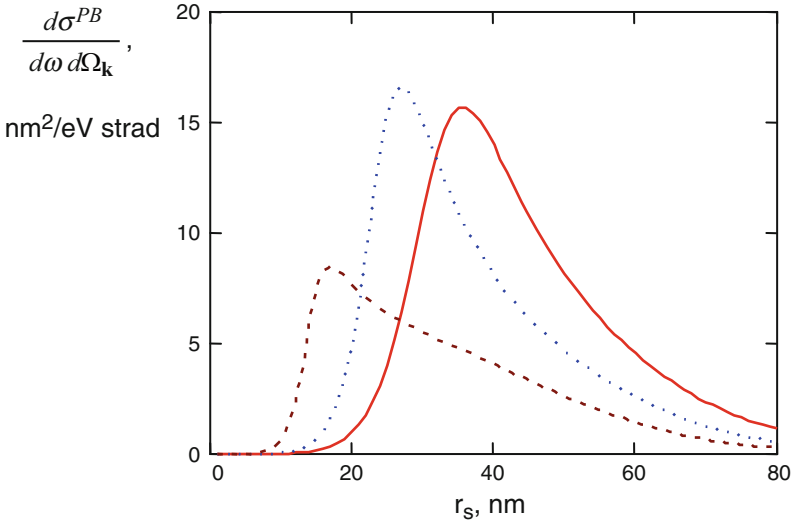

Fig. 8.10 The PBs cross-section for electron scattering by a silver sphere in glass as a function of the sphere radius for v = 50 a.u., $\theta = \pi/2$. *Solid line* – $\hbar\omega = 2.6$ eV, *dotted line* – $\hbar\omega = 2.8$ eV, *dashed line* – $\hbar\omega = 3.0$ eV

radiation. For lower electron velocities the effect of narrowing of the angular PBs distribution also takes place, though it is not so pronounced.

Thus in this section polarization bremsstrahlung on metal spheres in a dielectric medium is investigated theoretically with the use of the Mie theory of light scattering.

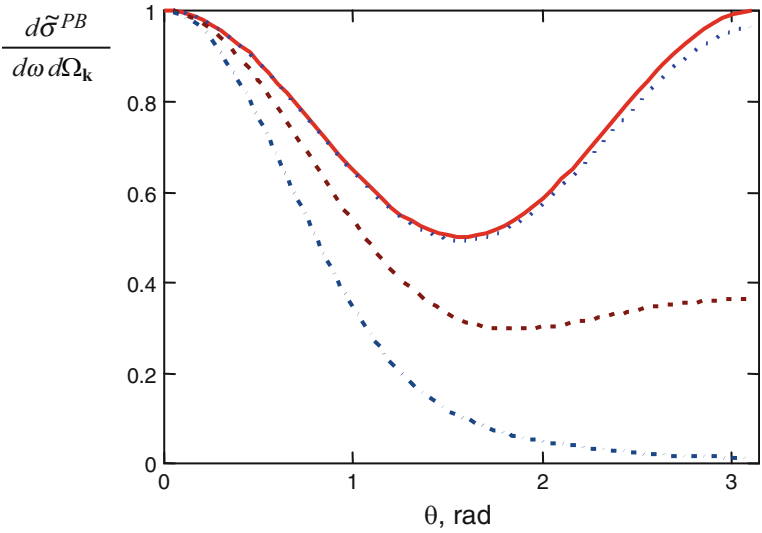

Fig. 8.11 The angular dependence of the normalized PBs cross-section for electron scattering by a silver sphere in glass for $v = 91$ a.u., $\hbar\omega = 2.8$ eV. *Solid line* is the dipole dependence $(1 + \cos^2\theta)/2$, *dotted line* $-r_s = 10$ nm, *dashed line* $-r_s = 50$ nm, *dash-and-dot line* $-r_s = 90$ nm

The spectral-angular distribution of PBs is calculated in the vicinity of a surface plasmon resonance for different radii of nanospheres and IP velocities. It is shown that the spectral line shape for PBs and the angular dependence are modified with the increase of the target radius. The carried out analysis makes it possible to determine an optimum region of parametric variation, in which the use of PBs spectroscopy for investigation of the structure and physical properties of metal nanoparticles in a dielectric matrix is most promising.

8.3 Bremsstrahlung of Fast Electrons on Graphene

8.3.1 Cross-Section of Bremsstrahlung on Graphene

8.3.1.1 General Expression for the Cross-Section of the Process on an Ensemble of Atoms

The cross-section of a photoprocess on an ensemble of target atoms looks like (in case of a monatomic target) [14]:

$$d\sigma_{target} = \left| \sum_j \exp\left(i\,\mathbf{q}\,\mathbf{r}_j\right) \right|^2 d\sigma_{atom}, \tag{8.34}$$

where the sum is over all target atoms being in the volume of interaction, $d\sigma_{atom}$ is the differential cross-section of the process on one atom under consideration,

$$\mathbf{q} = \left(\mathbf{p}_f - \mathbf{p}_i\right)/\hbar + \mathbf{k}$$

is the wave vector transferred from an incident electron to the target, $\mathbf{p}_i$, $\mathbf{p}_f$ are the initial and finite electron momenta, $\mathbf{k}$ is the wave vector of a photon.

In the state of thermodynamic equilibrium the squared absolute value in the formula (8.34) should be properly averaged:

$$\left|\sum_j \exp\left(i\,\mathbf{q}\,\mathbf{r}_j\right)\right|^2 \to \left\langle \sum_{j,j'} \exp\left(i\,\mathbf{q}\,\left(\mathbf{r}_j - \mathbf{r}_{j'}\right)\right)\right\rangle.$$

8.3.1.2 Structure Factor of a Three-dimensional Crystal

The structure factor of a medium in a three-dimensional case (a three-dimensional single crystal, the angle brackets mean averaging over atom positions) [14]:

$$\left\langle \sum_{j,j'} \exp\left(i\,\mathbf{q}\,\left(\mathbf{r}_j - \mathbf{r}_{j'}\right)\right)\right\rangle = N\left(1 - \exp\left(-u^2\,q^2\right)\right) + N\,n_a\,(2\pi)^3 \sum_{\mathbf{g}} e^{-u^2\,g^2}\,|S(\mathbf{g})|^2\,\delta^{(3)}(\mathbf{q}-\mathbf{g}), \quad (8.35)$$

where $N = N_0\,N_{cell}$ is the full number of atoms in the volume of interaction, N_0 is the full number of cells in the volume of interaction, N_{cell} is the number of atoms in a cell, $\mathbf{g}$ is the wave vector of a reciprocal lattice, $n_a = N_{cell}/\Delta_{cell}$ is the volume concentration of atoms, Δ_{cell} is the volume of a unit cell.

In the formula (8.35) the value $S(\mathbf{q})$ is introduced – the *normalized* structure factor of a unit cell of a crystal on the wave vector $\mathbf{q}$, $S(\mathbf{q}=0) = 1$, $\delta^{(3)}(\mathbf{q}) = \delta(q_x)\,\delta\left(q_y\right)\,\delta(q_z)$ is the three-dimensional delta function of the wave vector transferred to the target.

It should be noted that in the book [14] the *nonnormalized* structure factor of a cell is used.

8.3.1.3 Structure Factor of a Two-dimensional Crystal

In going to a two-dimensional case (we assume that a two-dimensional single crystal lies in the $x\,y$ plane, the z coordinate is fixed: $z = z_0$; graphene), when:

$$\mathbf{q}\,\mathbf{r}_j = q_z\,z_0 + \mathbf{q}_{\|}\,\rho_j,$$

for the structure factor of the target by analogy with the three-dimensional case we have

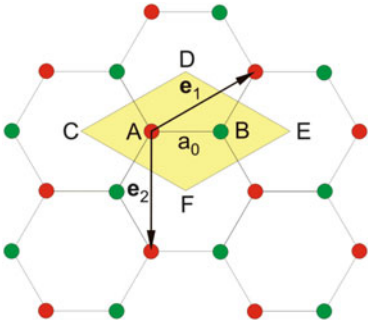

Fig. 8.12 The crystal structure of graphene. A unit cell (CDEF) and elementary translation vectors ($\mathbf{e}_1$, $\mathbf{e}_2$) are shown (The author Alexander Mayorov, InterNet)

$$\left\langle \sum_{j,j'} \exp\left(i\,\mathbf{q}_{\|}\left(\rho_j - \rho_{j'}\right)\right)\right\rangle = N\left(1 - \exp\left(-u^2\,q_{\|}^2\right)\right) + N\,n_s\,(2\pi)^2 \sum_{\mathbf{g}} e^{-u^2\,g^2}\,|S(\mathbf{g})|^2\,\delta^{(2)}\left(\mathbf{q}_{\|} - \mathbf{g}\right), \tag{8.36}$$

where ρ_j is the radius vector of an atom in the plane of the two-dimensional crystal, $\boldsymbol{\rho} = (x, y)$, $\delta^{(2)}\left(\mathbf{q}_{\|}\right) = \delta(q_x)\,\delta\left(q_y\right)$ is the two-dimensional delta function, n_s is the two-dimensional concentration of atoms, u is the root-mean-square deviation of atoms from the equilibrium position. The case $u = 0$ corresponds to going to a perfect crystal.

In Fig. 8.12 the crystal structure of graphene is presented.

The following values are introduced: $a = \sqrt{3}\,a_0 = 0.246$ nm is the lattice constant for graphene, $a_0 = 0.142$ nm is the distance between the nearest atoms (the distance between the atoms in a unit cell, graphene has *two atoms* in a unit cell).

8.3.1.4 Structure Factor of a Unit Cell of Graphene

We assume that an atom A (Fig. 8.12) is at the origin of coordinates, then

$$S(\mathbf{q}) = \frac{1}{2}[1 + \exp(i\,\mathbf{q}\,\mathbf{r}_B)]. \tag{8.37}$$

From Fig. 8.12 it follows that

$$\mathbf{r}_B = \frac{2}{3}\,\mathbf{e}_1 + \frac{1}{3}\,\mathbf{e}_2,$$

where $\mathbf{e}_1 = \left(\frac{\sqrt{3}\,a}{2}, -\frac{a}{2}\right)$ and $\mathbf{e}_1 = (0, a)$ are the basis vectors if the y-axis is directed straight down. Displacing a unit cell by these vectors, it is possible to reproduce the

whole crystal lattice of graphene. Then for the graphene reciprocal lattice vectors we have

$$\mathbf{g}_1 = \left(4\,\pi\Big/\sqrt{3}\,a, 0\right),\ \ \mathbf{g}_2 = \left(2\,\pi\Big/\sqrt{3}\,a, 2\,\pi/a\right), \tag{8.38}$$

so $\mathbf{e}_i\,\mathbf{g}_j = 2\,\pi\,\delta_{ij}$ according to the definition of the reciprocal lattice vector.

In the Cartesian coordinates ($y_B = 0$) it can be written:

$$\mathbf{g}\,\mathbf{r}_B = g_x\,x_B + g_y\,y_B = g_x\,x_B = g_x\,a\Big/\sqrt{3},$$

where the reciprocal lattice vector is:

$$\mathbf{g} = n_1\,\mathbf{g}_1 + n_2\,\mathbf{g}_2, \tag{8.39}$$

$n_{1,2}$ are the integers and

$$g_x = n_1\,g_{1x} + n_2\,g_{2x}.$$

Thus the scalar product included in determination of the structure factor of a unit cell of graphene (Eq. 8.37) is

$$\mathbf{g}\,\mathbf{r}_B = \frac{4\,\pi}{3}\,n_1 + \frac{2\,\pi}{3}\,n_2. \tag{8.40}$$

Accordingly, the structure factor of a unit cell of graphene is

$$S(\mathbf{g}) = \frac{1}{2}\left[1 + \exp\left(i\,(2\,n_1 + n_2)\,\frac{2\,\pi}{3}\right)\right]. \tag{8.41}$$

Hence for the squared absolute value of the structure factor of graphene we find

$$|S(\mathbf{g})|^2 = \frac{1}{2}\left[1 + \cos\left(\frac{2\,\pi}{3}\,(2\,n_1 + n_2)\right)\right]. \tag{8.42}$$

The magnitude of the graphene reciprocal lattice vector can be determined in view of the above expressions:

$$g(n_1,\,n_2) = \frac{4\,\pi}{\sqrt{3}\,a}\,\sqrt{n_1^2 + n_2^2 + n_1\,n_2}. \tag{8.43}$$

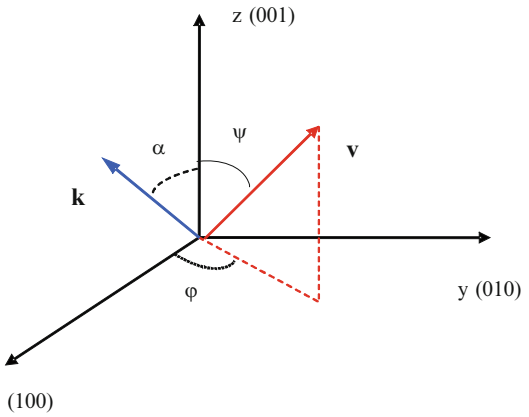

Fig. 8.13 The geometry of the process: α is the angle of photon emission with respect to the normal of the graphene plane, ψ is the polar angle of electron incoming with respect to the normal of the graphene plane, φ is the azimuth angle of electron incoming

The two-dimensional concentration of graphene atoms that is included in the structure factor of the two-dimensional crystal is

$$n_s = \frac{N_{cell}}{S_{cell}}.$$

The number of atoms in a unit cell of graphene is $N_{cell} = 2$, the area of a unit cell is $S_{cell} = \frac{\sqrt{3}\,a^2}{2}$, so

$$n_s = \frac{4}{\sqrt{3}\,a^2}. \tag{8.44}$$

Let us consider bremsstrahlung arising as a result of electron scattering by the two-dimensional plane of graphene. The geometry of the process is shown in Fig. 8.13.

8.3.2 *Cross-Section of Polarization Bremsstrahlung on a Carbon Atom*

The cross-section of polarization bremsstrahlung on an atom, differential with respect to the frequency and the solid angle of photon escape, is

$$\frac{d\sigma_a^{(PB)}}{d\omega\, d\Omega_{\mathbf{k}}} = \frac{e^2}{\hbar\,\omega}\,\frac{c}{\pi^2\,\mathrm{v}}\int \delta(\omega - \mathbf{k}\,\mathbf{v} + \mathbf{q}\,\mathbf{v})\,\frac{\left[\mathbf{s},\,\omega\,\mathbf{v}/c^2 - \mathbf{q}\right]^2}{\left(\mathbf{q}^2 - 2\,\mathbf{k}\,\mathbf{q}\right)^2}\left|\left(\frac{\omega}{c}\right)^2 \alpha(\omega,\,\mathbf{q})\right|^2 d\mathbf{q}, \tag{8.45}$$

where $\alpha(\omega,\,\mathbf{q})$ is the generalized dynamic polarizability of an atom, $\mathbf{s} = \mathbf{k}/|\mathbf{k}|$ is the unit vector in the direction of photon emission.

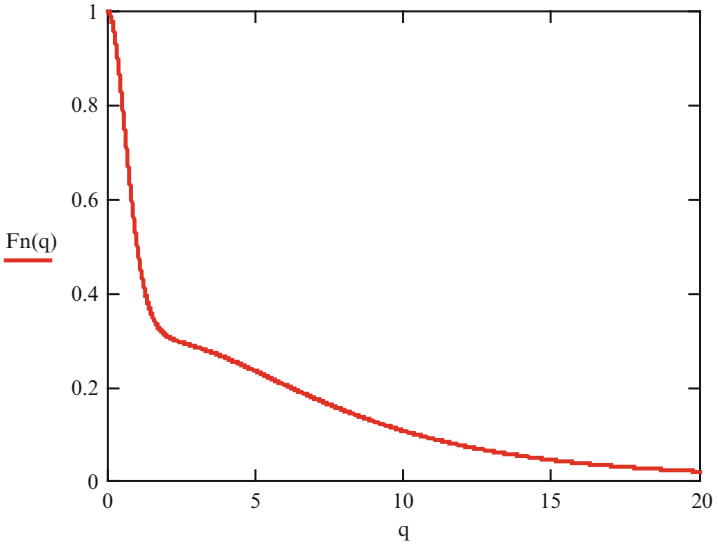

Fig. 8.14 The normalized form factor of a carbon atom, the X-axis is plotted in atomic units

In the multiplicative approximation the generalized dynamic polarizability of an atom is expressed in terms of the dipole polarizability and the atomic form factor:

$$\alpha(\omega, \mathbf{q}) = \alpha(\omega)\,\tilde{F}(q), \tag{8.46}$$

where $\tilde{F}(q)$ is the atomic form factor normalized by the condition $\tilde{F}(q = 0) = 1$.

To calculate the atomic form factor $F(q)$ that within the framework of the multiplicative approximation defines the dependence of the generalized polarizability of an atom on the value of a transferred momentum (of a wave vector), it is convenient to use the Slater wave functions of atomic orbitals. As shown in the work [15], the form factor calculated in such a way differs from its Hartree-Fock analog by no more than units of percents. Corresponding formulas look like:

$$\tilde{F}(q) = \frac{1}{Z}\sum_j N_j\, Q\left(q, \beta_j, \mu_j\right),\ Q(q, \beta, \mu) = \frac{\left[1 + (q/2\beta)^2\right]^{\mu}}{(\mu\, q/\beta)} \sin\left[2\,\mu\,\mathrm{atan}\left(\frac{q}{2\,\beta}\right)\right],$$

where N_j is the number of equivalent electrons in the j th atomic shell, β and μ are the Slater parameters of atomic shells.

The normalized form factor of a carbon atom calculated according to the above formulas is presented in Fig. 8.14 as a function of the magnitude of the transferred wave vector q. The nonmonotonicity of decrease of the form factor with growing value q is connected with the shell structure of an atom. Corresponding to high values of q is the contribution to $\tilde{F}(q)$ of the inner shell of a carbon atom with the principal quantum number $n = 1$. Corresponding to small values of q is the second (outer)

atomic shell. A bend of the dependence $\tilde{F}(q)$ at $q \approx 1$ corresponds to transition from one electron shell to another.

Since the dynamic polarizability of an atom is a complex value, the real and imaginary parts of which are related by the Kramers-Kronig relations, it is convenient to begin its calculation with the imaginary part. To obtain the frequency dependence of the imaginary part of the dipole polarizability, we proceed from its relation with the cross-section of radiation absorption $\sigma_{ph}(\omega)$ given by the optical theorem:

$$\mathrm{Im}(\alpha(\omega)) = \frac{c}{4\pi\omega}\,\sigma_{ph}(\omega). \tag{8.47}$$

In this book, to determine the spectral dependence of the photoabsorption cross-section $\sigma_{ph}(\omega)$, the data on the radiation absorption coefficient given at the Internet site of the Berkeley National Laboratory are used.

The real part of the atomic polarizability can be restored by the known imaginary part with the use of the Kramers-Kronig relation that for calculations is convenient to be presented as follows:

$$\mathrm{Re}(\alpha(\omega)) = \frac{2}{\pi}\int_0^\infty \frac{\omega\mathrm{Im}(\alpha(\omega)) - \omega'\mathrm{Im}(\alpha(\omega'))}{\omega^2 - \omega'^2}\,d\omega'. \tag{8.48}$$

This equation, due to the presence of the second summand in the numerator of the integrand, allows calculation of the principal-value integral appearing in the standard form of the Kramers-Kronig relations in terms of a punctured integral with a "puncture" eliminating the singularity of the integrand, which is convenient in practical calculations. At high frequencies the imaginary part of the polarizability decreases as $\omega^{-9/2}$, so the integral on the right side of the equation converges well at infinity.

The results of calculation of the dynamic polarizability of a carbon atom are presented in Fig. 8.15. Given for comparison in the same figure is the number of electrons in a carbon atom, tending to which in the high-frequency limit is the real part of the atomic polarizability normalized to the polarizability of a free electron with the opposite sign: $\alpha(\omega) \to \alpha(\omega)/\left(-e^2/m\,\omega^2\right)$.

From this figure it is seen that in the high-frequency limit the imaginary part of the polarizability tends to zero. The peculiarities on the curves of Fig. 8.15 correspond to potentials of ionization of electron subshells of a carbon atom.

8.3.3 Polarization Bremsstrahlung on Graphene

If the expression for the structure factor of graphene (Eq. 8.36) is substituted in the general formula for the cross-section of bremsstrahlung on a polyatomic target (Eq. 8.34), two terms will appear in the Bs cross-section that correspond to the incoherent (the first summand on the right side of Eq. 8.36) and coherent (the second summand on the right side of Eq. 8.36) parts of the structure factor.

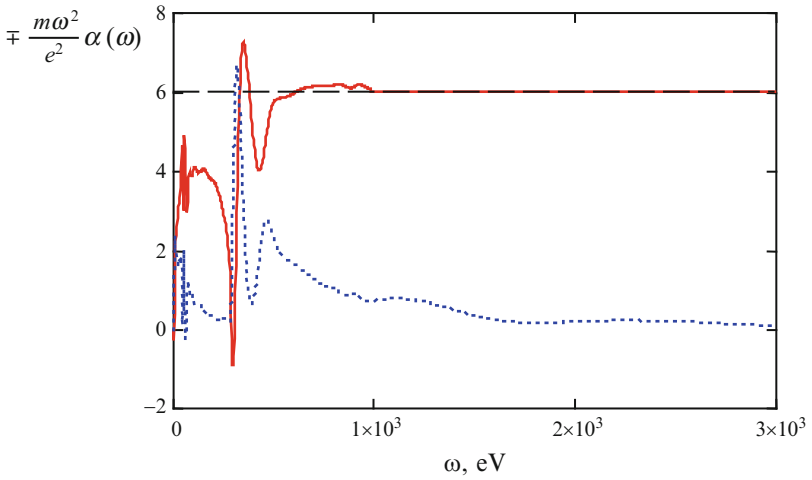

Fig. 8.15 The real (*solid curve*) and imaginary (*dotted curve*) parts of the dynamic polarizability of a carbon atom multiplied by the squared frequency, the Y-axis is plotted in dimensionless units, minus in the definition of the Y-axis relates to the real part and plus relates to the imaginary part of the polarizability

8.3.3.1 Incoherent PBs on Graphene

Substituting Eq. 8.36 in Eq. 8.34, we find that the cross-section of incoherent PBs on a target (in terms of one atom) is

$$\frac{1}{N}\frac{d\sigma^{(PB)}_{incoh}}{d\omega\, d\Omega_{\mathbf{k}}} = \frac{e^2}{\hbar\,\omega}\frac{c}{\pi^2\,\mathrm{v}}\int \delta(\omega - \mathbf{k}\,\mathbf{v} + \mathbf{q}\,\mathbf{v}) \times \left(1 - \exp\left(-u^2\,\mathbf{q}^2\right)\right)\frac{\left[\mathbf{s},\, \omega\,\mathbf{v}/c^2 - \mathbf{q}\right]^2}{\left(\mathbf{q}^2 - 2\,\mathbf{k}\,\mathbf{q}\right)^2}\left|\left(\frac{\omega}{c}\right)^2\alpha(\omega,\, q)\right|^2 d\mathbf{q}. \tag{8.49}$$

Integration on the right side of this equation with respect to the angles of the vector $\mathbf{q}$ in view of the presence of the delta function gives:

$$\frac{1}{N}\frac{d\sigma^{(PB)}_{incoh}}{d\omega\, d\Omega_{\mathbf{k}}} = \frac{2\,e^2}{\pi\,\mathrm{v}^2\,\mathrm{c}^3\,\hbar\omega}\int\limits_{q_{\min}}^{q_{\max}}\frac{dq}{q}\,I_{\varphi}(q,\,\mathrm{v},\,\omega,\,\theta)\left(1 - e^{-u^2\,q^2}\right)\left|\omega^2\,\alpha(\omega,\,q)\right|^2, \tag{8.50}$$

where

$$q_{\min}(\omega,\mathrm{v},\theta) = \frac{\omega}{\mathrm{v}}\left(1 - \frac{\mathrm{v}}{c}\cos\theta\right),\; q_{\max} = 2\mu\;\mathrm{v}/\hbar,$$

μ is the reduced mass of an electron and a target atom, $\theta = angle(\mathbf{k}, \mathbf{v})$ is the radiation angle,

$$I_\varphi(q, \mathrm{v}, \omega, \theta) = \frac{q^3\,\mathrm{v}}{2\,\pi}\int d\Omega_{\mathbf{q}}\,\delta(\omega - \mathbf{kv} + \mathbf{qv})\,\frac{\left[\mathbf{s}, \omega\,\mathbf{v}/c^2 - \mathbf{q}\right]^2}{\left(\mathbf{q}^2 - 2\,\mathbf{k}\,\mathbf{q}\right)^2} \tag{8.51}$$

is the dimensionless kinematic integral calculated in the explicit form in [5], $d\Omega_{\mathbf{q}}$ is the element of the solid angle around the vector $\mathbf{q}$. In the nonrelativistic limit $\mathrm{v}<<c$ the kinematic integral looks like

$$I_\varphi(q, \mathrm{v}, \omega, \theta) \cong \frac{1 + \cos^2\theta}{2} + \left(\frac{\omega}{q\,\mathrm{v}}\right)^2\,\frac{1 - 3\cos^2\theta}{2}. \tag{8.52}$$

In the general case the kinematic integral can be represented as a function of three variables $I_\varphi(q, \mathrm{v}, \omega, \theta) = \tilde{I}_\varphi(x = q\,c/\omega, \beta = \mathrm{v}/\mathrm{c}, \theta)$, where

$$\tilde{I}_\varphi(x, \beta, \theta) = \frac{x^2 f_1(x, \beta, \theta)}{\Delta^{3/2}(x, \beta, \theta)} + \frac{x^2}{4}\left[\frac{f_2(x, \beta, \theta)}{\Delta^{1/2}(x, \beta, \theta)} - 1\right], \tag{8.53}$$

$$f_1 = \left(x^2 + 2\,\tilde{x}\,\cos\theta\right)\left[\left(x^2 - \tilde{x}^2\right)\cos^2\theta + (\tilde{x} - \beta)^2\sin^2\theta\right] + 4\,\sin^2\theta\,\cos\theta\,(\tilde{x} - \beta)\left(x^2 - \tilde{x}^2\right),$$

$$f_2 = x^2 + 2\,\tilde{x}\,\cos\theta,\ \tilde{x} = q_{\min}\frac{c}{\omega} = \beta^{-1} - \cos\theta,$$

$$\Delta = \left(x^2 - 2\left(1 - \frac{\cos\theta}{\beta}\right)\right)^2 + 4\frac{1 - \beta^2}{\beta^2}\,\sin^2\theta.$$

In the relativistic limit ($\beta \to 1$) the function $\tilde{I}_\varphi(x, \beta, \theta)$ has a sharp maximum in fulfilment of the equation $x_{\max} = \sqrt{2\,(1 - \cos\theta/\beta)} \approx 2\,\sin(\theta/2)$, and the sharpness of the maximum increases for wide radiation angles $\theta \to \pi$. This maximum corresponds to exit of a photon "to the mass shell" in case of propagation of an electromagnetic field in a medium.

8.3.3.2 Coherent PBs on Graphene

The cross-section of coherent PBs on a two-dimensional periodic structure, which is graphene, (in terms of one atom) is

$$\frac{1}{N}\frac{d\sigma_{coh}^{(PB)}}{d\omega\, d\Omega_{\mathbf{k}}} = \frac{e^2}{\hbar\,\omega}\frac{c}{\pi^2\,\mathrm{v}}\left(\frac{\omega}{c}\right)^4 n_s\,(2\,\pi)^2\times$$
$$\sum_{\mathbf{g}} e^{-u^2\,(\mathbf{g}+\mathbf{q}_\perp)^2}\,|S(\mathbf{g})|^2\int\delta(\omega-\mathbf{k}\,\mathbf{v}+\mathbf{g}\,\mathbf{v}+q_z\mathrm{v}_z)$$
$$\times\frac{\left[\mathbf{s},\,\omega\,\mathbf{v}/c^2-(\mathbf{g}+\mathbf{q}_\perp)\right]^2}{\left((\mathbf{g}+\mathbf{q}_\perp)^2-2\,\mathbf{k}\,(\mathbf{g}+\mathbf{q}_\perp)\right)^2}\,|\alpha(\omega,\,\mathbf{g}+\mathbf{q}_\perp)|^2 dq_z. \tag{8.54}$$

In derivation of this expression it was taken into account that integration with respect to the two-dimensional delta function $\delta^{(2)}\left(\mathbf{q}_\parallel-\mathbf{g}\right)$ gives:

$$\mathbf{q}_\parallel=\mathbf{g}, \tag{8.55}$$

and there remains integration with respect to the component of the wave vector dq_z transferred to the target, this component being normal to the graphene plane, the said integration is also "removed" due to the presence of the delta function $\delta(\omega-\mathbf{k}\,\mathbf{v}+\mathbf{g}\,\mathbf{v}+q_z\mathrm{v}_z)$ under the sign of integration. As a result, we find a fixed value for the normal (to the graphene plane) component of the wave vector transferred to the target as a function of the problem parameters:

$$q_z=-g\,tg\psi+\frac{\omega-\mathbf{k}\,\mathbf{v}}{\mathrm{v}\cos\psi}. \tag{8.56}$$

This value should be substituted in the expression for the coherent PBs cross-section ($|\mathbf{q}_\perp|=q_z$). Taking into account the fact that $(\mathbf{q}_\perp\,\mathbf{g})=0$ and in view of the relation (8.46), we obtain for the differential spectral-angular cross-section of coherent PBs on graphene the following expression:

$$\frac{1}{N}\frac{d\sigma_{coh}^{(PB)}}{d\omega\, d\Omega_{\mathbf{k}}}=\frac{4\,n_s}{\cos\psi}\left(\frac{e^2}{\hbar\,\omega}\right)\frac{\omega^4\,|\alpha(\omega)|^2}{c^3\,\mathrm{v}^2}$$
$$\times\sum_{\mathbf{g}} e^{-u^2\,\left(g^2+q_z^2\right)}\,|S(\mathbf{g})|^2\left|\tilde{F}\left(\sqrt{g^2+q_z^2}\right)\right|^2 P(\mathbf{g},\,\mathbf{k},\,\mathbf{q}_\perp), \tag{8.57}$$

where

$$P(\mathbf{g},\,\mathbf{k},\,q_z)$$
$$=\frac{\left(\frac{\omega\,\mathrm{v}}{c^2}\right)^2+g^2+q_z^2-2\,\frac{\omega\,\mathrm{v}}{c^2}(g\,\sin\psi+q_z\,\cos\psi)-\left[\frac{\omega\,\mathrm{v}}{c^2}\cos\theta-g\,\sin\alpha-q_z\,\cos\alpha\right]^2}{\left(g^2+q_z^2-2\,\frac{\omega}{c}\,(g\,\sin\alpha+q_z\,\cos\alpha)\right)^2}, \tag{8.58}$$

$$|S(\mathbf{g})|^2 = \cos^2\Big(\frac{\pi}{3}(2\,n_1 + n_2)\Big),\ |\mathbf{g}| = g(n_1,\,n_2) = \frac{4\,\pi}{\sqrt{3}\,a}\,\sqrt{n_1^2 + n_2^2 + n_1\,n_2}$$

$$\cos\theta = \cos\alpha\,\cos\psi + \cos\varphi\,\sin\alpha\,\sin\psi,\ n_s = \frac{4}{\sqrt{3}\,a^2},$$

and

$$q_z = -g\,tg\psi + \omega\frac{1 - (\mathrm{v}/c)\,\cos\theta}{\mathrm{v}\cos\psi}.$$

Summation over the reciprocal lattice vectors $\mathbf{g}$ implies summation over the integers $n_{1,2}$ defining the magnitude of $\mathbf{g}$.

It should be noted that in contrast to coherent PBs in a three-dimensional single crystal, when the radiated frequency is fixed by the condition

$$\omega_{\max}^{(3)} = -\frac{\mathbf{g}\,\mathbf{v}}{1 - \beta\,\cos\theta}, \tag{8.59}$$

hence we find for a cubic crystal ($n_{1,2,3}$ are the integers):

$$\omega_{\max}^{(3)} = -\frac{g\,\mathrm{v}\,(n_1\,\sin\psi\,\cos\varphi + n_2\,\sin\psi\,\sin\varphi + n_3\,\cos\psi\,)}{1 - \beta\,\cos\theta}, \tag{8.60}$$

the frequency of coherent PBs in a two-dimensional single crystal is not a fixed value. Nevertheless, in the two-dimensional case with fulfilment of certain conditions (see below) the PBs spectrum has sharp maxima. The frequencies of these maxima are defined by the zeros of the denominator $P(\mathbf{g},\,\mathbf{k},\,q_z)$ in the expression for the coherent PBs cross-section (Eq. 8.57).

For the denominator $P(\mathbf{g},\,\mathbf{k},\,q_z)$, taking into account the explicit form of q_z, we find:

$$\mathrm{Den}(\omega,\,\alpha,\psi,\beta,\theta) = \frac{g^4}{\cos^4\psi}\Big\{\Big(\frac{\omega}{g\,\mathrm{v}}\Big)^2\,\delta\,[\delta - 2\,\beta\,\cos\alpha\,\cos\psi] + 2\,\beta\,\frac{\omega}{g\,\mathrm{v}}\,\cos\psi\,[\cos\alpha\,\sin\psi - \sin\alpha - \frac{\delta}{\beta}\,tg\psi] + 1\Big\}^2, \tag{8.61}$$

where the contracted notations $\delta = 1 - \beta\,\cos\theta$, $\beta = \mathrm{v}/c$ are introduced, and the cosine of the radiation angle is $\cos\theta = \cos\alpha\,\cos\psi + \cos\varphi\,\sin\alpha\,\sin\psi$.

For the zero angle of electron incoming into the graphene plane ($\psi = 0$) the expression for the denominator is simplified to the form:

$$\begin{aligned}&\mathrm{Den}(\omega,\ \alpha, \psi = 0, \beta, \theta = \alpha)\\&= g^4 \left\{ \left(\frac{\omega}{g\,\mathrm{v}} \right)^2 (1 - \beta\,\cos\alpha)\,(1 - 3\,\beta\,\cos\alpha) - 2\,\beta\,\frac{\omega}{g\,\mathrm{v}}\,\sin\alpha + 1 \right\}^2 .\end{aligned} \tag{8.62}$$

The resonance condition for the coherent PBs cross-section in the general case looks like

$$\mathrm{Den}(\omega,\ \alpha, \psi, \beta, \theta) = 0. \tag{8.63}$$

If this equation is solved with respect to the radiation frequency, the following expression for the frequency of a spectral maximum in coherent PBs on graphene will be obtained:

$$\omega_{\max} = g\,\mathrm{v}\,F_\omega(\alpha, \psi, \theta, \beta). \tag{8.64}$$

Here the dimensionless function is introduced:

$$\begin{aligned}&F_\omega(\alpha, \psi, \theta, \beta)\\&= \frac{\cos\psi\,(\beta\,\sin\alpha + \delta\,tg\psi - \beta\,\sin\psi\,\cos\alpha) + \mathrm{sign}(\delta - 2\,\beta\cos\alpha\,\cos\psi)\,\sqrt{D}}{\delta(\delta - 2\,\beta\cos\alpha\,\cos\psi)},\end{aligned} \tag{8.65}$$

where $\delta = 1 - \beta\,\cos\theta, \beta = \mathrm{v}/c, D = \cos^2\psi\,(\beta\,\sin\alpha + tg\psi\,\delta - \beta\,\sin\psi\,\cos\alpha)^2 - \delta\,(\delta - 2\,\beta\cos\alpha\,\cos\psi)$ and

$$\mathrm{sign}(x) = \begin{cases} 1 & \text{for } x>0 \\ 0 & \text{for } x = 0\,. \\ -1 & \text{for } x<0 \end{cases}$$

In case of the zero angle of electron incoming into a two-dimensional single crystal ($\psi = 0$), we have the following expression for the function determining the dependence of the resonance frequency of radiation on the electron velocity and the angle of photon emission:

$$\begin{aligned}&F_\omega(\psi = 0)\\&= \frac{\beta\,\sin\alpha + \mathrm{sign}(1 - 3\,\beta\,\cos\alpha)\,\sqrt{(\beta\,\sin\alpha)^2 - (1 - \beta\,\cos\alpha)\,(1 - 3\beta\,\cos\alpha)}}{(1 - \beta\,\cos\alpha)\,(1 - 3\beta\,\cos\alpha)}.\end{aligned} \tag{8.66}$$

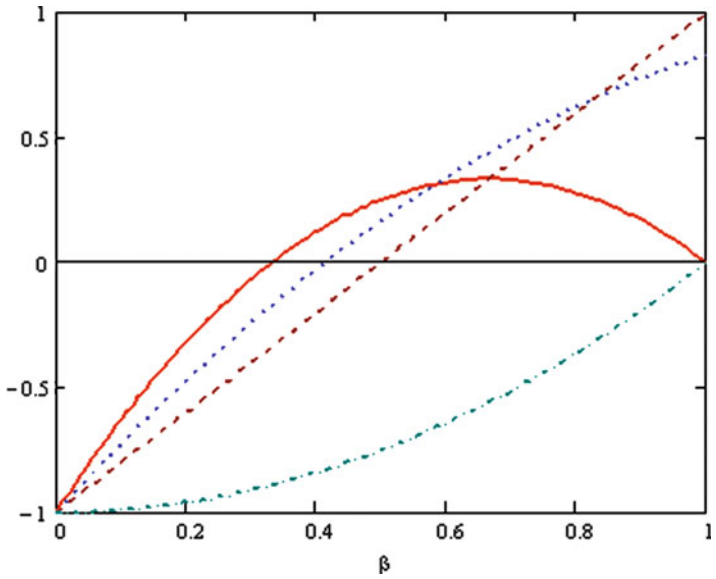

Fig. 8.16 The dependence of the discriminant (8.67) defining the resonance frequency of PBs for the zero angle of electron incoming $\psi = 0$ on the electron velocity ($.\gamma \propto r_s^3.$) for different radiation angles α: *solid line* – $\alpha = 0$, *dotted line* – $\alpha = \pi/4$, *dashed line* – $\alpha = \pi/3$, *dotted-dashed line* $\alpha = \pi/2$

For the positiveness of the discriminant in this expression

$$D\omega(\alpha, \beta) = (\beta \sin\alpha)^2 - (1 - \beta\cos\alpha)(1 - 3\beta\cos\alpha), \tag{8.67}$$

that is, for existence of a resonance frequency of coherent PBs the fulfilment of the condition is required:

$$\frac{1}{2\cos\alpha - 1} \geq \beta \geq \frac{1}{2\cos\alpha + 1}. \tag{8.68}$$

Following hence is the necessary condition of the presence of a resonance $2\cos\alpha + 1 > 1$, that is, $\alpha < \pi/2$ – radiation should go to the top hemisphere $z > 0$ (see Fig. 8.13).

The dependence of the discriminant (8.67) on the electron velocity for different radiation angles for the zero angle of electron incoming is presented in Fig. 8.16.

From this figure it is seen that with increasing radiation angle the range of electron velocity values decreases, in which the discriminant is positive, that is, there is a resonance in the cross-section of coherent PBs on graphene. For the angle $\alpha = \pi/2$ this range comes to the point $v = c$.

If the equation $1 - 3\beta\cos\alpha = 0$ is satisfied, then, as follows from the formulas (8.64) and (8.66), the resonance frequency of coherent PBs becomes infinite, that is, a resonance is absent. So the equation

$$\beta = \frac{1}{3\,\cos\alpha}\left(> \frac{1}{2\,\cos\alpha + 1}\ \text{for}\ \alpha < \pi/2\right) \tag{8.69}$$

means the absence of a resonance. In turn, it is possible if $\alpha < \arccos(1/3)$.

Thus the analysis of coherent PBs in case of normal electron incoming has shown in particular that for small enough radiation angles $\alpha < \arccos(1/3)$ with the condition $3\,\cos\alpha = c/\mathrm{v}$ satisfied spectral resonances in radiation are absent since the resonance frequency becomes infinite.

It should be noted that if the discriminant (8.67) is negative, but is close to zero, the cross-section of coherent PBs on graphene also has maxima, but not so sharp as in case of the positive discriminant.

The total cross-section of electron PBs on graphene in terms of one atom is equal to the sum of the incoherent and coherent parts:

$$\frac{1}{N}\,\frac{d\sigma^{(PB)}}{d\omega\,d\Omega_{\mathbf{k}}} = \frac{1}{N}\,\frac{d\sigma^{(PB)}_{incoh}}{d\omega\,d\Omega_{\mathbf{k}}} + \frac{1}{N}\,\frac{d\sigma^{(PB)}_{coh}}{d\omega\,d\Omega_{\mathbf{k}}}. \tag{8.70}$$

8.3.4 Static Bremsstrahlung on Graphene

The expression for the cross-section of static bremsstrahlung of a relativistic charged particle on an atom (without its excitation) in the first Born approximation looks like [16]:

$$\frac{d\sigma^{OB}_{el}}{d\omega\ d\Omega_{\mathbf{k}}} = \frac{1}{4\pi^2\,\omega}\,\frac{e_p^2}{\hbar\,c}\,Z^2\,r_e^2\left(\frac{p_f}{p_i}\right)\left(\frac{m}{m_p}\right)^2\int d\Omega_{\mathbf{p}_f}\left[1-\tilde{F}_a(q)\right]^2 J\left(\Omega_{\mathbf{p}_f}\right), \tag{8.71}$$

where m_p is the mass of an incident particle and $J\left(\Omega_{\mathbf{p}_f}\right)$ is the dimensionless function determined by the equations:

$$\begin{aligned} J\left(\Omega_{\mathbf{p}_f}\right) = \frac{m_p^2}{(\hbar\,q)^4}\Bigg\{ & \left(\frac{p_f}{\kappa_f}\right)^2\left(4\,\varepsilon_i^2-(\hbar qc)^2\right)\,\sin^2\theta' \\ & +\left(\frac{p_i}{\kappa_i}\right)^2\left(4\,\varepsilon_f^2-(\hbar qc)^2\right)\,\sin^2\theta+\frac{2(\hbar\omega)^2}{\kappa_i\,\kappa_f}\left(p_i^2\sin^2\theta+p_f^2\sin^2\theta'\right) \\ & -\frac{2p_ip_f}{\kappa_i\,\kappa_f}\left[2\left(\varepsilon_i^2+\varepsilon_f^2\right)-(\hbar qc)^2\right]\sin\theta\sin\theta'\cos\varphi\Bigg\}, \end{aligned}$$

$$\kappa_i = \varepsilon_i/c - c(\mathbf{kp}_i)/\omega,\ \kappa_f = \varepsilon_f/c - c\left(\mathbf{kp}_f\right)/\omega,$$

$$\hbar q = \sqrt{(\hbar k)^2 + p_i^2 + p_f^2 - 2p_i\hbar k\cos\theta + 2p_f\hbar k\cos\theta' - 2p_i p_f\left(\cos\theta\cos\theta' + \sin\theta\sin\theta'\cos\varphi\right)},$$

θ' is the angle between the vectors $\mathbf{p}_f$ and $\mathbf{k}$, φ is the angle between the planes $\mathbf{p}_i\,\mathbf{k}$ and $\mathbf{p}_f\,\mathbf{k}$, $r_e = \frac{e^2}{mc^2}$.

The approximate formula for the differential cross-section of SBs on an atom looks like:

$$\frac{d\sigma_{el}^{OB}}{d\omega\; d\Omega_{\mathbf{k}}} \approx \frac{1}{\pi}\,\frac{Z^2\,e^6\,(1+\cos^2\theta)\left(1-\left(\frac{\mathrm{v}}{c}\right)^2\right)}{m^2\,\hbar\,\omega\,\mathrm{v}^2\,c^3\left(1-\frac{\mathrm{v}}{c}\cos\theta\right)^2}\int\limits_{q_{\min}}^{q_{\max}}\frac{\left(1-\tilde{F}(q)\right)^2}{q}dq, \tag{8.72}$$

where

$$q_{\min}(\omega,\mathrm{v},\theta) = \frac{\omega}{\mathrm{v}}\left(1-\frac{\mathrm{v}}{c}\cos\theta\right),\; q_{\max} = 2\mu\;\mathrm{v}/\hbar,$$

μ is the reduced mass of an electron and a target atom, $\theta = angle(\mathbf{k},\,\mathbf{v})$ is the radiation angle.

The expression (8.72) has a characteristic error of 10–30 % in comparison with the formula (8.71). In derivation of Eq. 8.72 the approximate equation for electron energy change during bremsstrahlung was used:

$$\varepsilon_f - \varepsilon_i \approx \hbar(\mathbf{q}-\mathbf{k})\,\mathbf{v}.$$

In the nonrelativistic limit $\mathrm{v}<<c$ from the expression (8.72) the equation follows:

$$\frac{d\sigma_{el}^{OB}}{d\omega\; d\Omega_{\mathbf{k}}} \approx \frac{1}{\pi}\,\frac{Z^2\,e^6\,(1+\cos^2\theta)}{m^2\,\hbar\,\omega\,\mathrm{v}^2\,c^3}\int\limits_{q_{\min}}^{q_{\max}}\frac{\left(1-\tilde{F}(q)\right)^2}{q}dq. \tag{8.73}$$

For the incoherent part of the cross-section of SBs on graphene (in terms of one atom) we have:

$$\frac{1}{N}\frac{d\sigma_{incoh}^{OB}}{d\omega\; d\Omega_{\mathbf{k}}} \approx \frac{1}{\pi}\,\frac{Z^2\,e^6\,(1+\cos^2\theta)\left(1-\left(\frac{\mathrm{v}}{c}\right)^2\right)}{m^2\hbar\omega\,\mathrm{v}^2\,c^3\left(1-\frac{\mathrm{v}}{c}\cos\theta\right)^2}\int\limits_{q_{\min}}^{q_{\max}}\frac{\left(1-\tilde{F}(q)\right)^2}{q}\left(1-\exp\left(-u^2\,q^2\right)\right)dq. \tag{8.74}$$

Given in Figs. 8.17 and 8.18 is the comparison of the spectral cross-sections of PBs and SBs on a carbon atom and incoherent PBs and SBs on graphene for an electron velocity of 100 a.u. (this velocity corresponds to an incident electron energy of 240 keV).

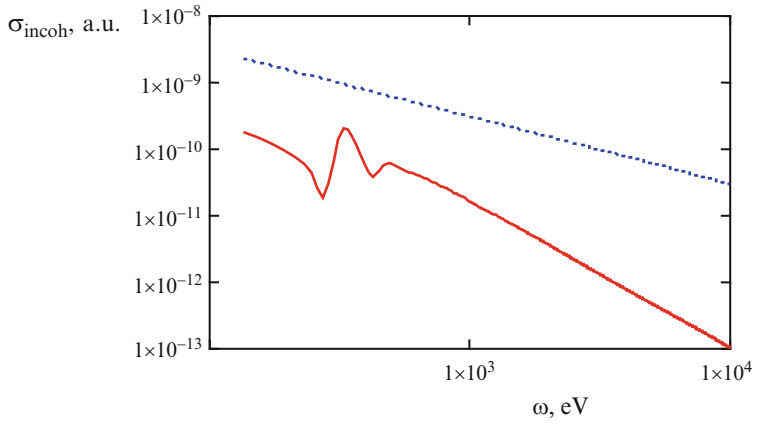

Fig. 8.17 The comparison of the spectral cross-sections of PBs (*solid curve*) and SBs (*dotted curve*) of an electron with a velocity of 100 a.u. scattered by a carbon atom, the radiation angle is $\theta = 30^\circ$, the abscissa is plotted in electron-volts, the ordinate is plotted in atomic units

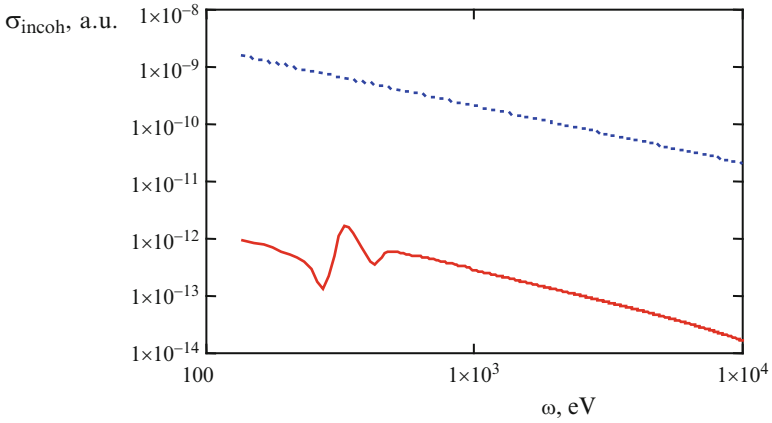

Fig. 8.18 The comparison of the spectral cross-sections of incoherent PBs (*solid curve*) and SBs (*dotted curve*) of an electron scattered by graphene (in terms of one atom), $v = 100$ a.u., the radiation angle is $\theta = 30^\circ$

From Fig. 8.17 it is seen that in case of a carbon atom the PBs cross-section at the maximum of the frequency dependence is about an order of magnitude less than the SBs cross-section. This circumstance is explained by relatively low dynamic polarizability of a carbon atom that defines the value of the PBs cross-section. With growing electron velocity the relative contribution of PBs will increase since the role of high impact parameters will increase.

The difference of incoherent channels of PBs and SBs on graphene is even more (Fig. 8.18) and is about two and a half orders of magnitude at the maximum of the spectral dependence of PBs. The latter circumstance is connected with the fact that the polarization channel is formed at long distances from a target, the contribution

of these distances to incoherent radiation is suppressed by the multiplier $1 - \exp(-u^2\, q^2)$ that is small for $q < 1/u$ (low impact parameters).

8.3.4.1 Coherent SBs on Graphene

For calculation of the coherent part of SBs on graphene it is necessary to express the cross-section of the process on an atom in terms of the integral with respect to the transferred wave vector **q**:

$$\frac{d\sigma_a^{OB}}{d\omega\; d\Omega_{\mathbf{k}}} \approx \frac{1}{2\,\pi^2}\,\frac{Z^2\, e^6\,(1+\cos^2\theta)\left(1-\left(\frac{\mathrm{v}}{c}\right)^2\right)}{\hbar\,\omega\, m^2\,\mathrm{v}\, c^3\left(1-\frac{\mathrm{v}}{c}\cos\theta\right)^2}\int\frac{\left(1-\tilde{F}(q)\right)^2}{q^2}\,\delta(\omega-\mathbf{k}\,\mathbf{v}+\mathbf{q}\,\mathbf{v})\,d\mathbf{q}. \tag{8.75}$$

Then the expression for the differential cross-section of coherent SBs on graphene (in terms of one atom) looks like:

$$\frac{1}{N}\,\frac{d\sigma_{coh}^{(OB)}}{d\omega\, d\Omega_{\mathbf{k}}} = \frac{Z^2\, e^6\,(1+\cos^2\theta)\left(1-\left(\frac{\mathrm{v}}{c}\right)^2\right)}{\hbar\,\omega\, m^2\,\mathrm{v}\, c^3\left(1-\frac{\mathrm{v}}{c}\cos\theta\right)^2}\, n_s \sum_{\mathbf{g}} e^{-u^2\,(\mathbf{g}+\mathbf{q}_\perp)^2}\,|S(\mathbf{g})|^2$$
$$\times\int\delta(\omega-\mathbf{k}\,\mathbf{v}+\mathbf{g}\,\mathbf{v}+q_z\mathrm{v}_z)\;\frac{\left[1-\tilde{F}(|\mathbf{g}+\mathbf{q}_\perp|)\right]^2}{(\mathbf{g}+\mathbf{q}_\perp)^2}\,dq_z. \tag{8.76}$$

The calculation of the integral on the right side of this equation in view of the delta function gives

$$\frac{1}{N}\,\frac{d\sigma_{coh}^{(OB)}}{d\omega\, d\Omega_{\mathbf{k}}} = frac2\, n_s \cos\psi\,\frac{Z^2\, e^6\,(1+\cos^2\theta)\left(1-\left(\frac{\mathrm{v}}{c}\right)^2\right)}{\hbar\,\omega\, m^2\,\mathrm{v}^2\, c^3\left(1-\frac{\mathrm{v}}{c}\cos\theta\right)^2}$$
$$\times\sum_{\mathbf{g}} e^{-u^2\left(g^2+q_z^2\right)}\,|S(\mathbf{g})|^2\,\frac{\left[1-\tilde{F}\left(\sqrt{g^2+q_z^2}\right)\right]^2}{g^2+q_z^2}, \tag{8.77}$$

where

$$q_z = -g\, tg\psi + \omega\frac{1-(\mathrm{v}/c)\,\cos\theta}{\mathrm{v}\cos\psi},\ \cos\theta = \cos\alpha\cos\psi + \cos\varphi\sin\alpha\sin\psi,$$

$$g(n_1,\, n_2) = \frac{4\,\pi}{\sqrt{3}\,a}\,\sqrt{n_1^2+n_2^2+n_1\, n_2}.$$

In view of the last equation summation over the reciprocal lattice vectors **g** in the formula (8.77) comes to summation over the set of the integers $(n_1,\, n_2)$.

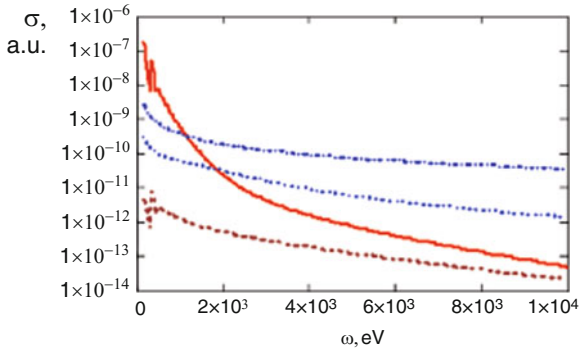

Fig. 8.19 The comparison of the cross-sections (in terms of one atom) of coherent and incoherent PBs and SBs of an electron on graphene for an electron energy of 30 keV ($v = 45$ a.u.), $\psi = 0$ and a radiation angle of 30°: *solid curve* – coherent PBs, *dotted curve* – coherent SBs, *dashed curve* – incoherent PBs, *dash-and-dot curve* – incoherent SBs

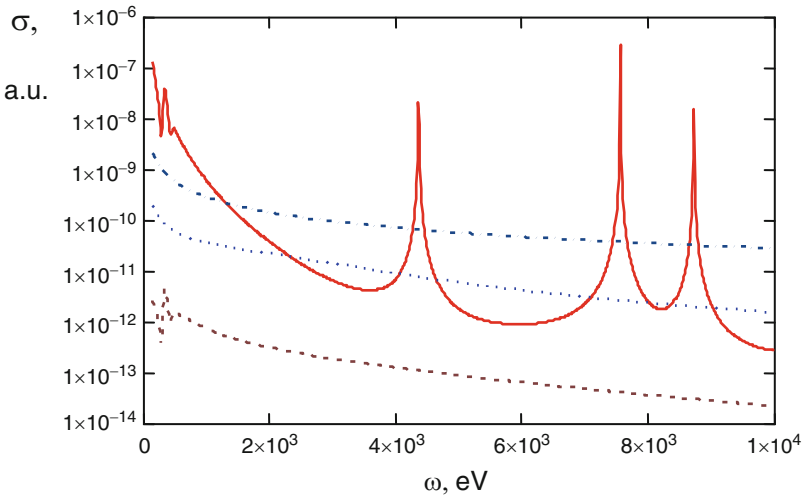

Fig. 8.20 The same as in Fig. 8.19 for an electron energy of 58 keV ($v = 60$ a.u.)

8.3.5 *Comparative Analysis of Contributions of Different Bremsstrahlung Channels in Electron Scattering on Graphene*

Let us calculate the contribution of different Bs channels in electron scattering on graphene with the use of expressions obtained in the previous section. The results of calculations are given in Figs. 8.19, 8.20, 8.21 and 8.22.

From Fig. 8.19 it follows that in case of a relatively low electron velocity of 45 a.u., which corresponds to the energy of 30 keV (at a specified radiation angle), spectral

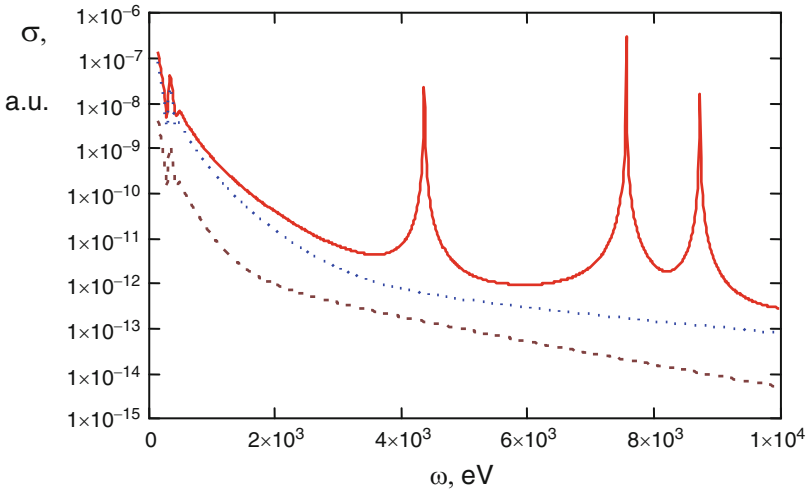

Fig. 8.21 The cross-section of coherent PBs of an electron on graphene for an electron energy of 58 keV (v = 60 a.u.), $\psi = 0$ and different radiation angles: *solid curve* – 30°, *dotted curve* – 60°, *dashed curve* – 120°

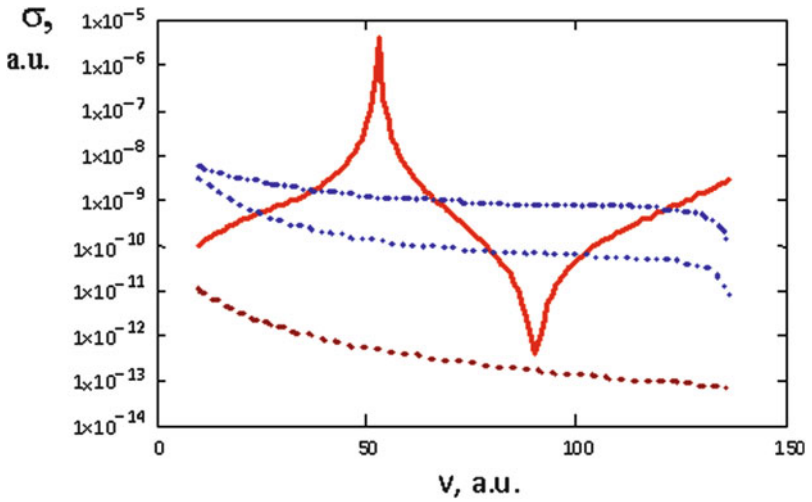

Fig. 8.22 The velocity dependences of coherent and incoherent PBs on graphene for the normal incidence of an electron, a photon energy of 272 eV, and a radiation angle of 30°: *solid curve* – coherent PBs, *dotted curve* – coherent SBs, *dashed curve* – incoherent PBs, *dash-and-dot curve* – incoherent SBs

resonances in the spectral range under consideration in the coherent PBs cross-section are absent. In this case coherent PBs prevails in the low-frequency region of the spectrum $\hbar\omega < 1 < 1$ keV, in the rest of the spectrum incoherent SBs prevails.

With growing electron velocity maxima appear in the coherent PBs cross-section at frequencies determined by the formulas (8.64) and (8.65) as seen from Fig. 8.20. Now near resonance frequencies a prevailing radiation channel is coherent PBs. With further increase of electron velocity the relative contribution of coherent PBs grows: it becomes comparable with incoherent SBs even far from resonances.

Given in Fig. 8.21 is the comparison of spectra of coherent PBs on graphene for a fixed electron velocity and different radiation angles.

It is seen that with growing radiation angle the maxima of the cross-section of coherent PBs in the spectral range under consideration disappear, and the value of the cross-section in a wide spectral range decreases.

The dependences of the cross-sections of different Bs channels on the electron velocity are presented in Fig. 8.22. From this figure it is seen that coherent PBs on graphene has sharp maximum and minimum. The velocity dependence of other Bs channels is monotonic. Deep minima in the cross-section of coherent PBs on graphene are caused by zeros of the function $P(\mathbf{g}, \mathbf{k}, q_z)$ (see the formula (8.58)) included in the expression for the cross-section (Eq. 8.57).

Thus the carried out analysis shows that the main contribution to bremsstrahlung of an electron on graphene is made by coherent polarization Bs and incoherent static Bs. It is found that the spectrum of coherent PBs of an electron on graphene for high enough velocities and small radiation angles contains sharp maxima corresponding to the vanishing denominator in the expression for the process cross-section. The spectral maxima in the cross-section of coherent PBs in a certain region of parametric variation take place in the angular and velocity dependences of the cross-section.

References

1. Lyalin, A.G., Solov'yov, A.V.: Polarization bremsstrahlung from atomic clusters. Rad. Phys. Chem. **75**, 1358 (2006)
2. Astapenko, V.A.: Bremsstrahlung of fast charged particles on clusters in a wide spectral range. JETP **101**, 3 (2005)
3. Astapenko, V.A., Buimistrov, V.M., Krotov, Y.A.: Bremsstrahlung accompanied by excitation and ionization of the scattering atoms. JETP **66**, 464 (1987)
4. Connerade, J.P., Solov'yov, A.V.: Giant resonances in photon emission spectra of metal clusters. J. Phys. B **29**, 3529 (1996)
5. Astapenko, V.A.: Polarization bremsstrahlung of heavy charged particles in polycrystal. JETP **99**, 958 (2004)
6. Shevelko, V.P., Tolstikhina, I.Y., Stolker, T.: Stripping of fast heavy low-charged ions in gaseous targets. NIM B **184**, 295 (2001)
7. Ishii, K., Morita, S.: Continuum x-ray produced by light-ion-atom collisions. Phys. Rev. A **30**, 2278 (1984)
8. Sonnichsen, C.: Plasmons in Metal Nanostructures. Cuvillier Verlag, Gottingen (2001)
9. Tsytovich, V.N., Oiringel, I.M. (eds.): Polarization Bremsstrahlung. Plenum, New York (1991)
10. Grishin, V.K.: Vestnik MGU **2**, 69 (2004) (in Russian)
11. Astapenko, V.A., Gostishev, N.A., Zhukova, P.N., Nasonov, N.N., et al.: Modification of the EDXD method for diagnostics of polycrystalline and fine-grained media. Bull. Russ. Acad Sci. Phys. **72**, 863 (2008)

12. Korol', A.V., Lyalin, A.G., Obolenskiy, O.I., Solov'ev, A.V.: The role of the polarization mechanism for emission of radiation by atoms over a broad photon frequency range. JETP **87**, 251 (1998)
13. Van de Hulst, H.C.: Light Scattering by Small Particle. Dover, New York (1981)
14. Ter-Mikaelian, M.: High Energy Electromagnetic Processes in Condensed Media. Wiley, New York (1972)
15. Shevelko, V.P., Tolstikhina, I.Y., Stolker, T.: Stripping of fast heavy low-charged ions in gaseous targets. Nucl. Instrum. Methods Phys. Res. B **184**, 295 (2001)
16. Berestetskii, V.B., Lifshitz, E.M., Pitaevskii, L.P.: Quantum Electrodynamics. Elsevier, Oxford (1982)

Chapter 9
Experimental Observation of Polarization Bremsstrahlung on Atoms, Clusters and Solids

9.1 Bremsstrahling on Atoms with Account for the Polarization Channel

9.1.1 Early Investigations

One of the first experiments for PBs on atoms was the work of the E.T. Verkhovtseva's group [1], studied in which was the contribution of the "atomic" component of Bs to the spectrum of bremsstrahlung of electrons with the energy 600 eV scattered by xenon gas in a photon energy range of 70–150 eV. In this spectral range a "giant resonance" takes place in the xenon photoabsorption $\sigma_{ph}(\omega)$, the said resonance being caused by the 4d-subshell of an atom, which according to the optical theorem

$$\mathrm{Im}\{\alpha(\omega)\} = \frac{c}{4\pi\omega}\,\sigma_{ph}(\omega) \tag{9.1}$$

is indicative of the high value of the imaginary part and, as a consequence, of the squared absolute value of the atomic polarizability $|\alpha(\omega)|^2$ that defines the contribution of the polarization channel to the total Bs. The last statement follows, for example, from the formula (3.24).

It should be noted that in early investigations of PBs several terms for designation of the polarization channel in bremsstrahlung were used in literature: polarization Bs, atomic Bs, dynamic Bs, parametric X-radiation, and transient Bs in plasma (see Chap. 1). For example, in the cited paper the polarization Bs channel was called the atomic channel.

Given in Fig. 9.1a from the paper [1] is the comparison of the intensity of polarization Bs on a xenon atom measured in a spectral range of 70–150 eV with PBs calculated by the formula analogous to Eq. 3.29. In Fig. 9.1b the dynamic polarizability of a xenon atom in a corresponding region of photon energies is presented. The squared absolute value of the dynamic polarizability included in

V. Astapenko, *Polarization Bremsstrahlung on Atoms, Plasmas, Nanostructures and Solids*, Springer Series on Atomic, Optical, and Plasma Physics 72,
DOI 10.1007/978-3-642-34082-6_9, © Springer-Verlag Berlin Heidelberg 2013

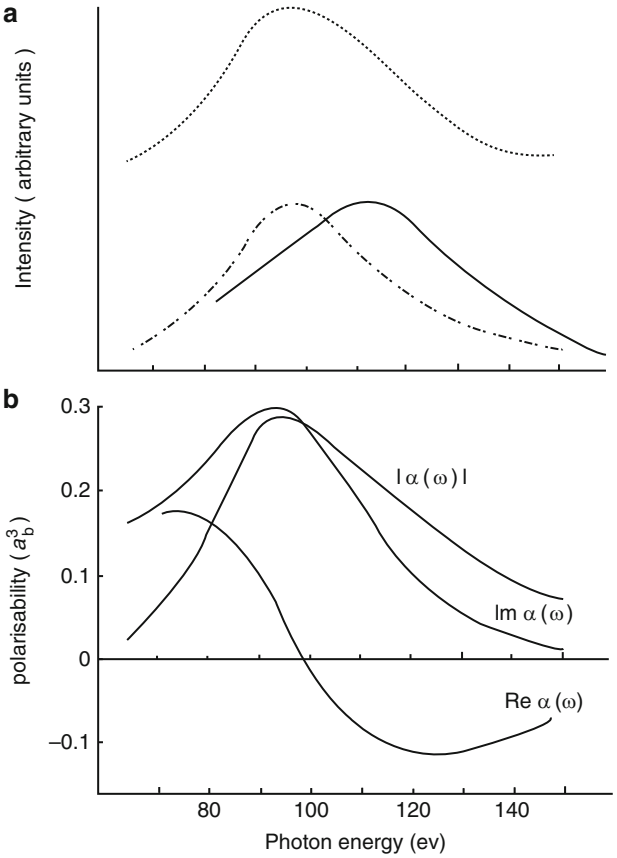

Fig. 9.1 (**a**) The comparison of the measured spectrum of atomic (polarization) Bs of an electron on a xenon atom (*solid curve*) with the calculated PBs spectrum (*dash-and-dot curve*), the photoabsorption spectrum is represented by a *dashed curve*; (**b**) the magnitude, the real and imaginary parts of the dynamic polarizability of a xenon atom calculated by the experimental value of the photoabsorption cross-section [1]

the expression for the PBs cross-section (Eq. 3.29) was calculated with the use of the optical theorem (Eq. 9.1) and the Kramers-Kronig relation for the real part of the polarizability

$$\mathrm{Re}\alpha(\omega) = \frac{1}{\pi}\,\mathrm{V.P.}\int_0^\infty \frac{\mathrm{Im}\alpha(\omega')}{\omega'^2 - \omega^2}\,d\omega'^2 \tag{9.2}$$

by the cross-section of photoabsorption $\sigma_{ph}(\omega)$ taken from the experimental work [2].

It should be noted that the electron energy was limited to the value 600 eV to avoid ionization of the 3d-subshell of xenon and resulting radiation at the transition

$4p^5 4d^9 \rightarrow 4p^6 4d^8$ in the spectral range under study. The concentration of particles in the interaction zone was $(5 \div 8) \times 10^{15}$ cm^{-3}, so the absorption of Bs on xenon atoms did not exceed 5 % in this frequency region.

To determine the atomic contribution to the process, from the spectrum of Bs of electrons on xenon the spectrum of Bs on argon was subtracted. This method is justified by the fact that PBs on argon in the spectral range under consideration is negligible.

From Fig. 9.1 the correlation of the measured PBs spectrum and the frequency dependence of the magnitude of the dynamic polarizability of a xenon atom in the spectral range under consideration is seen. In this case the maximum of the PBs spectrum fell on a photon energy of 113 eV, which considerably exceeds the energy of ionization of the 4d-subshell of xenon. The FWHM of the measured spectrum was 47 eV. The PBs intensity at the maximum of the frequency dependence was 70 % of the intensity of ordinary (electron) Bs according to the theoretical estimate made in the work [3].

PBs in the considered case is formed as a result of virtual excitation of xenon electrons to an ionization continuum above the threshold of ionization of the 4d-subshell. The authors of the work [1] connected the distinction between the obtained experimental data and the theoretical PBs spectrum (the dash-and-dot curve in Fig. 9.1) with a relatively low value of electron beam energy (600 eV) for validity of the PBs theory based on the Born approximation.

In the work [3] published a year before the paper [1], radiation of electrons with the energy of 500 eV scattered by metal lanthanum in a photon energy range of 100–140 eV was measured. In this frequency region the photoabsorption of metal lanthanum is close to atomic, which gave the authors of the cited paper reason to believe that the radiation spectrum is also of an atomic nature. A satisfactory agreement of the measured spectrum with the calculation based on the theory of PBs of fast electrons was found out.

The results of further experimental investigations of PBs of electrons on xenon atoms carried out by E.T. Verkhovtseva with co-authors are presented in the paper [4]. In this work the spectrum of radiation arising in electron scattering by xenon atoms in a photon energy range of 80–220 eV was measured. The energy of an electron beam varied within 300–900 eV.

In the cited work it was found that the position of the spectral maximum of radiation ω_{max} depends on the energy of scattered electrons and the radiation angle (between the electron velocity and the wave vector of a photon). This dependence is connected with the large width of the spectral maximum of radiation Γ that is in turn caused by a giant resonance in the spectrum of photoabsorption of a xenon atom in the spectral range under consideration (Fig. 9.2a).

In the Born-Bethe approximation, in the paper [4] the following expression for the shift of the PBs maximum with respect to the maximum of the frequency dependence of the squared absolute value of the dynamic polarizability of an atom ω_0 for a radiation angle of 90° was derived:

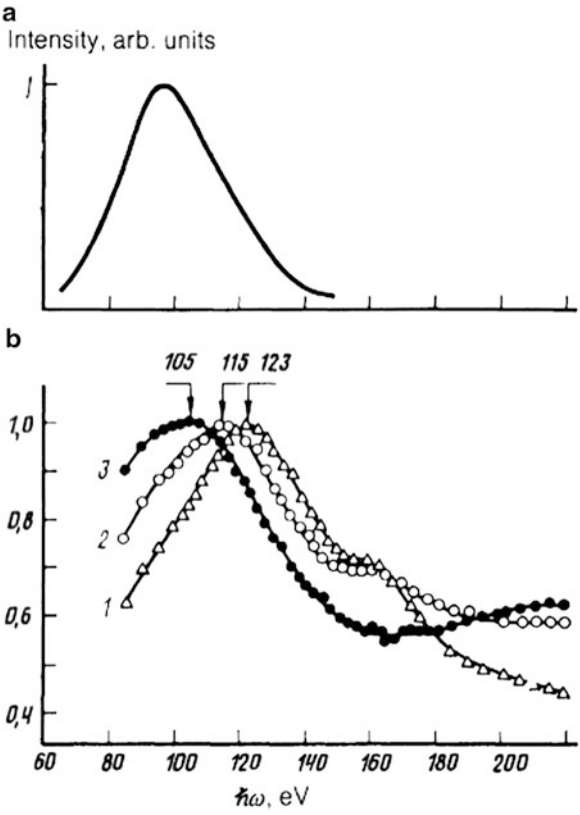

Fig. 9.2 (**a**) The spectrum of photoabsorption of a xenon atom; (**b**) Bs of electrons scattered by a xenon atom with different energies: *curve 1* – 300 eV, *curve 2* – 600 eV, *curve 3* – 900 eV. All spectra are normalized to their values at the maximum [4]

$$\omega_{\max} - \omega_0 \simeq \frac{2\,\Gamma^2}{\omega_0}\,\frac{1 + 5\,\varepsilon L/4}{1 + \left[1 - 5\,(\Gamma/\omega_0)^2/2\right]\varepsilon L}, \tag{9.3}$$

where $\varepsilon = m\hbar\,\omega/p^2$ (p is the initial electron momentum, $\hbar\,\omega$ is the energy of a bremsstrahlung photon), $L = \ln\left(\gamma\,\frac{\mathrm{v}^2}{\omega^2 R_a^2}\right)$ is the Coulomb logarithm (v is the initial electron velocity, R_a is the mean atomic radius, γ is the factor of the order of one). In the limit $\varepsilon \to 0$ the formula (9.3) for the frequency of the Bs spectrum maximum gives: $\omega_{\max} \to \omega_0 + 2\,\Gamma^2/\omega_0$. Thus even in the limit of high electron energies there is a shift of the Bs spectrum maximum with respect to the spectral maximum of the magnitude of the dynamic polarizability of an atom. From the obtained limiting relation it follows also that the spectral shift under consideration is noticeable if the ratio of the parameters Γ/ω_0 is great enough.

Since ordinary (electron) Bs is a smooth function of the photon frequency and the radiation angle, the shift of the spectral maximum is caused mainly by the polarization channel.

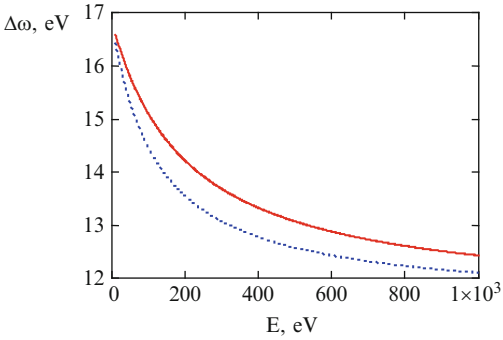

Fig. 9.3 The dependence of the shift of the spectral maximum of PBs in a photon energy range of 100–140 eV on the energy of an electron scattered by a xenon atom, for two values of the Coulomb logarithm: *solid curve* – L (the Coulomb logarithm) = 10, *dotted curve* – L = 6; the radiation angle 90°

From the Eq. 9.3 it follows that the shift of the spectral maximum of PBs for a radiation angle of 90° is always positive and decreases with growing electron energy. Both these facts are in conformity with the experimental data obtained in the work [4] (see Fig. 9.2b).

The plot of the function (Eq. 9.3) (depending on the electron energy) is presented in Fig. 9.3 for two values of the Coulomb logarithm and the following values of parameters: $\hbar\omega_0 = 100$ eV, $\hbar\Gamma = 24$ eV.

The comparison with experimental data shows that the theoretical shift of the frequency of the spectral maximum of PBs decreases with growing electron energy more slowly than it was observed in the work [4], which is apparently explained by insufficiency of the Born-Bethe approximation for quantitative description of Bs of electrons with a specified energy.

So experimentally demonstrated in the cited paper was the importance of taking into account the polarization channel in consideration of Bs on atom in the frequency range where the dynamic polarizability of an atom is high.

9.1.2 Measurements of the Absolute Value of the Cross-Section of Bs of Fast Electrons on Atoms

The measurements of the absolute double-differential Bs cross-section (depending on the frequency and the angle of photon emission) in scattering of electrons with an energy of 28 and 50 keV on atoms of noble gases were for the first time carried out in the work [5] in a wide spectral range from 5 keV to the kinematic limit, the radiation angle was 90°.

The results of experiments were compared with calculations of the cross-section of ordinary Bs and total Bs (in view of the polarization channel). Corresponding plots are presented in Figs. 9.4 and 9.5 [5].

The calculation of total Bs was carried out in the so-called “atom stripping” approximation (stripping approximation) [6]. The main idea of this approximation is that the PBs amplitude and the screening summand in the amplitude of ordinary

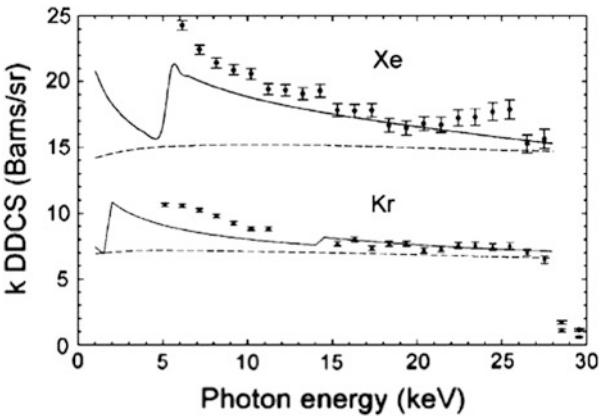

Fig. 9.4 The measured and calculated cross-sections of Bs of an electron with an energy of 28 keV scattered by krypton and xenon atoms [5]: *solid curves* – the calculated cross-section of total Bs in the stripping approximation; *dashed curves* – the calculated cross-section of ordinary Bs, *black circles* – the experiment [5]

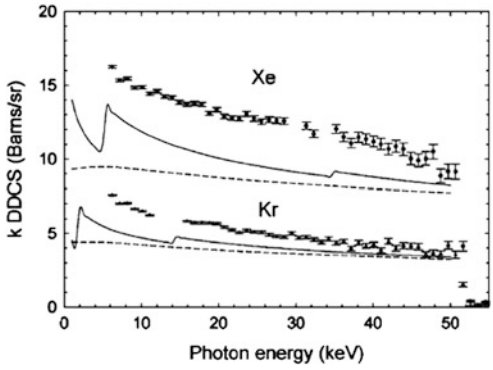

Fig. 9.5 The same as in Fig. 9.4 for an electron energy of 50 keV [5]

Bs on an atom cancel out [7], and the Bs process in the zeroth approximation proceeds as on a "bare" nucleus.

The cross-section of ordinary Bs was calculated in the relativistic approximation of partial waves, corresponding data are given in the work [8].

From the given figures it is seen that the measured cross-section exceeds considerably the calculated data, which to the greatest extent shows itself for a xenon atom, electron energy of 50 keV and in the low-frequency range. The exception is the case of a neon atom (Fig. 9.6) having a low value of dynamic polarizability, as a result, the measured contribution of PBs to the total cross-section of the process is negligible (practically is not visible in the range of an experimental error).

From the given plots it is seen that the experimental value of the total Bs cross-section, as a rule, exceeds its calculated value in the stripping approximation, which is most probably indicative of insufficiency of this approximation in the case under consideration.

As stated by the authors of the paper [5], the results of their work are strongly indicative of the essentiality of the polarization channel contribution to Bs of fast electrons on free atoms (with a considerable dynamic polarizability) in a wide spectral range.

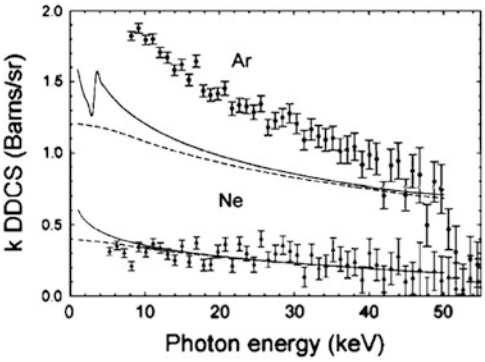

Fig. 9.6 The same as in Fig. 9.4 for Ar and Ne atoms and an electron energy of 50 keV [5]

9.1.3 PBs on Atomic Clusters

Theoretically the role of cooperative effects in Bs on atomic clusters in a wide spectral range was studied in the author's work [9] by the example of copper clusters (see the Sect. 8.1 of this monograph). In particular, it was shown that cooperative effects are of a considerable importance in PBs of relativistic electrons.

The experimental investigation of Bs of electrons with the energy of 700 eV on xenon atoms and clusters was carried out in the work [10], in which the influence of an ambient medium on the PBs spectrum was taken into account.

Under experimental conditions of [10] a cluster on the average consisted of 20 atoms, and the number of clusters in the volume of interaction was less than 2 % of the total number of particles. In case of changing experimental conditions the number of atoms in a cluster increased from several tens to 8,500.

The results of measurements and calculations of the cited paper are presented in Figs. 9.7 and 9.8.

Corresponding to Fig. 9.7 is a concentration of xenon atoms of 10^{15} atoms/cm^3. The average number of atoms in a cluster corresponding to Fig. 9.8 is 8,500.

From comparison of the plots of Figs. 9.7 and 9.8 it is seen that in case of clusters the maximum of the PBs spectrum is shifted by 10 eV towards lower photon energies and has a FWHM lesser than for PBs on individual atoms. In both cases the spectral maximum is of an asymmetric form.

The analysis of experimental data carried out in the paper [10] has shown that the reduction of the width of the spectral maximum of PBs with growing number of atoms in a cluster (N) at first is slow up to values $N \approx 200$–300. Then (for $N > 500$) the sharp reduction of the width of the maximum begins, and the width goes to saturation when the number of atoms in a cluster is several thousands. In this case the width of spectral maximum decreases approximately by 30 %.

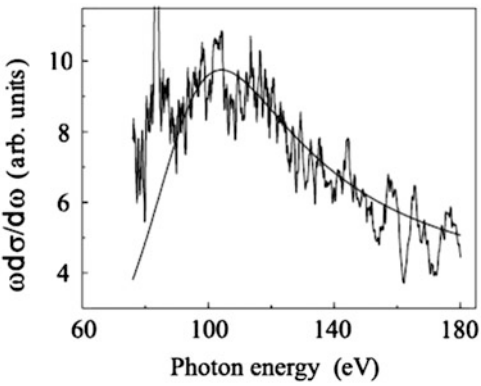

Fig. 9.7 The spectrum of PBs of an electron with the energy of 0.7 keV on a xenon atom: *"noisy" curve* – experiment, *smooth curve* – calculation in view of the dielectric permittivity of an ambient medium

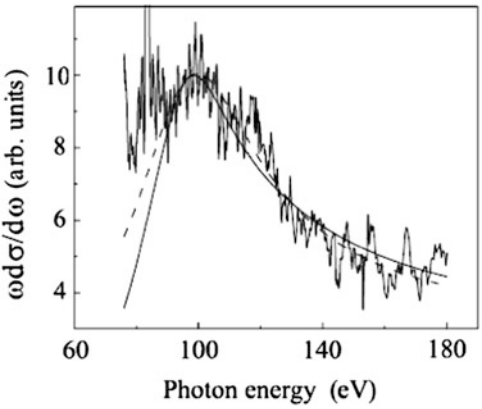

Fig. 9.8 The spectrum of PBs of an electron with the energy of 0.7 keV on a solid xenon cluster: *"noisy" curve* – experiment, *smooth solid curve* – calculation in view of the dielectric permittivity of an ambient medium, *dashed curve* – calculation in view of the frequency dependence of radiating dipole damping in a medium

The calculations of the cross-section of PBs on xenon atoms and clusters in the work [10] were carried out under the assumption that an atom/cluster is immersed in a gaseous or solid medium with a certain dielectric permittivity that influences the PBs spectrum. As a result, a good conformity between the experimental and calculated data was established.

So experimentally demonstrated in the paper [10] was the important role of PBs of electrons on xenon atoms and clusters in a spectral range corresponding to a giant resonance in photoabsorption, and cooperative effects were recorded that come to reduction of the PBs spectral maximum width with growing number of atoms in a cluster.

9.2 Bremsstrahlung on Solid-State Targets

9.2.1 PBs of Fast Electrons on Metal Foils

As was already noted in Chap. 1, one of the first works, in which PBs of fast (relativistic) electrons scattered by a metal foil was reliably recorded, was the paper

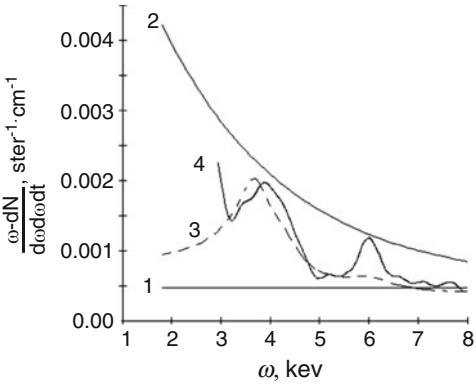

Fig. 9.9 The spectrum of electrons with an energy of 2.4 MeV scattered in polycrystalline aluminum: *straight line 1* – calculation of ordinary Bs, *curve 2* – calculation of PBs in amorphous aluminum, *curve 3* – calculation of PBs in polycrystalline aluminum, *curve 4* – results of the experiment of [11]

[11]. In this work the measurement of the spectrum of electrons with an energy of 2.4 MeV scattered in a polycrystalline aluminum target was carried out. The position of the spectral maximum of radiation falling on photon energy of 4 keV was exactly recorded (Fig. 9.9).

This maximum, as was predicted in the theoretical work [12], corresponds to the contribution of the polarization channel to total Bs. It corresponds to scattering of a virtual photon to a real photon by the crystallographic plane of target crystallites properly oriented, so that the Bragg condition (Eq. 5.19) is carried out for conversion of a virtual photon to a real photon (see Fig. 5.8). The Eq. 5.19 contains the target reciprocal lattice vector $\mathbf{g}$ that characterizes a crystallographic plane, by which scattering of a virtual photon occurs. It should be noted that the wave vector of a virtual photon forming the eigenfield of a relativistic electron is $|\mathbf{k}|\,\mathbf{v}/v$, where $\mathbf{v}$ is the electron velocity.

The maximum in the spectrum of PBs on a polycrystalline target is characteristic for relativistic electrons. Its central frequency is given by the formula (5.9). It should be noted that in case of nonrelativistic electrons the spectral maximum under consideration degenerates into a "frequency step" according to the formula (5.15).

The calculated curve 3 of Fig. 9.9 corresponds to taking into account three crystallographic planes (111), (220), (222). The spectral maximum at about 6 keV on the experimental curve 4 most probably corresponds to rescattered PBs from crystallographic planes with a high wave vector magnitude.

Further experimental investigation of the absolute cross-section of PBs of relativistic electrons with an energy of 7 MeV scattered by metal foils was carried out in the work [13], in which a source of an electron beam was a microtron. As targets, polycrystalline films of aluminum, copper and nickel were used. The film thicknesses were respectively 8.5 μm (aluminum), 15 μm (copper), 15 μm (nickel). The target was mounted at an angle of 45° to the beam axis, the radiation angle was 90°. Bs was recorded with the use of a Si-Li pin-detector. The angular acceptance of the detector was $1.5 \cdot 10^{-6}$ sterad. The intensity of the electron beam was measured by a Faraday cup placed at the end of the experimental system. The system was not

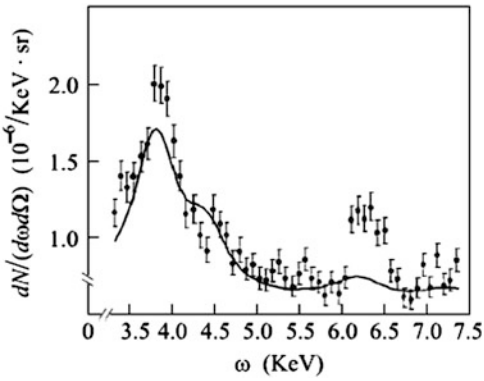

Fig. 9.10 The spectrum of electrons with an energy of 7 MeV scattered by an aluminum polycrystalline foil: *dots* – experiment, *solid curve* – calculation [13]

separated from the microtron as regards vacuum, inside it a pressure no more than 10^{-5} Torr was sustained.

The results of measurements (together with the value of the experimental error) and calculation of the spectrum of PBs of an electron with the energy of 7 MeV on a polycrystalline aluminum target are presented in Fig. 9.10. The experimental and theoretical data of this figure make it possible to separate three maxima in the PBs spectrum, the central energies of which are 3,782 ± 16, 4,560 ± 36, and 6,273 ± 19 eV. In the measured spectrum there is also an ambient background from the microtron that has two sources. The first of them is connected with incoherent PBs and ordinary Bs, its contribution is negligible. The second source is caused by secondary photons appearing as a result of reradiation at the inner walls of the target box and the photon channel. The contribution of this background is 2–4 % of the value of the main maximum in the PBs spectrum presented in Fig. 9.10. In the third spectral maximum there is the contribution of characteristic radiation of photons from the K-line of iron with an energy of 6,403 eV that were produced under the action of scattered electrons of the beam at the inner surface of the target chamber and the photon channel of the system.

Presented in Fig. 9.11 are the results of measurements and calculation of the spectrum of PBs of electrons with the energy of 7 MeV on a nickel target.

The experimental data of Fig. 9.11 are indicative of the presence of three maxima in the spectrum of PBs on a nickel foil, the centers of which have energies of 4,257 ± 15, 5,070 ± 16 and 5,735 ± 11 eV. There is also the contribution of the K-line of iron near a photon energy of 6,400 eV. The spectral maximum at the photon energy of 5,735 eV is of the known instrument origin. It results from ionization of the detector atoms by photons of the K-line of the nickel target since its central energy is exactly equal to the difference of energies of the K-line of nickel (7,475 eV) and silicon atoms (1,740 eV).

Thus in the cited paper the spectra of PBs of relativistic electrons on metal foils were measured and a satisfactory agreement with theoretical predictions for this phenomenon was obtained.

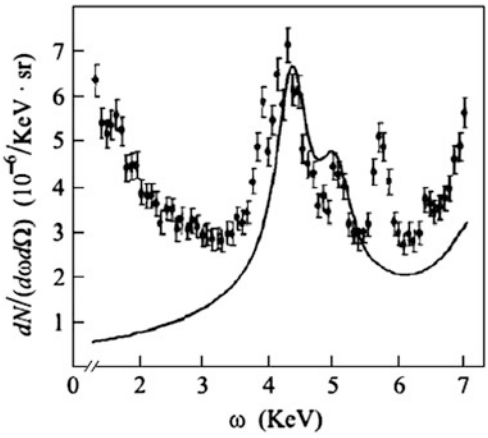

Fig. 9.11 The spectrum of electrons with an energy of 7 MeV scattered by a nickel foil: *dots* – experiment, *solid curve* – calculation [13]

Bs of nonrelativistic electrons with an energy of 53 keV scattered by gold foils of different thicknesses was studied experimentally and theoretically in the work [14] for four values of photon energy (15, 25, 35, 45 keV) and a radiation angle of 135°. The calculation was carried out with the use of the PENELOPE computer code [15] based on the Monte-Carlo method without considering the polarization channel. The PBs contribution was taken into account within the framework of the stripping approximation [6].

The results of measurements and the theoretical curves obtained in the cited paper are presented in Fig. 9.12 for two values of thickness of a gold foil.

It is seen that for a more thin foil the experimental data are satisfactorily described by the theory of Bs without considering the polarization channel. For a thicker target the experimental dots lie considerably higher than the predictions of the theory of ordinary Bs, however, they unsatisfactorily agree with the theoretical curve describing the PBs contribution within the framework of the stripping approximation.

It should be noted that from the theory of PBs on an atom it is known that the relative contribution of the polarization channel to total Bs decreases with growing energy of a bremsstrahlung photon (see Fig. 2.6). In the experiment of the work [14] the minimum photon energy, for which the measurements were carried out, is 10 keV. This value is represented by a too high quantity, at which the PBs intensity is already rather low. This circumstance is especially essential for nonrelativistic electrons used in the work since the lateral dimension of a virtual photon in this case is not large enough to excite in a coherent manner fluctuations of bound electrons in the target that are the source of PBs. Therefore for recording the contribution of the polarization channel it is preferable to study the low-frequency range of the spectrum of Bs of nonrelativistic electrons with photon energy not exceeding 10 keV.

The results of the paper [14] are also indicate that in the case under consideration a more exact theoretical approach to describe PBs should be used than the approach used in the stripping approximation.

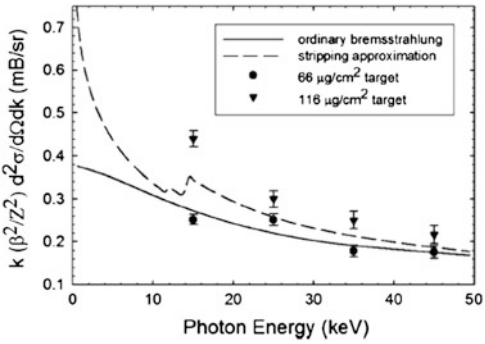

Fig. 9.12 The experimental and theoretical data on the spectrum of Bs of an electron with the energy of 53 keV scattered by gold films of different thicknesses [14]

9.2.2 PBs on Thick Metal Targets Under the Action of β-particles

In the work [16] bremsstrahlung arising in bombardment of metal targets under the action of β-particles from a ^{204}Tl radioactive source in a range of photon energies from 5 to 10 keV was investigated experimentally. To measure the spectral distribution of bremsstrahlung photons, the highly sensitive X-PIPS Si (Li) detector with an internal efficiency of 100 % and 97 % for photons with the energy of 5 and 10 keV respectively was used. The resolution of the detector was no less than 190 eV for photon energy of 5.9 keV. To decrease the influence of scattered photons and to restrict the background to a low level, a line of tin fragments and an aluminum foil was used for screening the detector. To obtain correct information on Bs from targets, a special method was used that made it possible to remove the influence of internal Bs and external background. Disks of aluminum (a mass thickness of 293 mg/cm^2), titanium (288 mg/cm^2), tin (281 mg/cm^2), and lead (286 mg/cm^2), each 4 cm in diameter, were used as targets.

It should be noted that in contrast to the above works, in which monoenergetic electron beams were used, in the case under consideration the ^{204}Tl source emits β-particles with energies continuously distributed in a range from 0 to 765 keV.

For comparison with the experiment, several Bs theory versions were used: the Bethe-Heitler theory without considering PBs with a modified Elvert factor for nonrelativistic particles (*EBH*), the Bethe-Heitler theory without considering PBs with a modified Elvert factor for relativistic particles ($F_{\text{mod}}\,BH$), and the Bethe-Heitler theory with a modified Elvert factor for relativistic particles with consideration for PBs ($F_{\text{mod}}\,BH + PB$). In the latter case PBs was calculated in the stripping approximation.

The experimental and theoretical results of the cited work for aluminum and lead targets are given in Figs. 9.13 and 9.14.

As seen from the given figures, the best agreement with experimental data is provided by the Bethe-Heitler theory with a modified Elvert factor for relativistic particles with consideration for the polarization channel (the curves 1 in Figs. 9.13 and 9.14).

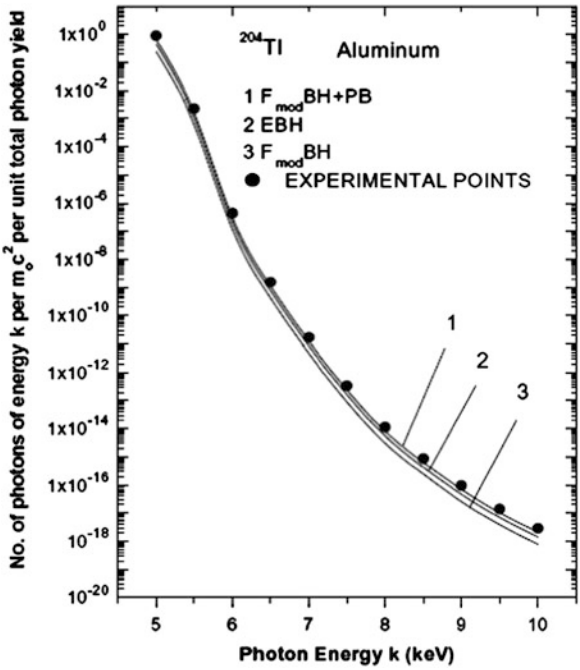

Fig. 9.13 The plots of the number of Bs photons normalized to the total photon yield as functions of the photon energy for aluminum target [16]

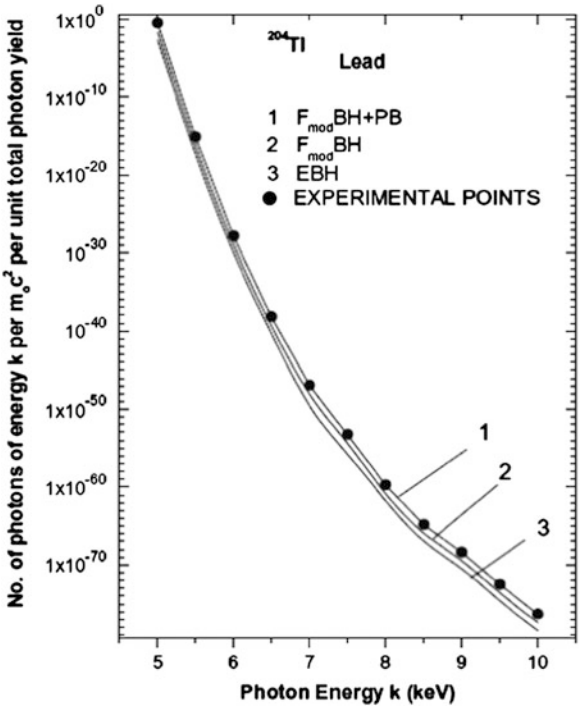

Fig. 9.14 The plots of the number of Bs photons normalized to the total photon yield as functions of the photon energy for lead target [16]

So the experiment carried out in the work [16] confirms the presence of the appreciable contribution of the polarization channel to total Bs in scattering of β-particles by thick metal targets. The relative value of the polarization contribution to Bs in the considered case is small and is on the average 10 % in a specified spectral range (5–10 keV), decreasing with growing photon energy, especially for targets of elements with a medium and high nuclear charge.

9.2.3 Proton Radiation on a Solid-State Target

In the work [17] the analysis of radiation arising in scattering of protons with energy of several MeV by aluminum target was given that confirmed the important role of PBs in the process under consideration. This analysis was based on the authors' experimental data on Bs of protons and light ions obtained in [18] and the formulas for PBs (called by the authors atomic Bs (AB)) and radiation ionization (RI) derived in the paper [17]. It should be noted that radiation ionization represents simultaneous emission of a photon and ionization of a target in collision with a charged particle. It is characteristic for processes with significant transfer of a momentum in collision.

In the cited work the contributions of different processes to total radiation were discussed. In case of light ions two mechanisms were usually taken into account: bremsstrahlung of secondary electrons (SEB) and Bs of quasi-free electrons (QFEB), the first of which has the boundary frequency $T_m = 2\,m_e\,\mathrm{v}_p^2$, and the second has the boundary frequency $T_r = T_m/4 = m_e\,\mathrm{v}_p^2/2$, where v_p is the velocity of an incident particle, m_e is the electron mass. Meant by QFEB is radiation of electrons of a target in their scattering in the field of an incident particle. In collision of heavy ions with a target the main role is played by molecular-orbital X-radiation and radiative capture (REC). Nuclear Bs can be neglected in case of fulfilment of the inequation $q\,a << m_T/m_e$ [17], where q is the wave vector transferred from an incident particle to the target, a is the mean atomic radius, m_T is the mass of the target nucleus. This inequation is satisfied in the X-ray range characteristic for physics of atomic collisions.

A new point in comparison with the previous works on radiation of ions on solid-state targets was the fact that the authors in interpretation of their experimental data took into account atomic (polarization) Bs. It was shown in particular that PBs of protons is essential not only in the spectral range near the potential of ionization of a target as was noted in the work [19], but also for high photon energies.

In the experiment [18] self-supporting aluminum foils with a mass thickness of 100 μg/cm^2 were used as a target. The thickness of the targets was measured with the use of the Rutherford scattering of protons with the energy of 1 MeV. A beam of incident ions was formed by the Van de Graaff accelerator with a voltage of 5 MV.

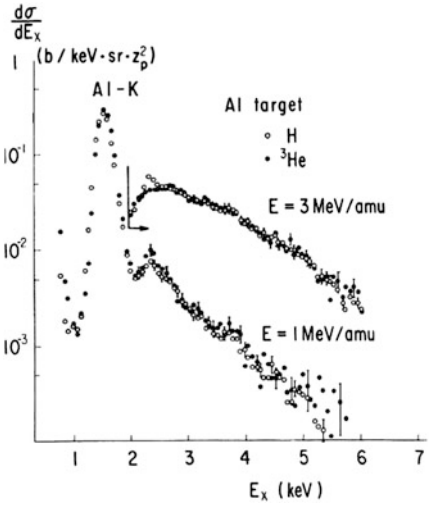

Fig. 9.15 The spectra of X-radiation in bombardment of aluminum target by protons and ^{3}He ions for two energies of incident particles, the detection angle is 90° [18]

The recording of the X-ray spectrum was carried out with the use of a Si-Li detector with a resolution of 205 eV at the photon energy of 6 keV and effective area of 12.5 mm^2.

The typical spectra of X-radiation obtained in the work [18] with bombardment of an aluminum target by protons and ^{3}He ions with an energy of 1 and 3 MeV per atomic mass unit (1, 3 MeV/amu) are presented in Fig. 9.15. The measurements were carried out for an angle of 90° between the velocity of incident ions and the direction to the photodetector (a detection angle). The angle of incidence of incident particles on the target surface was 45°.

In plotting in Fig. 9.15 the background spectrum was subtracted, but correction taking into account the absorption of X-radiation and the efficiency of the detector was not made. The ordinate was normalized to the squared charge number of an incident particle Z_p^2, so from Fig. 9.15 it follows that the measured continuous X-ray spectrum has a scaling with respect to the value Z_p^2. Seen in the figure are a maximum caused by characteristic K-radiation of an aluminum atom and a weak peak (at 2.307 keV) connected with the Kα-line of sulfur impurity atoms.

As was already noted, the analysis of the X-ray spectra obtained in the paper [18] was given in the work [17] with the use of the concept of polarization Bs that in the cited work was called atomic. The results of this analysis are given in Figs. 9.16 and 9.17 for two values of energy of protons incident on an aluminum target of 1 and 4 MeV and a detection angle of 90°.

The theoretical curves for PBs and radiating ionization were calculated by the formulas derived in the paper [17], Bs of free electrons was calculated with the use of the expression obtained in the work [20].

Arrowed in Figs. 9.16 and 9.17 are the boundary frequency for Bs of secondary electrons T_m and the boundary frequency for Bs of quasi-free electrons $T_r = T_m/4$.

From the given figures it is seen that in the high-frequency region of the measured spectrum the main channel of radiation is PBs. In case of 1 MeV protons

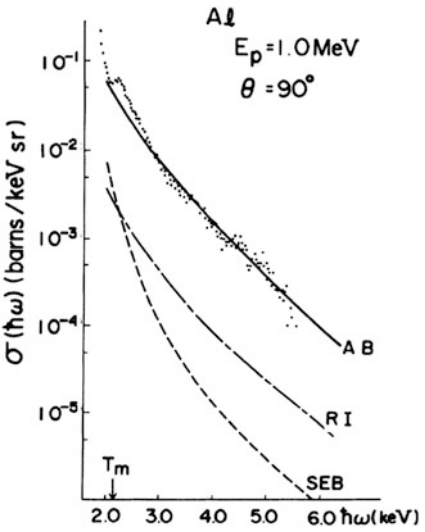

Fig. 9.16 The comparison of the theory with the experiment for Bs of protons with an energy of 1 MeV bombarding an aluminum target: *solid curve* – PBs (calculation [17]), *dash-and-dot curve* – radiating ionization (calculation [17]), *dashed curve* – radiation of secondary electrons (calculation [20]), *dots* – experiment [18]

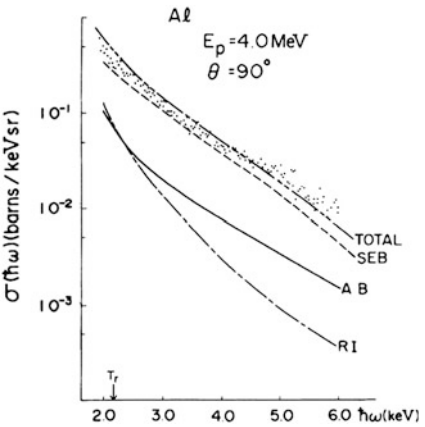

Fig. 9.17 The same as in Fig. 9.16 for a proton energy of 4 MeV, the *top curve* corresponds to the cross-section of total radiation [17]

this statement is true for $\hbar\omega > T_m$. For 4 MeV protons PBs prevails over other channels of radiation in the range $\hbar\omega > T_r = T_m/4$. In the frequency region $\hbar\omega < T_r$ in this case the cross-section of radiation ionization exceeds the PBs cross-section according to the calculations of the paper [17].

So the analysis of Bs of protons with an energy of 1 and 4 MeV scattered by the aluminum target that was carried out in the paper [17] has shown that among possible mechanisms of radiation PBs prevails in the high-frequency region of the spectrum $\hbar\omega > T_m$. In the range $T_m > \hbar\omega > T_r$ the main contribution is made by Bs of secondary electrons and, finally, in the frequency region $T_r > \hbar\omega$ radiation ionization prevails.

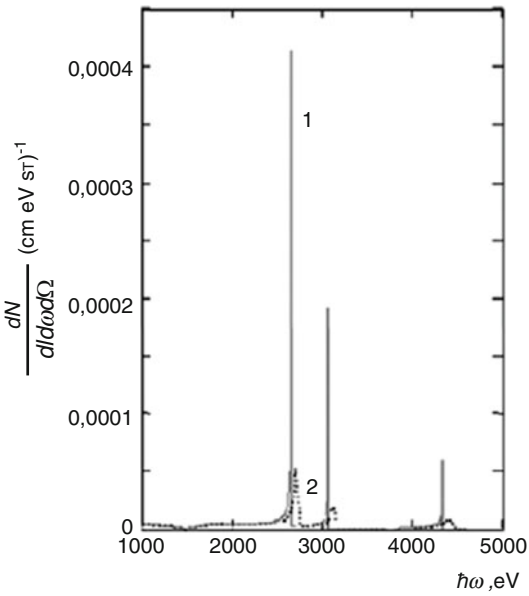

Fig. 9.18 An abnormal peak in the spectrum of PBs of an electron with an energy of 15 MeV in an aluminum polycrystal: *solid curve* (1) – the radiation angle $\theta = 180°$, *dotted curve* (2) – the radiation angle $\theta = 160°$ (From the paper [21])

9.2.4 *Experimental Observation of Coherent Spectral Peaks of PBs of Relativistic Electrons in a Polycrystal in Backward Radiation*

Theoretically predicted in the work [21] was a sharp increase of the intensity of PBs of a relativistic electron scattered in a polycrystal, when the angle θ between the wave vector of a bremsstrahlung photon and the electron velocity is 180° (backward radiation). The results of calculations of the PBs spectra carried out in the cited work are presented in Fig. 9.18 for an electron with the energy of 15 MeV scattered in an aluminum polycrystal for two radiation angles.

Three spectral maxima on the curves of Fig. 9.18 correspond to coherent PBs with transfer of the wave vector excess to different reciprocal lattice wave vectors (see the formula (5.15)).

In the work [21] the following expression was derived that describes the intensity of PBs of a relativistic electron in a polycrystal in the region of the spectral maximum as a function of the radiation angle and the electron velocity:

$$\Phi_{\max}(\theta,\, \gamma_*) \approx \frac{2\,\gamma_*\, \sin(\theta/2)}{\sqrt{\cos^2(\theta/2) - \cos\theta/\left(4\,\gamma_*^2\right)}}, \tag{9.4}$$

where γ_* is the Lorenz factor in a medium that takes into account the change of the phase velocity of radiation in a substance. From the formula (9.4) it follows that the value of a spectral peak for radiation angles far from 180° is proportional to the

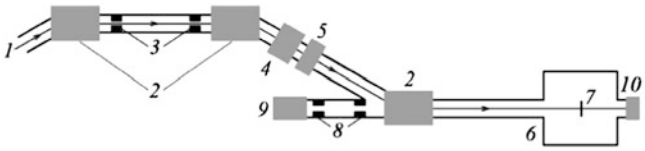

Fig. 9.19 The diagram of the modified "Roentgen" experimental system: *1* – vacuum channel for an electron beam; *2* – rotary magnets; *3, 8* – collimators; *4* – quadrupole lenses; *5* – beam corrector; *6* – vacuum chamber; *7* – target; *9* – X-ray detector; *10* – beam proportional chamber [22]

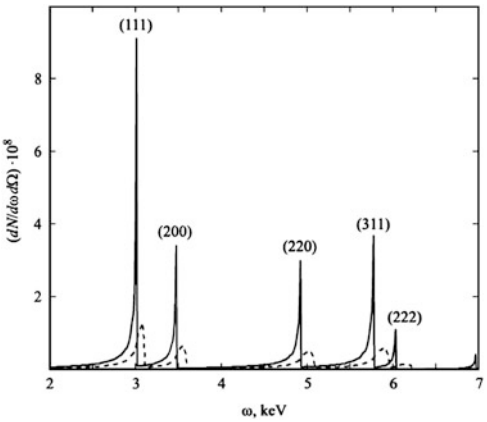

Fig. 9.20 The calculated spectrum of coherent PBs of a relativistic electron scattered by a copper polycrystal for two radiation angles: *solid curve* – $\theta = 180°$, *dashed curve* – $\theta = 160°$ (From the paper [22])

relativistic factor γ_*; and if $\theta = 180°$, then $\Phi_{max} \sim \gamma_*^2$, which in the limit $\gamma_* >> 1$ means a sharp increase of the PBs intensity.

In the paper [22] the experimental confirmation of the theoretical conclusions of the work [21] was obtained. The measurements of the spectra of PBs of electrons with an energy of 7 MeV scattered in a polycrystalline copper target were carried out for backward radiation. The basic diagram of the experimental system is given in Fig. 9.19.

Backward PBs was recorded by the PIN detector 9, the energy resolution of which was 152 eV. Serving as the target 7 was a foil of electrical copper with a thickness of 25 μm.

The results of calculation of the spectrum of coherent PBs of a relativistic electron in a copper polycrystal for the above problem parameters are presented in Fig. 9.20.

From the given figure it is seen that with the radiation angle approaching 180° the intensity of coherent PBs at the maximum of the frequency dependences sharply increases, and the width of a spectral peak decreases. Three numbers in the parentheses above spectral peaks number a crystallographic plane, by which a virtual photon of the electron eigenfield is scattered to a real Bs photon (see Fig. 5.8).

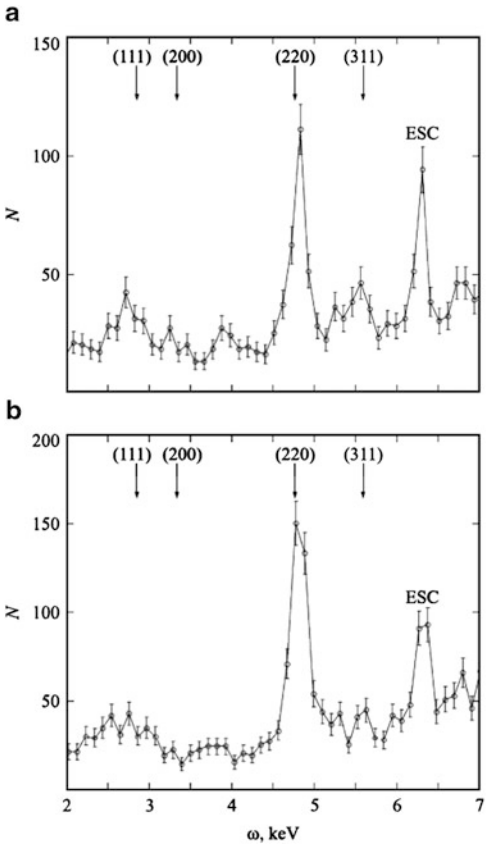

Fig. 9.21 The experimental spectra of PBs of a relativistic electron scattered by a copper foil in backward radiation: (**a**) normal orientation of the sample plane with respect to an electron beam, (**b**) random orientation of the target plane with respect to an electron beam, (**c**) another random orientation of the target (From the work [22])

It should be noted that the spectrum of coherent PBs presented in Fig. 9.20 corresponds to averaging over orientations of crystallites forming the polycrystal under the assumption of their isotropic distribution. This fact is expressed by the formula (5.14), in which the integral with respect to the normalized solid angle of the reciprocal lattice vector $d\Omega_{\mathbf{g}}/4\pi$ describes this averaging. In case of a texture crystal, when the isotropism of the distribution of the reciprocal lattice vectors $\mathbf{g}$ is violated, the polycrystal becomes partially oriented, it is necessary to introduce into the integral on the right side of the Eq. 5.14 the distribution function $f(\mathbf{g})$ reflecting a concrete texture of a polycrystal. A texture can appear in a polycrystalline sample such as a thin foil in the process of its manufacturing or by other reasons.

To investigate the microstructure of a target, in the work [22] the measurements of the spectra of coherent PBs were carried out for different orientations of a sample of a copper foil with respect to an electron beam. The results of these experiments are presented in Fig. 9.21a–c).

The comparison of the PBs spectra (Fig. 9.21) measured for a real target with the calculated spectrum (Fig. 9.20) obtained for a polycrystalline target (without texture) shows a change of the PBs photon yield (reflection) caused by different

crystallographic planes. For example, in Fig. 9.21a the (111) reflection yield is strongly suppressed in comparison with the theoretical data for an isotropic polycrystal and the (200) reflection yield is practically absent. At the same time from Fig. 9.21b it follows that at a specified orientation of a target with respect to an electron beam an increase of the (220) reflection yield is observed with other reflections suppressed. The PBs spectrum shown in Fig. 9.21c, corresponding to another abnormal orientation of a target, has another form differing from the spectra of Fig. 9.21a, b.

The comparison of reflection yields was made on the basis of comparison of the values of spectral maxima of PBs with the "instrument" spectral maximum at photon energy of 6.3 keV that in Fig. 9.21 is designated by the symbol ESC. The position of this spectral maximum is defined by the difference of the energy of a photon of the K-line of characteristic copper radiation and the energy of the silicon photoabsorption edge in the X-ray detector. It is seen that the spectral width of the "instrument" peak is comparable with the widths of peaks of coherent PBs of a relativistic electron with a specified energy (7 MeV) in backward radiation. Based on this fact, the authors of the paper [22] made an assumption that the real spectral width of PBs peaks in backward radiation is close to the spectral width of characteristic radiation of the copper K-line, which requires additional measurements of peaks under study by a detector with higher energy resolution.

It should be noted that according to the theoretical analysis carried out in the work [21], the spectral width for coherent PBs in backward radiation decreases in inverse proportion to the squared energy of an incident electron (with neglected saturation effect that is caused by changing phase velocity of radiation in a medium). For radiation angles less than 180° narrowing of the line of coherent PBs in a polycrystal is inversely proportional to the electron energy in the first degree.

Thus it can be concluded that narrow spectral maxima of coherent PBs recorded in the cited work were found to be rather sensitive to the structure of a polycrystalline target, which is of interest for development of a new energy dispersion method for substance structure diagnostics with the use of recording PBs spectra [23].

References

1. Verkhovtseva, E.T., Gnatchenko, E.V., Pogrebnjak, P.S.: Investigation of the connection between giant resonances and atomic bremsstrahlung. J. Phys. B At. Mol. Phys. **16**, L613 (1983)
2. Haensel, R., Keitel, G., Schreiber, P., Kunz, C.: Optical absorption of solid krypton and xenon in the far ultraviolet. Phys. Rev. **188**, 1375 (1969)
3. Amusia, M.Y., Zimkina, T.M., Kuchiev, M.Y.: Wide emission bands in radiation of atoms under influence of rapid electrons. Zh. Tekh. Fiz. **52**, 1424 (1982) (in Russian)
4. Verkhovtseva, E.T., Gnatchenko, E.V., Zon, B.A., Nekipelov, A.A., Tkachenko, A.A.: Bremsstrahlung in electron scattering by xenon. Zh. Eksp. Teor. Fiz. **98**, 797 (1990)
5. Portillo, S., Quarles, C.A.: Absolute doubly differential cross sections for electron bremsstrahlung from rare gas atoms at 28 and 50 keV. Phys. Rev. Lett. **91**, 173201 (2003)

6. Korol, A.V., Lyalin, A.G., Solovy'ov, A.V., Avdonina, N.B., Pratt, R.H.: On the stripping approximation in the bremsstrahlung process. J. Phys. B **35**, 1197 (2002)
7. Buimistrov, V.M., Trakhtenberg, L.I.: The role of atomic electrons in bremsstrahlung. Sov. Phys. JETP **46**, 447 (1977)
8. Kissel, L., Quarles, C.A., Pratt, R.H.: Shape functions for atomic-field bremsstrahlung from electrons of kinetic energy 1–500 keV on selected neutral atoms $1 \leq Z \leq 92$. At. Data Nucl. Data Tables **28**, 381 (1983)
9. Astapenko, V.A.: Bremsstrahlung of fast charged particles on clusters in a wide spectral range. JETP **101**, 3 (2005)
10. Gnatchenko, E.V., Nechay, A.N., Samovarov, V.N., Tkachenko, A.A.: Polarization bremsstrahlung from xenon atoms and clusters: a cooperative effect contribution. Phys. Rev. A **82**, 012702 (2010)
11. Blashevich, S., Chepurnov, A., Grishin, V., et al.: Polarization bremsstrahlung of relativistic electrons in aluminium. Phys. Lett. A **254**, 230 (1999)
12. Nasonov, N.N.: Collective effects in the polarization bremsstrahlung of relativistic electrons in condensed media. NIM B **145**, 19 (1998)
13. Astapenko, V.A., Kubankin, A.S., Nasonov, N.N., et al.: Measurement of the polarization bremsstrahlung of relativistic electrons in polycrystalline targets. JETP Lett. **84**, 281 (2006)
14. Williams, S., Quarles, C.A.: 1Absolute bremsstrahlung yields at 135° from 53-keV electrons on gold film targets. Phys. Rev. A **78**, 062704 (2008)
15. Salvat, F., Fernandez-Varea, J.M., Sempau, J., Llovet, X.: Monte Carlo simulation of bremsstrahlung emission by electrons. Radiat. Phys. Chem. **75**, 1201 (2006)
16. Singh, T., Kahlon, K.S., Dhaliwal, A.S.: Total bremsstrahlung spectral photon distributions in metallic targets in the photon energy range of 5–10 keV by 204Tl beta particles. NIM B **267**, 737 (2009)
17. Ishii, K., Morita, S.: Continuum x rays produced by light-ion-atom collisions. Phys. Rev. A **30**, 2278 (1984)
18. Ishii, K., Morita, S., Tawara, H.: Bremsstrahlung induced by proton and 3He-ion bombardments in the 1-4-MeV/amu energy range. Phys. Rev. A **13**, 131 (1976)
19. Amusia, M.Y.: "Atomic" bremsstrahlung spectrum. Comments At. Mol. Phys. **11**, 123 (1982)
20. Yamadera, A., Ishii, K., Sera, K., et al.: Quasifree-electron bremsstrahlung induced by the projectile field. Phys. Rev. A **23**, 24 (1981)
21. Astapenko, V., Nasonov, N., Zhukova, P.: Anomalous peak in the spectrum of polarizational bremsstrahlung from relativistic electrons moving through a solid target. J. Phys. B **40**, 1337 (2007)
22. Alekseev, V.I., Vokhmyanina, K.A., Eliseev, A.N., et al.: Measuring coherent peaks of polarization bremsstrahlung from relativistic electrons in polycrystalline targets in backscattering geometry. Tech. Phys. Lett. **38**, 294 (2012)
23. Astapenko, V.A., Gostishchev, N.A., Zhukova, P.N., et al.: Modification of the EDXD method for diagnostics of polycrystalline and fine-grained media. Bull. Russ. Acad. Sci. Phys. **76**, 863 (2008)

Chapter 10
Induced Bremsstrahlung Effect in an Electromagnetic Field with Account for Interference Phenomena

Considered in this chapter are spectral, angular, polarization, and amplitude peculiarities of the near-resonance bremsstrahlung effect on ions with a core in strongly inelastic electron scattering that arise due to the presence of the polarization channel of the process and its interference with the static channel. This phenomenon plays an important role in processes of energy exchange between plasma and a near-resonance laser field as well as in experiments on triple interaction on electron and atomic beams and storage rings.

The near-resonance case under consideration corresponds to high enough radiation frequency detunings from resonance in the ion core, so it is possible to neglect real excitation of the core, and yet to low enough detunings to be limited to the contribution of only one virtual transition of the subsystem of bound electrons to the process amplitude.

In contrast to the majority of previous works on resonance PBs, considered here is a bremsstrahlung effect on ions (including multiply charged ions) at relatively low velocities of a scattered particle, when the Born approximation is inapplicable, and the IP motion is more likely of a quasi-classical nature.

10.1 Near-Resonance Bremsstrahlung Effect (Including a Multiphoton Effect) in the Dipole Approximation for Interaction of a Quasi-Classical Incident Electron and the Ion Core

In this paragraph the calculation of the cross-section of multiphoton induced bremsstrahlung (IBs) in the dipole approximation for interaction of an incident electron with the ion core is carried out. The incident electron motion is supposed to be quasi-classical. The said limitations are adequate to laser field frequencies, near-resonance virtual transitions in the ion core with no change of the principal quantum number, and high enough charges of a target ion.

V. Astapenko, *Polarization Bremsstrahlung on Atoms, Plasmas, Nanostructures and Solids*, Springer Series on Atomic, Optical, and Plasma Physics 72,
DOI 10.1007/978-3-642-34082-6_10, © Springer-Verlag Berlin Heidelberg 2013

10.1.1 Prescribed Current Method in the Problem of Bremsstrahlung of a Quasi-Classical Electron on a Multiply Charged Ion (MCI)

The consistent quantum-electrodynamic solution of the set problem assuming summation of an infinite diagram series is connected with great mathematical difficulties. The approach developed below corresponds to approximate summation of such a series in a case of interest for us for collisions of a charged particle with a MCI. This approach is based on a possibility of description of radiative processes in electron scattering in the MCI field within the framework of the approximation of prescribed (not necessarily classical!) current. This model has a wide domain of applicability for a case of IBs in collision of charged particles with a MCI. A key condition of applicability of this approach is that in a region of space responsible for photon radiation in a laser mode the IP motion is only weakly disturbed both by the laser field (in comparison with disturbance of motion by the MCI field) and by an act itself of photon emission/absorption (of a real photon in static Bs or an equivalent photon in polarization Bs).

The smallness of the value of the laser field in comparison with the field of an ion in the region of space responsible for radiation imposes the following limitation on the amplitude of the intensity of an electric component in the laser beam (Ze is the ion charge):

$$E_0 < \frac{Ze}{r_\omega^2},$$

where the parameter r_ω is estimated as a characteristic distance, at which emission of a photon with the frequency ω in the MCI field occurs:

1. $r_\omega \approx \left[Z(Ry/\hbar\omega)^2\right]^{1/3} a_B$
   (here Ry is the Rydberg energy, a_B is the Bohr radius) for the case of high-frequency spectrum asymptotics in the quasi-classical case [1] ($\eta = Z e^2/\hbar \mathrm{v} > 1$ is the Born parameter, $\omega >> \omega_{Coul}$, $\omega_{Coul} \equiv m\mathrm{v}^3/Ze^2$ is the characteristic Coulomb frequency), and
2. $r_\omega \approx \mathrm{v}/\omega$
   for the Born case ($\eta << 1$) and low-frequency asymptotics in case of quasi-classical IP motion ($\eta > 1$, $\omega << \omega_{Coul}$).

We will give the results of the works [2] and [3] concerning opposite limiting cases of the IP motion nature.

The formula for the probability $W(n)$ of a n-photon static process in the Born case $\eta << 1$ that was for the first time obtained in [2] looks like:

$$W(n) = J_n^2(\mathbf{aq}), \tag{10.1}$$

where J_n is the n^{th}-order Bessel function, $\mathbf{a} = e\mathbf{E}_0/m\omega^2$ is the amplitude of electron oscillation in the laser field of frequency ω and amplitude $\mathbf{E}_0$, $\hbar\mathbf{q}$ is the change of an IP momentum in inelastic scattering by a MCI.

In case of quasi-classical motion ($\eta>>1$), in [3] the result is obtained that is similar in structure:

$$W(n) = J_n^2(|m\,\omega\ \mathbf{a}\mathbf{v}_\omega/\hbar|), \tag{10.2}$$

where $\mathbf{v}_\omega$ is the Fourier component of IP velocity on the classical trajectory in the field of an ion.

The relation between the formalism of the quasi-classical description of Bs and the prescribed current method was traced in [3] at a qualitative level for a radiative transition of an IP in its motion in the static central field. The rigorous quantum-mechanical substantiation of the prescribed classical current method for calculation of multiphoton IP transitions in the static central field in the presence of laser radiation was for the first time carried out by A.B.. Kukushkin within the framework of the method of two-dimensional quasi-classics [1] by the passage to the limit $\hbar \to 0$ in the quantum formalism of multiphoton transitions in the joint (with the author) work [4].

In the limit of *fast* collision ($\omega\tau_{\text{col}}<<1$) corresponding to weak inelasticity of the process, both results are represented, as was noted in [3], by a single formula of the form (10.1), in which now the vector $\hbar\mathbf{q}$ is the change of an IP momentum in scattering by a MCI both at $\eta<<1$ and at $\eta>>1$.

It turns out that the formula (10.1) can be extended to the region of strong inelasticity in terms of nonsmallness of the ratio of the total energy of emitted photons to the value E_i of the initial IP energy. In this case an actual limitation of its applicability is a weak disturbance of IP motion by an act of radiation in the region of space responsible for photon emission. As a matter of fact, such a generalization of the formula (10.1) covers, in addition to the said domain of its applicability, the region of strong inelasticity in case of quasi-classical motion of an IP, specifically of an electron. In the latter case, as shown by the generalization of the formalism of Kramers electrodynamics [1] to multiphoton processes [4], an actual condition of weak disturbance of electron motion is, according to the main conclusions of Kramers electrodynamics, weak *local* kinematic inelasticity

$$\mu \equiv n\hbar\omega/\mathrm{E}_{kin}(\mathbf{r}_\omega),$$

where r_ω is the characteristic radius of electron rotation around an ion near the point of the most approach, $\mathrm{E}_{kin}(\mathbf{r}_\omega)$ is the local kinetic IP energy. In case of quasi-classical electron motion that is characteristic just for collisions of electrons with multiply charged ions of practical interest, the condition of smallness of μ is found to be satisfiable in a wide range of frequencies. Really, $\mu \approx n\{\hbar\omega/Ry\}^{1/3}Z^{-2/3}$, so for characteristic frequencies of the Coulomb Bs spectrum ($\omega \approx m\mathrm{v}^3/Ze^2$) we have: $\mu \approx n/\xi$, and for the short-wavelength Bs limit we obtain $\mu \approx (n/\xi)^{2/3}$ ($\xi = \omega/\omega_{Coul}$).

The generalization of Eq. 10.1 to the case of strong inelasticity and arbitrary quanticity of IP motion can be justified from consideration of a matrix element of a multiphoton transition between true wave functions for IP motion in the static central field of an ion. Such a generalization is based on joining of descriptions in different regions of space $\{\hbar \mathrm{v}/Z e^2, n\hbar\omega/E_i\}$. The first step here is demonstration of truth of the description (Eq. 10.1) in the low-frequency limit ($\hbar\omega << E_i$, $\hbar\omega << E_f$) for an arbitrary η.

For a particular case of radiation of two photons in the Coulomb field this was done in [5] by difficult calculations developing the approach [6] (it should be noted that the formula for low frequencies and an arbitrary short-range potential given in [7]). The second step consists in extension of the low-frequency description to the case of arbitrary inelasticity within the framework of classical IP motion in the region $\eta >> 1$. This is achieved by the above substantiation of the prescribed classical current method (see Appendix 1 of [4]).

As a result of rigorous substantiations in the said regions of parameters and interpolation in the intermediate region, we obtain finally – throughout the region of truth of the prescribed current approximation – the following universal representation for the probability of multiphoton Bs in the static field of a target ion:

$$W_{stat}(n) = J_n^2\left[\left(4n_{\mathbf{k}\lambda}^{las} n_{\mathbf{k}\lambda}^{stat}\right)^{1/2}\right]. \tag{10.3}$$

Here $n_{k\lambda}^{las}$ is the occupation number for photons in a laser mode ($n_{k\lambda}^{las} >> 1$), $n_{\mathbf{k}\lambda}^{stat}$ is the occupation number for photons spontaneously emitted by an IP in the static field of an ion in the laser mode $\{\mathbf{k},\ \lambda\}$ with the wave vector $\mathbf{k}$ and polarization λ in the mode of ordinary *single-photon* Bs in inelastic (radiative) transition from the state with the initial momentum $\mathbf{p}_\mathrm{i}$ to the state with the direction of a momentum coinciding with the direction of the momentum $\mathbf{n}_f = \mathbf{p}_f \Big/ \left|\mathbf{p}_f\right|$ of the exact final quantum state (the momentum of which is $\mathbf{p}_\mathrm{f}$ and the energy is $E_f = E_i - n\,\hbar\omega$), and with an energy differing from the initial energy only by one photon:

$$n_{\mathbf{k}\lambda}^{stat} = \frac{2\pi}{\hbar}\left|\omega\left(\mathbf{e}\ \mathbf{d}_{if1}\right)\right|^2 \Big/ \left[V\frac{d\sigma_{scatt}}{d\Omega_f}\right], \tag{10.4}$$

where $\mathbf{d}_{if1}$ is the matrix element for the radiating dipole moment of an incident electron between the states $|i\rangle$ and $|f1\rangle$,

$$\begin{aligned} |i\rangle = |\mathbf{p}_i\rangle &= \left|E_i,\ \mathbf{n}_i\right\rangle = \left|p_i^2/2\,m,\ \mathbf{p}_i/|\mathbf{p}_i|\right\rangle,\ |f1\rangle \\ &= \left|E_i - \hbar\,\omega,\ \ \mathbf{n}_f = \mathbf{p}_f \Big/ \left|\mathbf{p}_f\right|\right\rangle, \end{aligned} \tag{10.5}$$

where V is the volume of quantization, $d\sigma_{scatt}/d\Omega_f$ is the cross-section of elastic IP scattering in the ion field from the state $|i\rangle$ to the state $|f1\rangle$.

As seen from Eq. 10.4, the extension of the prescribed current method (in the region of its truth) to the case of arbitrary quanticity of IP motion is achieved by replacement of the classical Fourier transform $\mathbf{j}_{\omega}^{projectile}$ for current produced by an IP to the quantum-mechanical expression

$$\frac{m<f|\mathbf{j}^{projectile}|i>}{2\pi\hbar\left(\sqrt{\frac{d\sigma_{scatt}}{d\Omega_f}}\right)}. \tag{10.6}$$

Really, at $\hbar \to 0$ by the correspondence principle [1] for single-quantum inelastic transitions of an IP in an arbitrary central field between states described by wave functions of the continuous spectrum we obtain the Fourier component of the classical trajectory in the argument of the Bessel function in the formula (10.2). And in the Born limit ($\eta<<1$) the formula (10.6) coincides with the value $\mathbf{q}/\omega$ in the formula (10.1) in the range of accuracy of this approximation itself based on weak inelasticity of the transition (a change of energy, that is, of the magnitude of a momentum vector, makes to $\hbar\mathbf{q}$ the contribution of the second order of smallness in comparison with the contribution of the angle of rotation of the momentum vector).

The formula for the process cross-section is obtained from Eq. 10.3 by proper summation over statistical weights of the final state of an IP, which corresponds to multiplication of the probability of radiation by the cross-section of Coulomb IP scattering in the MCI field:

$$d\sigma(n) = W(n)\, d\sigma_{Coul}. \tag{10.7}$$

10.1.2 Generalization of the Fermi Equivalent Photon Method to Multiquantum Processes

The basis for the generalization of the Fermi equivalent photon method to the multiphoton case formulated below is extension of the prescribed classical current approximation used in [3] for description of multiphoton *static* IBs at $\eta>>1$ to the process of *polarization* IBs and, besides, at an arbitrary quanticity of IP motion.

The equivalent photon method is (within the framework of its applicability) insensitive to the quanticity/classicity of motion of a charged particle producing a flux of equivalent photons. Therefore in the problem of multiphoton induced PBs it seems natural to take into account interaction of (of necessity quantized) radiated/absorbed field of real photons not only directly with IP current (as in ordinary static Bs), but also with polarization current induced by an IP in a target ion/atom. For the case of prescribed classical current (the generalization to the quanticity of IP motion – see

below) this gives an additional term in the Hamiltonian, so the equation for the wave function χ of one mode of the laser field in the interaction representation takes the form:

$$i\hbar\frac{\partial\chi}{\partial t} = -e\left(\frac{2\,\pi\,\hbar}{\omega\,V}\right)^{1/2}(\mathbf{e}_{k\lambda}\mathbf{j}^{total})(a_{k\lambda}(t) + a^{+}_{k\lambda}(t))\chi, \tag{10.8}$$

where a, a^{+} are the operators of annihilation and production of photons in the laser mode, $\mathbf{e}_{\mathbf{k}\lambda}$ is the unit vector of polarization of the intensity of an electric component of laser radiation, e is the electron charge, V is the volume of quantization.

The Fourier transform of total current including polarization current is given by the following expression:

$$\mathbf{j}^{total}_{\omega} = \mathbf{j}^{projectile}_{\omega} + \mathbf{j}^{polariz}_{\omega} \tag{10.9}$$

here $\mathbf{j}^{projectile}_{\omega}$ is the Fourier transform of IP current calculated at a classical trajectory, $\mathbf{j}^{polariz}_{\omega}$ is the Fourier transform of polarization current induced in the target.

The Eq. 10.9 corresponds to the dipole approximation both for interaction of laser radiation with a MCI and an incident electron and for interaction of an incident electron with a MCI. The first two conditions are expressed by the inequations: $\lambda > r_b$ and $\lambda > r(\omega)$, the third condition is expressed by $r(\omega) > r_b$ (λ is the laser wavelength, r_b is the radius of the orbit of a bound electron in a MCI, $r(\omega)$ is the characteristic distance from an IP to a MCI making the main contribution to radiation of frequency ω). It is can be seen that the dipole approximation is applicable in a wide range of frequencies.

The last condition ($r(\omega) > r_b$) defines also the fact that the field of an incident electron at the location of a bound electron is much less than the field of the MCI nucleus. Therefore in the rough the relation can be supposed to be satisfied:

$$\mathbf{j}^{polariz}_{\omega} \sim \chi(\mathbf{E}_0)\,\mathbf{j}^{projectile}_{\omega}, \tag{10.10}$$

where $\chi(\mathbf{E}_0)$ is the integral operator of susceptibility of the electronic system of multiply charged ions (in view of the influence of the laser field of amplitude $\mathbf{E}_0$) including the contribution of all harmonics of the IP field. This relation defines the linear connection between IP current and current induced in a MCI under the action of IP in the process of scattering, which justifies the choice of total current in the formula (10.10).

Further we will be interested in the case of a "developed" multiphoton nature of energy exchange between an IP and a laser field (strong enough, but, it will be recalled, still lower than the Coulomb MCI field in the effective region of radiation/absorption of a photon), at which the main contribution to polarization IBs is defined by the presence of single-photon near-resonance behavior of a laser field with MCI eigenfrequencies. This case corresponds to induced (under the action of a

laser field) scattering of n equivalent photons, each of energy $\hbar\omega$, "emitted" by an IP in its scattering in the Coulomb MCI field, by the core of a target ion with their transformation to n real photons. In the consistent quantum-electrodynamic consideration this process is described by the sum of "ladder" diagrams (see Appendix 2 of the work [4]), which results in nth order near-resonance behavior in the amplitudes of n-photon processes. Actually, corresponding to the said approach is realization of the principle of inducedness (stimulatedness, preference) of radiation of energy quanta at a frequency of the external field not only for (real) photons, but also for virtual photons "waiting" for their transformation to real photons.

The described approach, however, does not take into account the contributions from resonances in the core of an ion with higher laser frequency harmonics. Corresponding to this fact would be the appearance of polarizabilities of higher orders and, accordingly, the conversion of *one* virtual photon with the energy $n\hbar\omega$ to n real photons. In terms of diagrams, this process is represented by one (for a specified n) "comb" diagram and therefore corresponds (1) to disturbance of a target ion in a much more strict range of frequencies and (2) to a possibility only of the first-order resonance in the process amplitude.

In the approximation under consideration we obtain

$$\mathbf{j}_{\omega}^{total} = \mathbf{j}_{\omega}^{projectile} + \mathbf{j}_{\omega}^{polariz} = \left[1 - \left[\frac{m\omega^2}{Ze^2}\right]\alpha(\omega, \mathbf{E}_0)\right]\mathbf{j}_{\omega}^{projectile}, \tag{10.11}$$

where $\alpha(\omega, \mathbf{E}_0)$ is the first-order target polarizability at the frequency ω determined in view of disturbance of the target by the laser field of amplitude $\mathbf{E}_0$.

10.1.3 Probability of Multiphoton Bremsstrahlung in View of the Polarization Channel

A corollary of the Eqs. 10.8 and 10.9 is the following expression for the total probability of a n-photon process of radiation/absorption (W(n)) in the case $n^{las}>>1$ (n^{las} is the occupation number for photons in a laser mode), including the *static and polarization* channels:

$$W_{\sum}(n) = J_n^2\left\{2\left(n_{\mathbf{k}\lambda}^{las} n_{\mathbf{k}\lambda}^{stat}\right)^{1/2}[1-\delta]\right\}, \tag{10.12}$$

where J_n is the n^{th}-order Bessel function, and

$$\delta = \frac{m\omega^2\alpha(\omega, \mathbf{E}_0)}{Ze^2} \tag{10.13}$$

is the summand describing the contribution of the polarization mechanism of radiation to the process amplitude. In case of prevalence of radiation by the polarization channel we obtain:

$$W_{pol}(n) = J_n^2 \left\{ 2 \left(n_{k\lambda}^{las} n_{k\lambda}^{polariz} \right)^{1/2} \right\}, \tag{10.14}$$

where $n_{\mathbf{k}\lambda}^{polariz} = \delta^2 n_{\mathbf{k}\lambda}^{stat}$ is the occupation number for photons that are spontaneously emitted by an IP by the polarization channel in the laser mode $\{\mathbf{k},\ \lambda\}$ in collision of the IP with a MCI.

The formula (10.12) is the result of summation over both channels. The separation of the contribution of radiation by one of the channels in this expression is achieved by using the addition formula for Bessel functions. This makes it possible to copy the Eq. 10.12 as:

$$W_{\sum}(n) = \left| \sum_{\nu+m=n} J_\nu \left(\sqrt{4 n_{k\lambda}^{las} n_{k\lambda}^{stat}} \right) J_m \left(\sqrt{4 n_{k\lambda}^{las} n_{k\lambda}^{polariz}} \right) \right|^2. \tag{10.15}$$

The expression (10.12) for the probability of a multiphoton process is the generalization of the formulas obtained earlier by F.V. Bunkin and M.V. Fyodorov [2] in the Born approximation and by I.Ya. Berson [3] in the quasi-classical limit. The generalization is made (1) to the case of strong inelasticity of a multiquantum transition in a wide region of quanticity/classicity of IP motion covering the regions of truth of the results of [2, 3] and the whole domain of applicability of the prescribed quantum/classical current approximation, and (2) to taking into account the contribution of the polarization channel to the process of radiation in the prescribed quantum/classical current approximation for current produced by an IP.

It is significant that the result of Eq. 10.12 generalizes to the multiphoton case the known effect [8] of "stripping" a target ion consisting in partial (for an ion) or total (for an atom) descreening of a nucleus. This descreening occurs due to compensation of contributions of polarization radiation and the part of IP bremsstrahlung that is caused by Coulomb interaction of an IP with electrons of the core. Such a compensation exactly corresponds to disappearance of bremsstrahlung in the dipole approximation in collision of particles with equal charge-to-mass ratios.

The approach, within the framework of which the formula (10.12) was obtained, differs from the consideration of the work [9] carried out in the Born approximation by consistent taking into account the interaction of polarization current induced in a MCI with a quantized laser field and by generalization to the case of arbitrary values of the parameter η in the domain of applicability of the prescribed current formalism. However, it should be noted that the result of [9] has a strict physical analog. The direct comparison of Eq. 10.12 with the formula (10.2) from [9] carried out at the level of the cross-section of a corresponding process obtained by multiplication of probability by the cross-section of Coulomb IP scattering in the

MCI field is indicative of structure similarity. The main distinction consists in the form of multipliers representing the polarization channel that in [9] are expressed in terms of nonlinear susceptibilities of a target. This distinction is explained by different models used as the basis for description of the phenomenon under consideration.

The result obtained here (Eq. 10.12) corresponds, as mentioned above, to induced (under the action of a laser field) scattering of n equivalent photons, each of energy $\hbar\omega$, "emitted" by an IP in its scattering in the Coulomb MCI field, by the core of a target ion with their transformation to n real photons (here n^{th} order near-resonance behavior arises, see Appendix 2 of [4]). And corresponding to the approach of the work [9] – in the terms of the equivalent photon formalism – is the conversion of *one* virtual photon with the energy $n\hbar\omega$ to n real photons, at which only the first-order resonance is possible. For considered in this work multiphoton IBs in collision of a charged particle with a MCI in the presence of a strong laser field that is near-resonance with respect to single-photon transitions in the MCI core, the approximation we used is found to be more appropriate.

It should be noted that "odd" lines of virtual photons in "ladder" diagrams describing the conversion "n to n" increase the number of diagram vertices, but do not necessarily reduce the value of the process amplitude. In order for such a reduction to take place actually, an additional inequation should be satisfied that generalizes the known Born condition for a static scattering potential to a case of a time-dependent potential. This condition for a case of electron scattering by a MCI can be written as follows:

$$\frac{\alpha(\omega)\,E}{\mathrm{v}r_{\omega}} < 1. \qquad (*)$$

The inequation (*) can be called the dynamic Born condition. It was not used in the work [9].

The distinction of the formula (10.12) from the formulas of the work [10] is caused by the fact that in the said paper the wave function of a target was taken into account in the "dipole disturbance" approximation, which has defined taking into account emission of only one photon by the polarization channel.

The contribution of the polarization mechanism to the total probability of induced Bs becomes prevailing in case of near-resonance laser radiation. In this region generally determined by the condition

$$\gamma << |\omega - \omega_0| << \omega, \qquad (10.16)$$

where ω_0 is the eigenfrequency of a resonance electron transition in a MCI, γ is the total width of the considered transition, it is necessary to take into account the influence of a laser field on electrons of the MCI core that, as is known, can approximately be reduced to the known modification of MCI polarizability – to appearance in the denominator of the expression for the near-resonance MCI

polarizability of the generalized Rabi frequency: $\Omega_R = \sqrt{(\mathbf{dE}_0/\hbar)^2 + (\omega - \omega_0)^2}$. The near-resonance MCI polarizability can be described by the expression: $\alpha(\omega, \mathbf{E}_0) = d^2\, sign(\omega_0 - \omega)/\hbar\Omega_R$, here $\mathbf{d}$ is the matrix element of the dipole moment of the near-resonance transition. In terms of diagrams this can be shown by summation of a corresponding diagram series describing the interaction of laser radiation and a core ion. Accordingly, the expression for the value δ describing the contribution of the polarization channel to the total process amplitude can be represented as:

$$\delta = \left(\frac{m\omega^2}{Ze^2}\right)\frac{d^2\, sign(\omega - \omega_0)}{\hbar\Omega_R}. \tag{10.17}$$

Based on the above formulas, it is possible to write out the following condition of prevalence of the polarization channel over the static channel (in atomic units):

$$\Delta^2 + \frac{g_f}{g_i}\frac{f_0}{\omega}E^2 < \left(\frac{f_0\omega}{Z}\right)^2, \tag{10.18}$$

where f_0 is the oscillator strength, $g_{i,f}$ are the statistical weights of the initial and final states of the resonance transition, $\Delta = \omega - \omega_0$ is the detuning of laser frequency from resonance.

Following from the formula (10.18) is the expression for the saturating value of the laser field amplitude in the near-resonance case under consideration: $E_{sat} = \sqrt{\frac{g_i\omega}{g_f f_0}}\Delta$. For characteristic values of parameters included in this expression in the soft X-ray region and laser frequency detunings from resonance $\Delta \approx 10^{-3}$ (which exceeds the characteristic value for the Doppler broadening of the transition in the case under consideration), for the saturating field we have the estimation: $E_{\text{sat}} \approx 10^{-3}$ (a.u.).

From the above formulas we obtain the upper boundary for the value of the laser field for the region of prevalence of PBs over SBs in the near-resonance case:

$$E_h = \sqrt{\frac{2\omega}{f_0}\left[\left(\frac{\omega f_0}{2Z}\right)^2 - \Delta^2\right]}. \tag{10.19}$$

For $Z = 10$, $\omega \approx 2$ a.u., $f_0 \sim 1$ we find: $E_h \sim 0.1$ a.u.

In case of laser fields $E < E_{sat}$ we have the following condition of prevalence of PBs over SBs:

$$|\Delta| < \frac{f_0}{Z}\omega, \tag{10.20}$$

from which it follows that in this case a rather wide spectral range is covered.

Let us estimate the significance of the role of induced Bs, including polarization IBs, for a case of practical interest of coherent radiation generation in the soft X-ray band. We will give the numerical estimation for values of parameters reachable in modern experiments. Such an estimation is most appropriate to be given for the Kramers case, when $\omega \geq \omega_{Coul} \equiv \mathrm{v}^3/Z$.

In this case we obtain the following expression for the cross-section of a n-photon induced process (α is the angle between the initial IP velocity and the wave vector of a bremsstrahlung photon):

$$\sigma_n(\alpha) = \frac{(2Z)^{\frac{4}{3}}}{\mathrm{v}^2\,\omega^{\frac{2}{3}}} \int_0^{2\pi} d\phi \int \frac{dN}{N^{\frac{1}{3}}} J_n^2\left(\frac{|1-\delta|}{\omega^{\frac{5}{3}} Z^{\frac{1}{3}}} E\left(\frac{2^{5/3}}{\sqrt{3}}\right) N^{\frac{2}{3}} F(N,\alpha,\phi)\right) \tag{10.21}$$

where

$$F(N,\alpha,\phi) = \sqrt{\cos^2\alpha\;\; K_{2/3}^2\left(\frac{4}{3}N\right) + \cos^2\phi\,\sin^2\alpha\, K_{1/3}^2\left(\frac{4}{3}N\right)}$$

and $K_{2/3}$, $K_{1/3}$ are the Macdonald functions.

The analysis of the expression (10.21) shows the importance of interference effects between the static and polarization radiation channels. They result, in particular, in "dips" both on spectral and on amplitude dependences of the cross-section of the induced bremsstrahlung effect. These effects correspond to vanishing of the argument of the Bessel function in the formula (10.21) for $\delta = 1$. The last case can occur both due to a corresponding shift of the laser field frequency from the center of the emission line and (for negative detunings from resonance) due to dependence of the value δ on the amplitude of the laser field (see Eq. 10.17 and the expression for the generalized Rabi frequency).

Since the Bessel function reaches its maximum at the value of the argument approximately equal to the order of the function, for the probability of a multiphoton process to be comparable with the probability of a single-photon process it is necessary that the argument of the Bessel function in the above formulas is great enough. At the same time there is a top limitation on the value of a laser field (the formula (10.19)) for the relative contribution of the polarization channel to be not too small. So the contribution of PBs to the multiphoton process is noticeable against the background of the contribution of static IBs for a limited range of values of problem parameters. This ion-charge dependence for a lithium-like isoelectronic series of ions is presented in Fig. 10.1.

Given in Fig. 10.2 is the dependence of the differential cross-sections of induced bremsstrahlung of single-photon (curve 1) and two-photon (curve 2) processes on the intensity of a linearly polarized laser field for a zero angle between the field vector and the initial electron velocity vector.

Also given in the figure are the curves corresponding to the contribution only of the static channel (curves 3, 4) also are given. It is seen that in taking into account the polarization channel the cross-section of the two-photon process is compared

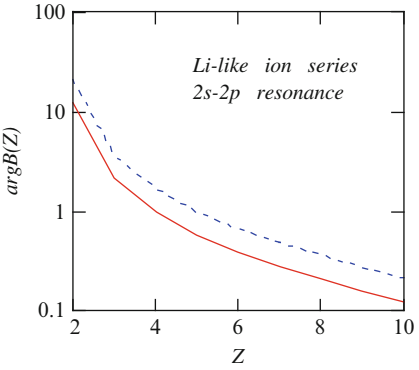

Fig. 10.1 The dependence of the argument of the Bessel function in the expression for multiphoton IBs near-resonance with respect to the transition *2s-2p* in a lithium-like ion on the charge of the ionic nucleus in case of equal amplitudes of the static and polarization channels. The relative detuning from resonance $5\%/Z$ for two values of IP velocity: $Z/3$ a.u. (*dotted curve*), $Z/\sqrt{3}$ a.u. (*solid curve*)

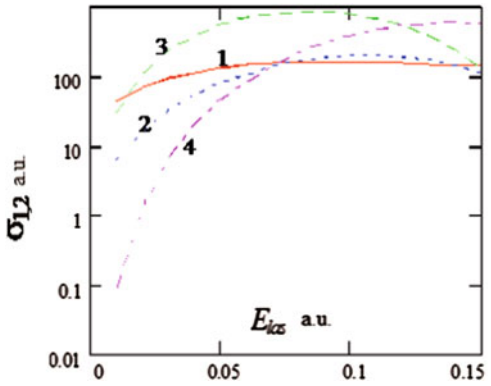

Fig. 10.2 The dependence of the differential cross-sections of IBs of single-photon, $\sigma_1(0)$ (*curve 1*) and two-photon, $\sigma_2(0)$ (*curve 2*) processes on the intensity of a linearly polarized laser field for the angle $\alpha = 0$, the ion charge $Z = 4$, the IP velocity $v = 0.447$ a.u., the laser frequency $\omega = 0.37$ a.u., the oscillator strength $f_0 = 0.69$, the relative frequency detuning $\Delta/\omega \approx + 0.014$. The curves corresponding to the contribution only of the static channel for single-photon (*3*) and two-photon (*4*) processes are also given

with the cross-section of the single-photon process at lower values of laser field intensity.

10.1.4 Cross-Section of a Single-Photon Process

Let us calculate the cross-section of induced bremsstrahlung/absorption for a single-photon process for laser field intensities, at which the argument of the Bessel

function in the formula (10.21) is less than one, so it is possible to retain the first term in the expansion of the said function. We will consider a case when the condition of (quasi-)classicity of motion of an incident particle ($\eta = Z e^2/\hbar \mathrm{v} > 1$) is satisfied. Then it is possible to perform integration with respect to impact parameters (or eccentricity of an orbit) in the closed form in the formula for the differential cross-section as it was for the first time done in [3]. Let us assume also that the condition of "Kramers behavior" of the process is satisfied, that is, the laser field frequency is much higher than the Coulomb frequency: $\omega >> \omega_{Coul}$ ($\omega_{Coul} \equiv m\mathrm{v}^3/Ze^2$). Under the said assumptions the expression for the cross-section of the single-photon process takes the form:

$$\sigma_1(\vartheta) = \frac{\pi^2}{\sqrt{3}} \frac{Z^2}{\mathrm{v}^2\omega^4} E_{las}^2 |1-\delta|^2 \left[\sin^2\vartheta + 2\left(3\cos^2\vartheta - 1\right)\right], \tag{10.22}$$

where ϑ is the angle between the vector of the initial velocity of an incident electron and the laser field intensity vector ($\mathbf{E}_{las}$), the value δ is given by the formula (10.17).

Further we will carry out calculation for a case of relatively cold recombining plasma, the temperature of which can be estimated according to the formula: $T \approx 0.025\, Z^2$. To be specific, we will consider the distribution of plasma electrons by velocities to be Maxwellian distribution. Then for the cross-section averaged over velocities (in the two-level approximation for a target ion) we find:

$$\sigma_1(E_{las}, \Delta) = \frac{2\sqrt{\pi}}{3\sqrt{3}} \left| 1 + \frac{\omega f_0\, sign(\Delta)}{2Z\sqrt{\Delta^2 + f_0 E_{las}^2/2\omega}} \right|^2 \frac{Z^2\, E_{las}^2}{T\,\omega^4}. \tag{10.23}$$

Here the explicit expression of the parameter δ for a near-resonance case is used, f_0 is the oscillator strength for the near-resonance transition.

We assume that the magnitude of the laser field frequency detuning from the frequency of the resonant transition in an ion ($\Delta \equiv \omega - \omega_0$) exceeds considerably both homogeneous and inhomogeneous broadening of the transition under consideration. It should be emphasized that the obtained expression (10.23) essentially depends on a sign of detuning from resonance, which defines the asymmetry of the process cross-section.

The cross-section of the static channel of the process under consideration is obtained from the formula (10.23) in case of dropping the second summand under the modulus sign. On the contrary, the polarization channel cross-section corresponds to the second summand under the modulus sign in Eq. 10.23.

We will give the results of calculations by the formula (10.23) for a case of bremsstrahlung absorption of a near-resonance laser field in scattering of electrons of relatively cold plasma ($T \approx 0.025\, Z^2$) by a lithium-like oxygen ion (O^{5+}) (Fig. 10.3).

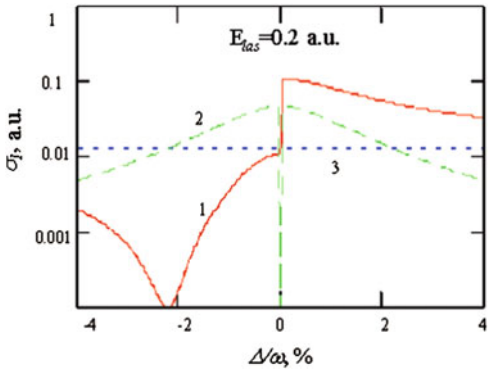

Fig. 10.3 The spectral cross-section of the single-photon induced bremsstrahlung effect for a quasi-classical electron on a *OVI* lithium-like ion in the laser field $E_{las} = 0.2$ a.u. that is near-resonance with respect to the transition *2s-3p* in the ion core. *Curve 1* – total cross-section, *curve 2* – contribution of the polarization channel, *curve 3* – contribution of the static channel

We assume that the laser frequency is close to the eigenfrequency of the transition *2s-3p* of this ion, but at the same time the detuning from resonance exceeds both homogeneous and inhomogeneous broadening of the transition in magnitude. In the case under consideration the values of the problem parameters are the following: $Z = 5$, $\omega = 3.037$ a.u. (86.2 eV), $T = 0.625$ a.u., $f_0 = 0.26$. Hence for the initial values of the Born parameter (η) and the "Kramers behavior" parameter ($\xi = \omega/\omega_{Coul}$) we have: $\eta = 4.47$ and $\xi = 10.87$. It should be noted that the final values of these parameters are inessential for applicability of the approximations used here.

For a possibility to neglect the spin-orbit splitting of the *3p*-state it is sufficient that the magnitude of the relative detuning from resonance ($|\Delta|/\omega$) is much higher than the relative value of this splitting (0.024 %). The relative value of the Doppler broadening in the case under consideration is about 0.01 %. Thus the two-level model works for $|\Delta|/\omega > 0.1$ %.

For applicability of the prescribed current approximation used here it is necessary that the intensity of the Coulomb field of an ion in a region of space responsible for radiation (E^{eff}_{Coul}) exceeds the laser field intensity. The estimation for E^{eff}_{Coul} gives: $E^{eff}_{Coul} \approx 7.5$ a.u. By this value the values of the laser field intensities are bounded above. On the other hand, the performed expansion of the Bessel function is true up to $E_{las} \leq 8$ a.u. So in our case the expansion of the Bessel function is true throughout the region of validity of the prescribed current approximation.

From Fig. 10.3 the asymmetry of the process spectral line shape is well seen. A "dip" in the low-frequency wing of the line corresponds to cancellation of the contributions of the polarization and static channels in case of their destructive interference. In the high-frequency wing of the line, on the contrary, the interference of the channels is constructive, and the total cross-section of the process exceeds the simple sum of the contributions of two Bs mechanisms.

Also following from this figure is the broadening influence of the laser field on the resonant transition in the ion core due to the presence of the Rabi frequency in the expression for the near-resonance polarizability of the target. This influence results in the fact that the resonance growth of the polarization channel cross-section is reduced for low enough detunings.

As will be shown in the following paragraphs, the dipole approximation in consideration of PBs for near-resonance transitions with changing principal quantum number and strongly inelastic electron scattering, generally speaking, is not sufficient since the penetration of an IP into the target core takes place. The above analysis can be considered as a zeroth approximation, in which the main features of the process are the most pronounced.

For near-resonance transitions in lithium-like ions the dipole approximation is more adequate, but in this case it is necessary to take into account the fine splitting of a radiating transition.

10.1.5 Taking into Account the Fine Splitting of the Upper Resonant Level

Here we will consider the influences of polarization of the ion core on induced bremsstrahlung in a situation when it is necessary to take into account simultaneously the influence of a strong near-resonance laser field on the polarizability of bound electrons and the fine splitting of the resonant transition. This case is characteristic for a MCI of a moderate charge ($Z_i \sim 10$) and near-resonance transitions with no change of the principal quantum number ($\Delta n = 0$). Really, for example, for a lithium-like *OVI* ion the ratio of the value of fine splitting to the medium transition frequency for transitions 2s $\rightarrow$ 2p and 2s $\rightarrow$ 3p is respectively 0.5 % and 0.024 %.

To describe the process under consideration, it is possible to use the following expression for the cross-section of the induced single-photon bremsstrahlung effect in view of polarization of the ion core, being the generalization of the formula (10.23) to a case of polarizability of the core of the general form:

$$\sigma_1(\omega, \mathrm{v}) = \frac{\pi^4}{6} \frac{Z^2 e^2}{\hbar^2 \omega^4 m^2 \mathrm{v}^2} E_{Las}^2 \left| 1 - \frac{m\omega^2 \alpha(\omega, E_{las})}{Ze^2} \right| F(\xi), \tag{10.24}$$

where Ze is the ion charge, v is the velocity of an incident plasma electron, $\xi = \omega/\omega_{Coul}$, and the function $F(\xi)$ is given by the expression:

$$F(\xi) = \xi \left| H_{i\xi}^{(1)}(i\xi) \right| H_{i\xi}^{(1)'}(i\xi),$$

where $H^{(1)}$ and $H^{(1)'}$ are the Hankel function of the first kind and its derivative with respect to the argument, $\alpha(\omega, E_{las})$ is the polarizability of the ion core in view of the

influence of a strong near-resonance laser field. It should be noted that in the Kramers region ($\xi >> 1$): $F(\xi) = 4/\left(\sqrt{3}\,\pi\right)$.

So in the case under consideration the resonance $|g> \rightarrow |e_1>, |e_2>$ takes place, where $|e_{1,2}>$ are the split upper states. We will assume that the magnitude of the splitting frequency $\Delta_0 = \omega_2 - \omega_1$ is much less than the resonance frequencies $\omega_{1,2}$ themselves. However, it can be great enough in comparison with the detunings $\Delta_{1,2} = \omega - \omega_{1,2}$ and is comparable with the resonance Rabi frequency $\Omega_0 = \mathbf{d}_0\,\mathbf{E}_{las}/\hbar$. Here d_0 is the matrix element of the dipole moment of the transition that we will assume to be the same for transitions to both split states. Further we will have to calculate the resonant polarizability $\alpha(\omega, E_{las})$ defining the contribution of the polarization channel to the process.

A strong near-resonance laser field results in mixing of lower and upper levels of the resonant transition and to appearance of so-called "dressed" states, into which the initial state of the ion core goes in case of adiabatic turning-on of the laser field (depending on the value and the sign of the detuning Δ). So three new states $|0>$, $|1>$, $|2>$ appear being the coherent superposition of the initial states $|g>$, $|e_1>$, $|e_2>$ with coefficients that are time-independent in the condition of applicability of the rotating wave approximation: $|\Delta|/\omega << 1$ that we assume to be satisfied.

With the use of a usual procedure of system Hamiltonian diagonalization (in the rotating wave approximation) the following characteristic equation for determination of the energy of "dressed" states can be obtained:

$$\lambda^3 - (\Delta_1 + \Delta_2)\lambda^2 - \left(2\Omega_0^2 - \Delta_1\Delta_2\right)\lambda + (\Delta_1 + \Delta_2)\Omega_0^2 = 0. \tag{10.25}$$

In derivation of the Eq. 10.25 it was assumed that $<e_1|d_{12}|e_2> = 0$.

The solutions (Eq. 10.25) can be obtained using the Cardano formula. The explicit form $\lambda_j = \lambda_j(\Delta_{1,2}, E_{las})$ is not given here because of its cumbersomeness.

Depending on the value Δ_1, the following transitions between the initial and "dressed" states of the resonant transition take place as a result of adiabatic turning-on of the laser field:

$$\Delta_1 < 0: \ |g> \Rightarrow |1>, \ |e_1> \Rightarrow |3>, \ |e_2> \Rightarrow |2> \tag{10.26a}$$

$$0 < \Delta_1 < \Delta_0: \ |g> \Rightarrow |3>, \ |e_1> \Rightarrow |1>, \ |e_2> \Rightarrow |2> \tag{10.26b}$$

$$\Delta_0 < \Delta_1: \ |g> \Rightarrow |2>, \ |e_1> \Rightarrow |1>, \ |e_2> \Rightarrow |3> \tag{10.26c}$$

From the formulas (10.26a), (10.26b) and (10.26c) it follows that the polarizability of the resonant transition in the ion core, according to in which electronic state an ion was before turning-on of the laser field, can be represented in terms of polarizabilities of the "dressed" states as a function of Δ_1 (it is obvious that $\Delta_2 = \Delta_1 - \Delta_0$) as follows:

$$\alpha_g(\Delta_1) = \alpha_1(\Delta_1)\,\Theta(-\Delta_1) + \alpha_2(\Delta_1)\,\Theta(\Delta_1)\,\Theta(\Delta_0 - \Delta_1) + \alpha_3(\Delta_1)\,\Theta(\Delta_1 - \Delta_0), \tag{10.27a}$$

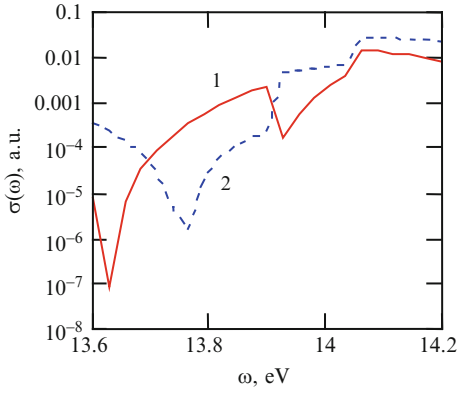

Fig. 10.4 The spectral cross-sections of the induced bremsstrahlung effect for quasi-classical electrons on a *FVII* ion in the laser field with the amplitude $E_{las} = 0.01$ a.u. (*curve 1*), $E_{las} = 0.02$ a.u. (*curve 2*) and a frequency close to the eigenfrequency of the transition $2s \rightarrow 2p$ in the electron core of the ion in view of the fine splitting of the upper level. The calculation is in the dipole approximation for IP interaction with the target core

$$\alpha_{e1}(\Delta_1) = \alpha_3(\Delta_1)\,\Theta(-\Delta_1) + \alpha_1(\Delta_1)\,\Theta(\Delta_1), \tag{10.27b}$$

$$\alpha_{e2}(\Delta_1) = \alpha_2(\Delta_1)\,\Theta(\Delta_0 - \Delta_1) + \alpha_3(\Delta_1)\,\Theta(\Delta_1 - \Delta_0). \tag{10.27c}$$

Here $\Theta(x)$ is the Heaviside theta function.

For polarizabilities of the "dressed" states α_j (j = 1,2,3) the following formulas are true:

$$\alpha_j\,(\Delta_1, E_{Las}) = -\frac{d_0^2}{\hbar}\frac{\left(W_j(\Delta_1, E_{Las})/\hbar + \Delta_1\right)^{-1} + \left(W_j(\Delta_1, E_{Las})/\hbar + \Delta_1 - \Delta_0\right)^{-1}}{(\Omega_0/2)^2\left\{\left(W_j(\Delta_1, E_{Las})/\hbar + \Delta_1\right)^{-2} + \left(W_j(\Delta_1, E_{Las})/\hbar + \Delta_1 - \Delta_0\right)^{-2}\right\} + 1}. \tag{10.28}$$

Shown in Fig. 10.4 are the spectral cross-sections for a *FVII* ion and two values of the amplitude of the laser field $E_{las} = 0.01$ a.u. (curve 1) and $E_{las} = 0.02$ a.u. (curve 2) calculated by the formulas (10.24), (10.25), (10.26a), (10.26b), (10.26c), (10.27a), (10.27b), (10.27c) and (10.28).

From this figure it follows that interference effects for frequencies inside the fine splitting take place for much larger average cross-sections of the process in comparison with a dip in the low-frequency wing that occurs also without considering the fine splitting of upper levels (for a laser field value lower than the saturating value).

To calculate the total cross-section of the process, it is necessary to perform averaging over the initial distribution of bound electrons of the ion core by the states $|g>$, $|e_1>$, $|e_2>$. This averaging in case of the Boltzmann distribution will

result in slurring of dips in the spectral cross-section of the process. However, for a temperature range characteristic for MCI, as a rule, the corona equilibrium is realized, in which the distribution by electronic states of the ion core will be defined by the ratio of the rates of excitation and deexitation of the states $|e_1>$, $|e_2>$. The estimation for the ratio $(N_e/N_g)_{corona}$ to $(N_e/N_g)_{Boltzm}$ (Ne/Ng) gives:

$$\frac{(N_e/N_g)_{corona}}{(N_e/N_g)_{Boltzm}} \approx 10^{-19} n_e \ [cm^{-3}]. \tag{10.29}$$

So from the relation (10.29) it follows that for a case of not too dense plasma in the corona equilibrium the population of the excited state of the resonant transition can be neglected in comparison with the population of the ground state.

10.2 Near-Resonance Bremsstrahlung of Quasi-Classical Electrons on Ions in the Coulomb Approximation: Taking into Account the Effects of Penetration into a Target Core

In this paragraph the interference-polarization effects in near-resonance Bs of quasi-classical electrons are analyzed in view of their penetration into the core of an ion, which is found to be rather essential for strongly inelastic processes. The approximations accepted here – the quasi-classical approximation for IP motion and the Coulomb approximation for field acting on an IP – are most adequate to scattering of plasma electrons by multiply charged ions. However, as the quantum analysis shows (see the following paragraph), the calculation below is approximately true also for ions of low charge.

The proposed quasi-classical consideration provides physical visualization making it possible to get the picture of a phenomenon under study that is not so obvious in the more exact quantum approach.

10.2.1 Main Relations

In the Sect. 10.1 the prescribed current method for calculation of the cross-section of Bs on multiply charged ions with a core for arbitrary values of the Born parameter $\eta = Z_i/v$ was justified. For slow enough incident particles, when the relation $\eta \geq 1$ is satisfied, good results are given by the so-called semiclassical approximation, in which the classical theory of Bs in combination with some quantum restrictions is used [1]. Here we use the semiclassical approximation also for calculation of the polarization channel of induced bremsstrahlung or absorption in the part concerning incident particles; for calculation of characteristics of bound electrons of the core, naturally, we use the consistent quantum-mechanical approach.

Within the framework of this picture the spectral amplitude of induced bremsstrahlung or absorption for the IP scattering angle ϑ (or the eccentricity of an orbit $\varepsilon = 1/\sin(\vartheta/2)$) is the sum of two summands, one of which is proportional to the temporal Fourier transform of the dipole moment of a scattered IP ($\mathbf{D}^{st}(\omega, \varepsilon)$ is the static channel), and the other is proportional to the Fourier transform of the dipole moment induced by the IP in the ion core ($\mathbf{D}^{pol}(\omega, \varepsilon)$ is the polarization channel).

Further we will consider induced bremsstrahlung or absorption at the frequency of outer radiation ω close to the eigenfrequency ω_0 of the transition in the electron core of an ion such as: $(n_i\ s) \rightarrow (n\ p)$, however, in this case we assume that the detuning $\Delta = \omega - \omega_0$ exceeds the transition line width, so the real excitation of the ion core can be neglected.

The corresponding formulas obtained in [11] in view of field broadening of the near- resonance transition look like:

$$d\sigma^{tot}(\omega, \varepsilon) = \frac{2\,\pi}{3}\,\frac{Z_i^2}{\mathrm{v}^4}\,\left|\mathbf{E}_0\,\mathbf{D}^{tot}(\omega, \varepsilon)\right|^2\,\varepsilon\,d\varepsilon \tag{10.30}$$

$$\mathbf{D}^{tot}(\omega, \varepsilon) = \mathbf{D}^{st}(\omega, \varepsilon) + \mathbf{D}^{pol}(\omega, \varepsilon) \tag{10.31}$$

$$D_j^{pol}(\omega, \varepsilon) = \frac{1}{6\,\pi}\,\frac{\langle n_i, l = 0 \,\|\, d \,\|\, n, l = 1\rangle}{\Omega} \times \int\limits_{-\infty}^{+\infty} dt\, e^{i\,\omega\,t}\,\frac{R_j(t, \varepsilon)}{R(t, \varepsilon)}\,\langle n, l = 1 \,\|\, a_1(r_{core}, R(t, \varepsilon)\,) \,\|\, n_i, l = 0\rangle$$

$$a_1(r, R) = \theta(R - r)\,\frac{r}{R^2} + \theta(r - R)\,\frac{R}{r^2}, \tag{10.32}$$

here $R_j(t, \varepsilon)$ is the j^{th} projection of the IP radius vector for a specified eccentricity of an orbit as a time function; $\Omega = \sqrt{\Delta^2 + \Omega_0^2}$ is the generalized Rabi frequency, $\Omega_0 = \mathbf{d}_0\,\mathbf{E}_0/\hbar$ is the resonance Rabi frequency, $\mathbf{d}_0$ is the matrix element of the dipole moment of the resonant transition; $\mathbf{E}_0$ is the amplitude of the electric field in outer radiation.

The time integral in the formula (10.32) is proportional to the temporal Fourier transform of the potential of interaction between an IP and the near-resonance transition in the ion core:

$$\varphi_{eg}(\mathbf{R}) = \langle e\|\mathbf{r} - \mathbf{R}|^{-1}|g\rangle,$$

here g and e is the set of quantum numbers of the lower and upper states of the electron transition under consideration.

In obtaining the formula (10.32), summation over magnetic quantum numbers and integration with respect to the angular variables of the ion core are performed.

It should be noted that the operation of taking the Fourier transform in the above formulas within the framework of the semiclassical approximation being used is equivalent to calculation of a matrix element from a corresponding operator in the consistent quantum-mechanical approach. The described procedure is the expression of the conformity principle for a matrix element of an arbitrary inelastic process calculated between the wave functions of the continuous IP spectrum generalized in [4] to a multiquantum case.

In the dipole approximation for interaction of an IP with an ion the formula (10.32) is reduced to the form:

$$D_j^{pol,\,dip}(\omega,\varepsilon) = \frac{1}{3}\frac{\langle n_i, l=0 \,\|\, d \,\|\, n, l=1\rangle}{\Omega}\frac{\omega^2}{Z_i}\, R_j(\omega,\varepsilon). \tag{10.33}$$

The expression (10.33) can be obtained from Eq. 10.32 in the limit of the zero radius of the ion core with the use of the formula:

$$\frac{-\omega^2 R_j(\omega,\varepsilon)}{Z_i} = \left(\frac{R_j(t,\varepsilon)}{R^3(t,\varepsilon)}\right)_\omega, \tag{10.34}$$

following from the equation of IP motion in the field of a *point* ion.

Following from the formula (10.33) is an important conclusion that the temporal Fourier transform of the dipole moment induced by the IP field in the ion core is proportional to a corresponding Fourier transform of the dipole moment produced by a scattered IP [8, Chap. 10]. This circumstance, true in the dipole approximation for IP interaction with an ion, formed the basis of the analysis of induced bremsstrahlung or absorption in the works [4].

Nondipole effects in induced bremsstrahlung or absorption in the work [12] were studied for a case of isotropic (by initial velocities) IP distribution, when the dependence of the process on polarization of external radiation disappears. It is just the purpose of this paragraph to take into account this dependence. Therefore we will calculate the cross-section of induced bremsstrahlung or absorption without averaging over the direction of the initial IP velocity. The expression for the cross-section integrated with respect to the IP scattering angle looks like:

$$d\sigma^{tot}(\omega,\alpha) = \frac{2\pi}{3}\frac{Z_i^2}{\mathrm{v}^4}\,\mathbf{E}_0^2 \int_1^\infty \left[\left(\left|D_x^{tot}(\omega,\varepsilon)\right|^2\right) f_x(\alpha,\varepsilon) + \left(\left|D_y^{tot}(\omega,\varepsilon)\right|^2\right) f_y(\alpha,\varepsilon)\right] \varepsilon^{-1}\, d\varepsilon, \tag{10.35}$$

where

$$f_x(\alpha,\varepsilon) = \cos^2\alpha + \frac{\varepsilon^2-1}{2}\sin^2\alpha;\; f_y(\alpha,\varepsilon) = (\varepsilon^2-1)\cos^2\alpha + \frac{1}{2}\sin^2\alpha.$$

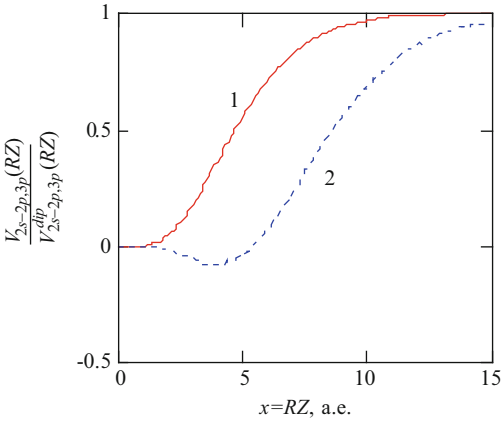

Fig. 10.5 The distinction of the potential of interaction of an incident particle with the transitions *2s-2p* (*curve 1*), *2s-3p* (*curve 2*) of a bound electron in a hydrogen-like ion from its dipole approximation (Z is the charge of the ion nucleus)

In this formula x, y are the axes of the focal coordinate system specified by the initial IP velocity vector [3], α is the angle between the initial IP velocity vector and the vector of the electric field vector of external radiation. In derivation of the expression (10.35) from the formula (10.30) integration with respect to the azimuth angle of scattering was performed.

The formulas (10.35), (10.31) and (10.32) are the main formulas for our investigation of polarization-interference effects in induced bremsstrahlung or absorption of quasi-classical electrons on ions with a core.

10.2.2 Influence of the Nondipole Nature of Interaction "IP-Target" on a Radiating Dipole Moment

A cause of arising polarization-interference effects under consideration is the nondipole nature of IP interaction with the near-resonance transition in the ion core. In the dipole approximation the interference summand in the Bs cross-section does not depend on polarization of external radiation [4]. Thus for appearance of this dependence the distinction of the potential of interaction "IP-ion core" from its dipole analog ("IP-point ion") is essential.

Given in Fig. 10.5 are the dependences of the ratio of the exact interaction potential to the dipole potential on the parameter $x = ZR$ (where R is the distance from an IP to the nucleus) in case of IP interaction with the transition *2s-2p* and with the transition *2s-3p* in a hydrogen-like ion. The calculation in the model potential approximation shows that similar dependences take place for transitions of an outer electron in a lithium-like ion.

From this figure it follows that the deviation from the dipole nature in IP interaction with the near-resonance transition occurs at the parameter values $x_0 \approx 12$ (for $\Delta n = 0$) and $x_1 = 16$ (for $\Delta n = 1$), while the value x corresponding to the radius of the *2p*-state of a hydrogen-like ion is about 4. So the dipole nature begins to show itself already at distances from an IP to the nucleus three times longer than the characteristic radius of the upper resonant state. As is known (see, for example, [1]), in the Kramers limit the region of the IP trajectory responsible for emission of a photon of frequency ω is localized at a distance of the order of $R_\omega(Z_i) \approx \left(\frac{Z_i}{\omega^2}\right)^{1/3}$ (for the Coulomb field) from the field center (this estimation corresponds to the "rotation" approximation [1]).

In case of lithium-like ions the eigenfrequency of the transition *2s-2p* can be approximated by the expression: $\omega_{2s-2p}(Z) = 0.0707\,Z - 0.120$ a.u. (Z is the charge of the nucleus of an ion). From the given expressions it is possible to estimate the parameter of nondipole behavior $\chi_{nd}(x_\omega) = \dfrac{V_{2s-2p}(x_\omega)}{V^{dip}_{2s-2p}(x_\omega)}$ (here $x_\omega(Z_i) = Z_i\ R_\omega(Z_i)$) as a function of the charge of a lithium-like ion Z_i for the near-resonance transition *2s-2p*. Simple calculations give: $\chi_{\mathrm{nd}}(1,2,3,4,5) = 0.25,\ 0.8,\ 0.96,\ 0.99$ for $\Delta n = 0$.

So this estimation based on the use of the "rotation" approximation shows that in lithium-like ions for transitions with no change of the principal quantum number the parameter of nondipole behavior for high enough charges of an ion ($Z_i \geq 4$) is close to one. An analogous estimation for the transition $\Delta n = 1$ shows that the corresponding parameter of nondipole behavior $x_\omega(Z_i)$ is much less than one for all Z_i.

However, it should be remembered that the "rotation" approximation corresponds to replacement of summation over the impact parameter of the contributions of different IP trajectories by IP radiation at a some effective distance $R_\omega(Z_i)$. It is not obvious beforehand that such a replacement is correct for taking into account the interference of the static and polarization channels occurring for each fixed impact parameter, especially in the region of destructive interference of these channels, where the value of the total cross-section is small. The calculations carried out in [12] in the prescribed Coulomb IP current approximation show that the "rotation" approximation, generally speaking, is insufficient for description of fine interference effects in the region of spectral-amplitude "dips". It is approximately true in the region of constructive interference of the static and polarization channels for transitions with no change of the principal quantum number. Therefore for correct description of this interference throughout the range of parameter values it is necessary to proceed from the general nonsimplified formula (10.35).

With the calculation of induced bremsstrahlung or absorption for *lithium-like* ions in mind, further we use the Coulomb approximation for IP current, in which the trajectory of IP motion is specified by the known classical expressions [3] of motion of a charged particle in the Coulomb field of attraction with the effective charge $Z_{eff} = Z_i + 1/2$.

The calculation of dependences of focal components of an induced dipole moment of the ion core on the eccentricity of the orbit of an incident particle – $D_{x,y}(\varepsilon)$ – shows that for transitions of bound electrons of an ion with no change of the principal quantum number the y-projection of the dipole moment is close to its dipole analog. At the same time the x-projection of the dipole moment for eccentricities close enough to unity differs greatly from the same value calculated in the dipole approximation. In particular, for some eccentricity of the orbit of an incident particle the x-projection of the dipole moment becomes zero and near $\varepsilon = 1$ changes sign.

The said difference underlies the dependence (being studied in this work) of polarization-induced effects in induced bremsstrahlung or absorption on the angle between the vector of the initial velocity of an incident particle and the vector of intensity of the electric field in an electromagnetic wave.

The physical cause of these peculiarities in behavior of the functions $D_x(\varepsilon)$ and $D_y(\varepsilon)$ consists in different influence of the effect of penetration of an incident particle into the ion core on the projections of the Fourier transform of an induced dipole moment in the focal coordinate system. Penetration into the ion core more strongly influences the x-component of the dipole moment than the y-component since it is the x-component of the radius vector of an incident particle that changes its sign in the process of motion of the incident particle from the point of minimum approach to the field center to infinity, while the y-component remains constant-sign at this section of the trajectory.

10.2.3 *Polarization, Spectral and Amplitude Dependences of Induced Bremsstrahlung or Absorption in View of Penetration of an IP into the Target Core*

The results of calculations of the cross-section of induced bremsstrahlung or absorption within the framework of the approach under consideration are presented in Figs. 10.6, 10.7 and 10.8. The calculations were carried out for the transitions *2s-2p* and *2s-3p* in a lithium-like N^{4+} ion. As wave functions of a valence electron, the functions of the model potential method were used.

In all figures the cross-sections of induced bremsstrahlung or absorption integrated with respect to the angle of IP scattering are given.

The spectral dependences of the cross-section of induced bremsstrahlung or absorption normalized to the static value near the transition eigenfrequency with no change of the principal quantum number in the ion core for two values of the angle α (between the vector of the initial velocity of an incident particle and the vector of intensity of the electric field in outer radiation) are shown in Fig. 10.6 for the initial IP velocity $v = 0.6$ a.u. From this figure it follows that interference effects are most pronounced for the angle $\alpha = \pi/2$, while for $\alpha = 0$ they are considerably reduced. And the distinction is greatest in the region of destructive

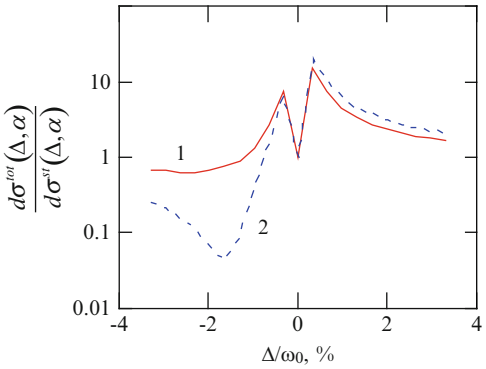

Fig. 10.6 The spectral dependences ($\Delta = \omega - \omega_0$) of the induced bremsstrahlung or absorption cross-section normalized to the static value for a quasi-classical electron on a N^{4+} ion for two values of the angle α ($\alpha = 0$ – *curve 1*, $\alpha = \pi/2$ – *curve 2*) between the initial IP velocity vector ($v = 0.6$ a.u.) and the vector of intensity of the electric field of outer radiation ($E_0 = 10^{-3}$ a.u.) for an outer field frequency near the eigenfrequency of the resonant transition in the ion core *with no change* of the principal quantum number (*2s-2p*)

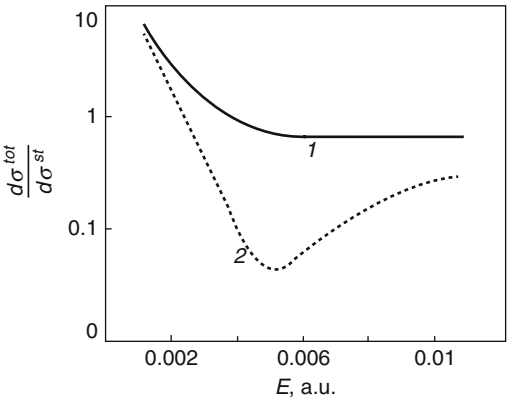

Fig. 10.7 The dependences of the induced bremsstrahlung or absorption cross-section normalized to the static value on the intensity of the electric field in outer radiation for two values of the angle α between the vectors of the initial electron velocity and of the electric field intensity ($\alpha = 0$ – *curve 1*, $\alpha = \pi/2$ – *curve 2*), negative detuning from resonance $(\omega - \omega_0)/\omega_0 = -0.3$ % near the eigenfrequency of the transition *2s-2p* in a N^{4+} ion for the IP velocity $v = 0.6$ a.u.

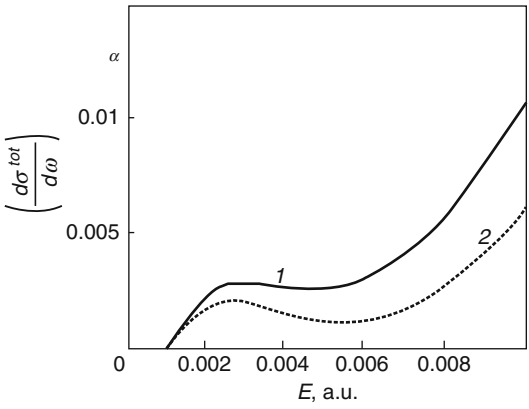

Fig. 10.8 The dependence of the cross-section of induced bremsstrahlung or absorption averaged over the angle α (for the angular distribution of the type $D_p(\alpha) = \cos^p\alpha/(p+1)$ with the distribution axis perpendicular to the polarization of outer radiation) on the intensity of the electric field of outer radiation for two values of the angular distribution parameter ($p = 2$ – *curve 1*, $p = 12$ – *curve 2*) in scattering of electrons with v = 0.6 a.u. by a N^{4+} ion for detuning of the external field frequency from the eigenfrequency of the transition 2s-2p in the ion core that is: $(\omega - \omega_0)/\omega_0 = -0.3$ %

interference of the static and polarization channels ($\omega < \omega_0$), where calculations in the dipole approximation for interaction of an incident particle with the core showed the presence of a deep minimum caused by cancellation of the polarization and static summands in the process amplitude. In the region of constructive interference ($\omega > \omega_0$) the distinction in the spectral dependence of the cross-sections for two values of the angle α is insignificant.

The cause of considered polarization peculiarities in the spectral cross-section of induced bremsstrahlung or absorption is connected with the distinction (discussed in the previous section) in influence of the nondipole nature of interaction of an incident particle with the near-resonance transition on the focal components of the radiating dipole moment induced in the ion core: in more strong influence on its x-component and weak influence (for the transition with $\Delta n = 0$) on the y-component. In case of $\alpha = 0$ the main contribution to radiation (for low enough velocities of an incident particle) is made by D_x, which is caused by the form of the functions $f_{x,y}(\alpha, \varepsilon)$ (the formula (10.34)). Really, if $\alpha = 0$, then $f_x(0, \varepsilon) = 1$ and $f_x(0, \varepsilon) = \varepsilon^2 - 1$. If now it is taken into account that for low enough values of the IP velocity (in the Kramers limit [1]) the main contribution to the process cross-section integrated with respect to the eccentricity of an orbit is made by $\varepsilon \approx 1$ (close collisions), from the previous equations it follows that $f_x(0, \varepsilon) >> f_y(0, \varepsilon)$.

The analogous reasoning shows that for $\alpha = \pi/2$ the inverse inequation $f_x(0, \varepsilon) << f_y(0, \varepsilon)$ is true, and, accordingly, the main contribution to the process is made by the y-component of the radiating dipole moment.

Thus the angle α "controls" the relative contribution of different focal components of radiating dipole moment. In the case that the main contribution to radiation is made by D_x, the strong influence of the nondipole nature of interaction of an incident particle with the ion core results in the fact that the cancellation of amplitudes of the static and polarization channels (in the region of their destructive interference $\omega < \omega_0$) takes place only for high enough values of the y of the orbit of an incident particle. For low enough eccentricities the said cancellation is no more true. Moreover, beginning with a some value ε_0, the function $D_x(\varepsilon)$ changes sign, and the interference of the static and polarization channels gets a constructive nature. As a result, the interference "dip" in the cross-section of induced bremsstrahlung or absorption integrated with respect to the eccentricity of the orbit of an incident particle is "slurred over", which is well seen in Fig. 10.6.

In the high-frequency wing of the spectral line $\omega > \omega_0$ the situation is opposite: high "manifestation" of channel interference results in a higher value of the cross-section of induced bremsstrahlung or absorption for the angle $\alpha = \pi/2$ in comparison with the value $\alpha = 0$. However, in this case the relative role of the interference summand is small since the total cross-section of the process is great. This circumstance is connected with closeness of the parameter of nondipole behavior χ_{nd} to unity (noted in the previous section) for $\Delta n = 0$ and $Z_i \geq 2$.

In the low-frequency wing of the spectral line, where the total cross-section is small, on the contrary, the role of interference is rather essential and the considered dependence of the cross-section of induced bremsstrahlung or absorption on polarization of outer radiation is most pronounced.

Similar spectral dependences were also obtained for the transition with changing principal quantum number: *2s-3p*. In this situation the distinction of the cross-sections in the region of destructive interference is not so great as for the transition with $\Delta n = 0$, which is explained by strong influence of the nondipole behavior on the value of the y-component of the dipole moment induced in the ion core, caused by the large radius of the *3p*-state in comparison with the *2p*-state.

Presented in Figs. 10.7 and 10.8 are the amplitude dependences of the cross-section of induced bremsstrahlung or absorption (from the intensity of the electric field in external radiation) integrated with respect to the IP scattering angle, for which polarization-induced interference effects of interaction of the static and polarization channels also take place.

Given in Fig. 10.7 is the amplitude dependence of the ratio of the total (including the polarization summand in the amplitude) cross-section of induced bremsstrahlung or absorption to its static analog for two values of the angle α ($\alpha = 0$ – curve 1, $\alpha = \pi/2$ – curve 2) in the region of destructive interference of the channels ($\omega < \omega_0$). As seen from the figure, in the first case interference effects are very low: they show themselves in the fact that with increasing intensity of the electric field the process cross-section tends to a value that is somewhat lower than the static

value due to destructive interference strongly suppressed by the nondipole behavior of interaction of an incident particle with the ion core. For $\alpha = \pi/2$ a strong interference effect is present: the amplitude dependence of the cross-section of induced bremsstrahlung or absorption has a wide "dip" caused by cancellation of the static and polarization summands in the process cross-section that is characteristic for consideration within the framework of the dipole approximation for interaction of an incident particle with the ion core [4, 12]. The cause of retention of "dipole features" in the amplitude dependence of the cross-section is the same as in the spectral dependence: for the angle $\alpha = \pi/2$ the main contribution to radiation is made by the y-component of the induced dipole moment that is weakly subject to the influence of the nondipole behavior for transitions with no change of the principal quantum number.

Given in Fig. 10.8 are averaged over the angular distribution of incident particles of the type

$$D_p(\alpha) = \cos^p \alpha/(p+1)$$

amplitude dependences of the total cross-section of induced bremsstrahlung or absorption for two values of the angular distribution parameter ($p = 2$, $p = 12$) for the angle $\pi/2$ between the distribution axis and the vector of intensity of the electrical field in an electromagnetic wave. The chosen kind of angular distribution of electrons is characteristic for the process of ablation of a solid-state target under the action of high-power laser radiation, and the angle $\alpha = \pi/2$ corresponds to the normal incidence of radiation on the solid surface.

From the figure it is seen that the interference effect is most pronounced for more "sharp" ($p = 12$) angular distribution, which was to be expected since in this case the average angle α is more close to $\pi/2$.

10.3 Quantum Approach to Description of Polarization-Interference Effects in Near-Resonance Strongly Inelastic Electron Scattering

The purpose of this paragraph consists in the quantum (for IP motion) calculation of spectral cross-sections (integrated and differential with respect to the electron scattering angle) of strongly inelastic electron scattering (with absorption and emission of photons) of thermal (relatively slow) electrons in a near-resonance external field and the analysis of influence of target polarization, channel interference, the nondipole nature of IP interaction with a target ion, and exchange effects on this process.

10.3.1 Method of Calculation

The primary formula for the cross-section of inelastic scattering of an electron from the state with the initial momentum $\mathbf{p}_\mathrm{i}$ to the state with the finite momentum $\mathbf{p}_\mathrm{f}$ in the solid angle $d\Omega_f$ by an ion under the action of the external field of amplitude $\mathbf{E}_0$ and frequency ω can be represented as (we use in this section atomic units $\hbar = m = e = 1$):

$$d\sigma(\mathbf{p}_\mathrm{f}) = \frac{1}{16\,\pi^2}\,|(M_\mathrm{fi})|^2\,\frac{p_f}{p_i}\,d\Omega_f, \tag{10.36}$$

here

$$M_{fi}(\omega) = \langle \mathbf{p}_\mathrm{f}|\,\frac{\mathbf{r}}{\mathrm{r}}\,\big(V_{st}(r) + V_{pol}(r,\omega,E_0)\big)|\mathbf{p}_\mathrm{i}\rangle\,\frac{\mathbf{E}_0}{\omega^2} \tag{10.37}$$

is the matrix element from the operator of disturbance of IP motion in the static field of the target and in the field of the induced dipole moment of the target. Here $\left|\mathbf{p}_{\mathbf{i},\mathbf{f}}\right\rangle$ are the wave functions of an IP in the central field of an ion normalized to the unit flux, $p_f = \sqrt{p_i^2 \pm 2\omega}$ is the magnitude of the final IP momentum, the plus sign relates to absorption, minus relates to emission of a photon as a result of inelastic scattering.

The expression (10.37) is obtained with neglected exchange effects, the contribution to the cross-section of which will be mentioned below.

In the formula (10.37) the function $V_{st}(r)$ is the magnitude of intensity of the static field of a target ion at the location of an IP, and $V_{pol}(r,\omega,E_0)$ is connected with the dynamic polarization of the electron core of an ion at the external field frequency ω and for the near-resonance case under consideration ($|\omega - \omega_0| << \omega_0$) looks like:

$$V_{pol}(r,\omega,E_0) = sign(\Delta)\,\frac{\omega^2}{\sqrt{\Delta^2 + (d_0E_0)^2/3}}\,\frac{d_0}{3}V_{ns,n'p}(r), \tag{10.38}$$

where $d_0 = \langle ns\|d\|n'p\rangle$ is the reduced matrix element of the dipole moment of the transition, $V_{ns,n'p}(r)$ is the reduced matrix element of the potential of IP interaction with the near-resonance transition $ns \to n'p$ in the ion core that is equal to:

$$V_{nsn'p}(r) = \big\langle ns\big\|\theta(r - r_b)r_b/r^2 + \theta(r_b - r)r/r_b^2\big\|n'p\big\rangle, \tag{10.39}$$

$\mathbf{r}_\mathrm{b}$ is the radius vector of a bound electron of the ion, $\theta(x)$ is the Heaviside function. Everywhere in the paper the ground s-state of the ion core is considered.

In calculation of the functions $V_{st}(r)$ and $V_{ns,n'p}(r)$ for an outer electron of the ion core the wave function of the model potential method was used, and for inner *2s*-electrons the Slater wave functions were used.

The main distinction of this consideration from previous quantum calculations of inelastic electron scattering in the near-resonance field is consistent taking into account the interference of contributions of the static and polarization channels in case of essentiality of the nondipole nature of IP interaction with a radiating transition in the ion core. The said nondipole nature is essential if the contribution of short distances (of the order of an ion size) exceeds the contribution of long distances or is comparable with it, which takes place in case of strong enough inelasticity of scattering that we assume in this chapter.

The wave functions of an IP can be calculated in the prescribed quantum IP current approximation by quantum number expansion of the orbital moment $\ell\ \hbar$. The external electromagnetic field is supposed to be weak enough, so the wave functions of the continuous spectrum of a scattered electron can be found by solution of a corresponding Schrödinger equation in the central field of a target ion.

The calculation was carried out for lithium-like ions in the ground state and for external radiation frequencies that are near-resonance with respect to the transition with no change of the principal quantum number.

The radial wave functions of the continuous IP spectrum were normalized according to their asymptotic form:

$$u(r \to \infty, l, p) \to \frac{2}{r} \sin\left(pr + \frac{Z_i}{p}\ \ln(2pr) - \frac{\pi}{2} l + \delta(l,p)\right), \tag{10.40}$$

here $\delta(l,p) = \delta^C(l,p) + \Delta\delta(l,p)$ is the total phase shift equal to the sum of the Coulomb $\delta^C(l,p)$ and non-Coulomb $\Delta\delta(l,p)$ phase shifts, the latter was calculated by the formula [13]:

$$\sin(\Delta\delta(l,p)) = \frac{1}{2p} \int_0^\infty \left(\frac{Z_i}{r} - |V_{st}(r)|\, r\right) u(r,l,p)\, u^{Coul}(r,l,p)\, r^2 dr, \tag{10.41}$$

where $u^{Coul}(r,l,p)$ is the solution of the radial Schrödinger equation with the Coulomb potential.

As a result, the integrated and differential cross-sections of inelastic scattering are represented as the sum (over the quantum number of the orbital angular momentum) of terms containing radial matrix elements of the total potential of disturbance of IP motion ($V_{st}(r) + V_{pol}(r, \omega, E_0)$):

$$R_{l,l\pm1} = \langle u(r,l,p_i) | V_{st}(r) + V_{pol}(r,\omega,E_0) \big| u\big(r, l \pm 1, p_f\big)\big\rangle \tag{10.42}$$

and corresponding phase shifts for the IP wave functions.

10.3.2 Inelastic Scattering Cross-Section Differential with Respect to Angle

After integration with respect to the directions of the IP radius vector the formulas (10.36) and (10.37) give:

$$\sigma(\Omega_f) = \frac{1}{16 p_f p_i^3} \left(\frac{E_0}{\omega^2}\right)^2 \left| \sum_{l=0}^{\infty} S_l^{fi}(\Omega_f) \right|^2 d\Omega_f. \tag{10.43}$$

For parallel polarization ($\mathbf{p}_i \,//\, \mathbf{E}_0$) the summands S_l look like:

$$S_l^{fi,par} = a_l \left[P_{l+1} R_{l,l+1} e^{i\left(\delta(l,p_i)+\delta\left(l+1,p_f\right)\right)} - P_l R_{l+1,l} e^{i\left(\delta(l+1,p_i)+\delta\left(l,p_f\right)\right)} \right], \tag{10.44}$$

where $P_l(\cos\theta)$ are the Legendre polynomials, θ is the angle of IP scattering, $a_l = l + 1$.

By analogy, in case of perpendicular polarization of the external field ($\mathbf{p}_i \perp \mathbf{E}_0$):

$$S_l^{fi,per} = e^{i\,\delta\left(l+1,p_f\right)} b_l \left[Y_{l+1,1} + Y_{l+1,-1} \right] \left\{ e^{i\,\delta(l,p_i)} R_{l,l+1} + e^{i\,\delta(l+2,p_i)} R_{l+1,l} \right\}, \tag{10.45}$$

where $b_l = \sqrt{\frac{\pi(l+1)(l+2)}{2l+3}}$, $Y_{nm}\left(\Omega_f\right)$ are the spherical functions.

Since for strongly inelastic scattering under consideration a considerable contribution to the cross-section is made by short distances to the nucleus of an ion, the calculation of radial matrix elements took into account the contribution of exchange processes in the polarization channel for two possible values of the total spin of the system "IP and ion core".

The results of calculation of spectral cross-sections normalized to the static cross-section and averaged over possible values of the total spin of colliding particles for different angles of inelastic IP scattering and two polarizations of the external field are presented in Fig. 10.9a, b for the incident electron energy 1 *Ry* and the external field strength $E_0 = 10^{-3}$ a.u., the field is near-resonance with respect to the transition *2s-2p* ($\hbar\omega_0 = 10$ eV) in the core of a N^{4+} ion.

From Fig. 10.9a it is seen that taking into account the nondipole nature of IP interaction with the radiating transition in the ion core for the case of parallel polarization of the external field results in the fact that the minimum in the spectral cross-section of the process caused by destructive interference of the static and polarization channels depends considerably on the angle of electron scattering. For small angles of IP scattering ($\theta < 90°$) the minimum falls on negative detunings ($\omega < \omega_0$), and for wide angles ($\theta > 140°$) it falls on positive detunings ($\omega > \omega_0$).

There is also a small range of angles ($\theta \approx 120°$), in which the interference minimum is absent. Accordingly, the "inversion" of spectral line shape asymmetry for the process cross-section with growing angle of IP scattering also occurs.

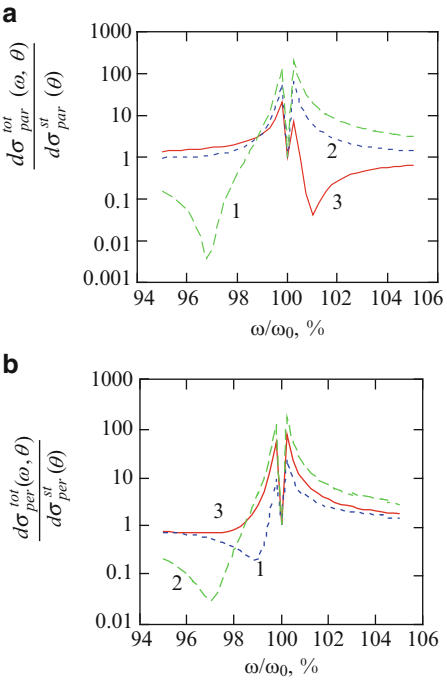

Fig. 10.9 The spectral cross-sections (averaged over the spin state of the system of colliding particles) of inelastic scattering (absorption) of an electron by a N^{4+} ion for different angles of IP scattering (*1* – θ = 57°, *2* – 120°, *3* – 140°), normalized to corresponding cross-sections of the static channel. Quantum calculation for IP motion: (**a**) parallel polarization of the external field $\mathbf{p}_i \,//\, \mathbf{E}_0$, (**b**) perpendicular polarization of the external field $\mathbf{p}_i \perp \mathbf{E}_0$

In case of perpendicular polarization ($\mathbf{p}_i \perp \mathbf{E}_0$) the interference minimum for all angles of IP scattering lies in the region of negative detunings of the external field frequency from resonance in the ion core (Fig. 10.9b), shifting to the center of the line with increasing scattering angle and disappearing at $\theta \approx 180°$.

The considered features of the spectral cross-section differential with respect to the IP scattering angle are connected with the dependence of the radial matrix element of nondipole polarization interaction on the quantum number of the orbital moment of an IP. The said matrix element changes sign in going from high moments to low ones. The role of these low moments is most essential in case of parallel polarization of the external field since then the contribution of an IP orbit section near the classical turning point increases.

On the contrary, for perpendicular polarization increases the role of long distances IP – ion (and accordingly, of high orbital moments), where the IP acceleration is found to be parallel to the vector of the external field strength.

Given in Fig. 10.10a, b are the spectral cross-sections for two angles of elastic IP scattering with photon absorption and two possible spin states of the system of colliding particles (without averaging over the total spin).

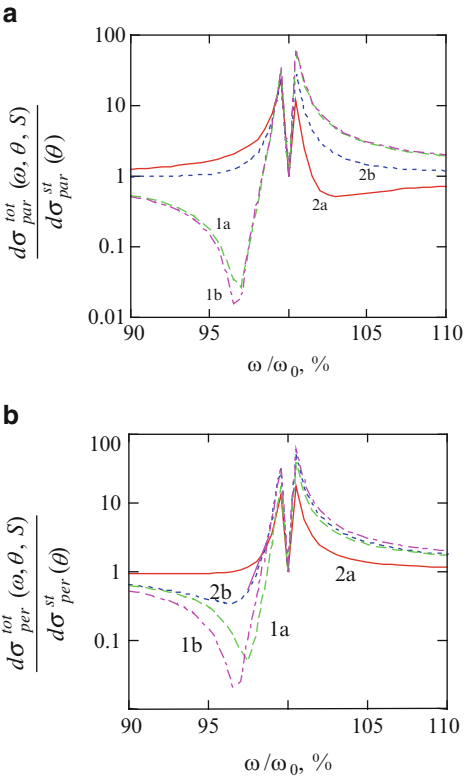

Fig. 10.10 The spectral cross-sections of inelastic scattering (absorption) of an electron by a N^{4+} ion for different angles of IP scattering ($1 - \theta = 57°$, $2 - 172°$), for the singlet ($S = 0$, *curves a*) and triplet ($S = 1$, *curves b*) states of the system of colliding particles. Quantum calculation for IP motion: (**a**) parallel polarization of the external field $\mathbf{p}_i \,//\, \mathbf{E}_0$, (**b**) perpendicular polarization of the external field $\mathbf{p}_i \perp \mathbf{E}_0$

It is seen that in case of parallel polarization of the external field exchange effects are most essential for wide angles of electron scattering, and in this case ($\theta = 172°$) the line shape asymmetry is more pronounced for the singlet state of the system ($S = 0$), for the triplet state ($S = 1$) the spectral shape of a scattering line is practically symmetric.

But in case of perpendicular polarization the exchange is noticeable also for small scattering angles and the interference minimum is found to be more deep for the triplet state. The line shape for a wide scattering angle is practically symmetric for the singlet state.

These features of the spectral cross-sections of inelastic IP scattering for different spin states of the system "IP + ion core" can be explained as follows. The exchange potential for the singlet state corresponds to effective attraction, so it reduces the amplitude of the polarization channel for those (high) orbital moments.

At such angles polarization interaction results from repulsion between an IP and the radiating transition in the ion core, which is true for perpendicular polarization (at any scattering angles) and in case of parallel polarization for small scattering angles.

And if an IP is scattered to wide angles in parallel polarization, polarization interaction results from an effective attraction between colliding particles, which is mathematically expressed in a change of the sign of a radial matrix element from the polarization potential for low ℓ. Therefore the exchange in the singlet state increases the polarization amplitude of the process. As a result, the asymmetry of the spectral cross-section of scattering for $S = 0$ is found to be more than in the triplet state, and in case of perpendicular polarization – quite the contrary.

It should be noted that the consideration of exchange interaction (only in the polarization channel) carried out in the work seems quite adequate for high enough degrees of ionization of a target, when the wave functions of an IP are mainly defined by the Coulomb attraction. In the opposite case this consideration may be insufficient. Nevertheless, the qualitative conclusions about the influence of spin effects on the spectral cross-section of strongly inelastic scattering given here should be retained.

10.3.3 Inelastic Scattering Cross-Section Integrated with Respect to Angle

For the spectral cross-section of induced inelastic scattering integrated with respect to the angle of IP scattering with parallel orientation of the vector of the external field strength and the vector of the initial IP momentum, after integration with respect to the solid angle $d\Omega_f$ the following expression can be obtained:

$$\int d\sigma_{\mathbf{p}_\mathrm{f}}^{par} = \frac{\pi}{4}\left(\frac{E_0}{\omega^2}\right)^2 \frac{1}{p_f\, p_i^2} \sum_{l=0}^{\infty} \frac{(l+1)^2}{2\,l+3}\, T_l{}^{par}\big(p_i,\, p_f\big), \tag{10.46}$$

where

$$T_l{}^{par}\big(p_i,\, p_f\big) = R_{l,l+1}^2 + \frac{2l+3}{2l+1}\, R_{l+1,l}^2 - 2 \times \frac{l+2}{l+1}\, R_{l,l+1}^2\, R_{l+2,l+1}^2\, \cos(\delta(l,p_i) - \delta(l+2,p_i)).$$

For the integrated spectral cross-section averaged over the polarization of the external field (or, which gives the same result, over the direction of the initial IP momentum) we have:

$$\int d\sigma_{\mathbf{p}_f}^{aver} = \frac{\pi}{4}\left(\frac{E_0}{\omega^2}\right)^2 \frac{1}{p_f\, p_i^2} \sum_{l=0}^{\infty} \frac{(l+1)}{3}\left(R_{l,l+1}^2 + R_{l+1,l}^2\right). \tag{10.47}$$

For a case of arbitrary orientation of the vector $\mathbf{E}_0$ with respect to the vector $\mathbf{p}_i$ (at the angle α) the following expression can be obtained:

$$\int d\sigma_{\mathbf{p}_f}(\alpha) = \frac{3}{2}\sin^2\alpha\left\{\int d\sigma_{\mathbf{p}_f}^{aver}\right\} + \frac{3\cos^2\alpha - 1}{2}\left\{\int d\sigma_{\mathbf{p}_f}^{par}\right\}. \tag{10.48}$$

It should be noted that the quantum calculation makes it possible to distinguish between the cross-sections of absorption and photon emission in IP scattering in the external field, which is important, for example, for the problem of energy exchange between plasma and radiation.

However, as carried out calculations show, the relative value of a corresponding difference cross-section (absorption minus photon emission) is maximum for directed IP motion and considerably decreases in case of averaging over the angle α between the field vector and the initial IP velocity vector.

The results of calculation of the spectral cross-section integrated with respect to the angle of IP scattering with absorption and emission of a photon for different polarizations of the external field are presented in Fig. 10.11. Scattering of an electron with an energy of 11 eV by a N^{4+} ion in the field that is near-resonance with respect to the transition *2s-2p* in the ion core was considered, $E_0 = 10^{-3}$ a.u.

From the given figures it follows that in the qualitative conformity with the conclusions of the quasi-classical consideration of the previous paragraph interference effects in the integrated cross-section of inelastic scattering are most pronounced for perpendicular polarization of the external field. At the same time, a spectral dip is found to be somewhat more smoothed and less deep in comparison with the results of the classical calculation.

For high detunings from resonance, where the static channel prevails, the sign of the difference cross-section corresponds to the results of calculation in the Born static approximation [14]: absorption exceeds radiation for perpendicular polarization and vice-versa for parallel polarization.

With decreasing frequency detuning the difference cross-section begins to be defined by interchannel interference that, as it was already mentioned, in the integrated scattering cross-section is most pronounced for perpendicular polarization of the external field. For example, in the frequency range of essentiality of destructive interference absorption considerably exceeds radiation for perpendicular polarization, as seen from Fig. 10.11 (bottom diagram) since the spectral minimum of scattering with photon emission is shifted towards higher detunings in comparison with absorption. However, the same shift results in the fact that with decreasing value of frequency detuning in the region $\omega < \omega_0$ the cross-section of radiation begins to exceed the cross-section of absorption. For $\omega > \omega_0$ ($\mathbf{p}_i \perp \mathbf{E}_0$) the situation becomes opposite.

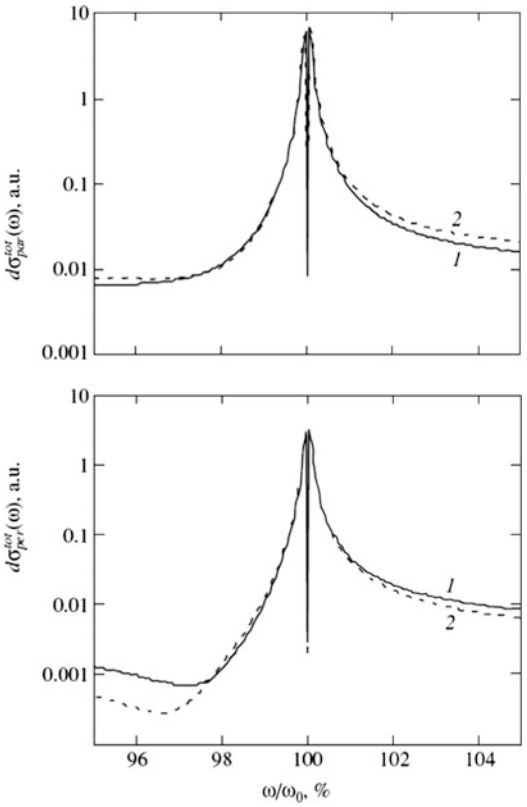

Fig. 10.11 The spectral cross-sections (integrated with respect to the scattering angle) of absorption (*curve 1*) and radiation (*curve 2*) in electron scattering ($p_i = 0.9$ a.u.) by lithium-like nitrogen in the external field ($E_0 = 10^{-3}$ a.u.) that is near-resonance with respect to the transition *2s-2p* in the core. Quantum calculation. *Top diagram* – parallel polarization of the external field $\mathbf{p}_i \,//\, \mathbf{E}_0$, *bottom diagram* – perpendicular polarization of the external field $\mathbf{p}_i \perp \mathbf{E}_0$

For parallel polarization ($\mathbf{p}_i \,//\, \mathbf{E}_0$) the value of the difference cross-section in the spectral range of essentiality of interference effects is much less (Fig. 10.11 (top diagram)) and has an opposite sign: absorption exceeds radiation for negative detunings low enough in magnitude ($\omega<\omega_0$) and vice-versa for $\omega>\omega_0$.

The calculation within the framework of the model under consideration shows that the difference cross-section of inelastic scattering averaged over the angle α and the total spin has an appreciable value near the resonance, where the process proceeds mainly by the polarization channel. The sign of the difference cross-section strongly depends on the IP energy: immediately near the threshold (in IP scattering with emission of a photon) radiation exceeds absorption, but even in case of small excesses of the IP energy over the threshold the situation becomes opposite.

The standard recalculation of the difference cross-section to the absorption/amplification coefficient shows that the value of the latter in the frequency range under consideration and for reasonable values of concentrations of colliding particles is extremely low and can be made appreciable only for very low detunings from resonance [15], where the specificity of the phenomenon under consideration disappears to a great extent. Nevertheless, it is possible that there will be such conditions, under which the obtained results can help also in the problem of amplification of electromagnetic radiation.

Thus in this paragraph within the framework of the prescribed quantum current approximation the spectral angular and integrated cross-sections of strongly inelastic scattering of thermal IP by an ion in the near-resonance external field are calculated.

It is shown that an essential role in the process under consideration is played by the nondipole nature of IP interaction with the near-resonance transition in the ion core. This nondipole nature results in the dependence of the nature of interchannel interference on such problem parameters as polarization of external radiation, the value of the initial IP velocity, and (for targets with a spin) on the total spin of the system of colliding particles.

The calculation of the cross-section differential with respect to the angle of IP scattering has found out the dependence of the spectral cross-section on the angle of IP scattering that is most strong for parallel polarization of external radiation, when with increasing scattering angle a peculiar kind of "inversion" of spectral line shape asymmetry occurs.

Confirmed on the basis of the quantum calculation was the conclusion of the quasi-classical consideration of the previous paragraph about the most manifestation of interchannel interference in the integrated cross-section of inelastic scattering for perpendicular polarization of the external field manifested in the asymmetry of the spectral cross-section and the presence of spectral dips.

The role of exchange effects in the spectral cross-section differential with respect to the angle of IP scattering was analyzed.

The features of the spectral dependences of the cross-section integrated with respect to the angle of IP scattering with absorption and emission of a photon for different orientations of the external field strength vector in relation to the initial IP velocity were investigated.

It was shown that the difference scattering cross-section (absorption minus radiation) averaged over the direction of the initial velocity is rather sensitive to the IP energy. In the near-threshold region of energies for frequencies near the resonance radiation exceeds absorption, but even in case of small excesses over the threshold the situation becomes opposite.

10.4 Experiments on Electron Scattering by Atoms in a Laser Field

In the processes of inelastic electron scattering by targets with a core in the presence of an external electromagnetic field an important role can be played, as it was theoretically predicted in [16], by a polarization mechanism, with which the transfer of energy from a field to an electron proceeds through virtual excitation of a target. Taking into account the contribution of the polarization channel made it possible to explain low laser breakdown thresholds for alkali metal vapor [17], atoms of which have high polarizability.

There is also another group of experiments on inelastic scattering of electrons by atoms in a laser field, in which the energy spectra of electrons scattered at a certain angle were measured, and for interpretation of which the calculation of the process cross-section based on the static approximation in a number of cases is found to be insufficient.

One of the first works of this kind [18] was dedicated to investigation of multiphoton processes in scattering of electrons by argon atoms in the presence of intensive radiation of a CO_2 laser (a peak power of 50 MW). The initial energy of electrons was 11 eV. It is essential that electrons were recorded at a wide angle of scattering (153°). In the experiment the number of scattered electrons with a specified energy was measured. It was found that the laser field results in significant redistribution of an originally monoenergetic electron beam by energies. The central peak corresponding to elastic scattering decreased approximately by 45 %. At the same time there arose additional maxima in the energy spectrum of scattered electrons, corresponding to absorption/emission of several laser photons up to $n = 3$.

The obtained experimental data were found to be in good agreement with predictions of the semiclassical phenomenon theory developed in [7]. In particular, it was shown that for the conditions of the carried out experiment the so-called "sum rule" is satisfied: the total probability of scattering summed over all photonicities of the process is a constant value.

The influence of target polarization and statistical properties of an electromagnetic field on the sum rule for multiphoton induced Bs was investigated in the work [19] within the framework of the first Born approximation. Meant by the sum rule in this case is a closure arising after summation of cross-sections corresponding to different numbers of photons emitted/absorbed by a target. This closure, without considering the polarization channel, is equal to the cross-section of elastic scattering of an electron by a target in the absence of radiation [20]. In the paper [19] it was shown that taking into account the polarization channel considerably modifies the sum rule for small enough angles of electron scattering. From the expression for the total scattering cross-section obtained in [19] it follows also that going from coherent radiation to stochastic radiation increases the role of polarization effects. The contribution of these effects to the transport cross-section of scattering has maximum for the perpendicular orientation of the external field vector with respect to the initial electron velocity vector.

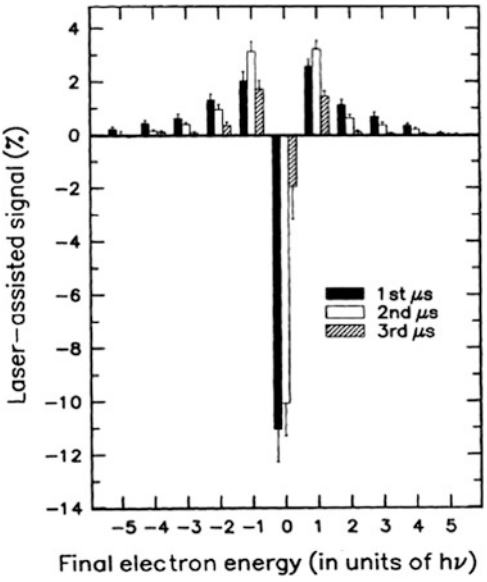

Fig. 10.12 The electronic spectra resulting from scattering of electrons by helium atoms in the laser field under conditions of the experiment [21]

The experimental investigation of electron scattering by helium atoms in a laser field was carried out in the work [21]. Radiation of a CO_2 laser with a power density of the order of 10^8 W/cm^2, the photon energy $\hbar\omega = 0.117$ eV, and an electron beam with the energy $E_i = 9.5$ eV were used. The viewing angle was 9°. The electron energy E_i was chosen so as, on the one hand, to satisfy the quasi-classical condition $E_i >> \hbar\omega$, and on the other hand, to avoid impact excitation of bound states of a helium atom with an energy about 19 eV.

As a result of measurements of the energy of an electronic signal, besides elastic scattering (with no change of electron energy), in the energy spectrum of scattered electrons maxima corresponding to absorption or emission of a whole number of laser photons were recorded. Emission/absorption of a photon in this case is an induced bremsstrahlung effect in a laser field, in the process of which electrons decrease or increase their kinetic energy.

The relative contribution of absorption/emission of laser photons in scattering measured within the first 3 s after beginning of a laser pulse is presented in Fig. 10.12. The typical temporal shape of a laser pulse is presented in Fig. 10.13.

It was found that the intensity of additional electron peaks corresponding to absorption/emission of laser photons by electrons in scattering exceeds considerably the values predicted by the theory [7] that does not take into account the polarization channel. The experimental conditions were chosen in [21] so as to satisfy to a maximum extent the criteria of applicability of the so-called Kroll-Watson approximation [7] and to exclude processes of excitation of the electron

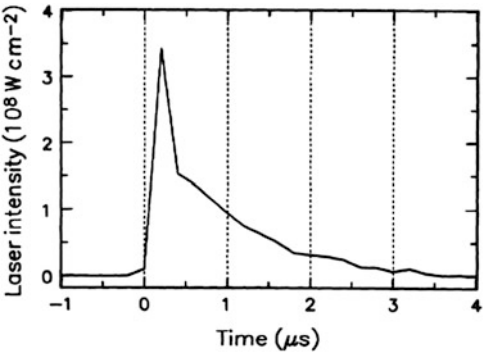

Fig. 10.13 The time dependence of a CO_2 laser pulse [21]

core of a target. The low value of polarizability of helium assumed also the minimization of polarization effects. Nevertheless, the results of [21] are indicative of insufficiency of the Kroll-Watson formula for explanation of the obtained experimental data and require taking into account additional mechanisms of radiation such as the polarization channel.

References

1. Kogan, V.I., Kukushkin, A.B., Lisitsa, V.S.: Kramers electrodynamics and electron-atomic radiative-collisional processes. Phys. Rep. **213**, 1 (1992)
2. Bunkin, F.V., Fedorov, M.V.: Bremsstrahlung in a strong radiation field. Sov. Phys. JETP **22**, 844 (1966)
3. Berson, I.Y.: Semiclassical approximation for stimulated bremsstrahlung. Sov. Phys. JETP **53**, 854 (1981)
4. Astapenko, V.A., Kukushkin, A.B.: Multiphoton static and polarization bremsstrahlung in collisions of charged particles with multiply-charged ions in a strong laser field. JETP **84**, 229 (1997)
5. Veniard, V., Gavrila, M., Maquet, A.: Two-photon free-free transitions in a Coulomb potential. Phys. Rev. A **32**, 2537 (1985)
6. Gavrila, M.: Elastic scattering of photons by a hydrogen atom. Phys. Rev. **163**, 147 (1967)
7. Kroll, N.M., Watson, K.M.: Charged-particle scattering in the presence of a strong electromagnetic wave. Phys. Rev. A **8**, 804 (1973)
8. Tsytovich, V.N., Oiringel, I.M. (eds.): Polarization Bremsstrahlung. Plenum Press, New York (1991)
9. Francken, P., Attaourti, Y., Joachain, C.J.: Laser-assisted inelastic electron-atom collisions. Phys. Rev. A **38**, 1785 (1988)
10. Astapenko, V.A.: Polarization-interference effects in the bremsstrahlung of quasiclassical electrons on ions with a core. JETP **88**, 889 (1999)
11. Astapenko, V.A.: Polarization-induced resonances in the stimulated bremsstrahlung spectrum of quasi-classical electrons scattered by multiply charged ions. Laser Phys. **8**, 1167 (1998)

12. Astapenko, V.A., Kukushkin, A.B.: Interference of stimulated static and polarization bremsstrahlung in electron–ion collisions in a strong laser field: line shape asymmetry and dips. Laser Phys. **8**, 552 (1998)
13. Messiah, A.: Quantum Mechanics. North-Holland, New York (1961)
14. Bunkin, F.V., Kazakov, A.E., Fedorov, M.V.: Interaction of intense optical radiation with free electrons (nonrelativistic case). Sov. Phys. Usp. **15**, 416 (1973)
15. Buimistrov, V.M., Trakhtenberg, L.I.: Free electron transition and light amplification. Opt. Commun. **8**, 289 (1973)
16. Zon, B.A.: Bremsstrahlung in collisions between electrons and atoms. Sov. Phys. JETP **46**, 67 (1977)
17. Rizzo, J.E., Klewe, R.C.: Optical breakdown in metal vapours. Br. J. Appl. Phys. **44**, 1137 (1966)
18. Weingartshofer, A., et al.: Direct Observation of multiphoton processes in laser-induced free-free transitions. Phys. Rev. Lett. **39**, 269 (1977)
19. Beilin, E.L., Zon, B.A.: On the sum rule for multiphoton bremsstrahlung. J. Phys. B **16**, L159 (1983)
20. Kruger, H., Jung, C.: Low-frequency approach to multiphoton free-free transitions induced by realistic laser pulses. Phys. Rev. A **17**, 1706 (1978)
21. Wallbank, B., Holmes, J.K.: Laser-assisted elastic electron-atom collisions. Phys. Rev. A **48**, R2515 (1993)

Chapter 11
Review of Possible PBs Applications for Structure Diagnostics and as an Effective Source of X-ray and UV Radiation

11.1 Procedure of Nanomaterial Diagnostics Based on PBs Spectroscopy

11.1.1 General Principles of Spectroscopy Based on PBs

Since polarization bremsstrahlung can be interpreted as scattering of virtual photons of a charged particle to a real photon by target electrons, PBs spectroscopy is in essence the generalization of ordinary spectroscopy and therefore has a number of features inherent in the latter. When the velocity of a charged particle approaches the velocity of light, this analogy becomes more exact since the electromagnetic field of a relativistic charge is close to the electromagnetic field of a real photon (a plane electromagnetic wave). One of manifestations of the said analogy is the Bragg condition for scattering of a virtual photon by crystal structures agreeing with the ordinary Bragg condition if it is considered that the wave vector of a virtual photon is directed along the velocity of an incident particle.

At the same time there is a number of distinctive properties in PBs spectroscopy that are connected first of all with the fact that the eigenfield of an incident particle has a continuous spectrum of virtual photons, and the dispersion law for a virtual photon differs from the dispersion law for a real photon. This allows obtaining a momentary "scan" of a recorded spectrum by all frequencies and wave vectors permitted by the energy conservation law. So instead of multiple spectral measurements by methods of ordinary spectroscopy, it is possible to carry out one measurement with the use of PBs spectroscopy that will contain the same or even greater body of information on an object under study.

From the practical point of view, an important distinction between PBs spectroscopy and traditional spectroscopy consists also in the fact that sources of fast electrons having in their electromagnetic field a wide set of virtual photons, as a rule, are more accessible than generators of real photons. This is especially true if the case in point is generation electromagnetic radiation in a wide spectral range including the X-ray wavelength range.

V. Astapenko, *Polarization Bremsstrahlung on Atoms, Plasmas, Nanostructures and Solids*, Springer Series on Atomic, Optical, and Plasma Physics 72,
DOI 10.1007/978-3-642-34082-6_11, © Springer-Verlag Berlin Heidelberg 2013

The next important distinguishing feature of the polarization spectroscopy method is a possibility of local excitation of a sample on the spatial scale much lesser than the wavelength of the optical range. Thus it is possible to increase considerably spatial resolution in comparison with traditional diffraction-limited spectroscopy.

Another important circumstance considerably enhancing the capabilities of PBs spectroscopy in comparison with traditional spectroscopy consists in the fact that the electromagnetic eigenfield of a charged particle contains a set of virtual photons with different angular momenta. It will be recalled that the angular momentum of a real photon is equal to one (in units of the Planck constant). This allows excitation of dipole-forbidden and intercombination transitions in a target under study that are inaccessible for investigation by traditional methods. Such an example is investigation of singlet-singlet transitions at NV (nitrogen-vacancy) centers in diamond samples that can not be exited by optical methods from the ground triplet state.

11.1.2 Recommendations for the Use of PBs Spectroscopy

The recommendations for development of a procedure of material diagnostics based on PBs spectroscopy are based on theoretical and experimental investigations carried out in the works of the last decade. The obtained expressions for intensity of PBs of fast electrons scattered by different types of targets, including single-crystal, polycrystalline, amorphous, cluster, nanostructured, two-dimensional targets, make it possible to determine a region of parametric variation, in which the use of PBs spectroscopy is most efficient as well as a procedure itself for investigation of structural, electronic and other properties of targets.

One of general recommendations for development of methods of nanomaterial diagnostics with the use of PBs following from theoretical consideration is a condition for a spectral region, in which the measurements of PBs spectra should be carried out. The optimum spectral range corresponds to the spectral maximum of the dynamic polarizability of atoms forming a target, which occurs usually near eigenfrequencies of target excitation or near thresholds of atomic ionization. Necessary information on dynamic polarization can be obtained on the basis of experimental data on photoabsorption with the use of the optical theorem and the Kramers-Kronig relations. In case of cluster targets, the use of quantum-chemical methods of calculation for the analysis of the electronic and spatial structure of a target is efficient. The most optimum approach for such a calculation is based on the density functional theory with the use of the hybrid three-parameter exchange Becke functional with the correlative Lee-Yang-Parr functional (B3LYP functional).

Another general recommendation in development of PBs spectroscopy methods consists in the fact that in spectral ranges corresponding to excitation of characteristic radiation PBs will be completely masked by it. Therefore, when choosing frequency ranges to record PBs, it is necessary to avoid proximity to characteristic peaks.

The recent works [1, 2], have allowed the development of experimental methods of nanomaterial diagnostics based on the use of a scanning electron microscope and photodetectors of different types for recording spectra in a wide spectral range.

The use of a scanning electron microscope makes it possible to realize the important advantage of PBs spectroscopy in comparison with traditional spectroscopy – high spatial resolution in investigation of nanostructures and usual materials. Scanning the surface of a sample allows obtaining a two-dimensional "PBs-image" of an object for short time intervals. Besides, the developed technology of scanning microscopy makes it possible to handle micro- and nanoobjects easily, which is an important advantage in nanostructure diagnostics.

The developed experimental procedure allows carrying out measurements in a wide temperature range, which is important in the presence of a strong electron–phonon or electron-vibron coupling in a target material as it is, for example, in case of NV centers in diamond samples that are promising for many applications of optical informatics.

PBs spectroscopy for investigation of nanomaterials (clusters, fullerenes, quantum dots, nanocoatings, metamaterials with different nanoinclusions, etc.) can be developed in the X-ray, UV, visible, and IR wavelength ranges with the use both of nonrelativistic and relativistic electron beams. PBs spectroscopy and spectroscopy of related radiative processes (ordinary Bs, transition radiation, cathode luminescence) assumes obtaining information on the structure and physical properties of a target not only on the basis of recording spectral regularities, but also by taking angular, velocity, and orientation dependences of radiation.

In investigation of the structure and physical properties of nanoinclusions in metamaterials (metal and semiconductor nanospheres, nanorods, nanodisks, etc.) it seems advisable to carry out measurements of PBs in the visible and near-UV spectral regions, where the photon energy varies from 2 to 6 eV. In this range polarization bremsstrahlung is formed due to excitation of surface plasmons [3]. For example, in case of silver nanospheres with a radius from several nanometers to several tens of nanometers the plasmon resonance lies in a photon energy range from 2.4 to 3 eV. The central frequency of the plasmon resonance is shifted to the region of lower photon energies with increasing size of a metal nanoparticle. The spectral width of the resonance in this case increases in connection with decreasing time of plasmon dephasing. Since the plasmon frequency is defined by the concentration of electrons in a target, it seems hardly probable to obtain its shift with changing target temperature. At the same time the width of the spectral resonance that depends on scattering of plasmons in a sample can show the temperature dependence. The optimum value of the electron beam energy for observation of PBs on metal clusters near the maximum of the frequency dependence, as a rule, is less than 100 eV. This value is 2 times less than the minimum energy of electrons in the Quanta 200 SEM (FEI).

PBs spectroscopy for investigation of a C_{60} fullerene should be carried out in two frequency ranges: in the low-frequency range (wavelength is 200–300 nm), where dipole-allowed transitions with highest oscillator strengths are concentrated, and

near the plasmon resonance energy ($\hbar\omega = 19\,\text{eV}$). In the latter case the maximum PBs cross-section is achieved at the electron energy of 167 eV. With growing electron beam energy the position of the spectral maximum is shifted to the region of high photon energies.

X-ray spectroscopy of PBs of structured nanomaterials for a case of nonrelativistic electrons is based on measurement of spectra peculiarities connected with the presence of optimum conditions for conversion of the IP eigenfield to a bremsstrahlung photon on the target structure. In case of a polycrystalline medium the structure of a target is defined by the crystal lattice of a sample material. Then the peculiarities of the PBs spectrum show themselves as a sawtooth structure reflecting "turning-off" of the contribution of the reciprocal lattice vector to the process, which is caused by the law of conservation of energy-momentum in coherent interaction (see Fig. 5.3 of this monograph). The energy of the first "tooth" of the spectral dependence is about 1.5 keV, it is defined by the spatial scale of the structure and the velocity of an incident particle. To find out this structure experimentally, it is necessary to use a photodetector with a resolution no more than 10 eV.

In case of a relativistic electron, in the spectrum of PBs on a structured target maxima appear with fulfilment of the Bragg condition describing scattering of a virtual photon of the IP eigenfield to a real bremsstrahlung photon (see Fig. 5.8 and the formula (5.18) of this book). The width of these peaks is proportional to the cotangent of the half-angle of radiation, so the PBs intensity is maximum in back radiation, which defines the requirement to the optimum conditions of the experiment [4].

11.1.3 PBs Spectroscopy of Nanoobjects

According to the results of carried out investigations and literature data, in scattering of relativistic electrons by fullerenes in the PBs spectrum in the X-ray range radiation intensity oscillations caused by interference effects should be observed. The period of these oscillations is defined by the IP velocity, the radiation angle and the fullerene radius, and the amplitude is defined by the electron energy [5]. Therefore it is possible to determine the size of a nanotarget by the PBs spectrum with specified parameters of scattering.

The peculiarities of PBs of fast charged particles on clusters in the X-ray spectral range are defined by cooperative effects in summation of process amplitudes from different atoms forming the cluster. In the carried out investigations it was shown that with growing IP energy the maximum of the spectral distribution of PBs on a cluster is shifted to the region of high frequencies. The form of the high-frequency part of the spectrum in the relativistic case strongly depends on the radiation angle. With reduction of this angle the Bs intensity decreases with growing frequency much more slowly than for wide angles. The analysis of the Bs intensity

as a function of IP velocity has shown that in the nonrelativistic case this dependence can be of different nature. In the limit of low IP velocities the role of cooperative effects in Bs on a cluster becomes negligible. The obtained results can be used in interpretation of experimental data on Bs of fast charged particles on clusters in the X-ray frequency range and in development of methods of investigation of the atomic cluster structure with the use of PBs.

The theoretical investigations carried out for the analysis of emission of fast electrons scattered by graphene [6] have laid the foundation for development of a PBs spectroscopy procedure in diagnostics of two-dimensional crystal structures. As shown in the Sect. 8.3 of this book, the spectrum of coherent PBs on graphene contains sharp peaks corresponding to transfer of a momentum proportional to one of the reciprocal lattice vectors to the two-dimensional crystal lattice. The relationship of the frequency of these maxima with the electron velocity and the angle of incident electron as well as with the angle of emission of a bremsstrahlung photon and the magnitude of the reciprocal lattice vector in the general case is given by the formulas (8.64), and (8.65), and in case of normal incidence of an electron on the graphene surface it is given by the formulas (8.64), (8.66). The obtained relationship makes it possible by known kinematic problem parameters to determine the parameters of a two-dimensional crystal structure, on which scattering and emission of electrons occurs, that is, to carry out target diagnostics. The condition of appearance of sharp maxima in the spectrum of coherent PBs is given by the inequations (8.68), from which it follows that for recording these spectral peaks two conditions should be satisfied: emission of a bremsstrahlung photon should be directed to the forward hemisphere, and the electron velocity should be high enough, though not necessarily relativistic. As follows from Fig. 8.20 of this monograph, at a radiation angle of 30° the electron energy of 58 keV is sufficient for appearance of sharp maxima in the spectrum of coherent PBs on graphene that can be used for target diagnostics. Thus it can be concluded that for diagnostics of PBs on two-dimensional structures the use of a transmission electron microscope for recording forward radiation and the use of electrons of high enough energy are optimum.

11.1.4 Diagnostics of Fine-Grained Media

The analysis of possibilities of fine-grained media diagnostics based on measurement of the spectrum of PBs of a fast electron was carried out in the work [7]. In motion of such an electron through a fine-grained medium the mechanism of Bragg scattering of the Coulomb field is not realized because of a small grain size. Under considered conditions the main thing is coherent scattering on a grain as a whole. This scattering is most efficient in a frequency-angular region, in which the length of radiation forming exceeds the grain size. Under considered conditions the use of the dipole approximation for the tensor of the photon Green function in a medium is more adequate. In the work [7] the following expression for PBs in a fine-grained

medium was obtained (here and further the velocity of light is assumed to be equal to one):

$$\omega\frac{dN}{dtd\omega d\Omega}=\frac{e^2}{\pi}n_c\ \omega^4|\alpha(\omega)|^2 \times\int\limits_{\sin\left(\frac{\theta}{2}\right)}^{\infty}\frac{dx\ x\exp(-4\omega^2u_T^2\sin^2\left(\frac{\theta}{2}\right)x^2)}{\left(1+4\omega^2R^2\sin^2\left(\frac{\theta}{2}\right)x^2\right)^2} \times\left[\overline{|T(k)|^2}-\frac{4\pi n_c}{k}\int\limits_0^{\infty}dr\ r(1-W(r))\sin(kr)\left|\overline{T(k)}\right|^2\right]f(\theta,\rho,x), \tag{11.1}$$

where

$$f(\theta,\rho,x)= =\left[\frac{1+\cos^2\theta}{\sqrt{(x^2-1)^2+\rho^2ctg^2\left(\frac{\theta}{2}\right)}}-2\sin^2\left(\frac{\theta}{2}\right)\left(1-\frac{x^2-1}{\sqrt{(x^2-1)^2+\rho^2ctg^2\left(\frac{\theta}{2}\right)}}\right) -\frac{\rho^2ctg^2\left(\frac{\theta}{2}\right)\cos^2\theta}{\left((x^2-1)^2+\rho^2ctg^2\left(\frac{\theta}{2}\right)\right)^{\frac{3}{2}}}\right]$$

is the auxiliary function , $T(\mathbf{k})=\sum\limits_n e^{i\,\mathbf{kr_n}}$ is the structure factor of a grain ($\mathbf{r}_n$ is the coordinate of the n^{th} atom in the grain), n_c is the grain density, $W(r)$ is the pair correlation function describing the probability of the centers of two grains being at the distance r (it is obvious that $W(r)=0$ at $r<L$ and $W(r)\to 1$ at $r>>L$, L is the characteristic grain size), $\rho=\sqrt{\gamma^{-2}+\left(\omega_p/\omega\right)^2}$ (γ is the relativistic factor, ω_p is the plasma frequency of the medium), the viewing angle θ exceeds ρ, the line in (11.1) means averaging over orientations of grains, $k=2\,\omega\,\sin(\theta/2)x$.

The formula (11.1) makes it possible to propose a new method of determination of the grain size by the position of a maximum in the spectrum of the coherent PBs peak (the maximum arises due to the multiplier ω^4 on the right side of Eq. 11.1 that suppresses the radiation yield in the region of small ω, in which the polarizability is $\alpha(\omega)\approx const$). For simplicity, let us consider a grain in the form of a cube, along the edge of which N atoms are located, the distances between which are equal (see Fig. 11.1).

In the case under consideration the value $\overline{|T(\mathbf{k})|^2}$ can be represented as $\overline{|T(\mathbf{k})|^2}=N^3T_N$, where

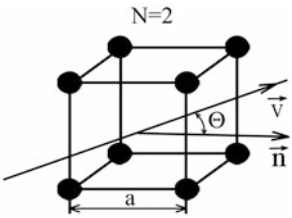

Fig. 11.1 The geometry of the process

$$T_N = 1 + \frac{6}{N}\sum_{j=1}^{N}(N-j)\eta(j) + \frac{12}{N^2}\sum_{j=1}^{N}(N-j)\sum_{l=1}^{N}(N-l)\eta(\sqrt{j^2+l^2}) +$$
$$+ \frac{8}{N^3}\sum_{j=1}^{N}(N-j)\sum_{l=1}^{N}(N-l)\sum_{p=1}^{N}(N-p)\eta(\sqrt{j^2+l^2+p^2}), \qquad (11.2)$$

and

$$\eta(\sqrt{j^2+i^2+p^2}) = \frac{\sin(2\omega\, a \sin(\theta/2)\sqrt{j^2+i^2+p^2}x)}{2\omega\, a \sin(\theta/2)\sqrt{j^2+i^2+p^2}x}.$$

The spectrum of PBs of 50 MeV electrons in fine-grained monodisperse tungsten calculated by the formulas (11.1) and (11.2) without considering correlations between grains ($W(r) = 1$) is given in Fig. 11.2 for the viewing angle $\theta = 0.3$ rad and three different values N.

The clear dependence of the position of a maximum in the spectrum on the size of a grain is seen. It is necessary to note very strong influence of dispersion of the dielectric susceptibility $\chi(\omega) = 4\pi\, n_c\, \alpha(\omega)$ on the form of the spectrum. To eliminate this influence, in the work [7] the function was analyzed:

$$\Phi(\xi, N) = \left(\frac{\sin^2(\theta/2)}{\omega\, a|\chi(\omega)|^2}\right) \times \frac{dN}{dtd\omega d\Omega} = \left(\frac{e^2}{64\pi^3}\right)\frac{\xi^2 P(\xi)}{N^3},$$

where $\frac{dN}{dtd\omega d\Omega}$ is the value measured in the experiment, $\xi = 2\,\omega\, a \sin(\theta/2)$, $P(\xi)$ is the integral on the right side of the Eq. 11.1.

Given in Fig. 11.3 are the curves of the dependence $\Phi\,(\xi, N)$ constructed by the formula (11.1) for fixed values of the viewing angle $\theta = 0.8$ rad and the parameter $\rho = 0.01 \approx \gamma^{-1}$, but for different values N. According to Fig. 11.3, the proposed method allows discerning grains of rather close sizes.

It is significant that the dielectric susceptibility $\chi(\omega)$ of a medium included in the function $\Phi(\xi, N)$ was determined experimentally in a wide range of frequencies for many elements, so it is possible to avoid model distortions of $\chi(\omega)$ in experimental data processing.

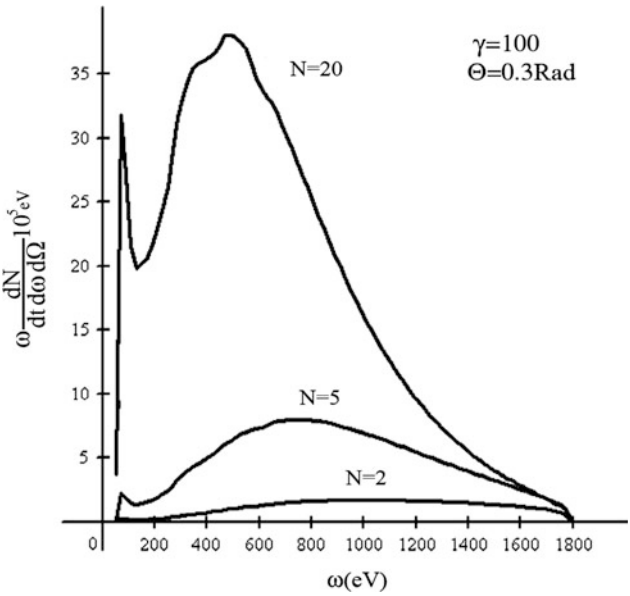

Fig. 11.2 The dependence of the spectrum of the coherent peak of PBs in fine-grained tungsten on the size of a grain. The electron energy is 50 MeV. The radiation angle is $\theta = 0.3$ rad [7]

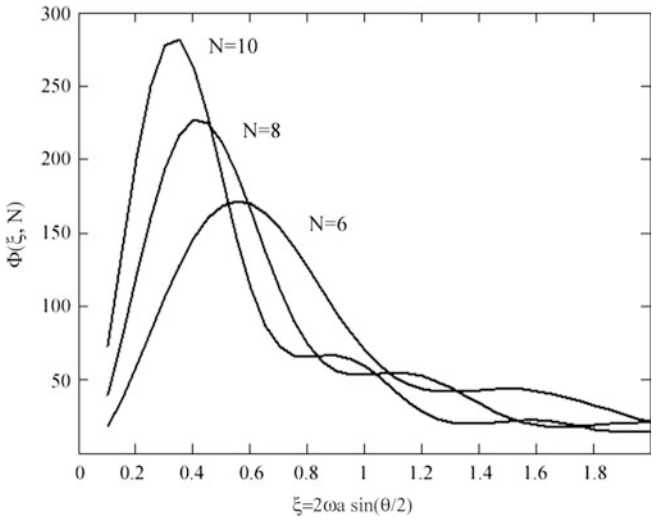

Fig. 11.3 The dependence of the position of a maximum in the spectrum of the modified PBs peak on the size of a grain [7]

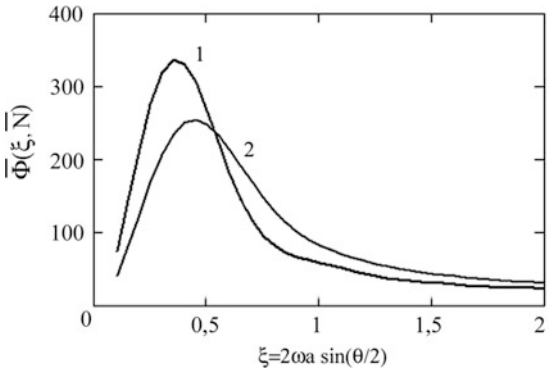

Fig. 11.4 The influence of the spread of grains in values on the position of a maximum in the spectrum of the modified PBs peak. The curves are calculated with the fixed value $\sigma = 3$ and different values $\bar{N}$. *Curve 1* corresponds to the value $\bar{N}$, *curve 2* corresponds to the value $\bar{N} = 6$

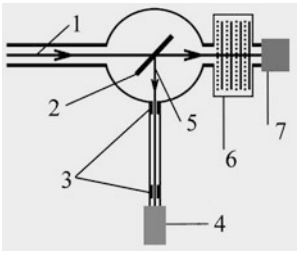

Fig. 11.5 The scheme of the experiment on diagnostics of the structure of a polycrystal based on PBs. *1* electron beam; *2* target; *3* collimators; *4* detector; *5* radiation; *6* proportional chamber; *7* Faraday cup

In real materials grains always have a spread both in values and in form. To estimate the sensitivity of the method to a medium size of a grain in a polydisperse material, the dependence was calculated:

$$\bar{\Phi}(\xi, \bar{N}) = \sum_{N \geq 1} \Phi(\xi, N) \frac{1}{\sqrt{\pi}\sigma} \exp\left(- \frac{\left(N - \bar{N}\right)^2}{\sigma^2} \right),$$

simulating PBs in a material with the Gaussian distribution of grains by sizes. The results of the calculation presented in Fig. 11.4 are indicative of retention of high sensitivity even for relatively high dispersion of the distribution.

The possibilities of the discussed method of diagnostics were checked experimentally by the example of scattering of the Coulomb field of relativistic electrons in polycrystalline media [7]. The scheme of the experiment is shown in Fig. 11.5 for the case that the angle between the velocity of a radiating electron and the direction of PBs photon escape is 90°.

In the experiments the electron beam current was measured, which allowed carrying out absolute measurements of radiation yield. The electron guide, the target chamber, and the photon channel for recording PBs were located in vacuum, which made it possible to avoid distortions of the measured photon spectrum photons due to absorption in air. The results of these experiments are presented in Fig. 11.6 for scattering of electrons with the energy of 7 MeV by an aluminum foil.

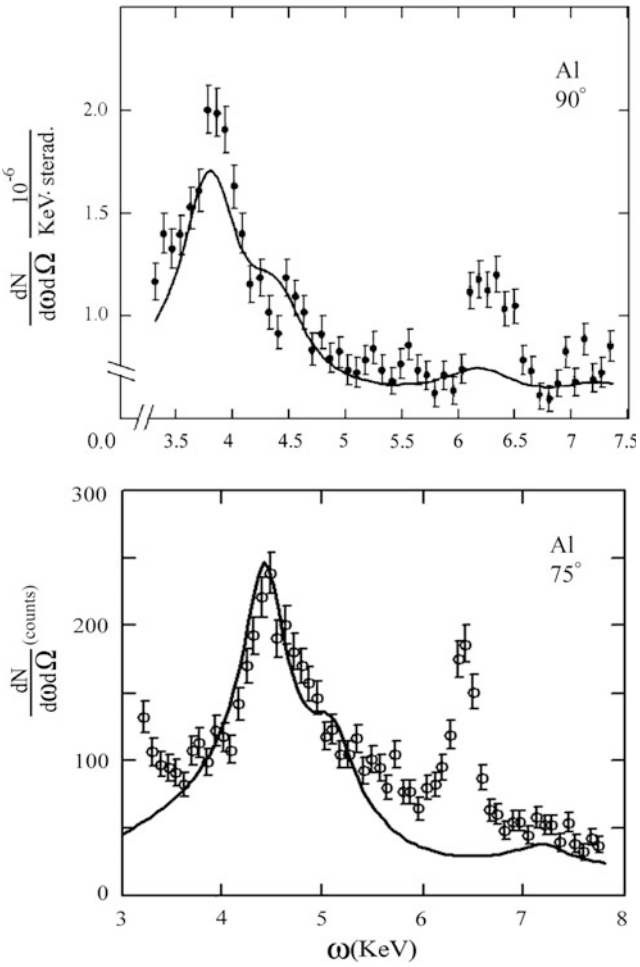

Fig. 11.6 The dependence of the position of a maximum in the spectrum of the coherent peak of PBs in an aluminum polycrystal with an effective thickness of 14 μm on the radiation angle. The electron energy is 7 MeV

The dependence of the position of a maximum of the coherent peak on the radiation viewing angle following from the theory developed in [7] was checked. Presented in Fig. 11.6 are the measured and calculated spectra of PBs from an aluminum film collimated at angles of 90° and 75°. The agreement of these measurements with theoretical predictions is seen, which proves the prospects for using the dependence of the position of the structural peak of PBs of relativistic electrons in polycrystals for identification of such peaks. The proposed method of measurement of sizes of grains in fine-grained media can be used in the nanomaterial industry.

11.2 Prospects for Using PBs for Development of Efficient Sources of X-radiation and UV Radiation

11.2.1 Near-Resonance PBs on Multiply Charged Ions with an Electron Core

As is known, a significant obstacle to development of laser sources of X-radiation is short lifetime of the upper operating level in a multiply charged ion.

In case of traditional lasers there should be real population of the upper operating level. The main idea of using near-resonance PBs of electrons (see the Sect. 2.42) on multiply charged ions as a source of short-wave radiation is that in this case real population of exited energy levels of ions is not required since radiation occurs as a result of *virtual* excitation of a target.

Near-resonance PBs with the frequency ω on an isolated atomic particle arises in fulfilment of the condition

$$\delta_{nf} << \left|\omega - \omega_{nf}\right| << \omega, \tag{11.3}$$

where ω_{nf} and δ_{nf} are the eigenfrequency and the width of the line of the transition $n \to f$ between two states of the discrete spectrum of the atomic core of an atom (ion). Since radiation frequency detuning is much higher than the transition line width, real population of the level $|f\rangle$ can be neglected.

The expression for the cross-section of near-resonance PBs in case of homogeneous broadening of the dipole-allowed transition with the oscillator strength $f_0 \neq 0$ on an atom is given by the formula (3.34) for a nonrelativistic incident particle.

The spectral cross-section of near-resonance PBs of a relativistic electron ($v \simeq c$, v is the electron velocity) in the Born-Bethe approximation is:

$$\frac{d\sigma^{res}}{d\omega} = \frac{4}{3}\frac{e^2}{\hbar c}\frac{r_e^2 f_0^2 \omega_0}{(\omega_0 - \omega)^2 + \delta_0^2}\ln\left(\frac{\gamma c}{\omega r_a}\right), \tag{11.4}$$

where $r_e = e^2/mc^2 \approx 2.8 \cdot 10^{-13}$ cm is the classical electron radius, γ is the Lorenz factor of an electron, r_a is the characteristic radius of the electron core of an atom (ion).

It should be noted that the formula (11.4) is true in fulfilment of the inequation

$$\omega < \frac{\gamma c}{r_a},$$

when the Born-Bethe approximation "works".

As an example of using the formula (11.4), we will consider an elementary case of PBs of a relativistic electron on a hydrogen-like ion (with the nuclear charge Ze) with natural broadening of a spectral line (the line width is defined by the Einstein

coefficient for spontaneous emission of radiation $\delta_0 = A_n$) for the near-resonance transition $1s \rightarrow np$ ($1s$ is the ground state, n is the principal quantum number of an exited state).

Then it is possible to use the analytical expressions for all values included in the formula (11.4). The oscillator strength of the transition under consideration is:

$$f_0 = f_n = n^5 \frac{2^8 (n-1)^{2n-4}}{3 (n+1)^{2n+4}}, \tag{11.5}$$

the eigenfrequency of the transition (in atomic units) is

$$\omega_0 = \omega_n = Z^2 \frac{n^2 - 1}{2 n^2}, \tag{11.6}$$

the width of the near-resonance transition line is

$$\delta_0 = A_n = Z^4 \frac{2^7 n (n-1)^{2n-2}}{9 (137)^3 (n+1)^{2n+2}}, \tag{11.7}$$

and the characteristic radius of the electron core in the exited state is $r_a \sim r_n = n^2 a_B/Z$ (a_B is the Bohr radius). It should be noted that the oscillator strength of a hydrogen-like ion (Eq. 11.5) does not depend on a nuclear charge.

From comparison of the formulas (11.6) and (11.7) it is seen in particular that with growing charge of the nucleus of a hydrogen-like ion in the considered case of natural broadening the line width grows faster than the eigenfrequency of the transition: $A_n/\omega_n \propto Z^2$.

Presented in Fig. 11.7 are the diagrams of the spectral cross-section of near-resonance PBs calculated by the formulas (11.4), (11.5), (11.6), (11.7) for $n = 2$ (the α-line of the Lyman series), $\gamma = 100$, and different charges of the nucleus of a hydrogen-like ion: Z 6, 10, 28. The logarithmic scale on both axes is used.

It should be noted that for Z 6 the resonance frequency is 367.2 eV, for Z 10 it is 1.02 keV and for Z 28 it is about 8 keV. In this case the natural line widths are respectively: $5.35 \cdot 10^{-4}$ eV, $4.13 \cdot 10^{-3}$ eV and 0.254 eV. Following from Fig. 11.7 are rather high value of the cross-section of near-resonance PBs and a narrow spectral line.

Besides, it should be noted that the angular directivity of PBs of a relativistic electron in the considered spectral range $\omega < \gamma c/r_a$ is of a dipole nature in contrast to ordinary Bs directed to a narrow cone with the axis parallel to the vector of the relativistic electron velocity. This circumstance is rather important for the practical use of near-resonance PBs.

The above case corresponds to special experimental conditions, when it is possible to neglect all kinds of broadening, except for natural broadening caused by spontaneous radiation.

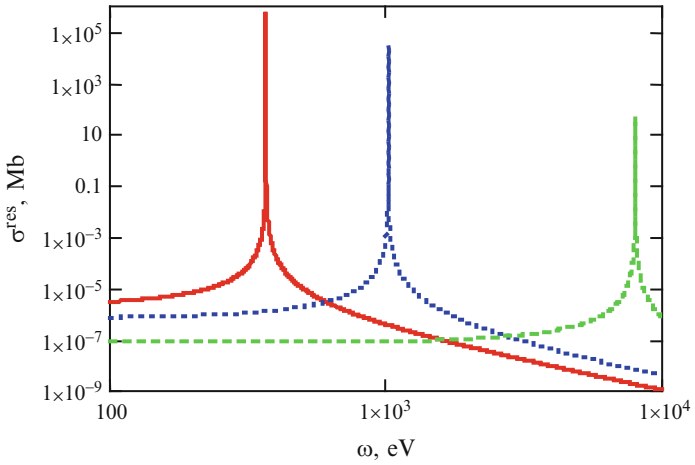

Fig. 11.7 The spectral cross-section of near-resonance PBs on a hydrogen-like ion calculated by the formula (11.4) for different nuclear charges: *solid curve* – Z 6, *dotted curve* – Z 10, *dashed curve* – Z 28

If PBs occurs on multiply charged ions in plasma, it is necessary to take into account a number of factors defining the form and width of the spectral line, such as the Doppler effect and the Stark effect. This requires a special consideration in each specific case, however, the main features of the spectral cross-section of near-resonance PBs will be retained, at least, at a qualitative level.

11.2.2 Resonance PBs in Crystals and Accompanying Radiative Processes

As was noted in Chap. 1 (see Table 1.2), coherent PBs of the X-ray range in crystals is called parametric X-radiation (PXR). This radiation has sharp spectral peaks in case of relativistic electrons and fulfilment of the Bragg condition for virtual and real photons (see the formula (5.18) and Fig. 5.8). The frequency of these spectral maxima is determined by the formula (5.9). The spectral-angular yield of PXR photons per unit trajectory length for an electron is given by the expression (5.8).

In contrast to the formula (5.8), in theoretical works on PXR (see, for example, the paper [8]) it is usually supposed that for the dynamic polarizability of an atom the high-frequency approximation can be used, when (see Appendix 1, the formula (A.16)):

$$\alpha_{\infty}(\omega) = -\frac{e^2 N_a}{m\,\omega^2}, \tag{11.8}$$

where N_a is the number of electrons in an atom. This is connected with the fact that in the X-ray range the frequency of radiation, as a rule, exceeds the

eigenfrequencies of atomic electrons, except for those that are most strongly bound with a nucleus. In other words, atomic electrons react to X-radiation as quasi-free charges.

It should be noted that the formula (11.8) is true in the dipole approximation, when radiation wavelength exceeds the average size of an atom. Otherwise X-ray photon (real or virtual) "knocks out" an electron from an atom. This takes place in the Compton effect and the collision ionization of atoms.

Using the formula (11.8) for description of PBs is equivalent to the approximation of dielectric permittivity of a medium by the plasma formula in the PXR theory, which "slurs over" the single physical nature of these radiative processes that practically describe the same phenomenon.

Experimentally, PXR was for the first time observed in the work [9] with the use of 900 MeV electrons that were generated at the "Sirius" synchrotron (Tomsk, Russia). As a target, a diamond crystal of thickness 0.08 cm was used. An electron beam was directed along the (100) axis of the crystal. The X-ray detector was located at the double Bragg angle $2\,\theta_B = 90^\circ$ with respect to the electron velocity vector $\mathbf{v}$ in the plane defined by the vectors $\mathbf{v}$ and τ, where the vector τ corresponded to the (220) crystallographic plane. For these conditions the photon spectrum recorded by the photodetector consisted of sharp maxima at frequencies multiples of photon energy of 6.96 keV. This set of resonance frequencies was determined by the formula [9]:

$$\omega_B^{(n)} = \frac{\pi\, n\, c}{d\, \sin\theta_B}, \tag{11.9}$$

where d is the distance between crystallographic axes on which conversion of a virtual photon of the electron eigenfield to a real PXR photon occurred, θ_B is the Bragg angle, $n = 1,\ 2,\ 3, \ldots$ is the natural number. (It will be recalled that the Bragg angle is determined by the equation $2\,d\,\sin\theta_B = n\,\lambda$, λ is the radiation wavelength).

As a result of the carried out experiment, the angular distribution of PXR photons was recorded that was in satisfactory agreement with predictions of the theory of this phenomenon [10].

In the dissertation [11] an extensive investigation of PXR was carried out to elucidate a possibility and optimum conditions of using this phenomenon for development of an efficient X-ray source convenient for a number of applications including medical ones.

Among medical applications, having a significant place is imaging of various organs with the use of a PXR source, specifically, mammography. In this connection, in the cited work a special emphasis was made on generation of X-radiation with the energy of 18 keV that is most convenient for mammographic purposes.

The comparison of the quality of X-radiation obtained with the use of a standard mammography device and PXR is presented in Table 11.1.

Used for comparison was electromagnetic radiation with an average energy of 17.5 eV, the distance from the source to the receiver, both placed in the vacuum

Table 11.1 Comparison of PXR and mammography device X-radiation qualities [11]

Quality	PXR	Mammography device
Energy tunability	Continuous	None
Polarized	Yes	No
Directionality	$1/\gamma$ 8.5 mrad	262 mrad
Limit of energy width	Photon lifetime	K_α transition
Yield [photon/e/cm^2]	$2{\cdot}10^{-6}$	$3{\cdot}10^{-8}$

chamber, was 50 cm. PXR was calculated for electrons with an energy of 60 MeV and a silicon target of thickness 500 μm with diffraction of virtual photons on the (220) crystallographic plane. Radiation from the mammography device was calculated by the Monte-Carlo method for electron energy of 30 keV and a molybdenum anode placed at an angle of 15° to the electron beam.

Used in a standard X-ray source is a rather large flow of electrons (an electric current of the order of several mA) that, colliding with the anode, cause characteristic radiation and bremsstrahlung of a target. To image, characteristic radiation is used that results from radiation filling of a vacancy in the inner atomic shell produced by an incident electron.

Bremsstrahlung is an accompanying process. In case of nonrelativistic electrons it has a broad pattern and, as a result, produces a background with a wide spectrum, an effect of which on living tissues may be adverse.

Thus from the point of view of practical application a PXR source has the following advantages in comparison with a standard mammography device: a possibility of X-ray photon energy tuning, specified polarization of radiation, narrow spectral-angular distribution, minimum bremsstrahlung background, and high photon yield.

From the above it follows that in the context of medical applications, such as imaging of a living organ, PXR improves an image contrast, reduces a radiation doze received by a patient. The last circumstance is connected with a possibility to obtain PXR photons of optimum energy for specified parameters of an organ under study [12].

11.2.2.1 Accompanying Radiative Processes

In scattering of relativistic electrons in a crystal, besides PXR and characteristic radiation, other types of radiative processes also occur [13]: coherent Bs, transition radiation, channeled electron radiation, Cherenkov radiation.

Given in Table 11.2 is the comparison of three types of radiation from the above-listed types.

Coherent ordinary bremsstrahlung is not considered here since for this bremsstrahlung much higher photon energy is characteristic.

Cherenkov radiation, on the contrary, is generated in a more long-wave range than the X-ray range. For its generation the fulfilment of the condition

Table 11.2 Comparison of three types of radiation [11]

Source	Bandwidth $\Delta\omega/\omega$	Emission direction	Energy tunability	Emission cone	Intensity [ph/s/mrad^2/1%bw]
Transition radiation	50 %	Forward	Not practical	γ^{-1}	10^8
Channeling radiation	10 %	Forward	Not practical	$\gamma^{-1}/3$	10^8
PXR	1 %	$2\,\theta_B$	Simple	γ^{-1}	10^8

$n(\omega) > c/\mathrm{v}$ (v is the electron velocity) is necessary, where $n(\omega)$ is the refractive index of a medium at a specified frequency that for X-rays is of the order of one and less than one.

11.2.2.2 Transition Radiation

Transition radiation (TR), by analogy with PBs, can be also considered as scattering of the eigenfield of a charged particle by inhomogeneities of dielectric permittivity of a medium. In case of TR arising at the media interface, reflection or refraction of a virtual photon of the charge eigenfield with conversion to a real photon takes place.

Thus PBs and TR belong to the same class of radiative processes that can be interpreted as conversion of a virtual photon of the eigenfield of a charged particle to a real photon either on atomic particles (PBs) or on optical inhomogeneities of a medium (TR).

The formula for the spectral-angular distribution of energy of transition radiation arising in case of incoming of a charged particle from vacuum ($\varepsilon_1 = 1$) into a substance with the dielectric permittivity $\varepsilon_2 = \varepsilon$ at a right angle to the flat surface (Fig. 11.8) looks like:

$$\frac{d\mathrm{E}_{\mathrm{tr}}^{(\mathrm{b})}}{d\omega d\Omega_k} = \frac{e^2\beta^2\sin^2 2\chi}{4\pi^2 c(1-\beta^2\cos^2\chi)^2}\left|\frac{(\varepsilon-1)\left(1-\beta^2+\beta\sqrt{\varepsilon-\sin^2\chi}\right)}{\left(1+\beta\sqrt{\varepsilon-\sin^2\chi}\right)\left(\varepsilon\cos\chi+\sqrt{\varepsilon-\sin^2\chi}\right)}\right|^2, \tag{11.10}$$

where ε is the dielectric permittivity of a medium, $\mathbf{k}$ is the photon wave vector, $\beta = \mathrm{v}/c$, $\mathbf{v}$ is the particle velocity, e is the particle charge, χ is the angle between the vectors $\mathbf{k}$ and $-\mathbf{v}$.

The formula (11.10) is obtained within the framework of classical electrodynamics in view of boundary conditions for intensity of the total electric field (charge field and radiation field) and the vector of electric induction at the media interface.

Transition radiation is polarized in the plane set by the electron velocity vector and the wave vector of an emitted photon.

The frequency dependence of transition radiation energy (11.10) is defined by the frequency dependence of the dielectric permittivity of a medium $\varepsilon(\omega)$. In the

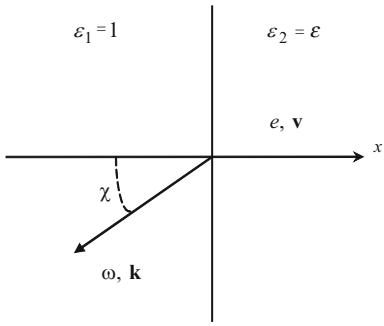

Fig. 11.8 Transition radiation in normal incidence of a charged particle on the vacuum/substance interface

high-frequency limit, when $\varepsilon \to 1$, the transition radiation energy tends to zero according to the expression (11.10). Really, in the case $\varepsilon = 1$ the interface disappears, and along with it transition radiation disappears too.

Let us consider limiting cases of the expression (11.10) that admit simple analytical representation. At the interface of vacuum with an ideal conductor $|\varepsilon| = \infty$, and the formula (11.10) is simplified to the form

$$\frac{d\mathrm{E}_{tr}^{(b)}}{d\omega d\Omega_{\mathrm{k}}} = \frac{e^2\ \beta^2\ \sin^2\ \chi}{\pi^2\ c(1 - \beta^2\ \cos^2\ \chi)^2}. \tag{11.11}$$

It should be noted that the right side of the Eq. 11.11 formally does not depend on frequency. Actually, the frequency boundary of applicability of this expression is defined by a spectral range, in which a medium can be considered to be an ideal conductor.

Shown in Fig. 11.9 is the angular distribution of transition radiation calculated by the formula (11.11) for different values of the parameter $\beta = \mathrm{v}/c$. The Y-axis is plotted in atomic units in the logarithmic scale. It is seen that in the nonrelativistic case ($\beta = 0.6$) the maximum of the angular dependence of radiation falls on $\chi\ 90^\circ$. With growing particle velocity the TR maximum is shifted to the region of small angles χ. In the ultrarelativistic limit radiation is directed antiparallel to velocity, that is, $\chi\ 0$. It should be noted that in this limit the charge electromagnetic field is similar to the plane wave field, and the said angular dependence of TR corresponds to reflection of the particle eigenfield back from the interface in case of normal incidence as it would be in reflection of a free electromagnetic field according to the Snell law.

From Fig. 11.9 it follows also that the intensity of transition radiation increases with charge energy. For nonrelativistic velocities intensity grows linearly with energy as it follows from the formula (11.11).

For high velocities, when $\gamma >> 1$ and transition radiation is mainly directed antiparallel to velocity ($\chi\ < 1$), the formula (11.10) can be represented as

$$\frac{d\mathrm{E}_{tr}^{(b)}}{d\omega d\Omega_{\mathrm{k}}} = \frac{e^2}{\pi^2 c}\left|\frac{\sqrt{\varepsilon} - 1}{\sqrt{\varepsilon} + 1}\right|^2 \frac{\chi^2}{\left[\chi^2 + \gamma^{-2}\right]^2}. \tag{11.12}$$

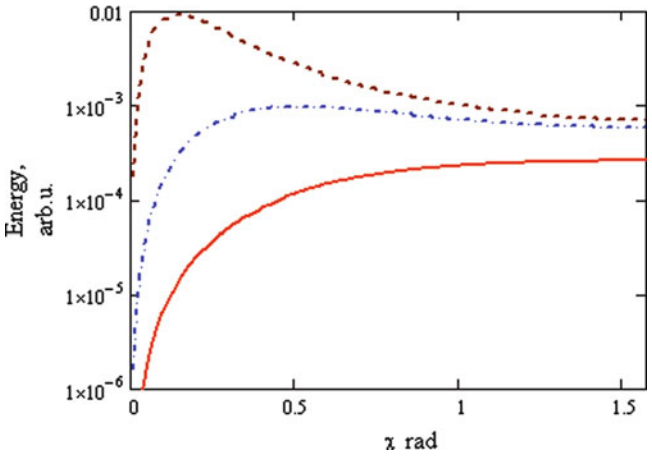

Fig. 11.9 The angular distribution of transition radiation energy in case of electron incoming from vacuum into an ideal conductor perpendicular to the interface for different electron velocities: *solid curve* – $\beta = 0.6$, *dash-and-dot curve* – $\beta = 0.9$, *dashed curve* – $\beta = 0.99$; $\beta = \mathrm{v}/c$

Hence it follows in particular that the width of the angular distribution of TR is of the order of $1/\gamma$ (see Table 11.2).

The energy of transition radiation of an ultrarelativistic particle integrated with respect to the angle (in case of incoming from vacuum into a substance) to the logarithmic accuracy is equal to

$$\frac{d\mathrm{E}_{tr}^{(b)}}{d\omega} = \frac{2e^2}{\pi c}\left|\frac{\sqrt{\varepsilon}-1}{\sqrt{\varepsilon}+1}\right|^2 1\mathrm{n}\gamma, \tag{11.13}$$

that is, increases with particle energy ($\gamma = E/mc^2$) logarithmically.

If the plasma formula for the dielectric permittivity of a substance $\varepsilon = 1-\left(\omega_p/\omega\right)^2$ is used, for frequencies $\omega >> \omega_p$ following from the formula (11.13) is the decrease of transition radiation energy with growing frequency as ω^{-4}. This means that the main contribution to back transition radiation is made by frequencies lower than the plasma frequency ω_p and of the order of it.

Thus TR of a charged particle with back radiation (Fig. 11.8) lies mainly in the visible and ultraviolet wavelength ranges.

Transition radiation in case of *escape* of a charged particle from a substance into vacuum (forward TR) is given by the formula analogous to Eq. 11.10, in which it is necessary to make the replacement $\beta \to -\beta$. In this case $\chi \to \theta$, where θ is the angle between the vectors **k** and **v** (the radiation angle).

In the ultrarelativistic limit $\beta = \mathrm{v}/c \to 1$ a corresponding expression for the spectral-angular distribution of forward TR takes the form

$$\frac{d\mathrm{E}_{tr}^{(for)}}{d\omega d\Omega_{\mathrm{K}}} = \frac{e^2\theta^2}{\pi^2 c}\left|\frac{\sqrt{\varepsilon}-1}{\left(\gamma^{-2}+\theta^2\right)\left(1-\beta\sqrt{\varepsilon^2-\theta^2}\right)}\right|^2, \tag{11.14}$$

where $\gamma = \left(1-(\mathrm{v}/c)^2\right)^{-1/2}$ is the relativistic factor. Hence it follows that transition radiation of an ultrarelativistic particle in case of escape from a medium into vacuum is concentrated in the region of small angles $\theta \le 1/\gamma$ along the direction of motion. The radiation energy in the region of *low frequencies* integrated with respect to the angle, when the dielectric permittivity differs noticeably from one, is

$$\frac{d\mathrm{E}_{tr}^{(for)}}{d\omega} = \frac{2e^2}{\pi c}\,1\mathrm{n}\gamma. \tag{11.15}$$

In the plasma dielectric permittivity model the spectral range, in which the expression (11.15) "works", is determined by the inequation: $\omega \le \omega_p$. Within the framework of this model in the range $\omega_p << \omega << \gamma\,\omega_p$ the formula (11.14) gives

$$\frac{d\mathrm{E}_{tr}^{(for)}}{d\omega} = \frac{2e^2}{\pi c}\,1\mathrm{n}\left(\frac{\gamma\omega_p}{\omega}\right), \tag{11.16}$$

and in the high-frequency region $\omega >> \gamma\,\omega_p$ we obtain

$$\frac{d\mathrm{E}_{tr}^{(for)}}{d\omega} = \frac{e^2}{6\pi c}\left(\frac{\gamma\omega_p}{\omega}\right)^4. \tag{11.17}$$

Thus in the case under consideration ($\gamma >> 1$) the frequency $\omega_{tr}^{(up)} = \gamma\,\omega_p$ is the upper frequency limit for forward transition radiation (in case of particle escape from a substance into vacuum).

The expressions (11.16) and (11.17) indicate that the main contribution to forward transition radiation is made by high frequencies $\omega \approx \gamma\,\omega_p$ in contrast to the above back transition radiation, when in the spectrum the low-frequency range $\omega \le \omega_p$ prevails.

The energy of forward transition radiation of an ultrarelativistic particle integrated with respect to the frequency is given by the simple formula

$$\mathrm{E}_{tr}^{(for)} = \frac{e^2}{3\hbar c}\gamma\hbar\omega_p. \tag{11.18}$$

Here the Planck constant is introduced to separate the expression for the photon energy at the plasma frequency $\hbar\omega_p$, the characteristic value of which in devices based on transition radiation is 20 eV.

From the expression (11.18) it follows that the total energy of TR of an ultrarelativistic charged particle ($\beta = v/c \to 1$) radiated forward in the direction of its motion grows linearly with particle energy. The linear growth of the total energy of forward TR is caused by two reasons: the increase of the spectral energy (Eq. 11.16) with increasing relativistic factor γ and the growth of the upper frequency limit.

An important role in technical applications is played by X-ray transition radiation (XTR) of relativistic and ultrarelativistic charged particles. In the X-ray range the dielectric permittivity of a medium is to a good accuracy given by the plasma formula. Intensive forward XTR arises in case of escape of a charged particle from a target. Then the total radiation energy is proportional to the relativistic factor γ (see the formula (11.18)), and the spectrum extends up to frequencies of the order of $\gamma\,\omega_p$. Thus the XTR energy can serve as a measure of the energy of a charged particle crossing the interface between media with different dielectric permittivities. This opens up a possibility to measure energy of elementary particles with the use of XTR.

The convenience of use of PXR of relativistic electrons in practical applications in comparison with TR is connected with the fact that the angular directivity of PXR is not rigidly bound with the direction of electron motion, but can be varied in a specified manner by changing the Bragg angle (see Table 11.2).

To optimize the PXR source for mammographic applications, in the work [11] experimental investigations of PXR were carried out with a 60 MeV linear accelerator in a photon energy range from 17 to 20 keV. The value of electron current varied from 10 nA to 1–1.5 μA. As targets, graphite and LiF, Si, Ge, Cu, and W single crystals were used. The spectral widths and PXR photon yield in conversion of virtual photons to real photons on different crystallographic planes of the above-listed crystals were measured. To determine the spectral width of a PXR line and photon energy, as a rule, the Si Amptek XR-100CR X-ray detector with a resolution of 350 eV for a photon energy of 17.5 keV and an area of 9 mm^2 was used.

A typical diagram of the experimental system used in the work [11] is given in Fig. 11.10 for a LiF target and the Bragg angle $\theta_B = 15°$.

In the case that the calculated line width was found to be so narrow that it could not be recorded with the use of the X-ray Si detector, for this purpose near-absorption edge transmission equipment was used. By this means the FWHM of the PXR spectrum was determined for a silicon target in conversion of a virtual photon on the (400) crystallographic plane (134 eV at a photon energy of 9.0 keV) and a silicon target in conversion of a virtual photon on the (220) crystallographic plane (540 eV at a photon energy of 17.7 keV).

As a result of the carried out experiments, it was shown that materials consisting of light atoms (graphite, LiF) are more suitable for generation of PXR photons since in them X-radiation is absorbed weaker, the bremsstrahlung background is less, and the cross-section of electron scattering is less. The highest yield of PXR photons was recorded in graphite, in a LiF crystal there was a narrowest emission line.

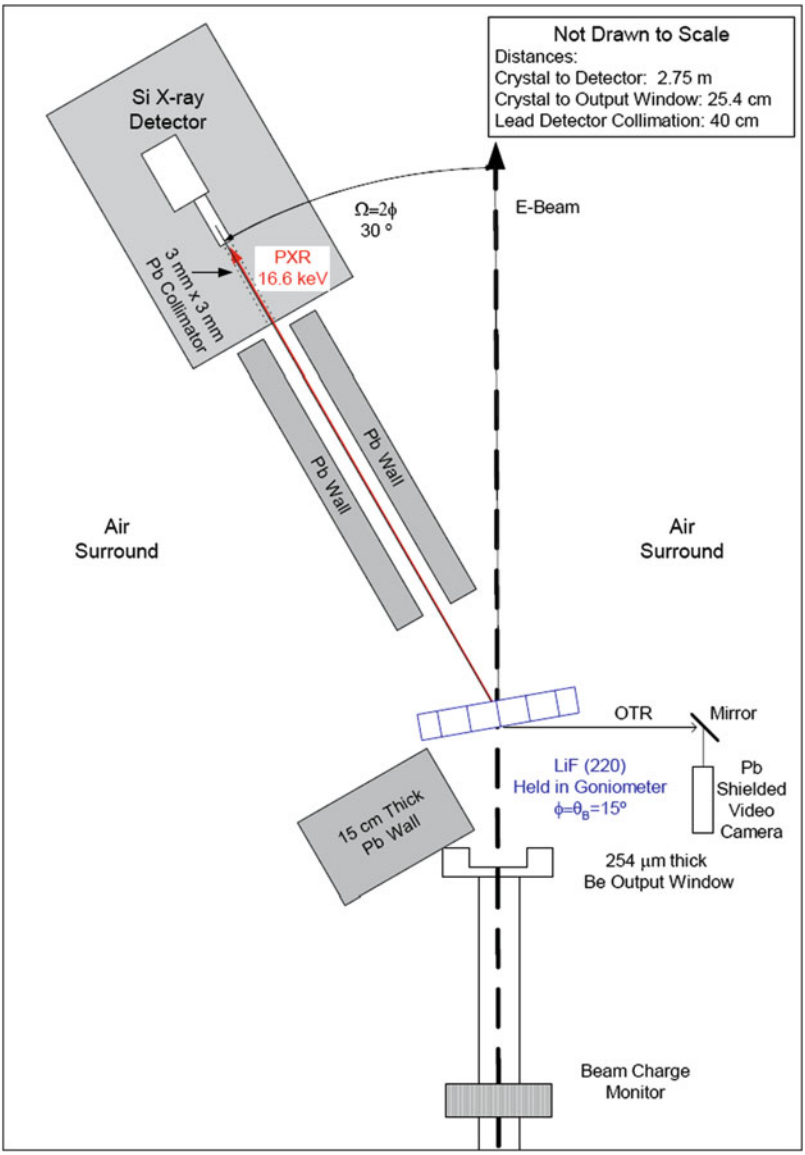

Fig. 11.10 The typical diagram of the experimental system for recording PXR [11]

Presented in Fig. 11.11 is the PXR spectrum measured on a LiF crystal, resulting from conversion of virtual photons of the eigenfield of an electron beam with an energy of 56 MeV on the (220) crystallographic plane.

From the given figure it is seen that in the actual spectral range (17–20 keV) there is a narrow PXR peak with a low background of bremsstrahlung.

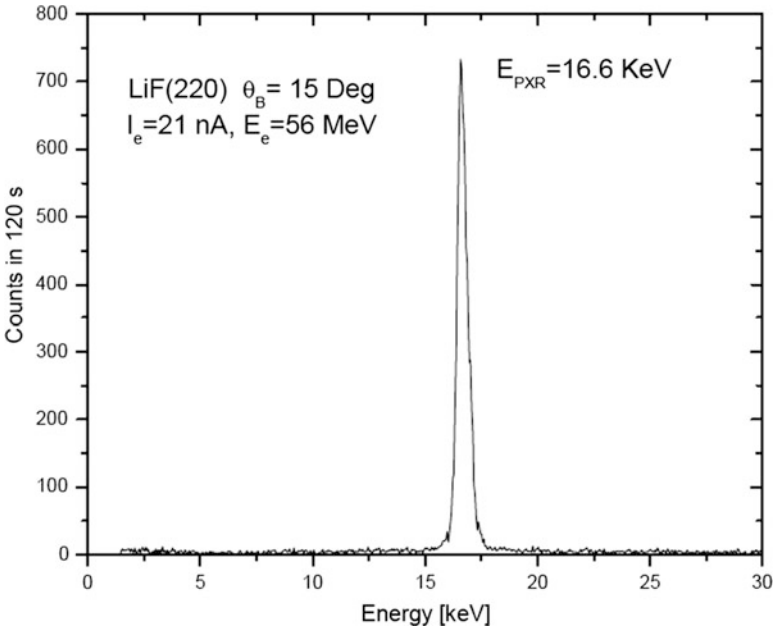

Fig. 11.11 The measured PXR spectrum from a LiF target at the Bragg angle $\theta_B = 15°$ [11]

Figure 11.12 demonstrates possibilities of imaging with the use of a PRX source based on a LiF crystal and a CCD camera [11].

The comparison of images obtained with the use of PXR and with the use of bremsstrahlung (from the same target) shows that in the first case much higher contrast is achieved. Images of a small fish (a biological object), a plastic electric switch, and a number of metal objects were also obtained.

In individual experiments the temperature of a target crystal was recorded, and it was shown that it grows rapidly under the action of an electron beam. Based on the carried out analysis, a conclusion was drawn that crystal cooling and short exposure time are required when using PXR for imaging if the beam current exceeds several μA.

Thus in the work [11] it was shown that with the use of a PXR source it is possible to generate wavelength- (photon energy)-tunable X-radiation with a narrow spectrum, with intensity sufficient for imaging objects of a different nature with the use of a X-ray CCD camera in a reasonable exposure time and with a high enough contrast.

11.2.3 PBs on Nanostructures

Considered in Chap. 8 of this book was PBs on nanostructures: atomic clusters, metal nanoparticles, and graphene. It was shown in particular that the spectrum of

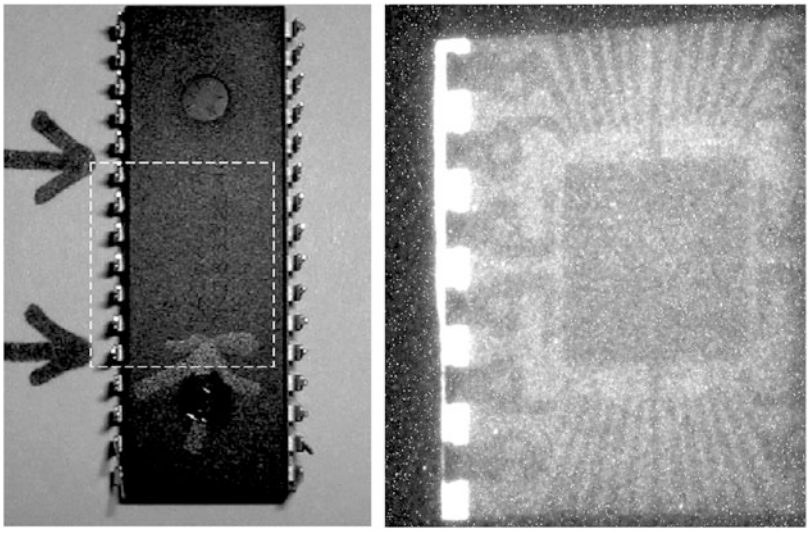

Fig. 11.12 At the *left*: the photo of a computer chip of length 4 cm with a separated square site of 1.6 cm; at the *right*: PXR of the image of the separated site of the computer chip obtained with the use of a (200) LiF target, the electron current is 3.2 μA, the exposure time is 25 s, the active surface of the CCD camera is 3 × 4 cm [11]

coherent PBs on graphene contains sharp maxima, the frequencies of which in the general case are determined by the formulas (8.64) and (8.65), and for the zero (relative to the normal of the graphene plane) angle of electron incoming they are determined by the more simple formula (8.66). The nature of these maxima is connected with coherent interaction of an incident electron and a two-dimensional graphene crystal.

As seen from the mentioned formulas, the resonance frequency of PBs on graphene is defined both by the reciprocal lattice vector g and by other problem parameters (see Fig. 8.13): the electron incoming angle ψ, the radiation angle α, and the electron velocity $\mathrm{v} = \beta c$ (c is the velocity of light in vacuum). In case of the zero incident angle, the dependence on the incoming angle ψ, naturally, disappears (see the formula (8.66)).

So, operating the above parameters, it is possible to change the resonance frequency of coherent PBs on graphene, which is very important for possible practical applications of the phenomenon under consideration.

A criterion for existence of resonance frequencies was also introduced that for the zero angle of electron incoming is given by the inequations (8.68). From these inequations it follows in particular that a necessary condition of existence of a resonance frequency is radiation of a PBs photon to the top hemisphere (Fig. 8.13), in other words, forward along the direction of electron motion ($\cos\alpha > 0$). It should be noted that the inequations (8.68) can be rewritten in the form that is explicit in relation to the radiation angle α:

$$\arccos\left(\frac{\beta^{-1}-1}{2}\right) \geq \alpha \geq 0. \tag{11.19}$$

It should be noted that the argument under the arc cosine sign on the left side of Eq. 11.19 is less than one for $\beta > 1/3$, that is, an incident electron should be fast enough, but not necessarily relativistic:

$$\mathrm{v} > \frac{c}{3}. \tag{11.20}$$

Following hence is the condition for the minimum kinetic energy of an electron T, at which sharp resonances in the spectrum of coherent PBs on graphene are still possible:

$$T > 30.968 \text{ eV}. \tag{11.21}$$

For an ultrarelativistic electron ($\beta \to 1$) the inequations (11.19) give $\pi/2 \geq \alpha \geq 0$, that is, the resonance frequency in the spectrum of coherent PBs on graphene exists for any radiation angle α.

The calculated spectra of different Bs channels in crossing the graphene plane by a fast electron are given in Figs. 8.19, 8.20, and 8.21 for different values of problem parameters. From the presented plots it follows that sharp resonances in the spectrum of coherent PBs on graphene (in the X-ray wavelength range) take place for nonrelativistic electrons and wide radiation angles. These characteristic features of the process under consideration make it very promising for various applications.

Presented in Fig. 11.13 is the dependence of the resonance frequency of coherent PBs on graphene on the electron velocity at the zero incoming angle for three values of the radiation angle α in scattering of a virtual photon by the crystallographic plane corresponding to the reciprocal lattice vector g (1,1).

It is seen that for each radiation angle α there is its minimum electron velocity, below which there is no sharp resonance in the spectrum of coherent PBs on graphene. The value of this velocity for the given radiation angles lies in the nonrelativistic range and decreases with decreasing angle α. Besides, according to the formula (8.69) that can be represented as (ψ is the incoming angle, see Fig. 8.13):

$$\mathrm{v}_{\mathrm{inf}}(\psi = 0) = \frac{c}{3\cos\alpha}, \tag{11.22}$$

for a specified radiation angle α there is an electron velocity, at which the resonance frequency becomes infinite, that is, sharp peaks in the spectrum of coherent PBs on graphene are absent.

So, operating the values of problem parameters (the electron velocity and the angular characteristics), it is possible to control the value of resonance frequency.

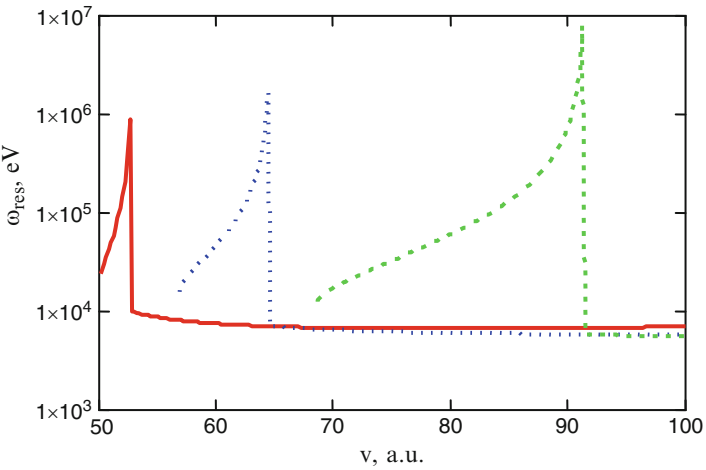

Fig. 11.13 The dependence of the resonance frequency of coherent PBs on graphene on the electron velocity at the zero incoming angle for three values of the radiation angle: *solid curve* – $\alpha = 30°$, *dotted curve* – $\alpha = 45°$, *dashed curve* $\alpha = 60°$, the reciprocal lattice vector is g (1,1)

To obtain intensive radiation in the UV range, it is possible to use PBs on metal nanoparticles placed in a dielectric medium. The calculation and analysis of the cross-section of this process for a case of silver nanospheres in glass are carried out in the Sect. 8.2 of this book in the spectral range corresponding to excitation of dipole plasmons on the surface of nanoparticles.

It was shown that the maximum of the spectral PBs cross-section caused by excitation of a surface plasmon depends on the radius of a nanoparticle. In the considered case the position of the spectral maximum is shifted from the region of the near-IR range to the region of the visible spectrum adjacent to the boundary with the UV range in case of reduction of the radius from 90 to 30 nm.

As follows from the formula for the frequency of the spectral maximum (8.33) caused by excitation of a dipole surface plasmon, when placing nanoparticles in a medium with lesser dielectric permittivity, the spectral maximum of PBs will be shifted towards high photon energies [14].

Presented in Fig. 11.14 are the results of calculation of the spectrum of PBs of electrons scattered by silver nanoparticles of different radii placed in a substance with the refractive index $n = 1.33$. It is seen that in this case the spectra are somewhat shifted to the region of higher values of photon energies in comparison with the case $n = 1.5$.

The X-ray and near-UV radiation sources under development can be used in X-ray lithography, medical diagnostics, microelement analysis of a substance in chemical and biological investigations. The advantages of such sources consist in a possibility of smooth emission line tuning and compactness of the system, which is caused by using accelerators for relatively low (in comparison with synchrotrons) electron energies. The trends of development of investigations in the field of X-ray sources are directed to creation of compact laboratory sources for industrial and

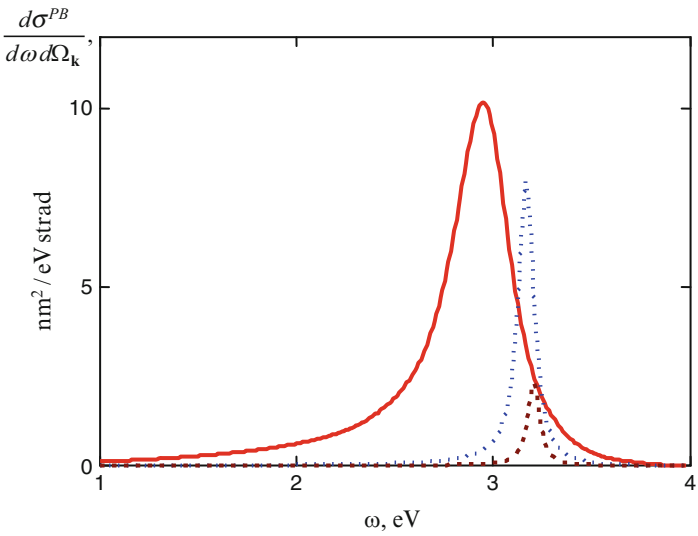

Fig. 11.14 The spectrum of PBs of an electron (v 30 a.u.) scattered by silver nanoparticles in a substance with the refractive index n = 1.33, the radiation angle is 30° for different nanoparticle radii: *solid curve* – 30 nm, *dotted curve* – 15 nm, *dashed curve* – 10 nm

diagnostic applications (a tabletop source). The vacuum ultraviolet range is intensively mastered, which is dictated, first of all, by biological investigations. The development of nanomaterial industry requires the development of efficient methods of diagnostics of such materials, so the intensification of research in this field should be expected.

References

1. Astapenko, V.A., Baturin, A.S., Korostylev, E.V.: Bremsstrahlung spectrum of nonrelativistic electrons scattered in metallic target: theory and experiment. J. Surf. Investig. X ray Synchrotron. Neutron. Tech. **4**, 193 (2010)
2. Astapenko, V.A., Baturin, A.S., Korostylev, E.V.: Bremsstrahlung of nonrelativistic electrons in metals with allowance made for the polarization channel. JETP **110**, 107 (2010)
3. Astapenko, V.A.: Polarization bremsstrahlung radiation on a nanosphere in a dielectric. Russ. Phys. J. **54**, 649 (2011)
4. Astapenko, V., Nasonov, N., Zhukova, P.: Anomalous peak in the spectrum of polarizational bremsstrahlung from relativistic electrons moving through a solid target. J. Phys. B **40**, 1337 (2007)
5. Grishin, V.K.: Polarization bremsstrahlung as a diagnostic means for fullerene structure. Vestnik MGU **2**(69) (2004) (in Russian)
6. Astapenko, V.A., Krotov, Y.A.: Bremsstrahlung of fast electron on graphene. J. Phys. C. **357**(012017) (2012)
7. Alekseev, V.I., Vokhmyanina, K.A., Eliseev, A.N., et al.: Measuring coherent peaks of polarization bremsstrahlung from relativistic electrons in polycrystalline targets in backscattering geometry. Tech. Phys. Lett. **38**, 294 (2012)

8. Nasonov, N.N.: Collective effects in the polarization bremsstrahlung of relativistic electrons in condensed media. NIM B **145**, 19 (1998)
9. Baryshevsky, V.G., Danilov, V.A., Ermakovich, O.L., et al.: Angular distribution of parametric x-rays. Phys. Lett. **110A**, 477 (1985)
10. Baryshevsky, V.G., Feranchuk, I.D.: Parametric x-rays from ultrarelativistic electrons in a crystal: theory and possibilities of practical utilization. J. Phys. **44**, 913 (1983). Paris
11. Sones, B.A.: Production of intense, tunable, quasi-monochromatic X-rays using the RPI linear accelerator. Ph. D. Thesis. Troy (2004)
12. Piestrup, M.A., Wu, X., Kaplan, V.V., et al.: A design of mammography units using a quasimonochromatic x-ray source. Rev. Sci. Instrum. **72**, 2159 (2001)
13. Ter-Mikaelian, M.: High Energy Electromagnetic Processes in Condensed Media. Wiley, New York (1972)
14. Sonnichsen, C.: Plasmons in Metal Nanostructures. Cuvillier Verlag, Gottingen (2001)

Chapter 12
Conclusions

12.1 General Provisions

This monograph considers polarization bremsstrahlung on atoms, nanostructures and solids with the use of the consistent quantum-mechanical approach in various regions of parametric variation. The cases both of spontaneous and induced PBs (in electron scattering by an atom/ion in the external field of radiation), PBs of incident particles with an own electron core are analyzed in details, the theoretical methods of description of this phenomenon and the experimental facts confirming a necessity to take into account PBs in a number of important physical situations are presented.

The main conclusion that can be drawn on the basis of the carried out consideration is that PBs is a fundamental radiative process resulting from scattering of virtual photons of an IP eigenfield by electrons of a target that should be taken into account for obtaining a full physical picture of Bs with participation of structural particles [1].

The material presented in the book demonstrates that the PBs concept covers a wide range of collisional-radiative phenomena that were earlier considered independently of one another, but actually representing the realization of PBs in various concrete physical situations.

According to its name, PBs of an electron on a target atom is defined by the generalized dynamic polarizability of a target $\alpha(\omega,\mathbf{q})$ depending both on the radiation frequency ω and on the wave vector $\mathbf{q}$ transferred to the target, so various methods of calculation of this value play a key role for quantitative description of the process under study. Together with quantum-mechanical methods of calculation of dynamic polarizability, presented in the book are simple semiclassical methods, such as the local plasma frequency approximation [2], that are to a great extent based on physical intuition, but give (under certain conditions) satisfactory quantitative description.

When going to PBs on ensembles of atoms/ions (in plasma, nanostructures and solids), for obtaining a quantitative result it is necessary to sum the amplitudes of

V. Astapenko, *Polarization Bremsstrahlung on Atoms, Plasmas, Nanostructures and Solids*, Springer Series on Atomic, Optical, and Plasma Physics 72,
DOI 10.1007/978-3-642-34082-6_12, © Springer-Verlag Berlin Heidelberg 2013

PBs on individual atoms with corresponding phase multipliers, which allows correct taking into account interference effects in the cross-section of PBs on nanostructures and in solids. Since (within the framework of the classical picture) PBs is defined by high impact parameters in scattering of an electron by a target with an electron core, the role of the above interference effects can be rather great. This is in contrast with ordinary (static) Bs, for which small impact parameters are characteristic, and the contribution of coherent interactions to the total SBs cross-section, as a rule, is insignificant.

For quantitative description of collective effects in PBs in plasma, an approach was developed that is based on the use of the dynamic form factor of a medium representing the spatio-temporal Fourier transform of the density-density correlator for plasma particles. The same approach can be used for PBs in other natural media and nanostructures in the high-frequency limit, when radiated frequency exceeds considerably the eigenfrequencies of target electrons.

12.2 PBs on an Atom

Within the framework of the consistent quantum-electrodynamic approach the expression was obtained for the amplitude of PBs of a relativistic incident particle on a one-electron atom with an arbitrary nuclear charge $Z \leq 137$ in a wide spectral range.

For frequencies $\hbar\omega << mc^2$ a rigorous passage to the limit in case of a nonrelativistic atomic electron was carried out, and the expression was obtained for the amplitude of PBs in the terms of the operator of electromagnetic field scattering by an atom, taking into account excitation and ionization of an atomic electron.

The equivalent photon method in calculation of the amplitude of PBs of a charged Born particle scattered by a multielectron atom (ion) was justified.

In the spectral range $I << \hbar\omega << m\,c^2$ (I is the characteristic ionization potential of atom) the expression for the total PBs cross-section in terms of the dynamic form factor of a target was obtained that is convenient for carrying out numerical calculations.

The expression for the spectral intensity of near-resonance PBs for a case of the band structure of the energy spectrum of a target was obtained.

The regions of essentiality of elastic and inelastic channels of polarization and static mechanisms of bremsstrahlung were determined.

Based on the analysis of the obtained expressions for the cross-section of total Bs of a relativistic charged particle, it was found that:

– The angular distribution of photons in the polarization channel of Bs of a relativistic IP in the region of essentiality of its integral cross-section (for frequencies $p_a \mathrm{v}_0 > \hbar\omega$, p_a is the characteristic momentum of an atomic electron, v_0 is the initial IP velocity) is of a dipole nature;

– In the frequency range $I << \hbar\omega << p_a \mathrm{v}_0$ the spectral cross-sections of Bs on a neutral atom by the polarization and static channels are approximately equal (accurate to the logarithmic factor);
– The spectral cross-section of polarization Bs grows logarithmically with the energy of relativistic IP;
– In the spectral range $p_a c << \hbar\omega << \gamma^2 p_a c$ ($\gamma >> 1$ is the relativistic factor) the angular distribution of bremsstrahlung photons emitted by the polarization channel gets the orientation along the IP velocity vector;
– In the frequency range $\hbar\omega \leq p_a \mathrm{v}_0$ the main contribution to the polarization channel is made by elastic processes (without excitation or ionization of a target), and if $\hbar\omega > p_a \mathrm{v}_0$, the main contribution is made by inelastic processes.

In the Born approximation for IP motion and in the Brandt-Lundqvist model [2], for the polarizability of the electron core of a target the expression for the PBs cross-section was obtained in the form of a local density functional for bound electrons. With the use of the Thomas-Fermi model for electron density of an atom it was shown that the spectral R-factor – the ratio of the cross-sections of Bs by the polarization and ordinary (static) channels – reaches its maximum value (of the order of unity) at the frequency $\hbar\omega_{\max} \approx Z m e^4 / \hbar^2$ ($Z|e|$ is the charge of an atomic nucleus).

The universal description of incoherent PBs of a fast charged particle on a multielectron atom is given on the basis of approximate scaling of the reduced Hartree-Fock profile of X-ray scattering, for which there is an extensive database allowing the calculations of corresponding cross-sections for all possible neutral atoms.

12.3 PBs of Fast Electrons in Plasma

Based on the microscopic consideration, the theory of PBs of a relativistic charged particle in partially ionized plasma is constructed in view of radiation on the Debye sphere and the influence of a medium on an electromagnetic field.

It is shown that the process cross-section can be expressed in terms of the dynamic form factors of plasma components describing the interaction between different kinds of particles, which allows taking into account mutual screening of plasma components with different charge signs in the process of bremsstrahlung.

The developed approach makes it possible in a single formalism to describe Bs of a fast charged particle in plasma with transfer of the energy-momentum excess to different plasma excitations including collective degrees of freedom.

As a result of the carried out analysis of the obtained cross-sections, it was found that:

– Studied earlier in the works of V.N. Tsytovich and A.V. Akopyan [3], transient Bs and polarization Bs on the Debye sphere around an ion in plasma have the same physical nature (practically coincide);

– PBs in plasma (with not too high concentrations) is not subject to the influence of the density effect suppressing static Bs of relativistic IP in the frequency range $\omega < \gamma\,\omega_{pe}$;
– The influence of a medium on the cross-section of PBs in plasma counts only in the logarithmed expression, which leads (for relativistic IP) in the frequency range $\omega < \gamma\,\omega_{pe}$ to leveling of logarithmic increase of the cross-section with energy.

Bs of fast electrons in dense plasma in the hard-sphere model was investigated in a wide spectral range, including the polarization and static channels of the process and their interference. The cases of fully and partially ionized plasma were considered. It was shown that the spectra of total Bs have maxima, the position and shape of which form depend on the density of plasma and the degree of ionization of a plasma ion.

12.4 Quasi-Classical Theory of PBs of Thermal Electrons on Atoms and Ions in Plasma

Within the framework of the local plasma model for target polarizability, a semi-quantitative approach to description of polarization effects in strongly inelastic Bs on a multielectron ion was developed.

Based on the developed approach, the analysis of the contribution of the polarization channel to spectral and total effective radiation was carried out for quasi-classical and quantum IP motion in view of penetration of an IP into the target core for different degrees of inelasticity of the process.

The generalized rotation approximation was constructed that makes it possible to estimate the value of the PBs cross-section (within the framework of the statistical model of a target ion) in a common manner for all nuclear charges and degrees of ionization.

In the high-frequency limit the analytical expression having a visual physical interpretation was obtained for total effective radiation of a quasi-classical IP on a multielectron ion in view of the polarization channel. The generalization of the target "stripping" effect to the case of classical IP motion is given.

A simple expression for total bremsstrahlung loss of thermal plasma electrons on the Debye cloud around an ion in plasma was obtained that extends the previous result for PBs of straight-flight superthermal particles and covers a case of nonideal plasma. It is shown that the ratio of the contributions of the polarization and static channels is a weak function of plasma electron density for a fixed value of the plasma perfectness parameter.

On the basis of the carried out analysis it was found that:

1. The contribution of the polarization channel to the cross-section of strongly inelastic Bs is maximum near the frequency of ionization of a target ion. The

maximum value of the R-factor (the ratio of the values of the channel contributions) within the framework of the Brandt-Lundqvist model for the polarizability of the ion core is approximately equal to two. The spectral R-factor, growing in the power manner in the region of low frequencies, sharply falls after reaching the extreme value due to the effects of IP penetration into the target core. The width of a corresponding maximum grows with inelasticity of the process. For characteristic frequencies of the order of a ionic charge (in atomic units) the R-factor is 10–15 %.

2. Interchannel interference in the spectral dependence of the Bs intensity is most essential near the potential of ionization of a target, being at extrema more than 60 % of the total intensity of the process. For frequencies lower than the ionization threshold, interference is of a destructive nature, for frequencies higher than the ionization threshold, it is of a constructive nature. The role of interchannel interference decreases with decreasing inelasticity of IP scattering since in this case the spatial regions of formation of Bs channels are more separated.
3. There is an optimum ionic charge (Z_i^{opt}), at which the value of the spectral R-factor at a frequency multiple of the characteristic frequency of ionization of an ion in the Thomas-Fermi model is maximum. This value Z_i^{opt} decreases with growing Bs frequency and grows with increasing ionic charge.
4. The integral with respect to the magnitude of the radius vector in the expression for the polarization bremsstrahlung loss of a quasi-classical IP converges at the lower limit of integration (in contrast to the divergent integral of the static channel), which reflects taking into account IP penetration into the electron core of a target. Thereby for polarization Bs the impossibility in principle of consistent calculation of bremsstrahlung loss by the static channel within the framework of classical physics is smoothed.
5. The values of the total static and polarization effective radiations calculated within the framework of the generalized rotation approximation are approximately equal up to IP energies of the order of an ionic charge (in atomic units) for targets with a low degree of ionization.
6. The polarization bremsstrahlung loss of thermal electrons on the Debye cloud around an ion in ideal plasma is about 10–15 % of the value of "static" bremsstrahlung loss and can be comparable with the latter only in case of nonideal plasma.

12.5 PBs of Fast Particles in a Solid

The general expression for the cross-section of PBs in a solid in terms of the structure factor of a medium is obtained, with the use of which it is possible to describe PBs in a single crystal, a polycrystal, and an amorphous substance. In case of a polycrystal, in the expression for the process cross-section averaging over the

direction of the reciprocal lattice vector was carried out, and in an amorphous medium the pair correlation function of medium atoms was used.

It is found that in the general case the cross-section of PBs in a crystal can be represented as the sum of two summands: coherent and incoherent. These summands reflect the nature of interaction of an incident electron with the crystal lattice of a target. In the coherent case a momentum equal to the momentum of the reciprocal crystal lattice is transferred to the target, and the radiated frequency is found to be fixed for specified values of problem parameters. The incoherent part of the cross-section is analogous to the cross-section of PBs on an individual atom in view of the Debye-Waller factor.

It is shown that the coherent part of PBs of a relativistic electron in a single crystal in the X-ray range of frequencies is nothing but parametric X-radiation theoretically predicted by Ya.B. Fainberg and N.A. Khizhnyak and experimentally discovered by V.G. Baryshevsky with co-authors [4].

As a result of investigation of PBs of nonrelativistic particles in polycrystals [5], it was shown that in the region of low photon energies $\omega << 2\pi \mathrm{v}/a$ (α is the crystal lattice constant), when the coherent component of the process prevails, PBs in a polycrystal is suppressed in comparison with radiation on an individual atom. This suppression is connected with the fact that low momenta transferred to the target and defining PBs on an isolated atom do not make a contribution to coherent scattering of a fast ion by a crystal lattice in the low-frequency range.

In the intermediate region of photon energies $\omega \geq 2\pi \mathrm{v}/a$ (2–6 keV) a well-discernible stepped structure in the PBs spectrum takes place – "frequency steps". This structure is connected with coherent scattering of an incident particle by a crystal lattice, in which a momentum equal in magnitude to one of the reciprocal lattice vectors is transferred to a target. A frequency step results from "turning-off" of the contribution of one of the reciprocal lattice vectors (g) to the process, when a minimum transferred momentum defined by the conservation laws in magnitude exceeds g. The position and the value of frequency steps reflect the features of the structure of a target, depend on the incident particle velocity and the angle of photon emission.

In the high-frequency spectral region $\omega >> 2\pi \mathrm{v}/a$ ($\omega > 8$–10 keV) the incoherent component of PBs prevails, and the radiation spectrum approaches the spectrum on an isolated atom.

The consistent quantum-mechanical calculation of the intensity of PBs of a relativistic electron in an amorphous medium has shown the important role of the effect of suppression of radiation of a fast charged particle. This effect is a result of destructive interference of the contributions to the process amplitude from different atoms of a substance that are chaotically arranged in the region of formation of an elementary radiative act. According to this physical picture, the suppression of PBs should be the more essential, the more atoms of a medium are in the region of formation of radiation, that is, for low frequencies, high IP energies and small radiation angles. This conclusion is confirmed by the results of the numerical analysis carried out in this paper for a number of targets and different problem parameters.

In the book different types of PBs of a fast hydrogen-like ion in a single crystal are calculated and analyzed. It is shown that radiation results from scattering of eigenfields of colliding charges to a bremsstrahlung photon by bound electrons of a target and an IP. The presence of a crystal structure results in the fact that the process of radiation can proceed both due to coherent interaction of an IP with a target and in an incoherent manner. As a result, four types of PBs take place: coherent and incoherent PBs on target electrons and coherent and incoherent PBs on an IP electron. In the coherent case a wave vector equal to one of the reciprocal lattice vectors $\mathbf{g}$ is transferred to a single crystal. In this case radiation occurs at a fixed coherent frequency (with specified $\mathbf{g}$, IP velocity and angle of photon emission). The frequency of incoherent PBs is not fixed, and the intensity of radiation is maximum in the near-resonance region near the eigenfrequencies of a bound IP electron. From the obtained expressions it follows that with growing charge of the IP nucleus the contribution of PBs by the second channel to the total radiation decreases, and the spectral range of its essentiality is shifted to the region of higher frequencies. At the same time the relative value of the considered types of PBs weakly depends on the charge of nuclei of target atoms, with increase of which the intensity of each of them grows proportionally.

By the example of a target of a copper foil, Bs of an electron with an energy of 10–30 keV was studied theoretically and experimentally in view of the ordinary and polarization channels, interchannel interference, photon absorption, scattering and loss of electron energy in a target. It is shown that with growing thickness of a target the nature of the Bs spectrum changes. For a thin target, with increasing photon energy a monotone decrease of Bs yield takes place with a peculiarity near the threshold of ionization of the electron shell of target atoms due to the influence of PBs. In case of a thick target the Bs spectrum is a curve with a maximum that is well pronounced if the thickness of the target is more than the photon and electron path length. With increasing initial electron energy the position of a spectral maximum is shifted to the region of high photon energies. The physical cause of appearance of maxima in the spectrum of Bs from a thick target consists in the competition of influences of photon absorption and energy loss by an electron on the Bs process.

It is found that with growing target thickness the yield of Bs photons reaches saturation faster for lower photon energies. For example, for $\hbar\omega = 1.36$ keV and an initial electron energy of 30 keV the "saturation thickness" is about 0.4 μm. With decreasing initial electron energy the "saturation thickness" increases a little.

The contribution of the polarization channel is most essential near the threshold of ionization of the L-shell of target atoms, that is, in the considered case for a photon energy about 1.5 keV. The variation of the initial energy of an electron beam results in a change of the relative PBs contribution to the total photon yield (in view of interchannel interference) within 45–65 %, and the maximum of the polarization contribution is reached for the energy $E_0 = 30$ keV. With growing photon energy the PBs contribution decreases, so for $\hbar\omega = 10$ keV it does not exceed 10 %. The change of the viewing angle β rather weakly influences the PBs contribution to the total photon yield. The calculation shows that with a growth of the angle β from 10° to 80° the PBs contribution decreases approximately by 15 %.

The carried out analysis indicates that the contribution of the polarization channel depends weakly on the thickness of a target.

The experimental identification of the PBs contribution to the total photon yield in the considered case is complicated by the fact that the spectra of PBs and Bs of a nonrelativistic electron, generally speaking, are similar. The distinction in spectral curve shapes is most essential for thin targets near the threshold of ionization of atomic shells, where Bs is masked by a strong maximum of characteristic radiation. Beyond this spectral region the PBs contribution can be recorded by carrying out absolute measurements of the Bs spectrum. An alternative approach to investigation of PBs can be based on taking the spectra of radiation in the region of the threshold of ionization of atomic shells with a temporal resolution for separation of a practically momentary Bs response from characteristic radiation with a finite relaxation time.

12.6 PBs on Nanostructures

Based on the carried out analysis of radiation of electrons on nanoclusters, it is possible to draw a conclusion about essentiality of cooperative effects in Bs of a fast (including relativistic) charged particle scattered by a polyatomic cluster in a wide range of frequencies. These effects caused by constructive interference of contributions of atoms to the process by the polarization channel result in nonlinear growth of the PBs intensity as a function of the number of atoms in a cluster. At the same time for the ordinary (static) mechanism of Bs the contribution of different atoms to radiation is incoherent, which is caused by the smallness of impact parameters, on which ordinary Bs is formed. The value of cooperative effects as a function of the number of atoms in a cluster is investigated. The dependence of the number N_{sat} (beginning with which the nonlinear growth of the PBs intensity ceases) on the main problem parameters is established. In particular, it is shown that for relativistic IP the value N_{sat} strongly grows with decreasing radiation angle.

It is shown that cooperative effects result in considerable modification of the main characteristics of Bs on a cluster in comparison with a monatomic case. For example, in the high-frequency range with growing number of atoms the PBs pattern is narrowed, and for large enough clusters the angular dependence of PBs of relativistic particles becomes nonmonotonic: a maximum appears at nonzero radiation angles.

With growing IP energy the maximum of the spectral distribution of PBs on a cluster is shifted to the region of high frequencies. The form of the high-frequency part of the spectrum in the relativistic case strongly depends on the radiation angle. With decrease of this angle, the Bs intensity with growing frequency decreases much more slowly than for wide angles.

An analytical expression was obtained for the spectral-angular cross-section of PBs of a charged particle scattered by a metal nanosphere placed in a dielectric medium. The derived formula contains the cross-section of scattering of an

electromagnetic field, for which in the developed approach the result of the Mie theory is used.

Within the framework of the proposed method of calculation, polarization bremsstrahlung on a silver sphere with a radius from 10 to 100 nm in glass and other matrices was analyzed. A wide range of incident electron velocities from 1 a.u. to the value equal to the velocity of light in a matrix material was considered. The calculations of the PBs cross-section differential with respect to the frequency and the radiation angle are carried out in the region of excitation of a plasmon resonance on the surface of a silver nanosphere (the photon energy is 1–4 eV), where the spectral characteristics of the process are most sensitive to the target and matrix parameters and the polarization channel of radiation prevails. The main spectral, velocity, and angular regularities of the process under consideration that are necessary for development of PBs spectroscopy are established. In particular, it is shown that the position and width of the spectral maximum in the PBs cross-section are defined by the radius of a nanosphere, the dielectric permittivity of a matrix, and the velocity of a scattered electron. It is shown that for large enough sphere radii in the high-frequency part of the PBs spectrum an additional maximum appears that is caused by excitation of quadrupole plasmons.

The carried out analysis makes it possible to establish an optimum region of parametric variation, in which the use of PBs spectroscopy for investigation of the structure and physical properties of metal nanoparticles in a dielectric medium is most promising.

Polarization bremsstrahlung and static (ordinary) bremsstrahlung (SBs) of a fast electron scattered by graphene are investigated theoretically. Coherent and incoherent interactions between an electron and a two-dimensional graphene lattice as well as the dynamic polarizability and the form factor of the core of a carbon atom are taken into account.

It is shown that the spectral features of the PBs cross-section depend on the electron velocity, the angle of IP incidence, and the radiation angle. In the said region of problem parameters sharp maxima in the PBs spectrum are predicted. For the normal incidence of an electron on the graphene plane the analytical description of resonance frequencies as functions of velocity and radiation angles is obtained.

In the low-frequency range coherent PBs is prevailed by the process without momentum exchange between an IP and graphene. In this range coherent PBs is comparable with or higher than incoherent PBs. Our analysis shows that prevailing channels of bremsstrahlung of a fast electron on graphene are coherent PBs and incoherent SBs.

12.7 Induced Bremsstrahlung Effect in an Electromagnetic Field

The induced bremsstrahlung effect in a near-resonance laser field in strongly inelastic scattering of electrons by ions with a core is calculated and analyzed, including the multiphoton process. The contributions of the ordinary (static) and polarization Bs mechanisms to the process cross-section are taken into account.

Particular attention is given to interference effects caused by interaction of the channels.

It is shown that IP penetration into the target core strongly influences the interference effects.

As a result of the carried out investigations, it was found that:

- Interference between the static and polarization channels in near-resonance Bs results in asymmetry of the process spectral line shape, so in the low-frequency wing of the line a "dip" appears;
- The form and depth of the spectral "dip" essentially depend on the intensity of the external field in the region of its "saturating" values and on the energy of a resonant transition;
- An interference "dip" occurs in the dependence of the cross-section of near-resonance induced Bs on the amplitude of the external electromagnetic field with negative detuning of radiation frequency from resonance ($\omega < \omega_0$);
- The effects of IP penetration into the target core result in dependence of the process spectral line shape on the angle between the vector of the initial IP velocity and the vector of the electric field of near-resonance radiation, so interference effects are most pronounced in case of perpendicular orientation of the said vectors and are strongly reduced in case of their parallel orientation;
- In the cross-section of near-resonance Bs differential with respect to the angle of IP scattering a peculiar kind of "inversion" of process spectral line shape asymmetry occurs as the angle of IP scattering increases due to the change of the sign of the nondipole polarization potential;
- Based on the quantum calculation, the conclusion of the quasi-classical consideration about the most manifestation of interchannel interference in the integrated cross-section of inelastic scattering is confirmed for perpendicular polarization of the external field expressed in the asymmetry of the spectral cross-section and the presence of spectral dips;
- The role of exchange effects in the spectral cross-section differential with respect to the angle of IP scattering is analyzed;
- The features of the spectral dependences of the cross-section integrated with respect to the angle of IP scattering with absorption and emission of a photon for different orientations of the vector of the external field strength in relation to the initial IP velocity are investigated.

12.8 Experimental Investigation of the Polarization Channel in Bremsstrahlung

The most dramatic proofs of essentiality of PBs were obtained in experiments with relativistic electrons scattered by solid-state targets, both single-crystal and polycrystalline [6] and amorphous, as well as in Bs on atoms in the region of a giant resonance in photoabsorption [7].

In case of a single-crystal target, when, as a rule, instead of PBs the term *parametric X-radiation* is used, sharp maxima in the radiation spectrum were recorded that are caused by conversion of virtual photons to real photons on the crystallographic planes in fulfilment of the Bragg condition. The width and intensity of these maxima were found to be comparable with the spectral width and intensity of characteristic radiation [8]. In contrast to unpolarized characteristic radiation having a wide angular distribution and a fixed central frequency of a maximum, PBs is polarized and has a narrow pattern, and the central frequency of its spectral maximum can be controlled by changing the problem parameters.

In the experimental spectra of relativistic electrons in polycrystals maxima are also found that are defined by the Bragg condition for a specified radiation angle [9]. In contrast to the case of a single-crystal target, these maxima have a large width and much lower intensity [10] that, however, in the region of the maximum exceeds the intensity of ordinary Bs (see Fig. 9.9).

The absolute measurements of the cross-section of Bs of nonrelativistic electrons on atoms of noble gases [11] in a wide spectral range from 5 keV to the kinematic limit have shown that the obtained results are not described by the standard Bs theory (without considering the polarization channel) (see Figs. 9.4, 9.5 and 9.6). In the work [11] it is shown that in the considered case taking Bs into account improves the agreement between experimental and theoretical data. Based on the carried out analysis, the conclusion was drawn that the obtained experimental dependences are unambiguously indicative of the considerable contribution of the polarization channel to Bs of fast electrons on free atoms.

The absolute measurements of the yield of bremsstrahlung photons in scattering of an electron with the energy of 53 keV by gold films of different thicknesses were carried out in the work [12] for a radiation angle of 153°. In this case it was found that the theory of ordinary Bs (without considering PBs) gives a good agreement with the experiment in contrast to the results of the work [11] on measurement of Bs on free atoms and experiments on emission of relativistic electrons on metal foils [10]. It should be noted that the theoretical data in the paper [11] were obtained within the framework of the atom "stripping" approximation and, as the authors of the paper note, for verification of the obtained conclusions a more consistent theoretical approach is needed. Such an approach for a polycrystalline target is described in the Sect. 5.3 of this book. Besides, for detection of "frequency steps" in the spectrum of PBs of a nonrelativistic charged particle scattered by a polycrystal (see Figs. 5.3 and 5.4) high enough resolution of the photodetector is necessary. Otherwise the said structure will be "slurred over" by the instrument function of the photodetector, and characteristic features of PBs predicted by the theory will disappear in the experiment.

Thus it can be concluded that reliable experiments intended to reveal the PBs contribution to radiation of nonrelativistic electrons on polycrystalline targets need the use of more perfect measuring equipment.

The interference of coherent ordinary Bs and coherent PBs in scattering of nonrelativistic electrons with the energy from 50 to 100 keV by a thin target of a silicon single crystal was observed in the work [13] in the X-ray range. The

experiment was carried out for a sliding angle of radiation with respect to the surface of a target to decrease photon absorption in the target material. Shown in the cited work was a possibility of frequency tuning of X-radiation due to the change of conditions of interference between the ordinary and polarization channels of coherent Bs.

In conclusion it should be noted that the important property of PBs – independence from an IP mass – was still insufficiently used in experimental investigations. The exception is the work [14]. At the same time PBs of multiply charged ions can have wide practical applications both for obtaining new types of sources of short-wave radiation and for diagnostics of materials.

References

1. Tsytovich, V.N., Oiringel, I.M. (eds.): Polarization Bremsstrahlung. Plenum Press, New York (1991)
2. Brandt, W., Lundqvist, S.: Atomic oscillations in the statistical approximation. Phys. Rev. **139**, A612 (1965)
3. Tsytovich, V.N., Akopyan, A.V.: Bremsstrahlung in a nonequilibrium plasma. Sov. J. Plasma Phys. **1**(4), 371 (1975)
4. Baryshevsky, V.G., Danilov, V.A., Ermakovich, O.L., et al.: Angular distribution of parametric x-rays. Phys. Lett. **110A**, 477 (1985)
5. Astapenko, V.A.: Polarization bremsstrahlung of heavy charged particles in polycrystal. JETP **99**, 958 (2004)
6. Blashevich, S., Chepurnov, A., Grishin, V., et al.: Polarization bremsstrahlung of relativistic electrons in aluminium. Phy. Lett. A **254**, 230 (1999)
7. Verkhovtseva, E.T., Gnatchenko, E.V., Zon, B.A., Nekipelov, A.A., Tkachenko, A.A.: Bremsstrahlung in electron scattering by xenon. Zh. Eksp. Teor. Fiz. **98**, 797 (1990)
8. Sones, B.A.: Production of intense, tunable, quasi-monochromatic X-rays using the RPI linear accelerator. Ph.D. Thesis. Troy, New York (2004)
9. Nasonov, N.N.: Collective effects in the polarization bremsstrahlung of relativistic electrons in condensed media. NIM B **145**, 19 (1998)
10. Astapenko, V.A., Kubankin, A.S., Nasonov, N.N., et al.: Measurement of the polarization bremsstrahlung of relativistic electrons in polycrystalline targets. JETP Lett. **84**, 281 (2006)
11. Portillo, S., Quarles, C.A.: Absolute doubly differential cross sections for electron bremsstrahlung from rare gas atoms at 28 and 50 keV. Phys. Rev. Lett. **91**, 173201 (2003)
12. Williams, S., Quarles, C.A.: Absolute bremsstrahlung yields at 135° from 53-keV electrons on gold film targets. Phys. Rev. A **78**, 062704 (2008)
13. Baryshevsky, V.G., Batrakov, K.G., Feranchuk, I.D., et al.: Experimental observation of frequency tuning of X-ray radiation from nonrelativistic electrons in crystals. Phys. Lett. A **363**, 448 (2007)
14. Ishii, K., Morita, S.: Continuum x-ray produced by light-ion-atom collisions. Phys. Rev. A **30**, 2278 (1984)

Appendix 1 Dynamic Polarizability of an Atom

Definition of Dynamic Polarizability

The dynamic (dipole) polarizability $\alpha(\omega)$ is an important spectroscopic characteristic of atoms and nanoobjects describing the response to external electromagnetic disturbance in the case that the disturbing field strength is much less than the atomic electric field strength $E<<E_a = m_e^2 e^5/\hbar^4 \cong 5.14 \cdot 10^9$ V/cm, and the electromagnetic wave length is much more than the atom size.

From the mathematical point of view dynamic polarizability in the general case is the tensor of the second order α_{ij} connecting the dipole moment **d** induced in the electron core of a particle and the strength of the external electric field **E** (at the frequency ω):

$$d_i(\omega) = \sum_j \alpha_{ij}(\omega)\, E_j(\omega). \tag{A.1}$$

For spherically symmetrical systems the polarizability α_{ij} is reduced to a scalar:

$$\alpha_{ij}(\omega) = \alpha(\omega)\, \delta_{ij}, \tag{A.2}$$

where δ_{ij} is the Kronnecker symbol equal to one if the indices have the same values and to zero if not. Then the Eq. A.1 takes the simple form:

$$\mathbf{d}(\omega) = \alpha(\omega)\, \mathbf{E}(\omega). \tag{A.3}$$

The polarizability of atoms defines the dielectric permittivity of a medium $\varepsilon(\omega)$ according to the Clausius-Mossotti equation:

$$\frac{\varepsilon(\omega) - 1}{\varepsilon(\omega) + 2} = \frac{4}{3}\, \pi\, n_a\, \alpha(\omega), \tag{A.4}$$

V. Astapenko, *Polarization Bremsstrahlung on Atoms, Plasmas, Nanostructures and Solids*, Springer Series on Atomic, Optical, and Plasma Physics 72,
DOI 10.1007/978-3-642-34082-6, © Springer-Verlag Berlin Heidelberg 2013

where n_a is the concentration of substance atoms. For simplicity it is assumed in Eq. A.4 that a medium consists of atoms of the same kind.

It should be noted that the basis for a number of experimental procedures of determination of the dynamic polarizability $\alpha(\omega)$ is its connection with the refractive index of a substance (that for a transparent nonmagnetic medium is determined by the equation $n(\omega) = \sqrt{\varepsilon(\omega)}$).

Dynamic polarizability defines the shift of the atomic level energy ΔE_n in an external electric field. In the second order of the perturbation theory for the nonresonant external field E and a spherically symmetric electronic state a corresponding correction to energy looks like

$$\Delta E_n^{(2)} = -\frac{1}{2}\,\alpha_n(\omega)\,E^2. \tag{A.5}$$

The formula (A.5) describes the quadratic Stark effect. In the case that the external field frequency coincides with the eigenfrequency of an atom, the energy shift is found to be linear in electric field intensity – the linear Stark effect. The linear Stark effect is realized also in case of an orbitally degenerate atomic state as it takes place for a hydrogen atom and hydrogen-like ions.

Static polarizability, that is, polarizability at the zero frequency $\alpha(\omega = 0)$ defines the level shift in a constant electric field and, besides, the interatomic interaction potential at long distances (the Van der Waals interaction potential). Since static polarizability is a positive value (see below), from the Eq. A.5 it follows that the energy of a nondegenerate atomic state decreases in the presence of a constant electric field. The potential of interaction of a neutral atom with a slow charged particle at long distances is also defined by its static polarizability:

$$V_{pol}(r) = -e_0^2\,\frac{\alpha(0)}{2\,r^4}, \tag{A.6}$$

where e_0 is the particle charge. With the use of Eq. A.6 it is possible to obtain the following expression for the cross-section of elastic collision of a charged particle with an atom in case of applicability of the classical approximation for description of motion of an incident particle with the energy E:

$$\sigma_{scat}^{el}(E) = 2\,\pi\,e_0\,\sqrt{\frac{\alpha(0)}{2\,E}}. \tag{A.7}$$

It should be noted that the Eq. A.7 follows (accurate to the factor equal to 2) from Eq. A.6 if the effective scattering radius r_E is determined with the use of the equation

$$E = \left|V_{pol}(r_E)\right|. \tag{A.8}$$

Thus the knowledge of dynamic polarizability is very important for description of a whole number of elementary processes.

Expression for the Dynamic Polarizability of an Atom

Let us calculate the dipole moment of an atom $\mathbf{d}$ in the monochromatic field $\mathbf{E}(t) = 2\mathrm{Re}\{\mathbf{E}_\omega \exp(-i\,\omega\, t)\}$ that by definition is

$$\mathbf{d}(t) = 2\mathrm{Re}\{\alpha(\omega)\,\mathbf{E}_\omega \exp(-i\,\omega\, t)\}. \tag{A.9}$$

The Fourier component of the dipole moment is given by the expression

$$\mathbf{d}_\omega = \alpha(\omega)\ \mathbf{E}_\omega. \tag{A.10}$$

In the formulas (A.9) and (A.10) $\mathbf{E}_\omega$ is the complex electric field vector in monochromatic radiation being a Fourier component of $\mathbf{E}(t)$.

The dipole moment of an atom in the absence of external fields is equal to zero in view of spherical symmetry, so the value of an induced dipole moment can serve as a measure of disturbance of an atom by an external action. The linear dependence $\mathbf{d}(t)$ on electric field intensity (A.9) is true in case of smallness of the field strength E from the standpoint of fulfilment of the inequations $E<<E_a$. Thus for low enough field strengths the response of an atom to electromagnetic disturbance can be characterized by its polarizability $\alpha(\omega)$.

For description of the electromagnetic response of an atom – a quantum system – within the framework of classical physics, it is convenient to use the *spectroscopic conformity principle*. It can be formulated as follows: an atom in interaction with an electromagnetic field behaves as a set of classical oscillators (transition oscillators) with eigenfrequencies equal to the frequencies of transitions between atomic energy levels. This means that each transition between the atomic states $|j\rangle$ and $|n\rangle$ is assigned an oscillator with the eigenfrequency ω_{jn} and the damping constant $\delta_{jn}<<\omega_{jn}$. The contribution of the transition oscillators to the response of an atom to electromagnetic action is proportional to a dimensionless quantity called *oscillator strength* – f_{jn}, the more is the oscillator strength, the stronger is a corresponding transition. Transitions with the oscillator strength equal to zero are called forbidden transitions.

According to the spectroscopic conformity principle, the change of an atomic state is made up of the change of motion of transition oscillators. The inequation $E<<E_a$ means the smallness of perturbation of an atomic electron state as a result of action of the electromagnetic field. Thus it is possible to consider the deviations of the transition oscillators from the equilibrium position under the action of the field $\mathbf{E}(t)$ small, so for a nth oscillator the equation of motion in the harmonic approximation is true:

$$\ddot{\mathbf{r}}_n + \delta_{n0}\,\dot{\mathbf{r}}_n + \omega_{n0}^2\,\mathbf{r}_n = \frac{e}{m} f_{n0}\,\mathbf{E}(t), \tag{A.11}$$

where $\mathbf{r}_n$ is the radius vector corresponding to the deviation of the transition oscillator from the equilibrium position; δ_{n0}, ω_{n0}, f_{n0} are the damping constant, eigenfrequency and the oscillator strength. For simplicity we consider a one-electron atom in the ground state, the dipole moment of which is equal to $\mathbf{d} = e\,\mathbf{r}$. (In case of a multielectron atom the dipole moment is equal to the sum of dipole moments of atomic electrons.) In view of the conformity principle the induced dipole moment of an atom is made up of induced dipole moments of the oscillators of transitions to the nth state $\mathbf{d}_n$: $\mathbf{d} = \sum\limits_n \mathbf{d}_n = e \sum\limits_n \mathbf{r}_n$. Going in this equation to Fourier components, we have

$$\mathbf{d}_\omega = e \sum_n \mathbf{r}_{n\omega}, \tag{A.12}$$

where $\mathbf{r}_{n\omega}$ is the Fourier transform of the radius vector of the transition oscillator deviation from the equilibrium position. The expression for this value follows from the equation of motion (A.11):

$$\mathbf{r}_{n\omega} = \frac{e}{m} \frac{f_{n0}}{\omega_{n0}^2 - \omega^2 - i\,\omega\,\delta_{n0}}\,\mathbf{E}_\omega. \tag{A.13}$$

Substituting the formula (A.13) in the Eq. A.12 and using the definition of polarizability (A.10), we find for it the following expression:

$$\alpha(\omega) = \frac{e^2}{m} \sum_n \frac{f_{n0}}{\omega_{n0}^2 - \omega^2 - i\,\omega\,\delta_{n0}}. \tag{A.14}$$

Hence it follows that the dynamic polarizability of an atom represents, generally speaking, a complex value with a dimensionality of volume. The imaginary part of polarizability is proportional to the damping constants of the transition oscillators. The sum on the right of the Eq. A.14 includes both summation over the discrete energy spectrum and integration with respect to the continuous energy spectrum. The imaginary part of polarizability is responsible for absorption of radiation, and the real part defines the refraction of an electromagnetic wave in a medium. The expression (A.14) describes not only a one-electron atom, but also a multielectron atom. The multielectron nature of an atom is taken into account by the fact that in definition of the oscillator strength the dipole moment of an atom is equal to the sum of dipole moments of its electrons.

From the Eq. A.14 several important limiting cases can be obtained. For example, if the frequency of the external field is equal to zero, the formula (A.14) gives the expression for the static polarizability of an atom:

$$\alpha_0 \equiv \alpha(\omega = 0) = \frac{e^2}{m} \sum_n \frac{f_{n0}}{\omega_{n0}^2}. \tag{A.15}$$

Hence it is seen that static polarizability is a real and positive value. It has a large numerical value if in the atomic spectrum there are transitions with high oscillator strength and low eigenfrequency as it is, for example, for alkaline-earth atoms.

In the opposite high-frequency limit, when $\hbar\omega >> I_P$ (I_P is the ionization potential of atom) and the eigenfrequencies in the denominators of Eq. A.14 can be neglected, from the formula (A.14) in view of the golden rule of sums, according to which the sum of oscillator strengths is equal to the number of electrons in an atom N_a, we obtain

$$\alpha_\infty(\omega) = -\frac{e^2 N_a}{m\,\omega^2}. \tag{A.16}$$

Hence it is seen that the high-frequency polarizability of an atom is a real and negative value that decreases quadratically with growing frequency of the external field.

If the external field frequency is close to one of eigenfrequencies of the transition oscillators, so that the resonance condition

$$|\omega - \omega_{n0}| \leq \delta_{n0} \tag{A.17}$$

is satisfied and one resonant summand in the sum (A.14) can be retained, then from Eq. A.14 the expression for resonant polarizability follows:

$$\alpha_{res}(\omega) = \left(\frac{e^2}{2\,m\,\omega_{n0}}\right) \frac{f_{n0}}{\omega_{n0} - \omega - i\ \delta_{n0}/2}. \tag{A.18}$$

In derivation of Eq. A.18 from Eq. A.14 in nonresonance combinations the distinction of the external field frequency from the transition eigenfrequency was neglected. Resonant polarizability is a complex value, the real part of which can be both positive and negative.

The Eq. A.10 determining dynamic polarizability after the Fourier transformation can be rewritten as

$$\mathbf{d}(t) = \int_{-\infty}^{\infty} \alpha(\tau)\,\mathbf{E}(t-\tau)\,d\tau, \tag{A.19}$$

where $\alpha(\tau)$ is the real time function, the Fourier transform of which is equal to the dynamic polarizability $\alpha(\omega)$. The most simple expression for $\alpha(\tau)$ follows from the formula (A.18):

$$\alpha_{res}(\tau) = \frac{e^2 f_{n0}}{2 m \omega_{n0}} (-i)\, \theta(\tau)\, \exp(-i\, \omega_{n0}\, \tau - \delta_{n0}\, \tau/2), \tag{A.20}$$

where $\theta(\tau)$ is the Heaviside step function. The time dependence of the induced dipole moment $\mathbf{d}(t)$ coincides with the time dependence of the right side of the Eq. A.20 for the delta pulse of the field: $\mathbf{E}(t) = \mathbf{E}_0\, \delta(t)$, where $\delta(t)$ is the Dirac delta function. In the general case the expression for $\beta(\tau)$ can be obtained by replacement of the frequency $\omega_{n0} \to \sqrt{\omega_{n0}^2 - (\delta_{n0}/2)^2}$ and summation over all transition oscillators. It should be noted that the decrease of the eigenfrequency of oscillations in view of damping following from the said replacement is quite natural since friction (the analog of damping) reduces the rate of motion.

Concerned above was dipole polarizability that describes the response of an atom to a spatially uniform electric field. In the case that the characteristic size of the spatial nonuniformity of a field is less than the size of an atom, dipole polarizability should be replaced by the *generalized* polarizability of an atom $\alpha(\omega,\ q)$ depending on the momentum $\hbar\,\mathbf{q}$ transferred as a result of interaction. The spatial scale of the field nonuniformity λ is inversely proportional to the value of the wave vector $\lambda \sim 1/q$. With the use of the generalized polarizability of an atom $\alpha(\omega,\ q)$ the formula (A.3) is modified to the form

$$\mathbf{D}(\omega) = \int \alpha(\omega,\ q)\, \mathbf{E}(\omega,\ \mathbf{q})\, \frac{d\mathbf{q}}{(2\,\pi)^3}, \tag{A.21}$$

where $\mathbf{E}(\omega,\ \mathbf{q})$ is the spatio-temporal Fourier transform of the electric field vector. For the spatially uniform field $\mathbf{E}(\omega,\ \mathbf{q}) = \mathbf{E}(\omega)\, \delta(\mathbf{q})$ the Eq. A.21 (in case of a spherically symmetric atomic state) goes to Eq. A.1 in view of the fact that $\alpha(\omega) = \alpha(\omega,\ \mathbf{q} = 0)$.

Appendix 2 Methods of Description of the Electron Core of Multielectron Atoms and Ions

Slater Approximation

For definition of the effective field and the concentration of a atomic core, for simple estimations, and in a number of applications, in which the behavior of wave functions of atomic electrons at long distances is essential, nodeless Slater functions of the following form are used:

$$P_\gamma(r) = \sqrt{\frac{(2\beta)^{2\mu+1}}{\Gamma(2\mu+1)}} r^\mu e^{-\beta r}, \tag{A.22}$$

where $\gamma = (nl)$ is the set of quantum numbers characterizing an electronic state, β, μ are the Slater parameters. The wave functions (A.22) are normalized, have correct asymptotics at long distances. The main advantage of the functions (A.22) consists in their simplicity.

To determine the parameters β, μ, Slater proposed empirical rules that for shells more than half-filled look like

$$\beta_\gamma = \frac{Z - S_\gamma}{\mu_\gamma}, \tag{A.23}$$

where Z is the atomic nucleus charge, S_γ is the screening constant, the values of which, together with the parameter μ_γ and the number of electrons N_γ for different electron shells, are given in Table A.1.

For shells that are half-filled or less than half-filled, the best results are given by another rule:

$$\mu = \text{half-integer value nearest to } Z\Big/\sqrt{2|E|}, \beta = \mu\, 2|E|/Z, \tag{A.24}$$

V. Astapenko, *Polarization Bremsstrahlung on Atoms, Plasmas, Nanostructures and Solids*, Springer Series on Atomic, Optical, and Plasma Physics 72,
DOI 10.1007/978-3-642-34082-6, © Springer-Verlag Berlin Heidelberg 2013

Table A.1 Slater parameters of atomic shells

Shell $\gamma = (nl)$	S_γ	μ_γ	N_γ
$1s^2$	0.30	1	2
$2(sp)^8$	4.15	2	8
$3(sp)^8$	11.25	3	8
$3d^{10}$	21.15	3	10
$4(sp)^8$	27.75	3.5	8
$4d^{10}$	39.15	3.5	10
$5(sp)^8$ без 4f	45.75	4	8
$4(df)^{24}$	44.05	3.5	24
$5(sp)^8$ с 4f	57.65	4	8
$5d^{10}$ с 4f	71.15	4	10

where E is the electronic state energy in atomic units.

With the use of the functions (A.22) the radial distribution of the electron density of an atom in the Slater approximation can be obtained as

$$\rho(r) = \sum_\gamma N_\gamma P_\gamma^2(r). \tag{A.25}$$

The atomic (Slater) potential corresponding to this electron density is

$$U_S(r) = -\frac{\zeta_S(r)}{r}, \tag{A.26}$$

where $\zeta_S(r)$ is the effective charge of the core:

$$\zeta_S(r) = Z - \int_0^r \rho(r')dr' - r\int_r^\infty \frac{\rho(r')}{r'}dr'. \tag{A.27}$$

It is possible to make sure that the potential of Eqs. A.26 and A.27 satisfies the electrostatic Poisson equation with the boundary conditions:

$$\zeta_S(0) = Z, \quad \zeta_S(\infty) = Z_i, \tag{A.28}$$

where Z_i is the charge of an ion that is equal, naturally, to zero for a neutral atom. Substituting in Eq. A.27 the formulas (A.22), (A.25) and performing integration, we find

$$\zeta_S(r) = Z - \sum_\gamma N_\gamma \left[1 - e^{-2\beta r}\sum_{k=0}^{2\mu-1}\frac{2\mu-k}{2\mu}\frac{(2\beta r)^k}{k!}\right]_\gamma. \tag{A.29}$$

So the expressions (A.26), (A.29) give the atomic potential in the Slater approximation.

Quantum-Mechanical Methods of Calculation of the Structure of Multielectron Atoms

Consistent quantum-mechanical methods of calculation of the structure of multielectron atoms are based on solution of the Schrödinger equation with a multiparticle Hamiltonian taking into account electron-nucleus and electron–electron interaction that contains direct and exchange components. The multielectron wave function of an atom Ψ depends both on the spatial coordinates $\mathbf{r}_i$ and on the spin variables of atomic electrons $\mathbf{s}_i$. The general form of the function Ψ for atoms with two and more electrons is unknown. This reflects the impossibility in principle to solve a many-body problem. So different approximate methods are used that are based on one or another choice of a general form of the atomic wave function that is then substituted in the Schrödinger equation.

With neglected exchange effects, the elementary form of the multiparticle function $\Psi(\mathbf{r}_i, \mathbf{s}_i)$ is a multiplicative form of the one-particle coordinate wave functions ψ_{γ_i} depending on "their" spatial variables. This approach was proposed by Hartree at the initial stage of the quantum theory of multielectron atoms (the Hartree approximation). This approximation was extended by V.A. Fock to account for exchange interelectron interaction. The corresponding approach – the Hartree-Fock method – has found wide application in calculations of the structure of electron shells of atoms. In this method the multiparticle wave function is written as the Slater determinant:

$$\Psi = \frac{1}{\sqrt{N!}} \det_N \{\psi_i(x_k)\}, \tag{A.30}$$

where $\det_N$ designates a determinant of the Nth order (N is the number of atomic electrons) with the line number i and the column number k, x_k is the set of spatial and spin coordinates of the kth electron. The representation (A.30) automatically takes into account the properties of antisymmetry of the full wave function of an atom with respect to rearrangement of coordinates of electrons (including their spins). Physically the approximate expression for the multiparticle wave function (A.30) is connected with the idea of a self-consistent field, according to which each separated atomic electron moves in a spherically symmetric electric field produced by a nucleus and other atomic electrons.

In case of the ground nondegenerate state of an atom, its wave function is given by one Slater determinant such as Eq. A.30 with a specified electron configuration, that is, with specified distribution of electrons by shells. In the general case it is necessary to consider the linear superposition of the functions (A.30). For the ground state, using the substitution of the determinant of Eq. A.30 in the multiparticle Schrödinger equation, the following integro-differential system of the Hartree-Fock equations can be obtained:

$$-\frac{\hbar^2}{2m}\Delta_i\varphi_i(\mathbf{r}_i)-\frac{Ze^2}{r_i}\varphi_i(\mathbf{r}_i)+\frac{e^2}{2}\sum_{j\neq i}\frac{\left|\varphi_j(\mathbf{r}_j)\right|^2}{\left|\mathbf{r}_i-\mathbf{r}_j\right|}\varphi_i(\mathbf{r}_i)-\frac{e^2}{2}$$
$$\sum_{j\neq i}\frac{\varphi_j^*(\mathbf{r}_j)\varphi_i(\mathbf{r}_j)}{\left|\mathbf{r}_i-\mathbf{r}_j\right|}\varphi_j(\mathbf{r}_i)=\varepsilon_i\,\varphi_i(\mathbf{r}_i), \tag{A.31}$$

where $i,j=1\div N$, N is the number of electrons in an atom, $\varphi_i(\mathbf{r}_i)$ are the one-electron wave functions, ε_i are their associated one-electron energies. The first and the second summands in Eq. A.31 are one-particle terms connected with the kinetic energy operator and the Coulomb potential of an atomic nucleus respectively. The second two summands describe two-particle electron–electron interaction, the third summand relating to direct interaction and the fourth summand relating to exchange interaction. It is essential that the potential of direct interelectron interaction is local, that is, depending on an electron coordinate at a given point. At the same time the potential of exchange interaction is nonlocal and is defined by the distribution of the electron density of the electronic state under consideration in the whole space, which considerably complicates the solution of the system (A.31). It should be noted that this system without the last summand on the left side of the equations is a system of the Hartree equations that does not take into account exchange interaction between electrons that, generally speaking, is rather essential for correct calculation of an atomic structure.

Practically for determination of the one-electron orbitals φ_i and their associated energies ε_i, instead of the Hartree-Fock equations (A.31), a variational method is often used that is equivalent to them, in which the minimization of a corresponding energy functional is carried out by the iterative method. The computational complexity of the Hartree-Fock method grows rapidly with the number of atomic electrons, so the corresponding calculated time for heavy atoms is found to be too long even when using modern computers. Another disadvantage of this method is that it does not take into account the correlation interaction between electrons depending on the difference of their coordinates. Taking into account the correlation interaction is beyond the scope of the self-consistent field approximation that is a physical basis of the Hartree-Fock method.

The said disadvantages can be to some extent overcome with the use of approaches, in which the localization of the exchange potential is carried out. One of such methods is the local electron density approximation, in which the electron density $n(\mathbf{r})$ is considered as a basic value defining the properties of the ground state of an atom. Within the framework of this approximation it is possible to a certain extent to take into account also the correlation interelectron interaction by introducing a single exchange-correlation potential. A corresponding system of equations looks like:

$$\left[-\left(\hbar^2/2m\right)\Delta+V_{eff}(\mathbf{r})\right]\varphi_i(\mathbf{r})=\varepsilon_i\,\varphi_i(\mathbf{r}), \tag{A.32}$$

$$V_{eff}(\mathbf{r}) = -\frac{Z e^2}{r} + e^2 \int \frac{n(\mathbf{r}')}{|\mathbf{r} - \mathbf{r}'|} d\mathbf{r}' + \frac{\delta E_{xc}[n]}{\delta n(\mathbf{r})}, \tag{A.33}$$

$$n(\mathbf{r}) = \sum_{i=1}^{N} |\varphi_i(\mathbf{r})|^2, \tag{A.34}$$

where $E_{xc}[n]$ is the exchange-correlation energy functional depending on the local electron density. The exchange-correlation energy is obtained as a result of functional differentiation of the functional $E_{xc}[n]$ as seen from Eq. A.33. Since the exact form of $E_{xc}[n]$, as a rule, is unknown, different approximations are used for this form. In the method under consideration the exchange-correlation energy is written as

$$E_{xc}[n] = \int n(\mathbf{r})\, \varepsilon_{xc}[n(\mathbf{r})]\, d\mathbf{r}, \tag{A.35}$$

where ε_{xc} is the exchange-correlation energy per one electron. The approximation (A.35) results in the local exchange-correlation potential:

$$V_{xc}(\mathbf{r}) = \frac{\partial}{\partial n(\mathbf{r})} \{n(\mathbf{r})\, \varepsilon_{xc}[n(\mathbf{r})]\}. \tag{A.36}$$

In practice, instead of Eq. A.36, the following simple expression (in atomic units) is often used:

$$V_{xc}(\mathbf{r}) = -\frac{0.611}{r_s(\mathbf{r})} - 0.0333 \ln\left(1 + \frac{11.1}{r_s(\mathbf{r})}\right), \tag{A.37}$$

where the function $r_s(\mathbf{r})$ is determined from solution of the equation $(4/3)\,\pi\, r_s^3 = n^{-1}(\mathbf{r})$. In view of Eq. A.37, the Eqs. A.32, A.33, and A.34 become much more simple than the Hartree-Fock equations A.31, in which the nonlocal exchange interaction is present.

Statistical Methods of Description of the Structure of Multielectron Atoms

As noted above, the Hartree-Fock approximation becomes extremely laborious with growing number of atomic electrons. At the same time, it is for description of multielectron atoms ($N \geq 20$) that there is an alternative approach based on the statistical model of the atomic core. The most known model of such a kind is the Thomas-Fermi approximation. There are different methods to derive this

approximation. Here we will give one of them, based on the plasma model for a subsystem of bound electrons of an atom. An argument for such an approach is the fact that plasma models of an atom retain their attractiveness for investigations in the field of atomic physics for years, in spite of rapid development of computing methods. An obvious advantage of these models is their simplicity and universality making it possible to describe many properties of complex atoms and ions on a single basis. Among such properties are potentials of interaction of atoms with charged particles, cross-sections of photoionization of atoms, their static and dynamic polarizabilities, and other parameters.

The Thomas-Fermi distribution for a multielectron atom can be obtained following the works of A.V. Vinogradov with collaborators, from solution of the Vlasov self-consistent equations that are traditionally used in plasma physics. A corresponding system of equations looks like (in this item we use atomic units $\hbar = e = m_e = 1$):

$$\frac{\partial f}{\partial t} + \mathbf{p}\frac{\partial f}{\partial \mathbf{r}} - \nabla U \frac{\partial f}{\partial \mathbf{p}} = 0, \tag{A.38}$$

$$\Delta U = 4\pi[Z\,\delta(\mathbf{r}) - n(\mathbf{r})], \tag{A.39}$$

$$n(\mathbf{r}, t) = \int f(\mathbf{r}, \mathbf{p}, t)\, d\mathbf{p}, \tag{A.40}$$

where $f(\mathbf{r}, \mathbf{p}, t)$ is the electron distribution function, $U(\mathbf{r}, t)$ is the electron energy in the self-consistent field, $n(\mathbf{r}, t)$ is the electron density distribution, Z is the atomic nucleus charge. In absence of an external electromagnetic field, for the function of distribution of electrons and their energy we have: $f(\mathbf{r}, \mathbf{p}, t) = f_0(r, p), U(\mathbf{r}, t) = \varphi(r)$, $n(\mathbf{r}, t) = n_0(r)$. Then the solution of the Eq. A.38 can be represented as

$$f_0(r, p) = \frac{2}{(2\pi)^3}\theta(E_F - E), \quad E = p^2/2 + \varphi(r) \tag{A.41}$$

In writing Eq. A.41 the presence of the Fermi energy E_F for degenerate electron gas of atomic electrons following the Pauli principle was taken into account. Substituting Eq. A.41 in the formulas (A.39) and (A.40) gives the Thomas-Fermi distribution:

$$n_0(r) = \frac{p_F^3}{3\,\pi^2}, \quad p_F(r) = \sqrt{2\,(E_F - \varphi(r))}, \tag{A.42}$$

$$E_F - \varphi(r) = \frac{Z}{r}\,\chi\left(\frac{r}{r_{TF}}\right), \quad r_{TF} = \frac{b}{\sqrt[3]{Z}}, \quad b = \sqrt[3]{\frac{9\,\pi^2}{128}} \cong 0.8853, \tag{A.43}$$

where $\chi(x)$ is the Thomas-Fermi function being a solution of the equation of the same name

$$x^{1/2}\,\frac{d^2\chi(x)}{dx^2} = \chi(x)^{3/2}$$

with the boundary conditions; $\chi(0) = 1$ and $\chi(\infty) = 0$; r_{TF} is the Thomas-Fermi radius.

It should be noted that for a neutral atom the Fermi energy is equal to zero: $E_F = 0$. As a result, from Eqs. A.42 and A.43) we have the distribution of the electron density of a Thomas-Fermi atom:

$$n_{TF}(r) = Z^2 f_{TF}(x = r/r_{TF}), \tag{A.44}$$

where the function of the dimensionless distance to the nucleus is introduced that is

$$f_{TF}(x) = \frac{1}{4\,\pi\,b^3}\left(\frac{\chi(x)}{x}\right)^{3/2}. \tag{A.45}$$

The representation of electron density in the form of Eq. A.44 is common for all statistical models. The form of the function $f(x)$ depends on a concrete approximation. For example, in the statistical approach proposed by Lenz and Jensen the following expression for $f(x)$ is obtained (the Lenz-Jensen model):

$$f_{LJ}(x) \cong 3.7\,e^{-\sqrt{9.7\,x}}\,\frac{\left(1 + 0.26\,\sqrt{9.7\,x}\right)^3}{(9.7\,x)^{3/2}}. \tag{A.46}$$

It should be noted that for $x \leq 1$ the formulas (A.45) and (A.46) give practically coincident results, at high x the Lenz-Jensen function results in a somewhat more realistic reduction of the electron density of an atom with distance than the Thomas-Fermi function.

The most simple statistical model corresponds to the exponential decrease of the electron density on the Thomas-Fermi radius, in this case

$$f_{\exp}(x) = \pi^{-1}b^{-3}\exp(-2x). \tag{A.47}$$

The model of the atomic core of Eqs. A.44 and A.47) is often used in consideration of interaction of an electromagnetic field with atoms in solids.

Given in Fig. A.1 is the radial electron density of a krypton atom calculated within the framework of different approximations.

It is seen that the statistical Lenz-Jensen model (A.44) and (A.46) in a smoothed manner renders the quantum-mechanical dependence obtained in the Hartree-Fock approximation, without considering peculiarities connected with the shell structure

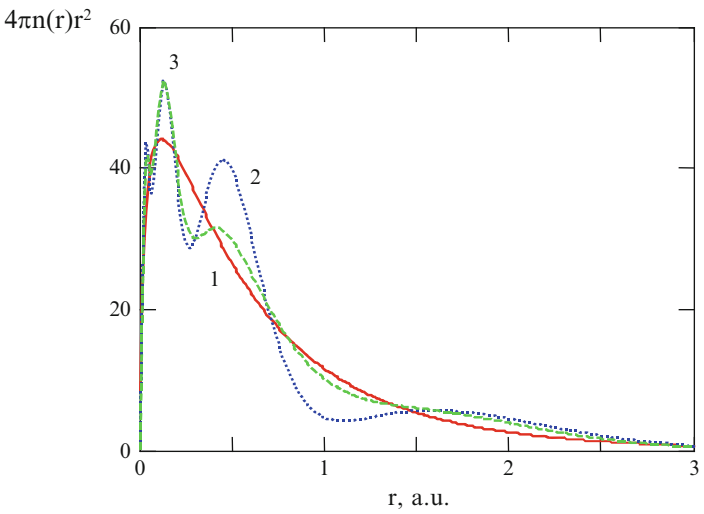

Fig. A.1 The radial density of the electron core of a krypton atom calculated within the framework of different models: *1* Lenz-Jensen, *2* Hartree-Fock, *3* Slater

of an atom. The Slater model (A.22), (A.23), (A.24), and (A.25) to some extent detects the radial fluctuations of electron density, especially in the region of small distances to a nucleus.

Approximations of the Thomas-Fermi Function for Neutral Atoms and Multielectron Ions

The Thomas-Fermi function $\chi(x)$ determining the potential and the electron density of an atom in the Thomas-Fermi model has no exact analytic representation, but there are its numerous approximations. Let us give here for the function $\chi(x)$ the Sommerfeld approximation describing not only neutral atoms, but also multielectron ions:

$$\chi(x,q) = \chi_0(x)\left[1 - \left(\frac{1+z(x)}{1+z_0(q)}\right)^{\lambda_1/\lambda_2}\right], \quad z(x) = \left(\frac{x}{\sqrt[3]{144}}\right)^{\lambda_2}, \tag{A.48}$$

where $q = Z_i/Z$ is the degree of ionization, $x_0(q)$ is the reduced radius of an ion, $\lambda_1 = \left(7+\sqrt{73}\right)/2$, $\lambda_2 = \left(-7+\sqrt{73}\right)/2$, $\chi_0(x)$ is the Thomas-Fermi function for a neutral atom, for which the following expression can be used:

$$\chi_0(x) = \frac{1}{(1+z(x))^{\lambda_1/2}}. \tag{A.49}$$

The parameter $x_0(q)$ can be determined from solution of the transcendental equation $q = -x\,d\chi/dx$, in which for the function $\chi(x,q)$ the formulas (A.48) and (A.49) are used. For high enough degrees of ionization a good result is given by the approximation of the reduced radius of an ion obtained in the Thomas-Fermi-Dirac model:

$$x_0(q) = 2.96\left(\frac{1-q}{q}\right)^{2/3}, \quad 0.2 < q \leq 1. \tag{A.50}$$

The Thomas-Fermi-Dirac model generalizes the Thomas-Fermi approximation to the consideration of exchange interaction between electrons. This interaction is a matter of principle for the statistical model of a neutral atom since it results in the finite size of the atom. It should be noted that in the Thomas-Fermi model the radius of an atom is equal to infinity. In the Thomas-Fermi-Dirac approximation the relation is true:

$$x_0(q=0) \approx 4\,Z^{0.4}, \tag{A.51}$$

and thus the radius of an atom within the framework of this model is finite.

Appendix 3 Dynamic Form Factor of Plasma Particles

Longitudinal Dielectric Permittivity of Plasma

Longitudinal waves, in which the electric field vector is parallel to the wave vector can propagate only in a substance. This follows from the Maxwell equation $\mathrm{div}\mathbf{D} = 0$. Really, from this equation in case of vacuum ($\varepsilon = 1$) for the longitudinal wave ($\mathbf{k} \parallel \mathbf{E}(\mathbf{k}, \omega)$) we obtain $(\mathbf{k} \cdot \mathbf{E}(\mathbf{k}, \omega)) = k E(\mathbf{k}, \omega) = 0 \rightarrow E(\mathbf{k}, \omega) = 0$. In a medium, generally speaking, $\varepsilon \neq 1$, so a longitudinal wave can exist if the equation is satisfied:

$$\varepsilon^{(l)}(k, \omega) = 0. \tag{A.52}$$

In writing this relation taken into account are spatial dispersion and the fact that the connection between the longitudinal components of electric induction and electric field intensity is given by the longitudinal component of dielectric permittivity $\varepsilon^{(l)}(k, \omega)$.

The Eq. A.52 represents the law of dispersion of a longitudinal electric wave in a medium. Solving it, it is possible to obtain the dependence $\omega(k)$ being the characteristic of the wave process in a substance under consideration with a specified longitudinal dielectric permittivity.

To obtain the dispersion dependence $\omega(k)$, it is necessary to know the explicit form of the function $\varepsilon^{(l)}(k, \omega)$. In case of plasma the dielectric permittivity is defined by free charges, the motion of which is subject to the laws of classical mechanics. To describe an ensemble of classical particles, the distribution function $f(\mathbf{r}, \mathbf{v}, t)$ is used that by definition is equal to the number of particles per unit phase volume at a specified point of phase space and a specified instant of time. In this case meant by the phase space is the six-dimensional space formed by the geometrical space and the velocity space. The velocity space integral of the distribution function gives the concentration of particles at a specified spatio-temporal point:

V. Astapenko, *Polarization Bremsstrahlung on Atoms, Plasmas, Nanostructures and Solids*, Springer Series on Atomic, Optical, and Plasma Physics 72,
DOI 10.1007/978-3-642-34082-6, © Springer-Verlag Berlin Heidelberg 2013

$$n(\mathbf{r},t) = \int f(\mathbf{r},\mathbf{v},t)\, d\mathbf{v}.$$

The distribution function defines all properties of the ensemble of particles including the contribution of this type of particles to the dielectric permittivity of a medium. In case of plasma the dielectric permittivity is defined by electrons and ions. Further in this section, unless otherwise indicated, by plasma particles we will mean electrons.

According to the Liouville theorem, the distribution function of the Hamiltonian system does not vary along any trajectory in the phase space. As applied to plasma, the Hamiltonian properties mean neglect of collisions. Thus in collisionless plasma for each kind of particles (electrons, ions) the following equation for the distribution function (the kinetic equation) is true:

$$\frac{df}{dt} \equiv \frac{\partial f}{\partial t} + \mathbf{v}\,\frac{\partial f}{\partial \mathbf{r}} + \frac{\mathbf{F}}{m}\,\frac{\partial f}{\partial \mathbf{v}} = 0, \tag{A.53}$$

where $\mathbf{F}$ is the force acting on a particle, m is the particle mass. For charged plasma particles $\mathbf{F}$ is the Lorentz force

$$\mathbf{F} = e\,\mathbf{E} + \frac{e}{c}\,[\mathbf{v}\,\mathbf{B}],$$

where e is the charge of the kind of particles under consideration, $\mathbf{E}$, $\mathbf{B}$ are the electric field strength and the magnetic induction acting on plasma particles.

If collisions can not be neglected, on the right side of the Eq. A.53 there should be the collision integral $St\{f\}$ representing an integral operator that is quadratic for the distribution function.

Let us consider the response of isotropic plasma to the longitudinal electric field of a plane wave $\mathbf{E} = \mathbf{E}(\omega,\mathbf{k})\exp\{i(\mathbf{k}\,\mathbf{r} - \omega)\}$. Let the wave vector $\mathbf{k}$ and the field intensity $\mathbf{E}$ be parallel to the axis x. Then, according to the definition of the electric induction and the longitudinal component of dielectric permittivity, we have ($\mathbf{P}$ is the plasma polarization):

$$D_x = \varepsilon^{(l)}\,E_x = E_x + 4\,\pi\,P_x, \tag{A.54}$$

hence

$$P_x = \frac{\varepsilon^{(l)} - 1}{4\,\pi}\,E_x. \tag{A.55}$$

On the other hand, from the equation $\rho = -\mathrm{div}\mathbf{P}$ for the Fourier component of polarization the equation is true:

$$P_x(\omega, k) = -i\frac{\rho(\omega, k)}{k}, \tag{A.56}$$

where $k \equiv k_x$. The obtained formulas give

$$\varepsilon^{(l)}(\omega, k) = 1 + \frac{4\pi i}{k}\frac{\rho(\omega, k)}{E(\omega, k)}. \tag{A.57}$$

Thus for determination of the explicit form of $\varepsilon^{(l)}(\omega, k)$ it is necessary to find the density of the polarization charge $\rho(\omega, k)$ induced in plasma by the longitudinal electric field $E(\omega, k)$. The desired density is connected with perturbation of the function of the plasma distribution δf arisen under the influence of the field:

$$\rho = e\int \delta f\, d\mathbf{v}. \tag{A.58}$$

The perturbed distribution function is $f = f_0 + \delta f$ (f_0 is the unperturbed distribution function). Further we assume that $\delta f << f_0$. Substituting the perturbed distribution function $f = f_0 + \delta f$ in the Eq. A.53, we find

$$\frac{\partial \delta f}{\partial t} + \mathbf{v}\frac{\partial \delta f}{\partial \mathbf{r}} = -\frac{e\,\mathbf{E}}{m}\frac{\partial f_0}{\partial \mathbf{v}}. \tag{A.59}$$

In derivation of Eq. A.59 the product $\mathbf{w}\,\delta f$ was neglected as a second-order term, and it was taken into account that the unperturbed distribution function is supposed to be isotropic, homogeneous and stationary (depends only on the magnitude of particle velocity and does not depend on the coordinate and time $f_0(\mathbf{r}, t, \mathbf{v}) = f_0(\mathrm{v})$).

In the case under consideration, when plasma is perturbed by a plane wave, the space-time dependence of perturbation of the function of the distribution of plasma particles in the approximation linear with respect to field looks like

$$\delta f \propto \exp\{i(\mathbf{k}\,\mathbf{r} - \omega)\}.$$

Substituting this dependence in the Eq. A.59, we find:

$$\delta f = \frac{i\,\mathbf{w}\,\partial f_0/\partial \mathbf{v}}{\mathbf{k}\,\mathbf{v} - \omega}. \tag{A.60}$$

Hence for the density of a polarization charge induced by the external field we have

$$\rho = i\frac{e^2}{m}\int \frac{\mathbf{E}\,\partial f_0/\partial \mathbf{v}}{\mathbf{k}\,\mathbf{v} - \omega}\, d\mathbf{v}. \tag{A.61}$$

Substituting the obtained expression in the Eq. A.57, we find for the longitudinal component of the dielectric permittivity of plasma:

$$\varepsilon^{(l)}(\omega,k) = 1 - \frac{4\,\pi\,e^2}{m\,k} \int\limits_{-\infty}^{\infty} \frac{(\partial f_0(\mathrm{v}_x)/\partial \mathrm{v}_x)}{k\,\mathrm{v}_x - \omega - i\,0}\, d\mathrm{v}_x, \tag{A.62}$$

where

$$f_0(\mathrm{v}_x) = \int\int f_0(\mathbf{v}) d\mathrm{v}_y\, d\mathrm{v}_z.$$

The infinitesimal imaginary additive in the denominator of Eq. A.62 is necessary for integral convergence. Its sign can be determined from the following reasoning. Let the electric field in the infinite past be equal to zero ($E(t \to -\infty) = 0$) and be turned on infinitely slowly. This means that the time dependence of intensity looks like

$$E(t) \sim \exp\{-i\,\omega\,t + \gamma\,t\} = \exp\{-i\,(\omega + i\gamma)\,t\},$$

where $\gamma \to +0$, that is, for taking into account the said field turning-on it is necessary to make the replacement $\omega \to \omega + i\,0$ as is done in Eq. A.62.

If the Sokhotsky's formula is used:

$$\frac{1}{x - i\,0} = V.P.\frac{1}{x} + i\,\pi\,\delta(x),$$

then for the real and imaginary parts of the longitudinal component of the dielectric permittivity of plasma it can be obtained:

$$\mathrm{Re}\left\{\varepsilon^{(l)}(\omega,k)\right\} = 1 - \frac{4\,\pi\,e^2}{m\,k} V.P. \int\limits_{-\infty}^{\infty} \frac{(\partial f_0(\mathrm{v}_x)/\partial \mathrm{v}_x)}{k\,\mathrm{v}_x - \omega}\, d\mathrm{v}_x, \tag{A.63}$$

$$\mathrm{Im}\left\{\varepsilon^{(l)}(\omega,k)\right\} = -\frac{4\,\pi^2\,e^2}{m\,k^2} \frac{\partial f_0(\mathrm{v}_x = \omega/k)}{\partial \mathrm{v}_x}. \tag{A.64}$$

It will be recalled that the symbol $V.P.$ means the principal integral value.

The distribution function in the expression for the imaginary part of dielectric permittivity (A.64) is taken for the x-projection of the electron velocity equal to the phase velocity of an electric wave $\mathrm{v}_{ph} = \omega/k$.

In view of the explicit form of the function of the electron velocity distribution in Maxwell plasma

$$f_0(\mathrm{v}_x) = \frac{m_e\, n_e}{\sqrt{2\,\pi\, T_e}} \exp\left\{-\frac{m_e \mathrm{v}_x^2}{2\, T_e}\right\} \tag{A.65}$$

from the formula (A.62) the following expression can be obtained for the complex longitudinal component of dielectric permittivity in view of the electron contribution:

$$\varepsilon^{(l,e)}(\omega, k) = 1 + \frac{1}{k^2\, r_{De}^2}\left[1 + F\left(\frac{\omega}{\sqrt{2}\, k\, \mathrm{v}_{Te}}\right)\right], \tag{A.66}$$

where

$$F(x) = \frac{x}{\sqrt{\pi}} \int\limits_{-\infty}^{\infty} \frac{\exp(-z^2)}{z - x - i\,0}\, dz, \tag{A.67}$$

$\mathrm{v}_{Te} = \sqrt{T_e/m_e}$ is the average thermal velocity of plasma electrons, $r_{De} = \sqrt{T_e/(4\,\pi\, e^2\, n_e)}$ is the electron Debye radius. The plot of the function (A.67) is presented in Fig. A.2.

Two characteristic ranges of variation of parameters for the dielectric permittivity of plasma can be separated: (1) the high-frequency range $\omega >> k\, \mathrm{v}_{Te}$ and (2) the low-frequency range $\omega << k\, \mathrm{v}_{Te}$. In the first case spatial dispersion is low in comparison with frequency dispersion. In other words, the electric field is quasi-uniform in space and essentially nonstationary. In the second case, on the contrary, the field is practically constant, but essentially nonuniform in space.

In the high-frequency range we have $x>>1$, and for the function (A.67) the expansion is true:

$$F(x>>1) \approx -1 - \frac{1}{2\,x^2} - \frac{3}{4\,x^4} + i\,\sqrt{\pi}\, x\, \exp\left(-x^2\right),$$

the imaginary part being close to zero. This can be seen from the diagrams of Fig. A.2. Then for the longitudinal part of dielectric permittivity we find:

$$\varepsilon^{(l,e)} \simeq 1 - \frac{\omega_{pe}^2}{\omega^2}\left[1 + 3\,(k\, r_{De})^2\right]. \tag{A.68}$$

Hence in the long-wavelength limit $k\, r_{De}<<1$ the elementary plasma formula for dielectric permittivity $\varepsilon(\omega) = 1 - \omega_p^2/\omega^2$ follows.

In the low-frequency range ($x<<1$) for the function (A.67) it is possible to obtain

$$F(x) \approx -2\,x^2 + i\,\sqrt{\pi}\, x.$$

Hence in the zeroth approximation $F = 0$, and the formula (A.66) gives

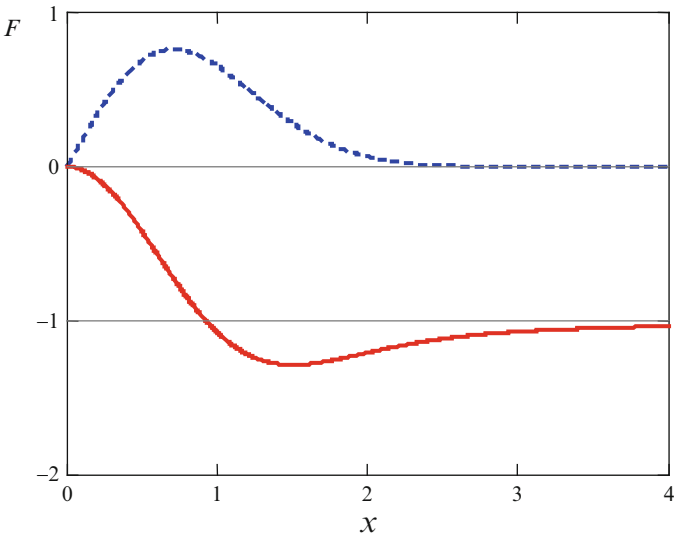

Fig. A.2 The real (*solid curve*) and imaginary (*dotted curve*) parts of the function (A.67) determining the longitudinal dielectric permittivity of Maxwell plasma

$$\varepsilon^{(l,e)} = 1 + \frac{1}{k^2\, r_{De}^2}, \tag{A.69}$$

that is, the low-frequency longitudinal dielectric permittivity does not depend on frequency.

The function (A.69) describes screening of the electric field of a static charge placed in plasma. It is possible to be convinced of this, calculating the spatial Fourier transform of the potential of a screened charge $\varphi = q\, \exp(-r/r_D)/r$ and dividing it by the Fourier transform of the potential of a point charge in vacuum. The low-frequency dielectric permittivity (A.69) indicates that long-wave perturbations ($k << r_{De}^{-1}$) are strongly screened in plasma $\varepsilon^{(l,e)} >> 1$, and short-wave perturbations ($k >> r_{De}^{-1}$), on the contrary, are weakly screened: $\varepsilon^{(l,e)} \simeq 1$.

The longitudinal part of the dielectric permittivity of Maxwell plasma in view of the contribution of ions looks like:

$$\varepsilon^{(l)}(\omega, k) = 1 + \frac{1}{k^2\, r_{De}^2}\left[1 + F\left(\frac{\omega}{\sqrt{2}\, k\, \mathrm{v}_{Te}}\right)\right] + \frac{1}{k^2\, r_{Di}^2}\left[1 + F\left(\frac{\omega}{\sqrt{2}\, k\, \mathrm{v}_{Ti}}\right)\right], \tag{A.70}$$

where the function $F(x)$ is given by the expression (A.67), $\mathrm{v}_{Ti} = \sqrt{T_i/m_i}$, $r_{Di} = \sqrt{T_i/\left(4\,\pi\, e_i^2\, n_i\right)}$ is the ionic Debye radius (e_i is the charge of a plasma ion).

It should be noted that since $v_{Te} >> v_{Ti}$, an electric wave that is high-frequency in comparison with the ionic component of plasma can be low-frequency in comparison with plasma electrons.

Determination and Calculation of the Dynamic Form Factor

Expressed in terms of longitudinal dielectric permittivity is an important characteristic of plasma called the *dynamic form factor* (DFF) or the *spectral density function*. The dynamic form factor defines the probability of electromagnetic interactions with participation of plasma particles, during which the subsystem of plasma electrons or ions absorbs the energy-momentum excess. An example of such processes is radiation scattering in plasma, bremsstrahlung and polarization bremsstrahlung on plasma particles including an induced bremsstrahlung effect and a number of other phenomena.

The determination of the DFF of a specified plasma component looks like

$$S(\omega, \mathbf{k}) = \frac{1}{2\pi} \int_{-\infty}^{\infty} dt\, e^{i\,\omega t} \langle \hat{n}(\mathbf{k}, t)\, \hat{n}(-\mathbf{k}) \rangle, \tag{A.71}$$

where $\hat{n}(\mathbf{k})$, $\hat{n}(\mathbf{k}, t)$ are the spatial Fourier transforms of the operator of concentration of plasma particles of a specified type in the Schrödinger and Heisenberg representations, the angle brackets include quantum-mechanical and statistical averaging.

It will be recalled that the Heisenberg representation of quantum-mechanical operators implies taking into account their time dependence in contrast to the Schrödinger representation, in which the whole time dependence is transferred to the wave function of the system. The connection between these representations for an arbitrary operator $\hat{Q}$ is given by the relation:

$$\hat{Q}(t) = \exp\left(i\,\hat{\mathrm{H}}\,t/\hbar\right) \hat{Q}\, \exp\left(-i\,\hat{\mathrm{H}}\,t/\hbar\right),$$

where $\hat{\mathrm{H}}$ is the Hamiltonian of the quantum-mechanical system. In this paragraph, however, the quantum-mechanical formalism will not be used, the quantum terms and designations are given only for completeness of statement.

The Eq. A.71 can be obtained from the formula

$$S(\omega, \mathbf{k}) = \sum_{f,i} w(i)\, \delta\left(\omega + \omega_{fi}\right) \left| n_{fi}(\mathbf{k}) \right|^2, \tag{A.72}$$

in which in the explicit form averaging over initial $|i\rangle$ and summation over final $|f\rangle$ states of plasma particles is performed ($w(i)$ is the probability of a plasma particle

being in the *i*th state). The delta function in Eq. A.72 reflects, as usual, the energy conservation law.

Depending on the type of plasma particles, the DFF can be electron, ionic, and mixed. In case of the mixed DFF in the definition (A.71) the product of the density operators for electrons and ions appears.

By its physical meaning the DFF defines the probability of plasma absorption of the four-dimensional wave vector $k = (\omega, \mathbf{k})$ in terms of the action of external disturbance *on a specified plasma component*. In case of uniform charge distribution in plasma this probability would be equal to zero since then the Fourier transform of the density of charged particles is reduced to the delta function $n(\mathbf{k}) \to n\,\delta(\mathbf{k})$. Thus the DFF is connected with charge fluctuations in plasma.

The dynamic form factor reflects the dynamics of plasma particles interacting with each other through the long-range Coulomb forces. In this case the interaction both in the ensemble of particles of one type and between electrons and ions is taken into account.

In case of uniform plasma it is convenient to introduce the DFF of the unit volume (the normalized DFF) by the formula

$$\tilde{S}(\omega, \mathbf{k}) = \frac{S(\omega, \mathbf{k})}{V}, \tag{A.73}$$

where V is the volume of plasma. This equation follows from the fact that for a uniform medium the pair correlation function of concentration depends only on the relative distance between spatial points:

$$Kn(\mathbf{r}, \mathbf{r}', t) \equiv \langle \hat{n}(\mathbf{r}, t)\, \hat{n}(\mathbf{r}', 0) \rangle = Kn(\mathbf{r} - \mathbf{r}', t).$$

To calculate the normalized DFF, it is convenient to use the fluctuation-dissipative theorem connecting the DFF of plasma components with the function of plasma response to the external electromagnetic disturbance. This theorem for the electron DFF is expressed by the equation:

$$\tilde{S}_e(\omega, \mathbf{k}) = \frac{\hbar}{\pi e^2} \frac{\mathrm{Im}\{F_{ee}(\omega, \mathbf{k})\}}{[\exp(-\hbar\omega/T) - 1]}, \tag{A.74}$$

where $F_{ee}(\omega, \mathbf{k})$ is the linear function of the electron component response to the fictitious external potential acting only on plasma electrons, T is the temperature of plasma in energy units. The imaginary part of the response function appearing in Eq. A.74 describes energy dissipation in plasma, which is the reason for the name of the theorem.

Let us introduce the second linear function of the response to the external potential $F_{ei}(\omega, \mathbf{k})$ that describes the response of the electron component of plasma under the action of the fictitious external potential acting only on plasma ions. Here for

convenience we use the Coulomb gauge of the electromagnetic field, in which the divergence of the vector potential is equal to zero (div$\mathbf{A} = 0$) and the charge density is related only to the scalar potential of the electromagnetic field φ via the Poisson equation. So let the external potential $\varphi_{ext}(k)$ act on plasma, where $k = (\omega, \mathbf{k})$ is the four-dimensional wave vector. Then the density of the electron charge induced in plasma is expressed in terms of the introduced response functions as follows:

$$\langle \hat{\rho}_e(k) \rangle = [F_{ee}(k) + F_{ei}(k)]\, \varphi_{ext}(k), \tag{A.75}$$

$\left\langle \hat{\rho}_j(k) \right\rangle = e_j \left\langle \hat{n}_j(k) \right\rangle$ is the density of the charge of the jth type of plasma particles. The Eq. A.75 indicates that the electron density of a charge arises in plasma both due to direct action on plasma electrons of the external potential (the first summand in the square brackets of Eq. A.75) and as a result of action of the external potential on plasma ions that are connected with electrons by Coulomb forces. If the interaction between particles of the kind i and of the kind j is weak, it is possible to express F_{ij} in terms of the characteristics of noninteracting particles. For this purpose the new response function $\alpha_j(k)$ is introduced – the function of the response of particles of the kind j to the *total potential* in plasma. It takes into account the action on charged particles of the potential $\varphi_{ind}(k)$ induced in plasma that appears because of redistribution of charged particles under the action of the external potential. With the use of the function $\alpha_j(k)$ the induced charge density for the jth component can be expressed in terms of the total potential as follows:

$$\left\langle \hat{\rho}_j(k) \right\rangle = \alpha_j(k)\, \varphi_{tot}(k). \tag{A.76}$$

As the response function $\alpha_j(k)$ describes the action on plasma particles of the total potential, for its calculation the characteristics of noninteracting particles can be used since the interaction between them is already taken into account in the total potential. This technique is widely used in plasma physics in description of screening and initiation of collective excitations. In the approach under consideration the response function $\alpha_j(k)$ can be expressed in terms of the function $Q_j(k)$ characterizing the noninteracting particles $\alpha_j = e_j^2\, Q_j$, where

$$Q_j(k) = \int \frac{n_j(\mathbf{p} + \hbar\,\mathbf{k}) - n_j(\mathbf{p})}{E_j(\mathbf{p} + \hbar\,\mathbf{k}) - E_j(\mathbf{p}) - \hbar\,\omega - i\,0}\, \frac{2\,d\mathbf{p}}{(2\,\pi\,\hbar)^3}. \tag{A.77}$$

Here $n_j(\mathbf{p})$ is the dimensionless function of the distribution of plasma particles of the kind j by momenta, $E_j(\mathbf{p}) = p^2/2\,m_j$. Further we should know the imaginary part of the function $Q_j(k)$ that can be determined from Eq. A.77 with the use of the Sokhotsky's formula. For the Maxwell distribution of electrons by velocities we find

$$\mathrm{Im}\{Q_j(k)\} = \pi \left(e^{-\hbar\omega/T} - 1\right) n_j \frac{\exp\left\{-\omega^2 \Big/ 2\,k^2\,\mathrm{v}_{Tj}^2\right\}}{\sqrt{2\,\pi}\,k\,\mathrm{v}_{Tj}}. \tag{A.78}$$

The introduced functions of the response to the total potential are related to the longitudinal part of dielectric permittivity as follows:

$$\varepsilon^{(l,j)}(k) = 1 - \frac{4\,\pi}{\mathbf{k}^2}\,\alpha_j(k). \tag{A.79}$$

Now let us solve the set problem: we will find the function $F_{ee}(\omega, \mathbf{k})$ expressing it in terms of the function of the response to the total potential. For this purpose we will introduce the fictitious external potential φ^*_{ext} acting only on electrons. Then according to the definition $F_{ee}(\omega, \mathbf{k})$ we have

$$\left\langle \hat{\rho}^*_e(k) \right\rangle = F_{ee}(k)\,\varphi^*_{ext}(k). \tag{A.80}$$

On the other hand, $\left\langle \hat{\rho}^*_e \right\rangle$ can be expressed in terms of α_e:

$$\left\langle \hat{\rho}^*_e(k) \right\rangle = \alpha_e(k)\left[\varphi^*_{ext}(k) + \varphi^*_{ind}(k)\right], \tag{A.81}$$

where φ^*_{ind} is the potential induced under the action of φ^*_{ext}, determined in terms of the density of all plasma charges with the use of the Poisson equation:

$$\varphi^*_{ind}(k) = \frac{4\,\pi}{\mathbf{k}^2}\left[\left\langle \hat{\rho}^*_e(k) \right\rangle + \left\langle \hat{\rho}^*_i(k) \right\rangle\right], \tag{A.82}$$

where

$$\left\langle \hat{\rho}^*_i(k) \right\rangle = \alpha_i(k)\,\varphi^*_{ind}(k), \tag{A.83}$$

since the potential φ^*_{ext} is assumed to act only on electrons. Solving the system of the Eqs. A.80, A.81, A.82, and A.83, we find the following expression for F_{ee}:

$$F_{ee}(k) = \frac{\alpha_e(k)\left[1 - \left(4\,\pi/\mathbf{k}^2\right)\alpha_i(k)\right]}{1 - \left(4\,\pi/\mathbf{k}^2\right)\left[\alpha_e(k) + \alpha_i(k)\right]}. \tag{A.84}$$

Substituting Eq.A.84 in Eq. A.74 and using Eqs. A.78 and A.79, we obtain

$$\tilde{S}_e(k) = \left|\frac{\varepsilon^{l(i)}(k)}{\varepsilon^l(k)}\right|^2 |\delta n_e(k)|^2 + z_i^2 \left|\frac{1 - \varepsilon^{l(e)}(k)}{\varepsilon^l(k)}\right|^2 |\delta n_i(k)|^2, \tag{A.85}$$

where

$$\left|\delta n_{e,i}(k)\right|^2 = \frac{n_{e,i}}{\sqrt{2\pi}\,\mathrm{v}_{Te}\,|\mathbf{k}|}\exp\left(-\frac{\omega^2}{2\,\mathbf{k}^2\,\mathrm{v}_{Te,i}^2}\right) \tag{A.86}$$

are the spatio-temporal Fourier transforms of the squared thermal fluctuations of electron and ionic components of plasma calculated on the four-dimensional wave vector $k = (\mathbf{k},\, \omega)$, z_i is the charge number of plasma ions, it is implied that the quasi-neutrality condition is satisfied, so $n_e = z_i\, n_i$.

The expression for the ionic normalized DFF is found in exactly the same way as for the electron DFF. For this purpose it is necessary to make the replacement of the indices $e \rightleftarrows i$ and to take into account the fact that now in the denominator of the formula (A.74) the ion charge $e_i = z_i\, e$ appears, then we obtain:

$$\tilde{S}_i(k) = \left|\frac{\varepsilon^{l(e)}(k)}{\varepsilon^{l}(k)}\right|^2 |\delta n_i(k)|^2 + z_i^{-2}\left|\frac{1-\varepsilon^{l(i)}(k)}{\varepsilon^{l}(k)}\right|^2 |\delta n_e(k)|^2. \tag{A.87}$$

The mixed normalized DFF is given by the equation:

$$\tilde{S}_{ei}(k) = z_i^{-1}\left|\frac{1-\varepsilon^{l(i)}(k)}{\varepsilon^{l}(k)}\right|^2 |\delta n_e(k)|^2 + z_i\left|\frac{1-\varepsilon^{l(e)}(k)}{\varepsilon^{l}(k)}\right|^2 |\delta n_i(k)|^2 \tag{A.88}$$

that follows from the fluctuation-dissipative theorem (A.74) (with the replacement $e^2 \to e\, e_i$) and the formula for the linear response function F_{ei} describing the initiation of an electron charge induced by the fictitious potential that acts only on ions. This formula looks like:

$$F_{ei}(k) = \frac{\left(4\,\pi/\mathbf{k}^2\right)\alpha_i(k)\alpha_e(k)}{1-\left(4\,\pi/\mathbf{k}^2\right)\left[\alpha_e(k)+\alpha_i(k)\right]}. \tag{A.89}$$

The Eq. A.89 is obtained with the use of similar reasoning that led to the formula (A.84).

Let us explain the physical meaning of the expression (A.85) for the electron DFF. The first summand is connected with the deficiency of electron charge around the electron density fluctuation caused by electron–electron repulsion. The second summand in this expression describes the electron charge screening the fluctuation of the ionic plasma component, it results from electron-ion attraction. By analogy, in the expression (A.87) for the ionic DFF the second summand describes the ionic charge screening the fluctuation of electron density, and the first summand describes the deficiency of ionic charge around the ionic fluctuation. Finally, in the formula (A.88) for the mixed DFF the first summand describes the ionic charge screening the fluctuation of electron density, and the second summand describes the electron charge screening the fluctuation of ionic density.

Let us consider the explicit form of the electron DFF in fulfilment of the inequations $k\,v_{Te} >> \omega >> k\,v_{Ti},\ \omega_{pi}$. Then for the longitudinal electron dielectric permittivity of plasma the low-frequency approximation is true, and for the ionic component the high-frequency approximation is true. Using the formulas (A.68), (A.69), (A.70), and (A.85), we find

$$\tilde{S}_e(k) \simeq \left(\frac{k^2 r_{De}^2}{1 + k^2 r_{De}^2}\right)^2 |\delta n_e(k)|^2 + \frac{z_i^2}{\left(1 + k^2 r_{De}^2\right)^2} |\delta n_i(k)|^2. \tag{A.90}$$

From this formula it is seen that in case of long-wave fluctuations, when $k^2 r_{De}^2 << 1$ ($k = 2\pi/\lambda$), the first summand describing the deficiency of electron charge around the fluctuation of electron density is small. The second summand connected with electron screening of ionic density fluctuations is great. Hence it follows that in the long-wavelength limit the transfer of energy-momentum to plasma proceeds through the electron charge of the Debye sphere around a plasma ion that reacts in a coherent manner to the electric field, that is, the interaction is of a collective nature. In the short-wave case $k^2 r_{De}^2 >> 1$ the situation is opposite: the electromagnetic interaction is realized through excitation of individual plasma electrons, into which the Debye sphere "falls apart" because of strong spatial nonuniformity of the electric field.

Index

V. Astapenko, *Polarization Bremsstrahlung on Atoms, Plasmas, Nanostructures and Solids*, Springer Series on Atomic, Optical, and Plasma Physics 72,
DOI 10.1007/978-3-642-34082-6, © Springer-Verlag Berlin Heidelberg 2013